Towards novel Au(III) porphyrins: Synthesis and characterization of a range of *meso*-tetraalkylporphyrins

Submitted in fulfilment of the requirements for the degree of

MASTER OF SCIENCE

By

Rosanne C. Salmond
BSc. (Hons) (UKZN)

September 2007

School of Chemistry
University of KwaZulu-Natal
Pietermaritzburg

Declaration

I hereby certify that this research is as a result of my own investigations which has not already been accepted in substance for any degree and is not submitted in candidature for any other degree.

Signed.....

Rosanne C. Salmond

I hereby certify that this statement is correct.

Signed.....

Professor O. Q. Munro

Supervisor

School of Chemistry
University of KwaZulu-Natal
Pietermaritzburg

September 2007

Acknowledgments

First and foremost, I would sincerely like to thank my supervisor, **Prof Orde Q. Munro** for his time, patience, expert advice and guidance. Thank you for your help and support throughout this work.

I would also like to take this opportunity to thank:

Craig Grimmer: for recording and helping to interpret my NMR spectra; as well as for his assistance (and patience) in averting many PC crises.
Shawn Ball and Hashim Desai: for their efficiency and willingness to help.
Raj Somaru and Fazel Sheik: for their help and invaluable assistance in the laboratory.
Michelle Francis and Karen Kader: for their help in all circumstances.
Dr André van der Hoven: for our weekly conversations and her encouragement.
Paul Forder and Clarence Mortlock: for all my new and repaired glassware.
The Warren Organic Laboratory Researchers: for their help whenever needed.
The Inorganic Laboratory Researchers: for their help and assistance; as well as providing a friendly and fun environment for lab work.
Irene, Arina, Nomandla, Madira, Allan, Tyler, Matt, Brad, Santham, Jude, Siphamandla, Zimbili: for the helping hand whenever needed.
Kristy-Lyn de Boer: for her time, help and understanding. Thank you for being there no matter what the situation. Your input and support have been invaluable to me.
Hilary Wilson: for her proof reading of this work. (Thanks also to **Neil** and **Kerry**.)

Those who helped from far: **Ylenia, Janine N., Lynette, Venashree, Kuveshnee, and Eloïse.**

As well as: **Jo, Lindsay, Cass, Liz, Kerry, Janine S., Gabz, Belinda, Helen, Mark, Vonnie, Karin, Kirst, Sarah, Steve and Suzanne.**

Clyde and Hilary Wilson: for their support, help and generosity.

NRF: The financial assistance of the National Research Foundation (NRF) toward this research is hereby acknowledged. Opinions expressed and conclusions arrived at, are those of the author and are not necessarily to be attributed to the NRF.

Mintek: for project funding at the end of my work.

Sheryn, Dylan and Jessica: thank you for your support and for all that you did to make these last few years easier. Thank you for getting me through the worst and for being there for the best.

My Wonderful Parents: thank you for allowing me the opportunity to begin this era of my life. Thank you for your support (in all the different ways you provided it) and for your continuous encouragement. Without you, this would never have been possible!

Neil: Thank you for your support and understanding. Thank you for keeping me laughing and for always being so encouraging.

Conference Proceedings

A poster of this work has been presented at the following South African Chemical Institute Conferences:

- The 12th Inorganic Conference held in Pietermaritzburg (2005); and
- The 13th Inorganic Conference held in Cape Town (2007).

The title of these posters was: Synthesis and characterization of some new meso-tetraalkylporphyrins.

List of Abbreviations and Symbols

2D	Two Dimensional
$BF_3 \cdot OEt_2$	Boron trifluoride etherate
bp	Boiling point
^{13}C NMR	Carbon Magnetic Resonance
CSD	Cambridge Structural Database
c.t.	Charge transfer
DCM	Dichloromethane
DDQ	2,3-dichloro-5,6-dicyano-1,4-benzoquinone
DFT	Density Functional Theory
DMF	*N, N*-dimethylformamide
Etio	2,7,12,17-methyl and 3,8,13,18-ethyl substituted porphyrin
EtOD	Ethyl alcohol-*d*
FMO	Frontier molecular orbital
FT	Fourier transform
^1H NMR	Proton Magnetic Resonance
HOMO	Lowest Unoccupied Molecular Orbital
HPLC	High Performance Liquid Chromatography
HRP	Horseradish peroxidase
$H_2T(iBu)P$	*meso*–Tetraisobutylporphyrin
$H_2T(CH_2Ph)P$	*meso*–Tetrabenzylporphyrin
$H_2T(iPent)P$	*meso*–Tetraisopentylporphyrin
$H_2T(CHPh_2)P$	*meso*–Tetradibenzylporphyrin
$H_2T(iPr)P$	*meso*–Tetraisopropylporphyrin
$H_2T(cyHx)P$	*meso*–Tetracyclohexylporphyrin
H_2TMP	*meso*–Tetramesitylporphyrin
H_2TPP	*meso*–Tetraphenylporphyrin
H_2TPyP	*meso*–Tetra-4-pyridylporphyrin

Hz	Hertz
IR	Infrared
ISC	Inter system crossing
J	Coupling constant
KBr	Potassium bromide
LD-MS	Laser-desorption mass spectrometry
LIS	Lanthanide Shift Reagents
LUMO	Lowest Unoccupied Molecular Orbital
µs	Micro seconds
ml	Milliliters
mmol	Millimoles
mM	Millimolar
MOs	Molecular Orbitals
MP2	Møller-Plesset perturbation theory
ms	Millisecond
NMR	Nuclear Magnetic Resonance
ns	Nanoseconds
PDT	Photo Dynamic Therapy
Ph	Phenyl
rf	Radio frequency
RIS	Ring current Induced Shifts
rR	resonance Raman
σ	Shielding constant
TFA	Trifluoroacetic acid
THF	Tetrahydrofuran
TLC	Thin layer chromatography
UV	Ultraviolet
vis	Visible
VT	Variable-temperature
v/v	Volume to volume ratio

Abstract

The principal goal of this work was to synthesize and fully characterize a range of free base *meso*-tetraalkylporphyrins due to the fact that the chemistry of these derivatives is underdeveloped relative to their *meso*-tetraaryl counterparts. Three novel porphyrins, $H_2T(iBu)P$, $H_2T(CH_2Ph)P$ and $H_2T(CHPh_2)P$, as well as three known porphyrins, $H_2T(iPent)P$, $H_2T(iPr)P$ and $H_2T(cyHx)P$, (where iBu, iPent, iPr, cyHx = isobutyl, isopentyl, isopropyl, cycloxehyl, respectively) were synthesized using an improved method developed in our laboratory. Yields up to 20% were obtained depending on the aldehyde starting material used in the condensation reaction with pyrrole.

The structures (particularly the conformations of the macrocycles) and spectroscopic properties of the porphyrins in this series were elucidated using several methods. For those porphyrins for which X-ray quality crystals could be obtained, X-ray structures were determined. Although only one structure was refined to a complete publication-quality model ($H_2T(CH_2Ph)P$), the other structures served to confirm the successful synthesis of the porphyrin and the geometry of its conformation. DFT simulations (B3LYP functional, 6-31G** basis set) in conjunction with the X-ray data suggest that crystal packing effects may have an effect on the porphyrin conformation. The trend in geometry observed from the DFT simulations for this type of porphyrin was predominantly a ruffled conformation. The porphyrins were also characterized using UV-vis, IR and NMR spectroscopy and comparisons were made with relevant literature. DFT simulations were used to obtain theoretical IR frequency data and NMR shielding tensors. The DFT-predicted frequencies and chemical shifts compared favourably with the experimental data and helped in the assignment of the experimental spectra of the porphyrins.

Preliminary fluorescence emission spectra were recorded for each of the porphyrins at room temperature and at 77 K. Emission from both the Q and B excited singlet states was observed in all the spectra. At 77 K, the emission spectra were well-resolved, permitting a preliminary analysis of the vibrationally excited states of the ground electronic state to be made, particularly in the case of $H_2T(CHPh_2)P$. Lifetimes were

determined for each of the emission maxima. The steady-state emission spectra were consistent with the emission spectra reported for other porphyrins in the literature (e.g., H_2TPP, where H_2TPP = 5,10,15,20-tetraphenylporphyrin). However, the excited state lifetimes of the present series of *meso*-tetraalkylporphyrins were substantially longer (at least one order of magnitude) than those typical of *meso*-tetraarylporphyrins (ca. 5–15 ns). The shortest and longest lifetimes measured in dichloromethane were 0.12(2) μs (Q band, $H_2T(CH_2Ph)P$, 298 K) and 1.05(1) μs (B band, $H_2T(CHPh_2)P$, 298 K), respectively. No significant differences in the excited state lifetimes were observed in degassed dichloromethane solutions.

The long term goal of this work is to metallate the present series of free base *meso*-tetraalkylporphyrins (including several others) with gold(III). The gold(III) derivatives will be screened *in vitro* (and possibly *in vivo*) for their efficacy as DNA-intercalating anticancer drugs. A preliminary successful metallation for one of the porphyrins is presented in this work. Proof of successful metallation was demonstrated using UV-vis, IR and NMR spectroscopy; however, no X-ray quality crystals have been obtained to date in on-going experiments.

Contents

Chapter 4 – NMR Spectroscopy

Chapter 5 – X-ray Crystallography

Chapter 6 – Photoluminescence

Chapter 7 – DFT Simulations

1. Introduction

1.1 Porphyrins in General

Colours form an imperative part of our lives; however, their origin is rarely questioned. One particularly extraordinary and large group of coloured compounds is the **porphyrins**, which are involved in many different fields including chemistry, biochemistry, medicine, geology, chemical engineering, paleobiology, alternative energy, and microelectronics. These porphyrins are a collection of intensely coloured (deep red/purple) compounds that can be described as fluorescent, crystalline pigments.[1] Their name is derived from the ancient Greek word porphura[2] which referred to the colour purple. However, this word seems to have its origins in an earlier Semitic word used by the Phoenicians to describe a type of mollusc from which they extracted a special dye that was used to give the purple colour to the attire worn by the Phoenician Royal Families.[1] Porphyrin in biochemistry now refers to *any of various nitrogen-containing, heterocyclic organic compounds occurring widely in plant and animal tissues.*[2]

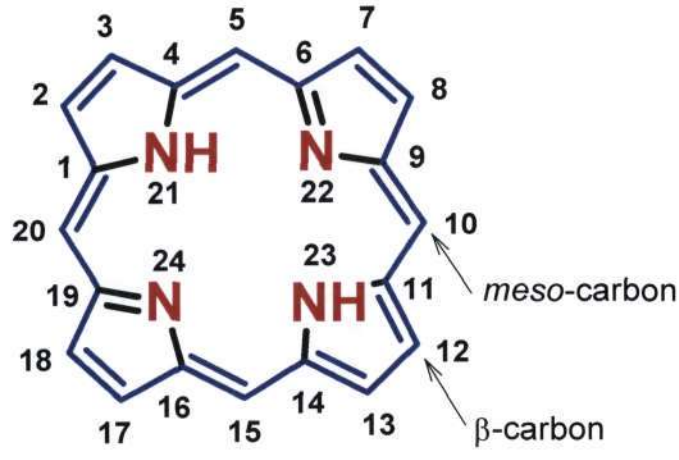

Figure 1.1: The unsubstituted porphyrin macrocycle and its IUPAC numbering scheme.[1]

The common feature of porphyrins is their central aromatic macrocycle, consisting of twenty carbon atoms and four nitrogen atoms. This macrocycle contains four smaller pyrrole rings connected by bridging carbon atoms (Figure 1.1). The macrocycle is an

aromatic system containing 22 π-electrons, but only 18 of these are delocalized, thus it obeys Hückel's rule for aromaticity (4n+2 π-electrons, where n=4).[3] Aromatic character for these compounds has been confirmed by measurements of their heats of combustion.[4] In 1912 this cyclic tetrapyrrole structure was first suggested by Küster;[5] however, it was thought that such a large ring would be fundamentally unstable.[1,4] Hence not even the man who later became known as the father of modern porphyrin chemistry, Hans Fischer, agreed with him.[1] Fischer did, however, have a part in the final proof, which was supplied by the total synthesis of protohaem in 1929.[6] Leading up to this synthesis there was other experimentation with pyrrole and its derivatives; one in particular in 1927 produced a porphyrin-type compound, which was called "porphyrin" $C_{36}H_{34}O_8N_4Br$.[7]

The porphyrin macrocycle is highly conjugated and a number of resonance forms can be written.[4] Porphyrins are generally flat, stable molecules and their solutions are relatively unstable to light. The porphyrin nucleus is stable towards concentrated sulfuric acid and neat trifluoroacetic acid (which are often used to remove metals coordinated at the centre of a porphyrin), but may be destroyed by perchloric acid, chromic acid, permanganate, or hydriodic acid.[4] The porphyrin has properties that are more than the sum of its parts and therefore their physical and chemical properties cannot be derived from those of pyrroles.[1] This can be seen by the difference in their colour; pure pyrroles are commonly clear when liquid or off-white as solids, very different to the intense purple colour of the porphyrins.

There are many examples where the macrocycle can become bent with major deformations from planarity due to the complexing of a variety of metal ions in the central cavity.[1] If the metal ion is too small, as in the case of the nickel(II) ion, or too large, as in the case of Pb^{2+} and Tl^{3+}, to fit the cavity then twisting of the ring in order to allow better binding is possible. The conformational effects of metal ion size have been examined. These studies highlight the importance of non-bonding repulsions between the axial ligands with the porphyrin core[8,9] and the variance of large metal ions with the restricted porphyrin cavity size.[10,11,12,13,14,15.] When all four of the central nitrogen atoms are protonated in combination with bulky peripheral substituents the macrocycle can also twist. Other substantial distortions may be caused by substitution

of groups onto the central nitrogen atoms and loss of aromaticity due to oxidation of the porphyrin.[1]

The main role played by porphyrins and porphyrin-type compounds found in nature is the binding of metal ions which act as active centres for important biochemical processes.[1] Thus porphyrin-based films on metal or semi-conductor surfaces are particularly attractive for application as chemical and gas sensors,[16,17,18] along with nanoporous catalytic materials[19,20] in novel synthetic biomimetic devices. Protoporphyrin-IX in haem complexes iron (Figure 1.2 [a]), which binds reversibly with oxygen so that it may be transported in the blood stream around the body for use (haemoglobin) or stored within muscle tissue (myoglobin). The interaction of molecular oxygen with haemoproteins is crucial in respiratory and metabolic processes. The most intriguing point about this course of action is the *reversible* binding of oxygen in haemoglobin and myoglobin (Scheme 1.1).[1]

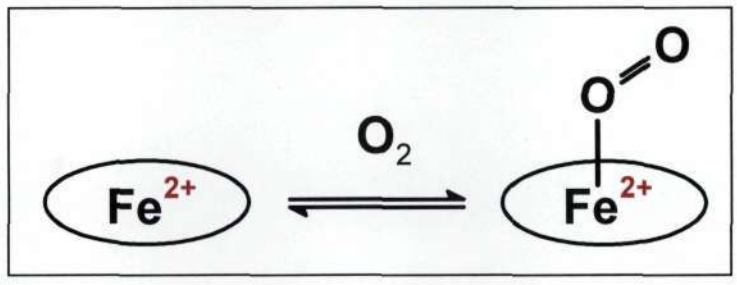

Scheme 1.1: The role of iron in the uptake and release of oxygen in haemoglobin and myoglobin.[21]

The system transporting oxygen has to take it up as effectively as possible from the gas phase in its ground state form ($^3O_2$) and take it to where it needs to be completely released. The supply and demand of oxygen changes, which makes it an even more difficult task. However, the cooperative effect[22] guarantees efficient transport of oxygen when and where needed, with more complete release into storage when there is a lack of O_2 being transported.[21] For haemoglobin and myoglobin the iron centre has two axial sites, one is occupied by a five-membered imidazole ring (*proximal* histidine), leaving the other essentially available for oxygen coordination. A "spin crossover" of the iron is induced from high- to low-spin state by the coordination of the weak oxygen ligand, either O_2 or $O_2^{\bullet-}$ (formed after inner-sphere electron transfer).[21]

When binding with the oxygen the iron does not irreversibly change its oxidation state.[1] Under normal circumstances this change would be expected; the most simple iron(II)-porphyrin complexes react irreversibly with oxygen and will form oxo-bridged dimers via peroxo intermediates.[21] In addition, iron is usually oxidized from Fe(II) to Fe(III) in the presence of air and water (e.g. rust). However, with the combination of porphyrin ligand and protein environment the iron's redox potential changes and thus does not allow the complexing with water. Taken together, these factors inhibit the usual oxidation of iron. To a certain extent the mode of iron binding is altered and thus results such unusual iron chemistry.[1]

The enzymic reductive activation and consequent utilization of oxygen in the oxidation of small molecules, for example the P450 cytochrome mono-oxygenases, has also received attention. For cytochrome *c* the iron progresses through the two oxidation states, +2 and +3, while carrying out electron transfer in cell respiration.[1] The only fully established, naturally occurring organometallic (contains a metal-carbon bond) compound, vitamin B_{12} coenzyme, uses cobalt to reduce organic species and in reactions that involve the transfer of hydrogen atoms.[1] The incorporation of cobalt is remarkable due to the fact that it is the least abundant first row (3d) transition metal in the earth's crust and in sea water; thus a special functionality is to be expected. The cobalt-carbon bond displays an individual reactivity viz. the *enzymatically controlled* creation of reactive primary alkyl radicals.

The process of photosynthesis supplies the majority of the energy needed to power living things and, as a by-product, it produces the oxygen needed to breathe. The macrocycle, chlorophyll, involved in this process has the metal magnesium bound at its centre (Figure 1.2 [b]), which has the main role in contributing to the particular arrangement of pigments (three-point fixing for defined spatial orientation). Due to immobilization and a defined orientation of pigments and reaction centres being essential for the success of photosynthesis, all chlorophyll molecules (which differ somewhat according to their substituents) feature a long aliphatic phytyl side chain for anchoring in the hydrophobic phospholipids membrane.[21] Chlorophyll captures photons ('light-harvesting') of light in visible spectrum (the near-ultraviolet (400 nm) and the red (650–700 nm) regions) and uses them to convert carbon dioxide and

water into energy-rich carbohydrates.[1] Pheophytins (metal free) are also found in the photosynthetic apparatus of plants and bacteria.[23]

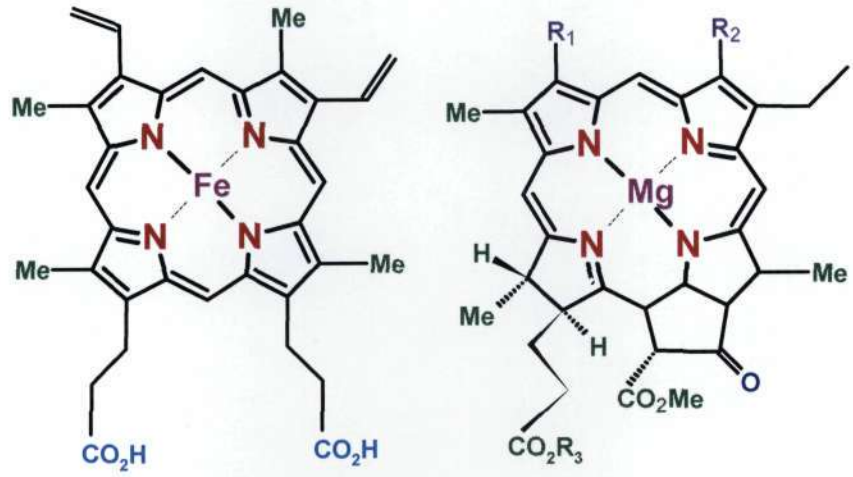

[a] **[b]**

Figure 1.2: The structure of haem (the iron(II)protoporphyrin-IX complex) **[a]** and chlorophyll **[b]**. (R1, R2 and R3 represent different hydrocarbon substituents for the different varieties of chlorophyll.)

There are two motivations behind the synthesis of certain model porphyrin compounds. The first is to help in the understanding of their features and the way that they operate in natural systems. The second involves application; models that are able to mimic the potential of enzymes for binding substrates, recognition and catalysis are assembled. Thus it may be possible to find practical application for the models themselves, e.g., oxidation of organic compounds.[24,25,26] The synthesis of synthetic porphyrins began serendipitously with phthalocyanines; these are blue-green pigments used in inks, surface coatings, dyes and even high temperature lubricants for space vehicles.

As our knowledge about porphyrins, their synthesis, their characteristics and their functions progresses, the number of possible applications therefore expands. The fact that only small deviations on a porphyrin's basic structural theme of the tetrapyrrolic macrocycle can result in a wide range of biological functions is one of its most fascinating features. The success of synthetic porphyrins in technological applications is fairly recent, but they continue to find their way in diverse areas of science including

medicine, electronics, and alternative energy generation.[1] Porphyrins have been found to connect many different areas of research including catalysis, spectroscopy, solar energy conversion, and the development of organic metals.[27] They are already used in energy storage devices, sensors, selective electrodes, molecular memory devices, organic conductors, solar energy devices, molecular switches, and non-linear optical materials.[28,29,30,31] They have also found excellent application in photodynamic therapy (PDT) for the treatment of cancer.[32,33]

Porphyrins play a part in a wide range of biological processes. They have the ability for their physical and chemical properties to be customized at the molecular level according to the type of process that they are involved in. This includes very large dipole moments, polarizability, non-linear optical response, absorption spectrum, energy transfer and catalytic properties.[23] This makes porphyrins and metalloporphyrins extremely versatile synthetic base materials which can be used for research projects in a variety of different fields of chemistry and physics. The many applications known for porphyrins and metalloporphyrins are expected to develop all the more as our knowledge about porphyrins, and porphyrin-type compounds, continues to advance.

1.2 Development of Porphyrin Synthetic Methods

There has been a dramatic development of synthetic approaches to porphyrin compounds since their introduction in the early twentieth century. Some porphyrins can be synthesized using open chain tetrapyrrolic intermediates and others by monopyrrole self-condensation, depending on the extent of molecule symmetry.[34] Fischer's school in Munich introduced several highly efficient methods in the 1920's and 1930's—these methods usually involved condensations of pyrromethenes (now known as dipyrromethenes, or more recently, dipyrrins) (Figure 1.3 [a]).[34] Despite symmetry limitations being intrinsic in this notion of porphyrin synthesis, numerous syntheses of photohaem and chlorophyll degradation products were produced by the Munich school. In the cases where syntheses were ambiguous and resulted in mixtures of porphyrins, separation was necessary and then even the most trivial by-products were examined and characterized.[34] The Fisher methods, however, relied

upon rather harsh reaction conditions and thus developments in the methods involved milder synthetic procedures.

From the time when Fischer's methods were being produced and after the break in research between 1940 and about 1960, it became less accepted to use syntheses which formed mixtures of porphyrins.[34] Except for McDonald's studies,[35] which also involved synthesis of porphyrins from pyrromethanes (now known as dipyrromethanes) (Figure 1.3 [b]), there was then also more interest in the formation of isolable open-chain tetrapyrrolic intermediates. In particular, to find conditions that would allow relatively labile side-chains to be carried from beginning to end of the reaction undamaged.[34]

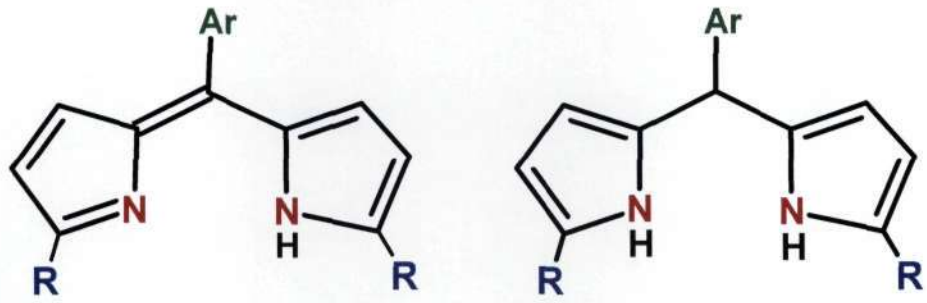

[a] [b]

Figure 1.3: The structure of a dipyrromethene (dipyrrin) **[a]** and a dipyrromethane **[b]**.

Porphyrin synthesis offers a basis for the study of an expansive range of scientific fields. Determining porphyrin structures using X-ray diffraction was a major experimental undertaking in the earlier days of research. Recent advances in this method (significant enhancements in data collection, structure solution and refinement procedures) and other methods, due to the development in digital computers and other electronic devices, have made determining porphyrin structures fairly routine nowadays. There has been an increase in the number of porphyrin structure determinations as they are now also used to confirm that the correct porphyrin has been synthesized. There are more than 3000 porphyrin and similar structured known compounds.[36]

Desired porphyrins can be obtained by two general methodologies, the first being modification of naturally occurring or existing porphyrins, and the second, the more

popular method of total synthesis.[37] Over time old methodologies have been tailored and there has also been development of new methods for the functionalization of porphyrins and their derivatives; with the formation of several new compounds that could otherwise only have been acquired from total synthesis.[38] The expansion of suitable functionalization reactions has been and is being explored. This is in an attempt to try and pass information and results from the sizeable area of functionalization of common, simple aromatic systems onto porphyrins.[39]

The modification of naturally occurring porphyrins can be more convenient, but also limiting, as certain substituents cannot be easily modified. However, in most cases these limitations can be overcome by total synthesis using pyrrole subunits that have the necessary substituents.[37] Total synthesis of porphyrins involves the use of diverse starting materials resulting in an arrangement of various substituents in particular positions. The two most commonly substituted macrocycles are the β-substituted and the *meso*-substituted porphyrins.[40] Commonly used methods for total synthesis include: tetramerization of monopyrroles, condensation of dipyrrolic intermediates and cyclization of open-chain tetrapyrroles.[37]

In order to obtain particular types of porphyrins with specifically placed substituents, the synthesis must be controlled to produce structures that are suitable for their intended applications. For effective execution of a 1-flask porphyrin reaction, optimization of the numerous reaction parameters is required. Porphyrin synthesis is a condensation involving polymerization and cyclization (Scheme 1.2). The condensation occurs when using pyrrole as one component and a compound with an aldehyde functional group as the other. Pyrrole and the aldehyde undergo acid-catalyzed condensation and cyclization which results in a porphyrinogen; this in turn is converted into a porphyrin by the addition of an oxidant—a commonly used example is 2,3-dichloro-5,6-dicyano-1,4-benzoquinone (DDQ).

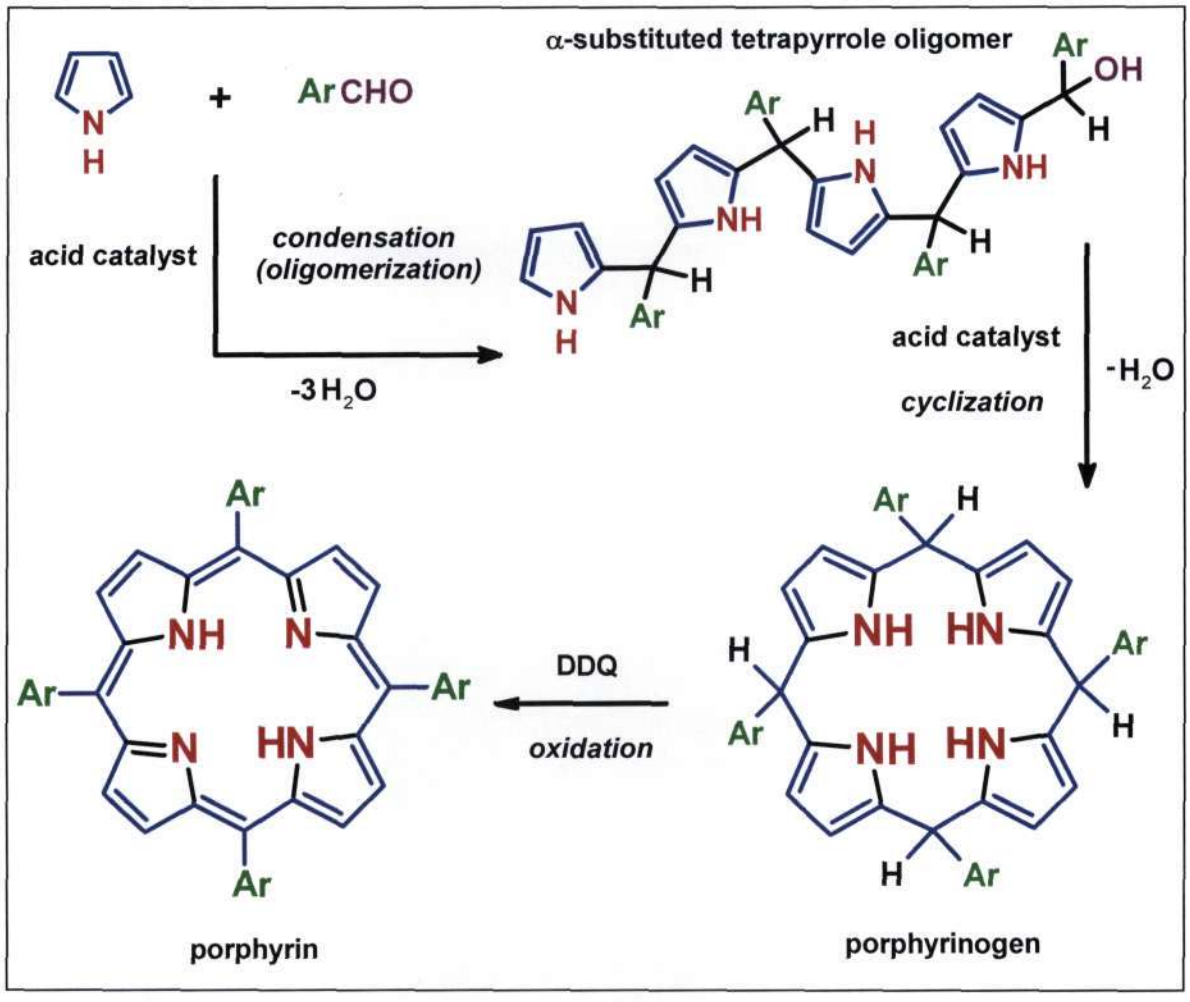

Scheme 1.2: Porphyrin synthesis: pyrrole and aldehyde condensation involving polymerization and cyclization.[41]

DDQ is used chiefly for fused carbocyclic ring systems, as a dehydrogenation agent[42,43] (dehydrogenation is commonly the last step in the synthesis of polycyclic aromatic hydrocarbons and their derivatives). The 1-electron reduction potential (in acetonitrile vs. saturated calomel electrode at 25°C) for DDQ is +0.51 V.[44] Thiele and Günther were the first to report on DDQ in 1906, including preparation, melting point, boiling point etc.[45] However, not much interest was shown in this compound until it was found to be a superior reagent for the dehydrogenation of hydroaromatic compounds by Linstead, Braude, and co-workers.[46] Using DDQ for the oxidation of several β-substituted porphyrinogens (an intermediate in porphyrin synthesis) results in yields of over 80% for the porphyrin.[47,48]

The various other uses of DDQ include: (1) establishing the oxidation level of hydroporphyrins,[49] (2) oxidizing dipyrromethanes to their corresponding dipyrromethenes,[50] (3) dehydrogenation of bilirubin to biliverdin,[51] and (4) DDQ has also found significant application in the steroid field.[42] The porphyrin is a stable aromatic product formed from the oxidation of the porphyrinogen, which has 4 benzylic positions at each of the *meso*-carbons.[40] The porphyrinogen is a hexahydroporphyrin and DDQ is a $2e^-$, $2H^+$ oxidant, thus it is necessary to have three molar equivalents of DDQ for stoichiometric oxidation to occur; therefore at least a three-quarter mole ratio with regard to the starting materials (0.75:1). If the quinone is used in less than a stoichiometric ratio, the isolation of partially oxidized porphyrinic intermediates is usually not possible.[40] Also, if DDQ is added to the reaction mixture too soon then it is possible that it might inhibit porphyrin formation by oxidizing precursors before they can form an intermediate (porphyrinogen).

The rate at which oxidation occurs is obviously an important aspect of the oxidizing agent; the rate is found to increase according to the one-electron reduction potential of the quinone. When DDQ and *p*-chloranil are compared with respect to their reaction rates in the dehydrogenation of 1,2-dihydronaphthalene, DDQ reacts 5500 times faster.[52] The reaction of tetrachloro-*o*-benzoquinone reacts 4200 times faster than *p*-chloranil in the same reaction under identical conditions.[52] Thus this vast difference between *o*- and *p*-tetrahaloquinones suggests that the unknown dichlorodicyano-*o*-benzoquinones might possibly be even better than DDQ in dehydrogenation reactions.[42]

Although for now DDQ seems to be the better choice, it has been reported that several substituted aldehydes in the presence of quinones, particularly DDQ, will produce side reactions. These unwanted side reactions include the oxidation of amines[53] and alteration or cleavage of some protecting groups (which may be used advantageously for selective deprotection[54,55]). The pyrrole-aldehyde condensation may, however, be monitored using the swift reaction of the porphyrinogen with DDQ. This is done by taking periodic samples of the reaction mixture and adding excess DDQ at room temperature for a few seconds; the yield of porphyrin from this oxidation can then be verified by using UV-vis spectroscopy.[27]

Some methods for porphyrin synthesis were developed that used one-step instead of the common two steps; in this case attention to the order of reagent addition was necessary. However, even under the best possible conditions identified, the yields were lower than those obtained when using the two-step synthesis. An example that illustrates this is the use of 0.1 M reactants with 10 mM BF_3·etherate, the yields are 18% (one-step) and 29% (two-step).[56] The yields in both these methods should be identical if the oxidant was selectively oxidizing only the porphyrinogen. Therefore, due to the discrepancy in yields, it is assumed that there is premature oxidation of porphyrinogen precursors, which subsequently inhibits the process of porphyrin production.[40]

At the end of the reaction procedure the porphyrin will not be the only compound present in the solution; it is undoubtedly contaminated by oxidized linear oligomers, unreacted aldehyde, diverse by-products, and quinone and hydroquinone species (from the oxidant). The quinone and hydroquinone species are likely to be present in a stoichiometric quantity, but the type and quantity of the by-products present will vary.[40] In an attempt to reduce these quinonoid species an aerobic oxidation process may be utilized. During porphyrin biosynthesis molecular oxygen receives the 6 electrons and 6 protons transferred by aerobic organisms from the porphyrinogen. Molecular oxygen can sometimes be an effective oxidant;[56] however, to function as an efficient room-temperature oxidant for the intermediate porphyrinogen it must be activated.

The underlying drive for many earlier structural studies of porphyrin derivatives was due to the significance of porphyrins in biological systems.[36] The β-substituted porphyrins bear a resemblance to the porphyrins found in biological systems, but the *meso*-substituted show no direct connection to naturally occurring porphyrins.[40] The porphyrins that predominantly possess biological importance are metalloporphyrins, primarily iron and magnesium porphyrin derivatives.[36] The *meso*-substituted porphyrins are, however, useful as biomimetic models and as practical components in materials chemistry.[40] In Nature, haemin and its biosynthetic precursors are modified to manufacture an assortment of biologically important molecules; therefore many synthetic porphyrin compounds (and their modified versions) have found application as natural porphyrin system models.[38]

The reason for widespread interest in *meso*-substituted porphyrins is due to their simple synthesis and the potential they hold for synthetic expansion. *meso*-Substituted porphyrins are known with various substituents including alkyl, aryl, heterocyclic, organometallic groups, or even other porphyrins. Some of these porphyrins can be synthesized by easy one- or two-step methods; some by simply using a one-pot synthesis from pyrrole and an aldehyde of choice. The more detailed and elaborate structures, having selected patterns, thus require more complicated methods. There is no necessity to make use of involved and lengthy processes to obtain precursors due to the variety of aldehydes commercially available. These aldehydes are also easily manipulated and therefore result in an assortment of porphyrins.[40]

Theoretical chemists have been captivated by porphyrins and related macrocycles for decades now. Porphyrins have been used as excellent natural testing grounds for, amongst other things, new quantum chemical theories and methods. Their relatively large molecular sizes, high symmetry (up to D_{4h}), and rich light absorption and emission properties allow for this. There are numerous driving forces behind theoretical research using porphyrins, like most aspects of porphyrin chemistry. These include their extensive coordination chemistry, the great biological importance of these molecules, and their increasing number of practical applications.[57]

meso-Tetraarylporphyrins have been involved in different synthetic projects as flexible starting materials. Their high solubility and convenient synthesis has allowed them to be of use in the determination of coordination properties of porphyrins.[58] However, *meso*-tetraalkylporphyrins have not been given as much attention as the *meso*-tetraarylporphyrins, which is surprising, considering that the synthetic method for symmetric *meso*-tetraalkylporphyrins is relatively straightforward. Descriptions of these procedures also began more than 70 years ago.[59,60,61] Recently, more extensive effort has been dedicated to the synthesis and characterization of numerous metalloporphyrins that have *meso*-alkyl substituents (these include fluorinated and chiral groups). These compounds have found uses as catalysts, amino acid receptors, and, in the case of nonplanar Ni(II) complexes, possible nano-scale molecular machines (Figure 1.4).[10]

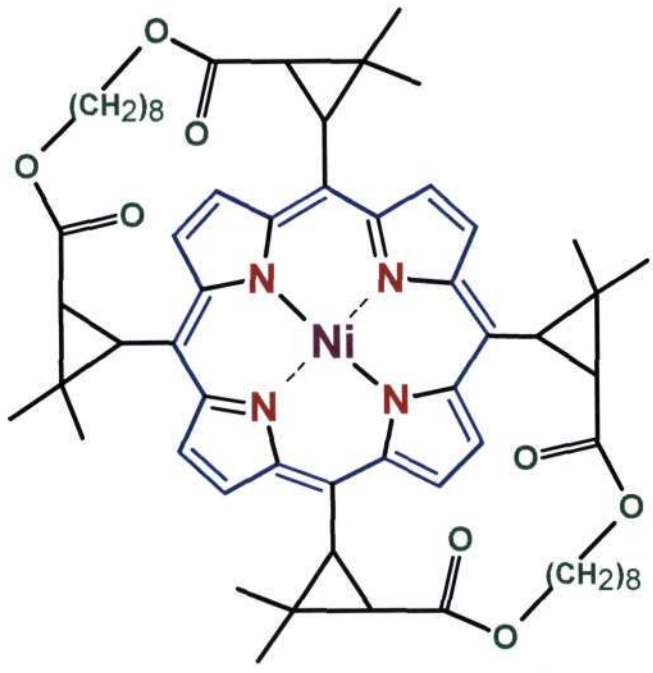

Figure 1.4: Structure of a potential molecular nanotweezer, the bridled chiroporphyrin, NiBCP-8.[10]

Another interest developed in the research of *meso*-tetraalkylporphyrins concerning the studies of non-planar conformations (and their biological relevance).[62,63,64] This was due to the belief that, *in vivo*, subtle modifications of the porphyrin chromophore conformations by the protein scaffold may perhaps be able to explain the diverse functions of porphyrin-type chromophores. It is thought that the conformational differences affect the highest occupied (HOMO) and lowest unoccupied (LUMO) molecular orbital levels and thus alter redox potentials and light absorption properties.[65] Their possible biological significance in proteins has been suggested numerous times.[66,67,68,69] The significance of these nonplanar haem structures is underscored due to the haem only being nonplanar when the surrounding protein exerts the necessary external forces on the prosthetic group. However, in solution the isolated haem is planar.[70] Therefore, the idea that nonplanar porphyrins and protein-induced changes in the nonplanarity may provide a mechanism for protein modulation of biological properties is realistic.[71]

These out-of-plane distortions are characterized by displacements along the lowest-frequency out-of-plane normal coordinates of the D_{4h}-symmetry of the macrocycle.[72] The degree of distortion from planarity depends on the type and number of

substituents, charge, aggregation, packing effects in crystals and the metal and axial ligands.[64] This distortion has an effect on various spectral properties, for instance optical, redox behaviour (in the ground and excited singlet and triplet states), EPR, NMR, vibrational, and electron-transfer.[63,65,73,74] Even though significant differences were noted in the physicochemical properties for porphyrins with nonplanar macrocyclic conformations, their general chemical behaviour was however similar to that of planar porphyrins.[13] The first studies involved dodecasubstituted porphyrins (substituted at all *meso*- and β-positions), which mainly presented severely distorted conformations with a saddle-shaped macrocycle.[65,73,74,75,76] There were, however, a few that crystallized in ruffled conformations, these were dodecasubstituted porphyrins bearing *meso*-alkyl groups.[77] Senge and co-workers soon discovered that introduction of extremely bulky substituents only at the *meso*-position also gave considerable conformation distortions.[13]

Therefore, much research has begun regarding porphyrins with sterically demanding *meso*-alkyl substituents to study their conformational properties. It was shown in a publication by Ema *et al.*[78] that the *meso*-carbons of 5,10,15,20-tetrakis(*tert*-butyl)porphyrin easily underwent nucleophilic attack resulting in porphodimethenes. However, this reaction was not detected for other porphyrins.[78] The reason for this was determined by Senge *et al.*[58] to be a heavily ruffled macrocycle conformation; it had the highest degree of *ruf*-distortion known for any other free base porphyrin system at the time. In-plane rotations of the pyrrole rings and considerable out-of-plane displacements of the *meso*-carbon atoms characterize these ruffled porphyrins.[79] There have been a number of reports published on the photophysical properties[80,81] as well as on theoretical calculations[14] for this and other related porphyrins.[58]

Highly nonplanar conformations have been reported for the corresponding 22,24-dihydroporphyrins (22*H*+,24*H*+-porphyrindiium salts) of N-protonation of 5,10,15,20-tetraalkylporphyrins with *n*-butyl, isobutyl, isopropyl, 1-ethylpropyl or *tert*-butyl substituents.[82] Generally the free base structures are planar or moderately ruffled (primary or secondary alkyl residues); however, for tertiary alkyl groups severe ruffling may be seen. X-ray crystallography was used to demonstrate the effect that certain substituents had on the porphyrin conformation when porphyrins were protonated. The

four N–H groups cause steric congestion within the macrocycle which therefore induces pyrrole ring out-of-plane tilting and the formation of nonplanar porphyrin conformations with highly distorted saddled geometries.

1.2.1 The Rothemund Method

Studies of the chemistry of *meso*-substituted porphyrins in particular started in 1935 due to the work of Rothemund. His first paper[61] was a communication to the editor entitled "Formation of porphyrins from pyrrole and aldehydes". It dealt with the formation of porphyrins from acetaldehyde or formaldehyde in methanol, using methods with slight variations with regard to temperature and reaction time. From the resulting crystalline porphyrin, he produced the copper and iron complexes. He then continued to perform the same type of reaction investigating a variety of other aldehydes. Rothemund then reported in more detail his attempt at the synthesis of porphine, for which he obtained a yield of 0.9%.[59] He reacted formaldehyde and pyrrole (both solutions in methanol) in a sealed container in pyridine at 90–95 °C for 30 hours under nitrogen. Rothemund then prepared the phyllin (magnesium), haemin (iron) and copper complexes of porphine. Further work using this method gave crystalline porphyrins from benzaldehyde, *n*-butyraldehyde, α-furaldehyde, and propionaldehyde. However, using the same method, porphyrin formation for another small group of aldehydes (*o*-nitrobenzaldehyde, *p*-dimethylaminobenzaldehyde, glyoxylic acid, chloral hydrate and vanillin) was detected only by spectroscopic means.[59]

The porphyrins containing *meso*-substituents like methyl, propyl, butyl, isobutyl, phenyl, 3-methoxy-4-hydroxyphenyl, 2-hydroxyphenyl, 3-hydroxyphenyl, and 4-methoxyphenyl groups were synthesized from relevant starting materials at temperatures of 140–150 °C for 24 hours.[60] Rothemund then gave a detailed description of his method for the synthesis of *meso*-tetraphenylporphyrin [H_2(TPP)] in 1941. Pyridine, pyrrole and benzaldehyde were heated in a sealed vessel at 220 °C under nitrogen for 48 hours. Enough pyridine is needed in order to keep the impurities in solution; however, too much pyridine may dissolve the porphyrin. Upon slow cooling of the reaction mixture for roughly 10 hours, lustrous deep-blue needles crystallized in

the crude reaction mixture. For longer cooling times (up to 18 hours) some needles as long as 2 cm were formed. Yields of 7.5–9%, depending on allowed cooling time, resulted from this method.[83]

The supporting analytical data used by Rothemund for the greater part of his earlier work was simply spectrographs and measured HCl partition coefficients (e.g. *meso*-tetraphenylporphine had a hydrochloric acid number of 13.5). Therefore only when these reactions were later more precisely examined by other methods was another porphyrin-type product detected, and in much higher yield (10–20%) by comparison to the porphyrin.[60] Using chromatography this contaminant was isolated and described as a chlorin.[84,85,86] Chlorins (Figure 1.5) are porphyrins that have one reduced pyrrole nucleus, but they can easily be converted into the corresponding porphyrin by oxidation. This can be done using DDQ[87,88] which will work for both the free base and the metal chelate.[89]

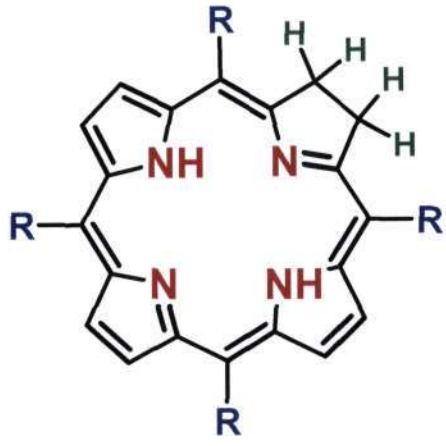

Figure 1.5: The structure of a *meso*-substituted chlorin.

Aronoff and Calvin[84] managed a more comprehensive separation of the isomers described by Rothemund[60] and showed the likelihood of six porphyrin-type compounds rather than just two. Calvin and co-workers, while further examining the reaction products, showed that the use of zinc acetate in this reaction gave an almost doubled porphyrin yield as compared to without it.[85,86] The product when using zinc acetate is expectedly the zinc complex; however, the removal of zinc to produce the free base is simply and readily performed by the action of 6 N hydrochloric acid.[85,86] For two other reactions, namely those of *p*-tolualdehyde and *p*-nitrobenzaldehyde,[90]

zinc acetate did not give improvements in yield, thus it was not always a valuable additive. However, this was the start of many more reports[86,90,91,92,93,94] showing positive results and increased yields due to the presence of different metals during pyrrole-aldehyde condensation (the most commonly used being magnesium, copper and zinc).

The distinctive features of Rothemund's methods include the lack of an additional oxidant, high temperatures and high concentrations in a sealed container.[40] The conditions for the Rothemund method were clearly based on the argument that the porphyrin is aromatic; aromatic compounds are stable and therefore it was expected that the porphyrin would be formed at high temperatures by simply cracking the initially formed adducts of benzaldehyde and pyrrole.[27] These Rothemund methods attained reaction at high concentrations; nonetheless, they did not give very high yields. Thus due to their extreme conditions as well, they could not be used for the conversion of all the various available substituted aldehydes to their porphyrin counterparts. The low yields were also a disadvantage as they restricted the extent of application for the resulting porphyrins.

Methods have been developed that bypass the use of solvent completely; three such examples follow. (1) Heating pyrrole with 1-3 equivalents of an aldehyde in a sealed vessel at high temperatures (150–250 °C) in the presence of a condensing agent, such as a metal salt, for 5–75 hours.[92] (2) Using an acidic solid support such as silica gel or clay and irradiating in a microwave oven or digester.[95] (3) Injecting pyrrole into a vial in an air atmosphere, containing one equivalent of aldehyde in the gas phase, and heating to temperatures 10–15 °C above the boiling point of the starting aldehydes.[96]

Other modifications made to the Rothemund method include drying of reagents, chemical oxidation of isolated chlorin by DDQ,[87,97] change in solvent from pyridine (bp 115 °C) to 2,4,6-collidine (bp 171–172 °C) and exposing the reaction to air.[98] Rothemund's method did not receive much interest in the quarter century following his first attempts; however, there are records of positive results obtained from the use of his methods, and variations thereof, in the 1960's, even more so in the 1980's, some in the 1990's and subsequently also in the early twenty-first century.[40]

1.2.2 The Adler Method

The method for the synthesis of *meso*-substituted porphyrins was further researched by Adler, Longo and co-workers in the 1960s. They refluxed pyrrole with one equivalent of benzaldehyde open to the atmosphere in a range of acidic solvents, including acetic acid, trifluoroacetic acid, acetic acid with a metal salt or benzene containing chloroacetic acid.[99] The yields for these methods were relatively good; however, the addition of the metal salts did not particularly enhance the results in contrast to a range of other porphyrin condensation reactions.[90,91,93,94,96] The highest yield obtained (50%) was in benzene containing chloroacetic acid; here a Dean-Stark trap was used to eliminate the water during a reaction time of 36 hours. Other elevated yields of about 30–40% were achieved in acetic acid or acidified benzene; unacidified benzene gave no porphyrin yield.[99]

From these results and additional research, further modification to these methods was made by Adler and Longo.[100] They noted that the yield and rate of H_2TPP production depended on a number of factors, including temperature, solvent, acidity and availability of oxygen. The most convenient method (although not the highest yielding) to obtain relatively pure H_2TPP involved the replacement of the solvent with propionic acid (bp 141 °C) and an increase of the pyrrole and aldehyde concentrations. After half an hour of reflux, open to the atmosphere, the isolation of porphyrin crystals was obtained after cooling, filtering and washing of the reaction mixture. Using this method there was a noticeable increase in the yields (up to 20%) due to the milder reaction conditions and it allowed a wider selection of substituted benzaldehydes to be converted to their respective porphyrins.[27,99] This type of reaction also allows large-scale synthesis and many porphyrins have been produced in multigram quantities.[27]

This type of process is thus now known as the Adler or Adler-Longo method. However, it is not without complexity. Due to the harsh conditions, those benzaldehydes with sensitive functional groups will not give positive results. The Adler method usually produces a contamination of about 2–10% chlorin along with the resultant porphyrin,[40] which then needs to be removed (as previously mentioned).[87,88] Another problem, which is less easily removed, is the production of large quantities of tar. This often poses a problem during purification, particularly for the porphyrins that

do not precipitate or crystallize easily. Finally, the batch-to-batch reproducibility for this type of the reaction is often somewhat meager.[27]

Adler and co-workers were, however, still interested in researching the diverse mechanistic features[101] of their reactions and found a number of factors that affected the yields and rates. Reacting under nitrogen dropped the yield to 5% from 35–40% in open atmosphere, thus showing the need for atmospheric oxygen in the reaction. The concentration at which the best yield occurred in acetic acid was 0.05 M; an increase in concentration saw the yield slowly degenerate up to 0.2 M, but a sharp decline was noted for a decrease in concentration at 0.01 M. The highest yields were obtained when using equimolar quantities of pyrrole and the aldehyde. Their studies also showed that the mole fraction of acetic acid in benzene was directly proportional to the reaction rate. The rates of reactions for some *p*-substituted tetraarylporphyrins were compared and were found to increase with the electron-withdrawing nature of the *p*-substituent.[102] This kinetic study took into account the rate of formation of the porphyrin; thus all the steps of the reaction were considered.

They also tested the role of acidity by using different acidic solvents: propionic acid, butyric acid and acetic acid. Although the reaction was faster in propionic acid (20% yield), the yield was higher in acetic acid (40%). In propionic acid the resulting porphyrin was much purer due to easy crystallization and less chance of the acid salt forming. The yields were the lowest in butyric acid and the product contained more impurities than either of the other two solvents. Therefore selection of solvent must take into account the numerous roles of reaction and crystallization solvent, and possible catalyst.[101]

Using the Adler method, many *meso*-substituted porphyrins, particularly with diverse aryl substituents, can be easily synthesized, and rather elaborate aldehydes converted to their subsequent porphyrins. The most popular of the three solvents—propionic acid, acidified benzene and acetic acid—was propionic acid due to its ability to solubilize a range of aldehydes and allow the formation of crystalline porphyrins in the tarry reaction mixture. Using propionic acid, average yields of about 20% or more have been obtained.[40] For the usual workup in propionic acid, filtration is used to collect the crystalline product that forms in the reaction mixture. However, isolation

becomes more problematic when no crystalline product formation occurs. The propionic acid then has to be distilled or removed by evaporation under vacuum, with subsequent use of recrystallization or chromatographic techniques to isolate (and purify) the porphyrin. Another alternative to collect the porphyrin from the reaction mixture is to add 10 N ammonium hydroxide; this neutralizes the solution and the black precipitate that forms can be washed with methanol prior to dissolution in an organic solvent (e.g. methylene chloride or chloroform). Final purification is then done using chromatography on an alumina column.[103]

The yields when using the Adler methods with *o*-substituted benzaldehydes are generally lower compared to those of *p*-substituted aryl aldehydes.[102] In order to deal with problems that arose for some aldehydes with this method, reaction conditions or work-up methods had to be changed and sometimes protecting groups had to be utilized.[40] (An instance where protective groups have been frequently put into practice is for hydroxybenzaldehydes; one particular example is shown in Scheme 1.3.) When choosing a protective group care must be taken in order to ensure that the correct porphyrin product, *o*-, *m*- or *p*-substituted, will be obtained.[104]

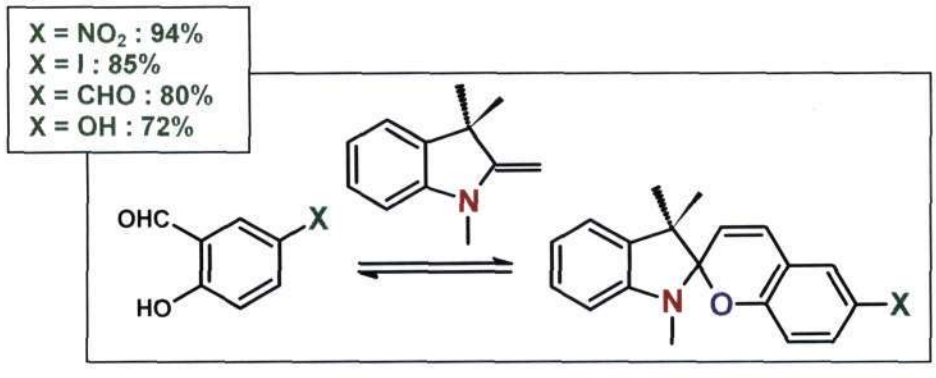

Scheme 1.3: An example of protecting hydroxybenzaldehydes in the formation of spiropyrans, showing the yields for different protecting groups.[105]

The basic Adler method involves acid-catalyzed condensations of pyrrole with an aldehyde, generally at elevated temperatures open to the atmosphere and in a solvent from which a crystalline form of the porphyrin may be obtained. Some adjustments to certain conditions have been made. For milder reaction conditions pyrrole will undergo a Mannich reaction (Scheme 1.4) when reacted with imines derived from

formaldehyde and dialkylamines, resulting in the α-dialkylaminomethyl derivative.[106] After 6 days at room temperature, the reaction gave the corresponding porphyrin (oxidation by air) in yields of 7–22% (based on the Soret band).[107] (This particular approach was studied primarily for preparing *meso*-tetraalkylporphyrins.)

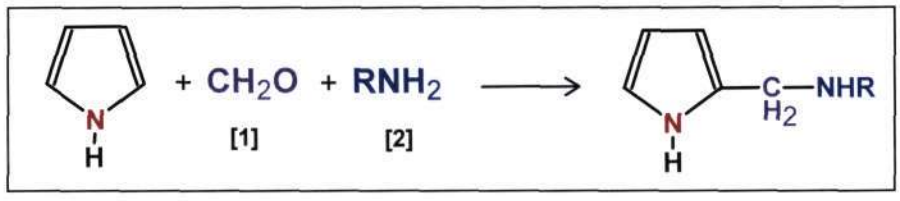

Scheme 1.4: The Mannich reaction of pyrrole and an immine (formed from formaldehyde [1] and a dialkylamine [2]).[34,106]

Higher reaction temperatures were allowed when using acidified xylenes due to their boiling points (bp of xylenes ~ 140 °C, bp of benzene 80 °C).[108] Using $AlCl_3$ as a catalyst in refluxing *N,N*-dimethylformamide (DMF) for 2 hours, on cooling to room temperature adding a small volume of ethanol gave pure, chlorin-free H_2TPP (30% yield). DMF could be replaced with dimethylsulfoxide, but other acids such as HCl, H_2SO_4, BF_3·etherate/ethanol, $FeCl_3$ and P_2O_5 did not have the same effect.[109] Treibs and Häberle used a double-solvent, acetic acid and pyridine, 2:1 (v/v). Their yield was similar to those obtained in propionic acid. Both alkyl and heterocyclic aldehydes gave moderate yields (≥ 5%).[110]

Pyrrole-carbinols are believed to be key intermediates in the pyrrole-aldehyde condensation. These pyrrole-carbinols have been studied to make a comparison with the pyrrole-aldehyde condensation and also for preparative functions.[40] There are different possible routes for the formation of pyrrole-carbinols.[111,112,113,114] There are a range of conditions under which pyrrole-carbinols will undergo self-condensation and form the porphyrin. Using the conditions of the Adler method several pyrrole-carbinols were reacted in hot propionic acid.[111] The yields of these porphyrins were analogous to those using the pyrrole-aldehyde condensation. The rates of the reactions were also found to support this theory of the Adler reaction having pyrrole-carbinol intermediates. This was due to the formation of coloured intermediates in the pyrrole-carbinols self-condensation being comparable to water formation in the pyrrole-aldehyde condensation.[111]

1.2.3 The Lindsey Method

There is a continual need to improve the range of model porphyrin systems that can be synthesized and hence the requirement for a method that uses milder reaction conditions to produce *meso*-substituted porphyrins. This synthetic method needs to be appropriate for those more sensitive porphyrins that are not easily prepared via alternative techniques. The need for mild reactions was based on the attempt to attain equilibrium during condensation and to try and avoid any side reactions occurring during any of the steps in the porphyrin production.[40] Methods using BF_3·ethanol as the catalyst proved that high temperatures are not necessary to overcome steric barriers to condensation or oxidation. The effect of these increased temperatures seems to preferably force the conversion of starting materials to dipyrrins (dipyrromethenes), rather than increasing the yields of porphyrin.[115]

The development of the Lindsey method involved a vantage point very different to that of either Rothemund or Adler and Longo and was inspired by various factors.[27] Firstly, the relatively high reactivity of both pyrrole and aldehyde was considered; due to this it should not be necessary to use high temperatures to promote their condensation.[27] Pyrrole is a flat and aromatic heterocycle, and it is electron-rich due to the lone pair of electrons on the heteroatom. It is a weak base and will be protonated in an acidic solution. Pyrrole is a good nucleophile, thus readily attacked by electrophiles.[3] There are examples where products are formed easily from the reaction of aryl aldehydes with nucleophiles using an acid catalyst at room temperature; specifically, the formation of Schiff Bases and acetals.[40] Secondly, the reaction conditions that are mild enough to attain equilibrium should also be compatible for a range of substituted aldehydes in order to allow the production of the subsequent porphyrins in good yields.[27] Another important consideration is that the reaction conditions that assist in the achievement of equilibria before oxidation occurs, should support high yields because the porphyrin should be the thermodynamically favoured product when pyrrole and the aldehyde are condensed.[27]

Methods for an approach to the synthesis of *meso*-substituted porphyrins by using a sequential process of condensation and oxidation steps were developed by Lindsey and co-workers.[27,56,115,116,117] The yields obtained ranged from 30–50% for H_2TPP[56,116,117] and 29% for H_2TMP.[115] The original general synthetic method[116] uses

dry dichloromethane under N_2 with benzaldehyde, pyrrole and TFA at equimolar concentrations (or BF_3 at one tenth molar ratio) and finally the addition of *p*-chloronil followed by column chromatography. These reactions were found to have sensitivity towards concentration. If the solution was either too concentrated or too dilute the percentage yields decreased.[27,56] This percentage decrease for the more concentrated solutions could be partly attributed to the increase that occurs in the acid catalyst concentration. It has also been found that reactions taking place at concentrations of 10 mM often leave as much as 15–20% unreacted aldehyde starting material. However, higher concentrations (100 mM) decreased this to negligible amounts.[117]

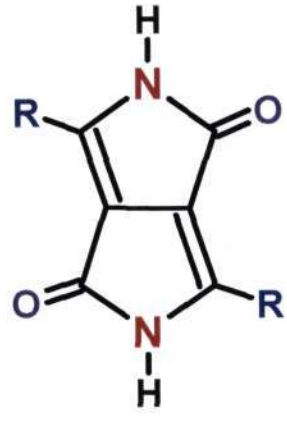

Figure 1.6: *The structure of pyrrole-red.*

Unfortunately the pyrrole-aldehyde condensation is not a straightforward reaction and there are some unfortunate side reactions that take place, some as a result of facile protonation of pyrrole. Pyrrole in the presence of a strong acid *or p*-chloranil affords a red mixture and in the presence of an acid *and* p-chloranil, a black mixture. Both these products, "pyrrole-red" (Figure 1.6) and "pyrrole-black", are distinctively coloured, but are poorly characterized substances.[40] When using Lindsey conditions at 10 mM pyrrole (1 mM BF_3·etherate or 20–50 mM TFA),[27] there will be no pyrrole-red formation. Conversely, at higher concentrations of pyrrole with higher acid concentrations it will be produced.[56] Not much else is known about these non-porphyrin compounds (by-products) that are formed from these side reactions. However, one other particular product that forms has been more specifically studied.

Using absorption spectroscopy, the presence of dipyrromethene chromophores is easily noted for the Lindsey method;[27] these compounds can be formed from either oxidation or tautomerization.[115] Dipyrromethenes (Figure 1.3 [a]) can be potentially damaging to the porphyrin yield when sometimes formed as the dominant side reaction. However, the use of a truly benign catalyst would produce polypyrromethane and porphyrinogen and avoid formation of dipyrromethene.[115] They typically terminate chain growth; the end of the dipyrromethane chain has an unsubstituted α-position which is unreactive with regard to additional substitution. Chain growth is also affected by dipyrromethenes that are produced by tautomerization, which are expected to have methylene groups at one α-position. This will also have a negative effect on cyclization.[40] The structures of dipyrromethenes formed via tautomerism are not as well characterized as similar reaction by-products that have been produced by the Rothemund method and subsequently isolated.[118,119,120] Recent developments in dipyrromethane methods and isolated structures have also been reported.[121,122]

In some cases where the reaction conditions were changed (e.g. concentration or temperature) and the yield of the porphyrin decreased, then a clear increase of dipyrromethene was seen. This is seemingly a result of catalyst-induced tautomerism rather than oxidation. At room temperature the porphyrin is found to be the predominant product; however, at higher temperatures (as used for Rothemund methods) this is reversed, giving porphyrin in a yield that is lower than that of dipyrromethene.[115] However, not all dipyrromethenes are expected to deplete the yield of porphyrin. Essentially they will not inhibit formation of a porphyrin precursor when they are at the centre of an oligomer. In the process of oxidation that leads to porphyrin production, a likely intermediate is a porphyrinogen (Figure 1.7) that in fact contains a dipyrromethene component.[40]

The general biosynthesis of porphyrins involves condensation, the neatening and adaptation of side chains, and oxidation in deliberate sequential steps. This process is expected to proceed via a porphyrinogen intermediate (Figure 1.7).[123] Experiments done by Dolphin provide convincing evidence that the key intermediate in the formation of porphyrins, from pyrrole and an aldehyde, is porphyrinogen.[124,125] In 1956 it was shown that uroporphyrinogen is enzymically converted to protohaem,[126] which

sparked the preparation of different porphyrinogens to be used as substrates in enzymic experiments. The intermediacy of porphyrinogens in both the synthesis and biosynthesis has been documented for many years;[124,125,127,128,129,130] however, their thermodynamic stability and ease of formation have not been extensively investigated with regard to the design of synthetic approaches for porphyrin production.[27] Porphyrinogens are considerably less stable than their aromatized analogs and are readily isomerised in hot acids.[127,128]

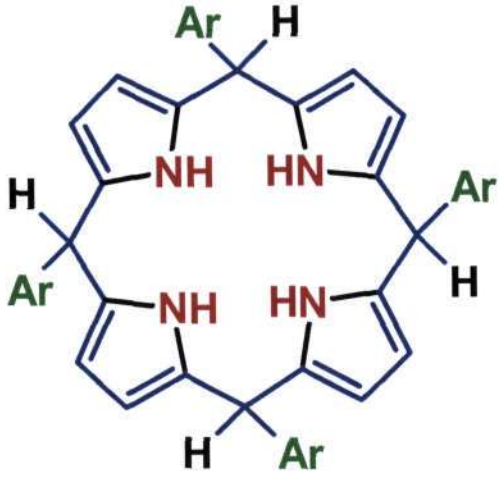

Figure 1.7: The structure of porphyrinogen.

Studies have been carried out on the pyrrole-aldehyde condensation to determine whether the formation of porphyrinogens is reversible. This was done using a simple exchange reaction for different aldehydes with pyrrole. In all instances, porphyrinogen exchange took place. The stability of the porphyrinogen macrocycle therefore had to be considered. To do this, double-labelling crossover experiments were used.[27] ^{13}C NMR labelling experiments were used to monitor the reversibility of the first step. The results showed that when the reaction mixture formed from pyrrole and ^{13}C-formyl labelled benzaldehyde was treated with excess (natural abundance) benzaldehyde there was no verifiable formation of the ^{13}C-formyl labelled benzaldehyde.[117] These results play a role in proving that near the beginning of the pyrrole-aldehyde condensation there is already an irreversible process, namely porphyrinogen formation.

During the biosyntheses of porphyrins, numerous enzymes are used for their condensation, but it has been found that without enzymes porphyrinogen can self-condense.[127,128] For efficient formation of the porphyrinogen the condensation of pyrrole and the aldehyde must be effectively catalyzed without promoting any harmful or more predominant side reactions. The choice of solvent, catalyst and reaction conditions must therefore be made to favour the pyrrole-aldehyde condensation without allowing for the formation of pyrrole-red (Figure 1.6) or other possible by-products.

The Lindsey method uses milder conditions at room temperature for the condensation and oxidation steps and therefore can be applied to a wider range of aldehydes (and pyrroles) producing a variety of *meso*-substituted porphyrins. Their yields can be as high as 50%, depending on the aldehyde used. However, as is the case for most methods, there were some exceptions. The reported applications (and failures) using this synthetic approach through 1992 have been assembled.[131] This compendium gives the results for numerous aldehydes using the standard Lindsey method, as well as the results for any modifications made to the method.

1.2.4 Catalyzed Lindsey Method

One particular exception using the Lindsey method was that of mesitaldehyde and pyrrole, which would not produce any of the corresponding porphyrin with either catalyst, BF_3 or TFA, in dichloromethane. It was, however, noted that if a change in solvent was made from CH_2Cl_2 to $CHCl_3$, with BF_3·etherate as the catalyst, then the reaction would produce the tetramesitylporphyrin. The yield for this reaction in chloroform ranged from 20% at 61 °C to 31% at room temperature.[115,132] This impressive difference in reactivity caused purely by a change in solvents was traced to the presence of ethanol in the chloroform. The commercial source of chloroform contains 0.75% (v/v) ethanol as a stabilizer, while dichloromethane does not.[115] When chemical treatment was used to remove the ethanol from the chloroform (as simple distillation was ineffective) there were no results from the chloroform either. However, the placement of ethanol in either one of the pure solvents resulted in a reaction.[115]

Equivalent percentages of ethanol in the two solvents gave very similar results; using 0.1% ethanol, the yield of tetramesitylporphyrin was 23% in dichloromethane and 25% in chloroform.[115] Therefore the presence of a co-catalyst system (like BF_3·etherate/ethanol) allows these reactions to proceed at room temperature for a number of different aldehydes. When the concentrations of the mesitaldehyde, pyrrole and BF_3·etherate were increased so did the yields; however, the amount of ethanol stayed comparatively steady.[133] These findings indicate that mesitaldehyde and similar aldehydes tend to be rather selective in their catalytic requirements, but that the reactions are not thermodynamically hindered.[40]

When an aldehyde does not react as expected, determining the exact cause is not clear-cut. It could be due to maladjusted reaction conditions or it could be a result of intrinsic structural restrictions caused by substituents of the aldehydes. Each of the different aldehydes will obviously have its own special reactivity pattern. Thus slight changes in catalysis, temperature and oxidant can give very different results, only slightly different results, or possibly no results at all, depending on the aldehyde.[115] The fact that some aldehydes needed the ethanol present for a reaction to occur and that others didn't initiated a comparison between mesitaldehyde and benzaldehyde (benzaldehyde gives favourable results with or without the addition of ethanol).[115]

Using IR spectra, in both dichloromethane and chloroform, proved hydrogen bonding with ethanol was not the basis for the dissimilar reactivity between the two aldehydes (the lack of solvent dependence was shown in the carbonyl stretching frequencies).[115] Attention was then directed at binding affinities; the red-shifted absorption band in the adducts was used to monitor the binding of BF_3 to the aldehydes.[134] The apparent association constant in dichloromethane for benzaldehyde and BF_3 was found to be 100 times less than the association constant for mesitaldehyde and BF_3.[115] (The pK_a of protonated mesitaldehyde (determined from sulphuric acid media by a spectrophotometric method) is –4.7 and for protonated benzaldehyde is –7.1, a difference of 2.4 units.[135] The basicity constant for protonated pyrrole is determined as pK_a = –3.80,[136,137] pyrrole is usually less basic than benzaldehydes.) Similar reactivity and binding behaviour were found for both mesitaldehyde and benzaldehyde when ethanol was added. The need for ethanol for reactivity of some aldehydes stems from some unusually stable aldehyde-BF_3 complexes.[115]

The major difference between benzaldehyde and mesitaldehyde is basicity,[135] which results in the strong affinity of mesitaldehyde for BF_3. Although the presence of ethanol does encourage porphyrin synthesis by aiding the displacement of BF_3 from the complex, BF_3 ethanolysis is then inevitable.[115] The results of tetramesityl-porphyrin formation in the presence of different volume percentages of ethanol were carried out to find the optimal addition. Although the mere presence of ethanol gave a result, it was necessary to determine the volume of ethanol with which the highest yield of porphyrin would be produced and the least ethanolysis would occur. Volumes were added from 0.1% ethanol up to 5%. The result was an increasing yield with an increasing percentage of ethanol up to a maximum yield at 0.75%, where the ethanol to BF_3 ratio is ~ 50:1.[115]

One possible explanation of the co-catalysis data is that the catalytic mechanism or event concerns a Brønsted acid (resulting from BF_3 and ethanol)[138] rather than polarization of the carbonyl through Lewis acid-base complexation.[139] Formation of a strong Brønsted acid from BF_3·etherate with an alcohol is shown in Scheme 1.5 above; this formation was confirmed with the use of ethyl alcohol-*d* (EtOD) and BF_3·etherate to give the deuterated porphyrin (at the β-positions).[140] Why this BF_3·ROH derived Brønsted acid would assist the reaction is not yet exactly known. Further work is necessary in order to determine the kind of the BF_3·ROH species that causes catalysis of the pyrrole-aldehyde condensation.

$$BF_3{\cdot}OR_2 + XH \rightleftharpoons BF_3{\cdot}XH + OR_2$$

$$BF_3{\cdot}XH \rightleftharpoons BF_3X^- + H^+$$

Scheme 1.5: An example of a Brønsted acid formation by means of dissociation of the BF_3·XH complex, where XH is a co-catalyst.[115,138]

Another interpretation has to do with acetals, after it was found that acetic acid and *tert*-butyl alcohol also gave a reaction. This shows the proton donor effect not to be specific to ethanol. It was also discovered that if concentrations were increased then H_2TMP could be produced without addition of alcohol. Results of these experiments

exclude the idea of elite mechanisms that happen via acetals or with a Brønsted acid derived from BF_3·ethanol.[115] Therefore we expect there to be many different conditions (and catalytic methods) under which the porphyrinogen can be synthesized from pyrrole and mesitaldehyde. It should be noted that some steric hindrance has still been seen in the mesityl derivatives, despite the use of improved catalysis.[141]

1.2.5 Other co-catalyst systems

The results of porphyrin synthesis at room temperature using pyrrole-aldehyde condensation have relied to a certain extent on efficient catalytic conditions. Mostly only one catalyst is necessary to produce good quality results; however, it has been noted that there are certain cases where the combination of catalysts either gives better results than one on its own, or are, in fact, required for the reaction to proceed. Differences in the production of porphyrins, from the usage of either TFA or BF_3·etherate as the reaction catalyst,[41,142,143,144] showed fairly complementary catalytic features between them. This therefore prompted research into using the two catalysts together.[145] Each of these two catalysts has shown itself to be appropriate for wide varieties of aldehydes.

The co-catalyzed reaction gave a remarkable increase in the yield of tetraphenylporphyrin, from 40% (using TFA) and 26% (using BF_3·etherate) to about 50 to 55% (using both).[145] From the results for the yield of H_2TPP (UV-vis), the yield of N-confused H_2TPP (HPLC), the level of unreacted aldehyde (TLC) and the oligomer composition (LD-MS), it was shown that this co-catalyzed reaction contained features that are associated to each acid individually.[145] Other possible co-catalysis reactions were observed when using methanol in conjunction with either TFA or BF_3·etherate (which produced ~ 40% yield of H_2TPP) and the addition of salts to BF_3·etherate catalyzed reactions.[145]

The addition of a minimal volume of ethanol to the reaction mixture creating a co-catalyst system resulted in better yields.[115] The use of a variety of salts also showed improvements in the yields.[117] It was, however, noted that in both scenarios the conditions of these co-catalysts had to be quite precise, as too little or too much gave poorer yields. The use of co-catalysts is a well known concept, particularly for a Lewis

acid and either protic species or salts. It was the synthesis of polymers that first showed co-catalysis with a Lewis acid and a protic additive.[146,147,148,149] These co-catalyst systems provide an increase in yields, rates of reaction and/or change the selectivity of the catalyst. Some of the Lewis acids that have been included in these co-catalyst reactions are BF_3, BF_3·etherate, $SnCl_4$, lanthanide triflates, and Cu(II) complexes. Usually water or an alcohol was used as the co-catalytic additive; however, stronger Brønsted acids were also sometimes used, for example acetic acid or HCl.[145]

There are a variety of mechanistic justifications for these types of co-catalysis: (1) the catalytic species is actually a strong Brønsted acid that is formed from the Lewis acid and the protic agent, (2) the co-catalyst helps to regenerate the Lewis acid, or (3) there is cooperation between the Lewis and Brønsted acids.[145] The co-catalytic process mechanisms have not yet been identified in pyrrole-aldehyde condensations. One reason for the difficulty in assigning mechanisms is that the data gives only the yields of the porphyrins and the aldehydes used. However, laser-desorption mass spectrometry (LD-MS) has now been used to probe the oligomers that are found to form in these porphyrin reactions.[41,142,143,144]

Studies involving the system of BF_3·etherate/ethanol co-catalysis have helped to outline the scope of the co-catalysis mechanism, but have not completely revealed it. Other forms of this co-catalysis have been successful using BF_3·etherate and ethylene glycol,[133] 2-methoxyethanol,[133] and the methanol adduct of borontrifluoride (20% yield).[150] There were also a number of attempted reagents that did not give the desired co-catalytic activity. These included protic reagents with a higher acidity than ethanol (trifluoroacetic acid, acetic acid, 2,2,2-trifluoroethanol, phenol), that were more hindered than ethanol (isopropanol, *t*-butyl alcohol) or those that contain thiol or amino functional groups.[133] Other examples of this type of co-catalysis in other areas of chemistry are commonly credited to the formation of Brønsted acids upon BF_3·ROH interaction.[138,140,146,147,148,149,151]

1.3 Other Remarkable Synthetic Porphyrins

In 1975, Collman and co-workers developed one of the most celebrated *meso*-substituted porphyrins, *meso*-tetra($\alpha,\alpha,\alpha,\alpha$–*o*-pivalamidophenyl)porphyrin. This porphyrin, synthesized from *o*-nitrobenzaldehyde and pyrrole and then reduced with stannous chloride, became known as the "picket fence porphyrin" (Figure 1.8).[152] The reason for the development of this type of porphyrin was the intention of favouring five-coordination and simultaneously inhibiting bimolecular reactions. Thus it has uneven steric bulk which creates a nonpolar cavity on one side of the porphyrin. A hindered cyclophane porphyrin had been previously reported; however, copper complexes were characterized, not iron.[153] The amines of these *o*-aminophenyl porphyrins are readily obtained. Using this simple, yet rugged and versatile porphyrin as a foundation, many more superstructured porphyrin model systems have been built.[154] In 1996, Rose *et al.* showed the synthesis of the "double picket fence" 5,10,15,20-Tetrakis(2',6'-dinitro-4'-tert-butylphenyl)-porphyrin.[155]

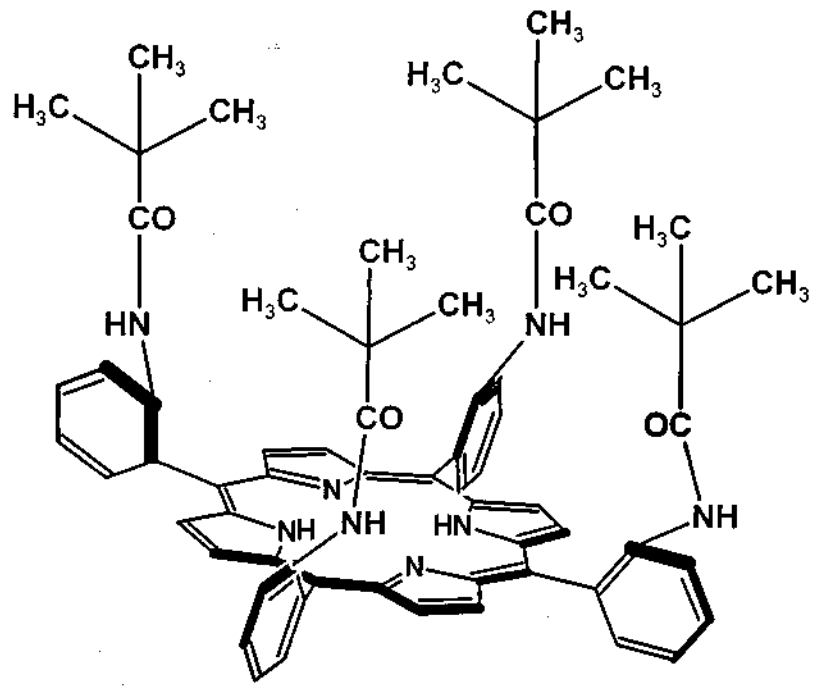

Figure 1.8: The structure of the "picket fence" porphyrin; *meso*-tetra($\alpha,\alpha,\alpha,\alpha$–*o*-pivalamidophenyl)porphyrin.

Other significant porphyrin chemistry includes the direct synthesis of capped and co-facial porphyrins. The condensation of pyrrole with a linked dialdehyde may produce a

porphyrin with the linker reaching over adjacent or alternating *meso*-positions. It is possible for the porphyrinogen to be locked from undergoing oxidation to produce the porphyrin if the linker that joins the aldehydes is too short.[40] A capped porphyrin has a bridging group over the top face of the porphyrin that is attached to each of the *meso*-substituted groups. Baldwin reacted a tetraaldehyde with pyrrole to form one of these capped porphyrins in a 2% yield (based on aldehyde).[156] Subsequently, Kagan and co-workers produced a novel Cyclophane system. They did this by condensing pyrrole and a porphyrin-tetraaldehyde (which had been synthesized from 4-(2-hydroxyethoxy)-benzaldehyde and pyrrole); this resulted in a co-facial porphyrin dimer (two porphyrins one on top of the other connected by their *meso*-substituents), in yields up to 8%.[108] Using the least number of conversions, these types of convergent syntheses produced super-structured porphyrins.

The methods discussed so far produce porphyrins with four identical substituents, but there are a number of applications that require a porphyrin with multiple substituents regiospecifically substituted around the porphyrin macrocycle.[40] To achieve this, a different type of method is necessary; one simple method takes the form of a mixed-aldehyde condensation. There are also possible mixed-pyrrole reactions; however, they are not utilized as commonly as mixed-aldehyde reactions. This is likely a consequence of the greater range of substituted aldehydes available in comparison to the lack of substituted pyrroles. There is, however, a disadvantage to mixed-aldehyde methods because there are likely to be six different porphyrin products formed (the two "parent" and the four "hybrid" porphyrins). Successful separation relies on two particular factors; the variation in polarity and the degree of facial encumbrance of the *meso*-substituents.[40]

When a porphyrin is required for practical purposes (necessary for application), a certain level of purity is preferred. This therefore restricts mixed-aldehyde or mixed-pyrrole reactions to binary condensations. There have been a few recorded methods for ternary mixed-reactions, but they produce low-yields (0.1%[157] and 0.7%[158]). Another method is solid phase synthesis which is restricted to aldehydes with a functional group for attachment to a solid-phase resin. This approach tries to minimize the chromatographic separation, which is normally essential for mixed condensations, by allowing one aldehyde to covalently attach to a solid phase.[159]

1.4 Events in Porphyrin History

The following time-line summarizes the key synthetic milestones for the synthesis of porphyrins.

1912 - Küster first suggested the cyclic tetrapyrrole structure of a porphyrin.[1,4]

1929 - Total synthesis of protoheme by Fischer.[6]

1935 - Rothemund synthesized porphyrins from pyrrole and aldehydes.[61]
1936 - Rothemund synthesized Porphine in a 0.9% yield.[59]
1939 - Rothemund studied the structure of the Porphine ring system.[60]
1941 - Rothemund gave a detailed method for *meso*-tetraphenylporphyrin synthesis (7.5-9% yield).[83]
1943 - Isolation and characterization of chlorin by Aronoff and Calvin.[84]
- Zinc acetate used to improve porphyrin yields.[85,86]

1956 - Uroporphyrinogen is enzymically converted to protoheme.[126]

1964 - Development of the Adler-Longo method.[99,100]

1970 - Dolphin showed porphyrinogen to be an intermediate in porphyrin synthesis.[124]
1975 - Synthesis of the "picket fence porphyrin" by Collman *et al.*[152]
- Baldwin and coworkers produced a capped porphyrin.[156]
1977 - A co-facial porphyrin dimer was constructed by Kagan and co-workers.[108]

1986 - Porphyrin synthesis under mild conditions: The Lindsey method.[116]
1988 - Attention devoted to porphyrins with severely distorted conformations.[65]
1989 - Lindsey method catalysed with a small volume of ethanol.[115]

1993 - Clays were used to improve yields of the Lindsey method.[168]
1994 - Investigation of a possible one-step synthesis.[56]
- A compilation of reported applications and failures of the Lindsey method.[131]

1997 - Investigation of the effect on yields of using different salts.[117]
1999 - Renewed interest in Synthesis, Reactivity and Structural chemistry of tetraalkylporphyrins.[58]

2001 - Studies using TFA and BF_3-etherate as a co-catalyst system.[145]

2007 - DFT simulations and Fluorescence spectra for *meso*-tetraalkylporphyrins in this work.

1.5 Synthetic Methods

Comparison of the Main Synthetic Methods

A direct comparison cannot be made for all the preparation methods discussed, due to not all the methods being used to prepare the same *meso*-substituted porphyrins from the same aldehydes. For each of the methods, some further modification has also been made to the original conditions and therefore the range of yields will also vary. Thus it seems more appropriate to compare the *scope* of the methods and their applicability. A defining feature of the scope of a method would be the failure rate, however these are results that are most often not recorded and therefore may exist only as "mute testimony"[40] to the limitations of the methods. A table has been drawn up to make a general comparison based on the common characteristics of each of the three main methods discussed.

From Table 1.1 it can be seen that although the Rothemund method was the founding technique it does not seem to have any type of distinctive advantages over the subsequent methods. The Adler method allows porphyrin synthesis from relatively stable aldehydes at the preparative scale; however, it does have its restrictions. There will be possible contamination of the porphyrin by chlorins when using this process; however, these can be easily removed by oxidation or chromatography. The method fails for many 2,6-disubstituted aryl aldehydes and various aliphatic aldehydes. The choice of solvent also causes concern for aldehydes that have substituents which may not endure the refluxing propionic acid and some porphyrins that will not crystallize from this solvent. The ability to effortlessly and swiftly obtain crystalline porphyrins, in yields around 20%, from the slow cooling mixture is what makes it such an appealing procedure.[40]

The Adler and Rothemund methods are both one-step methods concerning synchronized condensation and oxidation to produce the porphyrin. On the assumption that the intermediate is porphyrinogen, for these processes to succeed the condensation producing the porphyrinogen must be faster than the oxidation of precursors to obtain the porphyrinogen.[40]

Table 1.1: A comparison of the various experimental factors pertaining to each of the main synthetic methods for porphyrin production.[40]

	Rothemund method	Adler-Longo method	Lindsey method
Solvents	Pyridine	Propionic acid Acetic acid RCO_2H + benzene	CH_2Cl_2 $CHCl_3$
Concentration of reactants	3.6 M (pyrrole)	0.3–0.1 M	0.1–0.001 M
Catalyst	No catalyst	Solvent	BF_3·etherate BF_3·etherate/ethanol BF_3·etherate + salt TFA and other acids Clays
Oxidant	Excess aldehyde	Oxygen	DDQ or *p*-chloranil
Temperature	85-220 °C	141 °C	25 °C (room temperature)
Reaction time	10 to 48 hours	~ 1 hour	~ 1 hour
Stages	1-step	1-step	1-step or 2-step
Workup	Extract crystals	Filter crystals	Chromatography and removal of solvent
Yield	< 10%	~ 20–30%	Up to 40%
Scope	Restricted	Reasonable	Broad

The advantages of the Lindsey method include mild conditions, high yields (despite the necessity to remove large volumes of solvent at reactant concentrations of 0.01 M to 0.1 M) and the widest scope for application. However, there are still some aldehydes that will not succeed via this method. This procedure can be used for sensitive substituents, 2,6-disubstituted aryl aldehydes, aliphatic aldehydes and

expensive aldehydes (where total yield is of great significance).[40] One limitation of this method is that it usually involves a chromatographic workup. In the cases where both the Adler and Lindsey methods are successful, then other features such as availability of aldehyde and the ease of workup need to be examined.

A detailed list of the failures through 1992 can be found in Metalloporphyrin-Catalyzed Oxidations, written by Lindsey (1994)[131] and since then more reported failures have been published.[160,161,162,163,164,165,166] Some of these failures may be attributed to poor intrinsic solubility of the aldehyde (in CH_2Cl_2 or $CHCl_3$) or possible precipitation upon complexation with the acid catalyst. Examples of this are the pyridyl carboxaldehydes, a range of other heterocyclic aldehydes and relatively polar aldehydes. Some reported cases where the Lindsey method fails are for 2,6-dicyanobenzaldehyde,[161] 3,5-bis(perfluorooctyl)-benzaldehyde[166] and reactions of propionaldehyde with various 3,4-disubstituted pyrroles did not produce the relevant porphyrins.[77] There are also a few reported failures (that have since been resolved by the adjustment of reaction conditions) regarding a few unsaturated aldehydes or bulky aliphatic aldehydes.

Methods for Particular Kinds of *meso*-Substituted Porphyrins

Many of the mentioned synthetic methodologies have also been applied to *meso*-tetraalkylporphyrins.[27,60,61,107,110,111,112,114,167,168,169,170,171] Some additions and developments for the *meso*-tetraalkylporphyrin methods are as follows. In 1971, Yalman patented a method for synthesizing porphine, *meso*-monomethyl-, *meso*-dimethyl-, *meso*-trimethylporphin and their metal chelates. He used a pyrrole-carbinol at 120–150 °C in DMF, using a metal acetate and a small quantity of an organic acid.[172] Improved yields were obtained by reducing the self-polymerization of the pyrrole-carbinol and controlling the temperature and the pH of the buffer. Yields of the porphyrins could also be improved to 75 to 85% by a demetallation process from the corresponding metal chelates. Von Maltzan produced a yield of 1% of *meso*-tetramethylporphyrin by reacting pyrrole in ethanol with the diethyl acetal of acetaldehyde in the presence of trifluoroacetic acid open to air.[173]

Ulman *et al.* reported facile synthesis of *meso*-substituted tetraalkylchlorin and tetraalkylporphyrin, by reacting diethyl acetals with pyrrole in glacial acetic acid

containing $Ni(OAc)_2$ and 2% acetic anhydride.[174] The product formed was a mixture of the nickel porphyrin and nickel chlorin (the ratio depended upon the metal and the amount of anhydride present). For acetaldehyde diethyl acetal the porphyrin to chlorin ratio was 1:4 (an overall yield of 1.6% was recorded). When the same reaction was done without exposure to air the result was tetramethylisobacteriochlorin in 1% yield and some tetramethyl-porphyrinogen.[175] However, for butanal diethyl acetal the yield went up to 5.4% with the porphyrin being the most predominant product. Li and Govind used pyrrole and aldehyde in a cobalt-zeolite to obtain the cobalt porphyrin.[176] Neya and Funasaki furthered the changes made on the Adler method by Treibs-Haberle, by the use of a mixed solvent (propionic acid, pyridine and addition of water, which helped in porphyrin isolation) and an excess of pyrrole. The synthesized porphyrins gave yields of 8–10%.[177]

Making comparisons and evaluations of the different methods is difficult because (as already mentioned) each of the methods has not been applied to the same alkyl aldehydes. There is a significant difference between alkyl groups that pass on good solubility or poor (e.g. methyl, ethyl) solubility to the porphyrin.

Notable observations:

1) *meso*-Tetraalkylporphyrins are generally produced in yields of only a few percent. For example, *meso*-tetrapropylporphyrin gave yields of 6.2%[157] and 2.8%.[178]
2) The Lindsey method using concentrations of 1 mM gave yields of up to 25% for longer chain aldehydes (e.g. hexanal, undecanal).[27]
3) In 1994, Smith and co-workers found that they could successfully react hindered alkyl aldehydes (e.g. *t*-butyl and isopropyl) with the Lindsey method using an increased concentration of BF_3·etherate.[58,78]
4) To obtain higher yields of *meso*-tetraalkylporphyrins from the Lindsey method, clays (e.g. montmorillonite K10) were used as catalysts for the condensation. (K10's efficient promotion of porphyrin synthesis is established to be mostly due to the mesoporosity rather than to its acid property).[168,170]
5) The self-condensation of pyrrole-carbinols using *p*-toluenesulfonic acid in benzene, azeotropic removal of water and oxidation by DDQ efficiently produces perfluoroalkyl porphyrins.[169]

6) When Johnstone, *et al.* reacted *n*-butanal with pyrrole and acetic acid in nitrobenzene at 120 °C they obtained the highest reported yield for tetrapropylporphyrin of 12%.[171]
7) Neya and Funasaki obtained the highest reported yields of *meso*-tetraalkylporphyrins with short groups (methyl, ethyl), in the range of 10%.[177]

There has been great interest surrounding porphyrins that have alkenes or alkynes at the *meso*-position. One feature that poses a problem for this conversion of α,β-unsaturated aldehydes to porphyrins is that rather than attack at the carbonyl group there is a tendency for conjugate addition. However, this conjugate addition can be suppressed to a certain extent, if the 3-position of the alkynyl aldehyde has a bulky substituent.[179] Another approach may be the temporary masking of the ethyne.[180]

Effects of Salts

During the investigation of aerobic oxidation systems it was unintentionally determined that the porphyrin yield for H_2TPP could be increased as much as two-fold in the presence of salts. Consequently there was an interest in the salt effect and a further twenty-eight different salts were investigated.[117] Of the 21 insoluble salts tested, 12 gave increases in yields; however, 6 had no noticeable effects and 3 actually diminished yields. Increased yields resulted from salts that contained a variety of cations; however, only some anions, e.g., Cl^-, Br^-, I^- and Ph_4B^-, showed favourable results. The anions SO_4^{2-}, F^- and BF_4^- did not improve yields. Yield increases of > 1.5 fold were seen for all 7 soluble salts examined[117] It was found that the salts had the effect of increasing not only yields, but also the rate of condensation (as measured by rate of benzaldehyde depletion and porphyrin production). The salts (both insoluble and soluble) had the best effect when they were used in conjunction with the catalyst BF_3·etherate. These results of increased yields at high concentrations are of course useful for many porphyrin forming reactions, particularly those for preparative work.

Once useful salts had been identified, the next step was to establish how flexible these salt effects were and if they could be used to obtain increased yields from porphyrin syntheses other than H_2TPP. A group of nine aldehydes were studied.[40] Six of these gave successful results, which included improvements in yields ranging from

two- to six-fold. Although the mechanism of the exact functioning of this salt effect was not determined during these experiments, one point of interest is the reaction medium. For the duration of the pyrrole-aldehyde condensation the reaction medium becomes heterogeneous, either with or without the presence of soluble salts.[40]

Synthetic Methods for Porphyrins Bearing from One to Four *meso*-Substituents

Although this is not particularly relevant to this work, it is noteworthy that porphyrins may be synthesized with different numbers (one to four) of *meso*-substituents. To control the number and type of *meso*-substituents in the synthesis of a porphyrin involves the sequential introduction of groups at the α-positions of pyrrole and pyrrole derivatives. Numerous tactics can be foreseen to carry this out. Dipyrromethane condensations are one of the more dominant approaches.[40]

Distinctions between Tetrabenzporphyrins, Phthalocyanines, Porphyrazines and Porphyrins

In order to make a comparison of these different methods, it is necessary to compare the members of the porphyrinic family (Figure 1.9). Tetrabenzporphyrin is like porphine or octaalkylpoprhyrins as it has four unsubstituted *meso*-positions, but like phthalocyanines it has four benzannulated pyrrole rings. Diverse methods have been used to prepare tetrabenzporphyrin.[181,182] Phthalocyanines are very similar to tetrabenzporphyrins, but they have nitrogen atoms at each *meso*-position as well. They are of colossal interest with regard to industry and thus many methods have been developed for synthesizing them. One of the first methods developed by Linstead, in his quarter century of studies beginning in 1934, has laid the basis for most methods thereafter.[183,184] Porphyrazines (i.e. tetraazaporphyrins) are just like phthalocyanines, but they do not have the benzannulated pyrrole units. There is a synthetic route that produces the corresponding magnesium porphyrazine from the treatment of a maleonitrile with magnesium alkoxide in an alcohol (such as *n*-propanol or *n*-butanol).[185,186,187,188]

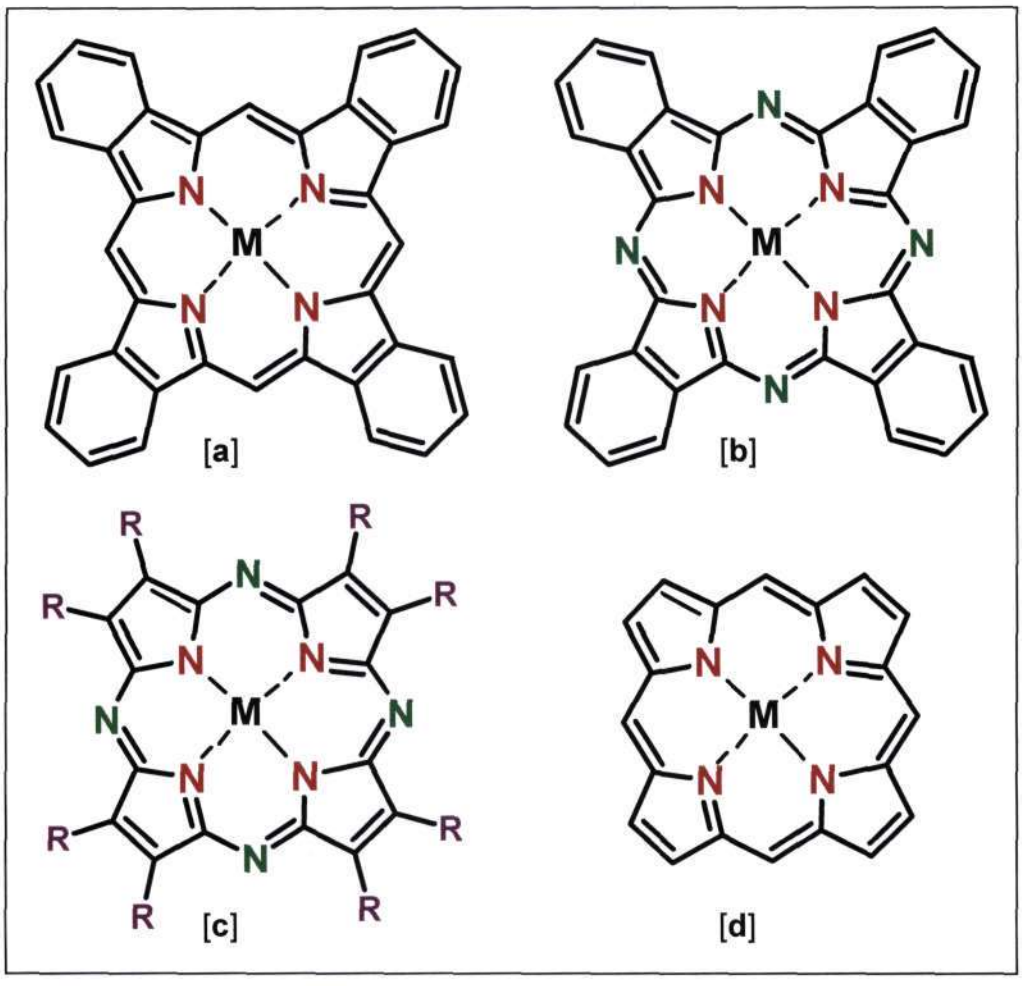

Figure 1.9: Comparison of the basic structures of tetrabenzporphyrins [**a**], phthalocyanines [**b**], porphyrazines [**c**], and porphyrins [**d**].[40]

The porphyrin forming pyrrole-aldehyde condensation stands in prominent distinction to the condensation of the other related members of the porphyrinic family mentioned above. This condensation starts with pyrrole and an aldehyde, which needs an oxidant (–6 electrons, –6 protons) to complete the conversion to the porphyrin; however, the other classes (tetrabenzporphyrin, phthalocyanine, porphyrazine) call for a reducing agent (+2 electrons, +2 protons). Unfortunately not a lot is known about the intermediates or mechanisms in each of these reactions.[40]

1.6 Objectives

In the porphyrin literature very little has been published and/or exists on the structures and physical properties of *meso*-tetraalkylporphyrins. Remarkable and innovative research, including beneficial characterization and interesting applications, has mostly been published for *meso*-tetraarylporphyrins. Therefore it is of interest to determine whether *meso*-tetraalkylporphyrins might have comparable properties and consequently similar, or possibly even better, functions and applications. Thus, the aim of this work is to alternatively synthesize and fully characterize a range of *meso*-tetraalkylporphyrins. These can then be compared in order to understand the impact of the different substituents on the properties and behaviour of the particular porphyrin. The geometrical conformations of these free base *meso*-tetraalkylporphyrins are of particular interest.

The method used to synthesize these porphyrins is also to be optimized (so that the yields that have already been quoted in the literature may be improved upon). There is also a desire to obtain crystal structures for any of the target porphyrins in order to extend the very small existing list of available *meso*-tetraalkylporphyrin crystal structures. Another interesting field is that of theoretical computations, the use of density functional theory (DFT) in particular. To date no calculations based particularly on *meso*-tetraalkylporphyrins can be found in the literature, which makes this a novel and pioneering focal point. Comparing these results to the experimental data has two advantages. It not only helps in the characterization and analysis of *meso*-tetraalkylporphyrins, but also shows the applicability of these DFT computations to *meso*-tetraalkylporphyrins. A third area of interest is fluorescence spectroscopy. In the literature, emission spectra and fluorescence lifetime data exist for *meso*-tetraarylporphyrins (mostly metallated, but some free bases as well). However, similar information for *meso*-tetraalkylporphyrins is absent from the literature. Thus it will be of interest to determine the type of emission and excited state lifetimes for a range of *meso*-tetraalkylporphyrins. A comparison can then be made with the existing data for *meso*-tetraarylporphyrins. A key question is whether alkyl substituents impart greater rigidity to the porphyrin macrocycle (relative to standard aryl groups) and thus modulate the excited state dynamics of these systems. Finally, a metallation with

gold(III) will be attempted in order to determine the properties of gold(III) *meso*-tetraalkylporphyrins with respect to their anticancer ability and cytotoxicity.

The principal objectives of this work were to:

(1) synthesize a range of free base *meso*-tetraalkylporphyrins (some novel and some currently known);

(2) optimize a method that could be used to synthesize the majority of *meso*-tetraalkylporphyrins simply and with the best possible yields;

(3) fully characterize all these porphyrins using UV-vis and IR spectra, as well as ^{1}H and ^{13}C NMR;

(4) obtain X-ray crystal structures and to perform DFT computational studies for each of these free base *meso*-tetraalkylporphyrins;

(5) observe and investigate any ruffling that occurred in the porphyrin ring using the DFT simulation data and X-ray structures;

(6) understand what factors may lead to planar or non-planar conformations for *meso*-tetraalkylporphyrins using X-ray and DFT methods to probe the structures and possible distortions of the synthesized *meso*-tetraalkylporphyrins;

(7) measure the emission spectra and lifetimes, for the first time, of *meso*-tetraalkylporphyrins and to gain a fundamental understanding of how the structural and conformational features of the compounds may impact on their luminescence; and

(8) perform a metallation of example *meso*-tetraalkylporphyrin(s) with gold(III) and attempt to fully characterize the gold complex.

2. Experimental

2.1 General Information

Solvents were obtained from Merk and were used as received, unless otherwise stated.

Hexane was dried and distilled over pressed sodium wire. THF was dried over Na/K alloy.

Pyrrole (Aldrich) was distilled from calcium hydride (CaH_2) using short path distillation apparatus and stored at 6 °C until use, which occurred prior to any discolouration.

BF_3·etherate was obtained from Aldrich, purified by short path distillation from calcium hydride CaH_2 under N_2, and then stored at 2 °C until use.

TFA, DDQ and Sodium tetrachloro-aurate(III) hydrate (all from Aldrich) were used as received.

The six aldehydes: 2-Methylbutyraldehyde, Phenylacetaldehyde (stored at 2 °C), 2-Ethylbutyraldehyde, Diphenylacetaldehyde, Isobutyraldehyde and Cyclohexane-carboxaldehyde (all from Aldrich) were all used as received.

$AgSbF_6$ was stored and dispensed under inert conditions in the glove box.

Concentration in *vacuo* was performed on a Buchi rotary evaporator.

Silica gel 60 (Merck) and aluminium oxide 90 (active, basic, Merk) were used for column chromatography.

Analytical thin layer chromatography (TLC) was carried out using Merck silica gel 60 F_{254} plates.

2.2 Instrumentation

Electronic UV-vis spectra were recorded using a Perkin-Elmer Lambda 45 double beam UV-vis scanning spectrometer. Dichloromethane was used in cuvettes of path length 1.0 cm. The IR samples for the compounds were made from KBr pellets and FT-IR spectra were obtained on a Perkin-Elmer Spectrum One spectrometer (3 scans, spectral resolution = 1.0 cm^{-1}). Peak assignments were based on calculated

vibrational modes at the B3LYP/6-31G** level of theory. ^{1}H and ^{13}C NMR spectra of saturated solutions of the compounds in $CDCl_3$ were recorded with a 500 MHz Varian Unity Inova spectrometer equipped with an Oxford magnet (11.744 T). The proton and carbon NMR spectra were assigned with the use of DEPT and 2D COSY and HSQC data. Coupling constants are averages calculated from peak separations measured with SpinWorks.[189] X-ray diffraction data were collected on an Oxford Diffraction Xcalibur2 CCD 4-circle diffractometer equipped with an Oxford Instruments Cryojet operating at 100(2) K. The data were collected at a crystal-to-detector distance of 50 mm using omega scans at θ = 29.389° with 20 to 35 s exposures taken at ~ 2 kW X-ray power with 0.75° frame widths. The data were reduced with the program *CrysAlis RED*[190] using outlier rejection, scan speed scaling, as well as standard Lorentz and polarization correction factors. Direct methods (SHELXS-97, WinGX32)[191,192] were used to solve the structures. All non-H atoms were located in the E-map and refined anisotropically with SHELXL-97.[193] The hydrogen atoms in each of the structures were included as idealized contributors in the least-squares process with standard SHELXL-97[193] parameters. Samples were analyzed using positive electrospray ionization (ESI+) on a Waters LCMS TOF LCT Premier spectrometer.

2.3 Fluorescence spectroscopy measurements

Luminescence studies

All emission spectra were recorded with a PTI TM-2 spectrofluorimeter using a Xeon lamp. Gated emission scan measurements were made at room temperature as well as at 77 K using a delay of 95 μs and an integration time of 100 μs. Each sample was dissolved in dichloromethane and had the concentration in the range of 10^{-7} mol dm^{-1}. The 77 K data were collected using a quartz finger dewar filled with liquid nitrogen. For optimal resolution, the spectral measurements were obtained with slit settings ranging from 5 to 14 nm for both the excitation and emission beams. The excitation wavelength used for both the room temperature and 77 K measurements was the shortest wavelength Q band (~ 520 nm).

Lifetime studies

The method for extracting lifetimes made use of a photomultiplier detector and the excitation source was a Xeon lamp. The decay curves were acquired in the time domain from 99 μs to 139 μs. The Soret band or lowest wavelength (greatest intensity) Q band was used for excitation. FeliX32 Analysis software[194] was used to capture the decay. The internal response function used for the lifetime fits was LUDOX (colloidal silica, SiO_2) at very dilute concentrations excitation and emission at 420 nm with the same magnitude of intensity as the sample. The data were fit by standard nonlinear least squares regression methods to single exponential decay (first order) functions.

2.4 Free base porphyrin synthetic methods

2.4.1 Syntheses of $H_2T(iBu)P$ (Porphyrin 1)

(1) Method with $BF_3{\cdot}OEt_2$ as the catalyst:

In a 1-L three-neck round-bottom flask, distilled pyrrole (4.86 ml, 0.070 moles) and 2-methylbutyraldehyde (7.50 ml, 0.070 moles) were stirred in distilled dichloromethane (750 ml) at room temperature for half an hour under nitrogen. $BF_3{\cdot}OEt_2$ (1.45 ml, 0.070 moles) was then added drop-wise to the reaction flask and then stirred for a further 18 hours at room temperature, covered in foil. DDQ (11.30 g, 0.050 moles) was then added and the reaction mixture was brought to reflux for 1 hour, after which it was cooled to room temperature. The product was put through a silica plug and then through an aluminium oxide plug (solvent system: dichloromethane:hexane, 40:60). Finally, the reduced product was placed on a column of silica gel and eluted with the same solvent system as before (dichloromethane:hexane, 40:60). TLC was used to determine the purity of the obtained fractions. The pure fractions were allowed to evaporate away from light and were then collected, combined and weighed. Isolated yield: 0.2191 g, 2.3 %.

(2) Method with co-catalyst system:

In a 1-L three-neck round-bottom flask, distilled pyrrole (0.694 ml, 20 mM, 0.01 moles) and 2-methylbutyraldehyde (1.071 ml, 20 mM, 0.010 moles) were stirred in dichloromethane (500 ml) at room temperature for 5 minutes under nitrogen. A solution of triflouroacetic acid (1.156 ml, 30 mM, 0.015 moles) and $BF_3{\cdot}OEt_2$ (0.040 ml, 0.6 mM, 0.0003 moles) in ~ 10 ml of dichloromethane was then added over a period of 15 minutes. The reaction was then covered in foil & left to stir for 1 hour. After the addition of DDQ (2.270 g, 20 mM, 0.01 moles) the mixture was allowed to stir for half an hour, then immediately run through an aluminium oxide plug. The product was reduced on the rotary evaporator and the column was eluted with the recycled dichloromethane. The final reduced product was then put through a silica gel column (solvent system = 100% chloroform, initially, switching to 100% dichloromethane at the end). The first fraction showed no trace of the porphyrin by TLC, but it was present in the later fractions, which were collected and combined after evaporation of the solvent. Isolated yield: 0.0352 g, 3.3 %.

(3) Method with 0.1% Ethanol:

In a 1-L three-neck round-bottom flask, dichloromethane (500 ml) and ethanol (0.50 ml) were stirred with pyrrole (0.694 ml, 10 mmol) and 2-methylbutyraldehyde (1.071 ml, 10 mmol) under nitrogen for 5 minutes at room temperature. Then TFA (0.770 ml, 10 mmol) was added and the mixture was stirred for 1 hour covered in foil. After the addition of DDQ (1.703 g, 7.5 mmol) the reaction stirred for 20 minutes at room temperature and was then immediately put through an aluminium oxide column. The product was reduced on the rotary evaporator and the solvent was used to wash the plug. After satisfactory washings, the resulting product was placed on a silica column and eluted first with chloroform and finally with dichloromethane. TLC was used to determine the purity of the obtained fractions, showing greater purity in the later collected fractions. After evaporation of the solvent the fine crystalline material was collected and combined. A sample of this pure product was dissolved in THF, put in a test tube and layered with hexane. After 6 days single crystals were obtained, some of which proved to be of X-ray quality and thus a structure was determined. Isolated yield: 0.0500–0.1000 g, 3.8–7.2 % (range from several reactions).

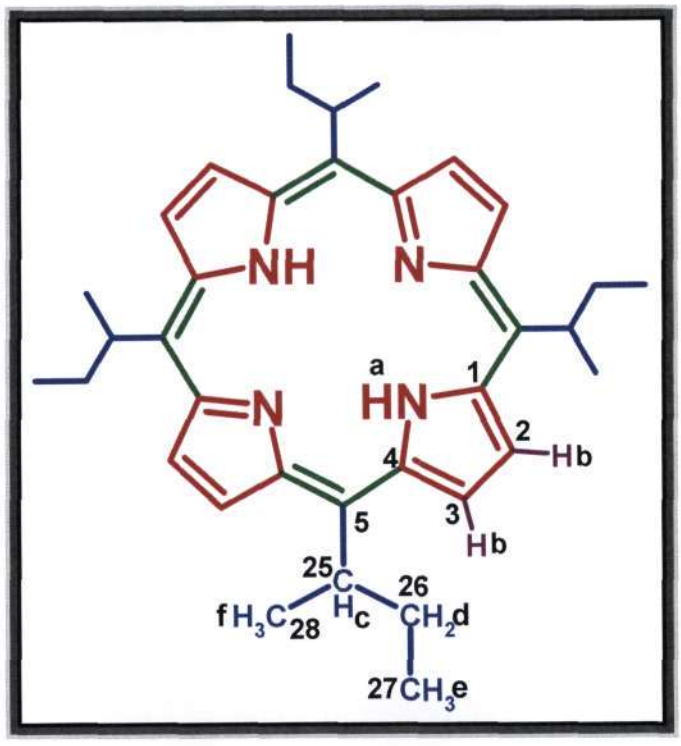

Figure 2.1: Structure of Porphyrin 1, $H_2T(iBu)P$.

Porphyrin 1, $H_2T(iBu)P$:

UV–vis (CH_2Cl_2) [λ_{max}, nm (ε, $M^{-1}cm^{-1}$]: 420.5 (564 × 10^3), 491.5 (sh), 513.0 (15.5 × 10^3), 559.0 (8.5 × 10^3), 602.0 (4.7 × 10^3), 658.5 (4.6 × 10^3). ^1H NMR (500 MHz, $CDCl_3$) [δ, ppm]: –1.937 (2H, s, br, *a*), 1.029 (24H, t, $^3J_{de}$ = 7.4, *e*), 1.256 (4H, t, $^3J_{cd}$, *c*), 2.358 (24H, d, $^3J_{cf}$ = 7.3, *f*), 2.729, 2.808 (8H, multiplet, *d*), 3.724 (8H, q, $^3J_{cde}$ = 7.0, *d*), 5.052 (4H, sextet, $^3J_{cdf}$ = 7.4, *c*), 9.471 (8H, s, *b*). ^{13}C NMR (125 MHz, $CDCl_3$) [δ, ppm]: 14.14 (C-27), 18.43 (C-25), 27.01 (C-28), 35.42 (C-26), 42.76 (C-25), 58.48 (C-26), 122.71 (C-5), 128.96 (C-2,3), 144.691 (C-1,4). IR (KBr pellet, cm^{-1}): 3329 (m, ν(N-H)), 3146 (w, ν_s(pyrrole C-H)), 3128 (w, ν_{as}(pyrrole C-H)), 2960 (s, ν_{as}(C-H)), 2927 (s, ν_{as}C-H)), 2869 (s, ν_s(C-H)), 1558 (w, ν(Cβ-Cβ and Cα-C_{meso})), 1453 (s, δ_{oop}(C-H), ν(C_α-C_{meso}) and ν(C_{meso}-C_{alkyl})), 1374 and 1325 (m δ_{ip}(pyrrole C-H), δ_{ip}(alkyl C-H)), 1151 (w), 967 and 902 (m, ν(Cα-Cβ), δ_{ip}(pyrrole C-H and N-H)), 794 and 731 (s, δ_{oop}(pyrrole N-H), δ_{oop}(pyrrole C_β-H)), 642 (w, ν(C_{meso}-CH), δ_{oop}(pyrrole N-H)). Mass (M+H): found 535.3800; calculated 535.3801 for $C_{36}H_{47}N_4$.

2.4.2 Syntheses of $H_2T(CH_2Ph)P$ (Porphyrin 2)

(1) Method with $BF_3 \cdot OEt_2$ as the catalyst:

In a 1-L three-neck round-bottom flask, distilled pyrrole (4.86 ml, 0.070 moles) and the phenylacetaldehyde (7.50 ml, 0.070 moles) were stirred in distilled dichloromethane (750 ml) at room temperature for half an hour under nitrogen. $BF_3 \cdot OEt_2$ (1.45 ml, 0.070 moles) was then added drop-wise to the reaction flask and the solution stirred for a further 18 hours at room temperature, covered in foil. DDQ (11.30 g, 0.050 moles) was then added and the reaction mixture was brought to reflux for 1 hour, and then cooled to room temperature. The product was put through a silica plug and then through an aluminium oxide plug (solvent system: chloroform). Finally, the reduced product was placed on a column of silica gel and eluted with the solvent system dichloromethane:hexane (60:40). TLC was used to determine the purity of the obtained fractions. No fractions were found to be pure and thus purification was attempted by crystallization in test tubes with a solvent system dichloromethane:hexane (ca. 1.5 ml CH_2Cl_2 : 15 ml hexane. Isolated yield: 0.0598 g, 0.51 %.

(2) Method with co-catalyst system:

In a 1-L three-neck round-bottom flask, distilled pyrrole (0.347 ml, 10 mM, 0.005 moles) and phenylacetaldehyde (0.585 ml, 10 mM, 0.005 moles) were stirred in dichloromethane (500 ml) at room temperature for 5 minutes under nitrogen. A solution of trifluoroacetic acid (0.900 ml, 15 mM, 0.0075 moles) and $BF_3 \cdot OEt_2$ (0.020 ml, 0.3 mM, 0.00015 moles) in ~ 10ml of dichloromethane was then added over a period of 15 minutes. The reaction was then covered in foil & left to stir for 1 hour. After the addition of DDQ (1.135 g, 10 mM, 0.005 moles) the mixture was allowed to stir for half an hour, then immediately run through an aluminium oxide plug (a mixture of dichloromethane and chloroform was used to wash the plug). The product was reduced on the rotary evaporator and was then put through a silica gel column (chloroform solvent system, switching to dichloromethane at the end). TLC was used to determine the purity of the obtained fractions. The pure fractions were allowed to evaporate away from light. However, this only yielded powders and thus test tubes

were set up (dichloromethane/hexane) and a single crystal of X-ray quality was formed in one of the test tubes after 9 days. Isolated yield: 0.0182 g, 1.1 %.

(3) Method with 0.1% Ethanol:

In a 1-L three-neck round-bottom flask, dichloromethane (500 ml) and ethanol (0.50 ml) were stirred with pyrrole (0.694 ml, 10 mmol) and phenylacetaldehyde (1.170 ml, 10 mmol) under nitrogen for 5 minutes at room temperature. TFA (0.770 ml, 10 mmol) was added and the mixture was stirred for 1 hour covered in foil. After the addition of DDQ (1.703 g, 7.5 mmol) the reaction mixture was stirred for 20 minutes at room temperature and was then immediately put through an aluminium oxide column. The product was reduced on the rotary evaporator and the solvent used to wash the plug. After satisfactory washings, the reduced product was placed on a silica column and eluted first with chloroform and finally with dichloromethane. TLC was used to determine the purity of the obtained fractions, the middle set of collected fractions showed improved purity. Isolated yield: 0.0364–0.0506 g, 2.2–3.0 % (range from several reactions).

Porphyrin 2, $H_2T(CH_2Ph)P$:

UV–vis (CH_2Cl_2) [λ_{max}, nm (ε, $M^{-1}cm^{-1}$]: 422.5 (457 × 10^3), 489.5 (sh), 520.0 (19.9 × 10^3), 555.5 (5.8 × 10^3), 600.5 (3.9 × 10^3), 658.5 (2.7 × 10^3). ^{1}H NMR (500 MHz, $CDCl_3$) [δ, ppm]: –2.343 (2H, s, br, *a*), 6.342 (8H, s, *c*), 7.120 (4H, t, $^3J_{ef}$ = 7.2, *f*), 7.188 (8H, t, $^3J_{def}$ = 7.6, *e*), 7.315 (8H, d, $^3J_{ef}$ = 7.7, *d*), 9.386 (8H, s, *b*). ^{13}C NMR (125 MHz, $CDCl_3$) [δ, ppm]: 40.43 (C-25), 115.17 (C-5), 125.86 (C-29), 128.44 (C-27,28,30,31), 128,56 (C-2,3), 144.90 (C-1,4). IR (KBr pellet, cm^{-1}): 3317 (m, ν(N-H)), 3059 (w, ν_s(pyrrole C-H)), 3023 (m, ν_{as}(pyrrole C-H)), 2924 (m, ν_{as}C-H)), 2856 (w, ν_s(C-H)), 1600 (m, ν(Cβ-Cβ and Cα-C_{meso})), 1493 and 1452 (m, δ_{oop}(C-H), ν($C_α$-C_{meso}) and ν(C_{meso}-C_{alkyl})), 1116 (w), 939 and 916 (m, ν(Cα-Cβ), δ_{ip}(pyrrole C-H and N-H)), 780 and 717 (s, δ_{oop}(pyrrole N-H), δ_{oop}(pyrrole $C_β$-H)). Mass (M+H): found 671.3184; calculated 671.3175 for $C_{48}H_{39}N_4$.

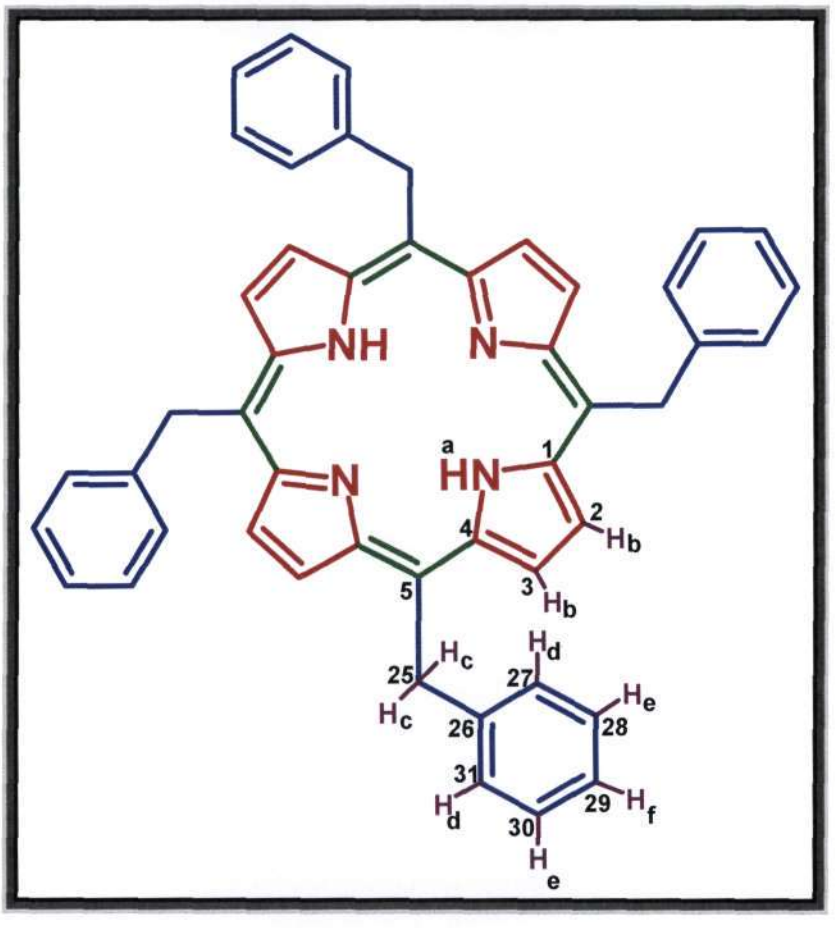

Figure 2.2 : Structure of Porphyrin 2, $H_2T(CH_2Ph)P$.

2.4.3 Syntheses of $H_2T(iPent)P$ (Porphyrin 3)

(1) Method with co-catalyst system (dilute):

In a 1-L three-neck round-bottom flask, distilled pyrrole (0.347 ml, 10 mM, 0.005 moles) and 2-ethylbutyraldehyde (0.815 ml, 10 mM, 0.005 moles) were stirred in dichloromethane (500 ml) at room temperature for 5 minutes under nitrogen. A solution of TFA (0.900 ml, 15 mM, 0.0075 moles) and $BF_3{\cdot}OEt_2$ (0.20 ml, 0.3 mM, 0.00015 moles) in ~ 10 ml of dichloromethane was then added over a period of 15 minutes. The reaction was covered in foil & left to stir for 1 hour. After the addition of DDQ (1.135 g, 10 mM, 0.005 moles) the mixture was allowed to stir for half an hour, then immediately run through an aluminium oxide plug and washed with dichloromethane. The product was reduced on the rotary evaporator and the column was eluted with the recycled dichloromethane. The final reduced product was then put

through a silica gel column (solvent system chloroform, using dichloromethane at the end). TLC was used to determine the purity of the obtained fractions. The pure fractions were allowed to evaporate away from light and all produced small purple crystals. Isolated yield: 0.0785 g, 10.6 %.

(2) Method with co-catalyst system:

In a 1-L three-neck round-bottom flask, distilled pyrrole (0.694 ml, 20 mM, 0.01 moles) and 2-ethylbutyraldehyde (1.229 ml, 20 mM, 0.10 moles) were stirred in dichloromethane (500 ml) at room temperature for 5 minutes under nitrogen. Then a solution of trifluoroacetic acid (1.800 ml, 30 mM, 0.015 moles) and $BF_3{\cdot}OEt_2$ (0.040 ml, 0.6 mM, 0.0003 moles) in ~ 10 ml of dichloromethane was added over a period of 15 minutes. The reaction was then covered in foil and left to stir for 1 hour. After the addition of DDQ (2.270 g, 20 mM, 0.01 moles) the mixture was allowed to stir for half an hour, then immediately run through an aluminium oxide plug and washed with dichloromethane. The product was reduced on the rotary evaporator and the column was eluted with the recycled dichloromethane. The final reduced product was then put through a silica gel column (solvent system = 100% chloroform, initially, switching to 100% dichloromethane at the end). TLC was used to determine the purity of the obtained fractions. The pure fractions were allowed to evaporate away from light and were then collected, combined, weighed and characterized. Isolated yield: 0.1219 g, 8.74 %.

(3) Method with 0.1% Ethanol:

In a 1-L three-neck round-bottom flask, dichloromethane (500 ml) and ethanol (0.50 ml) were stirred with pyrrole (0.694 ml, 10 mmol) and 2-ethylbutyraldehyde (1.791 ml, 10 mmol) under nitrogen for 5 minutes at room temperature. Then TFA (0.770 ml, 10 mmol) was added and the mixture was stirred for 1 hour covered in foil. After the addition of DDQ (1.703 g, 7.5 mmol) the reaction stirred for 20 minutes at room temperature and was then immediately put through an aluminium oxide column. The product was reduced on the rotary evaporator and the solvent used to wash the plug. After satisfactory washings, the resulting product was placed on a silica column and eluted first with chloroform and finally with dichloromethane. The first fractions were shown by TLC to be reasonably pure, with purity decreasing for the last set of

collected fractions. These purer fractions were allowed to evaporate away from light and were then collected and combined. A sample of this pure product was dissolved in THF, put in a test tube and layered with hexane. After 5 days single crystals were obtained, some of which proved to be of X-ray quality and thus a structure was determined. Isolated yields: 0.2200–0.2800 g, 15–20 % (range from several reactions).

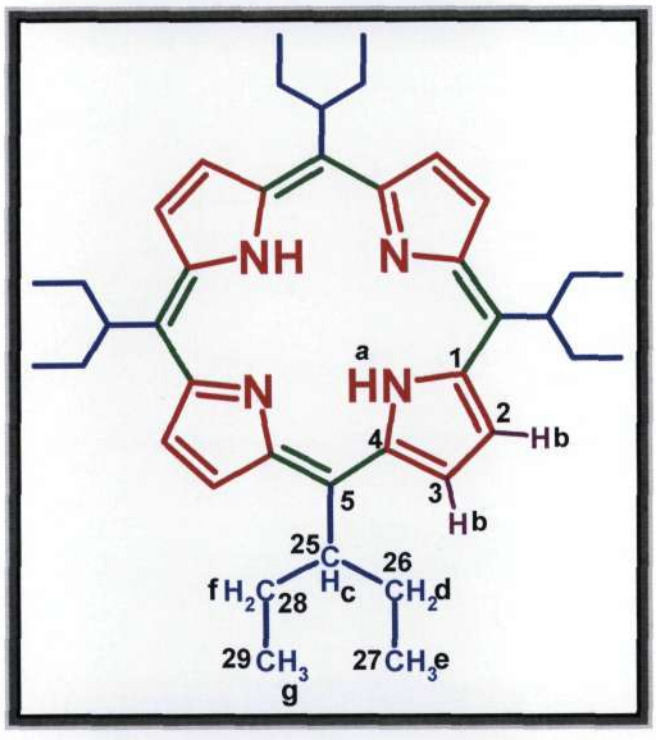

Figure 2.3: Structure of Porphyrin 3, $H_2T(iPent)P$.

Porphyrin 3, $H_2T(iPent)P$:

UV–vis (CH_2Cl_2) [λ_{max}, nm (ε, $M^{-1}cm^{-1}$]: 423.5 (896 × 10^3), 493.5 (sh), 527.5 (28.3 × 10^3), 563.5 (15.2 × 10^3), 609.0 (7.8 × 10^3), 666.5 (6.5 × 10^3). ^1H NMR (500 MHz, $CDCl_3$) [δ, ppm]: –2.247 (2H, s, br, *a*), 1.002 (24H, t, $^3J_{de,fg}$ = 7.4, *e,g*), 2.780 (8H, septet, *d*), 2.895 (8H, septet, *f*), 4.888 (4H, quintet, $^3J_{cdf}$ = 7.5, *c*), 9.537 (8H, s, *b*). ^{13}C NMR (125 MHz, $CDCl_3$) [δ, ppm]: 14.29 (C-27,29), 34.46 (C-26,28), 50.537 (C-25), 121.25 (C-5), 128.81 (C-2,3), 145.11 (C-1,4). IR (KBr pellet, cm^{-1}): 3328 (m, ν(N-H)), 3150 (w, ν_s(pyrrole C-H)), 3128 (w, ν_{as}(pyrrole C-H)), 2962 (s, ν_{as}(C-H)), 2926 (s, ν_{as}C-H)), 2869 (s, ν_s(C-H)), 1558 (w, ν(Cβ-Cβ and Cα-C_{meso})), 1460 (s, δ_{oop}(C-H), ν($C_α$-C_{meso}) and ν(C_{meso}-C_{alkyl})), 1376 and 1334 (m δ_{ip}(pyrrole C-H), δ_{ip}(alkyl C-H)), 1150 (w), 968 and 914 (m, ν(Cα-Cβ), δ_{ip}(pyrrole C-H and N-H)), 791 and 731 (s, δ_{oop}(pyrrole

N-H), δ_{oop}(pyrrole C_β-H)), 642 (w, $\nu(C_{meso}$-CH), δ_{oop}(pyrrole N-H)). Mass (M+H): found 591.4424; calculated 591.4427 for $C_{40}H_{55}N_4$.

2.4.4 Syntheses of $H_2T(CHPh_2)P$ (Porphyrin 4)

(1) Method with co-catalyst system:

In a 1-L three-neck round-bottom flask, distilled pyrrole (0.694 ml, 20 mM, 0.01 moles) and diphenylacetaldehyde (1.790 ml, 20 mM, 0.10 moles) were stirred in dichloromethane (500 ml) at room temperature for 5 minutes under nitrogen. A solution of TFA (1.800 ml, 30 mM, 0.015 moles) and $BF_3{\cdot}OEt_2$ (0.040 ml, 0.6 mM, 0.003 moles) in ~ 10 ml of dichloromethane was added over a period of 15 minutes. The reaction was then covered in foil & left to stir for 1 hour. After the addition of DDQ (20 mM, 0.01 moles) the mixture was allowed to stir for 20 minutes, then immediately run through an aluminium oxide plug and washed with dichloromethane. The product was reduced on the rotary evaporator and the column was eluted with the recycled dichloromethane. The final reduced product was then put through a silica gel column (solvent system chloroform, using dichloromethane at the end). When using TLC, the purity of the obtained fractions was found to be low. Test tubes for diffusion were set up (dichloromethane/hexane), however only a powder layer on the glass sides resulted. Isolated yield: 0.0672 g, 2.8 %.

(2) Method with 0.1% Ethanol:

In a 1-L three-neck round-bottom flask, dichloromethane (500 ml) and ethanol (0.50 ml) were stirred with pyrrole (0.694 ml, 10 mmol) and diphenylacetaldehyde (1.791 ml, 10 mmol) under nitrogen for 5 minutes at room temperature. TFA (0.770 ml, 10 mmol) was then added and the mixture was stirred for 1 hour covered in foil. After the addition of DDQ (1.703 g, 7.5 mmol) the reaction stirred for 20 minutes at room temperature and was then immediately put through an aluminium oxide column. The product was reduced on the rotary evaporator and the solvent used to wash the plug. After satisfactory washings, the resulting product was placed on a silica column and eluted first with chloroform and finally with dichloromethane. The purity of the fractions

was determined by TLC. Isolated yield: 0.1100–0.2810 g, 4.5–11.5 % (range from several reactions).

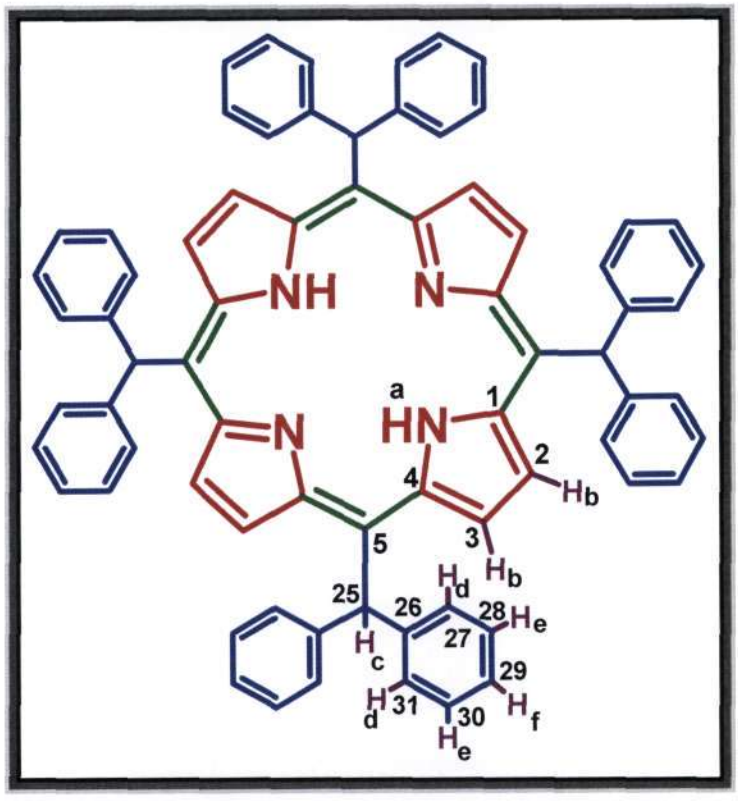

Figure 2.4: Structure of Porphyrin 4, $H_2T(CHPh_2)P$.

Porphyrin 4, $H_2T(CHPh_2)P$:

UV–vis (CH_2Cl_2) [λ_{max}, nm (ε, $M^{-1}cm^{-1}$]: 414.0 (291 × 10^3), 514.0 (18.8 × 10^3), 549.5 (6.9 × 10^3), 590.0 (5.9 × 10^3), 643.0 (1.8 × 10^3). ^1H NMR (500 MHz, $CDCl_3$) [δ, ppm]: –2.253 (2H, s, br, *a*), 7.173 to 7.555 (40H, m, *d, e, f*), 9.040-9.294 (8H, m, *b*). ^{13}C NMR (125 MHz, $CDCl_3$) [δ, ppm]: 29.69, 56.18, 119.49 (C5), 128.45 (C-27,28,29,30,31), 132.38 (C-2,3), 146.41 (C-1,4). IR (KBr pellet, cm^{-1}): 3232 (w, ν(N-H)), 3058 (w, ν_s(pyrrole C-H)), 3023 (w, ν_{as}(pyrrole C-H)), 2924 (w, ν_{as}(C-H)), 1597 (m) and 1535 (w) (ν(Cβ-Cβ and Cα-C_{meso})), 1493 (s) and 1444 (m) (δ_{oop}(C-H), ν(C_α-C_{meso}) and ν(C_{meso}-C_{alkyl})), 1165 (w), 960 and 917 (m, ν(Cα-Cβ), δ_{ip}(pyrrole C-H and N-H)), 788 and 740 (s, δ_{oop}(pyrrole N-H), δ_{oop}(pyrrole C_β-H)). Mass (M+H): found 975.4423; calculated 975.4427 for $C_{72}H_{55}N_4$.

2.4.5 Synthesis of $H_2T(iPr)P$ (Porphyrin 5)

(1) Method with 0.1% Ethanol:

In a 1-L three-neck round-bottom flask, dichloromethane (500 ml) and ethanol (0.50 ml) were stirred with pyrrole (0.694 ml, 10 mmol) and isobutyraldehyde (0.910 ml, 10 mmol) under nitrogen for 5 minutes at room temperature. TFA (0.770 ml, 10 mmol) was then added and the mixture was stirred for 1 hour covered in foil. After the addition of DDQ (1.703 g, 7.5 mmol) the reaction solution was stirred for 20 minutes at room temperature and was then immediately put through an aluminium oxide column. The product was reduced on the rotary evaporator and the solvent used to wash the plug. After satisfactory washings, the resulting product was placed on a silica column and eluted first with chloroform and finally with dichloromethane. TLC was used to determine the purity of the obtained fractions. The pure fractions were allowed to evaporate away from light and were then collected, combined, weighed and characterized. Crystallization was achieved by dissolving the product in CH_2Cl_2 and layering 1.5 ml aliquots of the solution with ca. 15 ml of hexane in test tubes. A crystal was obtained after about a week, for which a structure was determined. Isolated yield (crystals that started to form in mother liquor before a column was run): 0.1582 g, 13.2 %. Isolated yield: 0.0150–0.0220 g, 1.5–7.7 % (range from several reactions).

Porphyrin 5, $H_2T(iPr)P$:

UV–vis (CH_2Cl_2) [λ_{max}, nm (ε, $M^{-1}cm^{-1}$]: 419.5 (229 × 10^3), 488.5 (sh), 522.00 (8.1 × 10^3), 557.5 (4.3 × 10^3), 601.5 (2.2 × 10^3), 658.5 (2.3 × 10^3). ^1H NMR (500 MHz, $CDCl_3$) [δ, ppm]: –1.786 (2H, s, br, *a*), 2.331 (24H, d, $^3J_{cd}$ = 7.4, *d*), 5.319 (4H, septet, $^3J_{cd}$ = 7.4, *c*), 9.466 (8H, s, *b*). ^{13}C NMR (125 MHz, $CDCl_3$) [δ, ppm]: 28.67 (C-26,27), 35.20 (C-25), 123.67 (C-5), 129.02 (C-2,3), 143.757(C-1,4). IR (KBr pellet, cm^{-1}): 3320 (m, ν(N-H)), 3144 (w, ν_s(pyrrole C-H)), 2961 (s, ν_{as}(C-H)), 2930 (s, ν_{as}C-H)), 2871 (s, ν_s(C-H)), 1558 (m, ν(Cβ-Cβ and Cα-C_{meso})), 1455 (s, δ_{oop}(C-H), ν(C_α-C_{meso}) and ν(C_{meso}-C_{alkyl})), 1386 and 1365 (m δ_{ip}(pyrrole C-H), δ_{ip}(alkyl C-H)), 1149 (w), 969 and 914 (m, ν(Cα-Cβ), δ_{ip}(pyrrole C-H and N-H)), 789 and 732 (s, δ_{oop}(pyrrole N-H), δ_{oop}(pyrrole C_β-H)), 641 (w, ν(C_{meso}-CH), δ_{oop}(pyrrole N-H)). Mass (M+H): found 479.3173; calculated 479.3175 for $C_{32}H_{39}N_4$.

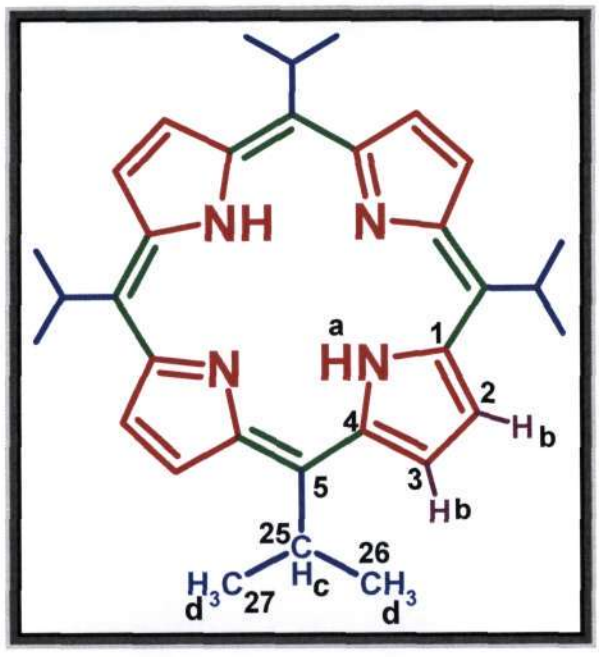

Figure 2.5 : Structure of porphyrin 5, $H_2T(iPr)P$.

2.4.6 Syntheses of $H_2T(cyHx)P$ (Porphyrin 6)

(1) Method A with 0.1% Ethanol:

In a 1-L three-neck round-bottom flask, dichloromethane (500 ml) and Ethanol (0.50 ml) were stirred with pyrrole (0.694 ml, 10 mmol) and cyclohexanecarboxaldehyde (1.1217 ml, 10 mmol) under nitrogen for 5 minutes at room temperature. Then TFA (0.770 ml, 10 mmol) was added and the mixture was stirred for 5 hours covered in foil. After the addition of DDQ (1.703 g, 7.5 mmol) the reaction was refluxed for one and a half hours, then cooled and run through an aluminium oxide column. The product was reduced on the rotary evaporator and the solvent used to wash the plug. After satisfactory washings, the resulting product was placed on a silica column and eluted with solvent system of 1:1 dichloromethane:hexane. None of the fractions were found to be pure, and nor was the porphyrin the predominant product. However on evaporation of the solvent only trace quantities of the porphyrin remained.

(2) Method B with 0.1% Ethanol:

In a 1-L three-neck round-bottom flask, dichloromethane (500 ml) and ethanol (0.50 ml) were stirred with pyrrole (0.694 ml, 10 mmol) and cyclohexanecarboxaldehyde

(1.1217 ml, 10 mmol) under nitrogen for 5 minutes at room temperature. TFA (0.770 ml, 10 mmol) was then added and the mixture was stirred for 1 hour covered in foil. After the addition of DDQ (1.703 g, 7.5 mmol) the reaction solution was stirred for 20 minutes at room temperature and was then immediately put through an aluminium oxide column. The product was reduced on the rotary evaporator and the solvent used to wash the plug. After satisfactory washings, the resulting product was placed on a silica column and eluted first with chloroform and finally with dichloromethane. The first fractions were shown by TLC to contain a lot of impurities with the porphyrin; however the last fractions proved to have a higher purity of the porphyrin. After evaporation of the solvent fine crystals were present in these beakers. However, they were found to be too thin to be of X-ray quality. Isolated yield: 0.0320–0.0970 g, 2.0–6.2 % (range from several reactions).

Porphyrin 6, H_2T(cyHx)P :

UV–vis (CH_2Cl_2) [λ_{max}, nm (ε, $M^{-1}cm^{-1}$]: 423.0 (282 × 10^3), 492.5 (sh), 526.5 (11.8 × 10^3), 562.5 (7.6 × 10^3), 604.0 (3.4 × 10^3), 660.5 (4.9 × 10^3). ^{1}H NMR (500 MHz, $CDCl_3$) [δ, ppm]: –1.605 (2H, s, br, *a*), 1.858 (12H, multiplet, H_{4a}, H_{3a}), 2.117 (12H, d, $^2J_{4a4e}$ = 9.1 H_{4e}), 2.218 (12H, d, $^2J_{3e3a}$ = 11.7, H_{3e}), 2.595 (8H, d, $^2J_{2e2a}$ = 13.3, H_{2e}), 2.979 (8H, q, $^2J_{2e2a}$ = 12.6, H_{2a}), 4.765 (4H, t, $^3J_{12}$ = 12.6, $^4J_{13}$ = 3.5 H_1), 9.470 (8H, s, *b*). ^{13}C NMR (125 MHz, $CDCl_3$) [δ, ppm]: 26.73 (C-27,28,29), 28.58 (C-27,28,29), 38.70 (C-26,30), 46.91 (C-25), 122.54 (C-5), 129.27 (C-2,3), 143.76 (C-1,4). IR (KBr pellet, cm^{-1}): 3301 (m, ν(N-H)), 3145 (w, ν_s(pyrrole C-H)), 2923 (s, ν_{as}C-H)), 2849 (s, ν_s(C-H)), 1555 (w, ν(Cβ-Cβ and Cα-C_{meso})), 1473 (m) and 1447 (s) (δ_{oop}(C-H), ν(Cα-C_{meso}) and ν(C_{meso}-C_{alkyl})), 1341 (m δ_{ip}(pyrrole C-H), δ_{ip}(alkyl C-H)), 1162 (w), 972 and 919 (m, ν(Cα-Cβ), δ_{ip}(pyrrole C-H and N-H)), 785 and 724 (s, δ_{oop}(pyrrole N-H), δ_{oop}(pyrrole $C_β$-H)). Mass (M+H): found 639.4422; calculated 639.4427 for $C_{44}H_{55}N_4$.

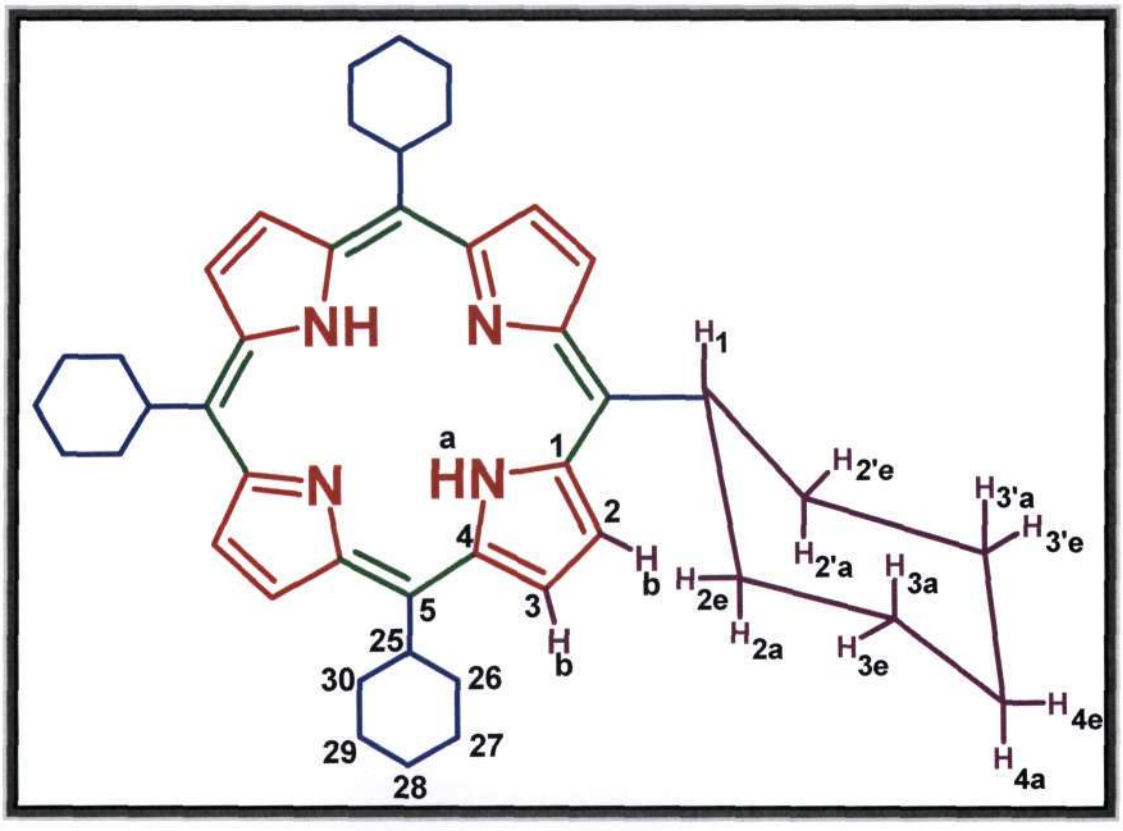

Figure 2.6: Structure of Porphyrin 6, $H_2T(cyHx)P$, showing an expanded substituent for straightforward labelling.

2.5 Discussion of the Methods examined

The success of room-temperature *meso*-tetraalkylporphyrin synthesis is controlled by choice of the correct reaction conditions. This includes finding an effective catalyst for the pyrrole-aldehyde condensation, which will give rise to good percentage yields. Other factors to consider are choice of oxidant, duration of condensation period, concentrations of the acid, pyrrole, and aldehyde, the presence of water in the solvent and number of steps involved. Oxidation can be achieved by use of either DDQ or *p*-chloranil. *p*-Chloranil is the milder of these two oxidants, and hence requires more reaction time (1 hour or more) but may offer higher yields than DDQ.[27] However, unfortunately, when a method is successful for one aldehyde it does not necessarily mean that it will be successful for all aldehydes and thus all methods (and conditions) must be tested for each individual aldehyde. Each of the different aldehydes will obviously have its own special reactivity pattern. Thus slight changes in catalysis,

temperature and oxidant (or other reaction conditions) may result in different yields for each of the different aldehydes.

After research was done into the various methods that have been used for the synthesis of these porphyrins, a few were chosen and tried. The first synthesis[10] that was attempted used distilled dichloromethane, BF_3·etherate as the catalyst, long stirring times and rather large quantities of both pyrrole and aldehyde (0.070 moles). There was a total reaction time (excluding time needed for filtration through silica or alumina plugs and columns etc.) of 18½ hours, which included reflux of the reaction mixture after addition of DDQ (equimolar quantity). The resulting percentage yields of the first two porphyrins from our choice of aldehydes were very low (~ 2%), although the paper stated yields of about 7% for their porphyrins that had been synthesized.[10]

In an attempt to improve these yields another method was found. This second method[145] was quoted with larger percentage yields (in the range of 50% for H_2TTP), and gave better yields for most of our porphyrins than the first attempted method did. These better yields were also obtained using far more dilute solutions in distilled dichloromethane than were used in the first attempt. The reaction time was less than two hours; this was due to no reflux after addition of DDQ, but excluded time needed for filtration through a silica plug and column. The method did not use a lone catalyst, but rather a mixture of two of the most prominent catalysts used in these types of syntheses, BF_3·etherate and TFA (trifluoroacetic acid). This use of combination catalysts often gave better yields than the use of either catalyst separately; other combinations (and different ratios) were found in the literature.[145]

The series of papers by Geier *et al.*[41,142,143,144] in 2001 showed that percentage yields for the catalysts (TFA and BF_3·etherate) on their own were both less than the result of the combined catalysts. Differences in the results from the usage of either TFA or BF_3·etherate thus prompted the research into the collective use of the two catalysts. The results were a remarkable increase in the yield of tetraphenylporphyrin, from 40% (TFA) and 26% (BF_3·etherate) to about 50 to 55% for the co-catalysis. When various aspects of the reaction, including the oligomer composition (LD-MS), yield of H_2TTP (UV-vis), yield of N-confused H_2TTP (HPLC), and level of unreacted aldehyde (TLC) in the co-catalytic reaction were examined, it was found that there were combined

features of those observed with each acid individually. Each of the two catalysts used has shown itself to be appropriate for wide varieties of aldehydes, mostly only one of the catalysts is necessary to produce results. However, it has been noted that there are cases where the combination of catalysts either gives better quality results than one on its own or are required for the reaction to in fact proceed.[145]

An attempt was then made to double the concentrations of the reaction mixture and note any differences. The resulting percentage yields from these higher concentrations proved to be very similar to that of the dilute method for certain porphyrins. Doubled concentrations gave a quicker colour change after addition of catalyst compared to single concentrations and thus a faster reaction time is probable.

The final method tested in this work involved the addition of 0.1% volume ethanol[195] to the reaction mixture with only TFA as the catalyst, which also gave improved yields. The yields, when using the 0.1% ethanol method, mostly doubled from the co-catalyst method and the two aldehydes that had produced ineffective results with the co-catalyst method gave acceptable yields. The paper stated the method with reflux after addition of DDQ; however, after certain tests with reflux and only using different stirring times, it was found that optimum yields were obtained without reflux for a stirring time of only 15 to 20 minutes.

It was found that the shorter the reaction time with DDQ, the better the results obtained. If reflux was introduced or the time frame was allowed over the 1 hour mark, then the product yield actually started to deplete. As a result it was decided to pass the solution through a plug of basic alumina gel directly after a stirring time of 20 minutes following addition of the DDQ. It was also noted that if silica was used instead of basic alumina for this plug then a green solution was obtained instead of the expected red solution. This is due to formation of the porphyrin diacid salt and thus it was necessary to add either morpholine (or ethylamine) to deprotonate the porphyrin diacid and hence obtain the red solution. After this plug the solvent was reduced on the rotary evaporator and the concentrated product was then run down a silica gel column for final purification.

The method was also modified from the original paper regarding concentration, one eighth of the solution volume was used, but only one quarter of starting reagents' mole ratios, and thus we doubled the concentrations. However, this still gave extremely favourable results, the best of the three methods. It allowed us to produce quantities of around 0.010 to 0.100 g of the porphyrins at one time. These 2–20% yields depended on the particular aldehyde that was used in the reaction.

The products obtained from the different methods of synthesis (used for each of the six *meso*-tetraalkylporphyrins) were all found to be the same by TLC and ^{1}H NMR for each particular porphyrin. For $H_2T(iPr)P$ (P5) only one method yielded the porphyrin. A summary of the different resulting yields from each method applied are given in Table 2.1 below. These yields are the highest obtained for each method used and from this table it is obvious that the best yielding method for each of the *meso*-tetraalkylporphyrins in this series is where 0.1% EtOH has been added to the reaction. There is no particularly obvious correlation between the structure of the *meso*-group and the yield.

Table 2.1: The highest percentage yield obtained for each porphyrin from each of the attempted methods.

	Method using $BF_3 \cdot OEt_2$ as the catalyst	Method using a co-catalyst system	Method with addition of 0.1% EtOH
$H_2T(iBu)P$	2.3 %	3.3 %	7.2 %
$H_2T(CH_2Ph)P$	0.5 %	1.1 %	3.0 %
$H_2T(iPent)P$	–*	8–10 %	19.1 %
$H_2T(CHPh_2)P$	–*	2.8 %	11.5 &
$H_2T(iPr)P$	–*	No result	7.7 %
$H_2T(cyHx)P$	–*	Trace	6.2 %

* = this method was abandoned after two syntheses due to comparably poor yields.

2.6 Synthesis of Gold(III) Porphyrin Complexes

2.6.1 First attempted synthesis [196]of [Au(T{iPent}P)Cl]

This method follows a procedure used for the synthesis of [Au(TPP)Cl] complex as used by Rothemund and Menotti.[197]

$H_2T(iPent)P$ (P3) (0.20 g, 0.338 mmol) was boiled under reflux with $NaAuCl_4.nH_2O$ (0.10 g, 0.276 mmol) in acetic acid (50 ml) for one hour and tested for complete reaction by TLC. The unreacted free base porphyrin was, however, still present. After another 2 hours of reflux the solution was then cooled. The solvent was distilled in vacuum, and the residue was treated with chloroform. The complex was precipitated by the addition of methanol and then dissolved in a small amount of chloroform. It was purified by chromatography on a column of Al_2O_3 with chloroform as an elutent. The result was a large fraction of pure $H_2T(iPent)P$ and a smaller fraction of a more polar compound which had to be removed from the column with methanol. The solvent evaporated from this fraction to afford an intractable brown oil, from which no definitive results could be obtained.

2.6.2 Second attempted synthesis[198] of [Au(T{iPent}P)Cl]

This procedure was taken from the preparation of five Au(III) porphyrin complexes according to a previously described literature method[199,200] *with some modifications.*

$NaAuCl_4.nH_2O$ (0.20 g, 0.553 mmol) and sodium acetate (0.22 g, 2.69 mmol) were stirred in acetic acid (20 ml) for 15 minutes. Thereafter a solution of $H_2T(iPent)P$ (P3) (0.25 g, 0.423 mmol) in acetic acid (10 ml) was added drop-wise. The mixture was then heated to reflux for 2 hours; on TLC the free base porphyrin was still present, but other compounds were also visible. Thus the solvent was removed under vacuum and the residue was dissolved in dichloromethane (40 ml). It was chromatographed on a neutral 90-alumina packed column using dichloromethane as elutant to remove the unreacted free base porphyrin, and the suspected gold(III) porphyrin complex. Unfortunately this second attempt gave results similar to those above.

2.6.3 Synthesis of [Au(T{iPent}P)Cl]

DMF (20 ml) was placed in a 100 ml round-bottomed flask with $NaAuCl_4.nH_2O$ (0.15 g, 0.415 mmol). $H_2T(iPent)P$ (P3) (0.20 g, 0.338 mmol) was added and the mixture was heated to reflux for 1 hour. The reaction mixture was tested by TLC and a single brown spot was noted with no sign of the original porphyrin. Thus heating was halted and water (100 ml) was added to the reaction mixture, which was in turn filtered through a frit and washed with hot water. This was then left to dry in air (3 days) and was collected. On TLC the product now gave two spots and thus it was run through a column to purify it using dichloromethane containing 10% hexane as the elutant. Isolated yield: 0.1076 g, 0.131 mmol, 38.7 %. All attempts to grow X-quality crystals failed.

[Au(T{iPent}P)Cl]:

UV-vis (CH_2Cl_2) [λ_{max}, nm (ε, $M^{-1}cm^{-1}$]: 412.5, 493.5 (sh), 517.5, 556.0, 581.0, 640.0. ^1H NMR (500 MHz, $CDCl_3$) [δ, ppm]: 0.97, 1.10, 1.97, 2.50, 2.80, 2.94, 4.22, 4.29, 4.72, 4.85, 4.99, 5.20, 5.30, 7.05, 7.47, 8.95, 9.04, 9.32, 9.64. IR (KBr pellet, cm-1) 3447 (w), 3255 (w), 3118 (w), 2960 (s, ν_{as}(C-H)), 2926 (s, ν_{as}C-H)), 2869 (s, ν_s(C-H)), 2360 (w, KBr stretch), 1608 (w), 1458 (s, δ_{oop}(C-H), $\nu(C_\alpha$-$C_{meso})$ and $\nu(C_{meso}$-$C_{alkyl})$), 1376 and 1332 (m δ_{ip}(pyrrole C-H), δ_{ip}(alkyl C-H)), 1237 (w), 1054 (w), 962 and 914 (m, ν(Cα-Cβ), δ_{ip}(pyrrole C-H and N-H)), 810 (s), 741 (w).

2.6.4 Synthesis of $[Au(T\{iPent\}P)]SbF_6$ - Metathesis of the chloride counter ion

To increase the probability single crystal formation it was necessary to replace the chloride counter ion of the metalloporphyrin with a hexafluoroantimonate counter ion according to the following reaction:

$$[Au(T\{iPent\}P)]Cl + AgSbF_6 \rightarrow [Au(T\{iPent\}P)]SbF_6 + AgCl(s)$$

The metalloporphyrin [Au(T{iPent}P)Cl] (60 mg, 0.0731 mmol) was placed in a clean, dry round-bottomed flask (100 ml), under nitrogen. Under inert conditions, in a glove box, 1.1 molar equivalents of $AgSbF_6$ were added (28 mg, 0.0804 mmol). Once out of

the glove box, dry THF (50 ml) was added using cannula transfer. The mixture was stirred for 2 hours before the THF was removed under vacuum and replaced by an equivalent volume of dry dichloromethane. The solution was then filtered, using a cannula filter, into a second clean, dry round-bottomed flask (100 ml) to remove the insoluble silver chloride. The dichloromethane was removed *in vacuo* and replaced by dry THF. The change of solvent was required due to the decreased solubility of the silver salts in dichloromethane as opposed to THF.

3. Spectroscopy – UV-vis and IR

3.1 UV-vis Spectroscopy

3.1.1 Introduction

It is not possible to separate quantum mechanics from spectroscopy. Spectroscopy is the analysis of transitions between defined states of energy of a system, typically a molecule or an atom, and the type of spectroscopy used is relevant to the energy state. The techniques for detection of the absorption or emission of radiation by a sample vary significantly. This depends on the kind of transition to be detected and on the particular frequency range that is involved.[201] For a number of decades ultra-violet and visible spectrometry have been extensively used in the qualitative and quantitative determination of substances.[202] The only criterion for these spectra is that the compound or its derivative should obey Beer's law in the range of concentrations to be considered.[203] The obtained UV-vis spectra help to elucidate the sample characterization by observing certain bands at certain expected wavelengths.

The spectral region associated with these spectra is defined at its lower frequency end by the limits of visibility (ca. 800 nm, 3.75 x 10^{14} Hz) and at its high frequency end by the fact that normal prisms and lenses, and air, become opaque above 200 nm, 1.5 x 10^{15} Hz.[201] The human eye is sensitive to the visible region of the range of wavelengths between 400 and 800 nm. The ultra-violet region is subdivided into two spectral sections; between 200 and 400 nm is referred to as the near ultra-violet region, and below 200 nm is called the far or vacuum ultra-violet region.[203]

When light energy interacts with an organic molecule the light disappears. This absorption of the light energy brings about a transition from the molecule's ground state to an ionic, electrically excited state. The frequency of the light absorbed is determined by the difference in energy between these states.[202] The larger the

difference, the larger the frequency (or the shorter the wavelength) of light absorbed. The intensity of an absorption band is determined partly by the probability of occurrence of this interaction which results in the transition from ground to excited state. The polarity of the excited state also has an effect, when large electric moments are involved in the transition a strong absorption results.[202]

The origin of colour in compounds is dependent on the occurrence of one or more unsaturated linkages, called chromophores. There are also certain groups which—although they do not confer colour on compounds when by themselves—seem to increase the colouring power of a chromophore. These are known as auxochromes.[203] Some typical examples of chromophores are: C=C, C=O, N=N and of auxochromes are: C-Br, C-OH, C-NH_2.[203]

A survey of the electronic spectra of organic molecules shows some generalities. There is no absorption in the near UV and visible regions (200–800 nm) for saturated organic molecules.[203] The electrons of unsaturated bonds cause the absorption of light in the near ultraviolet region (200 to 400 nm) or in the visible region (400 to 800 nm).[202] The presence of a chromophore usually causes absorption in the 200–800 nm region—for each chromophore the absorption maximum varies. The features that influence the maximum for chromophores are the relative ease in forming the double bond and the difference in the electro-negativities of the elements that form the double bond. If an auxochrome is introduced to a saturated system, then it generally results in a shift to longer wavelength for the absorption maximum.[203]

For C=O, N=O, -N=N, and C=S, as well as for similar "chromophoric" groups, absorption takes place at wavelengths longer than 200 nm. These absorption bands are generally of weak intensity in this region; bands in the higher-energy (shorter-wavelength) region are strong. Groups such as -C=C-, -C≡C-, and –C≡N usually only absorb in this region; however, if they are conjugated with another unsaturated, intense absorption then they may be found at wavelengths longer than 200 nm. An increase in conjugation causes shifts to longer wavelength (known as bathochromic shifts)[202] and increases the intensities. Auxochromes generally generate bathochromic shifts as well, owing to interaction between the electrons of the chromophoric groups and those of the substituents. The largest of these bathochromic shifts and increased

intensities are caused by unsaturated substituents or groups with unshared electrons (e.g. OH, NH_2, OCH_3).[202]

Electrons that form single bonds, σ electrons, have characteristic functions and charge densities that are rotationally symmetrical with respect to the bond axis. The characteristic functions and charge densities of the electrons responsible for double bonds, π electrons, have an oscillation nodal plane through the bond axis.[203] It is predominantly the π electrons in unsaturated systems that determine the energy states of the electrons which are excited by the absorption of light (visible or ultra-violet). In molecules that contain atoms like nitrogen or oxygen there are the unshared or nonbonded electrons. These electrons are usually called *n* electrons, which are the *p* electrons in the case of the first two rows of the periodic table.[203]

The interactions between σ and π electrons are negligible; however, those between *n* and π or π and π electrons are substantial. The σ electrons are bound more strongly than the π electrons in the bonding electrons; however, in the antibonding levels, the π^* level has a lower energy than the σ^* level. In addition, non-bonded electrons are less strongly bound than bonding electrons.[203]

Shown in Table 3.1.1 are the different types of transitions that occur. The first is the N $\rightarrow$ V transition. There may be more than one for a molecule as this is a large class. The $\sigma \rightarrow \sigma^*$ transitions are observed only in the far ultra-violet region, whereas most $\pi \rightarrow \pi^*$ transitions are observed in the near ultra-violet region with only some in the far ultra-violet region. These $\pi \rightarrow \pi^*$ bands may be displaced to longer wavelength by suitable substitution on the molecule.[203]

Table 3.1.1 Transitions responsible for electronic spectra.[203]

Type of Transition	Description of Transition	Region and example in electronic Spectra
N → V	From a ground state bonding orbital to a higher energy antibonding orbital Between σ orbitals: $\sigma \rightarrow \sigma^*$ Between π orbitals: $\pi \rightarrow \pi^*$ (often called K or A or E bands)	 Vacuum ultra-violet e.g. methane: 125 nm Ultra-violet e.g. ethylene: 180 nm
N → Q	From the excitation of a nonbonding orbital localized on an atom to a higher energy antibonding orbital. To σ orbitals: $n \rightarrow \sigma^*$ To π orbitals: $n \rightarrow \pi^*$ (often called R bands)	 Far ultra-violet and sometimes near ultra-violet e.g. acetone: 190 nm Near ultra-violet and visible e.g. acetone: 277 nm
N → R	From ground state orbital to one of high enough energy for the molecule ion core to resemble an atomic ion.	Vacuum ultra-violet

The next class of N → Q transitions is generally weaker than the N → V transitions; the $n \rightarrow \pi^*$ transitions are always found at fairly long wavelengths (near ultra-violet or visible regions) whereas the $n \rightarrow \sigma^*$ transitions are normally in the far or near ultra-violet region. Saturated molecules containing singly bonded basic groups with atoms possessing unshared pairs of electrons give $n \rightarrow \sigma^*$ transitions. The $n \rightarrow \pi^*$

transitions are found in molecules that include a hetero atom that is multiply bonded to another atom and has unshared electrons. These $n \rightarrow \pi^*$ transitions are forbidden transitions and thus their intensities are usually far below those of $n \rightarrow \sigma^*$ and $\pi \rightarrow \pi^*$ transitions.[203] The last group is found in the far end of the vacuum ultra-violet region, these N → R transitions are seen as a progression of bands (Rydberg series) which terminates in ionization (continuum).[203]

Compounds containing multiple bonds absorb at longer wavelengths than saturated systems and they also have lower ionization energies. Unsaturated heterocyclic compounds exhibit a very intense band due to the diene absorption below 220 nm, and a low intensity band at longer wavelengths; for pyrrole these bands are at 210 and 350 nm respectively. Chlorophylls (green colour in plants) and haemin (red colour of blood) contain pyrrole rings, as do our synthesized porphyrins.[203]

3.1.2 UV-vis Spectroscopy of Porphyrins

The presence of colour in compounds usually makes their identification much easier in view of the fact that their colour almost always implies the existence of certain types of chromophoric groups. Intensities of the absorption bands may also be used as a defining factor; however, it is then necessary to have completely pure samples.[203]

There have been a number of theories regarding colour since the first isolation of a dye.[204] In 1876 there was a proposal by Witt that certain chromophoric groups, such as unsaturated linkages, should necessarily be present in organic compounds to lend them colour. Then in 1888 Armstrong suggested, basing his argument on a simple compound like *p*-benzoquinone being coloured, that the quinoid structure might have something to do with compound colouring. However, it is now known that the true cause of compound colouring is the $n \rightarrow \pi^*$ transition (R-band) of chromophoric groups in some of the simple organic compounds.[203] The role that porphyrins play in photosynthetic mechanisms shows that these molecules have the ability to mediate visible photon-electron energy transfer processes.

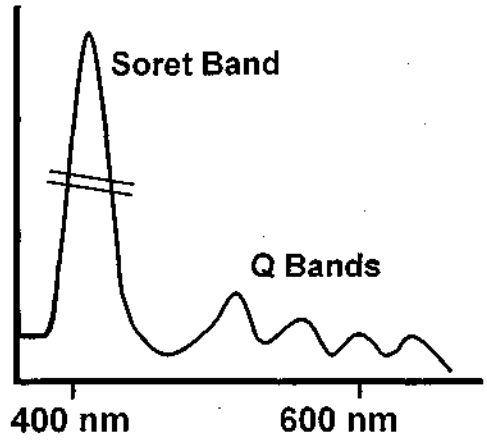

Figure 3.1.1: A typically shaped UV-vis spectrum for a porphyrin.

The UV-visible absorption spectra of porphyrins are distinctive; a typically shaped spectrum is shown in Figure 3.1.1 above. These highly conjugated, intensely coloured macrocycles give an intense band at about 400 nm known as the Soret band. This intense absorption band was first discovered in haemoglobin by Soret[205] in 1883 and was later observed in porphyrins by Gamgee[206] in 1897. This main absorption band usually has very high extinction coefficients to the value of around 400,000 M^{-1} cm^{-1} often being recorded. It is found in all tetrapyrroles that have fully conjugated nuclei and is therefore considered to be characteristic of this macrocyclic conjugation, thus possible rupture of the macrocycle would result in its disappearance.[4]

The Soret band is then followed by several weaker absorbing bands known as the Q bands in the higher wavelength region from about 450 to 700 nm. The general absorption bands for porphyrins are around 430, 487, 518, 561 and 613 nm;[207] of these bands, only the first and the last are believed to be due to pure electronic interactions.[208] Slight changes to these absorptions, in intensity and wavelength, may be caused by different substituents on the porphyrin ring. If the two central nitrogen atoms are protonated or the porphyrin is metallated then there will also be a change, usually a more significant change, in the spectrum's appearance. Certain features of porphyrins may be determined with the use of absorption spectra.[37]

Transition moments to the excited state configurations may either (1) add together, resulting in a higher-energy band with a very large net transition moment (the B band) or (2) almost cancel each other, resulting in a lower-energy band with a small net

transition moment (the Q band). The orbitally-allowed one-electron excitations from the four highest filled singly-degenerate π molecular orbitals (MOs) to the lowest lying doubly degenerate π^* MO of the porphyrin are the most realistic description of the porphyrin $\pi \rightarrow \pi^*$ transitions.

Gouterman's four-orbital MO model for porphyrins and metalloporphyrins predicts excited states and symmetries for transitions occurring in the visible and UV region (Figure 3.1.2). The left and the right sides of the energy level diagram represent the excited states before and after configuration interaction mixing, respectively. The ground (ν_0) and first excited (ν_1) vibrational states for each of the electronic states are depicted. This MO model is not only useful for predicting the main $\pi \rightarrow \pi^*$ transitions in porphyrin and metalloporphyrin spectra; but it also gives reasonably accurate results when predicting the transition frequencies.

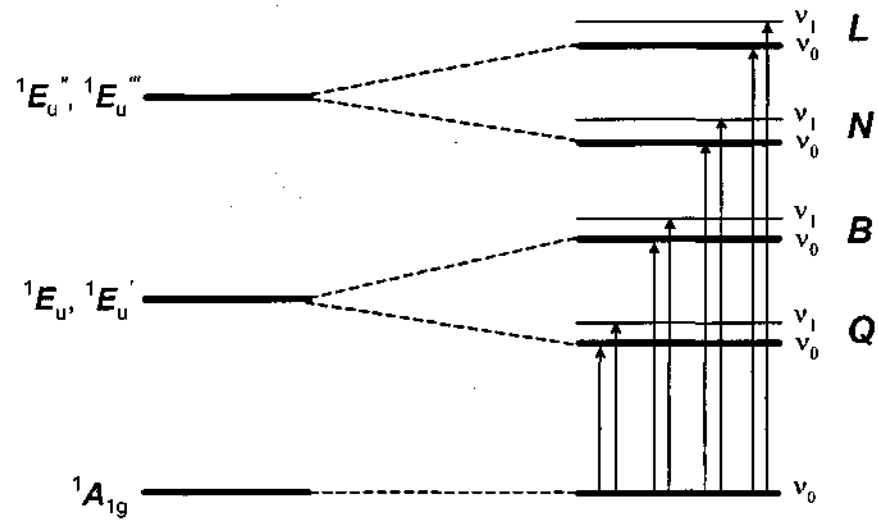

Figure 3.1.2: Gouterman's four-orbital MO model for porphyrins and metalloporphyrins.

Calculations performed on the porphine ring by the method of Pariser, Parr, and Pople (Pariser-Parr-Pople method)[209] substantiate the earlier deductions of Gouterman and Platt that the bands of the porphine absorption spectrum, both Soret and visible, can be explained using a four-orbital model.[210] This model shows the lowest two pairs of excited configurations to be accidentally degenerate. It is the extensive interaction between them that accounts for the weakness of the visible bands and the great intensity, by comparison, of the Soret band. Interaction with higher configurations is

negligible. This four-orbital model has been further extended to give successful accounts of the absorption spectra of porphyrins. More elaborate calculations (that use extensive configuration interaction) are able to produce remarkable qualitative agreement with the porphine triplet-triplet absorption spectrum. However, configuration interaction is consistently overestimated, and therefore the calculated splitting of visible and Soret bands is always too large. Additionally, singlet-triplet splitting is overestimated in the same way.

An attempt to apply this four-orbital model to porphyrin molecules was made by Gouterman *et al.* This model was a combination of L.C.A.O.-M.O. and a simplified treatment of configuration interaction. Qualitative agreement between this model and the calculations with the observed spectra was obtained. The application of this model to the calculation of chemical and magnetic properties was also further discussed.[211] Gouterman presented a model for the excited states of porphine, which are considered to arise from two configurations which can be mixed to varying degrees.[212] The triplet excited states of porphine have been classified as either singly or doubly excited electron configurations (the latter are discussed in detail by Gouterman[213]). Intensity changes and energy shifts for three porphyrins (derived from the basic skeleton) are related to the properties of the highest two occupied and lowest two unoccupied empty π orbitals.[214]

3.1.3 Objectives

The aims of this chapter were to:

(1) obtain UV-vis spectra for each of the six synthesized *meso*-tetraalkylporphyrins;
(2) record the wavelengths of all the visible bands and determine the extinction coefficients for each, according to Beers Law; and
(3) form the basis on which further work will be performed to determine the fluorescence and lifetimes of the porphyrins.

3.1.4 Results and Discussion

The UV-vis spectra were recorded for each of the six synthesized *meso*-tetraalkylporphyrins. A representative UV-vis spectrum (for the novel porphyrin $H_2T(CH_2Ph)P$) is shown in Figure 3.1.3 and the spectra for all the porphyrins are available in **Appendix B1**. The purple crystals of each gave a pale yellow solution in dichloromethane from which the spectra were produced. Their spectra were all in the expected form of those of typical porphyrins with a Soret band in the region of 420 nm and four other weaker bands at around 520, 555, 600 and 655 nm. These are known collectively as the Q bands, the two with the lower wavelengths are known as Q(1,0) bands and the two with the longer wavelengths are known as Q(0,0) bands. Due to the two-fold symmetry that exists in the free base porphyrin structure, the transition moment operator is split into x and y components. Hence, this is why each Q band is split into two components in the spectrum. The exact values for each of the specific bands for each of the six *meso*-tetraalkylporphyrins porphyrins are given in Table 3.1.2.

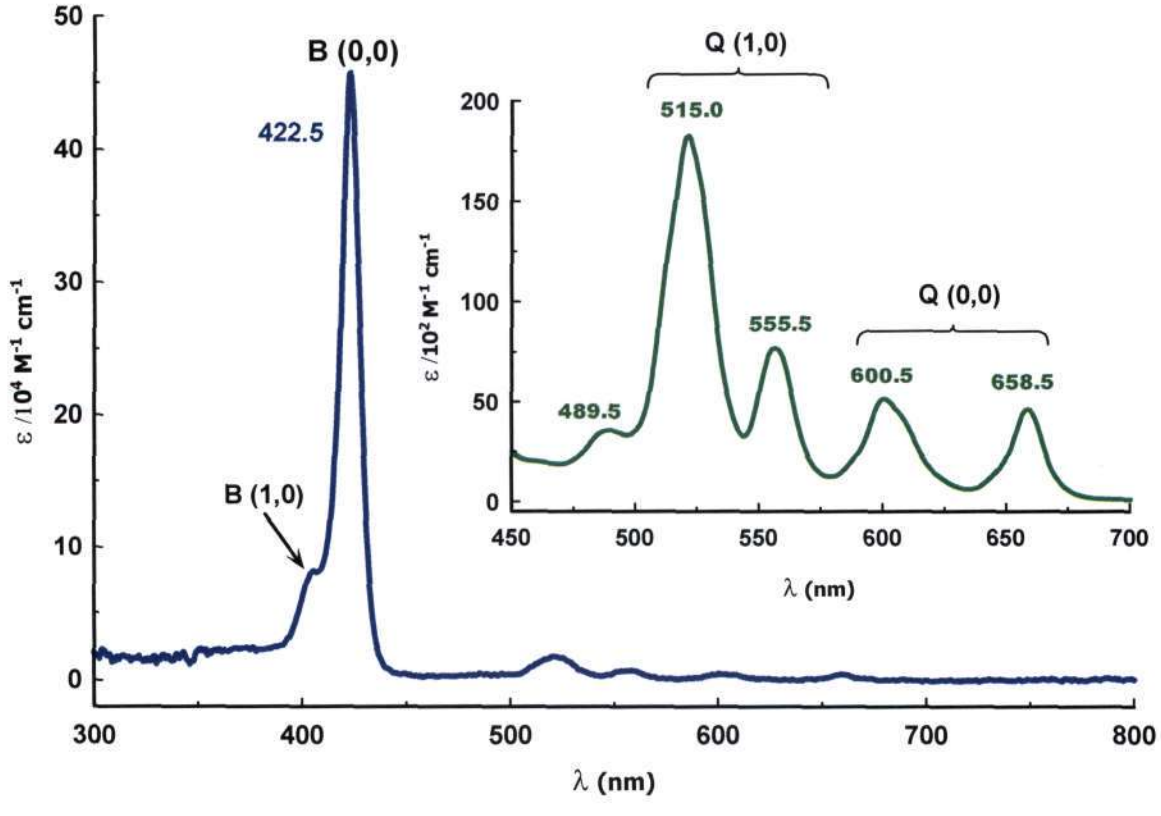

Figure 3.1.3: Representative UV-vis spectrum for $H_2T(CH_2Ph)P$ with an enlarged area from 450 to 700 nm for better clarity of the Q bands.

The wavelengths at which the Soret band is observed for each of the six porphyrins are all within a range of 10 nm of each other. They also all have similar intensities at similar concentrations (as noted during Beers Law experiments). The porphyrin with the largest *meso*-substituent, $H_2T(CHPh_2)P$, has the shortest B(0,0) wavelength, yet the porphyrins with the second and third largest *meso*-substituents, $H_2T(CH_2Ph)P$ and $H_2T(cyHx)P$, have two of the longest B(0,0) wavelengths. Thus it is see that the bulkiness of the *meso*-substituent does not have a specific effect on the position of the Soret band. It is possible that the conformation of the porphyrin may have a greater effect on the position of the UV-vis bands as opposed to the actual substituents.

Table 3.1.2 UV-visible spectral bands present for each of the six synthesized porphyrins in CH_2Cl_2 at 25 °C.[a]

Porphyrin	Soret band	Visible bands				
			Q(1,0)		Q(0,0)	
$H_2T(iBu)P$	420.5 (564×10^3)	491.5 (sh)	513.0 (15.5×10^3)	559.0 (8.5×10^3)	602.0 (4.7×10^3)	658.5 (4.6×10^3)
$H_2T(CH_2Ph)P$	422.5 (457×10^3)	489.5 (sh)	520.0 (19.9×10^3)	555.5 (5.8×10^3)	600.5 (3.9×10^3)	658.5 (2.7×10^3)
$H_2T(iPent)P$	423.5 (896×10^3)	493.5 (sh)	527.5 (28.3×10^3)	563.5 (15.2×10^3)	609.0 (7.8×10^3)	666.5 (6.5×10^3)
$H_2T(CHPh_2)P$	414.0 (291×10^3)	–	514.0 (18.8×10^3)	549.5 (6.9×10^3)	590.0 (5.9×10^3)	643.0 (1.8×10^3)
$H_2T(iPr)P$	419.5 (229×10^3)	488.5 (sh)	522.0 (8.1×10^3)	557.5 (4.3×10^3)	601.5 (2.2×10^3)	658.5 (2.3×10^3)
$H_2T(cyHx)P$	423.0 (282×10^3)	492.5 (sh)	526.5 (11.8×10^3)	562.5 (7.6×10^3)	604.0 (3.4×10^3)	660.5 (4.9×10^3)

[a]All wavelengths in nm; molar absorptivities have units of M^{-1} cm^{-1}.

Also present in all the spectra, except for $H_2T(CHPh_2)P$, was a shoulder to the first of the Q bands in the region around 490 nm, as shown in Table 3.1.2. Otherwise the same pattern is seen in each experimental spectrum with regard to the Q-band intensities; the first band (with the lower wavelength) has an almost doubled intensity of any of the other three (which all have rather similar intensities). For the individual wavelengths of the Q bands in each porphyrin there is also no specific trend followed according to the size and type of the *meso*-substituents. This is true, except when the wavelength for one Q band of a particular porphyrin is greater than the corresponding

Q band of another porphyrin, then it is likely that this divergence will be seen for each of its Q bands relative to the other porphyrin. In general, the four Q bands seen for each porphyrin are within about 20 nm of their matching band for the other porphyrins in the series.

3.1.5 Comparison with Porphyrin Spectra in the Literature

As was expected, no data could be obtained for the three novel structures of $H_2T(iBu)P$, $H_2T(CH_2Ph)P$ and $H_2T(CHPh_2)P$. However, data concerning the bands for the UV-vis spectra of $H_2T(iPent)P$, $H_2T(iPr)P$ and $H_2T(cyHx)P$ were all found. Some sources also gave extinction coefficients for each of the bands. However, these values were only reported for porphyrins $H_2T(iPent)P$ and $H_2T(iPr)P$. The values obtained from our experimental procedure for the UV-vis bands of these three porphyrins and for the extinction coefficients acquired from Beers Law experiments are all compared to those obtained from the literature in the following tables.

Table 3.1.3 Literature and experimental UV-vis bands and extinction coefficients for $H_2T(iPent)P$.[a]

	Soret	**Visible bands**			
Experimental	423.5 (896×10^3)	527.5 (28.3×10^3)	563.5 (15.2×10^3)	609.0 (7.8×10^3)	666.5 (6.5×10^3)
Reference 58	419 (417×10^3)	522 ?	559 (14.1×10^3)	601 (8.9×10^3)	664 (10.0×10^3)

[a]All wavelengths in nm; molar absorptivities have units of M^{-1} cm^{-1}.

One reference[58] was found for $H_2T(iPent)P$ that gave the UV-vis bands; it also gave the extinction coefficients. The wavelengths for the bands differed from those obtained in this work by about 5 nm for each; this magnitude of deviation is not serious. However, the 5 nm difference between the literature values and this work for $H_2T(iPent)P$ exceeds that for either $H_2T(iPr)P$ or $H_2T(cyHx)P$. The solvent used for this work and for the literature was CH_2Cl_2 and therefore this discrepancy cannot be attributed to a solvent shift. All the wavelengths for the UV-vis bands for $H_2T(iPent)P$

are, however, consistently smaller in the literature. The value for the extinction coefficient for the wavelength of 522 nm in this particular paper is unfortunately believed to be a typographical error, hence no value is quoted and therefore no comparison can be made for this particular wavelength. However, the values for the other extinction coefficients of the other bands compare well. They are each of the same orders of magnitude as their corresponding experimental value. The experimentally determined extinction coefficients for the other five synthesized porphyrins all have bands with extinction coefficients with similar orders of magnitude as seen here. And this trend will also be seen for $H_2T(iPr)P$ and $H_2T(cyHx)P$, Tables 3.1.4 and 3.1.5.

Table 3.1.4 Literature and experimental UV-vis bands and extinction coefficients for $H_2T(iPr)P$.[a]

	Soret	**Visible bands**			
Experimental	419.5 (229×10^3)	522.0 (8.1×10^3)	557.5 (4.3×10^3)	601.5 (2.2×10^3)	658.5 (2.3×10^3)
Reference 13	420 (186×10^3)	524 (12.3×10^3)	560 (6.4×10^3)	602 (3.8×10^3)	656 (4.2×10^3)
Reference 58	420 (209×10^3)	522 (11.0×10^3)	557 (7.1×10^3)	602 (4.0×10^3)	658 (4.0×10^3)
Reference 78	420	524	560	602	656

[a]All wavelengths in nm; molar absorptivities have units of M^{-1} cm^{-1}.

Both references 13 and 78 reported identical wavelength values, which correlate well with our experimental findings; the largest variation is only 3.5 nm, which is negligible. This cannot be attributed to solvent shifts, as the same solvent was used in all cases. The wavelengths for these UV-vis bands are also all consistently larger for the literature values. Reference 58 reported some slightly different values; however, these values were in better agreement with those obtained by us experimentally (with an average difference of only 0.5 nm). Two of the literature references[13,58] reported data for the extinction coefficients, all of which compared favourably, with regard to orders of magnitude, to our experimentally obtained values.

The UV-vis data for $H_2T(cyHx)P$ were found in two sources[195,215] of the same origin, which therefore gave identical values for the wavelengths of the UV-vis bands. Our experimental data were in good agreement with the literature, with the largest difference between literature and experimental values being only 1.5 nm, which is again negligible. The wavelengths for the UV-vis bands in the literature were all slightly higher than those determined experimentally. No values for the extinction coefficients were available.

Table 3.1.5 Literature and experimental UV-vis bands for $H_2T(cyHx)P$.[a]

	Soret	**Visible bands**			
Experimental	423.0 (282×10^3)	526.5 (11.8×10^3)	562.5 (7.6×10^3)	604.0 (3.4×10^3)	660.5 (4.9×10^3)
References 195 and 215	422	525	562	603	660

[a]All wavelengths in nm; molar absorptivities have units of M^{-1} cm^{-1}.

3.1.6 Summary

This work provides the band maxima and extinction coefficients for three novel porphyrins ($H_2T(iBu)P$, $H_2T(CH_2Ph)P$ and $H_2T(CHPh_2)P$). This data was also obtained for three currently known porphyrins ($H_2T(iPent)P$, $H_2T(iPr)P$ and $H_2T(cyHx)P$). Generally good agreement between the present data and that in the literature exists. Finally, the absorption data in this chapter provides the required experimental excitation wavelengths for studying the excited state behaviour of this class of porphyrins (*vide infra*).

3.2 IR Spectroscopy

3.2.1 Introduction

In 1800 Sir William Herschel first showed in Scientific Literature the existence of IR Radiation.[216] The finding of suitable prism materials, the development of adequately sensitive detectors, and finally—at the beginning of the 20th century—the introduction of the Echelette grating, were all fundamentally important factors in making the measurement of well-resolved spectra possible.[217] In 1937 Lehrer developed the first fully automated spectral photometer at BASF AG in Luwigshafen on the Rhine.[218] After 1940 there was advancement of industrial techniques, particularly in the USA, and as a result it has been possible since 1950 to record well-resolved IR spectra within the course of a few minutes. In 1946 the first complete and systematic record of infrared absorption spectra for analytical purposes was published.[217] The first commercial FT spectrometer, however, appeared only after 1960.[217]

A molecule's energy can be divided into three additive parts: (1) the rotation of the molecule as a whole, (2) the motion of the electrons in the molecule, and (3) the vibrations of each atom in the molecule. The basis for this separation is due to the difference in time scales between the transitions. Electronic transitions occur on a shorter time scale than vibrational transitions and rotational transitions on a longer time scale. There is, strictly, also a translational component for the molecule; however, it is not spectroscopically important because it is essentially not quantized.[219]

Our main concern is with vibrational transitions observed in IR spectra. These vibrational energy levels have a small separation and thus transitions will be seen at the low frequencies (10^2 cm^{-}1 to 10^4 cm^{-1}) in the infrared region. These transitions originate from vibrations of the nuclei constituting the molecule. The electronic levels are generally far apart and the transition frequencies (10^4 cm^{-1} to 10^6 cm^{-1}) are seen in the visible and ultraviolet regions. The rotational levels are relatively close together and transitions between these levels are observed in the microwave and far-infrared regions at low frequencies in the microwave region, i.e. long wavelengths (1 cm^{-1} to

10^2 cm^{-1}). This type of distribution is, however, rather subjective, as it is possible for pure rotational spectra to materialize in the far-infrared region (when transitions to higher excited states are concerned), and for pure electronic transitions to emerge in the near-infrared region (close spacing of electronic levels).[219,220]

The section of the electromagnetic spectrum between the visible and microwave regions is broadly referred to as infrared radiation. The portion that is most useful to chemists is the region between 400 and 4000 cm^{-1}. However, some interest has been shown in the near-infrared (4000–14,290 cm^{-1}) and the far-infrared regions, 200–700 cm^{-1}.[221] IR spectrometry is primarily important due to a spectrum's high content of information and because of the variety of possibilities for sample preparation and measurement. This makes IR spectroscopy one of the most important and useful methods for preparative as well as analytical chemists.[217] Characteristic infrared spectra are usually observed as absorption spectra in the infrared region, and originate in transitions between two vibrational levels of the molecule in the electronic ground state.[220] Not all transitions between these levels will be possible, so determination of which may be "allowed" and which are "forbidden" must be done using the relevant selection rule, which is determined by the symmetry of the molecule.[219]

Two types of molecular vibrations exist, stretching and bending. In IR spectroscopy it is only those that result in a rhythmical change in the dipole moment of the molecule that will be observed. The spectrum of even a simple molecule may be rather complex, with numerous bands being present. However, the actual number of bands that are seen in a spectrum may be reduced by a variety of factors. These factors include bands that may occur outside the range of 400–4000 cm^{-1}, some bands may be too weak to be clearly seen, and some may even disappear into other bands.[221]

In vibrational spectra, rotational transitions are common. However, for most polyatomic molecules rotational fine structure will not be seen due to the rotational levels being closely spaced on account of relatively large moments of inertia. Samples in solution do not exhibit rotational fine structure in their vibrational spectra due to

molecular collisions which occur before a rotation may be completed, and the levels of the individual molecules are perturbed differently.[219]

IR radiation will be absorbed by a molecule to excite certain atomic movements in the molecule; the energy for such vibrational motions is definite for a particular molecule, but differs for dissimilar substances.[217] The position and the intensity of the absorption bands are also specific to each substance. This makes the IR spectrum highly characteristic for each substance and hence can be used for identification. The high specificity is based on the good reproducibility with which the coordinates of the absorption maxima—generally wavenumber and transmittance—can be measured. The best absorption bands to help with identification are those of the carbon back-bone of the molecule, which are frequently found in the easily accessible range of 650–1500 cm^{-1}, known as the "fingerprint region".[217]

The IR spectrum incorporates all the particulars about the molecular structure of a compound and, as a result, the spectrum contains a surplus of information about that compound.[217] Hence, attempting a total spectral analysis is a very complicated procedure, one which succeeds only after extensive calculation for even the simplest compounds. In most cases, one has to be content with merely a partial interpretation and bases conclusions on empirical rules. This is, however, mostly accepted due to the use of other methods for compound characterization and not only IR spectroscopy.

3.2.2 IR Spectroscopy of Porphyrins

Vibrational spectra of metalloporphyrins and other related compounds have been studied at length due to their biological importance as prosthetic groups of haem proteins.[220] Free base porphyrins are, however, far less studied and their spectra are therefore not as well documented. The IR spectrum for porphine itself (the simplest porphyrin) has not even been completely recorded or fully understood. However, a comparatively reliable assignment of the infrared active vibrations has been obtained by means of a normal coordinate analysis.[222] Porphine has 105 (3 x 37 – 6) normal vibrations which have been characterized; as expected the bands between 1700 and 950 cm^{-1} are due to ν(C-C), ν(C-N), δ(C-H) and δ(CCN) modes and are strongly

coupled to each other.[220] Many studies have been performed on complexes of H_2TPP because of their relatively high synthetic yields and convenient purification. The IR spectra of these complexes are particularly difficult to assign due to the fact that the phenyl group vibrations will be either mixed with or overlapped by the porphyrin core vibrations.

A simple metalloporphyrin that has D_{4h} symmetry has vibrational behaviour that is typical of the porphyrin part of more complex molecules. Thus this molecule may be used to obtain an indication of the expected vibrations, despite the fact that unsubstituted porphyrins play only a small role in porphyrin chemistry. The 105 possible vibrations can be classified,[222] as in Table 3.2.1. As a result, a maximum of 35 Raman lines and 24 infrared absorptions are likely to be observed. The addition of substituents to the porphyrin macrocycle will increase the number of observable vibrations; this is due to the larger number of atoms and the possible lowering of symmetry.[223]

Table 3.2.1: Table of vibrations for a porphyrin macrocycle.[223]

In-plane vibrations		Out-of-plane vibrations	
a_{1g} (Raman active)	**9**	a_{1u}	**3**
a_{2g}	**8**	a_{2u} (Infrared active)	**6**
b_{1g} (Raman active)	**9**	b_{1u}	**5**
b_{2g} (Raman active)	**9**	b_{2u}	**4**
e_u (Infrared active)	**18**	e_u (Raman active)	**8**
	71		**34**

The spectra of metalloporphyrins will differ from those of free base porphyrins due, to the fact that they usually exhibit fewer bands and sharper infrared absorptions owing to their higher symmetry. These differences are more obvious for the vibrations of the porphyrin skeleton as opposed to those of the inner vibrations of the peripheral substituents. The differences are most noticeable in the far infrared where the M-N vibrations of metalloporphyrins are found; however, these cannot be considered isolated because they are coupled with skeletal bending modes.[223]

The vibrations of the porphyrin ring substituents are more prominent than the absorptions that arise from motions of the macrocycle skeleton; however, the spectra of porphyrins (or other types of similar molecules) will have some comparable peaks between them due to this central macrocycle. It is, however, not possible for any two spectra, except those of enantiomers, to be exactly the same. The classification of porphyrins does not rely on IR spectra alone and thus it is not necessary to assign each separate peak; however, the presence of specific peaks does help to elucidate already made characterizations.[221] In Table 3.2.2 a few of the most commonly encountered peaks are listed. It may be noted that hetero-aromatics containing an N-H group usually show an N-H stretching absorption in the region of 3220–3500 cm^{-1}.[221]

Table 3.2.2: Expected general IR absorption bands.

Vibration	Absorption (cm^{-1})	Reference
ν(N-H)	3300–3360 (generally)	**223**
	3320 (porphine)	**223**
	~ 3300 (*meso*-tetraalkylporphyrins)	**This work**
$\nu(C_\beta\text{-}H)$	3000–3150	**221, 223**
ν(C-H)	2840–2970	**221, 223**
$\nu(C_\beta\text{-}C_\beta)$, $\nu(C_\alpha\text{-}C_{meso})$	1550–1600	**223, DFT**
δ_{ip}(N-H)	1110	**223**
δ_{oop} (pyrrole N-H) δ_{oop} (pyrrole C_β-H)	770–800	**223, DFT**
δ_{oop}(N-H)	638, 739	**223**

3.2.3 Sample Preparation

Before the interpretation of a spectrum it should first be examined to check for errors, impurities and anomalies. At first glance it is possible to detect if too much or too little sample has been used during preparation (only the most intense bands will be visible if insufficient amounts were used).[217] The shape of the absorption bands also helps to draw conclusions about the sample preparation quality. In pellet spectra, if there is an increase in the background absorption (reduced transmittance), then it implies large crystals and hence that the sample had been poorly pulverized. An embedding process can be seen when a single band's shape is distorted in such a way that the transmittance on the long-wavelength side is smaller than on the short-wavelength side. Organic materials at good resolution usually display 30 to 40 bands in the 400 to 2000 cm^{-1} region, mainly concentrated in the fingerprint region. A few wide, intense bands typically indicate an inorganic substance.[217]

The most commonly used of the halogenides to make up IR pellet samples is potassium bromide (KBr), due to its permeability down to 400 cm^{-1} (this was used for all our presented spectra). KBr is known to be hygroscopic, particularly when it has been finely crushed in the production of the sample pellets, due to the larger surface area. The adsorption of moisture will give interfering bands at around 3450 cm^{-1} and 1640 cm^{-1} (as well as to a decline of the background above 1000 cm^{-1}). If the sample is too concentrated then there will be a lot less adsorption. This and other possible extraneous signals are listed in Table 3.2.3.[217]

Table 3.2.3: Positions of some possible extraneous bands in the IR spectra.

Wavenumber (cm^{-1})	Type of contaminant	Comments
3450–3330	H_2O	water in the substance or in KBr
~ 2345	CO_2	atmospheric non-compensation for samples and background spectrum
1640	H_2O	liquid water
1355	$NO_3^{\ominus}$	from KBr, H_2O residues etc.
837	$NO_3^{\ominus}$	from KBr, H_2O residues etc.
667	CO_2	atmospheric non-compensation for samples and background spectrum

3.2.4 Objectives

The goals of this chapter were to:

(1) present experimental IR modes for the six synthesized *meso*-tetraalkylporphyrins;

(2) present calculated IR absorption data for the six compounds based on high-level DFT simulations on geometry optimized structures;

(3) use the simulations to assist in the assignment of key experimental IR-active modes for the six *meso*-tetraalkylporphyrins; and

(4) find any correlations between the six *meso*-tetraalkylporphyrins.

3.2.5 Results and Discussion

3.2.5.1 Calculated and experimental IR modes

In all of the spectra, the pyrrole type N-H stretch was clearly present in the expected region, along with the symmetric and asymmetric C-H stretching modes. It was also possible to assign some definitive C-H modes of the pyrrole rings. The finger print region was more complicated; however, with the help of the theoretical spectra it was possible for some of the most prominent and common peaks to be assigned. The computed vibrations could be assigned exactly even if there was no marked evidence of these peaks in the experimental spectrum. A representative IR spectrum (for the novel porphyrin $H_2T(CH_2Ph)P$) showing the experimental and calculated data is shown in Figure 3.2.1. All the experimental IR spectra for each of the six synthesized *meso*-tetraalkylporphyrins are available in **Appendix B2**.

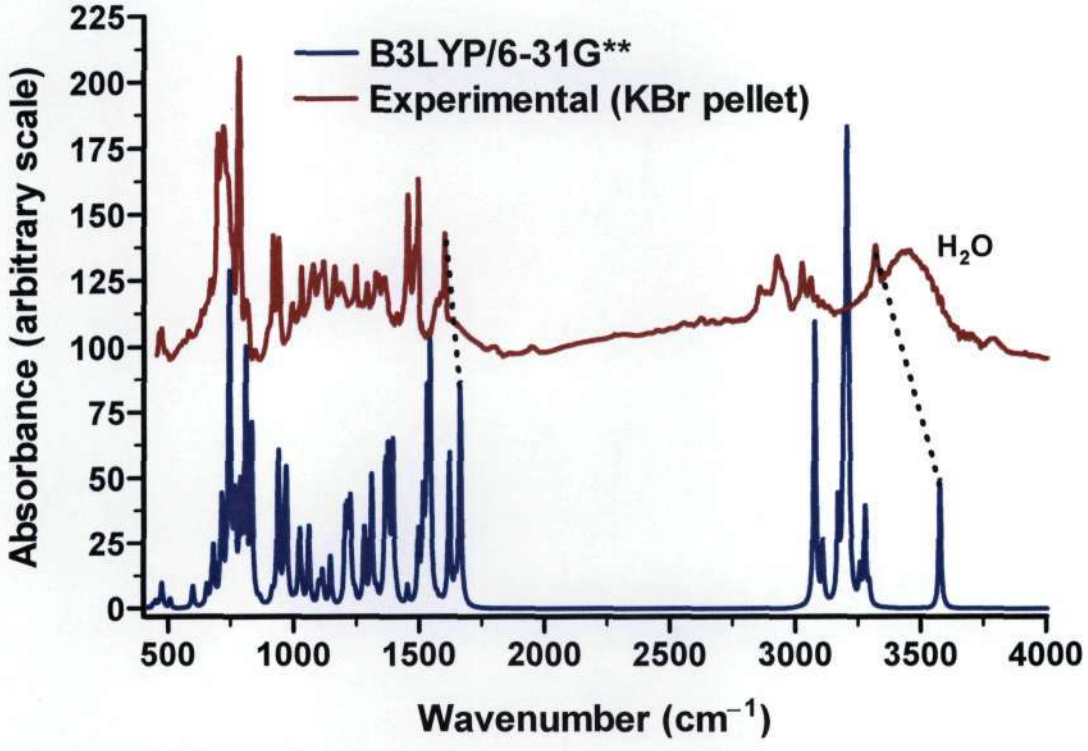

Figure 3.2.1: Representative IR spectrum for $H_2T(CH_2Ph)P$ showing the experimental and DFT-calculated plots.

The comparison of the two IR spectra in Figure 3.2.1 shows good agreement between the experimental and calculated absorption envelopes, except for a few apparent

divergences. The DFT calculations do not take into account the water present in the prepared sample, and therefore the large water band seen for the experimental data is absent in the computed data. Another obvious difference between the spectra is that of the strong intensity calculated for one of the C-H stretches in the region of 3200 cm^{-1}; this band in the experimental data is not nearly as intense. Besides these few differences the spectra are very similar, particularly in the fingerprint region, and therefore the expected IR spectrum for this novel porphyrin has successfully been predicted.

However, the comparison between the fingerprint and higher frequency regions must be noted. An example for the difference between two corresponding peaks in the fingerprint region and two corresponding peaks in the higher frequency region has been depicted. The angle for the connecting line in the higher frequency region is clearly much greater than that in the fingerprint region. Thus a graph for the differences between two corresponding frequencies was plotted against the observed (experimental) data (Graph 3.2.1).

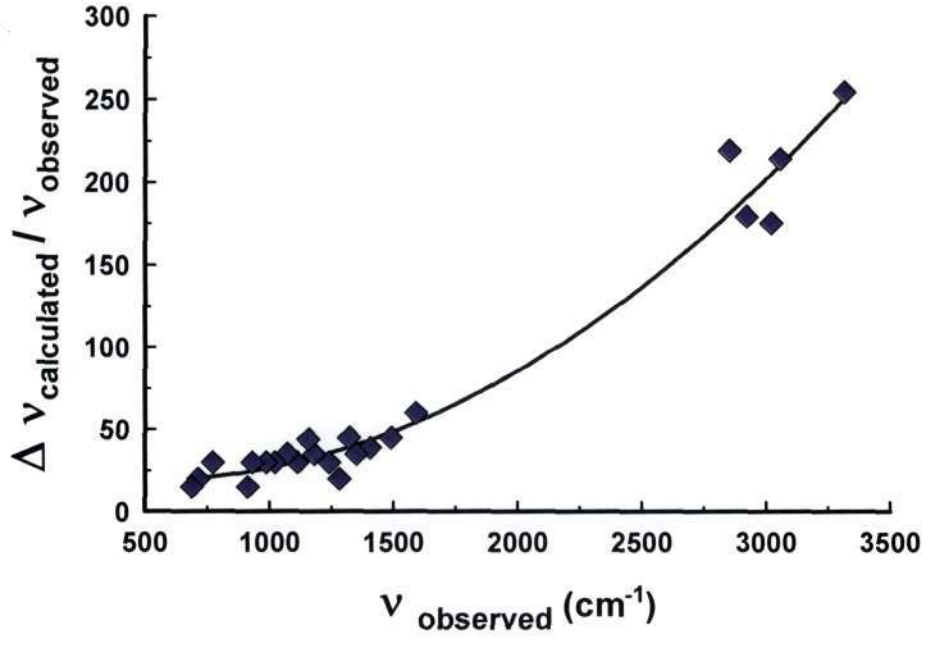

Graph 3.2.1: *Difference between calculated and observed versus observed band.*

If there was a consistent difference between observed and calculated data then a straight, horizontal line would be evident. Here a definite curve with greater differences

at higher frequencies is observed. Thus better correlation is seen in the fingerprint region than at higher frequencies. The greater concentration of bands in the fingerprint region usually makes allocating particular bands more difficult, but here the DFT-calculated data will assist in assignment. Also plotted are the DFT-calculated values versus the experimental values for some of the bands for the novel porphyrin $H_2T(CH_2Ph)P$ (Graph 3.2.2). This shows the extent of the correlation between the computed and observed bands. The difference between the two methods (RMSD) for the values at lower frequencies is more than six times less than that at higher frequencies. Although at higher frequencies this greater difference (RMSD) is seen, there is still a good correlation between the two methods according to the correlation coefficient (0.999) and the slope (1.091) that is near unity.

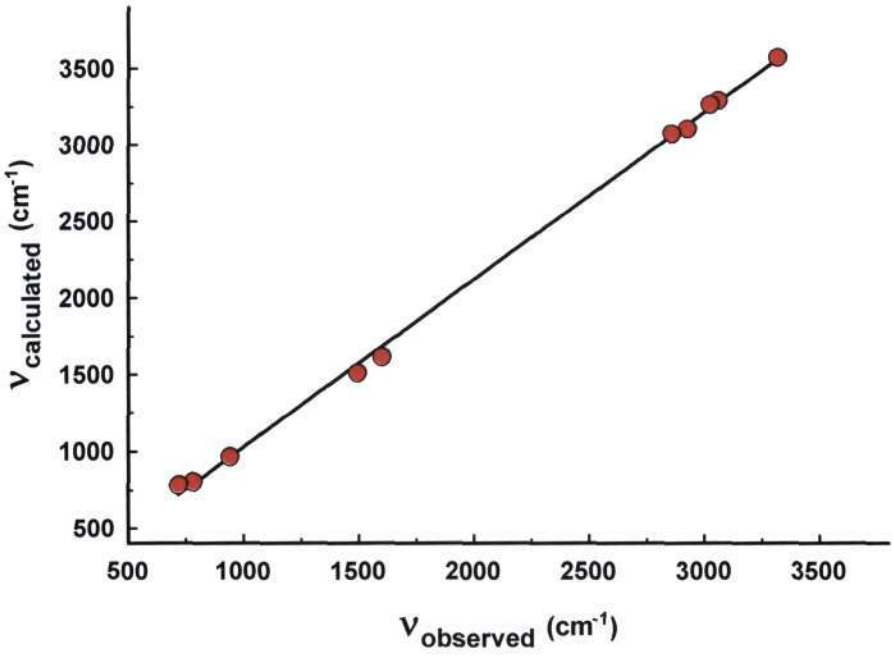

Graph 3.2.2: The correspondence between ten of the calculated and observed band frequencies for the IR spectrum of the novel porphyrin $H_2T(CH_2Ph)P$. The slope is 1.091 and the RMSD is 505 cm^{-1} for the high frequency region and 82 cm^{-1} for the low frequency region. The correlation coefficient is 0.999.

3.2.5.2 Assignment of the IR modes

In order to make assignments for vibrations of the porphyrins in the IR region, the experimental spectra were compared with the vibrations calculated from the DFT computations (Chapter 7). This type of computation was performed for each of the six

meso-tetraalkylporphyrins, with the exception of $H_2T(CHPh_2)P$, due to refinement difficulties associated with its large size. These calculated vibrations were first corrected for the type of theory used by means of the factor 0.9613.[224] There was also an associated intensity for each of these vibrations; this needed to be taken into account when making assignments because it gave an indication of the probability that a particular vibration would be visible in the spectrum. Each of the computed vibrations can be exactly displayed for the particular molecule using GaussView 3.09,[225] thus allowing accurate assignment of the type of calculated vibration occurring at a given wavenumber.

For porphyrins 1–6: $H_2T(iBu)P$, $H_2T(CH_2Ph)P$, $H_2T(iPent)P$, $H_2T(CHPh_2)P$, $H_2T(iPr)P$ and $H_2T(cyHx)P$, the experimental IR spectra exhibited one prominent peak in the region 3300 to 3330 cm^{-1}, close in energy to the water band. This peak was attributed to the stretching mode of the N-H groups at the centre of the porphyrin macrocycle (Table 3.2.4). The theoretical DFT calculations showed two vibrations in the region 3420 to 3480 cm^{-1} (for the corrected values). However, the intensity for one of these peaks was either zero or very close to it, and therefore the band was not expected to be present in the IR spectrum.

Table 3.2.4: Experimental and theoretical peaks for the N-H stretch.

N-H stretch	ν(N-H) (cm^{-1})	ν_s(N-H) (cm^{-1})			ν_{as}(N-H) (cm^{-1})		
	Experimental value	DFT	DFT_{corr}	Int.	DFT	DFT_{corr}	Int.
$H_2T(iBu)P$	3329	3610	3470	0.03	3561	3423	54.0
$H_2T(CH_2Ph)P$	3317	3615	3475	0.00	3572	3434	49.4
$H_2T(iPent)P$	3328	3613	3473	0.12	3564	3426	53.9
$H_2T(CHPh_2)P$	3232	–	–	–	–	–	–
$H_2T(iPr)P$	3320	3614	3474	0.00	3566	3428	53.4
$H_2T(cyHx)P$	3301	3609	3469	0.12	3559	3421	57.0

DFT_{corr} = corrected value for the DFT calculation using the factor 0.9613.
Int. = the intensity of the DFT calculated values in arbitrary units.

If there is no change in the dipole moment, then the mode is calculated, but it has an intensity of zero, and will instead be seen in the resonance Raman spectra of the compound. On further inspection, it was clear that in each case it was the symmetrical stretch (ν_s(N-H)) that would not be observed (IR inactive; Raman active). The asymmetrical stretch (ν_{as}(N-H)), however, had, in each case, an approximate intensity of around 50 units. The experimental values obtained for the N-H asymmetrical stretches for each porphyrin were ~ 100 cm^{-1} less than those for the corrected DFT values. This was noted as an acceptable error due to the consistency of this shortfall for each of the six *meso*-tetraalkylporphyrins.

In the region 3000 to 3150 cm^{-1} it is sometimes possible to observe peaks related to the symmetric and asymmetric stretching of the pyrrole ring C-H groups. Mostly, both these peaks can be clearly observed; however, this is not the case for the spectra of P5 and P6 (Table 3.2.5). The symmetric peak is clearly present in these two spectra, whereas the asymmetric peak, although somewhat visible, is very weak (P5 = H_2T(iPr)P) or is partly hidden by the symmetric peak (P6 = H_2T(cyHx)P). However, it was possible to determine the expected asymmetric peak vibration for P5 and P6, using the DFT calculations. This gave an accurate prediction due to there being favourable comparison—in most cases—between the vibrations given by the corrected values of the DFT computations and the experimental data. Generally there was only a difference of about 20 to 50 cm^{-1} between them; however, for P2 (H_2T(CH_2Ph)P) the deviations were as high as 125 cm^{-1}. It was also common to find two DFT calculated vibrations (of similar magnitude, within 25 cm^{-1}) that were responsible for the same vibration (symmetric or asymmetric) in the molecule according to the display when using GaussView 3.09.[225] In such cases both of these wavenumbers were reported in Table 3.2.5.

Table 3.2.5: Experimental and theoretical peaks for the pyrrole ring C-H modes.

Pyrrole ring C-H	ν_s(C-H) (cm^{-1})		ν_{as}(C-H) (cm^{-1})	
	Experimental	DFT_{corr}	Experimental	DFT_{corr}
$H_2T(iBu)P$	3146	3185 3160	3128	3144 3134
$H_2T(CH_2Ph)P$	3059	3163	3023	3147 3127
$H_2T(iPent)P$	3150	3165 3162	3128	3158 3146
$H_2T(CHPh_2)P$	3058	–	3023	–
$H_2T(iPro)P$	3144	3173 3162	w/p	3157 3145
$H_2T(cyHx)P$	3146	3178 3167	n/p	3152 3134

DFT_{corr} = corrected value for the DFT calculation using the factor 0.9613.
w/p = weak peak.
n/p = no visible peak.

Interestingly, the experimental symmetric and asymmetric pyrrole C-H vibrations for $H_2T(CH_2Ph)P$ (P2) and $H_2T(CHPh_2)P$ (P4) both have a lower wavenumber relative to the other porphyrins. The other porphyrins have wavenumbers ~ 100 cm^{-1} higher than those for $H_2T(CH_2Ph)P$ and $H_2T(CHPh_2)P$, and all their values are in a small range of less than 10 cm^{-1}. None of these other four porphyrins have phenyl substituents, thus it seems that the substituent may perturb the pyrrole C-H stretching vibration. The DFT computed values do not differ according to the different substituents; they are similar for each of the porphyrins. This is true for the symmetric and asymmetric vibrations. It is therefore possible that any potential substituent effects are not well accounted for in the DFT calculations, or that their contribution to the spectrum is small. Another factor that should be taken into account is the conformation of the porphyrin macrocycle. As can be seen in Table 3.2.8, $H_2T(CH_2Ph)P$ (P2) was almost planar, whereas the other porphyrins, except for $H_2T(CHPh_2)P$ (P4) which was saddled, all displayed ruffled distortions. Therefore it is once again only $H_2T(CH_2Ph)P$ (P2) and $H_2T(CHPh_2)P$ (P4) that differ from the generally expected ruffled conformation.

The next prominent set of peaks seen in most of the experimental spectra are those for the symmetric and asymmetric C-H stretching modes in the region 2965 to 2850 cm^{-1} (Table 3.2.6). In most cases, three peaks are clearly visible in this region for each of the experimental spectra of the porphyrins; however, for P2 ($H_2T(CH_2Ph)P$) and P6 ($H_2T(cyHx)P$), only two definitive peaks were observed, and P4 ($H_2T(CHPh_2)P$) only gives one. The values for the first two peaks for each porphyrin were similar. The first band was at about 2960 cm^{-1}; the second in the small range of 2922 to 2930 cm^{-1}. However, the third band ranged from 2848.98 cm^{-1} (P6 = $H_2T(cyHx)P$) to 2869.31 cm^{-1} (P1 = $H_2T(iBu)P$).

Each of the computed DFT vibrations were easily assigned using GaussView.[225] However, three distinct peaks were not computed by DFT for this region, which made assignment of the experimental values slightly more complicated. Generally for C-H stretches there will be two sets of two bands; one set for the asymmetrical and another for the symmetrical modes. Hence four distinct bands are expected, with the asymmetrical modes at the higher wavenumber than the symmetrical modes. In our experimental spectra there is a difference of approximately 35 cm^{-1} between the first two peaks, and a difference of about 60 cm^{-1} between the second and third. When examining the spectra for each porphyrin, it was obvious that the first two peaks seemed to be grouped together, while the third was on its own, sometimes with a possible shoulder present. Therefore, once a comparison had been made between the experimental values and those computed by DFT for these C-H stretches, it was evident that the first two peaks correspond to the asymmetrical stretching mode. The third was a symmetrical stretching mode, with the fourth peak being too weak to be clearly observed.

Table 3.2.6: Tentative assignments of the experimental and theoretical peaks for symmetric and asymmetric stretching of the C-H groups.

	ν(C-H) (cm^{-1})	Assignment	ν(C-H)(cm^{-1})	Assignment
	Experimental		DFT_{corr}	
$H_2T(iBu)P$	2960	ν_{as}(C-H)	3023 – 2976	ν_{as}(pyrrole C-H)
	2927	ν_{as}(C-H)		
	2869	ν_s(C-H)	2964 – 2916	ν_s(pyrrole C-H)
			2929	ν_s(C-H) (CH_2 only)
			2922	ν_s(C-H) (CH_3 only)
$H_2T(CH_2Ph)P$	n/p	–	3083	ν_s(C-H) (phenyl
	n/p	ν_{as}(C-H)	3076 – 3043	ν_{as}(C-H) (phenyl ring)
	2924	ν_{as}(C-H)	2985	ν_{as}(C-H) (CH_2 of subst.)
	2856	ν_s(C-H)	2954	ν_s(C-H) (CH_2 of subst.)
$H_2T(iPent)P$	2962	ν_{as}(C-H)	3029 – 3014	ν_{as}(C-H) (CH_3 only)
			3005 – 2976	ν_{as}(C-H) (CH_2 and CH_3)
	2927	ν_{as}(C-H)	2972 2967	ν(C-H) (C-H only)
			2947 – 2938	ν_{as}(C-H) (CH_2 and CH_3)
	2869	ν_s(C-H)	2933 – 2903	ν_s(C-H) (CH_2 and CH_3)
$H_2T(CHPh_2)P$	w/p	ν_{as}(C-H)	–	–
	2924	ν_{as}(C-H)	–	–
	w/p	ν_s(C-H)	–	–
$H_2T(iPr)P$	2961	ν_{as}(C-H)	3028 2994	ν_{as}(C-H) (C-H and CH_3)
	2930	ν_{as}(C-H)		
	2871	ν_s(C-H)	2978	ν_s(C-H) (C-H only)
			2932	ν_s(C-H) (CH_3 only)
$H_2T(cyHx)P$	n/p	ν_{as}(C-H)	3001– 2900	ν_{as}(pyrrole C-H)
	2923	ν_{as}(C-H)		
	2849	ν_s(C-H)	2898	ν_s(pyrrole C-H)

DFT_{corr} = corrected value for the DFT calculation using the factor 0.9613.
w/p = weak peak.
n/p = no visible peak.

In the fingerprint region of the IR spectra, there are many more peaks and the spectra are therefore not as easily assigned. Fortunately, it is not realistic (nor necessary) to try and allocate each specific peak to a particular vibration. However, with the help of the DFT computations some common peaks in the spectra could be delineated and assigned, as shown in Table 3.2.7. Peaks with the greatest intensities that occurred in each or most of the six *meso*-tetraalkylporphyrin spectra were tabulated and examined. Tentative assignments for these peaks were then made possible by using their corresponding computed vibrations from the DFT calculations.

Table 3.2.7: Tentative assignments of common bands (cm^{-1}) in the fingerprint region of the experimental spectra using calculated DFT vibrations.

	$\nu(C_\beta\text{-}C_\beta)$ and $\nu(C_\alpha\text{-}C_{meso})$	δ_{oop}(alkyl C-H) $\nu(C_\alpha\text{-}C_{meso})$ and $\nu(C_{meso}\text{-}C_{alkyl})$		δ_{ip}(pyrrole C-H) δ_{ip}(alkyl C-H)	
$H_2T(iBu)P$	1558	1453	n/p	1374	1325
$H_2T(CH_2Ph)P$	1600	1493	1452	w/p	w/p
$H_2T(iPent)P$	1558	1460	n/p	1376	1334
$H_2T(CHPh_2)P$	1597 1535	1493	1444	w/p	w/p
$H_2T(iPr)P$	1558	1455	n/p	1386	1365
$H_2T(cyHx)P$	1556	1473	1447	1341	n/p

	$\nu(C_\alpha\text{-}C_\beta)$ δ_{ip}(pyrrole C-H and N-H)		δ_{oop}(pyrrole N-H) δ_{oop}(pyrrole C_β-H)		$\nu(C_{meso}\text{-}C\text{-}H)$ δ_{oop}(pyrrole N-H)
$H_2T(iBu)P$	967	902	797	731	642
$H_2T(CH_2Ph)P$	939	916	780	717	n/p
$H_2T(iPent)P$	968	914	791	731	642
$H_2T(CHPh_2)P$	960	917	788	740	w/p
$H_2T(iPr)P$	969	914	789	732	641
$H_2T(cyHx)P$	972	919	785	724	w/p

DFT_{corr} = corrected value for the DFT calculation using the factor 0.9613.
w/p = weak peak.
n/p = no visible peak.

One important frequency in the calculated output of the DFT calculations is the value for the lowest energy vibration determined for each porphyrin. If this value is negative, then the geometry optimization has located a transition state instead of a local minimum. For each of our computations, the lowest energy vibrations for each porphyrin was above zero (the smallest being around 6 cm^{-1}) and thus stable minima were computed in all cases. These values for each porphyrin and their respective assignments are shown below in the Table 3.2.8. The lowest vibrations for the porphyrins each have intensities much smaller than 1 unit (below 0.007 units). The vibration associated with each of these values according to the DFT computation is caused by the distorted motion of the porphyrin macrocycle and its substituents. The trend seen is that ground states with ruffled conformations have higher energy, low-frequency distortions than ground states with planar geometries. They therefore principally "resist" significant further distortion as they are already distorted; whereas planar conformations will still distort.

Table 3.2.8: The lowest energy DFT-computed vibration for each porphyrin.

	$\bar{\nu}$ (cm^{-1})	$\bar{\nu}_{corr}$ (cm^{-1})	Intensity	Ground state conformation	Distortion mode
$H_2T(iBu)P$	19.3	18.5	0.0032	Ruffled distortion	Ruffled → slightly more ruffled
$H_2T(CH_2Ph)P$	6.5	6.2	0.0035	Planar with slight wave distortion component	Planar → slight ruffle
$H_2T(iPent)P$	15.4	14.9	0.0065	Ruffled distortion	Ruffled → slightly more ruffled
$H_2T(CHPh_2)P$	–*	–*	–*	Saddled distortion	–*
$H_2T(iPr)P$	19.5	18.7	0	Ruffled distortion	Ruffled → slightly more ruffled
$H_2T(cyHx)P$	11.8	11.3	0.0019	Ruffled distortion	Ruffled → slightly more ruffled

*No DFT-computed vibrational data was obtained for $H_2T(CHPh_2)P$.

Due to each porphyrin having the same structure of the central macrocycle, the spectra are all rather similar. As well as the similarities already noted in the tables above, each porphyrin has a number of DFT calculated vibrations in the range 1590–1550 cm^{-1} at low intensities that also correlate to $\nu(C_\beta\text{-}C_\beta)$ and $\nu(C_\alpha\text{-}C_{meso})$ modes. There is, furthermore, a peak in the region 1110 to 1180 cm^{-1} for each porphyrin that could be assigned to the N-H in-plane bending vibration (δ_{ip}(N-H)). The tetraalkyl-substituents of each porphyrin do, however, differ, particularly those for $H_2T(CH_2Ph)P$ and $H_2T(CHPh_2)P$, since they include phenyl rings. For the other four porphyrins, although their substituents are different, they mostly have similar bonds. Thus their resulting IR spectra will all have similar bands in similar regions.

According to the computed DFT vibrations, the porphyrins which have ring systems as part of their substituents have some other variations in their spectra. $H_2T(CH_2Ph)P$ with four phenyl rings has a number of interesting DFT calculated vibrations. There are two related to the ν(C-C) and δ_{ip}(C-H) of the aryl ring at 1660 cm^{-1} (DFT_{corr} = 1596 cm^{-1}) and 1639 cm^{-1} (DFT_{corr} = 1576 cm^{-1}). Most of the peaks between the corrected DFT values of 1255 and 1320 cm^{-1}, particularly those at higher intensities, concern vibrations of the phenyl ring. This is also the case for the range between 1350 and 1465 cm^{-1} (corrected DFT values). $H_2T(CH_2Ph)P$ also has an out-of-plane bending vibration (δ_{oop}(C-H)) for the phenyl ring at 383.85 and 711.61 cm^{-1} (corrected DFT values), which were not easy to locate in the experimental spectrum.

Data could not be obtained for $H_2T(CHPh_2)P$; however, it is expected that similar peaks would be seen for the phenyl ring substituents as were observed for $H_2T(CH_2Ph)P$. $H_2T(cyHx)P$ also has a number of vibrations due to the cyclohexyl rings in the region 790 to 1000 cm^{-1}. These originate from the ring carbon-carbon stretch (ν(C-C)) and the CH_2 out-of-plane bending mode ($\delta_{oop}(CH_2)$).

3.2.6 Summary

The most prominent IR modes for the six *meso*-tetraalkylporphyrins were assigned using the vibration data obtained from DFT simulations. The differences between the theoretical and experimental data were in the range of 0.5–5%. It was observed that

the ground state conformations (ruffled or planar) of the porphyrin macrocycle had a measurable effect on the energy of the low-frequency modes in the IR spectra. Furthermore, the steric bulk of the *meso*-substituents tended to modulate some of the vibrational modes, as evidenced by small up- or down-frequency shifts for selected modes.

4. NMR Spectroscopy

4.1 Introduction

Nuclear Magnetic Resonance (NMR) spectrometry is another form of absorption spectrometry, analogous to that of IR or UV-vis spectrometry. A sample can absorb electromagnetic radiation in the radio frequency (rf) region at frequencies governed by its particular characteristics. This will take place in the presence of an applied *magnetic field* under suitable conditions.[221] Absorption is a function of certain nuclei in the particular molecule. Intensities of these absorption peaks plotted against their frequencies on the x-axis constitutes an NMR spectrum.[221]

Our concern is always with molecules in which the nuclei are surrounded by electrons and other atoms, thus the observed resonances are influenced in distinctive ways by these different environments of the monitored nuclei. As a result, diamagnetic molecules have an effective magnetic field at the nucleus that is then weaker than the externally applied field, i.e. the nuclei are magnetically shielded.[226] This small effect is measurable using the shielding constant, σ. The extent of magnetic shielding is determined by the shell (or shells) of electrons.[226] The reduction of the field and of the associated resonance frequency is shown by theory and experiment to be determined largely by the distribution of electron density in the molecule. Substituents will therefore affect chemical shifts by specifically influencing this electron distribution. While inductive and mesomeric substituent effects are conveyed through chemical bonds, interactions through space are also a possibility. An example of this is when the observed nuclei have magnetically anisotropic neighbours, for instance: a double or triple carbon bond, a carbonyl group or a phenyl ring. Furthermore, intermolecular interactions can also be contributing factors to the shielding.[226]

The shielding and deshielding in a molecule depends on its orientation with respect to the applied magnetic field as it depends on diamagnetic anisotropy. An example of diamagnetic anisotropy is the so-called "ring-current" effect which explains the large

deshielding of benzene ring protons. This effect indicates that a proton positioned directly above or below the aromatic ring ought to be shielded (Figure 4.1).[221] In benzene the proton signal is found at 7.27 ppm in the ^{1}H NMR spectrum and for ethylene at 5.28 ppm.[226] This is due to the position of the protons in the particular molecule; the protons in benzene are in the deshielding region (–) and thus their resulting resonance is downfield. The greatest effect by the ring current is achieved when the benzene ring is perpendicular to the field direction. It will be zero when one of the molecule's in-plane axes is parallel to the field, so that the magnetic field lines do not pass through the ring.

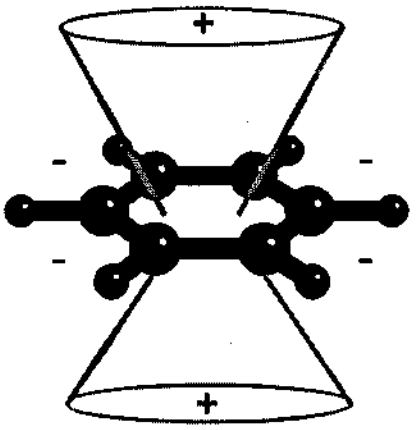

Figure 4.1: The shielding (+) and deshielding (–) zones of benzene.

This is not just an isolated case for benzene, but applies generally to arene protons, which are less shielded than those of alkenes. In large, unsaturated ring systems where the number of π-electrons satisfies the Hückel rule ($4n + 2$), effects are found which again signify the reality of a ring current.[226] The ring current is set up when the molecule and its delocalized π-electrons are placed in a magnetic field; the ring current induces an additional magnetic field. This magnetic field has lines of force at the centre of the arene ring in the opposite direction to the external magnetic field. This is what leads to protons in the vicinity of the arene molecule being in zones of increased and reduced shielding. Hydrogen atoms that are directly attached to the arene are in a position where the lines of force increase the field; there will be reduced shielding.[226]

Pauling[227] first presented the idea of an aromatic ring current in association with the very anisotropic diamagnetic susceptibilities of benzoid hydrocarbons. An induced circulation of the system's delocalized electrons in an applied magnetic field was used to explain these susceptibilities. The ring current effect generates induced magnetic fields which are dependent upon the orientation of the aromatic system in the applied magnetic field.[228] Pople was the first to apply this ring current approach to the calculation of NMR chemical resonances in 1956.[229] He used it to explain the strange (as compared to those of alkenes) chemical shifts of aromatic molecules.

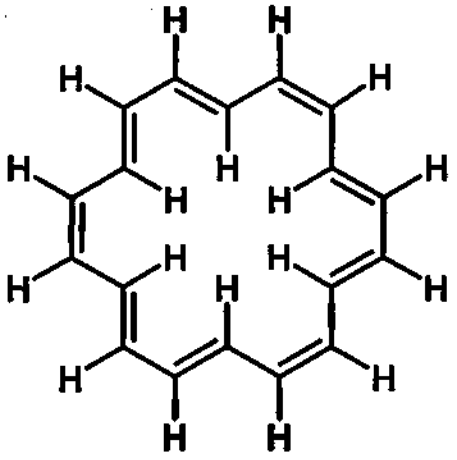

Figure 4.2: The structure of [18]-annulene.

Annulenes provide a spectacular example of shielding and deshielding by ring currents. The protons inside the ring are strongly shielded below zero (i.e. more shielded than TMS) and those outside the ring are strongly deshielded (~ 9 ppm). This type of ring current gives good evidence regarding planarity and aromaticity; at least for low temperatures.[221] In the [18]-annulene (Figure 4.2) the six inner protons are in the shielded cone of the molecule, whereas the twelve outer protons are outside of the cone and are therefore deshielded. The resulting chemical shifts in the spectrum are –1.8 ppm and a second of twice the intensity at 8.9 ppm. If a comparison is made with the value obtained for the non-planar, non-aromatic molecule cyclooctatetraene (a chemical shift of 5.7 ppm), the effect of the ring current can be clearly seen.[226] Another example is the signal of the methyl protons for the compound trans-10b,10c-dimethyldihydropyrene which is found at 4.25 ppm. This shows a definite representation of the effect caused by the ring current because without it these protons are expected to produce a signal at about 1 ppm instead.[226]

For ^{13}C NMR there is less of an effect by the ring current; it contributes only a few percent to the shielding in each case. An explanation for benzene, although over-simplified, is that the carbon atoms are a part of the "current loop", which is where the induced field will be zero.[226]

4.2 ^{1}H NMR and Porphyrins

The first NMR analysis on porphyrins was reported by Becker and Bradley,[230] they discussed the effects of ring currents on porphyrin NMR spectra. Other than some metallo-organic compounds, they were not aware of any other organic compounds at that time that could produce proton resonances as shielded as those of the porphyrins. Sixteen years later, in 1975, Scheer and Katz[231] published the first comprehensive review of NMR literature studies of porphyrins. After four years a second review by Dolphin with equally impressive coverage emerged; it dealt exclusively with NMR studies of diamagnetic porphyrins. Some other work considered to be revolutionary includes some of the first porphyrin NMR spectra that were reported by Ellis *et al.*[232] and an early review by Caughey and Koski[233] on an assortment of porphyrins (twenty-two porphyrins, the metal complexes of Ni(II), Pd(II), and Zn(II), and a chlorin).

Since about 1960 there have been rapid advances made in proton NMR spectroscopy and this has had a firm influence on the study and classification of almost all categories of organic compounds, including porphyrins.[234] However, for only a small number of these classes can such an abundance of information be acquired from NMR spectra, as is the case for porphyrins. The reason being the large magnetic anisotropy (ring current) of the aromatic macrocycle of these particular types of compounds.[230,232,235]

The parent compound, porphine, has a 24-atom carbon/nitrogen skeleton over which 18 π-electrons are delocalized. In an external magnetic field these electrons circulate around the porphyrin ring to give a diamagnetic ring current. An induced magnetic field is then generated that will strongly oppose the applied field *inside* the porphyrin ring but will assist and align with it *outside* the ring.[1] Therefore the porphyrin macrocycle

ring current causes considerable deshielding (downfield shifting) of the *meso*- and pyrrole protons at the periphery of the ring and substantial shielding (upfield shifting) for the N-H protons at the centre of the porphyrin[228] (in the conic region as shown for benzene in Figure 4.1). These ring currents (and consequent changes in chemical resonances) are always present in porphyrins; evidence of this can be seen in their NMR spectra.

The ring current operates as an incorporated chemical shift reagent, and generally extends the proton magnetic resonance spectrum of porphyrins over a large range of around 15 ppm. Consequently it is likely to cause the ^{1}H NMR spectra to be first order, which then simplifies interpretation and assignment of the spectra. This therefore makes ^{1}H NMR a very sensitive survey of structural alterations. In depth scrutiny of molecular interactions of porphyrins in solutions is also made possible by the ring current effects. ^{1}H NMR was extensively used as an investigative means in the early relevance of NMR spectroscopy to porphyrins and the resulting structural information helped to refresh an interest in porphyrins and their chemistry. The coupling constants in porphyrins are quite standard; the ^{1}H NMR subspectra of different substituents are mostly first order. Long range coupling constants are generally only seen when the peripheral β-positions of the porphyrins are unsubstituted.[234]

Early ^{1}H NMR studies needed to use samples of high concentration to obtain suitable spectra,[231] and under these conditions porphyrins tend to self-aggregate. This made acquiring reliable chemical shift data rather complicated. The tendency that porphyrins have to self-aggregate is of substantial interest. There are quite a few common types of aggregation known to affect porphyrins; these include weak $\pi-\pi$ interactions in free base porphyrins, stronger $\pi-\pi$ interactions in metalloporphyrins, and strong metal-side chain interactions in porphyrins and chlorophylls.[236] Solvent, temperature and porphyrin concentration are some of the factors upon which the type of aggregate depends.

Additionally, in early ^{1}H NMR studies it was sometimes essential that the porphyrin solubility be increased, which was done using TFA. This then gave results for the corresponding dications rather than the free base porphyrins. These types of problems

have now been minimized due to modern spectrometers with higher sensitivity (results can be obtained at very low concentrations); however, porphyrin chemical shifts should still be viewed with caution except if obtained under strongly disaggregating conditions.[228] Nonetheless this dependence of porphyrin NMR spectra on concentration and solvent offers a chance to determine spectra under conditions where spectral overlap is minimized.[228]

Modern high magnetic field NMR spectrometers give the following advantages: (1) an increase in signal sensitivity; (2) better signal separation; and (3) increased symmetry of splitting pattern (approaches first-order), which facilitate in interpretation of spectra.[237] The division of chemical shifts increases due to overlapping being reduced by the fact that spin-spin coupling constants (*J*) are independent of magnetic field strength, thus a multiplet requires relatively less spectral width at higher fields.[237] The high sensitivity of modern spectrometers has happened largely due to higher magnetic fields and Fourier transform (FT) NMR spectroscopy; however, the default parameters used may not be optimized for porphyrins. When assessing porphyrin spectra a larger pulse angle and/or a shorter relaxation delay can be utilized to take advantage of their shorter T_1 times (0.25–1.0 seconds).[238,239] These types of alterations can significantly improve the signal-to-noise ratio of the spectrum and normally there will be little or no decrease in the accuracy of integration ratios.

The prominent difference between ^{1}H NMR chemical shifts of porphyrins and those of most other compounds can generally be accredited to modifications in the shielding constant's component of shielding from neighbouring groups because of the porphyrin ring current effect.[228] The chemical shifts in porphyrins depend on the proton's distance and orientation with regard to the delocalization pathway of the π-electrons and the degree to which they are shielded from the applied field.[228] An increase in shielding gives a lower local field and thus a lower transition frequency; thus producing an upfield shift. Protons that are inside or above and below the porphyrin ring are shielded by the ring current effect and those outside of this area are deshielded. This is clear in the case of free base porphyrins where the central protons on the nitrogen atoms are strongly shielded (~ –2 ppm) and the pyrrole protons are strongly deshielded (~ 9 ppm) by comparison.[221,228] This sensitivity to orientation and distance

with respect to the ring current makes a very useful probe for studying intramolecular and intermolecular interactions in porphyrins.

There are other examples of protons that exhibit large ring current effects due to their position relative to the porphyrin macrocycle. These include the protons of axial ligands or anions that are complexed to metalloporphyrins and the protons of porphyrin dimers or aggregates. Under these circumstances the effect is nearly always shielding due to the situation of the anion, ligand or other porphyrin more often than not being in the shielding cone above (or below) the plane of the porphyrin macrocycle.[228]

The effects that substituents on the porphyrin macrocycle will have on the ring current effect have been inspected using NMR studies. On the whole it was noted that *meso*-position substitution has a tendency to decrease the ring current more than substitution at the pyrrole β-positions.[240,241] An early study by Abraham *et al.*[240] (of dications of two particular porphyrin types: 5,10,15,20-tetraalkylporphyrins and 2,3,7,8,12,13,17,18-octaalkylporphyrins) reported on this difference in affect on the porphyrin ring current due to different substitution positions. They showed that substitution at the *meso*-position affected the whole current flow while for β-substitution the current flow could choose an alternate path via the nitrogen atoms. A more recent study found the same results using bis-amine cobalt(III) complexes of H_2OEP and H_2TPP.[228] Expectedly, the effects of very bulky substituents on the porphyrin ring current have been observed for substituents which can conjugate with the porphyrin π-system and upset the ring current flow.[242,243]

Additional investigations have focused on porphyrins that have been distorted from planarity by peripheral steric crowding and have deduced that this results in a decrease in the ring current effect as well.[244,245,246] In the case of these nonplanar porphyrins it is essential to look at changes resulting from the distortion, including the positions of the porphyrin ring current loops and the protons of the substituents (as well as other anisotropic substituents such as phenyl rings).[228] In a few studies of highly substituted porphyrins, the downfield shift of the N-H protons signal has been attributed to reduced ring current caused by nonplanarity.

The chemical resonance at a very high field of the central nitrogen protons is a diagnostic feature of free base porphyrins. Some porphyrins show a considerable downfield shift of this N-H signal to around –1.70 ppm[247] (e.g. $H_2T(iPr)P$ = –1.786 ppm and $H_2T(cyHx)P$ = –1.605 ppm in this work), from the generally expected region: –2.6 ppm.[231] Larger bulky groups (e.g. tBu) give an even larger downfield shift to around –1.58 ppm.[247] In the ^1H NMR spectra of porphyrins large changes in the chemical shifts are generally accredited to variations in the contribution from the porphyrin ring current effect.[228,231] Metal complexes of *meso*-tetraalkylporphyrins have been shown to have greater nonplanar distortions with larger alkyl substituents,[13,14] thus it seems reasonable to assume that the downfield shift of the N-H signals is due to a decrease in the porphyrin ring current.

This idea is, however, not completely ideal due to the fairly small (about 5%) ring current decrease that was found for some cobalt(III) complexes of $H_2T(tBu)P$.[248] These studies by Medforth *et al.* indicated that even severe distortion of the planarity brought about little or no decrease in the porphyrin ring current effect, this was quite the reverse to earlier studies on highly substituted porphyrins.[244,245,246] These earlier studies only used the chemical shift of the N-H protons to determine the porphyrin ring current effect, but Medforth *et al.* took other factors into account. This included nonplanarity-induced changes in the orientations and positions of substituents and current loops, as well as ring currents of axial ligands and *meso*-phenyl substituents. Additionally, an adjustment to the ring current would not be able to explain the modifications that are seen in these porphyrins concerning the activation energies for N-H tautomerism.

Porphyrin and chlorophyll aggregate structures have been determined with reasonable success using ring current models.[228] These models offer an outstanding means for the analysis of porphyrin aggregation, although it may not always be clear-cut. One difficulty is that the observed ring current may be a result of the average ring current shifts in aggregates with different structures or with diverse numbers of molecules; all of which on the NMR timescale are in fast exchange with each other.[228] Experimental values are averaged due to the continuous rapid motion of the molecules in solution.

The ring current model is only one of the likely models that can be used for interpreting the experimental results.[226] Although the chemical shifts of some protons are influenced by the inductive effect of the ring, this can not be the sole reason for the differences. There must be other factors involved, for instance the steric, electronic and anisotropic effects caused by substituents, structural changes (e.g., distortions of the porphyrin macrocycle), and variations in the degree and/or pattern of hydrogen bonding for the central nitrogen protons. However, the contributions that each of these components make to the chemical shifts are not exactly known.[228]

Due to the possible occurrence of these other factors, interpreting chemical shift differences based on ring current arguments should be approached carefully. Some of the latest research suggests that this is particularly true for the central nitrogen protons, which experience the greatest effect of the ring current. They have also been used to evaluate the porphyrin ring current effect in the past, although it has been discovered that they can also display prominent chemical shift changes due to other factors including hydrogen-bonding effects.[247,249] Furthermore, there have been strong intermolecular hydrogen-bonds with solvent molecules observed; based on the nonplanarity of the porphyrin ring.[249] It is also possible that less pronounced differences in hydrogen bonding are present in numerous porphyrins and hence need to be taken into account when examining the obtained chemical shifts.[228]

To delineate the changes in N-H chemical shifts and activation energies for N-H tautomerism, Somma *et al.* proposed an alternative model that also contains a considerable increase in intramolecular hydrogen bonding with increasing size of the substituents.[247] It is expected that this hydrogen bonding will generate a further downfield shift for the N-H protons and also lower the activation energies for tautomerism. This is due to intramolecular hydrogen bonding being equivalent to the transition state for tautomerism where the hydrogen atoms are co-shared (Figure 4.3) by neighbouring nitrogen atoms.[228,250] In the past this kind of strong intramolecular hydrogen bonding in porphyrins has not been proposed; however, this phenomenon has been suggested in an account of similar NMR behaviour in the porphyrin isomer porphycene by Vogel and co-workers.[251]

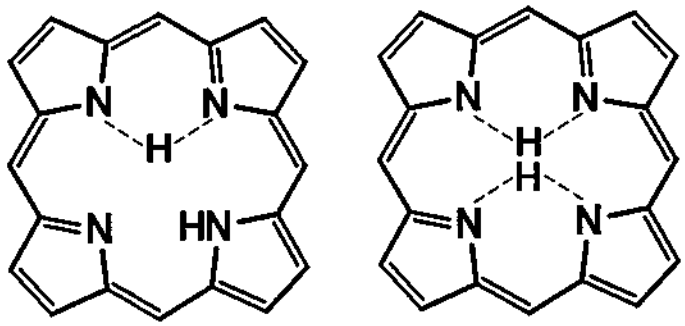

Figure 4.3: Tautomerism transition state showing the sharing of hydrogen atoms between two adjacent nitrogen atoms.[228,252]

It seems possible that increased intramolecular hydrogen bonding might result from bulkier alkyl substituents that force the porphyrin rings into increasingly ruffled conformations. This has in fact been observed for some metal complexes of related tetraalkylporphyrins.[13,14] Intramolecular hydrogen bonding would be enhanced due to the contracting of the porphyrin core and shortening of the distance between adjacent nitrogen atoms caused by this ruffling distortion. For the crystal structures that were determined by Somma *et al.*[247] it was shown that ruffling of the macrocycle increased with bigger substituents. This ruffling has a tendency to keep the nitrogen and hydrogen atoms in the plane of the porphyrin. It will also maximize core contraction, in comparison with other types of distortion styles.[15] Thus the crystal structures show the exact kind of nonplanar deformation that is expected to enhance intramolecular hydrogen bonding and generate the results observed in the ^{1}H NMR spectra.

A review done on a number of *meso*-tetraalkylporphyrin crystal structures showed some N-H tilting even in supposedly planar systems.[58] Studies[247] show that a particular type of nonplanar deformation (ruffling) can intensely enhance intramolecular bonding of hydrogen in porphyrins, and also offers another illustration of how the properties of porphyrins can be affected by nonplanarity, sometimes in unanticipated ways.[71] There has not been much attention focused on enhanced intramolecular hydrogen bonding in other nonplanar porphyrins due to their usual partiality to saddle conformations,[253] in which intramolecular hydrogen bonding will not be favoured as the pyrrole rings will be slanted out of the plane. Studies by Takeda *et al.* have shown in some solvents the downfield shifting of the N-H protons is because of an increase in the intermolecular hydrogen bonding.[254] Using this information on

hydrogen bonding and the studies proving that even great nonplanar distortions only give small decreases in the porphyrin ring current effect,[248] suggests again that care should be exercised when using chemical shifts of the N-H protons as an indicator of structurally induced changes in the porphyrin ring current.[247]

4.2.1 Changes brought about by *meso*-substitution

These include:

1) Reduction in the ring current. Generally the degree of this reduction does not depend on the features of the substituents.
2) In mono-substituted porphyrins, the methine proton opposite the *meso*-substituent will be more effectively shifted upfield than the neighbouring methine protons.
3) The protons in the locality of the substituent will experience further shielding effects.

The overall reduction of the ring current due to a *meso*-position substitution can be rationalized due to a barrier to conjugation being created affecting the full ring current and not only a section of it.[235] The main cause of reduction in the ring current of *meso*-substituted porphyrins seems to be the steric hindrance found between the *meso*- and β-pyrrole substituents. This is confirmed by the direct relationship of the decreasing size of the β-substituent with decreasing effect on the ring current. The further shielding effects that are experienced by protons that are near the *meso*-substituent are somewhat steric in origin as these groups are pushed out of the plane of the macrocycle. The leading role, however, seems to be played by magnetic anisotropies of the *meso*-substituent.[234]

4.2.2 Protons bonded to Nitrogen

Protons that are bonded to carbon differ from those bonded to an oxygen, sulphur or nitrogen atom. Carbon protons are not exchangeable and they are not subject to hydrogen bonding. The protons on a nitrogen (^{14}N) atom have cause to experience partial or complete decoupling by the electric quadrupole moment of the ^{14}N

nucleus.[221] Nitrogen protons may undergo rapid, intermediate or slow exchange. In the case of rapid exchange, the proton will be decoupled from the nitrogen atom which results in a sharp singlet. For the intermediate exchange rate a broad peak results from the N-H proton being partially decoupled. At a slow rate of exchange a broad peak is still present due to the electric quadrupole moment of the nitrogen nucleus inducing moderately efficient spin relaxation and thus an intermediate lifetime for the spin states of the nitrogen nucleus.[221]

4.3 ^{13}C NMR and Porphyrins

Other than ^{1}H NMR, the majority of studies involve ^{13}C; this is because carbon is a universal component of organic structures, has a comparatively high sensitivity and a comparatively low price in high isotopic purity.[234] Porphyrin carbon NMR spectra are usually acquired on natural abundance samples (^{13}C = 1.1%) with broadband decoupling of ^{1}H. The large chemical shift range and the narrow signals make spectral overlap an inconsequential problem in carbon spectra.[228] The ring current effect for ^{13}C is of the same absolute magnitude but is small relative to the intrinsic chemical shift magnitude. The ^{13}C chemical shifts are predominantly affected by paramagnetic contributions from low-lying excited states; the porphyrin ring current only plays a small role.[234] It has been found that the absolute magnitude of the ring-current effect for ^{13}C is the same as for ^{1}H chemical shifts when they are in the same point in space with respect to the aromatic electron cloud.[255] Originally off-resonance decoupling and selective ^{1}H decoupling experiments were used in the assignment of carbon signals. Nowadays, these techniques have been replaced by other, newer NMR experimental procedures. These processes involve establishing the number of attached protons (e.g. DEPT) or correlating the carbon and proton chemical shifts using *J*-couplings in 2D NMR experiments (e.g. HMQC and HMBC).[228]

The assignments of carbon atoms bearing hydrogen atoms can be easily made due to the beneficially spaced and well-assigned ^{1}H NMR spectra of porphyrins. There is a challenge related to the assignment of the quaternary carbons in large molecules because these carbons may be predicted to supply valuable information that cannot be obtained from ^{1}H NMR. Most, if not all, of the quaternary carbon atom resonances

are seen as resolute singlets. These singlets can be distinguished from one another in the undecoupled spectrum using their multiplicity and in the broad-band ^{1}H decoupled spectrum by their relatively low intensity as compared to the proton-bearing carbons (this is caused by the small nuclear Overhauser enhancement of the quaternary carbons and longer relaxation times).[234]

Ring current effects do not play such a significant role in ^{13}C NMR and in the determination of the relative magnitude of chemical shifts, weak self-aggregation of free base porphyrins has a much smaller effect. Accordingly, for ^{13}C NMR spectra at natural abundance, it is the generous amount of material necessary and the solubility limitations that are the major tribulations against the expansive use of this technique. For ^{13}C NMR spectra at natural abundance the sought-after concentration is 0.1 M (this can be increased if a high S/N ratio is preferred).[234]

It is necessary to differentiate between the resonances of the α- and β-pyrrolic carbons in order to be able to assign them. Difficulty may be encountered when trying to assign the α-carbon resonances due to the (exchange) broadening of the α-pyrrole ^{13}C signals in free base porphyrins.[256,257] This is expected to be caused by tautomeric N-H exchange; support for this is obtained from the spectra of the N-deuterated species.[258] A method to assign some of the quaternary ^{13}C resonances uses gradual structural changes[259] and utilizing ^{13}C–^{13}C couplings in highly enriched porphyrins makes some assignments in the surrounding area of the *meso*-carbons possible.[260] Modifications of the standard INDOR (heteronuclear double resonance) method is the most direct approach used for assignment of the quaternary carbon atoms.[261]

N-H tautomerism in free base porphyrins at room temperature shows exchange broadening of the pyrrole carbon signals. This can have quite a large effect on the signals and in some cases prevent the signals from being observed, particularly the α-carbon signals.[228] Free base porphyrins give two kinds of α- or β-pyrrole carbon signals when N-H tautomerism is slow on the NMR time scale at low temperatures. Between the two observed α-carbon signals there is a reasonably steady difference in chemical shift ($\Delta\,\delta$).

An example of this is the chemical shift difference between the same types of α carbon atoms in reference compounds pyridine = 150.2 ppm and pyrrole = 118.4 ppm; which gives a signal difference of $\Delta\delta$ = 31.8 ppm.[221] The difference in the β-carbon signals is a lot smaller (pyridine = 123.9 ppm and pyrrole = 108.0 ppm; $\Delta\delta$ = 15.9 ppm) and ranges over a few ppm. The same reference molecules may be used here, with the pyridine-type carbon atom again being assigned as downfield of the pyrrole-type carbon atom which has the lower value resonance.[178]

When protonating the porphyrins, H_2OEP and H_2TPP, to give dications, qualitatively different chemical shift changes were seen. A chemical shift solvent dependence was also noted for H_2TPP when significant downfield shifts were observed in TFA compared to in a solution of TFA in $CDCl_3$.[228] The largest variations in chemical shift are noted for the α-carbon atoms in H_2TPP complexes.[228]

4.3.1 ^{13}C Chemical shifts

In the ^{13}C spectra of porphyrins it is possible to make a division of the region where the chemical shifts resonate into four groups. These groups include the aliphatic carbon region (10–70 ppm); the methine carbon region (90–100 ppm); the aromatic and olefinic carbon region (130–170 ppm); and the carbonyl region (170–190 ppm) in the most strongly deshielded section of the spectrum.[234]

These are not set groups and therefore overlaps between them are possible; particularly in the lower field regions. These overlaps do not cause a problem for assignment as they can be resolved using the number and multiplicity of the resonances. In the high field region (between 0 and 70 ppm) all the sp^3 hybridized carbon atoms with protons will be seen; these chemical shifts are within the expected ranges.[234] The carbon atoms in the aliphatic side-chains resonate from 10–40 ppm. In both the ^{1}H and the ^{13}C spectrum the same order is noted for similar substituents.[261] The area dedicated to the methine carbons (90–100 ppm) contains signals that are closely spaced in alkyl- or vinyl-substituted compounds but are more spread out by β-substitution with other groups and in chlorins. In the aromatic and olefinic carbon region (130–170 ppm) the β-pyrrole carbons occur at a higher field and generally

without overlap with the α-carbon atoms. Again these two groups of resonances are closely spaced in alkyl-substituted porphyrins,[257,258,262] but are more expansive in less symmetrical substituted porphyrins and chlorins.

4.4 Tautomers in Porphyrins

NMR spectroscopy is of fundamental use in the investigation of porphyrin dynamic processes. Three particular groups of dynamic processes have been the subject of specialized detailed research; this comprises N-H tautomerism, rotational processes and macrocyclic inversion of nonplanar porphyrins.[228] N-H tautomerism is the longest and best known of the three and has been investigated in the most detail. Rotational processes of the porphyrin substituents have also received a lot of attention with many new processes being reported. The interactions of the substituent or ligand with the porphyrin macrocycle play a role in the activation energies for these processes and usually keep to predictable trends. Macrocyclic inversion was a recent addition to porphyrin dynamic processes, but only after the synthesis of porphyrins with highly nonplanar conformations.[228]

Tautomerism is defined as an intramolecular proton transfer route together with the migration of double bonds;[263] a dynamic process observed for all porphyrins. Typical free base porphyrins undergo rapid tautomerism at ordinary temperatures with the central hydrogen atoms exchanging between opposite pairs of central nitrogen atoms. This N-H tautomerism that occurs in porphyrins (Scheme 4.1) involves the shifting of highly conjugated double bond systems.[264,265,266,267] The switching between two tautomers is generally at such a fast rate, that only at very low temperatures is it possible to differentiate between the two tautomers spectroscopically.

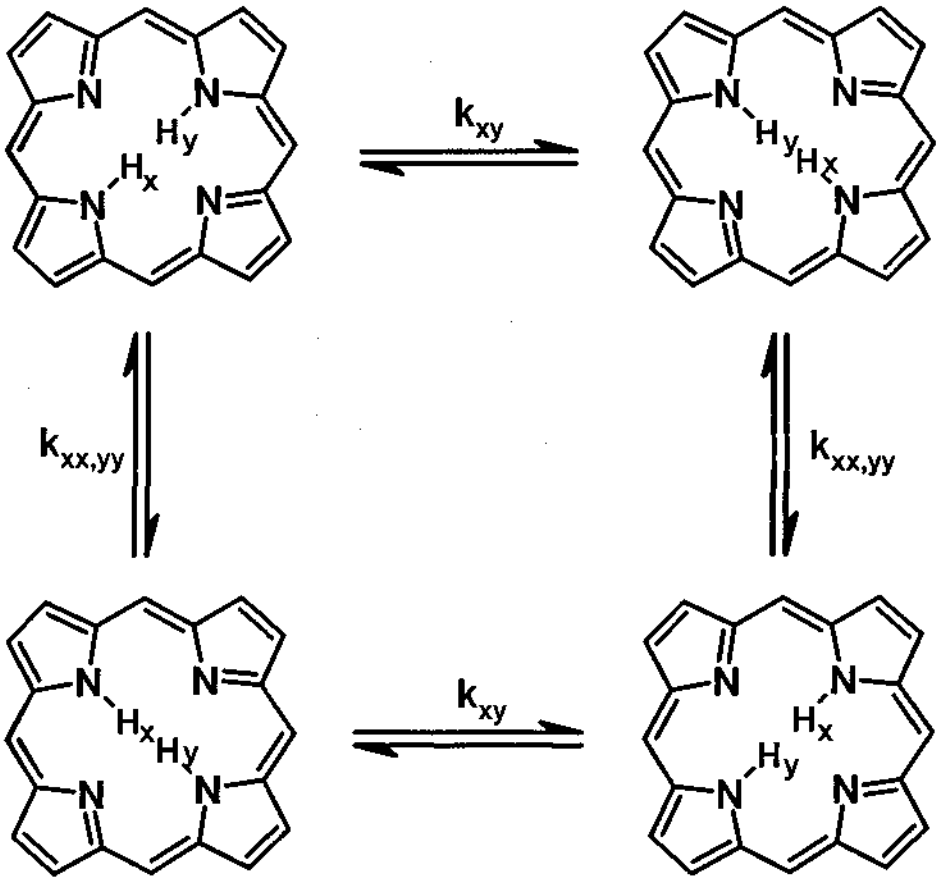

Scheme 4.1: N-H tautomerism in porphyrins.[263]

The existence of tautomers in porphyrins is not a new idea, free base porphyrins have been found to have a number of tautomers for some time now. This observable factor was first noted by Becker *et al.*[268] in 1961, when he used tautomerism to explain the magnetic equivalence of the methyl groups in H_2(Copro-I), even at low temperatures. This idea was again used in 1966 by Abraham and co-workers[269] to elucidate the methine signals in H_2(Copro-II).

Detailed studies of deuterium and tritium isotope effects on the rate of tautomerism were done by Limbach and co-workers.[270,271] Depending on the temperature, large isotope effects of 10–500 were seen for the rate constant. With temperature, the rate constants increase sharply, but Arrhenius plots (logarithm of the rate constant versus inverse temperature) show curvature as if the apparent activation energy increases according to temperature. These characteristics are considered together to be a sign of quantum mechanical tunnelling.[272]

During tautomerism among the four core nitrogen atoms in a porphyrin each tautomer has a similar stability and exists in the equilibrium; however, this would not be the case for N-confused porphyrins.[273] The early work carried out on N-H tautomerism focused on the measurement of activation energies in solution. There is an almost unvarying activation energy of about 50 kJ mol^{-1} in solution and solid state related to the tautomerism process; though, it may vary significantly with regard to structural changes to the porphyrin macrocycle.[228]

Early quantum chemical investigations considered whether each central proton in a free base porphyrin ring was attached to one nitrogen atom or bridged over two adjacent nitrogen atoms. In 1936 Robertson published an X-ray structure of phthalocyanine in which the central protons seemed to be bound equally to two nitrogen atoms.[274] However, Corwin and co-workers reasoned that, if the N-H system was equally bridged then a substantial difference in the absorption spectra would be expected in the case of etioporphyrin free base and N-methyl etioporphyrin.[275,276] But this is not so as the spectra were quite similar; this therefore supported the idea of normal localized N-H bonds.

Storm *et al.*[252] were the first to show the non-equivalence of neighbouring pyrrole rings as a result of slow N-H exchange; at low temperature they showed two resolved lines for the β-protons in H_2TPP. At a temperature of –53 °C the signals for H_2TPP combine and when the inner protons are substituted by deuterium the tautomerism shows an exceptionally high kinetic isotope effect.[252] Variable-temperature NMR studies, including ^{1}H, ^{13}C, and ^{15}N, were used to illustrate two distinct pyrrole rings; these corresponded to N-protonated and N-unprotonated rings in symmetrically substituted porphyrins at low temperatures.[264,266,267] When the temperature was increased, peaks started to coalesce consistent with fast tautomerism on the NMR time scale.[272] Showing two different central nitrogen atoms of a free base porphyrin proves each hydrogen is attached to one nitrogen because the central nitrogens would all be equivalent for the bridging structure. This was also shown with the use of X-ray photoelectron spectroscopy.[277]

From more recent X-ray studies the determined bond lengths of free base porphyrins correlate better to a structure where the two hydrogen atoms at the centre of the macrocycle are bonded to the opposite nitrogen atoms.[4] From the infrared spectra of a range of porphyrins, haems, and related compounds, it seems that the N-H groups are involved in considerable intramolecular hydrogen bonding.[278] The most stable form found from further infrared data and orbital overlap calculations[279] also seems to be when the porphyrin has two like opposite nitrogen atoms.

Using an NMR study at low-temperature,[252] it was possible to detect the two tautomers (with hydrogen atoms opposite and next-to each other). The less symmetrical form is expected to be less stable due to the breach of one hydrogen's van der Waals sphere by the other hydrogen.[4] Thereafter the rate of tautomerism was also determined[280] at three different temperatures for *meso*-tetraphenylporphyrin and for its N,N'-dideutero derivative. The kinetic parameters accompanied by the kinetic isotope effect show the process to be two-step. Some of the resonances in the ^{13}C NMR spectra of metal-free porphyrins show line broadening in deuterated chloroform solution; this has been attributed to N-H tautomerism (due to the spectra of the *N*-deuterated species) rather than possible ^{14}N quadrapole affects.[258,280]

The type of migration of the two central protons of the porphyrin was another important issue examined. In particular, whether this proton transfer occurs via the *cis*-intermediate (asynchronous mechanism) in a successive migration or concerned a simultaneous two hydrogen shift (synchronous mechanism).[228] The tautomerization mechanism by which interconversion occurs has been the theme for many theoretical and NMR studies and initially there was uncertainty between theoreticians and experimentalists. However, they now agree that the migration occurs in a stepwise manner proceeding via transient *cis*-porphyrin intermediates which quickly tunnel to the *trans*-tautomers.[281,282,283,284] In 1972 Storm published a review on N-H tautomerism in porphyrins and chlorins[264] and again the following year.[252]

Irving and Lapidot[285] made use of ^{15}N NMR spectroscopy in 1977 to examine N-H tautomerism in labelled porphyrins. Intramolecular exchange rates were determined from the temperature dependence of the ^{15}N resonances between 215 K and 320 K; these authors found a mechanism involving two consecutive proton jumps to be

superior. Eaton and Eaton[265] came to the opposite conclusion in that same year when they used (VT) proton NMR spectroscopy and lineshape analysis. They obtained large values of k_H/k_D which they attributed to a two hydrogen simultaneous exchange. Further investigations were made by Gust and Roberts,[286] also in 1977, and by Hennig and Limbach[287] in 1979; but neither gave conclusive reports on the mechanism.

This tautomerism of the mobility of the two inner protons, between the four nitrogen atom sites, takes place both in liquid and solid state.[265] The process of tautomerism has long served as a prototype for double proton transfer reactions. Along with the understanding of this mechanism comes the understanding of the mechanism for inserting a metal into the porphyrin core.[288] The ground state of *trans*-porphyrin has been shown to have textbook or close-to-textbook D_{2h} symmetry. The optimization of *cis*-porphyrin also gave a perfectly planar geometry with the highest possible symmetry of C_{2v}. An estimate (MP2) in 1995, by Ghosh and Almlöf showed *cis*-porphyrin to be about 7.6 kcal/mol higher in energy than the *trans*-tautomer. The difference between the two structures is mainly in the internal bond angles of the central $C_{12}N_4$ ring.[289] The transition state of monodeprotonated porphine was then calculated in 1997 by Vangberg and Ghosh to be approximately 11.84 kcal/mol above the ground state. Deformation of the porphyrin framework was seen during proton transfer and the internal angles underwent maximum changes.[288]

There is an interest in tautomeric systems and the process not only as a prototype of double proton migration but also due to their biological relevance, the mechanism involved, and the involvement of quantum mechanical tunnelling.[272] This interest also extends to their potential to function as memory-storage devices,[290] and porphyrin tautomers have already been used in photo-chemical hole burning.[291] Understanding the functioning of the core porphyrin protons might in future also find relevance in computational studies on the mechanism of the complexing of the free base porphyrins by the metal ion.[272]

Surprisingly, small tautomerism rate constants for a selection of porphyrins were reported by Asakawa *et al.*[263] They were assessed by using N-H line-shape analysis of variable-temperature dynamic ^{1}H NMR. This study showed that appropriate

adaptation of the *meso*-position group in free base *meso*-mono-substituted octaethylporphyrins can, surprisingly, lower the rate of tautomerism due to considerable improvement in each tautomer's kinetic stability. Recent studies have been performed using a range of modern NMR techniques. Much of the experimental evidence being contributions from Limbach and co-workers in the mid 1990s,[270,271,265,292] who interpreted and proved an asynchronous mechanism. Hydrogen tunnelling is also believed to contribute, which is significant at low temperatures and leads to nonlinear Arrhenius behaviour.[228]

4.5 Objectives

The aims of this work were to:

(1) fully characterize all synthesized porphyrins using ^{1}H and ^{13}C NMR spectroscopy (and where necessary DEPT and 2D spectra: COSY and HSQC);
(2) obtain the shielding tensors for each atom in each of the six porphyrins from calculations using DFT methods;
(3) compare these theoretical shifts to the experimental values; and
(4) make a comparison of the results to relevant literature.

4.6 Results and Discussion

4.6.1 Introductory remarks

The chemical shifts of hydrogen or carbon nuclei that are in similar bonding situations can be grouped together into characteristic regions. Accordingly, it is possible for conclusions to be reached about the structure of a molecule using the signal position.[226] This is then also true for the reverse, as in our case, where we have six porphyrins with similar characteristics; we expect that many of the signals for each porphyrin will be in similar regions of the spectra or at least correlate to each other. Despite rather comprehensive knowledge of the relationship that exists between the chemical shift and the structure of a molecule, exact theoretical predictions are rarely possible. The signals of more than 95% of the protons in organic molecules are found

to be contained by the narrow range of 0 to 10 ppm. Definitive limits for individual groups cannot be given, and therefore these categories usually overlap.[226]

Slight disagreement between the literature data and our experimental data can often be the result of differences in concentration. These types of concentration effects on chemical shifts are well known for porphyrins. In general, solvent and concentration effects do not cause more than a few ppm differences in the chemical shifts; on condition that there is no chemical interaction. Therefore results that are acquired in solvents such as benzene, carbon tetrachloride, chloroform or dichloromethane can be used in direct comparison with those of neat ligands. This is a fortunate situation due to the range and, in some cases, the unknown conditions under which some literature measurements have been made.[293]

As an example, we can look at the commonly discussed *meso*-tetraarylporphyrin, H_2TPP. In this system, the pyrrole protons experience more shielding than those in the benzoid rings.[294] For metal complexes of H_2TPP the pyrrole β-protons usually give a singlet peak between 9.05 and 9.20 ppm and the *meso*-phenyl group protons resonate in the region 7.8–8.4 ppm. Attached axial ligands will give peaks at a higher field in the region 1.5 to 6 ppm due to their location in the macrocycle's shielding zone.[230,295] In metallated complexes the chemical shift of the β-proton of the pyrrole in the porphyrin ring may be affected by the shielding cone to a small degree. However, these protons are usually positioned in the plane of the porphyrin and thus are more likely to be affected by the electron density donation and withdrawal that takes place to the metal (from electron rich and electron poor axial ligands, respectively). In the case of the carbon low temperature spectrum the *meso*-carbon signal of H_2TPP is at 119.5 ppm.[228]

Porphyrins exhibit both ^3J- and ^4J-couplings; ^3J-couplings between their β-pyrrole protons and small ^4J-couplings between the β-pyrrole and central nitrogen protons ("w-couplings").[228] The proton-proton coupling constants for attached substituents are generally similar to those seen in isolated substituent fragments and are therefore not particularly significant.[228]

The carbon signals that are seen for the α- and β-pyrrole carbon atoms can be related back to the signals that are seen for the unsubstituted (free) pyrrole molecules. These values for pyrrole are typically: 118.4 ppm (α-C) and 108.0 ppm (β-C).[221] The order of the α-C and β-C resonances is the same for the final porphyrin, although both the chemical resonances are shifted much further downfield. The assignment of the carbon signals to particular carbon atoms for each of the porphyrin molecules can be quite tricky, especially for the quaternary carbon atoms of the porphyrin core. Furthermore, N-H tautomerism in free base porphyrins at room temperature induces exchange broadening of the pyrrole signals. This can have quite a large effect on the signals and in some cases prevent the pyrrole carbon signals from being observed, particularly the α-carbon signals.[228] There have been suggestions to try and avoid these problems in free base porphyrins of exchange broadening and aggregation by evaluating carbon spectra for the zinc complexes with a disaggregating ligand such as pyrrolidine.[296]

4.6.2 Results and assignment

NMR of H_2T(iBu)P (Porphyrin 1)

The ^{1}H NMR spectrum for this porphyrin (Figure 4.4) is expected to have four different signals relating to the *meso*-substituents. This includes one chemical shift for the C-H group, one chemical shift for the CH_2 group and two signals for the two CH_3 groups. This is because each of the CH_3 groups lies in a unique molecular environment; their signals are found at 2.358 ppm (doublet) and 1.029 ppm (triplet). The CH_3 on the ethyl group is the signal at the "lower" ppm (upfield) because it is more shielded from the porphyrin ring and this can also be seen from its multiplicity. In the proton NMR spectrum the main signal for the C-H group is found at 5.052 ppm (sextet), and for the CH_2 group, a multiplet in the region of 2.729–2.808 ppm.

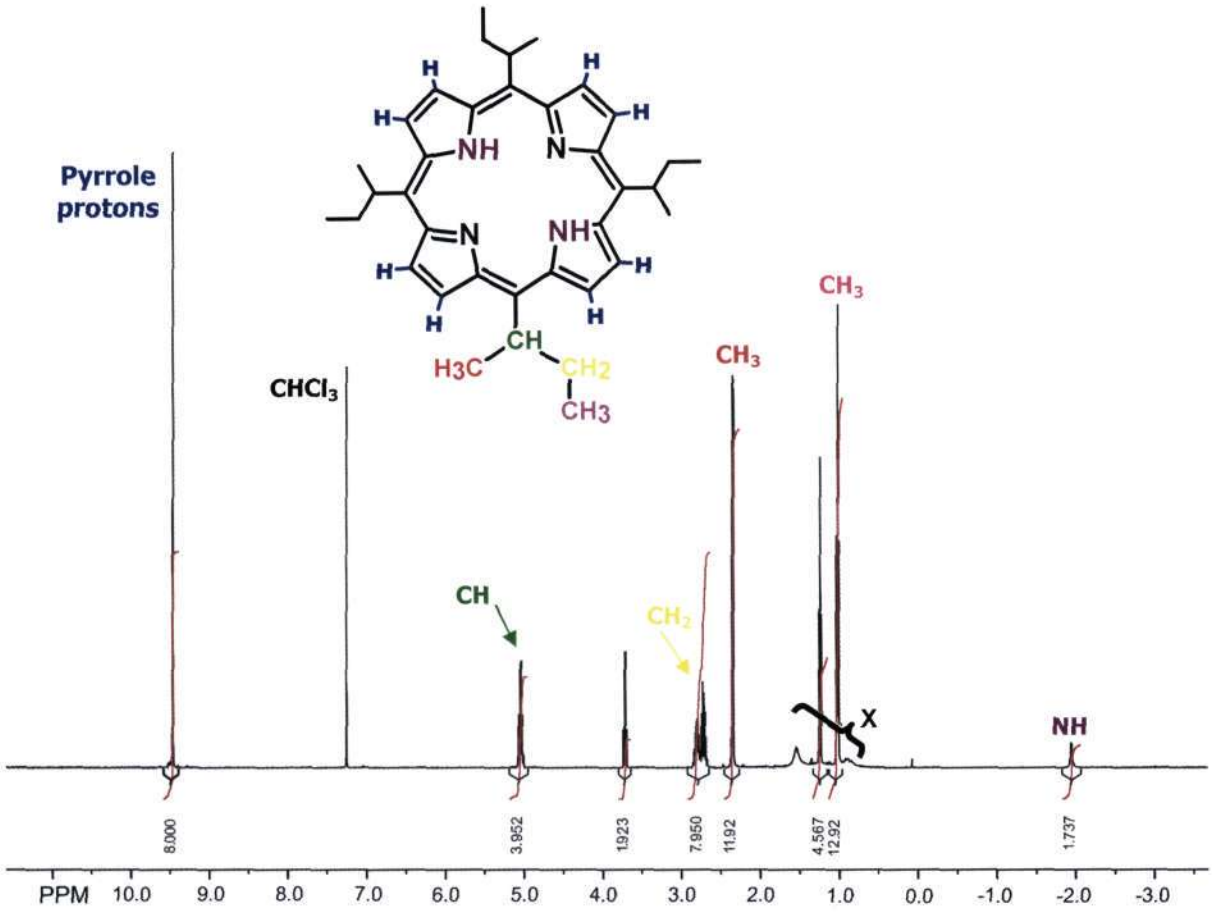

Figure 4.4: Assignment of the ^{1}H NMR spectrum of H_2T(iBu)P.

There are, however, two more signals to assign, one at 1.256 ppm (triplet) and the other at 3.724 ppm (quartet). They correlate to C-H/CH_3 and CH_2 groups, respectively, when assigned using the 2D DEPT and HSQC data. According to their chemical shifts, integrals and multiplicities they do not correspond to any porphyrin C-H/CH_3 and CH_2 groups. However, the chemical shifts of these two peaks (as well as their multiplicities) may correspond to those of ethanol (which was present as a catalyst in the reaction). In this spectrum impurities between 1 and 2 ppm are labelled X. The pyrrole protons and the protons on the centre nitrogen atoms give resonances in the expected high and low chemical shift regions due to the deshielding and shielding of the ring current, respectively. These values are 9.471 ppm and –1.937 ppm.

For the carbon NMR spectrum (Figure 4.5) it is a similar situation, with the main signal for the C-H group at 42.76 ppm and the CH_2 group at 35.42 ppm. Two subsequent signals are seen at 18.43 and 58.48 ppm for a C-H/CH_3 and a CH_2 group, respectively. Using the 2D spectra to assign these signals showed that these two

extra resonances correlated with the two extra resonances in the proton NMR spectrum. The signals for the carbon atoms of the centre macrocycle (α -, β - and *meso*-carbon atoms) were all clearly visible in the anticipated range of 120–150 ppm, at chemical shifts of 144.69, 128.96 and 122.71 ppm, respectively.

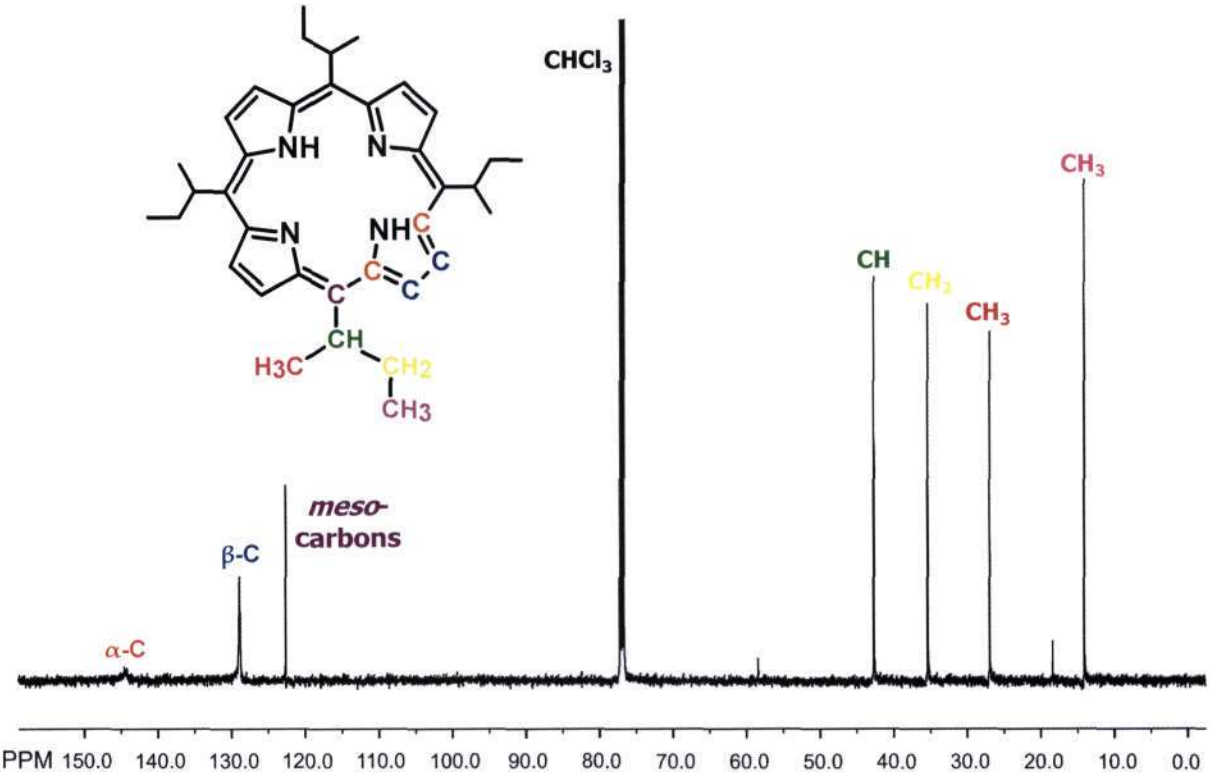

Figure 4.5: Assignment of the ^{13}C NMR spectrum of $H_2T(iBu)P$.

Further proton and carbon NMR spectra were obtained for the starting material, 2-methylbutyraldehyde, to determine whether these extra signals were possibly unreacted staring material. The starting material proton spectrum (Figure 4.6) clearly showed the presence of double signals in the spectrum for each of the C-H, CH_2 and one of the CH_3 groups. This splitting of the signals into two sets is due to the mixture of the R and S chiral centres present in this racemic starting material. These two sets are, however, very close to each other and are not separated by any other signals. They also look very similar to each other and have similar intensities, unlike the two extra signals found in the ^1H NMR spectrum of the porphyrin which have very different intensities, positions and appearances to the other signals present. The CH_3 groups, labelled *a* and *d*, are less affected by the chiral centre, and hence the splitting of the signals is substantially smaller. The two sets of signals for *a* can clearly be seen,

although closer than the other sets, and on enlarging the spectrum the two sets for *d* are also clearly resolved.

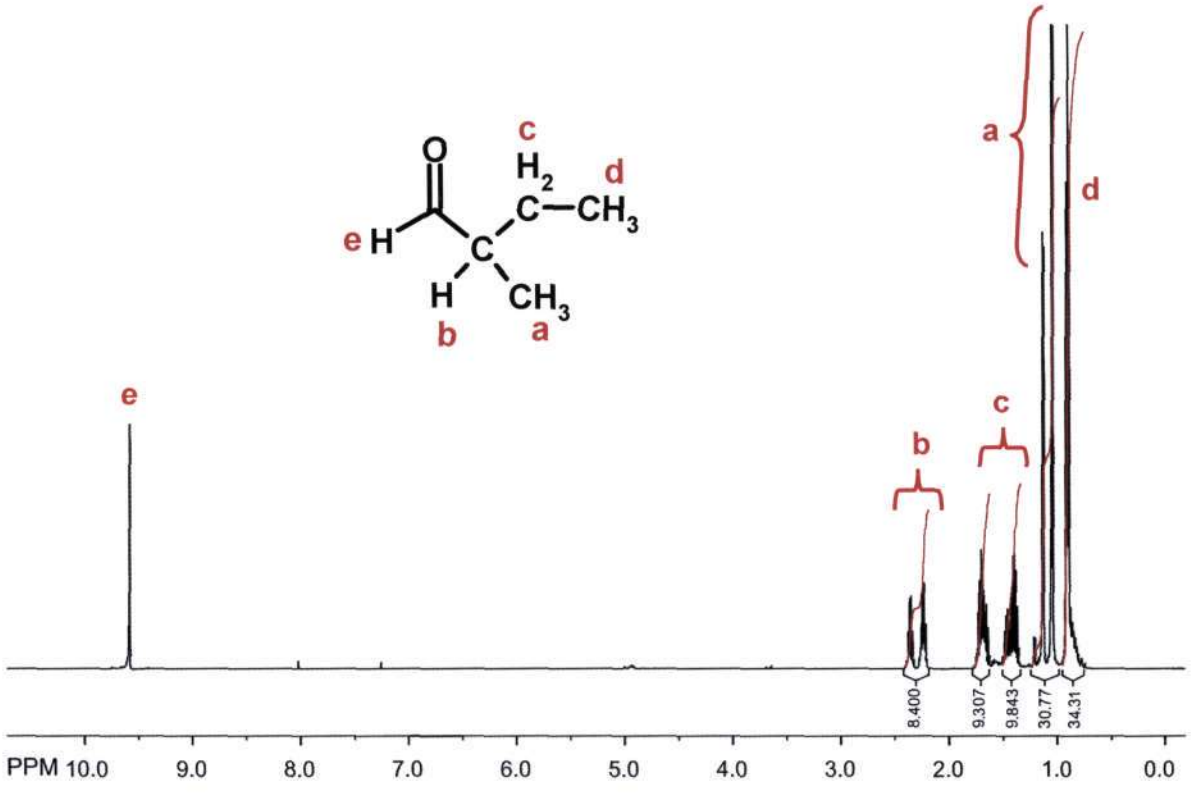

Figure 4.6: Assignment of the ^{1}H NMR spectrum of 2-methylbutyraldehyde.

When noting the exact resonance of each of these signals there is a definite shift between the starting material and the signals produced by the same proton groups in the final porphyrin molecule. These shifts are all downfield from the originals, and although some shifts are greater than the others, the order in which the signals appear stays the same. The signal for the CH_3 group, labelled *d*, shifts by less than 0.2 ppm; this is the smallest shift of all the signals. The CH_3 group, labelled *a*, shifts from 1.099 ppm in the starting material to 2.358 ppm in the porphyrin. The CH_2 shifts from 1.700 ppm to the range 2.729–2.808 ppm and the largest shift is seen for the C-H group by almost 3 ppm to 5.052 ppm, this is due to the attachment to the porphyrin ring now instead of the original aldehyde group. The C-H group of the *meso*-substituent also only gives one set of peaks rather than the two observed for the aldehyde. This may be due to the fact that it is no longer attached to the H-C=O group, but rather to the porphyrin ring which has no hydrogen atoms for splitting or coupling. The position of

the C-H group is likely to be close to or in the plane of the porphyrin macrocycle and hence will be deshielded. The shifts of these signals are all shown in Figure 4.7.

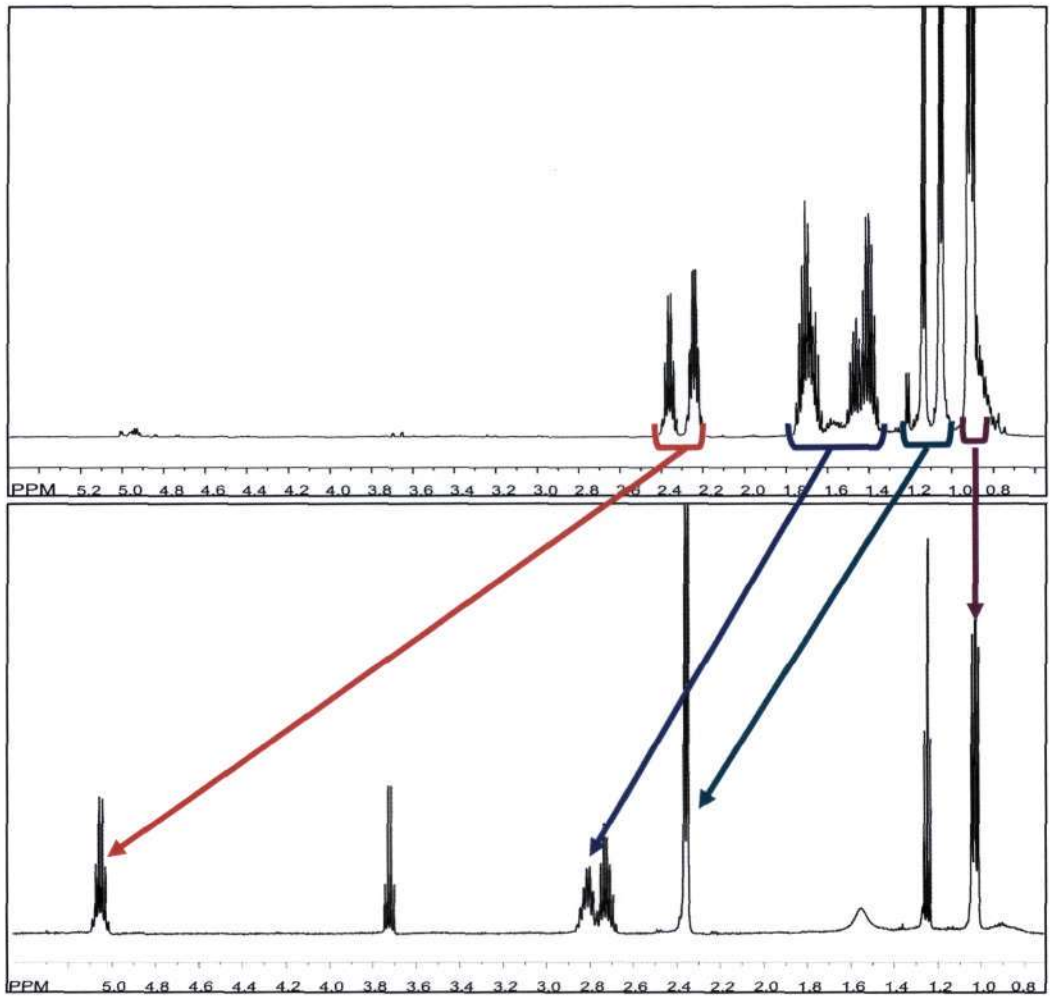

Figure 4.7: Illustration of the signal shifts from the starting material, 2-methylbutyraldehyde (top), to the subsequent porphyrin, $H_2T(iBu)P$ (bottom).

NMR of $H_2T(CH_2Ph)P$ (Porphyrin 2)

The ^1H NMR spectrum (Figure 4.8) for this porphyrin, $H_2T(CH_2Ph)P$, also contains impurities in the region 1–2 ppm; the region labelled X is ascribed to these impurities. At about 3.7 ppm the spectrum shows a broad unknown peak as well; however, this is of negligible intensity. On enlarging the spectra this broad band was also seen in the other porphyrin spectra. According to the 2D COSY spectrum these signals only correlate with each other and there is no sign of correlation to any of the porphyrin signals, consistent with the presence of a minor non-porphyrin contaminant. It must,

however, also be noted that these impurities seem to correlate with those already observed in the spectrum for $H_2T(iBu)P$ (and subsequently all the other ^1H NMR spectra presented here).

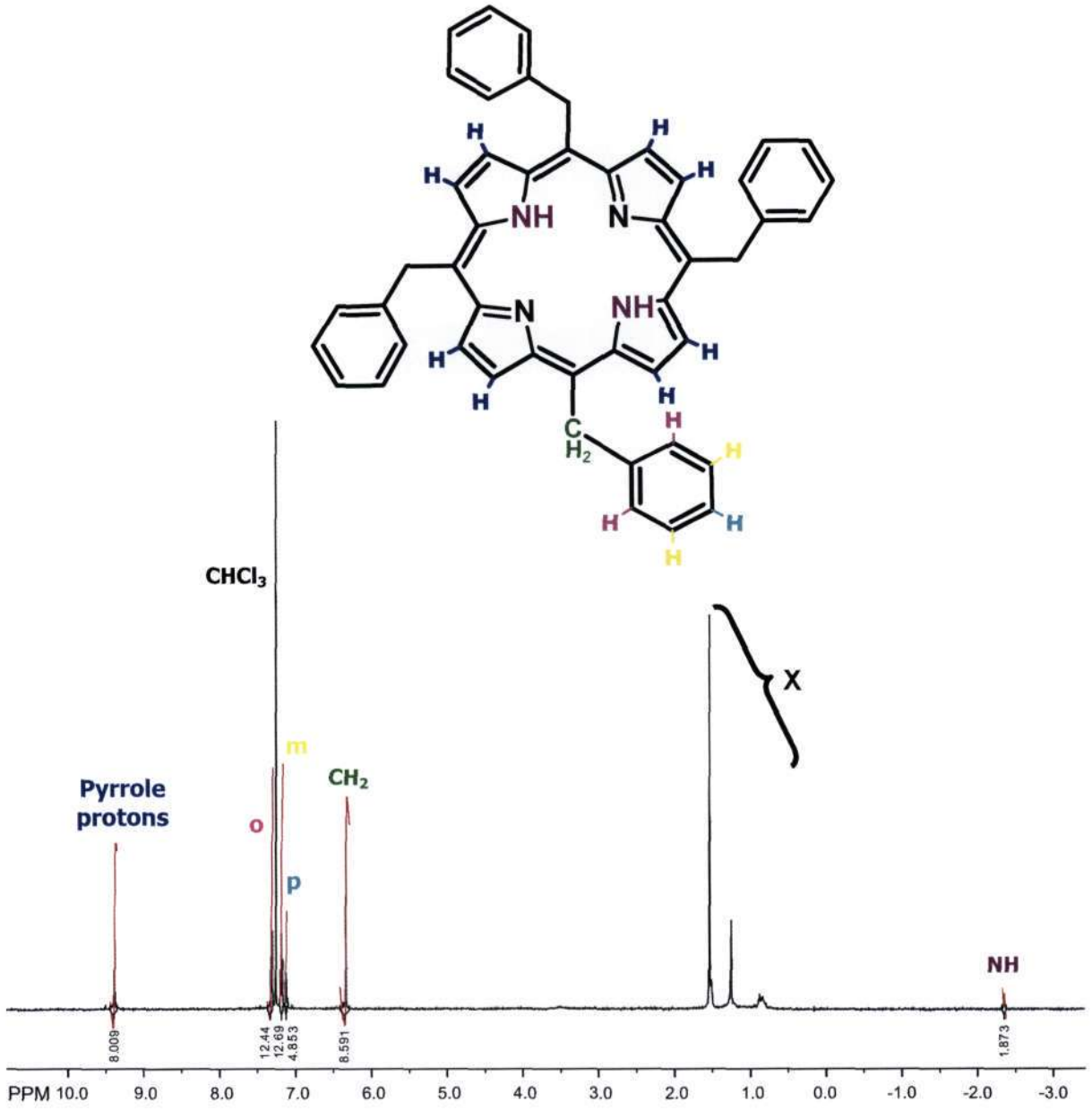

Figure 4.8: The assignment of the ^1H NMR spectrum of $H_2T(CH_2Ph)P$.

The spectrum once again shows the protons on the macrocycle in the expected ranges; pyrrole protons at 9.386 ppm and the N-H protons at –2.343 ppm. The aromatic region is between 7 and 7.5 ppm and this can clearly be divided into three different signals, with one representing each of the ortho-, meta- and para-positions for the benzene rings. On enlarging this region (Figure 4.9) one doublet and two

triplets are evident; their integrals are ~ 9, 8 and 3, respectively. The para-position will have the smallest integral and is expected to be a triplet, thus the triplet with an integral of 3 at 7.120 ppm may be assigned to this proton. Both the ortho- and meta-positions are expected to have an integral of 8, thus this corresponds to the remaining two signals. The difference here is, however, that the meta-position will be a triplet, like the para-position, but the ortho-position will only be a doublet. Thus the ortho- and meta-protons can be assigned to the chemical shifts of 7.315 and 7.188 ppm, respectively.

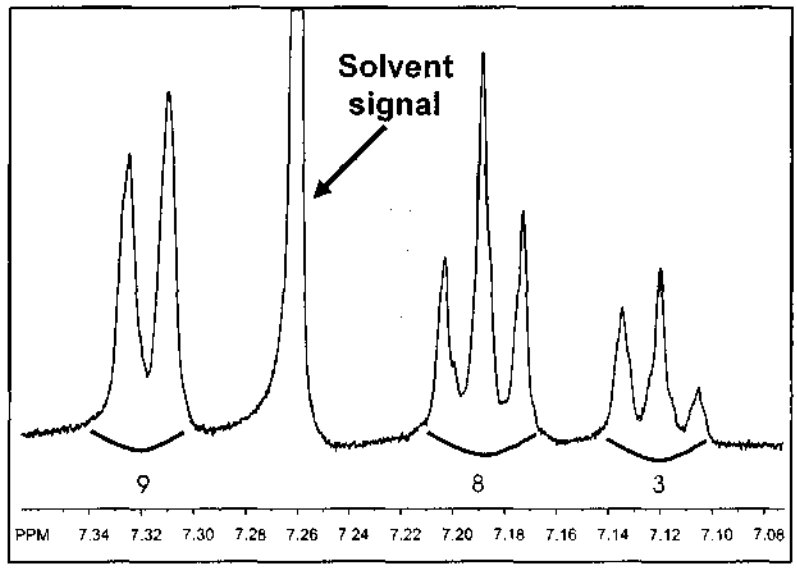

Figure 4.9: The phenyl ring signals enlarged with integrals.

There is a large downfield shift in the CH_2 group's signal for this particular porphyrin to 6.342 ppm. This means that the CH_2 group has been largely deshielded by comparison to the expected region (~ 2–3 ppm) for an average CH_2 group. This can be attributed to the two ring currents in this porphyrin. One produced by the porphyrin macrocycle and another by the phenyl ring of the *meso*-substituent. The CH_2 group is situated directly between them in the deshielding region of both currents. Thus it will experience deshielding effects from both the ring currents causing a large downfield shift in the expected resonance position.

The carbon spectrum for porphyrin 2 (Figure 4.10) was mostly very easy to assign using the 2D HSQC spectrum. The positions of the aromatic carbons could easily be assigned again. Although the ortho- and para-positions were found to overlap, an

enlargement of the signal clearly showed two separate peaks. There was no prominent signal found for the β-carbons in the expected 130 ppm region; however, when enlarging the para-signal a very small shoulder to the right of the base of the signal was present. It is possible that this may be the β-carbon signal. Otherwise it may also be obscured by the ortho- and para-carbon signals.

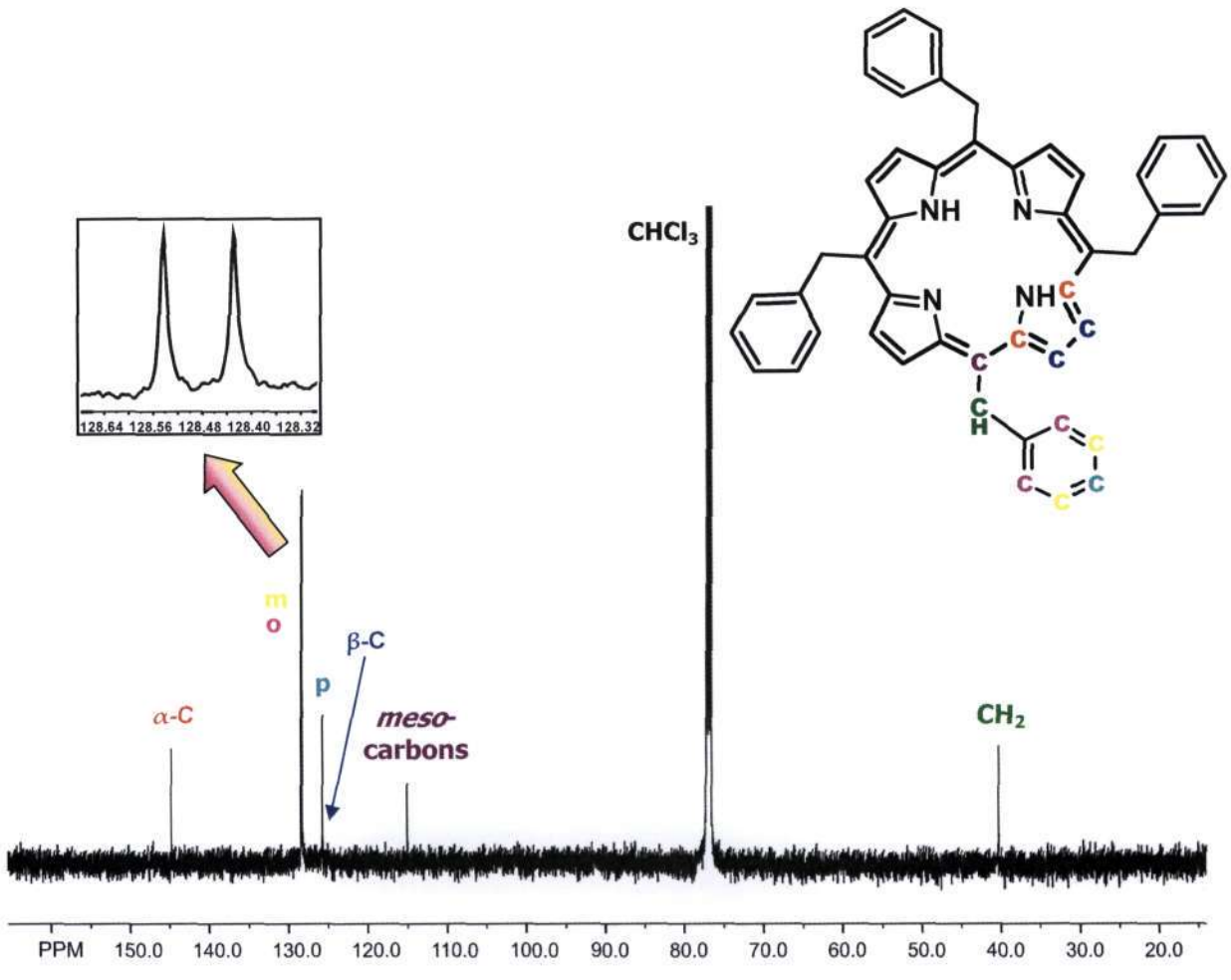

Figure 4.10: Assignment of the ^{13}C NMR spectrum of $H_2T(CH_2Ph)P$.

The two signals at 144.90 and 115.17 ppm do not have any correlation to signals in the proton spectrum according to the HSQC spectrum. Hence, due to their resonance values, they are assigned as the α- and *meso*-carbon resonances, respectively. The chemical shift for the first carbon of the phenyl ring also seems to be amiss, even when enlarging the spectrum, and thus the explanation can only be an overlap with the α-position carbon atoms as it would be expected in the region of about 140–145 ppm.

NMR of $H_2T(iPent)P$ (Porphyrin 3)

The assignment for the proton NMR for porphyrin 3 is shown below in Figure 4.11. Again there is the presence of the impurities labelled X around 1 and 2 ppm. The consistent signals for the protons on the macrocycle are found at 9.537 ppm (pyrrole protons) and –2.247 ppm (protons on the nitrogen atoms). The C-H and CH_3 groups are easily assigned to the multiplet at 4.888 ppm and the triplet at 1.002 ppm, respectively.

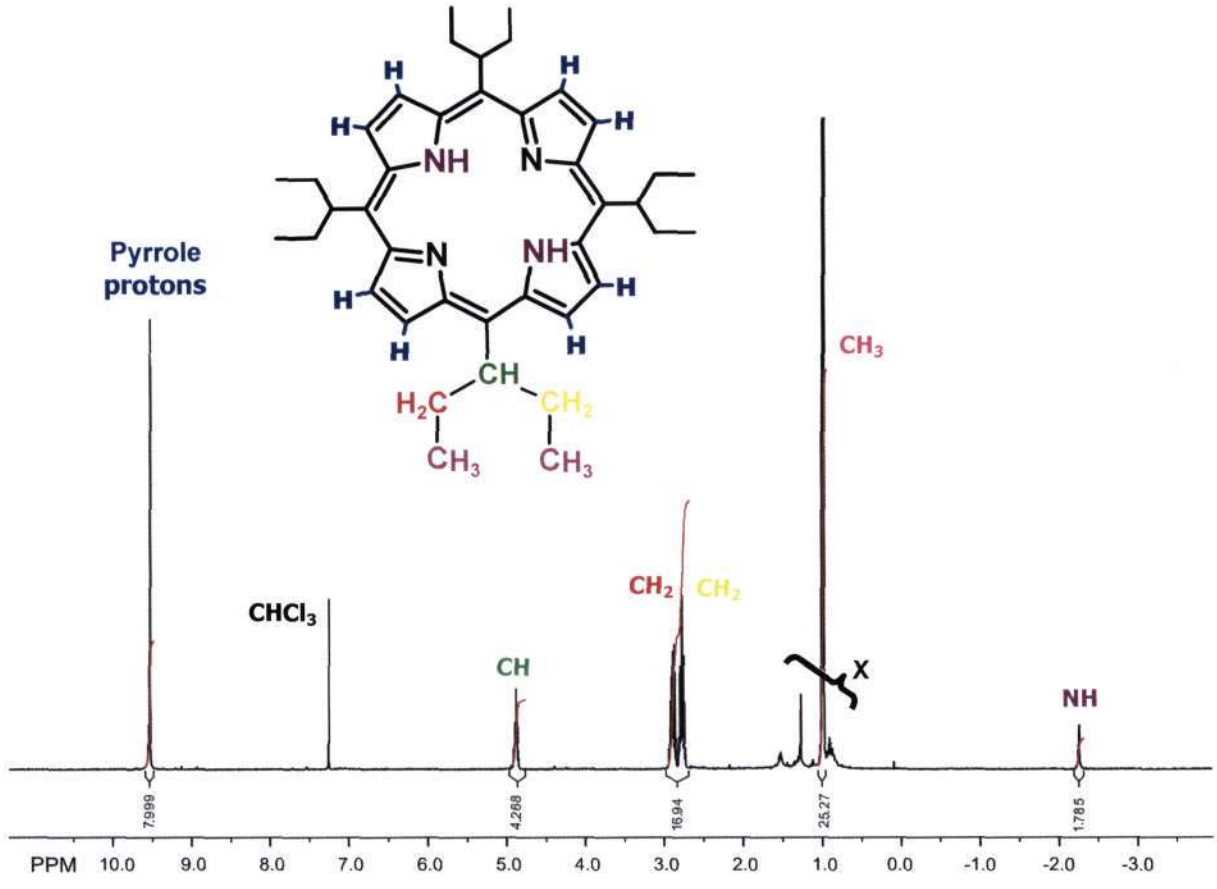

Figure 4.11: Assignment of the ^1H NMR spectrum of $H_2T(iPent)P$.

In the proton NMR spectrum for this porphyrin the CH_3 and CH_2 groups are expected to produce only one signal each due to the expected free rotation around the C_{meso}-C-H bond. This free rotation would result in the protons for each group being seen in the same environments and thus they can be considered equivalent. This seems to be the case for the CH_3 groups; however, not for the CH_2 groups. Instead, for the two CH_2 groups a set of closely spaced identical signals is evident and an enlarged spectrum shows them to be multiplets (possibly septets). It is possible that the porphyrin is still

in the slow exchange limit for rotation of the isopentyl groups at room temperature and thus further temperature dependant NMR studies were performed to check this. Specifically, these studies were done in order to determine if these two signals would coalesce into one, and if so, at what temperature region this would occur.

The starting temperatures chosen for this study were 25 °C and 100 °C. At first glance the two new spectra obtained looked very similar to that of Figure 4.11. However, on closer investigation it was noted that although there were still two sets of signals for these CH_2 groups there was a difference in their coupling constants. Enlargements of these signals at both temperatures are shown in Figure 4.12; there are differences in the separation and positions of these peaks. At the lower temperature the frequency separation between the two closest signals is 10.902 Hz and at the higher temperature it is 7.975 Hz. Therefore, with an increase in temperature, the signals start to move closer together. Between the furthest signals at lower temperature the frequency separation is 83.109 Hz and 80.269 Hz at higher temperature. In the two separate multiplets, a narrowing of the line widths is also evident. The increase in temperature also causes a slight downfield shift for this set of signals. At 25 °C the signal starts at about 4.01 ppm and ends at about 4.18 ppm, but at 100 °C, it starts around 4.05 ppm and ends at 4.22 ppm. Based on these observations, it is possible that on further increase of the temperature, these two signals will finally converge.

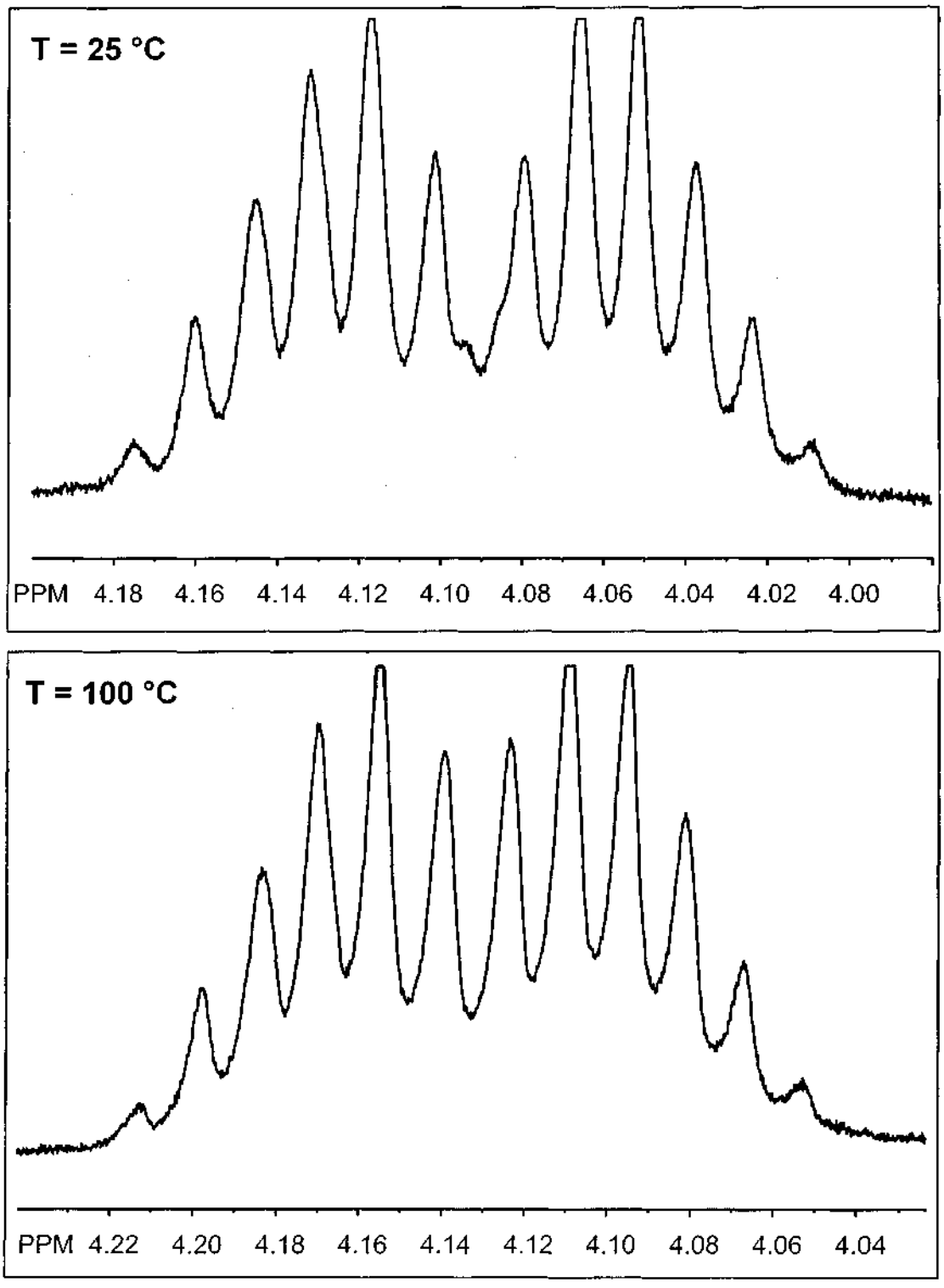

Figure 4.12: The two sets of ^{1}H NMR signals for the CH_2 groups of $H_2T(iPent)P$ at 25 °C (top) and 100 °C (bottom).

Two possible explanations for the data exist. (1) The isopentyl groups have a rotational barrier greater then ca. 30 kcal/mol such that free rotation is not observed even at 100 °C. (2) The two sets of multiplets are due to two distinct porphyrin

conformers that are in slow exchange, even at 100 °C. These might be, for example, planar and ruffled or ruffled and saddled forms. One significant observation is that the relative intensities of the two multiplets do not noticeably change with temperature. This would be expected for conformational switching between ruffled and planar or ruffled and saddled conformers.

If, on the other hand, we have an exchange equilibrium between inverted ruffled (or inverted saddled) conformers,

$$\text{ruf} \underset{}{\overset{k_{inv}}{\rightleftharpoons}} \text{ruf}^*$$

where ruf* is the inverted conformation of ruf, then a 1 :1 ratio of the two conformers will always be present, consistent with equivalent signal intensities for the two conformers. Coalescence of the multiplets will only occur if the barrier to inversion is surmountable in the temperature range that is studied. Coalescence of the signals would then reflect fast interconversion between the conformers on the NMR timescale such that we observe a signal from the average of the two conformations.

If the isopentyl group does not freely rotate, then CH_2 and CH_2' are in different magnetic fields and chemical environments and therefore this would explain their different chemical shifts. The rotations around the C-H–CH_2 bond would average out the CH_3 site differences for the two CH_3 groups and this would result in the same chemical shift. This is seen in the ^1H spectrum (Figure 4.11). These rotations would, however, not affect the CH_2 groups to any large extent. The literature reference for this porphyrin[58] shows very similar results to those obtained here, with a multiplet for the CH_2 group over the range of 2.72–2.98 ppm. As seen in Figure 4.13 the ^{13}C NMR spectrum showed no splitting of the CH_2 signal due to dynamic processes.

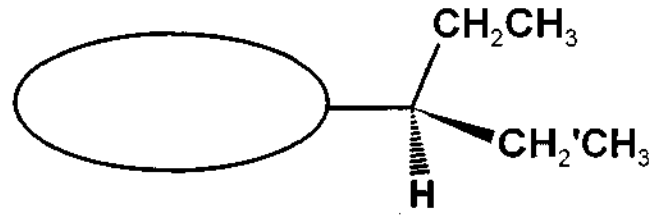

The carbon NMR spectrum for $H_2T(iPent)P$ (Porphyrin 3) has simple signals of good intensity that are considerably well-separated. The spectrum shows an unexpected and low intensity peak at about 30 ppm which, according to the DEPT spectrum, is a CH_2. In the HSQC spectrum there is correlation of this signal to part of the impurities clearly seen in the proton NMR, labelled X, and thus it is not of importance to us. The rest of the spectrum is easily assigned from the HSQC. The assignment of the C-H, CH_2 and CH_3 groups correlates well with the DEPT spectrum. The region from 116 to 148 ppm is expanded to give an enhanced view of the signals and therefore to allow for exact assignment of the alpha- beta- and *meso*-carbon atom chemical shifts. The COSY spectrum shows the expected correlation between the CH_2 and CH_3 groups and between the C-H and CH_2 groups.

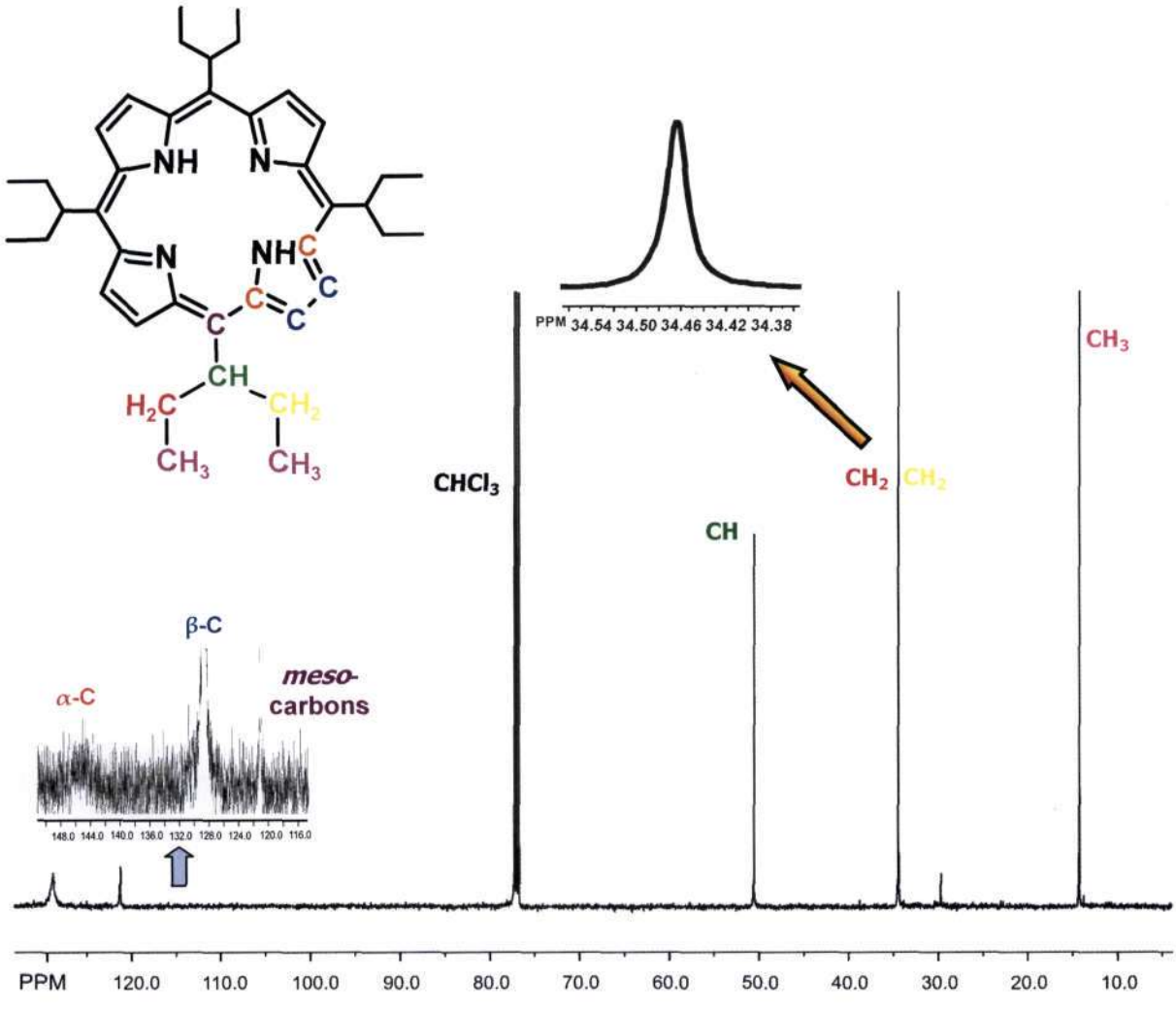

Figure 4.13: Assignment of the ^{13}C NMR spectrum of $H_2T(iPent)P$ (Porphyrin 3).

NMR of $H_2T(CHPh_2)P$ (Porphyrin 4)

This porphyrin was by far the most difficult to assign. Not only was it the most difficult to purify, but the two phenyl rings at each *meso*-position introduced significant steric bulk and an asymmetric conformation, which in turn gave numerous peaks in both the ^1H and ^{13}C NMR spectra. This made assignment of individual peaks rather difficult; however, the best possible assignments consistent with the experimental data are presented below.

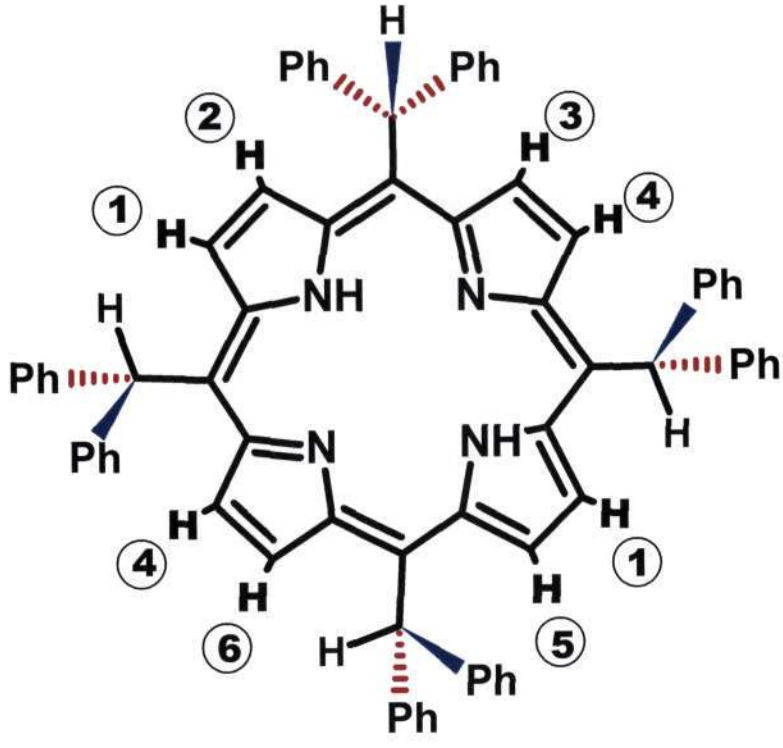

Figure 4.14: The structure of $H_2T(CHPh_2)P$ showing the most probable *meso*-group orientations.

The basic structure with orientations of the four *meso*-substituents is shown in Figure 4.14 above. Three of the *meso*-substituents are expected to have the same conformation, with the phenyl rings on either side of the porphyrin macrocycle plane and the methine hydrogen in the plane of the macrocycle. The fourth substituent has its own conformation with both phenyl rings on one side of the plane of the porphyrin macrocycle and the methine hydrogen atom on the other side. From this we expect to see one set of peaks representing the proton and carbon atoms in the three similar *meso*-substituent groups and another set of peaks for the differently orientated group. The assignment of the proton spectrum is given in Figure 4.15.

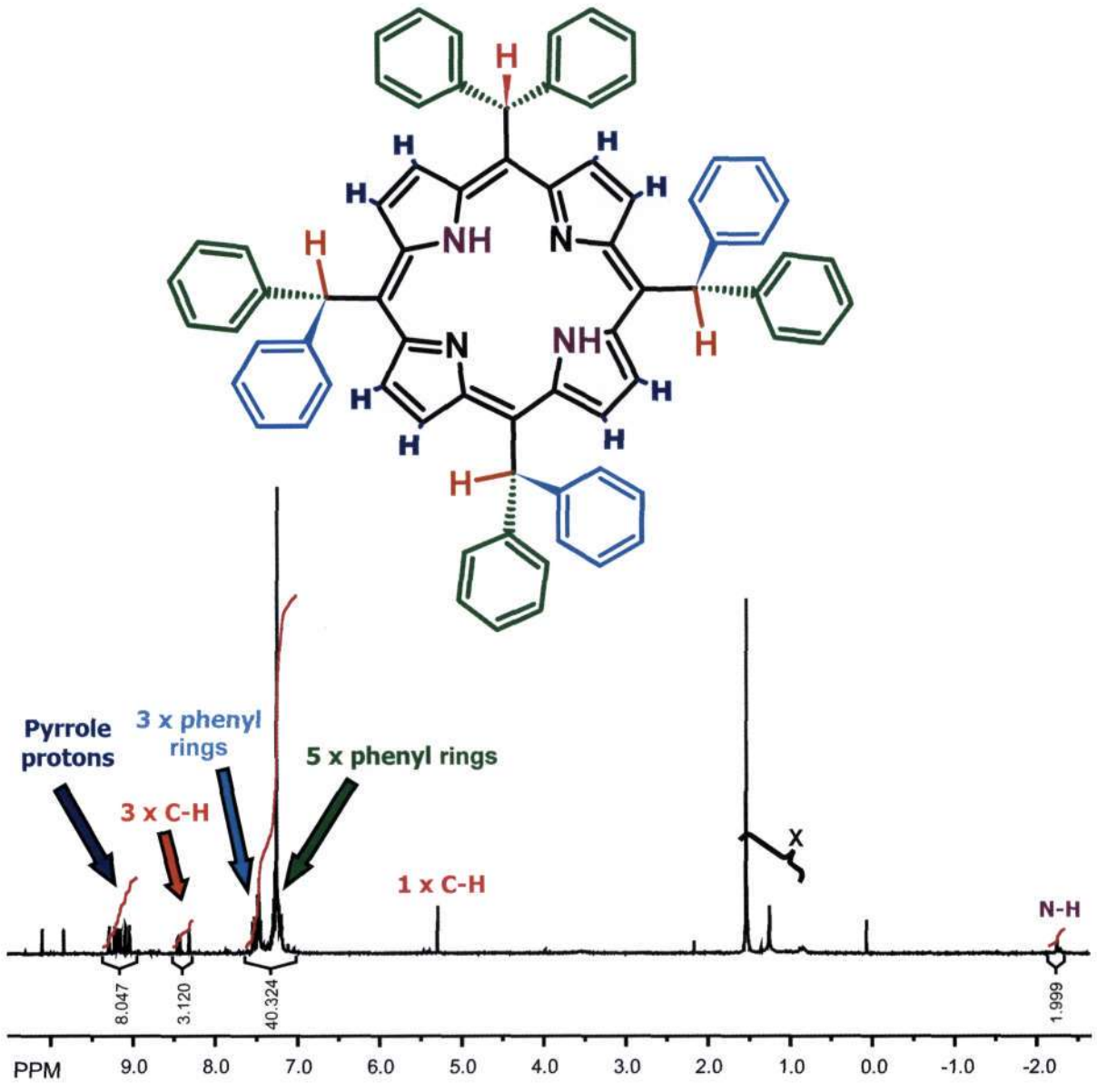

Figure 4.15: Attempted assignment of the 1H NMR spectrum of H2T(CHPh2)P.

The eight pyrrole protons are expected to resonate in the region at ~ 9 ppm, consistent with the other porphyrins in this work. However, when this region is enlarged only six doublets are visible (Figure 4.17 [a]). This can be explained if the assumption of fixed orientations of the *meso*-alkyl groups is made, as shown in Figure 4.14. (This assumption is not unreasonable considering the steric bulk of the *meso*-substituents.) There are four hydrogen atoms in their own distinct environments (2, 3, 5 and 6) due to their positions relative to the different *meso*-substituents. However, the pyrrole protons on opposite protonated or nonprotonated pyrrole groups orientated on either side of a pseudo centre of inversion (located at the centre of the macrocycle) are in the same chemical environments and have magnetically equivalent partners (1

and 4). Therefore there are only six magnetically distinct pyrrole protons. This therefore accounts for the six doublets, two of which integrate with slightly more than the other four. The order of the peaks will depend on the relative shielding of each of the chemically unique pyrrole protons. Each signal has to be a doublet due to the spin coupling to the adjacent proton on each pyrrole ring. We therefore believe that these six doublets account for all eight of the pyrrole protons; this is also supported by the integration across the whole region giving a total value of around 8 (when the N-H protons have been assigned a value of 2).

The magnetic environments of the C-H groups in the four *meso*-substituents are different. The conformation shows three in-plane C-H groups and one out-of-plane C-H group. Thus two separate peaks are expected, one which integrates to 1 and another with an integration of 3. The in-plane C-H groups will be highly deshielded compared to the one that is situated out-of-plane because it penetrates the conic region; this is represented in Figure 4.16. The three in-plane protons resonate in the 8.4 ppm region and the lone out-of-plane proton is shielded by almost 3 ppm upfield to 5.299 ppm (the same region where this signal is seen for the C-H group in the other porphyrins in this series). Each of these signals will be a singlet because there are no neighbouring hydrogen atoms to cause spin coupling. This is depicted in Figure 4.17 [b] for the three signals of the similarly orientated groups. Integrals of around 1 (relevant to the 2 N-H protons) for each of the four signals, shows the number of protons for the C-H groups to be correct.

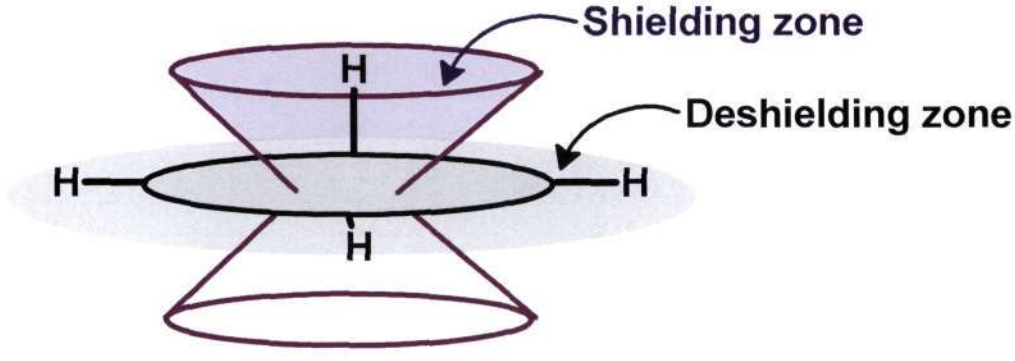

Figure 4.16: A schematic diagram of the porphyrin ring showing the deshielding and shielding of the three in-plane and one out-of-plane *meso*-substituent hydrogen atoms, respectively.

Assignment of the chemical resonances for the phenyl protons (found in the 7 ppm region) in the ^{1}H NMR spectrum was very difficult. This region has a doublet, a triplet and a multiplet (Figure 4.17 [c]) and although exact assignment of each peak is not possible, the region can be correctly allocated to the protons on the phenyl substituents. From the suspected conformation of the *meso*-substituents (Figure 4.14) there should be five phenyl rings on one side of the plane of the porphyrin macrocycle and three on the other side. Thus a ratio of 3:5 or integrations of 15 and 25 are expected, respectively. Integrating the area of the doublet and triplet together gives 13.61 (relative to 2 N-H protons). The multiplet is slightly more difficult to integrate because it also contains the solvent peak (CH_3Cl at 7.26 ppm); however, integrating in sections on either side results in 13.77 and 11.09. This then gives a total close to 25 and hence the 3:5 ratio between the two sets of peaks, as expected. This results in a total of about 40, which is also obtained when the whole section is integrated together. This value is correct for the five protons on each of the eight phenyl rings. Although this does still not help to fully resolve each signal, correct assignment of the whole region can at least be made.

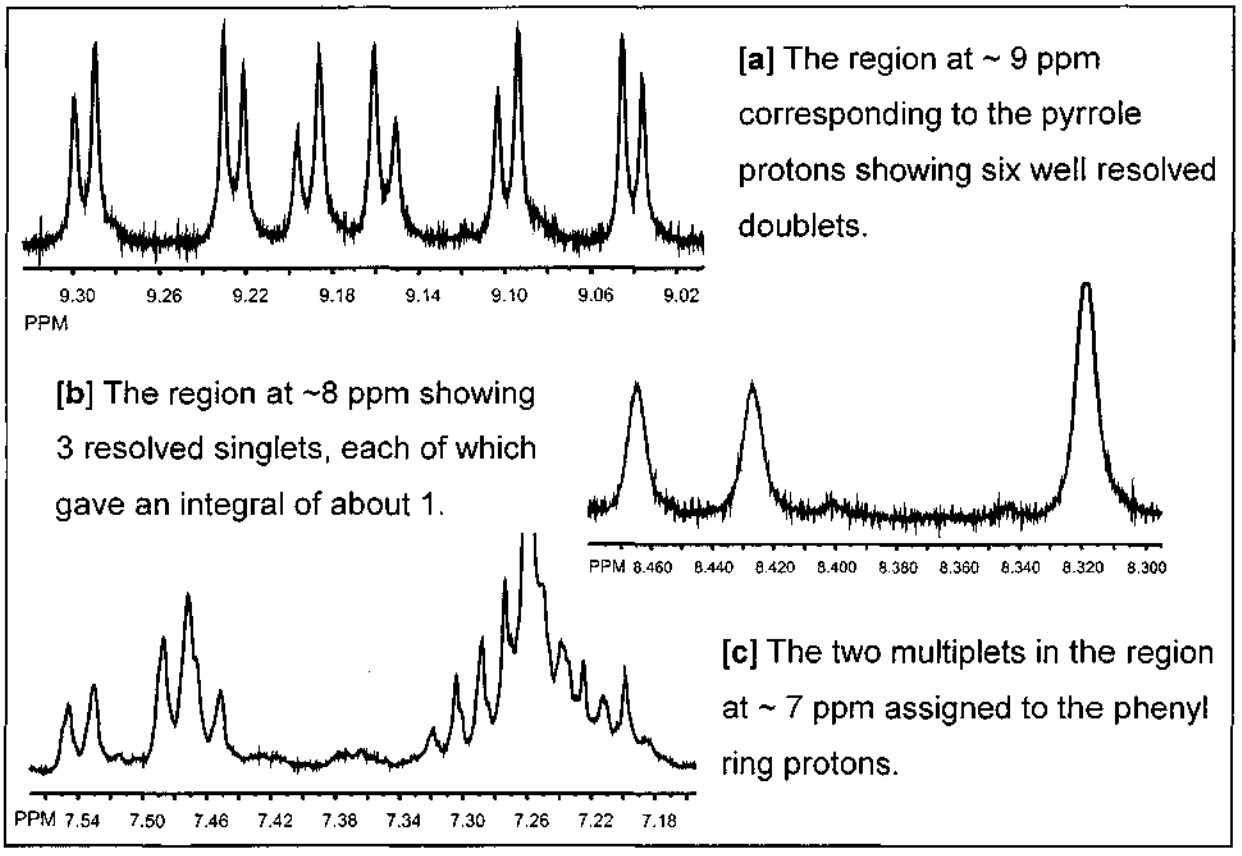

Figure 4.17: Expanded regions of the ^{1}H NMR spectrum of $H_2T(CHPh_2)P$.

The peak at –2.253 ppm, which is unquestionably assigned to the N-H protons due to its high upfield position, is in fact made up of two separate signals (–2.244 ppm and –2.284 ppm). This can be explained by the fact that there is no two-fold symmetry in the conformation of this porphyrin. Although the predicted conformation may not be as rigid as is shown in Figure 4.14, the idea of three similar (and one dissimilar) *meso*-substituents is correct according to the data. This would then rule out the possibility of any two-fold axis of symmetry. The minor peaks at 10.108, 9.845, 3.989, 2.173 and 0.073 ppm are all singlets and all give integral values of about 1 or less (when the N-H peak is assigned the value of 2) and therefore are assumed to be impurities. The spectrum also gives the same set of impurity peaks seen for each of the other porphyrins in the region 1 to 2 ppm, they are again assigned here as X.

The ^{13}C NMR spectrum was almost as difficult to assign (Figure 4.18). There are no simple regions with single peaks, which again reaffirms the idea of a low-symmetry conformation. The phenyl carbon signals will most likely hide the β-carbon signals, as was the case for Porphyrin 2 ($H_2T(CHPh_2)P$). In the upfield region of the spectrum there are only two prominent signal groups, one at ~ 26 ppm and the other at ~ 56 ppm. According to the HSQC, the signal at 26.70 ppm correlates to the peak at 1.206 ppm in the proton NMR spectrum (from the region labelled X) and is therefore assigned as an impurity. The three downfield signals at 57.28, 56.18 and 55.83 ppm (of which an enlarged section is shown in Figure 4.18) correlate to the singlet at 5.23 ppm and the three singlets at ~ 8 ppm in the proton NMR spectrum. Thus this region is assigned to the C-H group of the *meso*-substituent.

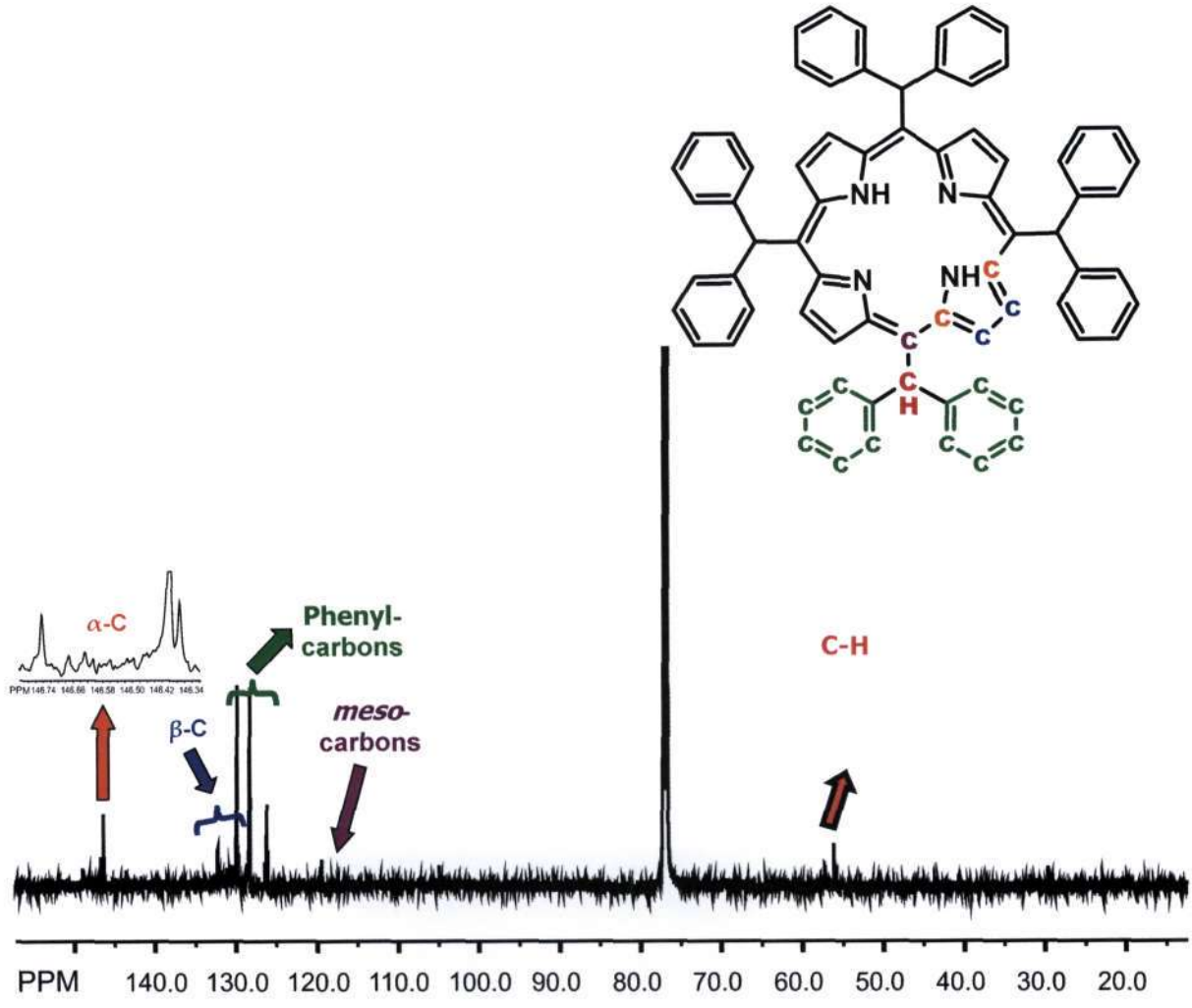

Figure 4.18: Attempted assignment of the ^{13}C NMR spectrum of $H_2T(CHPh_2)P$.

The set of most downfield signals in the carbon NMR spectrum show no correlation to any proton peaks in the HSQC. This is where the α-carbons have been found for the other porphyrins in this work. Thus this group of signals at ~ 146 ppm is assigned to the α-carbons. The *meso*-carbon signals, which will also show no correlation to any proton signals, are expected slightly upfield in the 120 ppm region, as has been found for the other porphyrins in this series. The signal region at 119.49 ppm is therefore assigned to the *meso*-carbons. The set of signals in the 130 ppm region cannot be unequivocally assigned. Correlation of the pyrrole protons in the HSQC spectrum was shown to be to the signals further downfield in this region, while the phenyl signals correlated with the upfield signals in this region. However, there was noticeable overlap and therefore exact assignment is not possible.

NMR of $H_2T(iPr)P$ (Porphyrin 5)

Assignment of the ^1H NMR spectrum of $H_2T(iPr)P$ was straightforward (Figure 4.19). The two CH_3 groups give a lone doublet signal around 2.3 ppm; this is expected due to them being equivalent protons. The C-H is a multiplet (as expected) which is shifted to the 5 ppm region, consistent with its situation in the deshielding zone of the porphyrin ring current. There is also a set of signals in the region 1–2 ppm, once again labelled X, which is assigned as impurities. The macrocycle protons present on the pyrrole rings and on the inner nitrogen atoms have chemical shifts of 9.466 ppm and –1.786 ppm, respectively.

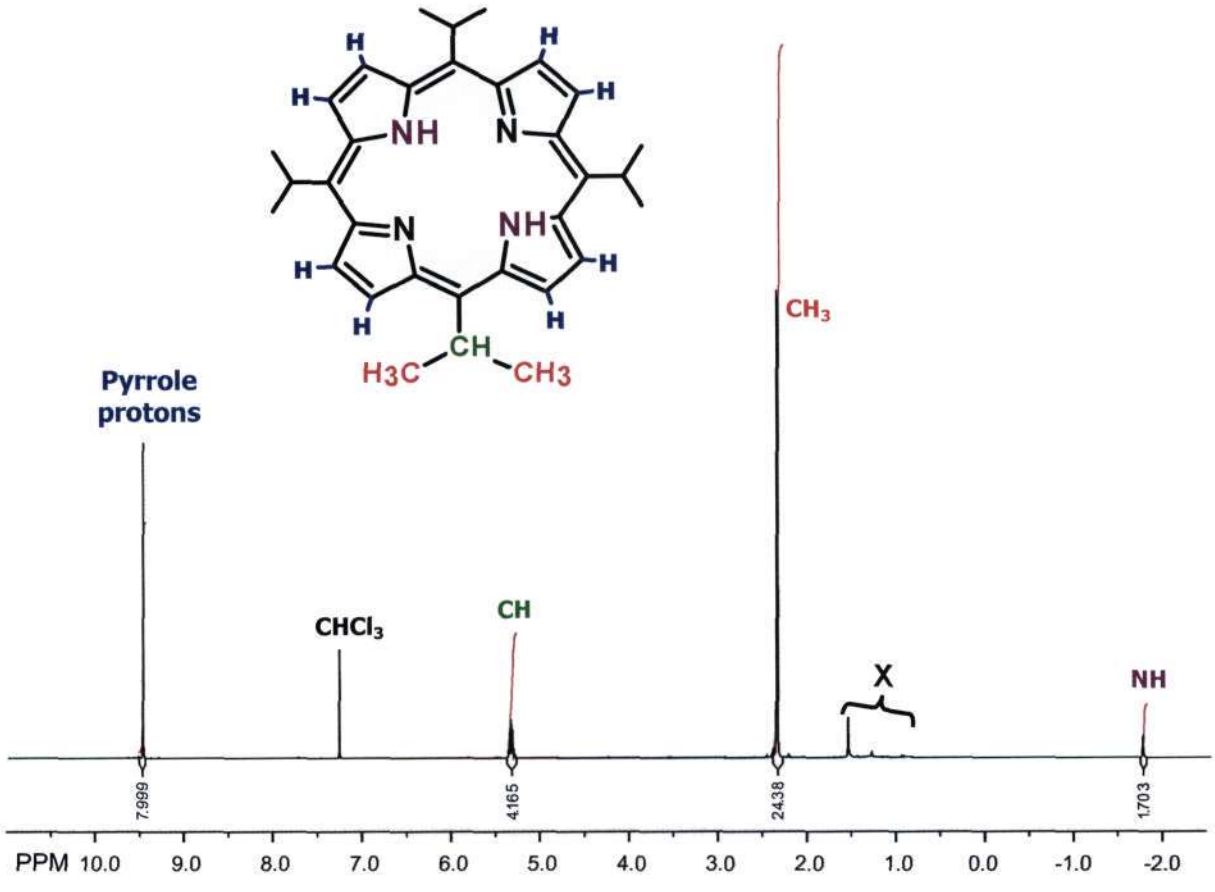

Figure 4.19: Assignment of the ^1H NMR spectrum of $H_2T(iPr)P$.

The ^{13}C NMR spectrum in Figure 4.20 was as simple as the ^1H NMR and therefore was easily assigned using the HSQC spectrum. The two CH_3 groups have one corresponding carbon signal for their single proton chemical shift and this is at 28.67 ppm. The signal for the C-H group is found at 35.20 ppm. The pyrrole β-carbon

atoms correspond to the signal at 129.02 ppm according to the HSQC spectrum. The two carbon signals with no protons that hence show no correspondence to the proton NMR, namely the *meso*- and α-pyrrole carbon atoms, give signals at 123.67 and 143.76 ppm, respectively. The COSY spectrum shows the expected correlation between the C-H and CH_3 groups, and also some correlation with the pyrrole protons on the β-carbons.

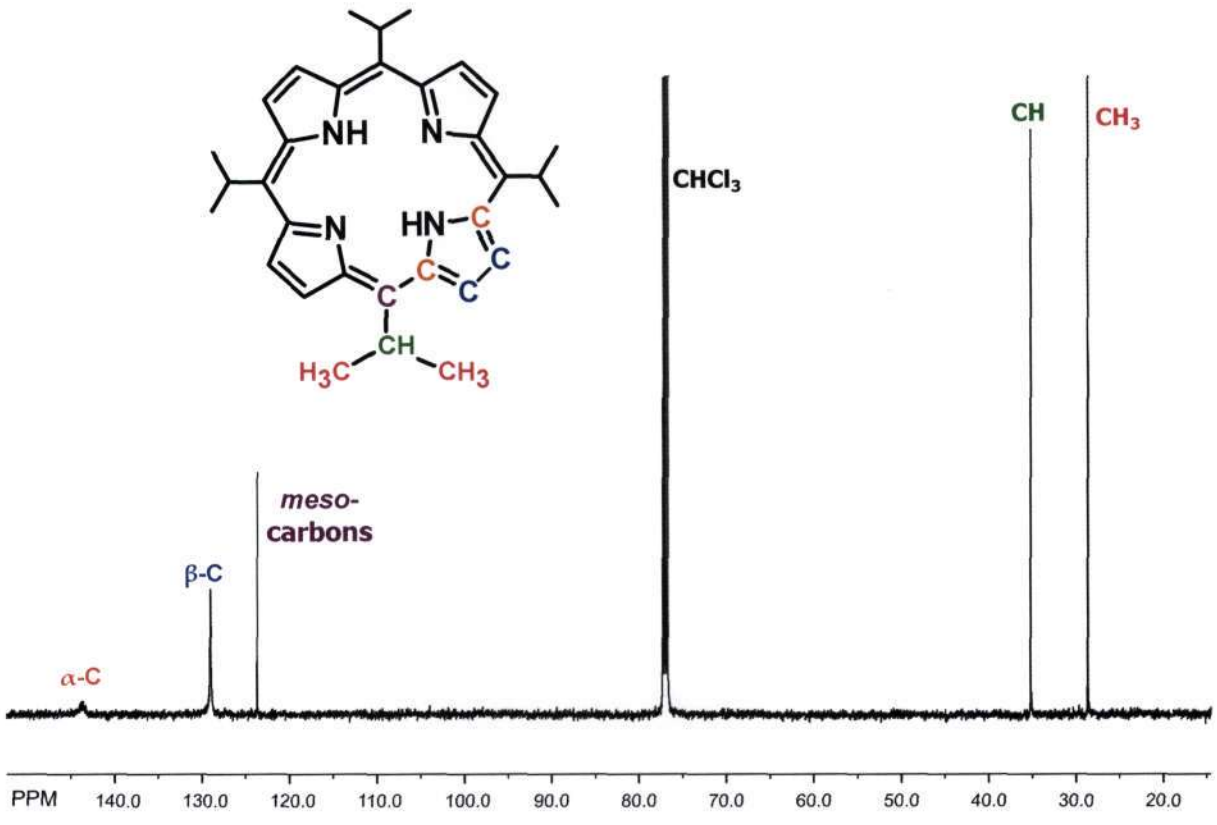

Figure 4.20: Assignment of the ^{13}C NMR spectrum of $H_2T(iPr)P$.

NMR of $H_2T(cyHx)P$ (Porphyrin 6)

Assignment of the spectra for porphyrin 6 was almost as complicated as it was for $H_2T(CHPh_2)P$ due to the chair conformation of the cyclohexane rings. This conformation caused unusual signals because, unlike a planar conformation, the opposite protons did not correlate. Veyrat *et al.*[195,215] have shown in previous syntheses of this porphyrin their NMR assignments for the cyclohexane rings. These NMR assignments were determined by employing the combination of 2D ^1H-^1H and ^{13}C-^1H correlation procedures along with temperature-dependent NMR spectroscopy.

Both the ^{1}H and ^{13}C NMR spectra are highly symmetric which is consistent with the fast averaging of equatorially bound cyclohexyl groups in a chair conformation. The possibility of the mean plane of the cyclohexyl substituents being coplanar with the porphyrin macrocycle is not likely due to the steric crowding that would occur between H_{2e} and H_{β}. Not much work has been dedicated to the free base porphyrin; however, the observed geometry for the Zn^{2+} complex of $H_2T(cyHx)P$ shows these planes to be approximately orthogonal. This then results in *gauche* conformations (±g, see below) of the C_{α}-C_{meso}-C_1-C_2 fragments being observed. Tiny rotations of the cyclohexyl groups off the strictly orthogonal orientation can successfully alleviate the repulsive interactions that will take place between hydrogen atoms that are in the axial positions on C_1 and the hydrogen atoms on the neighbouring β-carbons of the pyrrole ring.[215]

According to the assignment by Veyrat *et al.*, the resonances for each of the protons 2 and 2', 3 and 3' and for the pyrrole β-protons give a single peak at room temperature in both the ^{13}C and ^{1}H NMR spectra. On the NMR time scale in solution at room temperature this can imply fast rotation of the cyclohexyl groups and inversion of the nonplanar porphyrin. The H_1 proton gives a triplet of triplets signal and the two coupling constants give values that are in the anticipated range for axial-axial (J = 12.5 Hz) and axial-equatorial (J' = 3.4 Hz) interactions.[297] This is consistent with the equatorial bonding of the cyclohexyl substituents.[195,215]

The final assignments of the ^{1}H and ^{13}C NMR spectra for this porphyrin are given in Figures 4.21 and 4.22, respectively. The schematic view of $H_2T(cyHx)P$ has one cyclohexyl substituent expanded for better visibility of the atom labels and the stereochemistry of the cyclohexyl rings. In the proton spectra the pyrrole protons and the nitrogen protons can be easily distinguished at 9.470 and –1.605 ppm, respectively. The only other signal for which an immediate assignment can be made is that of the first C-H group on the cyclohexyl ring, which has a downfield signal at 4.765 ppm. The collection of signals between 1 ppm and 3.5 ppm are assigned as shown in the spectrum, according to the literature.[195,215]

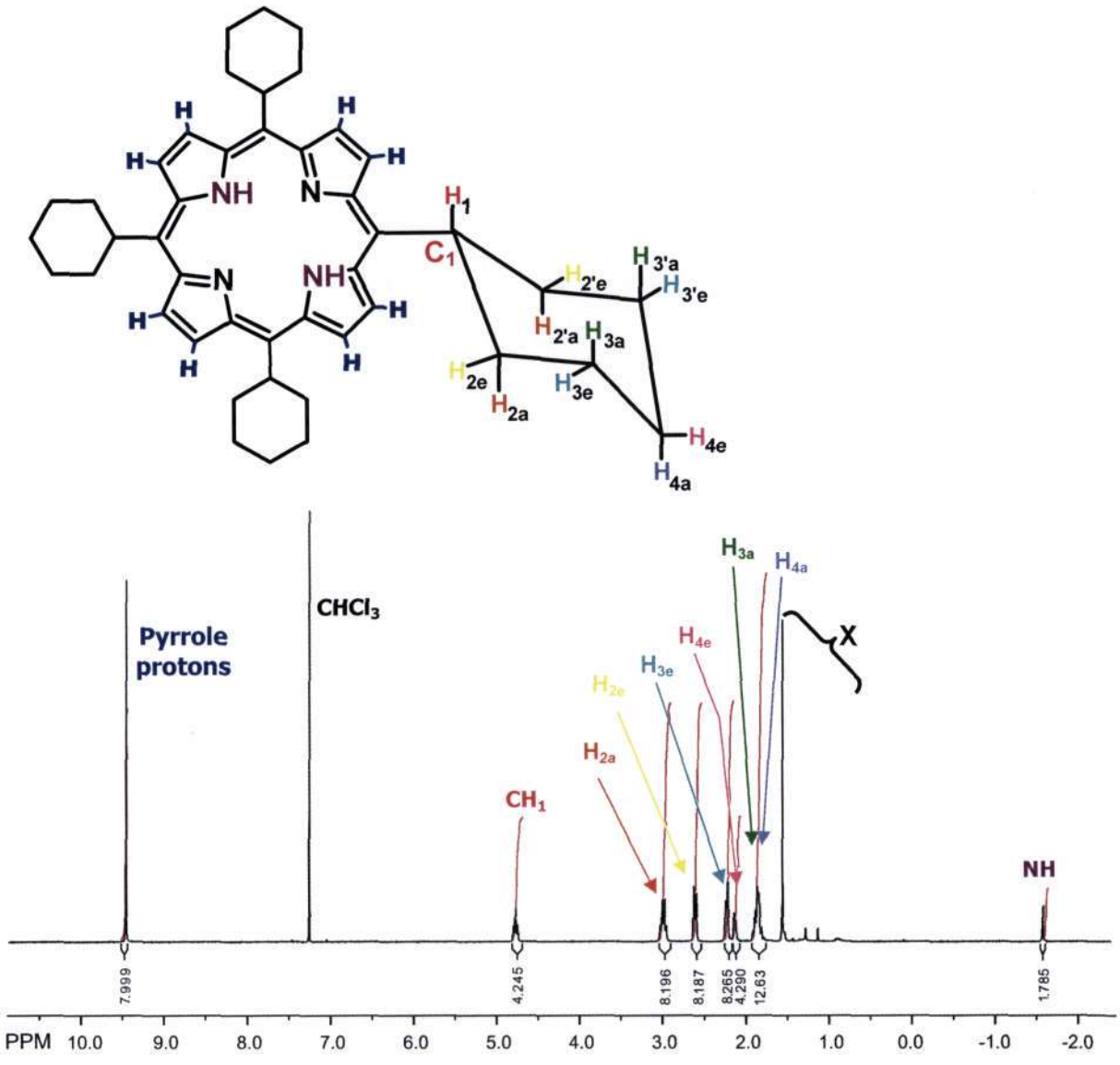

Figure 4.21: Assignment of the ^{1}H NMR spectrum of H_2T(cyHx)P.

In the carbon NMR spectrum, exact assignments for each of the carbon atoms in the cyclohexyl ring were possible using the literature and 2D spectra. The only C-H signal at 49.91 ppm was thus assigned to the carbon labelled 1 in the cyclohexyl ring. The three signals for the macrocycle carbons, the pyrrole alpha- and beta-carbons, and the *meso*-carbons were in the expected order in the range of 120–150 ppm. From the 2D HSQC spectrum it was possible to assign each of the CH_2 groups found by the DEPT spectrum in the region 20 to 40 ppm to either the ortho- meta- or para-positions around the ring.

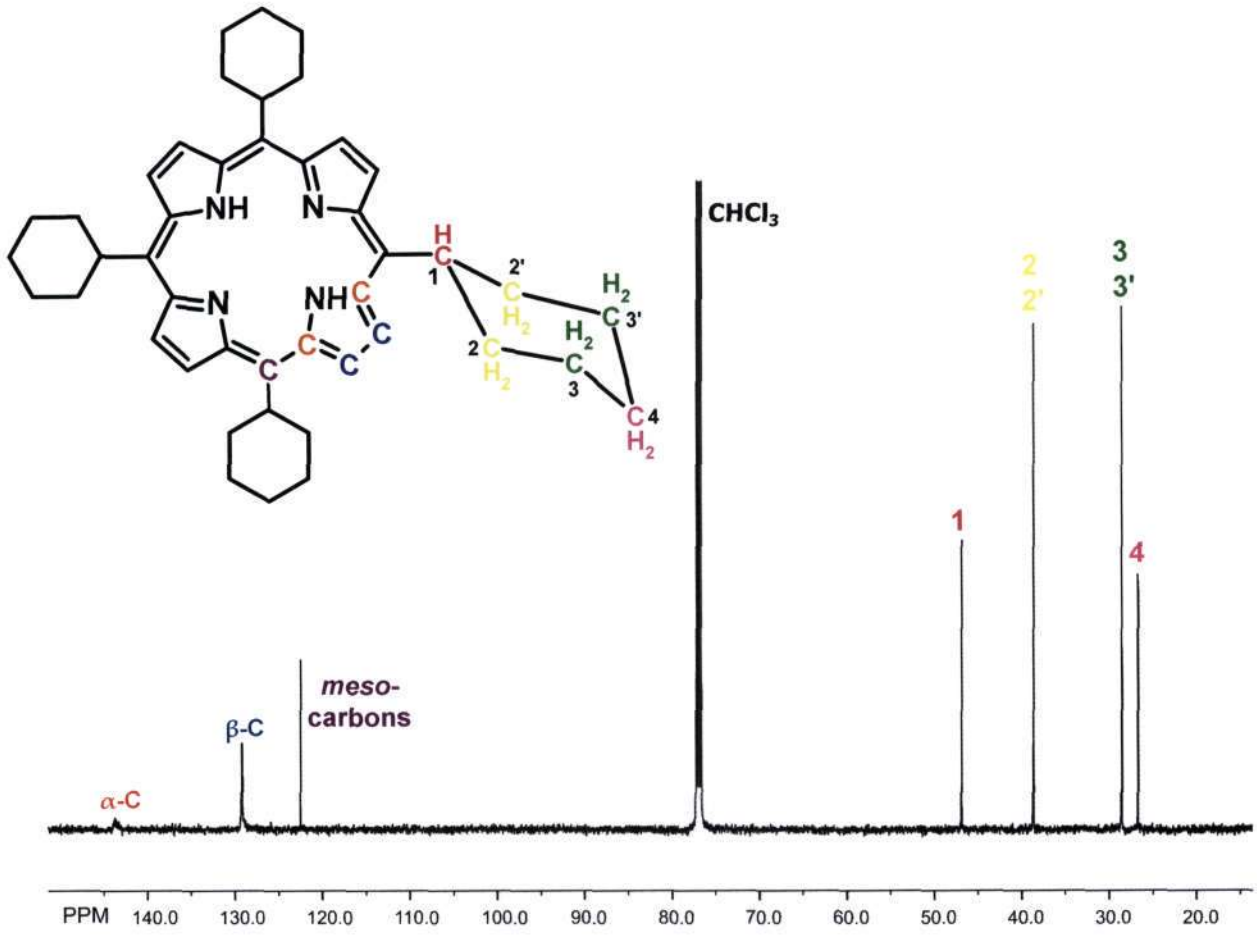

Figure 4.22: Assignment of the ^{13}C NMR spectrum of $H_2T(cyHx)P$.

4.6.3 Discussion

Impurities

Evidently, each of the synthesized porphyrins (1-6), exhibits some type of impurity around the region 1.0 ppm. The NMR samples were not always prepared from methods using the same solvent systems and thus it is difficult to try and assign these impurities to a particular solvent signal. However, Gottlieb *et al.*[298] show different solvent resonances and the one in specific that does seem to have a resonance that is consistent with these impurities is that of *n*-hexane in deuterated chloroform. It gives a signal for the CH_2 group as a multiplet resonating at 1.26 ppm and the CH_3 as a triplet at 0.88 ppm. Another that should also be noted is ethanol (particularly in the case of $H_2T(iBu)P$). Ethanol in deuterated chloroform will result in a triplet at 1.25 ppm (CH_3) and a quartet at 3.72 ppm (CH_2). (Ethanol was used as a co-catalyst in the porphyrin synthesis and is present as a stabilizer in the commercial grade chloroform used for

column chromatography.) Therefore it is possible that the upfield signal also exists in this region of 1–2 ppm.

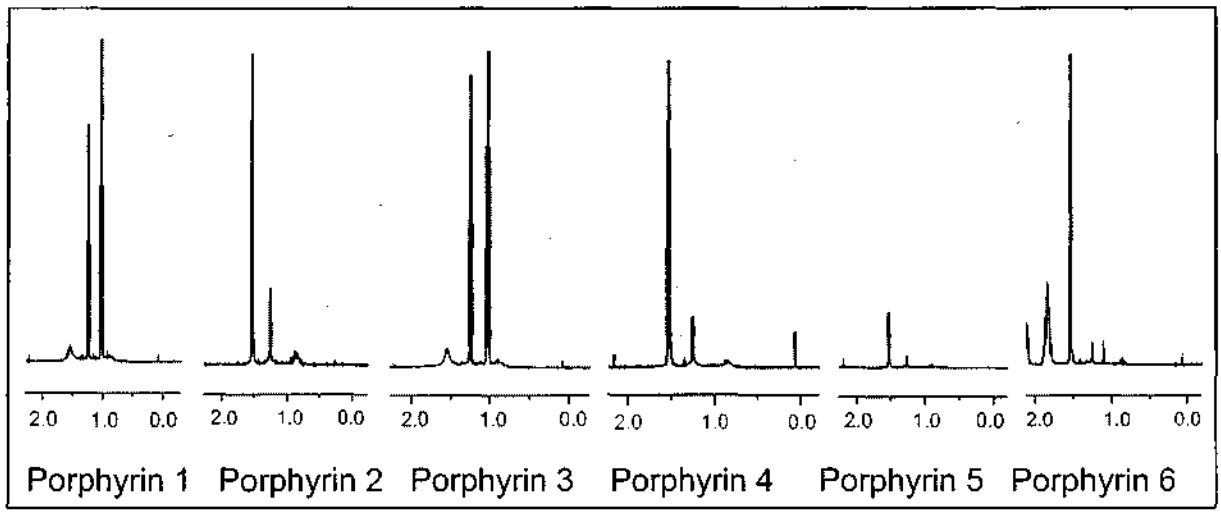

Figure 4.23: The 0.0–2.0 ppm region for each of the six porphyrins in this series.

The impurity signals in this region for each porphyrin are compared in Figure 4.23. Although the signals do not look exactly alike, and in some cases there are actual porphyrin signals within the same region (e.g. $H_2T(iBu)P$ and $H_2T(iPr)P$), they nonetheless all seem to be in a similar locale. In the 0.0–2.0 ppm sections of the six porphyrins, three signals at δ H ~ 0.8, 1.2 and 1.5 ppm are visible in almost each one. These signals sometimes have corresponding signals in the carbon spectrum in the region of about 20–40 ppm. The correlation in the HSQC spectrum shows in most of the spectra that the ~ 1.2 ppm signal in the ^1H spectrum corresponds to a signal at about 30 ppm in the ^{13}C spectra, which is consistent with a CH_2 group from the DEPT spectrum. The other two signals are not as intense and although some connection to the carbon spectrum is seen, no definitive correlations exist. The peak at ~ 1.5 ppm is weak in some spectra and more intense in others, it can, however, be assigned to water that is present in the chloroform solvent used to dissolve the samples. There is also a weak peak around 0 ppm, in some cases barley visible, which corresponds to either grease or oil.

Comparison of the NMR signals

The centre macrocycle has the same framework structure for each of the synthesized porphyrins; this consists of the 18 delocalized π electrons over the 24 atoms (carbon/nitrogen) in this skeleton structure. Thus it is expected that there will be some signals that will always be present in both the ^{1}H and ^{13}C NMR spectra and this has been noted for all the spectra in this work. These signals should not be overly affected by the type of substituent that is present on each porphyrin and therefore they are expected to be observed in the same chemical shift region for each spectrum. Specifically, in the proton NMR spectrum these signals are those for the pyrrole and nitrogen protons and in the carbon NMR spectrum, the α-pyrrole, β-pyrrole and *meso*-positioned carbon atoms.

^{1}H NMR signals

In the proton NMR spectra the two most common signals that would be seen for each porphyrin are the two centre protons on two opposite nitrogen atoms (~ –2 ppm) and the eight pyrrole protons (~ 9 pm). As mentioned, the signal for the N-H proton is in an unusual section of the spectrum (below 0.0 ppm) and is therefore a highly diagnostic feature of free base porphyrins. The exact value for each of the porphyrin's signals for the N-H proton is given below (Table 4.1). They follow in the order P6 > P5 > P1 > P4 > P3 > P2. The least shielded of the N-H protons are therefore those of P6 with cyclohexane at the *meso*-position (in chair conformation) and P5 (with the two methyl groups). The most shielded N-H protons are found for the porphyrins with phenyl groups (P2 and P4) and for P3. Between these two extremes is P1 at –1.937, which has one ethyl and one methyl group at the *meso*-position. There is therefore no obvious correlation that exists between the N-H shift and the steric bulk of the *meso*-substituent or indeed the conformation of the porphyrin macrocycle (e.g. degree of ruffling).

Table 4.1: The most common signals for the ^{1}H NMR spectrum.

^{1}H	H_2T(iBu)P **P1**	H_2T(CH_2Ph)P **P2**	H_2T(iPent)P **P3**	H_2T($CHPh_2$)P **P4**	H_2T(iPr)P **P5**	H_2T(cyHx)P **P6**
N-H	–1.937	–2.343	–2.247	–2.253	–1.786	–1.605
Pyrrole H	9.471	9.386	9.537	9.040–9.294	9.466	9.470
C-H	5.052	6.342 (CH_2)	4.888	5.299 and 8.4–8.5	5.319	4.765

The pyrrole proton signals all resonate further downfield, than simple aromatic rings. These signals span about 0.5 ppm and thus are very easily assigned. They are not greatly affected by the different alkyl-substituents and thus are all in the same region. The final common signal is one that is seen for five of the six synthesized porphyrins. It is the first carbon atom of the *meso*-substituent that usually carries the two substituent groups and one hydrogen atom. This signal is not seen for P2 (H_2T(CH_2Ph)P) as this first carbon is bonded to two hydrogen atoms instead. However, the resonance for this CH_2 group is shown in the table—it is further downfield than the C-H groups of the other five porphyrins. For the other five porphyrins, this peak is clearly visible in the same chemical shift region of the spectrum (~ 5 ppm) over a range of about 0.6 ppm. (Note: as discussed earlier, the magnetically inequivalent C-H groups for H_2T($CHPh_2$)P resulting from population of a low-symmetry conformational isomer in solution affords an additional signal in the 8 ppm range.)

^{13}C NMR signals

There are more carbon atoms than hydrogen atoms that make up the porphyrin skeleton, thus we expect to see more correlating signals in the carbon NMR than were in the proton NMR spectra. These include the α- and β-carbon atoms of each of the pyrrole rings, which are expected to resonate at ~ 144 ppm and ~ 128 ppm, respectively. This is seen in the table below (Table 4.2). These values for free pyrrole

are typically: 118.4 ppm (α-C) and 108.0 ppm (β-C).[221] Another prominent signal is obviously from the *meso*-carbons; this has a slightly more varied range due to the closer proximity to the substituent in comparison to the other skeleton carbons. The most common region seems to be around 122 ppm; however, P2 and P4 give signals at a chemical shift lower than 120 ppm (115.17 and 119.52 ppm, respectively) due to the presence of phenyl rings in their *meso*-substituents.

Table 4.2 The most common signals for the ^{13}C NMR spectrum.

^{13}C	$H_2T(iBu)P$ **P1**	$H_2T(CH_2Ph)P$ **P2**	$H_2T(iPent)P$ **P3**	$H_2T(CHPh_2)P$ **P4**	$H_2T(iPr)P$ **P5**	$H_2T(cyHx)P$ **P6**
Alpha	144.69	144.90	145.11	146.61	143.76	143.76
Beta	128.96	128.56	128.81	132.38	129.02	129.27
Meso	122.71	115.17	121.25	119.49	123.67	122.54
C-H	42.76	40.43 (CH_2)	50.54	56.18	35.20	49.91

The last signal of importance is the first carbon atom of the *meso*-substituent. The chemical shifts observed here vary over a range of about 15 ppm; this can be accounted for by the difference in the actual substituents attached to this carbon atom. These substituents will have an influence on the exact position of the carbon atom's resonance. Mostly one hydrogen atom and two identical groups (or at least similar groups as $H_2T(iBu)P$ (P1) has one methyl and one ethyl) are attached to this carbon. However, the porphyrin $H_2T(CH_2Ph)P$ (P2) does not have this single hydrogen atom, but instead a CH_2 group (with a resonance of 40.43 ppm) and one phenyl substituent.

Values obtained from DFT calculations

For each of the porphyrins in the series, DFT calculations (B3LYP/6-31G**, see Chapter 7) were employed to determine the predicted structures of the porphyrins,

along with providing data for the expected IR and NMR spectra in each case. The calculated NMR data were obtained for each of the porphyrins with no solvent (gas phase) and then for some using a solvent continuum model with chloroform ($H_2T(iBu)P$, $H_2T(iPr)P$ and $H_2T(cyHx)P$). Mostly the differences between a calculation with solvent or without were negligible. The isotropic shielding constants were converted to chemical shifts for each expected signal; then tabulated and grouped according to the type of signal. These chemical shifts were then averaged for each type and a comparison made with the experimental chemical shifts.

The DFT computation to obtain the NMR data for $H_2T(CHPh_2)P$ unfortunately failed. Despite numerous attempts only the optimization was successful. Therefore no correlation could be made between the experimentally obtained data and the theoretical chemical shifts. However, presented in Table 4.3 below are the experimental chemical shift values for the ^1H and ^{13}C NMR spectra.

Table 4.3: Experimental chemical shifts for the ^1H and ^{13}C NMR spectra of $H_2T(CHPh_2)P$.

^1H	N-H	C-H	para	meta	ortho	beta
experimental	–2.253	5.299 and 8.4–8.5	7.173–7.555			9.040–9.294

^{13}C	CH_2	*meso*	para	ortho	meta	beta	alpha
experimental	57.28, 56.18 and 55.83	119.49	128.45			132.38	146.41

Tables for the NMR spectra (proton and carbon NMR spectra) of the other five porphyrins in the series, with both the experimental values and the DFT-calculated values (Chapter 7), are given below in Tables 4.4 to 4.13 that follow. These tables also include the chemical shift difference between the calculated and observed chemical shifts for each compound.

Table 4.4: Experimental and DFT-calculated chemical shifts for the ^{1}H NMR spectrum of $H_2T(iBu)P$.

^{1}H	N-H	Ethyl-CH_3	Methyl-CH_3	CH_2	C-H	beta
experimental	–1.937	1.029	2.358	2.729, 2.808	5.052	9.471
DFT	–4.229	1.612	2.250	3.022	5.026	9.853
absolute Δ	2.292	0.583	0.108	0.008, 0.086	0.026	0.382

Table 4.5: Experimental and DFT-calculated chemical shifts for the ^{13}C NMR spectrum of $H_2T(iBu)P$.

^{13}C	Ethyl-CH_3	Methyl-CH_3	CH_2	C-H	*meso*	beta	alpha
experimental	14.14	27.01	35.42	42.76	122.71	128.96	144.69
DFT	15.12	26.02	37.96	46.78	122.01	125.04	138.82
absolute Δ	0.98	0.99	2.54	4.02	0.70	3.92	5.87

Table 4.6: Experimental and DFT-calculated chemical shifts for the ^{1}H NMR spectrum of $H_2T(CH_2Ph)P$.

^{1}H	N-H	CH_2	para	meta	ortho	beta
experimental	–2.343	6.342	7.120	7.188	7.315	9.386
DFT	–4.752	6.283	7.182	7.280	7.485	9.537
absolute Δ	2.409	0.059	0.062	0.092	0.170	0.151

Table 4.7: Experimental and DFT-calculated chemical shifts for the ^{13}C NMR spectrum of $H_2T(CH_2Ph)P$.

^{13}C	CH_2	*meso*	para	ortho	meta	beta	C-ring	alpha
experimental	40.43	115.17	125.86	128.54	128.54	128.43	144.90	144.90
DFT	43.87	114.29	120.44	128.44	128.44	124.77	141.43	142.81
absolute Δ	3.44	0.88	5.42	0.10	0.10	3.66	3.47	2.09

Table 4.8: Experimental and DFT-calculated chemical shifts for the ^{1}H NMR spectrum of $H_2T(iPent)P$.

^{1}H	N-H	CH_3	CH_2	C-H	beta
experimental	–2.247	1.002	2.780 2.895	4.888	9.537
DFT	–4.024	1.527	2.698	5.094	9.566
absolute Δ	1.777	0.525	0.082 0.197	0.206	0.029

Table 4.9: Experimental and DFT-calculated chemical shifts for the ^{13}C NMR spectrum of $H_2T(iPent)P$.

^{13}C	CH_3	CH_2	C-H	*meso*	beta	alpha
experimental	14.29	34.46	50.54	121.25	128.81	145.11
DFT	16.36	37.39	50.62	120.84	125.11	139.62
absolute Δ	2.07	2.93	0.08	0.41	3.71	5.49

Table 4.10: Experimental and DFT-calculated chemical shifts for the ^{1}H NMR spectrum of $H_2T(iPr)P$.

^{1}H	N-H	CH_3	C-H	beta
experimental	–1.786	2.331	5.319	9.466
DFT	–4.464	2.369	5.394	9.926
absolute Δ	2.678	0.038	0.075	0.460

Table 4.11: Experimental and DFT-calculated chemical shifts for the ^{13}C NMR spectrum of $H_2T(iPr)P$.

^{13}C	CH_3	C-H	*meso*	beta	alpha
experimental	28.67	35.20	123.67	129.02	143.76
DFT	29.87	40.18	121.05	124.85	138.96
absolute Δ	1.20	4.98	2.62	4.17	4.80

Table 4.12: Experimental and DFT-calculated chemical shifts for the ^{1}H NMR spectrum of H_2T(cyHx)P.

^{1}H	N-H	meta-a & para-a	para-e	meta-e	ortho-e	ortho-a	C-H	beta
experimental	–1.605	1.858	2.117	2.218	2.595	2.979	4.765	9.470
DFT	–3.967	1.950	2.026	2.451	2.487	3.120	4.967	9.843
absolute Δ	2.362	0.092	0.091	0.233	0.108	0.141	0.202	0.373

Table 4.13: Experimental and DFT-calculated chemical shifts for the ^{13}C NMR spectrum of H_2T(cyHx)P.

^{13}C	meta	para	ortho	C-H	*meso*	beta	alpha
experimental	28.58	26.73	38.70	49.91	122.54	129.27	143.76
DFT	28.65	27.84	39.08	47.35	122.24	125.46	138.85
absolute Δ	0.07	1.11	0.38	2.56	0.30	3.81	4.91

For all the porphyrins it is obvious from the tables that the worst correlation for the proton NMR signals between the calculated value and the experimentally obtained value is for the pyrrole N-H. In all cases, there is a difference between the two N-H proton values of more than 2 ppm. For each of these chemical shifts it is the DFT-calculated value that is always more shielded (more negative) and is therefore a consistent error for all six porphyrins. Thus it is possible that this consistent error in the computations is due to over-estimated shielding, by the ring current, of these N-H protons. It must also be noted that the other predicted resonances are for protons that are attached to carbon atoms (with a spin ½ nucleus), whereas this proton is attached to a nitrogen, which has a quadrupole nucleus. Studies by Takeda *et al.* have shown in some solvents the downfield shifting of the N-H protons because of an increase in the intermolecular hydrogen bonding.[254] Even so, the exact cause for this is still uncertain.

The rest of the calculated data for the ^{1}H NMR shifts compares well to our experimental data, with small discrepancies of only about 0.5 ppm or less. These

small differences between the values from the two techniques show good correlation. The predicted values with the least accuracy (other than the N-H signals) seem to be for terminal methyl groups and the pyrrole β-protons. For the carbon chemical shifts there was also very little difference (less than 6 ppm) between experimentally obtained and calculated values. The signals that have the greatest discrepancies between experimental and calculated values appear to be the pyrrole α- and β-carbons.

The difference between the observed and calculated chemical shift at the B3LYP/6-31G** level of theory is therefore small and of a consistent magnitude for each porphyrin. Use of a larger basis set, which would be at the expense of execution time, would reduce this error in the shielding tensor estimation further. The agreement between theory and experiment is nevertheless good at the chosen level of theory, particularly for the majority of the proton and carbon signals in each molecule. Thus it does not warrant a higher level calculation for these large molecules.

Shown in Graph 4.1 and 4.2 below are two examples for the plots of the DFT computed chemical shifts versus the experimental values. As shown by Graph 4.1, the slope of 1.24 is close to unity for the ^{1}H chemical shifts. The slope for the ^{13}C chemical shifts is 0.95 and closer still to 1.0 (Graph 4.2). Thus it seems that the ^{13}C chemical shifts have been calculated more accurately; however, this is not the case when we consider the RMSD. For the ^{1}H NMR values the RMSD is 2.43 ppm whereas for the ^{13}C values it is 8.48 ppm. Clearly, shielding tensors are therefore more accurately calculated for the protons than the carbon atoms despite the better correlation shown in the graph for the ^{13}C values. This observation is consistent with the expectation for the GIAO (Gauge-Independent Atomic Orbital) method.[299,300]

However, GIAO is not a particularly good term because these orbitals actually do include a factor reliant on the gauge; a better description would be from the proposed 'gauge-dependent atomic orbitals'.[301] This method uses gauge-invariant atomic orbitals, the real atomic basis functions are adapted according to a multiplicative complex factor (this factor is dependent on the gauge of the vector potential).[299] Use of such functions for problems involving molecular diamagnetism was first

documented in 1937[302] for ring currents in aromatic hydrocarbons and since then, they have been used in many more general investigations of magnetic properties.

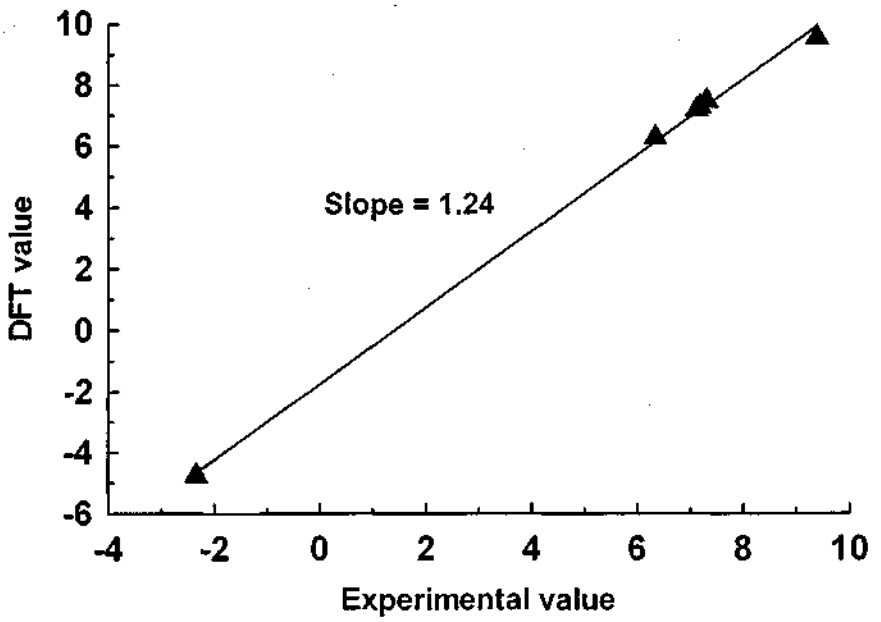

Graph 4.1: Correlation between DFT and experimentally determined ^{1}H NMR signals, for porphyrin 2 ($H_2T(CH_2Ph)P$).

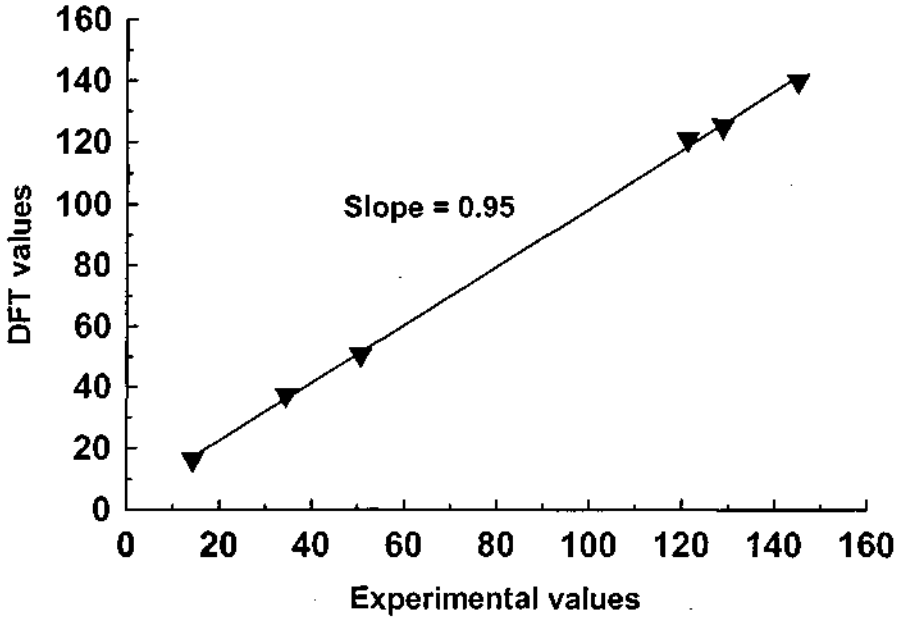

Graph 4.2: Correlation between DFT and experimentally determined ^{13}C NMR signals, for porphyrin 3 ($H_2T(iPent)P$).

Accurate computation of ^1H NMR shielding tensors was previously very difficult with large deviations from experimental values. The 4-31G level of theory is found to aptly predict the 'α-effect' (deshielding of the methane carbon when H is replaced by CH_3) and the difference in shielding at a carbon atom in a single (C-C) and a double (C=C) bond.[299] The GIAO method seems to converge faster than the localized techniques thus giving the same accuracy with a smaller basis, particularly for the individual tensor components.[300] In general, there is exceptional agreement between experimental values for NMR chemical shifts and those calculated by the 4-31G level of theory or higher.[299]

Table 4.14: Slopes for each fit between experimentally obtained and theoretically calculated NMR chemical shifts.

Porphyrin	Correlation Factor		
	Proton NMR		Carbon NMR
	All points	Without N-H	
$H_2T(iBu)P$	1.1684	1.0001	0.9516
$H_2T(CH_2Ph)P$	1.2419	1.0545	0.9392
$H_2T(iPent)P$	1.1167	0.9763	0.9475
$H_2T(CHPh_2)P$	–*	–*	–*
$H_2T(iPr)P$	1.2611	1.0612	0.9313
$H_2T(cyHx)P$	2.1211	2.7359	0.9667

*DFT geometry optimization failed.

Graphs for the correlation between experimental and DFT-computed ^1H and ^{13}C NMR chemical shifts for each of the porphyrins were all plotted. Table 4.14 gives the slope for each of these graphs. The slopes are all similar for the graphs of the proton resonance values and also for the graphs of the carbon resonance values. The proton slopes are all slightly more than 1 and the carbon slopes are all slightly less than 1. The slopes for the proton graphs were also calculated without the N-H points (due to this being the poorest correlating value) and the resulting slopes were better than when the chemical shift for the N-H proton was included. They were even better than those for the carbon graphs, except for $H_2T(cyHx)P$. Although the correlation for the

^{1}H NMR chemical shift graph of this porphyrin was already the worst, leaving out the N-H proton made the correlation even worse rather than improving it.

4.7 Comparison with NMR Spectra in the Literature

For each of the six synthesized *meso*-tetraalkylporphyrins, NMR spectra have been collected. These comprise ^{1}H and ^{13}C NMR spectra as well as certain 2D spectra including DEPT, COSY and HSQC data. Using these spectra, assignments for each porphyrin have been made. Literature reports for NMR values have been obtained for H_2T(iPent)P (Porphyrin 3), H_2T(iPr)P (Porphyrin 5) and H_2T(cyHx)P (Porphyrin 6). These results agree well with the experimentally obtained data (tables below). For porphyrins 3 and 5, there were no literature values for the carbon chemical shifts, but the literature proton chemical shifts showed good correlation with our experimental data, with the largest difference of only 0.5 ppm (Tables 4.15 and 4.16).

Table 4.15: Comparison of literature and experimental chemical shifts (^{1}H) for H_2T(iPent)P (porphyrin 3).

^{1}H	N-H	CH_3	CH_2		C-H	beta
This work	–2.247	1.002	2.780	2.895	4.888	9.537
Reference 58	–2.31	0.90	2.72	2.98	4.87	9.11
absolute Δ	0.063	0.102	0.060	0.085	0.018	0.427

Table 4.16: Comparison of literature and experimental chemical shifts (^{1}H) for H_2T(iPr)P (porphyrin 5).

^{1}H	N-H	CH_3	C-H	beta
This work	–1.786	2.331	5.319	9.466
Reference 58	–1.60	2.38	5.34	9.48
absolute Δ	0.186	0.049	0.021	0.014

The assignment for porphyrin 6 (H_2T(cyHx)P) is given above in the Results section, as determined by Veyrat *et al.*[195,215] The experimentally obtained spectra for both the

proton and carbon NMR were very similar to those reported by Veyrat *et al.* [195,215] The proton NMR spectra differed by less than 0.1 ppm and the carbon spectra had a largest discrepancy of about 3 ppm, thus these results are viewed as high-quality and reproducible. Fast rotation of the cyclohexyl groups is observed at room temperature in deuterated chloroform solution on the NMR time scale, and high symmetry is therefore seen in both the ^{13}C and ^{1}H spectra. It is expected that the ruffled porphyrin seen in the crystal structure[195,215] may also be present in solution and thus inversion of the macrocycle is most likely fast as well.

Table 4.17: Comparison of literature and experimental proton chemical shifts for $H_2T(cyHx)P$ (porphyrin 6).

^{1}H	N-H	meta-a & para-a	para-e	meta-e	ortho-e	ortho-a	C-H	beta
This work	−1.605	1.858	2.117	2.218	2.595	2.979	4.765	9.470
References 195,215	−1.60	1.83	2.14	2.14	2.58	2.96	4.76	9.46
absolute Δ	0.005	0.028	0.023	0.078	0.015	0.019	0.005	0.010

Table 4.18: Comparison of literature and experimental carbon chemical shifts for $H_2T(cyHx)P$ (porphyrin 6).

^{13}C	meta	para	ortho	C-H	*meso*	beta	alpha
This work	28.58	26.73	38.70	49.91	122.54	129.27	143.76
References 195,215	26.7	28.5	38.7	46.9	122.5	129.1	143.7
absolute Δ	1.88	1.77	0.0	3.01	0.04	0.17	0.06

This porphyrin can be considered to be a derivative of H_2TPP that has fully hydrogenated *meso*-substituents. Interest has been drawn to this particular porphyrin due to some unusual steric and electronic features which this macrocyclic ligand possesses. The non-planarity of the bulky *meso*-substituents is predicted to impact the stereochemistry of the porphyrin core.

The cyclohexyl groups are not planar, but rather in a chair conformation, thus they must be categorized in some way. This has been done with reference to the orientation of the C_1-H_1 vector (either clockwise or anticlockwise around the porphyrin centre), such that each of the cyclohexyl substituents is given either a comparative *g* or *–g* value, [195,215] consistent with the nomenclature adopted for other polycyclohexyl systems by Colombus and co-workers.[297,303,304] The result is four different conformers, these include (g,g,g,g), (–g,g,g,g), (–g, –g,g,g) and (–g,g, –g,g) (and the corresponding conformers acquired from the change of g for –g.) After averaging the four possible conformer signals, a 4-fold artificial symmetry may be seen. For the two metal complexes (zinc and nickel) that were synthesized by Veyrat *et al.*[195,215] temperature-dependent ^{1}H NMR spectra showed the most common conformer to be (–g,g–g,g) at low temperatures, and provided an estimate for the cyclohexyl group rotation barrier ($\Delta G_c^{\ddagger}$ = 10–12 kcal/mol) in this system. The experimental NMR data corresponds with that given in the literature and therefore it is possible that the (–g,g–g,g) conformation exists in solution. Moreover, the DFT optimization results in a conformation which is best described by the form (–g,g,–g,g).

4.8 Future Work

Atropisomers will be mainly found for two of the six *meso*-tetraalkylporphyrins in the series, namely $H_2T(CHPh_2)P$ and $H_2T(cyHx)P$. Therefore future work will involve:

(1) Variable temperature NMR studies;

(2) Quenched molecular dynamics simulations to locate all low-energy conformations (atropisomers) for the sterically hindered porphyrins; and

(3) DFT computations to determine accurate relative energies for the most stable atropisomers both in solution and *in vacuo*.

5. X-ray Crystallography

5.1 Introduction

The literature concerning the stereochemistry of porphyrins has expanded rapidly since the first report of an X-ray structure determination in 1959.[305] This structure was of nickel etioporphyrin II, [Ni(Etio(II))P], and was an exemplary, but uncertain, analysis of a highly disordered crystal. Prior to 1963, the best available model for the stereochemistry of the porphyrin skeleton in the porphyrins and metalloporphyrins was an *indirect product of Robertson and Woodward's classic X-ray analyses of the crystal* structure for phthalocyanine (1936).[306] The subsequent nickel(II)[307] and platinum(II)[308] derivatives were published in 1937 and 1940, respectively. From 1962 onwards, more frequent reports of X-ray structure determinations of porphyrins and metalloporphyrins appeared.[309] All, except one, reported X-ray analyses for the various porphine derivatives have been derived from the three-dimensional {hkl} data provided by single crystals.[309]

For the earliest of these studies, a determination of the porphyrin structure using X-ray diffraction was a monumental experimental undertaking; however, modern day advances using computers and other electronic devices have improved the methodology. Structure analysis has improved immensely in efficiency, selectivity, and precision, due to the lavish use of modern computers and CCD measurements of the diffracted intensities of the Bragg 'reflections'. Improvements in data collection, structure solution and refinement procedures have now made structure determination a routine and popular procedure.[309,310] As with all methods there are certain limitations in X-ray diffraction analyses.

The early studies involving porphyrin derivatives were performed because the derivatives usually had some connection to porphyrin importance in biological systems. X-ray structure determinations are used in the proof of synthesis or to show exact stereochemistry, many of which have been published in the literature (some not

with complete details).[310] The total number of porphyrins and porphyrin-related structures in the CSD (Cambridge Structural database)[311] is found to be greater than 3000 (Figure 5.1).

Studies of porphyrins have slowly moved away from those of the biologically derived protoporphyrin IX (and its related species) to derivatives of synthetic, symmetric porphyrins like H_2TPP, H_2OEP, H_2TPyP and H_2Etio. One reason for this is practical considerations, which include availability and the ease with which single crystals can be obtained for diffraction studies. Interest has also grown in another important class of porphyrins bearing peripheral substituents that result in superstructured products, designed to produce species with particular properties.[310] Such an example is the "picket fence" porphyrins[152] which were initially designed as models for the oxygen-carrying haemoproteins.[312]

According to the work by Fleischer and co-workers[313] in 1964, the naturally occurring porphyrin molecule is planar; however, it possesses low energy barriers to out-of-plane distortions, and thus is particularly sensitive to its packing environment. Arguments have been made[314] that ruffling seen in porphyrins is not due to these packing effects, but rather an attempt to reduce the strain in the σ-bonding network of the porphyrins. It is possible for either of these explanations to account for the out-of-plane deviations seen in many porphyrin structures. Electrostatic repulsion of the inner nitrogen atoms (assuming each of them to have a charge of + ½), which applies to solution as well as solid state species, has also been mentioned.[315] Some investigators feel that the molecule might be ruffled in the gaseous state due to the existence of a considerable amount of angular strain in the σ-bonding system of a strictly planar porphyrin nucleus.[315]

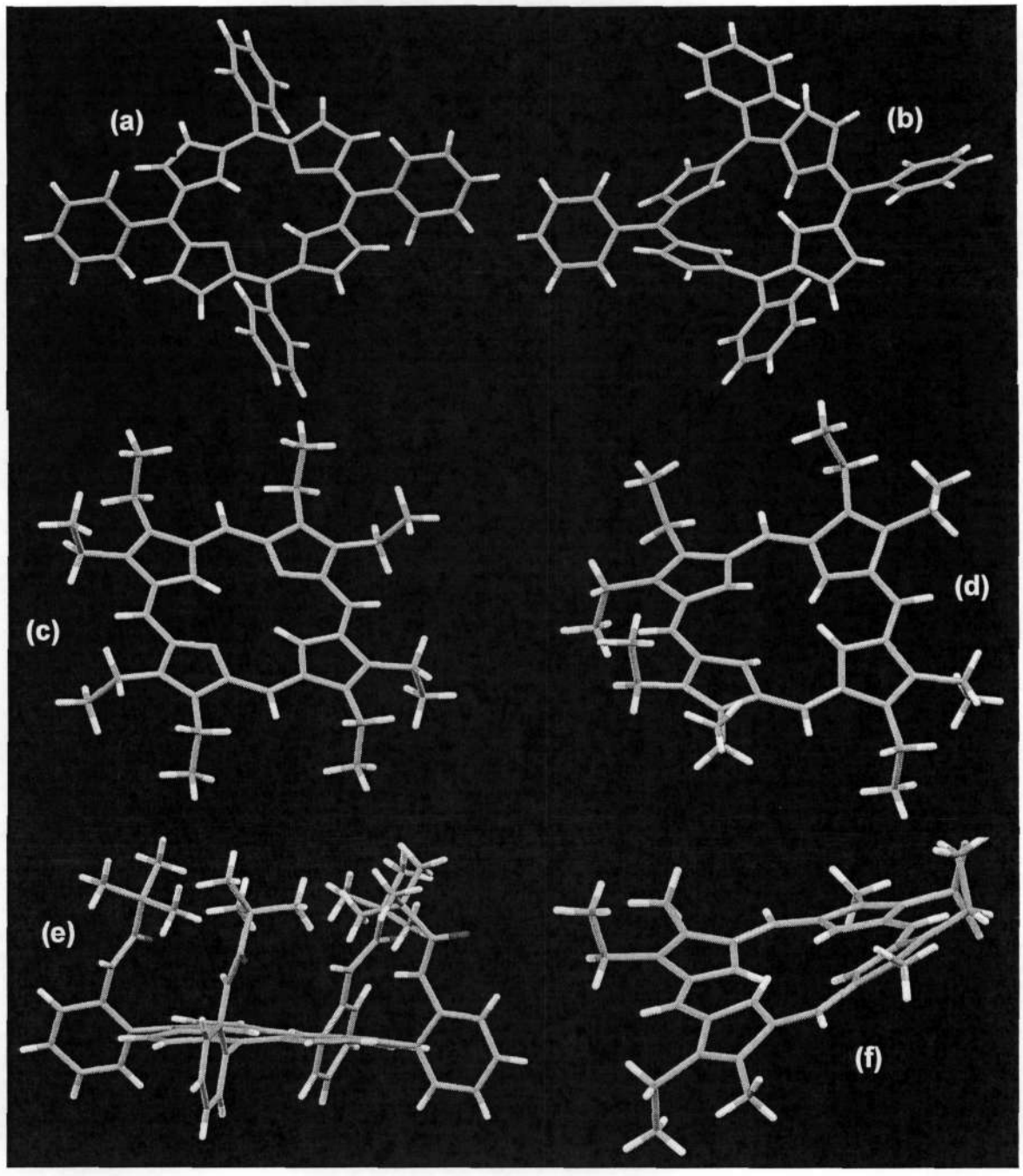

Figure 5.1: Some examples of well-known porphyrins found in the Cambridge Structural database (with their CSD codes): (a) H_2TPP (TPHPOR01), (b) $[H_4TPP]^{2+}$ (ASUNAD), (c) H_2OEP (OETPOR10), (d) $[H_4OEP]^{2+}$ (RUHQAM), (e) $[H_2TPivPP]^{2+}$ (LANTUQ), and (f) $[H_4Etio(II)P]^{2+}$ (REVROZ). The structures of the diacids (b) $[H_4TPP]^{2+}$, (d) $[H_4OEP]^{2+}$ and (f) $[H_4Etio(II)P]^{2+}$ are good examples of the saddle conformation, while the other three are predominantly planar.

The porphyrin core resists undue radial expansion or contraction but it can readily distort from a planar conformation; it is known to be quite flexible toward out-of-plane

deformation.[310] The 24-atom porphyrin core is easily distorted in a direction perpendicular to the mean plane as opposed to the radial (in plane) direction. Additionally, the pyrrole ring subunits are always themselves planar. *meso*-Substituted porphyrins seem to have a greater tendency towards distortion than β-substituted analogues; however, it should be emphasized that both types are equally capable of substantially distorted conformations. Steric crowding at the periphery also seems to cause substantial nonplanarity.[316]

The observed nonplanar conformations are caused by a variety of factors. These phenomena include: 1) packing constraints in the crystal, 2) steric crowding due to substituents on the porphyrin macrocycle, 3) effects of intermolecular interactions (typically between two of the ligands), 4) effects of the intramolecular interactions between the porphyrin core and the axial ligands, and 5) the coordination requirements of the central metal ion itself.[310] Many crystallographic studies show a fairly flexible macrocycle and thus planarity is rather an exception. Large deviations from planarity have particularly been observed for H_2TPP derivatives in which the pyrrole rings can be maximally twisted out of the plane (defined by the four central nitrogen atoms) in the dication at about 33°.[315] Extreme tilting of pyrrole rings allows aryl rings to become nearly coplanar with the porphine nucleus.[316] These different core conformations may result in profound influences on the magnetic and electronic properties of the molecule.[316]

Idealized terms can be used to describe the most common forms of core nonplanarity as S_4 (sometimes D_{2d}) ruffled (*ruf*, B_{1u}) and saddled cores (*sad*, B_{2u}), C_{4v} domed cores (*dom*, A_{2u}) and stepped or waved cores (*wav*, E_g), with a more recent addition of the propeller (*pro*, A_{1u}) distortion.[317] These idealized nonplanar conformations are schematically represented in Figure 5.2. It is mostly the case that the experimentally observed core conformations are often of lower symmetry than these described below. On visual inspection of the observed distortions, a mixture of the idealized conformations is often seen. Macrocyclic structures, even highly distorted porphyrins, may be accurately represented by displacements along only the lowest-frequency normal coordinates and the small displacements for other normal coordinates are also able to be discerned.[317]

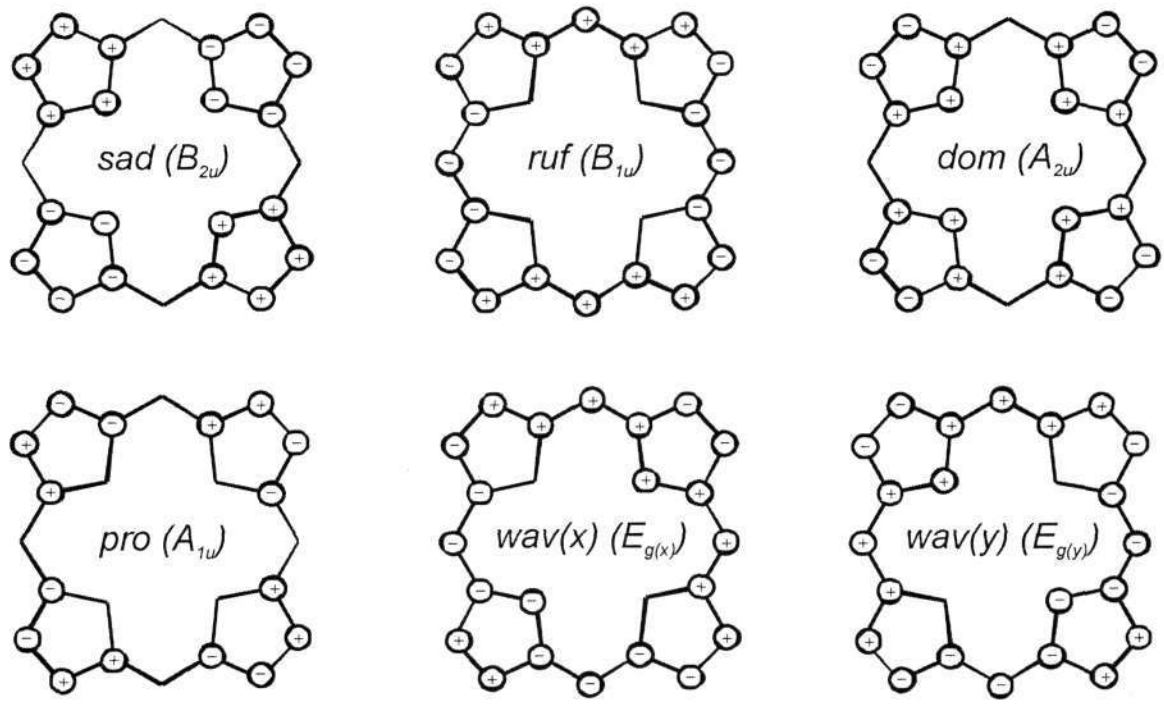

Figure 5.2: Idealized representations of the out-of-plane distortions found in porphyrin (and metalloporphyrin) species. The positive symbols represent displacement of atoms above the mean plane of the macrocycle and the negative symbols represent displacement below. The atoms that do not have a positive or negative displacement are situated in the mean plane.[310,317]

The importance of nonplanar porphyrins for their biological significance has been noted several times.[66,67,68,69] Thus it has further been suggested that a mechanism for protein modulation of biological properties may be deduced from distorted porphyrins and protein-induced changes in nonplanarity.[72] In 1995, Jentzen *et al.*[14] provided an outline for the process of classifying porphyrin distortions in terms of the equivalent displacements along the lowest-frequency normal coordinates of the porphyrin macrocycle. This has been used in the case of haemeprotein characterization according to the displacements along the lowest-frequency out-of-plane normal coordinates of the D_{4h}-symmetric macrocycle. These X-ray crystal structures were then analyzed using a computational procedure where the distortion has been accurately simulated by a linear combination of the above orthonormal deformations.[72]

The saddle-shaped distortion has a D_{2d}-ruffled core in which the pyrrole rings have been alternately displaced (above and below) from the mean plane. This is different to

the regular D_{2d}-ruffled core by a 45° rotation of the point group symmetry operators with respect to the major twofold axis, which is perpendicular to the mean plane. Doming (C_{4v}) has been described as a slight "stepping" of the core appropriate to inversion symmetry and a "roof" conformer[318] as folding along a line joining opposite *meso*-carbon atoms.[316]

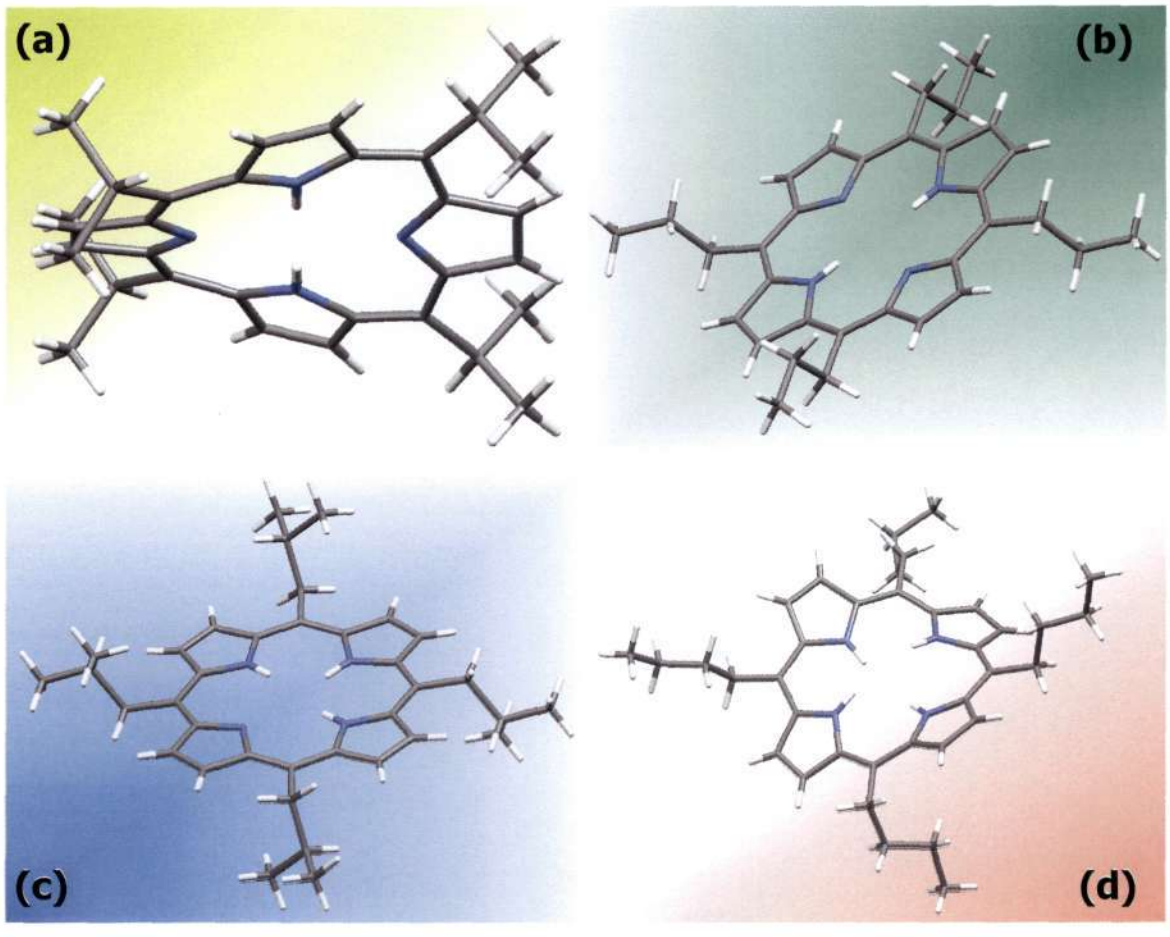

Figure 5.3: Four representative examples of the *meso*-tetraalkylporphyrins found in the Cambridge Structural Database. They are: (a) $H_2T(iPr)P$[247] (b) $H_2T(n\text{-}Pr)P$[319] (c) $H_2T(CH_2CH(CH_3)_2)P$[58] and (d) $H_2T(n\text{-}Bu)P$[82]. $H_2T(n\text{-}Pr)P$ and $H_2T(CH_2CH(CH_3)_2)P$ are planar, while $H_2T(iPr)P$ and $H_2T(n\text{-}Bu)P$ show some saddling distortion.

Crystal structures have been determined for some free base *meso*-tetraalkylporphyrins and many are of particular interest to the present work. Some examples of these are shown in Figure 5.3. Unfortunately, there are not many structures that exist to date in the CSD (Cambridge Structural Database),[311] due to the difficulty in obtaining crystals from these particular porphyrins. *meso*-

Tetraalkylporphyrins also have rather high internal *R* values associated with poor diffraction when crystals can be obtained. However, those that have been recorded, and for which data have been reported, are listed in Table 5.1.

Table 5.1: Reported X-ray crystal structures of *meso*-tetraalkylporphyrins.

CSD[311] Reference Code	*meso*-Tetraalkylporphyrin	Empirical formula	Space group	Lit. ref.	This work
MAHXAU	$H_4T(n\text{-Pent})P$	$C_{40}H_{54}N_4$	$P2_12_12_1$	247	
WODJEE	$H_2T(5\text{-ClPent})P$	$C_{40}H_{50}Cl_4N_4$	C2/c	[320]	
DOWJOO	$H_3T(iPent)P$	$C_{40}H_{54}N_4$	$P2_1/c$	58	**P3**
KIBLIQ	$H_4T(iPent)P$	$C_{40}H_{56}N_4$	$P\bar{1}$	82	**P3**
DOWBOG	$H_2T(n\text{-Bu})P$	$C_{36}H_{46}N_4$	$P2_1/c$	58	
KIBMAJ	$H_4T(n\text{-Bu})P$	$C_{36}H_{48}N_4$	P43	82	
DOWGEB	$H_2T(CH_2CH(CH_3)_2)P$	$C_{36}H_{46}N_4$	P2/n	58	
TPRPOR10	$H_2T(n\text{-Pr})P$	$C_{32}H_{38}N_4$	$P2_1/c$	319	
KIBMEN	$H_4T(iPr)P$	$C_{32}H_{40}N_4$	$P\bar{1}$	82	**P5**
MAHWUN	$H_2T(iPr)P$	$C_{32}H_{38}N_4$	Fdd2	247	**P5**

Each of the *R*-factors for these porphyrins ranges from 4% to just less than 10%; and most exhibit *R*-factors closer to 10% than to 4%. Most of them also possess some type of disorder in their structure. Some of these structures are planar, while others possess varying degrees of distortion from the mean plane. It must also be noted that not all of the structures are for the free bases as we have prepared in this work, but also for the diacids or monoacids. Structures for two of our synthesized porphyrins are represented in Table 5.1 as they have been previously reported, namely $H_2T(iPent)P$ and $H_2T(iPr)P$. However, it is the monoacid $H_3T(iPent)P$ and diacid $H_4T(iPent)P$ of our free base porphyrin ($H_2T(iPent)P$) that have been recorded and thus our structure,

although not fully resolved, is novel. Our space group for $H_2T(iPent)P$ agrees with the space group for the monoacid, $H_3T(iPent)P$, but not with the space group for the diacid, $H_4T(iPent)P$. Attempts to find a space group for the disordered $H_2T(iPr)P$ agree with neither of the two existing references for either the free base or diacid, $H_4T(iPr)P$.

5.2 Objectives

To determine and report the crystal structures of each of the six synthesized free base porphyrins, including a full analysis of each structure. This included reporting and analyzing relevant bond lengths, angles, torsion angles and other interesting features to establish correlations between *meso*-substituents and conformations for the present group of tetraalkylporphyrins. Three of the structures could be refined to an *R*-factor lower than 10%; however, only one porphyrin ($H_2T(CH_2Ph)P$) was refined to completion. And one other porphyrin ($H_2T(CHPh_2)P$) would not produce diffraction quality crystals by any means.

5.3 Results and Discussion

5.3.1 General

For the porphyrin structures discussed below, the following general notation (Figure 5.4) will be used to label the atoms of the central macrocycle. The α- and β-carbon atoms of the pyrrole rings are labelled C(a) and C(b) respectively, with C(m) being used for the *meso*-carbon atom. The hydrogen atoms will be named according to the atom to which they are bonded.

In this section on X-ray crystallography the determined structures of the porphyrins synthesized are discussed. Packing diagrams are presented to show the patterns in which the molecules are located in the solid state. Intensity measurements were carried out on the crystals, which were all air stable. The data were collected on an Oxford Diffraction Xcalibur2 CCD diffractometer in house. In solving the structures of the various crystals direct methods (SHELXS-97, OSCAIL V8, WinGX32) were used. There are relatively few crystallographically characterized *meso*-tetraalkylporphyrins

due to their generally poor crystal quality. Our strategy was to build porphyrins with some additional steric bulk on the *meso*-substituents in the hope that this would allow for substantially distorted free base porphyrin macrocycles.

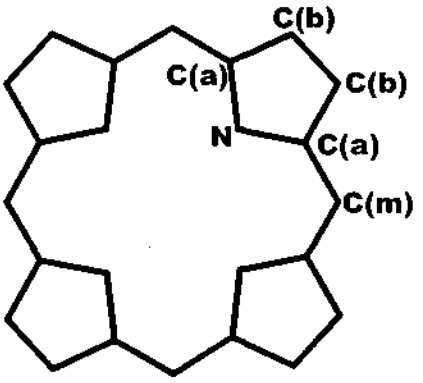

Figure 5.4: A skeleton of the macrocyclic centre showing the notation used for the chemically unique atoms in the *meso*-tetraalkylporphyrin structures.

From the six synthesized porphyrins, attempts were made to obtain diffraction quality crystals for each. The original crystals that were first used to collect diffraction data for $H_2T(iBu)P$, $H_2T(CH_2Ph)P$, $H_2T(iPent)P$, $H_2T(iPr)P$ and $H_2T(cyHx)P$ were formed after evaporation of the solvent (CH_2Cl_2). They were, unfortunately, found to be low quality, with intrinsically poor diffracting power. Thus, test tubes for solvent diffusion were set up using THF and hexane. These crystals were expected to have better data sets than the original crystals; however, the results proved to be very similar to earlier measurements, except for $H_2T(CH_2Ph)P$. This novel porphyrin gave a data set that refined to $R_1 < 7\%$. The final series of crystals obtained for $H_2T(iBu)P$, $H_2T(iPent)P$, $H_2T(iPr)P$ and $H_2T(cyHx)P$ were from the extremely slow evaporation of toluene. These had the best appearance (large with shiny sides) but alas, still no fully refined structures could be determined, and high *R*-factors were still present due to poor data to parameter ratios. The porphyrin, $H_2T(CHPh_2)P$, gave no diffraction quality crystals from any of the methods used, and although further attempts were made to obtain crystals, they all resulted in powder. Therefore all efforts with this porphyrin were finally abandoned.

5.3.2 X-ray structure for $H_2T(iBu)P$ (P1)

Obtaining a structure for this particular porphyrin without disorder is impossible due to the starting material being a racemic mixture. This starting aldehyde, 2-methylbutyraldehyde, had both R- and S-enantiomers present. Clearly, when synthesizing the porphyrin, it is possible for there to be different R and S chiral centres present at each of the *meso*-substituents. This results in several different feasible configurations, for example they could all be the R-enantiomer (R,R,R,R), or all the S-enantiomer (S,S,S,S), or there could be mixtures of the two enantiomers, e.g. (S,R,S,R), (S, S, R, R), (R, S, S, S), (S, R, R, R), etc.

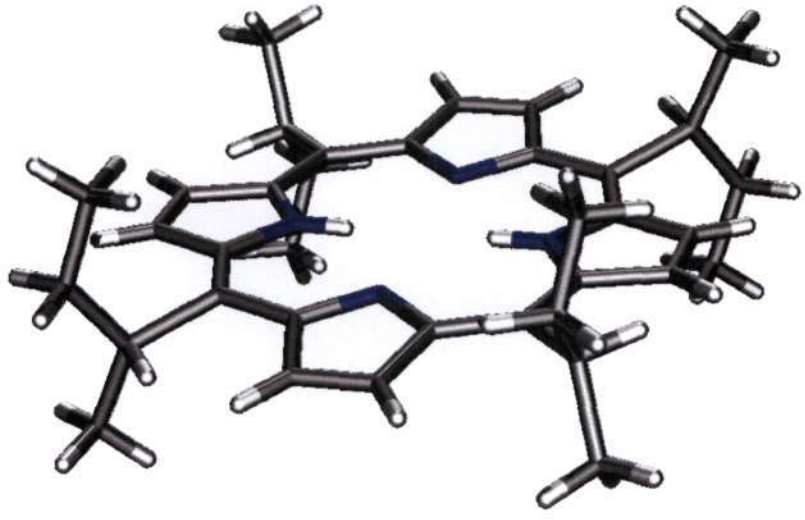

Figure 5.5: The structure of $H_2T(iBu)P$ (P1) as determined from X-ray diffraction.

Although it was possible to obtain an X-ray quality crystal which diffracted well, and despite the fact that the structure was refined with an internal *R*-value of less than 10%, the racemic disorder was too great for the structure to be refined to completion. The final structure was an average of all the possible different R/S configurations, and therefore the disorder could not be effectively modelled. The final observed structure (as seen in Figure 5.5) was planar with a slight wave component, whereas the resulting structure calculated using DFT methods (at the B3LYP/6-31G** level of theory) was ruffled.

5.3.3 X-ray structure for $H_2T(CH_2Ph)P$ (P2)

5,10,15,20-Tetrabenzylporphyrin (1) is a novel example of a structurally characterized *meso*-tetraalkylporphyrin. This porphyrin was found to exhibit a planar central macrocycle with only a very slight wave component and inversion symmetry. The central macrocycle was essentially flat except for a slight tilt of the pyrrole rings; this could be seen using either torsion angles (ranging from 0.6 to 3.73°) or a plane through the macrocycle using Mercury 1.4.[321] These deviations from the mean plane are shown in Figure 5.6 and most likely reflect very minor crystal packing effects.

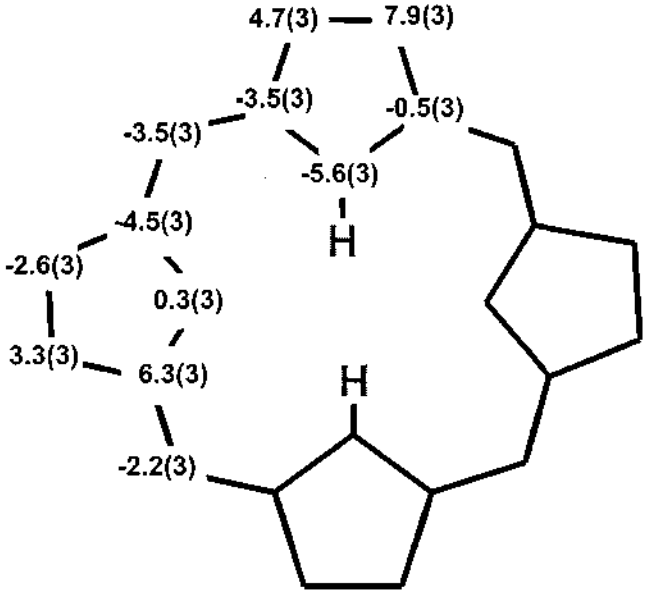

Figure 5.6: A schematic diagram showing the slight deviations (pm) of the chemically unique atoms from the plane of the central macrocycle of 5,10,15,20-tetrabenzylporphyrin (1).

Two adjacent *meso*-alkyl substituents project above the mean plane (on one side of the macrocycle face) and the remaining two project below the mean plane (on the opposite face) therefore resulting in inversion symmetry. The labelled X-ray crystal structure of (1) at 100 Kelvin is shown in Figure 5.7. In an unstrained porphyrin, a planar macrocycle is normally observed if crystal packing effects are slight. Therefore this structure represents a relatively unstrained porphyrin that is relatively free from crystal packing induced strain. This planarity is then likely to also be found in solution. The resulting structure that was calculated using DFT methods (at the B3LYP/6-31G** level of theory) also gave a planar conformation with a slight wave component

(Chapter 7), suggesting that a planar conformation is favoured on energetic grounds in the absence of crystal packing constraints.

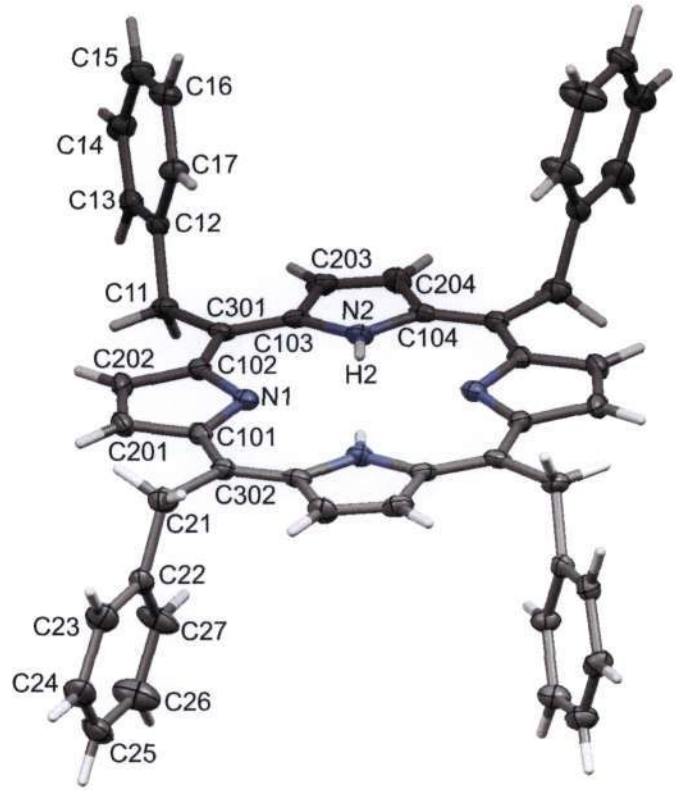

Figure 5.7: Partly labelled ORTEP view (displaying chemically unique atom labels for the asymmetric unit only) of the X-ray structure of (1) (50% probability displacement ellipsoids), showing the overall molecular conformation. (Hydrogen atom labels have been left out for clarity.)

Crystals of $H_2T(CH_2Ph)P$ were thin plates (0.02 × 0.15 × 0.20 mm^3). However, data were collected to 0.95 Å resolution owing to the small triclinic unit cell (a = 5.952(2) Å, b = 12.076(4) Å, c = 12.188(5) Å, α = 91.76(3)°, β = 100.16(3)°, γ = 97.75(3)°, V = 853.0(5) $Å^3$). The final structural model gave R_1 = 0.0698 and wR_2 = 0.1491 with the space group determined as $P\bar{1}$ (Table 5.2). The maximum and minimum electron densities on the final difference Fourier map were 0.268 (1.76 Å from H(2)) and -0.271 (0.97 Å from C(104)) e $Å^{-3}$, respectively. There are no peaks that are greater than 1 e $Å^{-3}$ and therefore it is clear that all non-hydrogen atoms have been located. The crystallographic details for this data collection and final crystal structure are listed in Table 5.2. Atomic coordinates, crystal data and structure refinement tables, as well as the IUCR[322] CIF check report, are available in **Appendix D1**.

Table 5.2: Crystallographic data and structure refinement for $H_2T(CH_2Ph)P$.

Empirical formula	$C_{48}H_{38}N_4$	
Formula weight	670.82 amu	
Temperature	100(2) K	
Wavelength	0.71073 Å	
Crystal system	Triclinic	
Space group	$P\bar{1}$	
Unit cell dimensions	a = 5.952(2) Å	α = 91.76(3)°
	b = 12.076(4) Å	β = 100.16(3)°
	c = 12.188(5) Å	γ = 97.75(3)°
Volume	853.0(5) $Å^3$	
Z	1	
Density (calculated)	1.306 Mg/m^3	
Absorption coefficient	0.077 mm^{-1}	
F(000)	354	
Crystal size	0.20 x 0.15 x 0.02 mm^3	
Theta range for data collection	4.12 to 25.05°	
Index ranges	$-6 \le h \le 7$ $-14 \le k \le 14$ $-14 \le l \le 11$	
Reflections collected	5627	
Independent reflections	2991 (R_{int} = 0.1051)	
Completeness to theta = 25.00°	99.3 %	
Absorption correction	None	
Max. and min. transmission	0.9985 and 0.9848	
Refinement method	Full-matrix least-squares on F^2	
Data / restraints / parameters	2991 / 0 / 236	
Goodness-of-fit on F^2	0.886	
Final R indices [$I > 2\sigma(I)$]	R_1 = 0.0698, wR_2 = 0.1491	
R indices (all data)	R_1 = 0.1383, wR_2 = 0.1724	
Largest diff. peak and hole	0.268 and -0.271 e $Å^{-3}$	

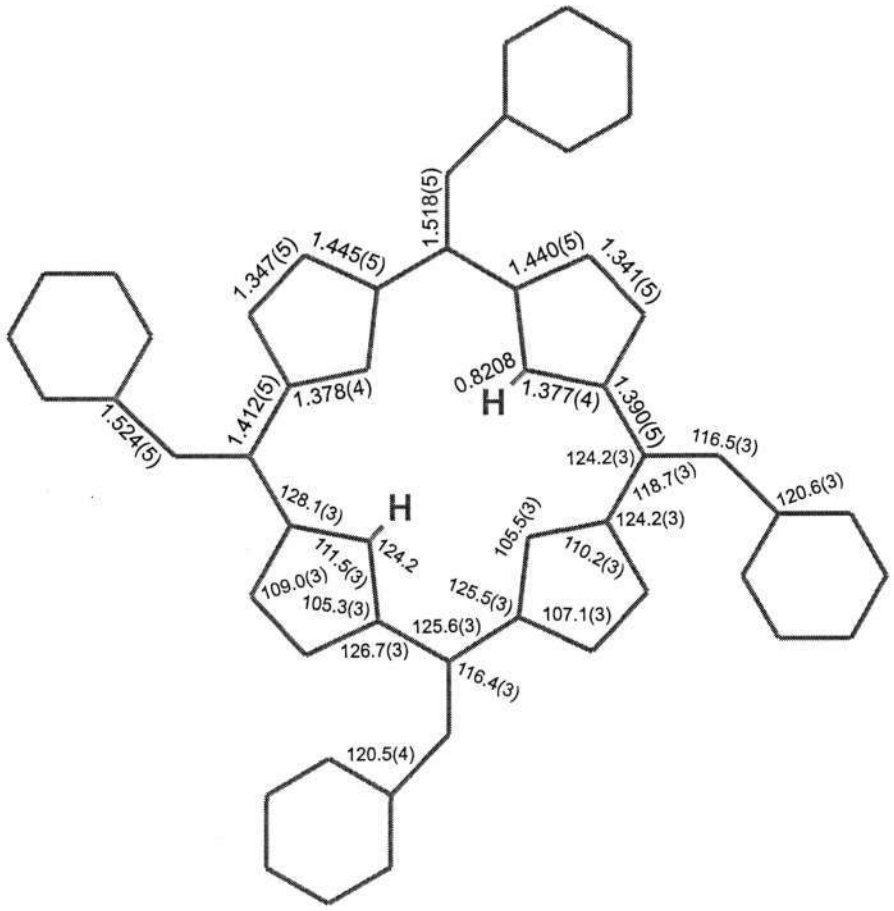

Figure 5.8: Skeletal diagram of (1) showing the average structural parameters for each chemically unique class of bond (Å) and angle (°) in the porphyrin macrocycle and *meso*-substituent (bonds on the top left half and angles on the lower right half of the molecule). The bond lengths and angles for the phenyl rings have not been labelled, the average values are 1.387(6) Å and 119.9°, respectively.

Figure 5.8 shows the average structural parameters for each chemically unique class of bond and angle in the porphyrin macrocycle and *meso*-substituent. The hydrogen atoms and hence their bond lengths and angles (other than N-H) were left out for clarity. The N-H bond lengths were 0.821 Å, which are shorter than any of the other bonds to hydrogen atoms in the structure. N-H bonds are shorter than C-H bonds, since nitrogen is more electronegative than carbon. The torsion angles for the *meso*-substituent aryl rings with regard to the porphyrin plane were determined. The rings opposite each other had the same dihedral angles due to the inversion symmetry of the molecule, but the rings next to each other differed slightly, resulting in two chemically unique groups. These values show the aryl rings are tilted slightly with respect to the porphyrin macrocyclic plane, with one set of rings having a greater

incline (118.22 and –64.92°) than the other (88.44 and –91.71°). These rather acute torsion angles mean that the phenyl rings are tipped over towards the adjacent pyrrole rings.

The packing symmetry and interactions for (1) are shown more clearly in Fig. 5.9, which depicts a perspective view of the unit cell. There is a full molecule positioned at the centres of two opposite cell edges of the unit cell that projects into the neighbouring unit cells. This results in two half molecules in each unit cell, and therefore there is one molecule in the triclinic unit cell (Z = 1). The crystal symmetry and occupancy of the asymmetric unit requires that the porphyrins are tilted equivalently with respect to the unit-cell axes, such that the molecular packing places the molecules in close van der Waals contact with each other.

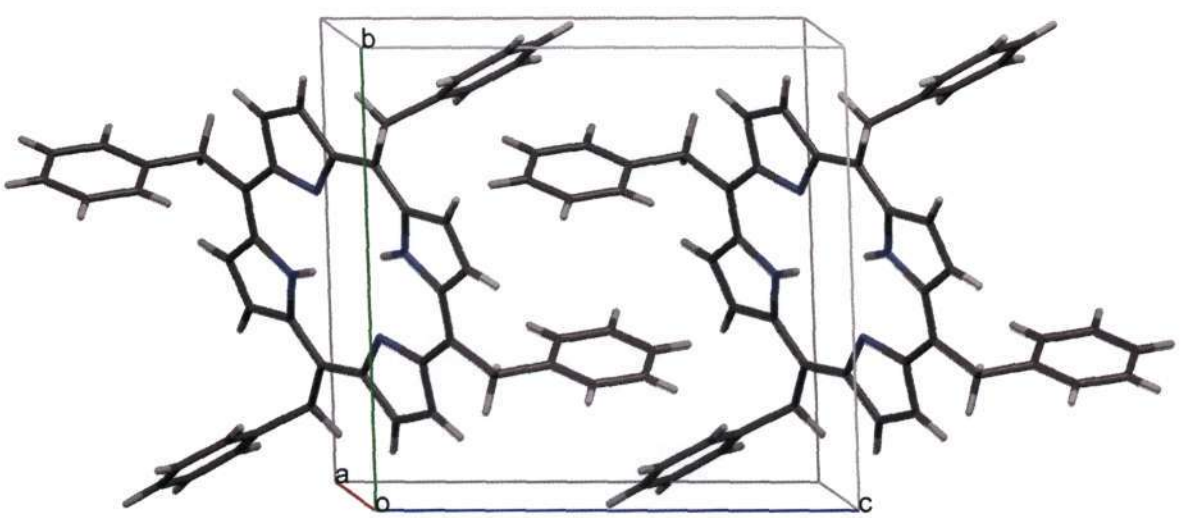

Figure 5.9: A perspective view of the unit cell of (1) illustrating the interaction in relation to the remaining unit-cell contents.

The crystal packing shows an interesting "staircase" or ladder-like arrangement of the macrocycles, which pack horizontally above each other with half of one molecule overlapping with the next. There is a short C-H$\cdots\pi$ contact that occurs between one of the two hydrogen atoms from the CH_2 group of the *meso*-substituent and a C(a) of the next molecule (at a distance of 2.556 Å). This C-H$\cdots\pi$ contact also occurs in reverse

from the neighbouring molecule to give a symmetrical interaction. Since aliphatic C-H donors are weakly acidic, the C-H··· π interaction is expected to be weak, and therefore will not necessarily exist in solution. The π-stacking present in this molecule has an interplanar distance of 3.418 Å, which compares favourably with the sum of the van der Waals radii of two carbon atoms (3.4 Å).

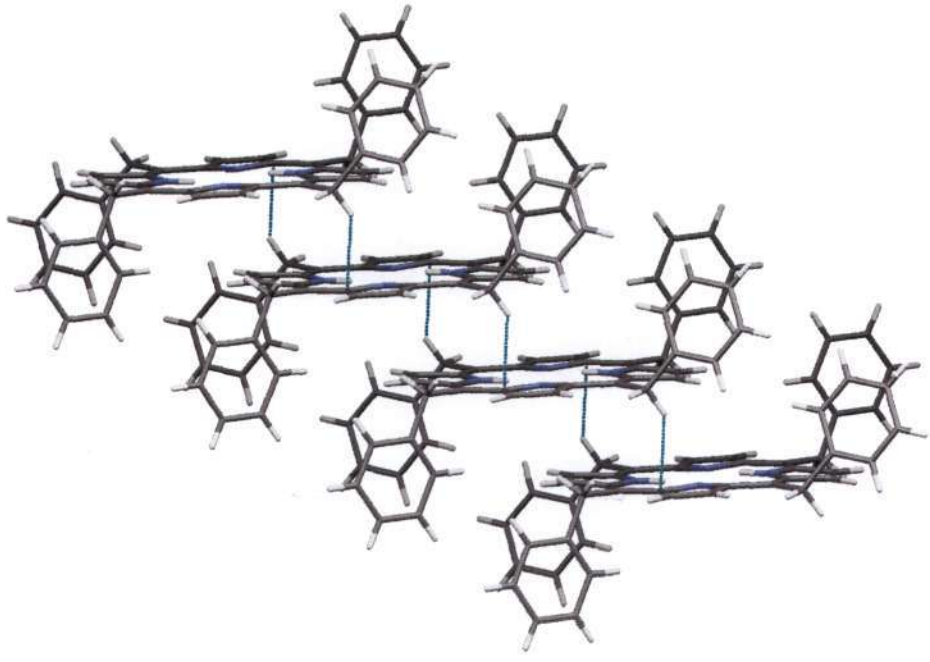

Figure 5.10: The packing "staircase" of the porphyrin, $H_2T(CH_2Ph)P$, showing short contacts between neighbouring porphyrins. The C-H··· π contacts measure 2.556 Å.

The H atom of the C-H donor to the π-system can be seen in the space-filling model in Figure 5.11. This model clearly shows how tight the interaction is. The next two atoms of the neighboring molecule can also be seen; a carbon atom (C102) above the CH_2 group hydrogen atom and a hydrogen atom (H21B) above a C(a) atom. This space-filling model also depicts the interesting "staircase" packing of three molecules and shows how they essentially interlock in a stepwise manner. A representative schematic diagram showing this particular "step-packing" pattern is shown in Figure 5.12.

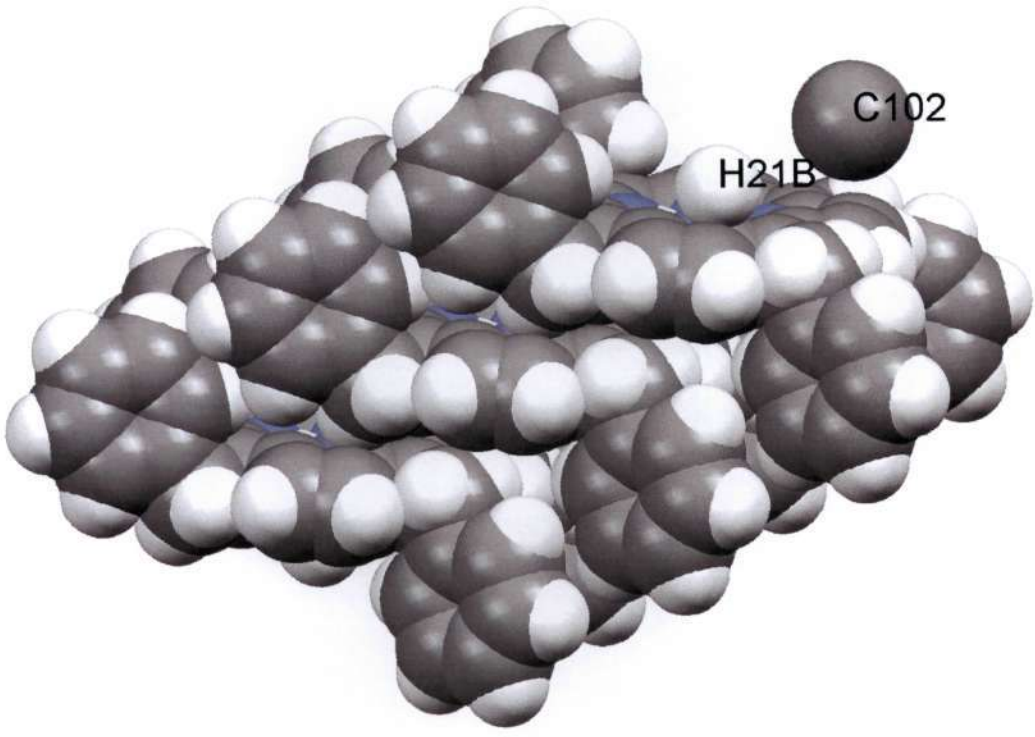

Figure 5.11: A space-filling plot (CPK model) of three neighbouring molecules of (1) in the crystal lattice showing the packing pattern and the two labelled short contacts of the top molecule.

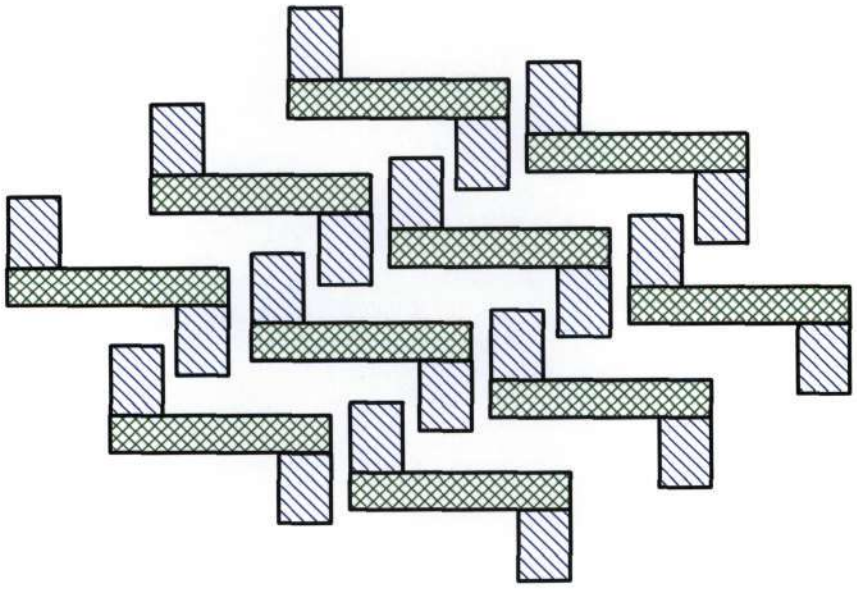

Figure 5.12: A schematic diagram to show the particular packing prototype in this crystal structure of 5,10,15,20-tetrabenzylporphyrin.

5.3.4 X-ray structure for $H_2T(iPent)P$ (P3)

The data for 5,10,15,20-tetraisopentylporphyrin (2) yielded a two-molecule monoclinic unit cell with an inversion plane along the central axis through the molecule. The final values for R_1 and wR_2 were 0.1340 and 0.3256, respectively, with the space group of $P2_1/c$. As noted previously, these high *R*-values reflect weak diffraction from the crystal and a low data to parameter ratio. This porphyrin showed an essentially planar central macrocycle, except for a slight wave component and the inversion symmetry. The slight tilt of the pyrrole rings was similar to that seen in the structure of $H_2T(CH_2Ph)P$, with torsion angles ranging from 0.56 to 3.2°. One pair of opposite pyrrole rings was tilted more out of the plane than the other pair. These deviations from the mean plane are shown in Figure 5.13 below.

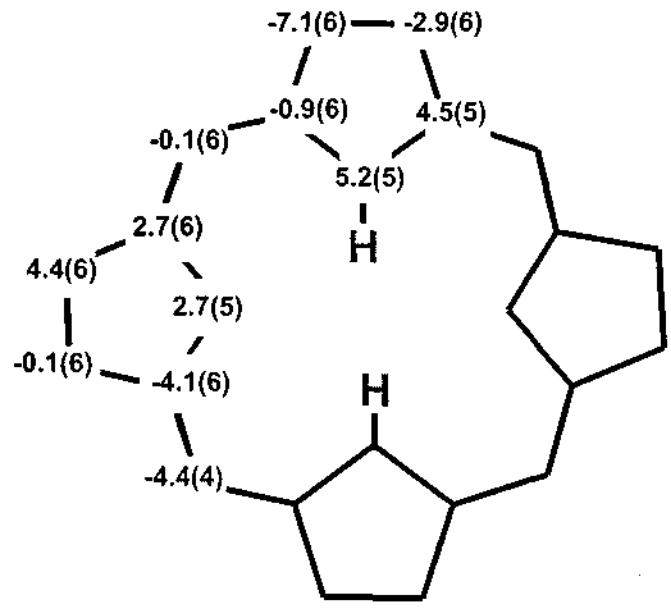

Figure 5.13: A schematic diagram showing the slight deviations (pm) from the plane of the central macrocycle for the chemically unique atoms of 5,10,15,20-tetraisopentylporphyrin (2).

If the slight deviation from planarity that is observed in the X-ray structure is not seen in solution, then it might be as a result of packing effects in the crystal lattice. The resulting structure for $H_2T(iPent)P$, calculated using DFT methods (at the B3LYP/6-31G** level of theory), however, gave a severely ruffled conformation (Chapter 7). This suggests that packing effects in fact have a tendency to flatten and actually reduce the deviation from planarity, rather than enhancing it for this particular

structure. This was also seen for the disordered structure of $H_2T(iBu)P$ (P1). Figure 5.14 shows the labelled X-ray crystal structure of (2) at 100 K.

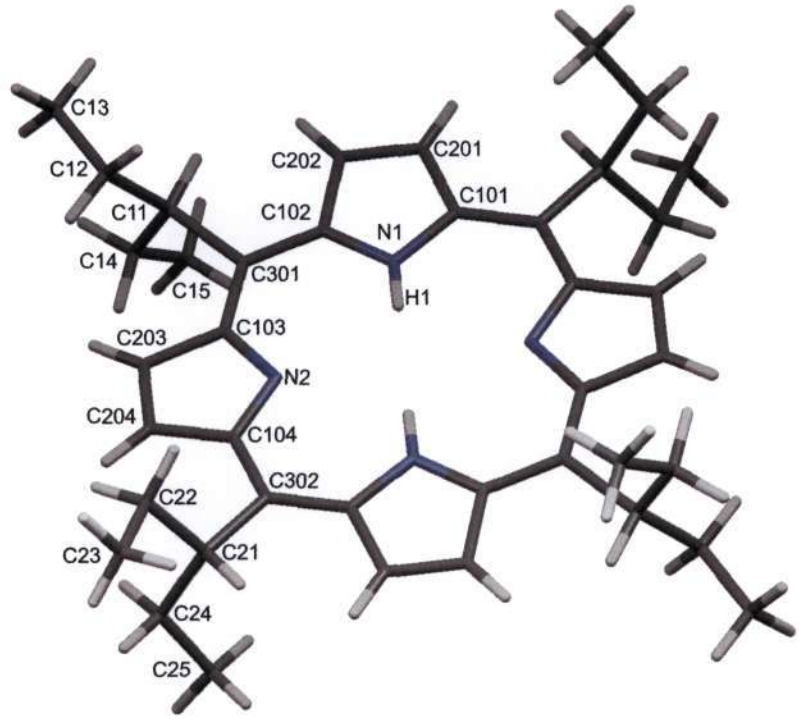

Figure 5.14: Labelled view of the X-ray structure of (2) for the asymmetric unit only, showing the overall molecular conformation. (Hydrogen atom labels have been left out for clarity.)

5,10,15,20-Tetraisopentylporphyrin (2) is not a completely new example of a structurally characterized *meso*-tetraalkylporphyrin, as it has previously been recorded by Senge *et al.* as the monoacid[58] (in the same space group as $H_2T(iPent)P$ in this work) and as a diacid[82] (space group $P\bar{1}$). However, the free base structure reported here has not been described in the literature and therefore, despite not being fully refined, is still a novel structure. These simple alkyl *meso*-substituents are not chiral and therefore they have an expected "balance" in their bulk and the subsequent strain which they will exert on the central macrocycle; however, there is an unanticipated symmetry pattern and consequent distortion from planarity. Adjacent substituents have the hydrogen groups on the same side, slightly distorted from the mean plane. Subsequently, the two ethyl groups of these neighbouring substituents are also in a similar conformation, with one up and the other down (with respect to the mean plane). In the case where the methine hydrogen atom is slightly below the plane of the molecule, the ethyl group at the top extends over the macrocycle, whereas the ethyl

group below extends away from the central core. This pattern is mirrored on the other side of the molecule by the remaining two substituents. Although the adjacent substituents are not completely identical and cannot be perfectly superimposed, the same basic outline is observed between opposite sets of substituents. This is depicted in Figure 5.15.

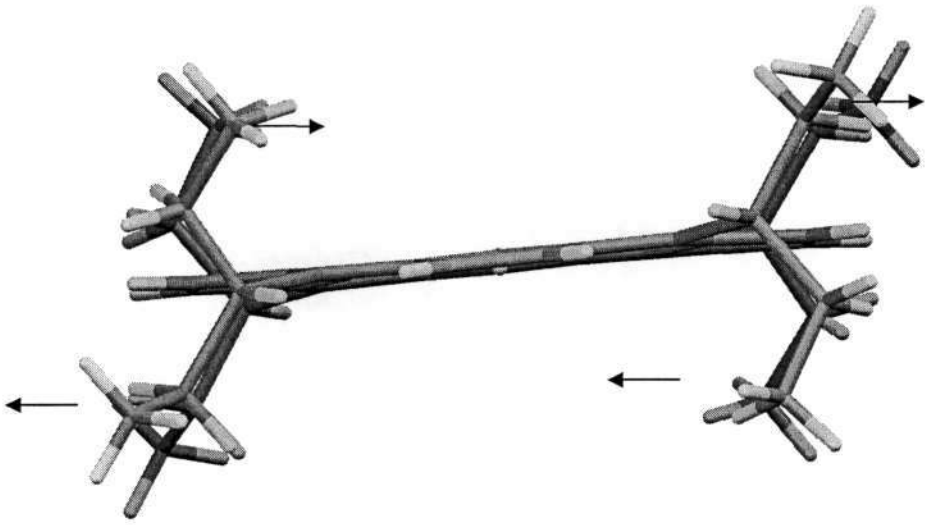

Figure 5.15: The two adjacent substituents on the left with the methine hydrogen atom slightly below the mean plane and the two on the right with the hydrogen group slightly above the plane. This shows the position of the ethyl groups, either extended over or away from the macrocycle.

The maximum and minimum electron densities on the final difference Fourier map were 1.077 (0.85 Å from H(15A)) and -0.364 (0.37 Å from H(1)) e $Å^{-3}$, respectively. The crystallographic details for this data collection and final crystal structure are listed in Table 5.3. Atomic coordinates, crystal data and structure refinement tables are available in **Appendix D2**.

Table 5.3: Crystal data and structure refinement for $H_2T(iPent)P$.

Empirical formula	$C_{40}\ H_{54}\ N_4$	
Formula weight	590.87 amu	
Temperature	100(2) K	
Wavelength	0.71073 Å	
Crystal system	Monoclinic	
Space group	$P2_1/c$	
Unit cell dimensions	a = 11.328(11) Å	α = 90°
	b = 10.448(10) Å	β = 98.02(8)°
	c = 14.179(12) Å	γ = 90°
Volume	1662(3) $Å^3$	
Z	2	
Density (calculated)	1.181 Mg/m^3	
Absorption coefficient	0.069 mm^{-1}	
F(000)	644	
Crystal size	0.40 x 0.30 x 0.02 mm^3	
Theta range for data collection	4.30 to 25.15°	
Index ranges	$-12 \le h \le 13$	
	$-12 \le k \le 11$	
	$-16 \le l \le 14$	
Reflections collected	9412	
Independent reflections	2944 [R_{int} = 0.1837]	
Completeness to theta = 25.00°	99.3 %	
Max. and min. transmission	0.9986 and 0.9730	
Refinement method	Full-matrix least-squares on F^2	
Data / restraints / parameters	2944 / 6 / 199	
Goodness-of-fit on F^2	0.971	
Final R indices [$I > 2\sigma(I)$]	R_1 = 0.1340, wR_2 = 0.3256	
R indices (all data)	R_1 = 0.2601, wR_2 = 0.3855	
Largest diff. peak and hole	1.077 and -0.364 e $Å^{-3}$	

Figure 5.16 shows the structure of $H_2T(iPent)P$ with the average structural parameters for the bonds and angles in the porphyrin macrocycle and *meso*-substituents. Averages are given for each of the chemically unique values. The hydrogen atoms for this structure were calculated and hence their bonds and angles are all standard, thus

they have been excluded for clarity. The angles and bond lengths of the pyrrole rings compare relatively well with those of the resolved structure for $H_2T(H_2Ph)P$, with the angles and bond lengths for the C(m) having even closer values. The ethyl groups show angles and bond lengths of the expected magnitude with no particular outliers. The torsion angles of the *meso*-substituents with respect to the macrocycle were measured and showed only slight differences of about 1° between the two unique groups, C(11) to C(15) and C(21) to C(25).

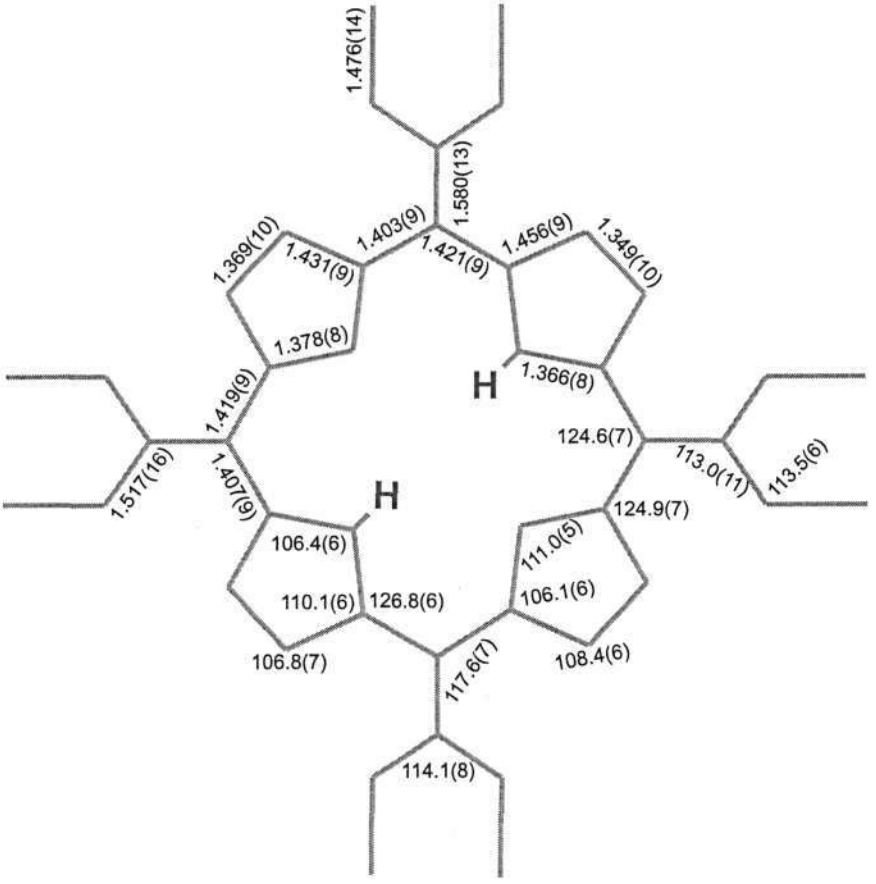

Figure 5.16: Skeletal diagram of (2), showing the average structural parameters for each chemically unique class of bond (Å) and angle (°) in the porphyrin macrocycle and *meso*-substituent. (Bonds on the top left half and angles on the lower right half of the molecule.)

The packing diagram shown in Figure 5.17 indicates how the molecules of (2) are arranged in the crystal lattice. The unit cell has eight molecules which are stacked in pairs at four sides of the unit cell; this is clearly shown in Figure 5.17. One quarter of each of these molecules is inside the unit cell which therefore gives the final Z-value of 2. The molecules are stacked in layers almost perpendicular to each other, as shown

in Figure 5.18, creating a step-like packing. Each of the individual layers forms its own structure with cavities in which the perpendicular structures fit. An example of one of these layers and the honeycomb-type pattern it forms is shown in Figure 5.18.

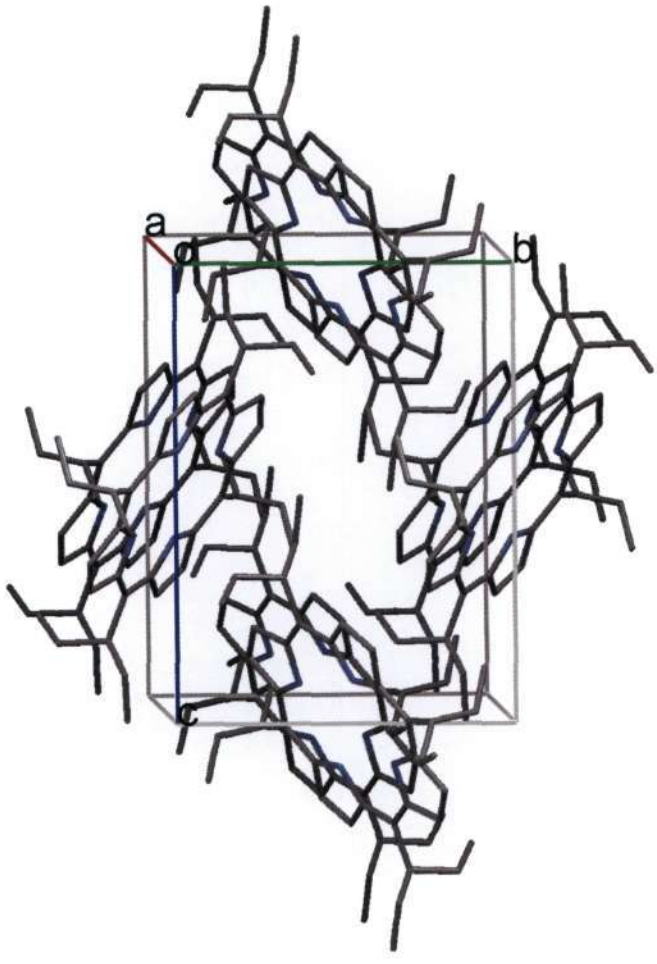

Figure 5.17: The packing of the porphyrin, $H_2T(iPent)P$. View of the unit cell packing approximately along the *a* axis. The H atoms have been left out for clarity.

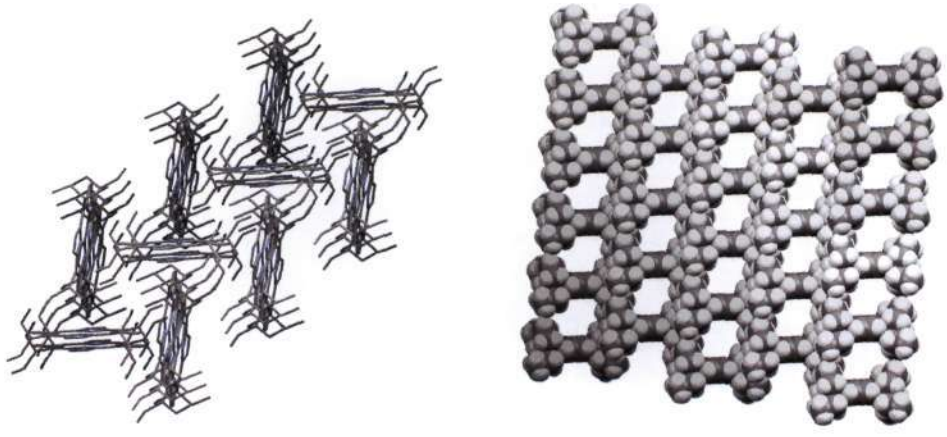

Figure 5.18: The step-like perpendicular packing and the honeycomb-type layers.

The short intermolecular contacts for $H_2T(H_2Ph)P$ are shown in Figure 5.19. There are four types of short contacts seen between the layers of porphyrin molecules: (1) terminal hydrogen atoms of the *meso*-substituents of one porphyrin with two C(b) atoms of the neighbouring porphyrin, (2) terminal hydrogen atoms of the *meso*-substituents of one porphyrin with terminal carbon atoms of the *meso*-substituents of the neighbouring porphyrin, (3) pyrrole hydrogen atoms with the C(a) and C(b) atoms of the neighbouring porphyrin, and (4) the terminal hydrogen atom of the *meso*-substituents of one porphyrin with a hydrogen atom of the CH_2 group of the *meso*-substituents of the neighbouring porphyrin. The distances for each of these short intermolecular contacts are as follows: (1) = 2.784 and 2.832 Å, (2) = 2.332 Å, (3) = 2.859 Å to C(a) atom, 2.879 Å to C(b) atom, and (4) = 2.899 Å.

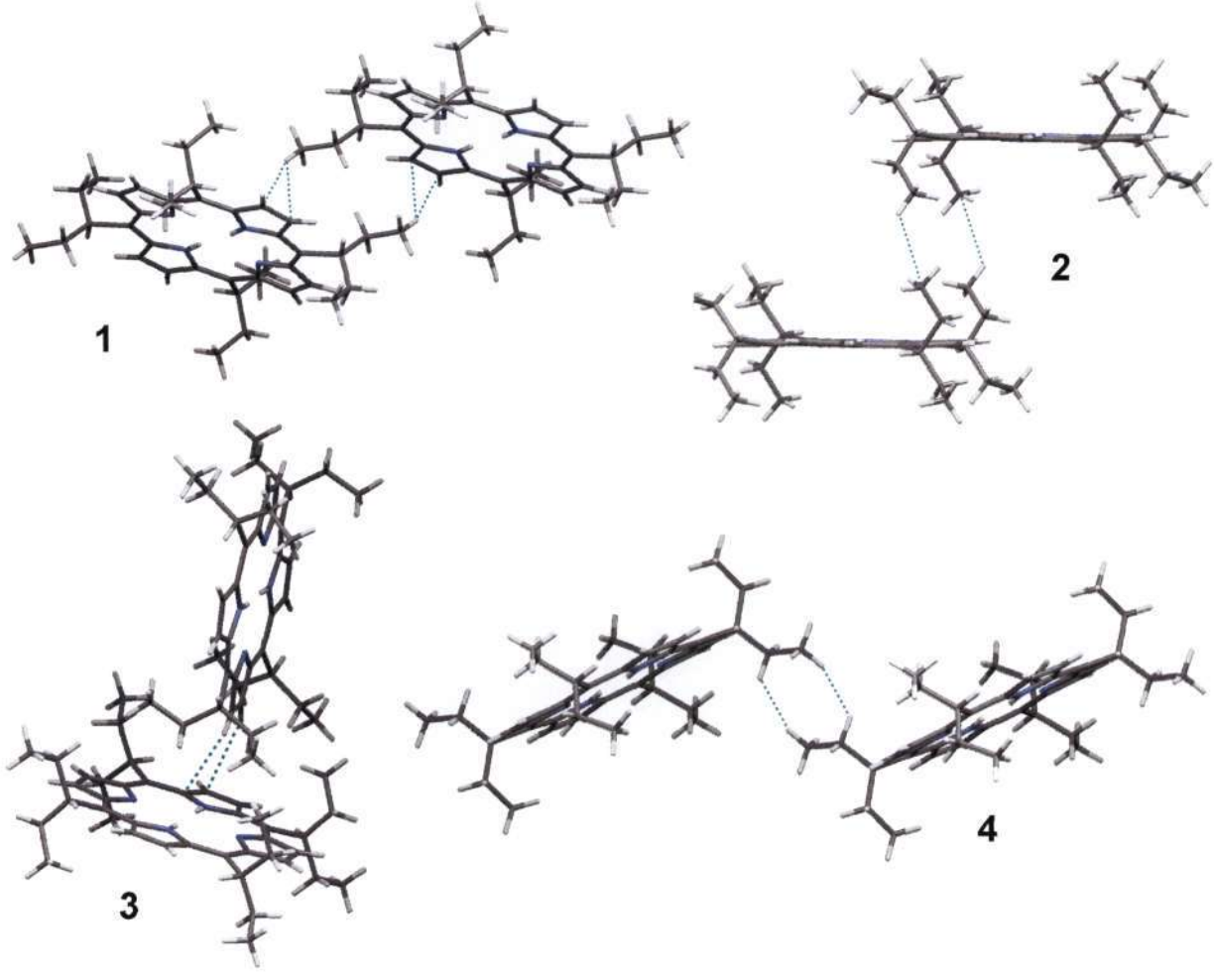

Figure 5.19: The four different short contacts between the molecules of 5,10,15,20-tetraisopentylporphyrin (2).

Of the above contacts, (1) and (2) also occur in reverse between the same two molecules; however, contacts (3) and (4) do not. There is only one set of this type of contact between any two molecules, but each particular molecule possesses two sets of this contact. This is because on opposite sides of molecule this contact occurs with different porphyrin neighbours, and hence it forms a type of chain connection. All the contacts occur between molecules in parallel planes, except for (3) which occurs between molecules that are perpendicular to each other. The shortest contact is (2) between a terminal hydrogen atom of the *meso*-substituents of one porphyrin and a terminal carbon atom of the *meso*-substituents of the neighbouring porphyrin. The longest is between a terminal hydrogen atom of the *meso*-substituents of one porphyrin and a hydrogen atom of the CH_2 group of the *meso*-substituents of the neighbouring porphyrin (4).

5.3.5 X-ray structure for $H_2T(iPr)P$ (P5)

This is one of the most fascinating *meso*-tetraalkylporphyrin structures. Despite the small and simple *meso*-substituents, there is rotational disorder that negates complete refinement of the alkyl groups. This disorder is due to the variety of different conformations that may be formed. The final crystal structure that is determined for this porphyrin is actually an average of two predominant conformations. The way in which this "averaging process" functions is depicted below in Figure 5.20.

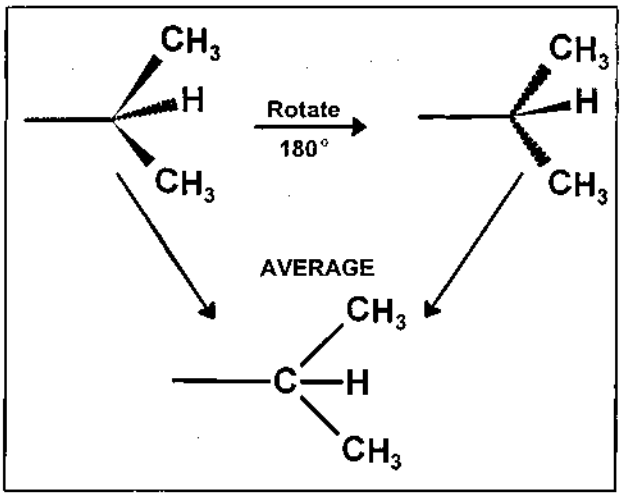

Figure 5.20: Conformational isomerism of the iPr substituents of $H_2T(iPr)P$.

The resulting refined structure, which is shown in Figure 5.21, therefore exhibits a "planar" iPr group that is clearly an average of two major conformations of the iPr group. The porphyrin macrocycle is therefore almost perfectly planar with inversion symmetry. Each of the substituents is in the same conformation with the hydrogen atom lying in the mean plane of the macrocycle, with one methyl group on either side of it. Thus the methyl groups are nearly mirror images of each other, with one directly below and one directly above the mean plane of the porphyrin macrocycle. However, they exhibit torsion angles (with respect to the mean plane) of not quite 90° (e.g. 95.16 and 86.19°) and therefore are not exactly lined up with each other.

In the literature, two structures for this particular porphyrin have been reported, one for the diacid and one for the free base. The diacid was solved in the space group $P\bar{1}$ and the free base had the space group Fdd2. In this work it was the free base porphyrin structure, $H_2T(iPr)P$, that was to be determined. The space group which gave the best results (R_1 = 0.0812 and wR_2 = 0.2048) for this structure was *I*23. The Fdd2 structure is ordered, while the present *I*23 structure is disordered. The data set could not be solved in Fdd2 and thus we have a novel polymorph of $H_2T(iPr)P$.

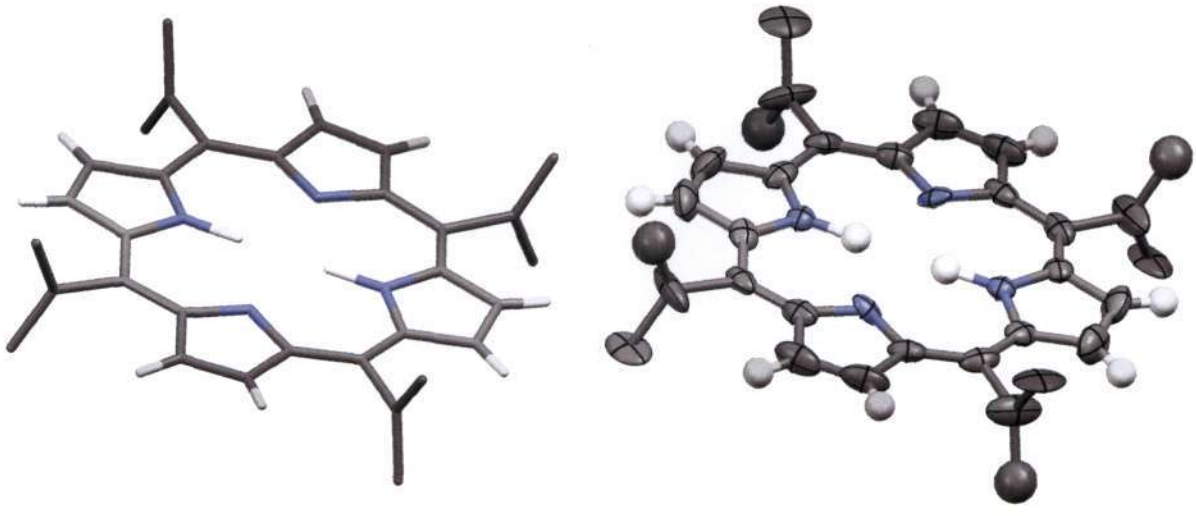

Figure 5.21: The X-ray structure of $H_2T(iPr)P$, showing the overall molecular conformation of the planar macrocycle and the average structure of two possible iPr group orientations (left). A thermal ellipsoid plot shows the disorder of the system (right). Non positive definite atoms are shown as spheres. (Substituent hydrogen atoms have been left out for clarity.)

In the thermal ellipsoid view of the structure, shown in Figure 5.21, there are four non-positive definite atoms which result from the anisotropic parameters not being reliable. The first carbon atom of the *meso*-substituent to which the two methyl groups are attached is a long, thin oval shape. This markedly elongated ellipsoid confirms the disorder present in the system.

5.3.6 X-ray structure for $H_2T(cyHx)P$ (P6)

Although this porphyrin, *meso*-tetracyclohexylporphyrin (3), has been previously synthesized and the iron,[323] nickel and zinc complexes have been reported and studied,[195,215] the X-ray structure for the free base itself has not been described in the literature. Unfortunately, the structure could not be fully refined in this work either; however, it was possible to solve from the weak diffraction the structure data to final values of 0.2285 and 0.4640 for R_1 and wR_2, respectively. The conformation of this X-ray structure was highly ruffled; the deviations from the mean plane of the macrocycle are shown in Figure 5.22 below.

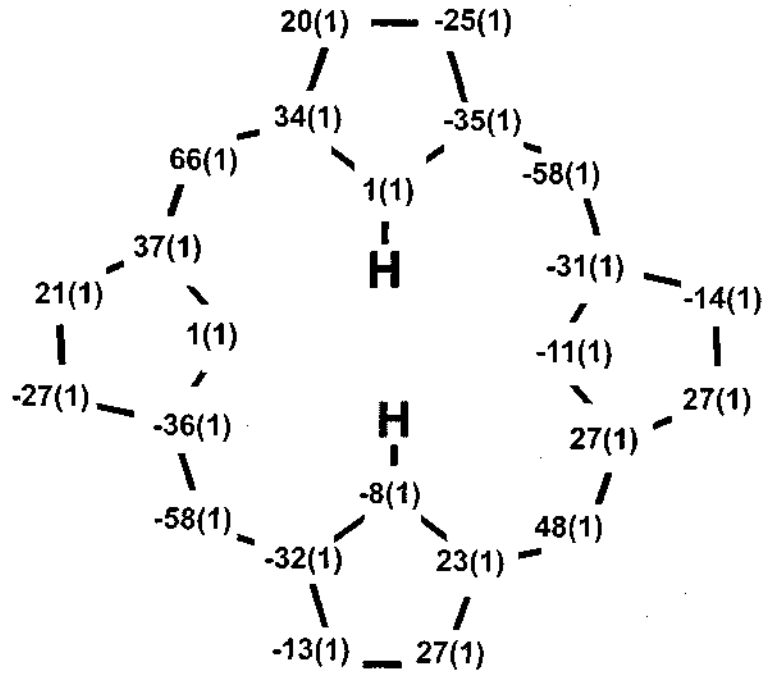

Figure 5.22: A schematic diagram showing the deviations (pm) of the atoms from the plane of the central macrocycle of 5,10,15,20-tetracyclohexylporphyrin (3).

The cause of this marked non-planarity is most likely due to the conformational strain introduced by four bulky cyclohexyl groups. The optimum or lowest energy conformer evidently accommodates the bulky cyclohexyl rings best if the porphyrin macrocycle is strongly ruffled. The structure of $H_2T(cyHx)P$ calculated using DFT methods (at the B3LYP/6-31G** level of theory) also gave a ruffled conformation (Chapter 7). This therefore suggests that the ruffling conformation is favoured on energetic grounds irrespective of whether the structure is in the gas or solid state.

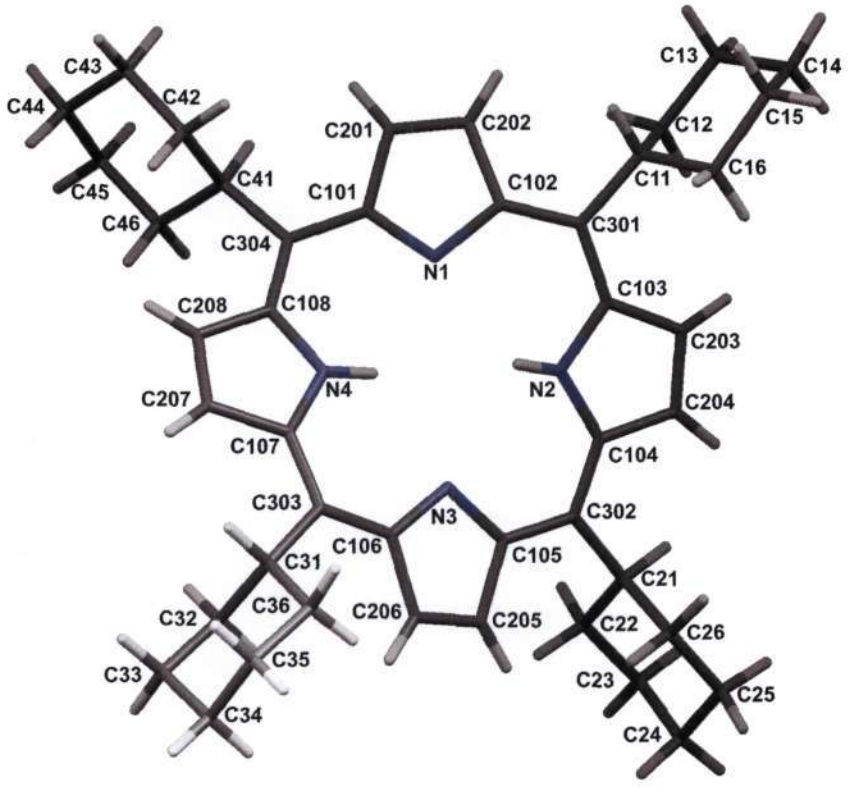

Figure 5.23: A labelled view of the X-ray structure of (3), showing the molecular conformation of the cyclohexyl rings and the overall molecular conformation. (Hydrogen atom labels have been left out for clarity.)

The X-ray crystal structure of (3) at 293 K is shown in Figure 5.23. The cyclohexyl rings are all in the chair conformation and not planar; thus it is necessary to categorize them in some way. This is done using the orientation of the C-H vector of the first carbon of the cyclohexyl ring, in a way that each of the cyclohexyl substituents is assigned a comparative *g* or *–g* value (*qauche conformations*).[195,215] The ruffling of the macrocycle in the X-ray structure causes an alternating deviation from the plane for the C(m) atoms and therefore also for the greater part of the *meso*-substituents. Two

opposite *meso*-substituents are above the mean plane and the remaining two are below. In each case if the C(m) atom is above the mean plane, then so too is the first hydrogen atom of the cyclohexyl ring and therefore the C-H vector is assigned a *g* value. Although these hydrogen atoms are not accurately perpendicular to the mean plane of the macrocycle, they are also not in the mean plane or parallel to it. Therefore their deviation from the mean plane is considered either as a positive value, *g*, or as a negative value, *–g*. Thus the X-ray structure for $H_2T(cyHx)P$ shows a definite (g,–g,g,–g) conformation. The structure determined by DFT for $H_2T(cyHx)P$ also shows the same (g,–g,g,–g) conformation. Due to the sideways position of the hydrogen atom, the cyclohexyl ring is almost perpendicular to the macrocycle of the porphyrin. These C-H vectors face clockwise for two adjacent *meso*-substituents and anti-clockwise for the remaining two.

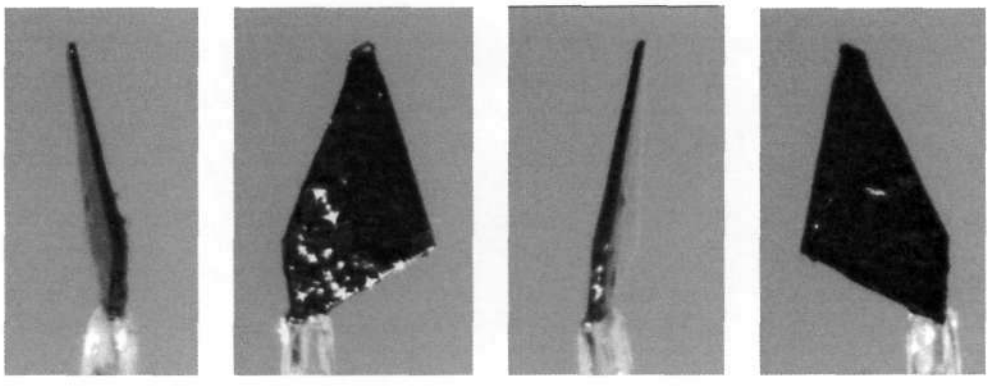

Figure 5.24: Different views to show the small crystal fragment of $H_2T(cyHx)P$.

Crystals of $H_2T(cyHx)P$ were extremely thin plates (0.05 × 0.3 × 0.5 mm^3), as shown in Figure 5.24. This therefore explains the rather limited diffraction data. The maximum and minimum electron densities on the final difference Fourier map were 0.55 (0.59 A from H(207)) and -0.65 (1.29 A from H(14A)) e A^3, respectively. The crystallographic details for this data collection and final crystal structure are listed in Table 5.4 on the following page. Atomic coordinates, crystal data and structure refinement tables are available in **Appendix D3.**

Table 5.4: Crystal data and structure refinement for $H_2T(cyHx)P$.

Empirical formula	$C_{44}H_{54}N_4$	
Formula weight	638.91 amu	
Temperature	293(2) K	
Wavelength	0.71073 Å	
Crystal system	Orthorhombic	
Space group	*P* bca	
Unit cell dimensions	*a* = 10.5218(12) Å	α = 90°
	b = 12.7805(14) Å	β = 90°
	c = 53.917(6) Å	γ = 90°
Volume	7250.4(14) $Å^3$	
Z	8	
Density (calculated)	1.171 Mg/m^3	
Absorption coefficient	0.068 mm^{-1}	
F(000)	2768	
Crystal size	0.05 × 0.3 × 0.5 mm^3	
Theta range for data collection	3.71 to 25.07°	
Index ranges	$-12 \le h \le 12$	
	$-15 \le k \le 15$	
	$-63 \le l \le 64$	
Reflections collected	65864	
Independent reflections	6407 [R_{int} = 0.1528]	
Completeness to theta = 25.00°	99.7 %	
Refinement method	Full-matrix least-squares on F^2	
Data / restraints / parameters	6407 / 0 / 441	
Goodness-of-fit on F^2	1.176	
Final *R* indices [$I > 2\sigma(I)$]	R_1 = 0.2285, wR_2 = 0.4640	
R indices (all data)	R_1 = 0.2769, wR_2 = 0.4785	
Largest diff. peak and hole	0.553 and -0.650 e $Å^{-3}$	

Although there was not any particular crystallographic symmetry in the molecule, chemically unique distances and angles have been averaged. Figure 5.25 shows the skeleton structure of $H_2T(cyHx)P$, with these average structural parameters for the bond lengths and the bond angles in the porphyrin macrocycle and *meso*-substituents. The hydrogen atoms for this structure were calculated and hence their bonds and angles are all standard, thus they have been excluded from the figure for clarity. The

angles and bond lengths of the pyrrole rings compare relatively well with those of the refined structure for $H_2T(H_2Ph)P$.

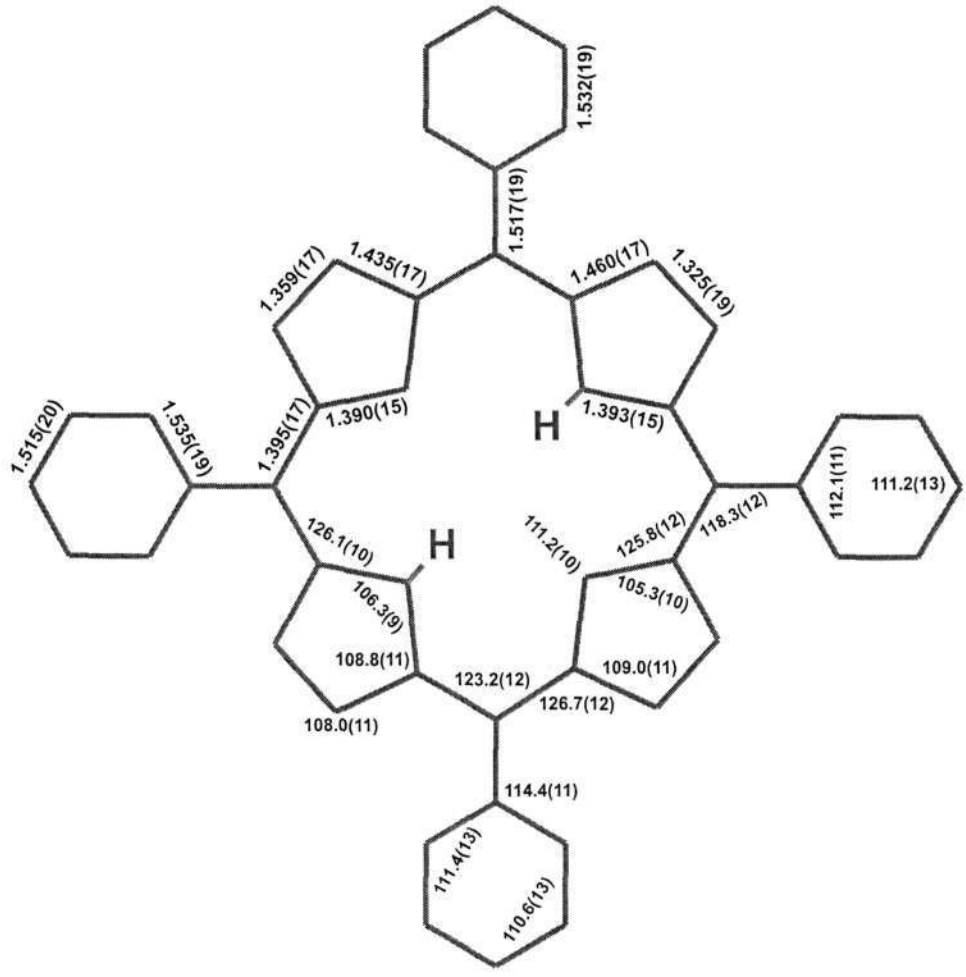

Figure 5.25: Skeletal diagram of (3), showing the average structural parameters for each chemically unique class of bond (Å) and angle (°) in the porphyrin macrocycle and *meso*-substituent (bonds on the top left half and angles on the lower right half of the molecule). The hydrogen atoms have been left out for clarity. These bond lengths and angles were calculated and are therefore the standard, average values.

This porphyrin, $H_2T(cyHx)P$ (P6), has a very large unit cell compared to that of $H_2T(CH_2Ph)P$ (P2). The Z value is 8 and these eight molecules can be seen in groups of two in the unit cell, Figure 5.27. These molecules are packed in two layers in a plane, with one running almost perpendicular to the other. The pattern in which they are packed is shown in Figure 5.28. The partial packing diagram in Figure 5.29 shows how the molecules of $H_2T(cyHx)P$ are arranged in the crystal lattice. There is a short C-H$\cdots\pi$ contact that occurs between one of the two hydrogen atoms at the *meta*-

position of the cyclohexyl ring of the *meso*-substituent and a C(b) atom of the next molecule (at a distance of 2.658 Å). This C-H$\cdots\pi$ contact does not occur in reverse from the neighbouring molecule but rather with another neighbouring molecule on the opposite side of the molecule. The hydrogen atom with which this short contact occurs is one at the *meta*-position of the cyclohexyl ring adjacent to the C(b) atom in the first short contact (Figure 5.29).

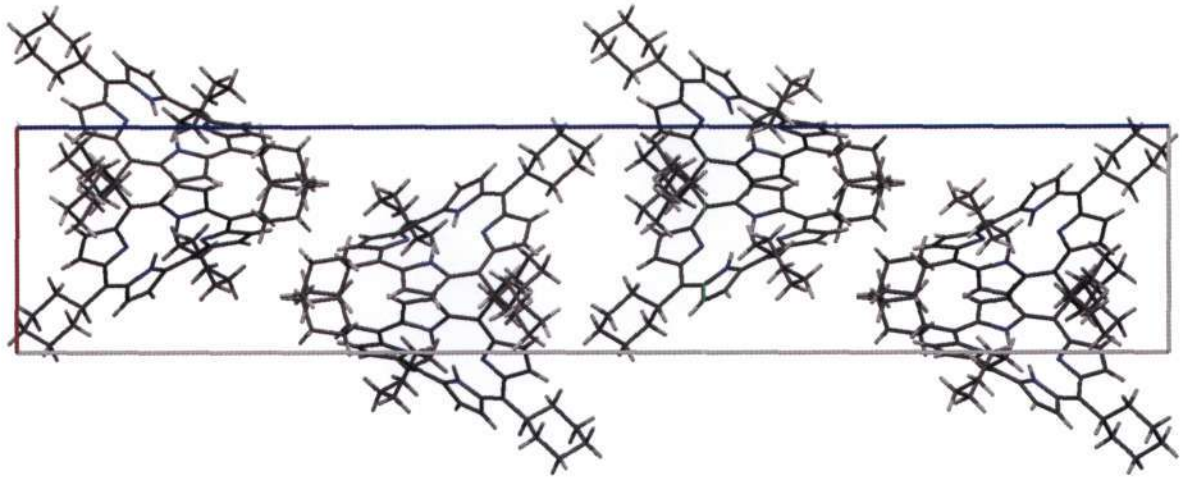

Figure 5.27: The packing of $H_2T(cyHx)P$ showing the eight molecules situated in the unit cell. This view along the b-axis shows how one set of four molecules is centred and the other four, although in line with the first set, alternate along opposite faces of the unit cell.

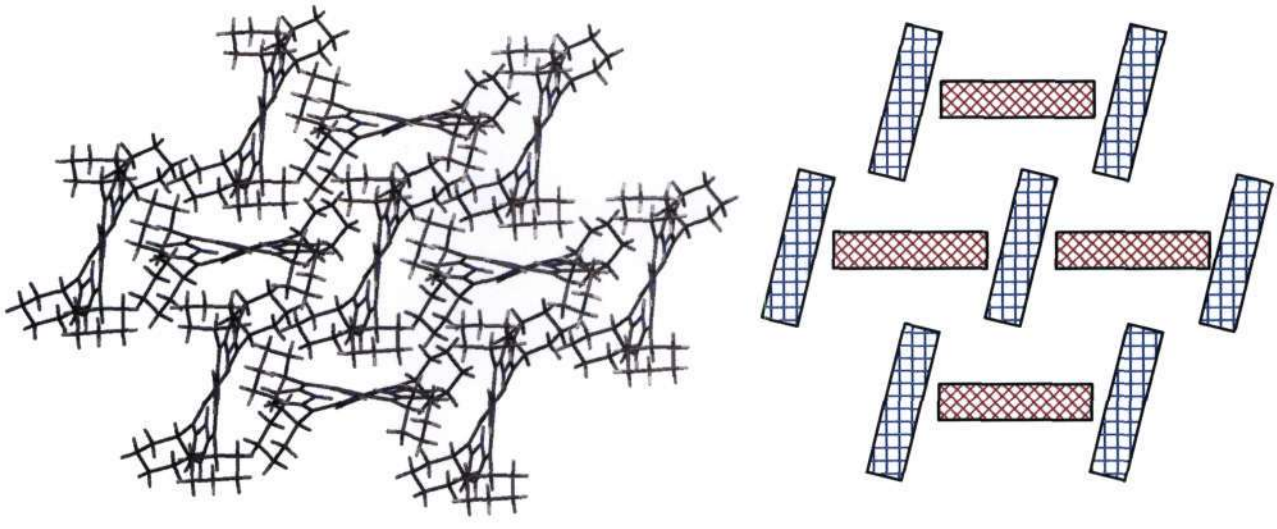

Figure 5.28: The packing pattern of $H_2T(cyHx)P$ showing the actual structure on the left and a representative schematic diagram on the right.

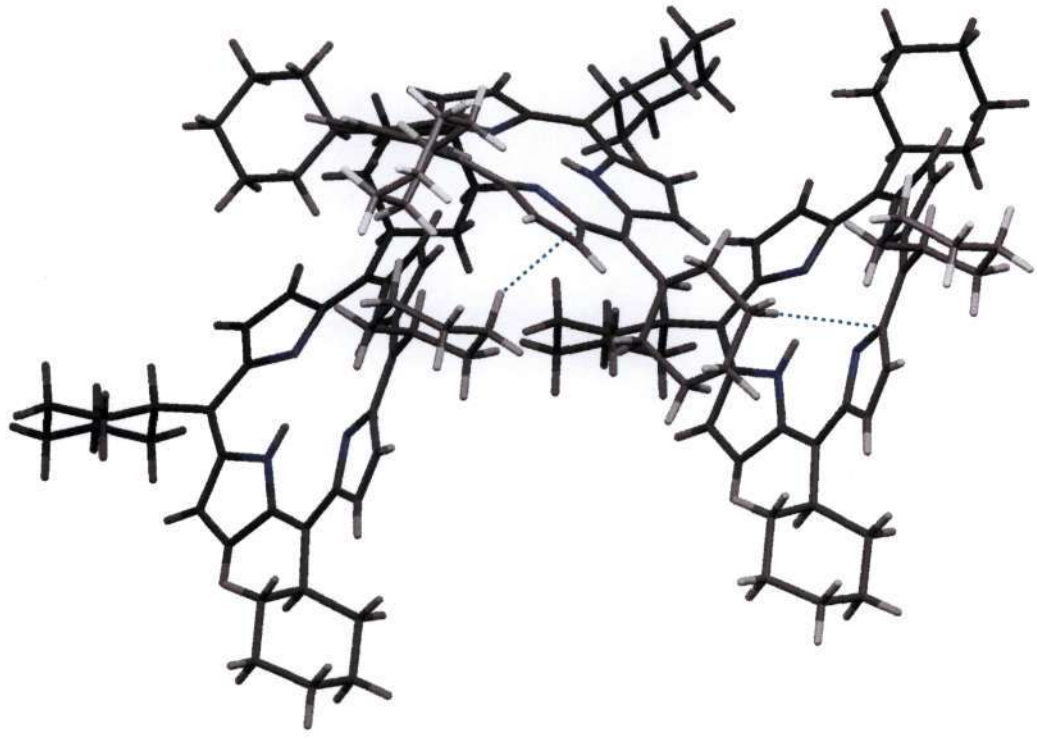

Figure 5.29: Partial packing diagram for $H_2T(cyHx)P$ showing short contacts between neighbouring porphyrins.

5.4 Summary

The porphyrin structures obtained using X-ray diffraction were generally planar, with $H_2T(cyHx)P$ being the only structure that exhibited significant atomic displacements from the plane of the macrocycle and a strongly ruffled conformation. However, when considering the DFT-computed structures, most of the porphyrins had ruffled conformations, with only one predominantly planar structure ($H_2T(CH_2Ph)P$) and one saddled conformation ($H_2T(CHPh_2)P$), as summarized in Table 5.5. Unfortunately, it was not possible to obtain an X-ray structure for $H_2T(CHPh_2)P$, and therefore the conformation in the crystal is not known.

The porphyrins $H_2T(CH_2Ph)P$ and $H_2T(cyHx)P$ both have similar conformations in the X-ray determined and DFT-calculated structures. The remaining three porphyrins: $H_2T(iBu)P$, $H_2T(iPent)P$ and $H_2T(iPr)$, all have a planar crystallographic conformation, while the DFT-computations suggest a ruffled lowest-energy conformer is likely.

According to DFT simulations a saddled conformation would be likely for $H_2T(CHPh_2)P$.

Table 5.5: The summary of the porphyrin properties according to X-ray and DFT calculations.

	Final R_1 factor	Space group	Conformation according to X-ray	Conformation according to DFT optimization
$H_2T(iBu)P$	0.0974	$P2_1/c$	Planar with slight wave distortion component	Ruffled distortion
$H_2T(CH_2Ph)P$	0.0698	$P\bar{1}$	Planar with slight wave distortion component	Planar with slight wave distortion component
$H_2T(iPent)P$	0.1340	$P2_1/c$	Planar with slight wave distortion component	Ruffled distortion
$H_2T(CHPh_2)P$	–	–	–	Saddled distortion
$H_2T(iPr)P$	0.0812	$I23$	Planar with slight ruffling	Ruffled distortion
$H_2T(cyHx)P$	0.2285	$Pbca$	Ruffled distortion	Ruffled distortion

For the planar conformations in the crystalline solid state, packing interactions and inversion symmetry preclude ruffling of the porphyrin macrocycle as suggested by the gas phase DFT simulations. For these porphyrins, the lattice energy readily overcomes the energy penalty associated with a planar macrocycle conformation. The asymmetric unit usually represents a half of the porphyrin structure, this is true for each of the porphyrins except for $H_2T(cyHx)P$. Due to disorder in many of these structures it was not possible to fully refine many of them; however, the structures have been presented because they still confirm the synthesis of the compounds and nonetheless provide some key conformational data.

6. Photoluminescence

6.1 Introduction

Previous chapters have been concerned with the phenomenon of light absorption; however, the *emission* of light can also be used in the study, characterization and structural clarification of various molecules. This type of work can provide further significant information about the molecule, including excited states, force constants, the geometry of molecular ground states and the mechanism of energy transfer between molecules or among different states in the molecule.[324]

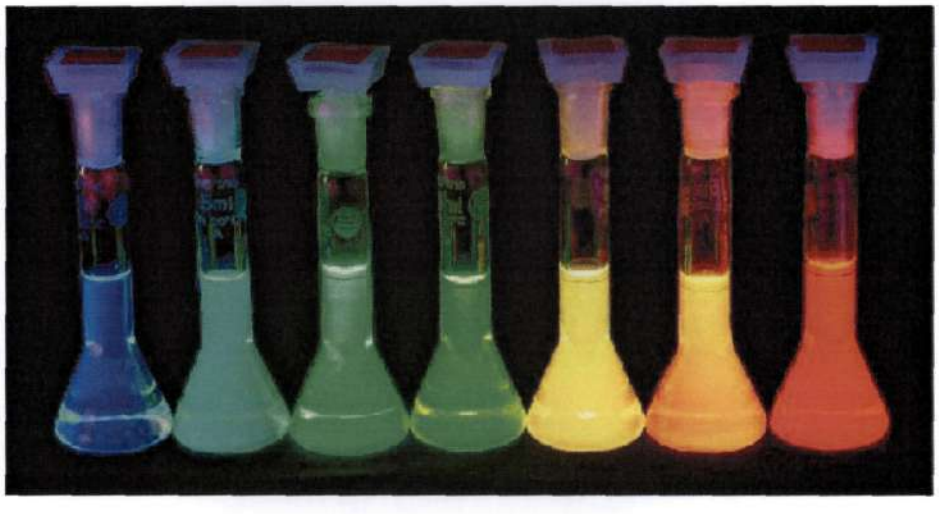

Figure 6.1: Fluorescence as seen for various sized Cadmium Selenide Quantum Dots.

A coloured sample has the ability to repeatedly absorb energy from electromagnetic radiation in the visible region. Thus, there must exist at least one procedure in which molecules are restored to the ground state from their excited state in order for the excitation process to be repeated.[325] An example of fluorescence is shown for an assortment of differently sized Cadmium Selenide Quantum Dots in Figure 6.1.[326] The concept of fluorescence is utilized in our everyday lives with the use of fluorescent lamps; they essentially function by the atomic excitation of mercury vapour. The gaps in the mercury spectrum are filled by the fluorescence of powders which coat the inside of the tube.[327]

Photoluminescence (often termed only as luminescence) encompasses both fluorescence and phosphorescence. It is the process that emits radiant energy when a molecule, ion, or atom returns to the ground state from the excited state after it has absorbed radiant energy.[328] This method re-emits radiation after it has been absorbed, due to stimulation caused by incident radiation. A vapour or a liquid will most likely discontinue re-emitting this light when the exciting light is stopped; however, for a solid this re-emission may persist, sometimes for hours. This phenomenon is called phosphorescence; it may also sometimes appear in a liquid with high viscosity.[329] In order for the exciting light to be emitted it needs first to be absorbed, this is what differentiates between scattering phenomena and fluorescence or phosphorescence.[329] The emitted energy is usually visible radiation, but may also be ultraviolet and infrared radiation. In a general case it would be ultraviolet radiation that is used to raise a sample to the excited state from its ground state.[328]

In 1565, the first record for the observation of fluorescence was noted by Nicolas Monardes, although it was at this time not understood. This fluorescence occurred when a certain wood had been used to make cups in which water was found to have a blue tinge under "room light". It is now understood that there was a soluble component in the wood which could be excited by the UV radiation (> 320 nm) in the "room light". This same solution, called "Lignum Nephriticum" was also described by Boyle in the mid 17th century.[328]

The equipment to show that radiation had been absorbed and then re-emitted wasn't available until 1852. It was around this time that the word *fluorescence* came into use due to a study being performed by George Stokes of Cambridge University, on the now well-known English Fluorite or Fluorspar mineral. However, it is ironic to note that not all naturally occurring fluorites will actually fluoresce.[328]

In the 1600s, the first phosphorescence was seen for the Bolognian stone, which was an artificial phosphor, prepared by an Italian alchemist, Vincenzi Cascariolo. He showed that exposing a sample to light caused light to be emitted later in the dark. He showed that a heated mixture of powdered barite ($BaSO_4$) with coal would glow for hours in the dark.[328] It was assumed that the sample merely absorbed and subsequently released light. Phosphorescence was characterized faster than

fluorescence, due to the slowness of the process which allowed visibility for longer time periods.[328]

Incandescence involves the emission of light due to high temperatures, but fluorescence needs no heat; in fact, heat can actually be detrimental to the process. Most substances will produce very little heat during fluorescence and hence it has been called "cold light".[330] Photoluminescence (phosphorescence and fluorescence) by definition must involve photoexcitation, which may occur from different forms of radiant energy: (1) sunlight, (2) ultraviolet radiation, (3) visible radiation (including room light), or (4) X-rays.[328]

Fluorescence spectroscopy is primarily concerned with electronic states and vibrational states. The species of interest will have a ground electronic state (low energy) and an excited electronic state (higher energy). Each of these electronic states has various vibrational states.[331] The molecule will be excited from its ground electronic state, S, to one of the various vibrational states in the higher energy level, S', by light absorption.[203] Luminescence is the method of emission of light by a sample which has gone through a spontaneous transition from an excited state to a lower energy level.[203] It is possible for the transition from the excited state to take place directly in a very short time; this is the process of fluorescence, of the order of 10^{-9} seconds. Or the transition may take place through an intermediate meta-stable triplet state of lower energy, T'. This process of phosphorescence would increase the life of the excited state to about ~ 10^{-3} seconds.[203] Due to the fast emission (10^{-6}–10^{-9} sec) during fluorescence it is not possible for it to been seen once the light source has been removed. On the other hand, phosphorescence can usually be observed after the light source has been removed, and for different time periods (depending on the sample type). It occurs more slowly (> 10^{-4} sec) and the emission time frame may vary greatly. The sample documented for the longest phosphorescence time period seems to be the mineral Willemite ($ZnSiO_4$), which lasted for 340 hours![328]

The definitive difference between these two emissions, phosphorescence and fluorescence, is whether or not a change in the spin of the excited electron will be observed. Therefore it is not the case that phosphorescence will always be observed

for all samples on removal of the radiation supply.[328] It is known as fluorescence when the excited electron *does not change* its spin on the conversion from the excited to ground state, and phosphorescence when the spin *does change*.[328] Fluorescence is commonly taken to mean emission of radiant energy when the sample moves from the lowest excited singlet state, S_1, to the singlet ground state, S_0, because most organic molecules are singlets. Phosphorescence is commonly taken to mean emission of radiant energy when the sample moves from the lowest excited triplet state, T_1, to the singlet ground state, S_0, i.e. any change in the spin of the excited electron.[328] This can be represented by a Jablonski diagram, as shown in Figure 6.2.

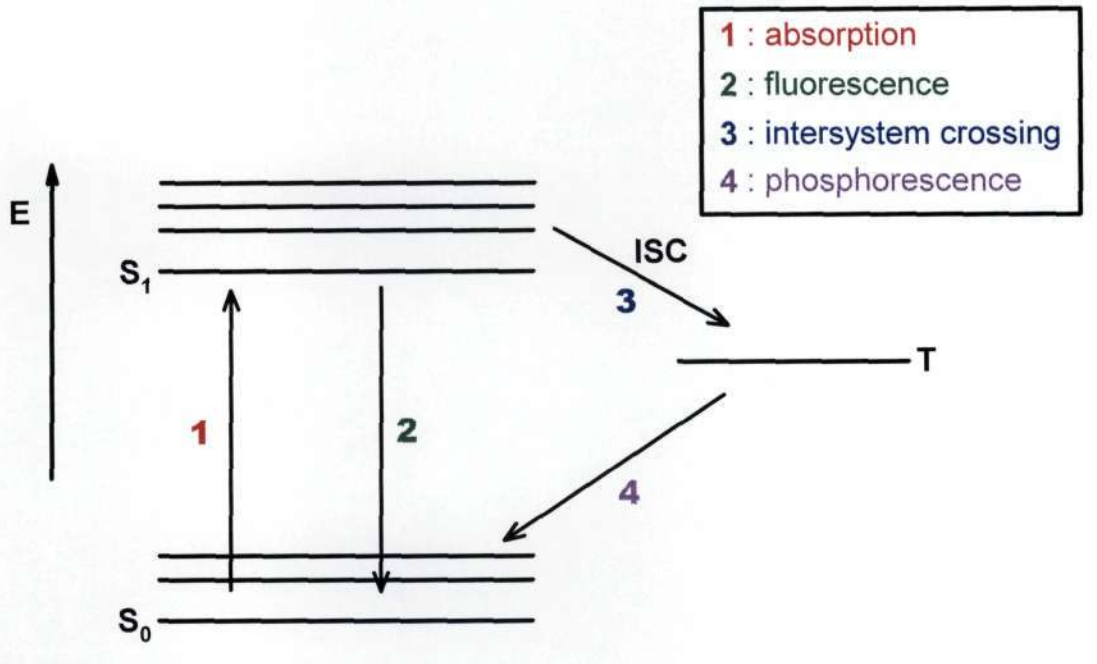

Figure 6.2: A basic Jablonski diagram.

The light emitted will have an intensity that depends on the number of atoms or molecules that are capable of absorbing that particular wavelength incident light; it will also follow the quantum rules of absorption. The emitted light must have either the same or less energy than that of the incident radiation; as stated by the law of conservation of energy.[329] The light emitted by the sample will generally be lower in energy than the light used to excite it. Wavelength is inversely proportional to energy and therefore the lower energy radiation of phosphorescence or fluorescence will be at longer wavelengths, in the UV (> 300 nm), or in the visible (380–750 nm), or possibly in the near infrared (> 750 nm).[328] This generalization that the emitted light

will have longer wavelength is known as 'Stokes Law'.[329] This 'Stokes Shift' refers to the shift in absorption and emission and is therefore related to the difference in equilibrium internuclear distances of the particular state.[332]

Excitation will take place from the ground *singlet* state to an upper *singlet* state due to change in spin multiplicity being forbidden by the selection rule; however, it is possible for excitation to take place to many different vibrational levels of the upper singlet state.[333] After this absorption of radiation and transfer to an excited state, the excited molecules will subsequently undergo deactivation and there are many ways that this energy can be lost. Chemical elements and changes in the physical environment can have an influence on the intensity, width of bands, or duration of emission during fluorescence. This is known as quenching, which can take place via different methods: external quenching, internal quenching, and concentration quenching.[203]

External quenching is when energy is transferred to other molecules via collisions.[333] If there is an increase in collisions between molecules, then the excitation energy may be partly or even wholly transferred to the other particle before it can be emitted and hence the state of excitation will be altered, deactivated or possibly entirely destroyed.[329] The colliding particles do not have to be of the same kind and therefore fluorescence will be inhibited by dissolved gases, e.g. O_2, SO_2, HCl and trimethylamine(5) or even solvent molecules.[203] Internal quenching is when a radiationless transfer (energy is neither lost nor gained) takes place to the ground singlet state in a highly excited vibrational level, from where vibrational energy is lost on return to the ground state.[333] Predissociative transitions can internally quench fluorescence in many saturated hydrocarbons, alcohols, ethers and acids. Internal conversion quenches fluorescence when inside the molecule radiationless electronic transitions take place. The increase of concentration in some samples may produce non-fluorescent dimers or higher aggregates.[203] It is possible for temperature to also quench fluorescence; e.g. fluorescein and rhoduline-orange, or the addition of potassium iodide.[203]

An intersystem crossing between a singlet and a triplet state will be allowed via spin-orbit coupling or under the influence of a paramagnetic species.[324] A relaxation to a spin triplet state (most likely at lower energy) may occur either before emission or

before it can be fully completed. Intersystem crossing is slower than internal conversion. It depends upon the two excited states' coupling mechanism, which is normally spin-orbit coupling.[332]

These external and internal energy conversions are both important models of deactivation.[324] There will be radiation emitted as this conversion occurs from the excited state to vibrationally excited levels of the ground state.[203] This drop down may occur to any of the vibrational levels of the ground state. Some transitions may be forbidden, but most will release photons with different energies and frequencies.[333] Thus the study of these different frequencies of light emitted can decipher the structure of these different vibrational levels.[331] If low temperatures and viscous solvents are used, then it is possible to reduce the quenching taking place in a sample.[203] From all the different factors that contribute to the process of quenching, insight can possibly be provided into the mechanism of the fundamental processes which occur in the interaction of atoms and molecules.[329]

An emission spectrum is obtained from the measurements of the different frequencies of fluorescent light emitted by a sample, when the excited light is held at a constant wavelength. An *excitation spectrum* is obtained by recording the sum of the fluorescent light that is emitted at all frequencies as a function of the frequency of the monochromatic incident light.[331] The quantum yield emission is the ratio of the number of photons emitted to the number actually absorbed by a sample, this is often close to one, which shows that radiationless transitions from S' and T' states to the ground state are not significant.[324]

The transitions that occur between the various electronic and vibrational states resulting in fluorescence and phosphorescence are commonly represented using a Jablonski diagram.[334] The electrons occupy molecular orbitals surrounding the nuclei which form the skeleton of the molecule. Each of the orbitals has its own definite energy and angular momentum, according to the motion of the electrons present. Electrons have spin owing to their rotation in relation to their axes, which is conveniently measured in units of ½ units of spin angular momentum. In simple systems the angular momentum of the electron itself and the angular momentum of its motion may be considered separately.[334]

Not all samples will exhibit fluorescence due to internal quenching being a predominantly faster process. The lifetime from the upper singlet state is generally in the range 1–100 ns. Molecules that fluoresce are usually flat and quite large with extensive π conjugation; internal quenching appears to be assisted by internal rotation.[333] Two samples that have similar structures may differ with regard to their fluorescence—phenolphthalein does not fluoresce, but fluorescein does. The only difference is that the two benzene rings are either allowed to rotate or not.[333]

The lifetimes of fluorescent states in fluids at room temperatures are of the order of nanoseconds to microseconds, and phosphorescent lifetimes of the order microseconds to milliseconds. Solid samples at lower temperatures are likely to have longer lifetimes.[332] Several mechanisms, including collisions, may reduce lifetimes of excited states.[332] Most excited states survive long enough in order to relax to their equilibrium states. For a forbidden d-d transition, excitation takes place to a higher vibrational state of the excited electronic state, although emission, if observed, will move down from the v' = 0 level of the excited electronic state.[332]

6.2 Photoluminescence in porphyrins

Some work has been done on lanthanide metalloporphyrins. Lanthanide porphyrin derivatives generally exhibit usual absorption spectra with Q and B bands. Little effect on the absorption spectra is caused by these rare earth ions; but small perturbations do occur according to which is present. They are a lot like those of other closed-shell metalloporphyrins.[335] Lanthanide(III) complexes with acetylacetonate and *meso*-tetraalkyltetrabenzoporphyrin (Ln(TATBP)acac; A = alkyl = $C_{12}H_{25}$) have been studied by Qi and Liu. Fluorescence lifetimes at room temperature were found to be in the range 0.014–0.022 ms.[336] In the same year the same authors also analyzed complexes of the lanthanide dysprosium(III) with *meso*-tetraalkyltetrabenzoporphyrin and acetylacetonate: Dy(TATBP)acac (A denotes any of the following alkyl groups: C_6H_{13}, C_8H_{17}, $C_{10}H_{21}$, $C_{12}H_{25}$, $C_{14}H_{29}$, $C_{16}H_{33}$ or $C_{18}H_{37}$). Fluorescence lifetimes at room temperature were found to be in the range 0.013–0.019 ms.[337]

Rusakove *et al.* studied complexes of ytterbium with an assortment of *meso*-tetrasubstituted porphyrins and found that for this ion the quantum yield and the lifetime of 4f-luminescence are elevated when the compound has aromatic and heteroaromatic *meso*-substituents, as opposed to n-alkyl ones. This is also true in the case where an acetylacetonate ion is an extra ligand.[338] Spectral-luminescent characteristics were examined for two particular lanthanide ions, Yb^{3+} and Nd^{3+}, complexed with porphyrins that have *meso*-positioned aromatic substituents.[339] More recently, in 2003, photoluminescent studies were performed on a new unsymmetrical diethyl malonate appended porphyrin and its Yb^{3+} , Er^{3+} and Nd^{3+} complexes ([Yb^{III}(*o*-DEM-C_4-O-TPP)(H_2O)], [Er^{III}(*o*-DEM-C_4-O-TPP)(H_2O)] and [Nd^{III}(*o*-DEM-C_4-O-TPP)(H_2O)]).[340]

A series of papers published by Gouterman *et al.* in the early 1970s discussed the luminescence properties of different porphyrins. This included different metallated octaethylporphin complexes,[341] a range of cobalt, nickel, palladium and platinum porphyrin complexes,[342] copper tetraphenylporphyrin, vanadyl etioporphyrin and vanadyl tetraphenylporphyrin.[343]

For PtOEP (2,3,7,8,12,13,17,18-octaethylporphyrin platinum(II)) a 200-fold increase in photoexcited phosphorescent emission has been seen when a polystyrene film on nanotextured silver surfaces is used. This causes a 5-fold increase in the triplet state lifetime.[344] Palladium(II) and platinum(II) porphyrin complexes were shown to emit strong phosphorescence at room temperature which is illustrated by long-wave spectra and long lifetimes of the order of milliseconds.[345] The excited-state molecular structural dynamics of three nickel porphyrins showed that the relaxed 3(d, d) state lifetimes for NiTPP, NiTMP and NiSWTP decreased according to substituent steric bulk and increased non-planarity of the porphyrin macrocycle.[346]

In the late 1970s a study on "Position-dependent and spin-dependent deuterium isotope effects on the triplet-state lifetime of porphyrin free bases" was published by Burgner *et al.*[347] In 1996 fluorescence lifetimes and time-resolved spectra were measured for Zn-porphyrin and Zn-chlorin dimers in a study by von Borcyskowski.[348]

Song *et al.* used static absorption and fluorescence spectroscopy and very fast transient absorption measurements in order to examine differing photophysical properties between two Si(IV) *meso*-tetraphenylporphyrins, $Si(TPP)(py)_2$ and $Si(TPP)Cl_2$.[349] The complex $Si(TPP)(py)_2$ has a 750-fold shorter excited-state lifetime than $Si(TPP)Cl_2$ (2.4 ps as opposed to 1.8 ns) in the same solvent (pyridine). This rapid deactivation may be due to the ruffled structure and the existence of low-energy excited states in its electronic manifold.

Optical absorption and lifetimes of the excited states of Cu(II) octaethylporphyrin and Cu(II) tetraphenylporphyrin have been studied at 77 K.[350] Other copper(II)porphyrins have been researched in more detail (amongst other things, lifetimes) by Cunningham *et al.*; these include: $Cu(TCl_2PP)$ [TCl_2PP denotes 5,10,15,20-tetra(2',6'-dichlorophenyl)porphyrin] and Cu(TMeOPP) [TMeOPP denotes 5,10,15,20-tetra(4'-methoxyphenyl)porphyrin].[351] Allison and Becker obtained low temperature emission spectra for Mg etioporphyrin II and Zn phthalocyanine, as well as for dimethyl ester of *meso*-porphyrin IX and its bivalent derivatives with Co, Ni, Cu, Zn, Pd, Cd, and Ba.[352]

Very few cases have involved free base porphyrins. They have been studied as aggregates of *meso*-tetraphenylporphyrin (H_2TPP), *meso*-tetra-4-carboxy-phenylporphyrin (H_2TPPC), and *meso*-tetra-4-pyridylporphyrin (H_2TPyP) under various conditions, by Khairutdinov and Serpone. Fluorescence lifetimes vary from 10^{-12} to 10^{-9} s and are smaller than those for the corresponding monomeric porphyrins.[353] Another Russian journal published the results for the phosphorescence of etioporphyrin I and some complexes with light metals, e.g. Mg and Al.[354] Barbosa and co-workers analyzed dynamic optical nonlinearities in free base tetrapyridylporphyrin (H_2TPyP) solutions. Flamingi and co-workers studied the photophysical properties of a new, stable corrole-porphyrin dyad consisting of a free-base corrole and a free-base porphyrin joined by an amide linker. A common lifetime is recorded for both states. This lifetime of 6.2 ns is shorter than the 9.9 ns of the lone porphyrin and longer than the corrole model lifetime, which was determined to be 3.9 ns.[355]

The series of papers[356,357,358,359] published by Harriman between 1979 and 1981 gave immense insight into the luminescence of *meso*-substituted porphyrins and metalloporphyrins, for *meso*-tetraphenylporphyrin in particular. The first paper[356] gave the lifetimes for H_2TPP and three common metal derivatives, as shown in Table 6.4. This was followed by an extension of the range of TPP metalloporphyrins[357] (Table 6.5) with other metalloporphyrins being studied at room temperature as well as at 77 K[358] (Tables 6.6 and 6.7, respectively).

The absorption spectra for each of the metalloporphyrins are all rather similar, which implies that any interaction between the metal and porphyrin is fairly weak. Both intensity and position of the Q and B bands would be affected by the extent to which metal *d*-orbitals interact with the porphyrin. Energy and oscillator strength decreases as the extent of interaction increases.[212] When making a comparison of the spectra it is obvious that Ni(II)TPP possesses a great deal of metal-porphyrin interaction, while Mn(II)TPP and Zn(II)TPP possess a lot less.[356]

The position of the emission maximum has been noted for the luminescence spectra of the various metal TPP complexes and a Stokes shift of 3900 ± 100 cm^{-1} has been observed. Corresponding *meso*-complexes all gave a Stokes shift of about 3200 ± 120 cm^{-1} (660 ± 60 cm^{-1} divergence when compared to H_2TPP). This is particularly true for Cu, VO and other metalloporphyrins where strong charge transfer (c.t.) interaction exists between the porphyrin π-system and the paramagnetic metal centre. It is therefore possible that for other metalloporphyrins a crude prediction can be made regarding the position of the emission maxima.[356]

Charge-transfer involves rearrangement of electron density and is classified according to the transfer between (1) porphyrin and metal, (2) metal and additional ligands, and (3) porphyrin and ligands. The most evident transitions take place between the metal ion orbitals and the porphyrin π-orbitals. Therefore these transitions can either be metal to porphyrin, which occurs from filled d-orbitals to vacant π^*–orbitals d $\rightarrow$ π^*, or porphyrin to metal, which takes place from occupied π-orbitals to empty d-orbitals π $\rightarrow$ d. The geometry of the complex and any axially coordinated ligands have a definite effect on the energy of the c.t. transitions. Calculations have been done for

metalloporphyrins in order to try and compute the energy of c.t. transitions; this has mostly been performed for iron complexes that resemble, and therefore make good models for, natural haems.[357]

The metalloporphyrins had different lifetimes to the free base H_2TPP; therefore showing metallation does have an effect on the porphyrin luminescence. The metals can be grouped according to the amount of c.t., but each metal also has a distinct effect. These papers[356,357,358] showed that the central metal ion does play a part in the resulting photophysical properties of metalloporphyrins. Luminescence and flash-photolysis techniques have been used to observe the degree of the effects of heavy-atom and paramagnetic perturbations induced by the metal ions. The rate constants for inter-system crossing can be related to the spin-orbital coupling constant of the metal ion for diamagnetic porphyrins.[356,358] (This intersystem-crossing refers to both singlet to triplet excited states and non-radiative deactivation of the triplet state at 77 and 293 K.) Paramagnetic porphyrins showed greater effects, as there was a relaxation of the spin-forbidden character of singlet-triplet transitions, due to the interaction of the porphyrin π-system with the central metal ion.[357]

Phosphorescence properties have not been as well studied or documented as fluorescence.[356] Phosphorescence properties for a few free base porphyrins at low temperature have been examined.[360] Quantum yields were rather low and it was necessary to use heavy atom perturbation techniques so that the emission could be resolved.[360] More easily characterized (particularly at low temperatures) are zinc porphyrins,[361,362] e.g. ZnTPP, due to their greater phosphorescence. There is an interesting difference between the free base porphyrin, H_2TPP, and the metallated, ZnTPP. The free base porphyrin has weak phosphorescence at about 865 nm, while the metallated porphyrin has more intense phosphorescence with two well resolved maxima at 780 and 875 nm. H_2TPP has a reasonably long lifetime, but ZnTPP has an even longer lifetime. The corrected excitation spectra are good matches with their absorption spectra at 77K and no changes are seen as the temperature is further lowered. All the reported spectra for H_2TPP P and ZnTPP agree[356,360] with the best resolved H_2TPP spectra presented by Harriman.[356]

Thus the lowest energy excited states for free base H_2TPP, Zn(II)TPP and Mn(II))TPP can be described in terms of 'normal' $\pi \rightarrow \pi^*$ character. The absence of luminescence from Ni(II)TPP has been attributed to the presence of a low energy (*dd*) singlet state. The rest of the first row transition metal porphyrins require that two other excited states are considered:[357] c.t. and tripmultiplet.[356] The ground-state absorption spectra and the porphyrin excited singlet and triplet state lifetimes were perturbed by the type of metal ion present. Paramagnetic metal ions had the greatest effect due to their strong interaction with the porphyrin π-system, which causes some relaxation into the spin-forbidden singlet-triplet transitions.[356,357,358]

The zinc, nickel and manganese metallated H_2TPP show very little c.t. between the metal and porphyrin ring, which gives simple $\pi \rightarrow \pi^*$ characteristics. The free base has a relatively long lifetime for low temperature luminescence, but the zinc complex has an even longer lifetime, with intense phosphorescence. These lifetimes are shown in Table 6.4. The manganese metallated porphyrin, although with a similar wavelength to free base H_2TPP, gave a much shorter lifetime than either. No low temperature luminescence lifetime could be acquired from the nickel complex; however, an upper limit was recorded. This has been attributed to the presence of a low energy *(dd)* singlet state.[356] Therefore the excited states of these metalloporphyrins can be regarded as normal porphyrin $\pi \rightarrow \pi^*$ singlet and triplet states.

Table 6.4: The quantum yields, lifetimes and wavelengths for free base H_2TPP and three metal derivatives in methylcyclohexane at 77 K.[356]

	ϕ_P	τ_P/ms	λ_{max}/nm
TPP	4×10^{-5}	6	865
ZnTPP	1.2×10^{-2}	26	778
Ni(II)TPP	$< 10^{-5}$	—	—
Mn(II)TPP	3×10^{-4}	0.2	840

$_P$ = phosphorescence

Further work by the same author[357] shows the luminescence of metalloporphyrins that exhibit appreciable c.t. in the excited states. The excited states with the lowest energy

will no longer be simple $\pi \rightarrow \pi^*$ states, but comprehensively mixed.[356] These metalloporphyrins have more pronounced effects in their luminescence properties. The luminescence spectra for these metalloporphyrins compared well with other studies in the literature. The manganese complex had a sharp luminescence spectrum, but a shorter lifetime than that for the copper complex. For the two iron complexes, the luminescence spectra were so similar that they were almost the same. The Fe(III) complex had a short lifetime and no luminescence could be determined for the Fe(II) complex (Table 6.5); this is likely due to the rapid oxidation of Fe(II) to Fe(III) caused by oxygen in the air.

Table 6.5: The quantum yields, lifetimes and wavelengths for five metallated TPP porphyrins in methylcyclohexane at 77 K.[357]

	ϕ_L	$\tau_L/\mu s$	λ_{max}/nm
Cr(III)TPP	7×10^{-4}	44[363]	850
Cu(II)TPP	6×10^{-2}	600	747
Fe(III)TPP	7×10^{-5}	< 100	718
Fe(II)TPP	$< 10^{-5}$	—	—
Mn(III)TPP	2×10^{-5}	<100	700

$_L$ = luminescence

The metals Fe(II), Fe(III) and Mn(III) will differ in the visible region with Mn(III)TPP and Fe(II)TPP having at least one extra band and Fe(III)TPP having two. Cr(III)TPP also has additional bands in the near UV region; however, Cu(II) porphyrins have no oddities in their spectra, illustrating no c.t. transitions in the visible or near UV regions. A direct absorption to the 'spin-forbidden' triplet state is also possible resulting from interactions between metal ion unpaired d-electrons and the porphyrin $\pi \rightarrow \pi^*$ triplet state.[357] This produces tripmultiplet states; described in detail by Gouterman and co-workers.[357]

The influence of heavy-atom metal ions on the luminescence properties of *meso*-tetraphenylporphyrin was also analyzed.[358] Typical metalloporphyrin fluorescence was

observed at room temperature for four of the five complexes, namely MgTPP, ZnTPP, CdTPP and PdTPP (Table 6.6). The results showed the lifetimes decreasing in the order: Mg > Zn > Cd ≈ Pd. This agrees with the expected heavy-atom effect. Consistent with this heavy atom effect, no definite fluorescence could be recorded for the Hg complex. Also noted was that different samples gave different quantum yield readings and therefore only a maximum may be quoted. Low temperature phosphorescence was also recorded for these samples (Table 6.7). These lifetimes again followed the same trend. At this temperature a value for the phosphorescence lifetime of the Hg complex could be recorded.

Table 6.6: The quantum yields and lifetimes for five more metallated TPP porphyrins in methylcyclohexane at room temperature.[358]

	ϕ_F	τ_F/ns
MgTPP	0.15	9.2
ZnTPP	0.03	2.7
CdTPP	4×10^{-4}	0.065
PdTPP	2×10^{-4}	0.020
HgTPP	$< 10^{-3}$	—

$_F$ = fluorescence

Table 6.7: The quantum yields and lifetimes for five more metallated TPP porphyrins in methylcyclohexane at 77 K.[358]

	ϕ_P	τ_P/ms
MgTPP	0.015	45
ZnTPP	0.012	26
CdTPP	0.04	2.4
PdTPP	0.17	2.8
HgTPP	0.01	0.2

$_P$ = phosphorescence

Work has been done on the effect that heavy-atom metal ions will have on the luminescence properties of *meso*-tetraphenylporphyrin.[358] Room temperature triplet-state absorption spectra and lifetimes have also been recorded (which were then

compared to previous work[356,357]). The reason for this type of work follows two directions: (1) to allow intensive study of intramolecular effects on photophysical properties and (2) to possibly use metalloporphyrins as photosensitisers for the dissociation of water into H_2 and O_2.[364] Gouterman and co-workers' study,[365] although comprehensive, was complicated by axial ligation, and therefore a simplified system where the axial ligands can be ignored is necessary for these intramolecular effects to be studied. The diamagnetic metalloporphyrins that have been analyzed possess properties that may result in applications for solar-energy devices.[366] A photosensitiser must absorb strongly throughout the visible region and have a relatively long excited-state lifetime in order to store sunlight in the form of H_2 fuel.[358]

Work has shown that there is little interaction between the porphyrin π-system and the metal for HgTPP, but that the interaction for PdTPP is fairly strong.[358] A blend of different aspects dictates the degree of interaction. These factors include metal ion size, geometry of the metalloporphyrin and electrostatic and inductive effects.[358]

There has been reasonable agreement in most areas of this research; however, as with all studies, there are still deviant systems, particularly for metalloporphyrins with the first row transition metals. What has already been established is that free base porphyrins and porphyrins metallated with zinc(II) will have both fluorescence and low temperature phosphorescence.[356] For the metalloporphyrins that contain copper(II) and vanadyl, only low temperature luminescence will be seen. Both low and room temperature excited states for these compounds have been well characterized by a range of authors.[367]

In the visible region of the absorption spectra of metalloporphyrins there are intense $\pi \rightarrow \pi^*$ transitions. In the region 500 to 600 nm occurs the origin of the first $\pi \rightarrow \pi^*$ transition (lowest energy excited singlet state), which is known as Q(0, 0). In the region 400 to 470 nm there is a B (0, 0) band which is the origin of the second $\pi \rightarrow \pi^*$ excited singlet state and is the most intense band.[356,357,358] Furthermore, there are also N, L and M bands present;[356] they are all assigned to $\pi \rightarrow \pi^*$ transitions (and nomenclature is according to Platt[368]). The extent of the porphyrin π-system and

metal ion interaction affects both the energy (E) and the intensity, as measured by the oscillator strength (f) of the Q (0, 0) band. The energy is proportional to the interaction, whereas the oscillator strength is inversely related. This provides an easy means to evaluate the relative degree of interaction between the metal and the porphyrin π-system.[357,358]

Previous work showed the effects on H_2TPP luminescence properties when halogens have been substituted onto the phenyl rings of H_2TPP.[361] The final paper of the Harriman series involved the free base H_2TPP and the effect of different substitutions on the phenyl *meso*-substituents, as seen in Table 6.8. Both electron withdrawing and electron donating groups were substituted onto the phenyl rings. Mostly the data for the quantum yields and lifetimes were similar to that for the unsubstituted phenyl rings; however, strong electron withdrawing or donating groups did reduce these values. The largest of these reductions was caused by the porphyrin-quinone compound; the lifetime was less than one fifth of that for the unsubstituted H_2TPP. The B band wavelengths were all very similar to each other. The resulting conclusion was that fluorescence properties of H_2TPP are not especially susceptible to these types of substitutions on the phenyl ring.[359]

Table 6.8: The quantum yields, lifetimes and wavelengths for H_2TPP and for some substituted free base H_2TPP porphyrins in out-gassed benzene solutions.[359]

Meso-substituent	ϕ_F	τ_S/ns	λ^B/nm
phenyl	0.13	15.7	419
p-CH_3-phenyl	0.15	14.0	421
p-$COOCH_3$-phenyl	0.13	13.9	422
o-NO_2-phenyl	0.020	6.4	421.5
p-NO_2-phenyl	0.045	8.3	422
p-$N(CH_3)_2$-phenyl	0.025	8.4	440
p-CN-phenyl	0.064	12.2	421
p-OCH_3-phenyl	0.15	12.3	421
p-CH_2OH-phenyl	0.14	13.4	421.5
1,4-OH-phenyl	0.030	7.5	422
1,4-O-phenyl	0.007	2.5	423

$_F$ = fluorescence
$_S$ = singlet-state
$_B$ = B band

In 1988, after the work by Harriman, a study was performed on *Factors Influencing Fluorescence Spectra of Free Porphyrins*. In this work the effect that pH, ionic strength, and solvent composition have on the fluorescence of porphyrins was determined.[369] This was done by recording fluorescence excitation and emission spectra of uro- and coproporphyrin. Fluorescence was found to have a dependence on pH; the greater the alkalinity, the less the fluorescence. Fluorescence is minimal when the pH is close to neutral for uroporphyrin and slightly acidic (~ 5) for coproporphyrin. Porphyrin fluorescence intensity was also found to be related to ionic strength.

The strong and characteristic absorption bands in the visible and near-ultraviolet are due to the presence of a conjugated double-bond system in the tetrapyrrole nucleus. Often this property has been used in the identification of porphyrins; one restriction is, however, the relatively high concentration necessary for accurate spectrophotometric measurement.[369] Free base porphyrins and their esters possess a very characteristic and significant property seen when irradiated with light around 400 nm; an intense red

fluorescence. The detection of most porphyrins can therefore occur at concentrations of about 10^{-8} mol/L. Fluorometric methods have been used to quantify tetrapyrroles due to the sensitivity and specificity of this method.[369]

Groundbreaking work in the luminescence of metalloporphyrins was presented by Becker and Allison.[352] This work gave the low temperature emission from many transition metal complexes with *meso*-porphyrin IX dimethyl ester. Further work, in the form of a series of authoritative papers, was produced by Gouterman and co-workers.[356] These papers included a wide variety of metalloporphyrins for which luminescence and theoretical calculations were described. Other work has been contributed by Gurinovich *et al.*, Quimby *et al.*[361] and Solov'ev *et al.*[356]

6.3 Objectives

The aims of this chapter were to:

(1) obtain the emission spectra for each of the six *meso*-tetraalkylporphyrins in the series;
(2) determine the wavelengths at which maximum emission occurred for each porphyrin;
(3) find the lifetimes at these wavelengths for each porphyrin; and
(4) investigate the dependence on the excited state lifetimes and emission maxima on the solvent and the physical state of the system (solid vs. solution).

6.4 Results and Discussion

6.4.1 Results

Solids easily phosphoresce at room temperature; however, this is not frequently the case with solutions of most organic compounds and many inorganic species. The problem often lies with possible collision with dissolved oxygen and therefore solutions are typically frozen at 77 K with liquid nitrogen (to form "rigid solutions" or "glasses").[328] Originally emission spectra in this work were obtained for samples open to the atmosphere, i.e. oxygen present, and also for samples which had oxygen removed and were therefore under a nitrogen atmosphere. There was no difference between these particular spectra and therefore it was deemed unnecessary to obtain spectra without oxygen. Thus all results presented were obtained with the sample open to the atmosphere. Some emission spectra were determined with excitation at different wavelengths, but this had very little effect on the emission spectra, thus proving no dependence on the wavelength of the excitation. Spectra were obtained for the solutions at room temperature as well as at 77 K, using liquid nitrogen to cool the samples.

After the emission spectra had been obtained for each of the porphyrins in the series, they were first corrected and then smoothed using a box car averaging algorithm. The resulting final spectra are presented in Figures 6.3 to 6.8 for both room temperature and 77 K measurements for each of the six free base *meso*-tetraalkylporphyrins. For the 77 K measurements of the original samples, the conditions had to be changed to get spectra on scale. This was due to the increases in intensity at lower temperatures caused by the normal and expected decrease in thermal vibrations.

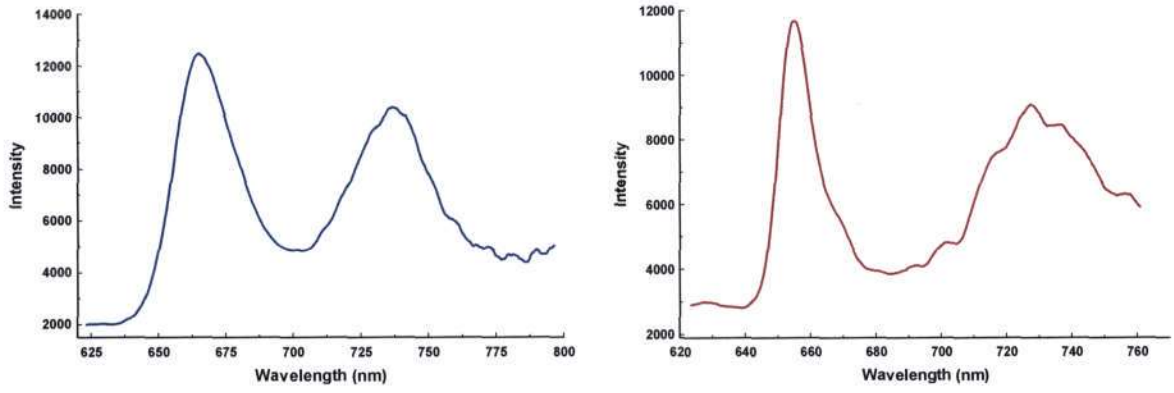

Figure 6.3: Emission spectra for $H_2T(iBu)P$ (porphyrin 1) at room temperature (left) and at 77 K (right).

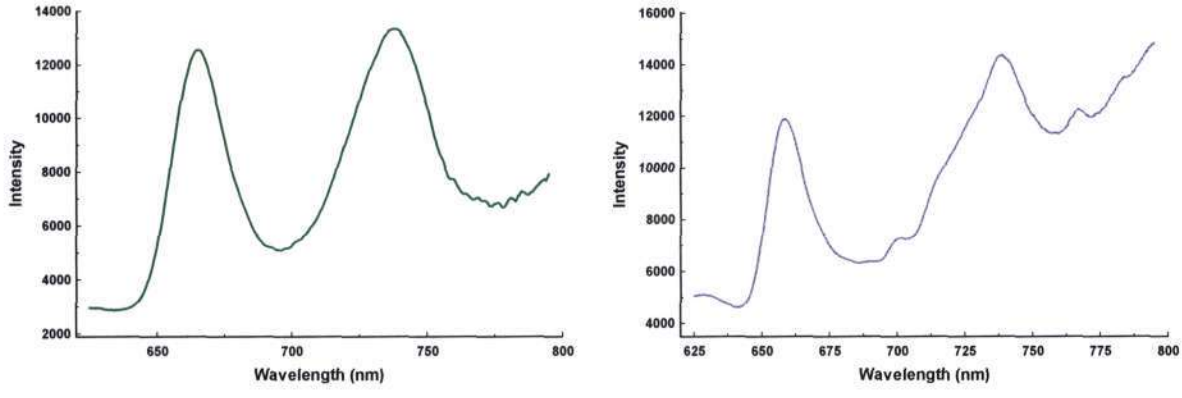

Figure 6.4: Emission spectra for $H_2T(CH_2Ph)P$ (porphyrin 2) at room temperature (left) and at 77 K (right).

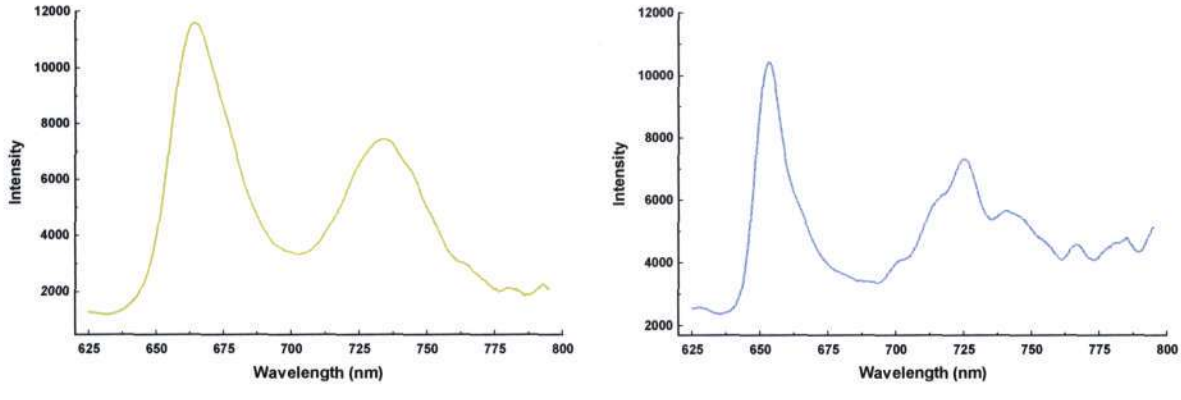

Figure 6.5: Emission spectra for $H_2T(iPent)P$ (porphyrin 3) at room temperature (left) and at 77 K (right).

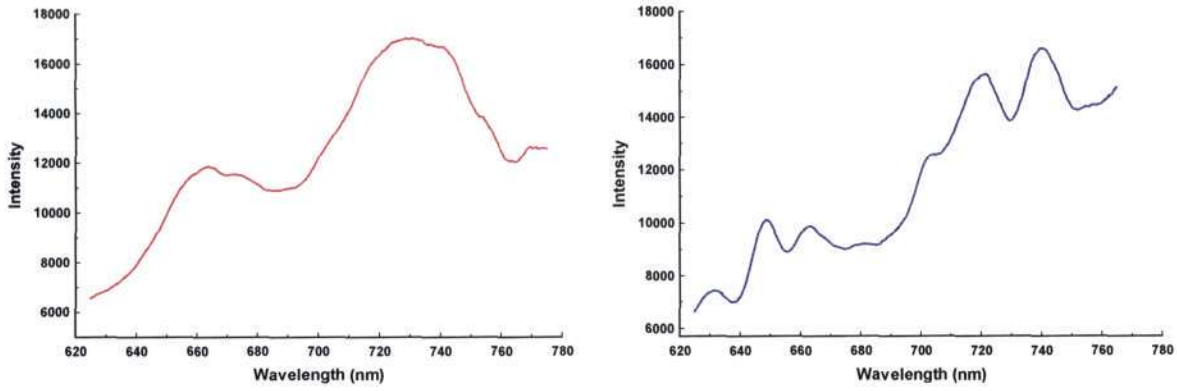

Figure 6.6: Emission spectra for $H_2T(CHPh_2)P$ (porphyrin 4) at room temperature (left) and at 77 K (right).

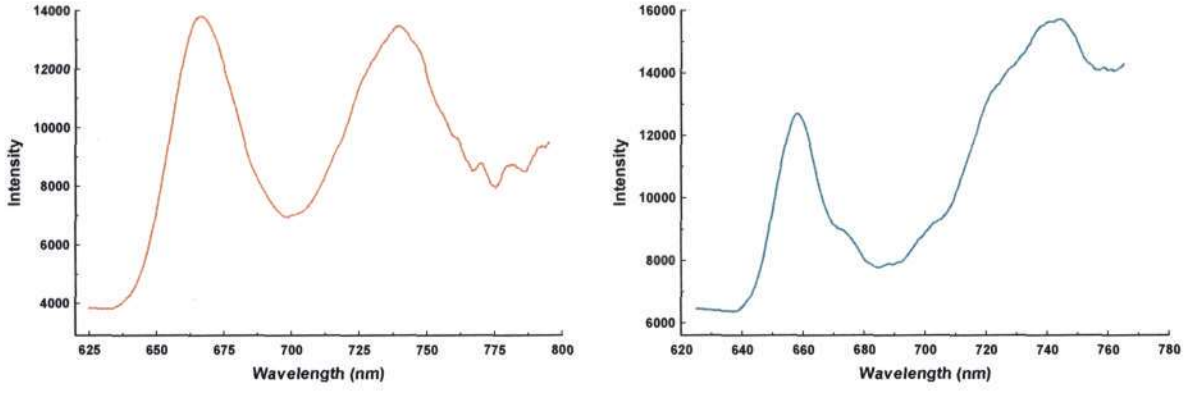

Figure 6.7: Emission spectra for $H_2T(iPr)P$ (porphyrin 5) at room temperature (left) and at 77 K (right).

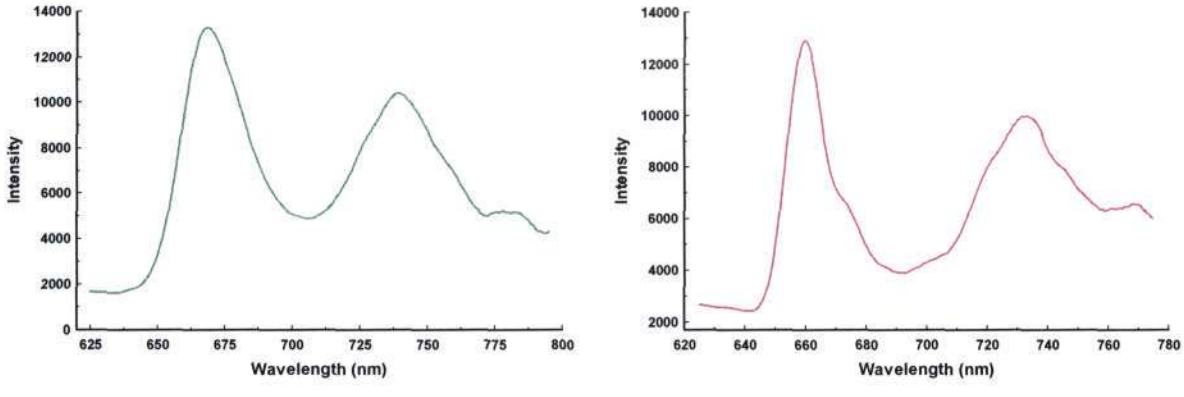

Figure 6.8: Emission spectra for $H_2T(cyHx)P$ (porphyrin 6) at room temperature (left) and at 77 K (right).

6.4.2 Discussion

For each of the six porphyrins at room temperature there are two definite, smooth emission bands in the emission spectrum; an example of this is shown for $H_2T(CHPh_2)P$ in Figure 6.9. However, the spectra at 77 K have more features, the bands are not as smooth and there are evidently additional bands relative to the spectra at room temperature. This is especially true for the spectrum of $H_2T(CHPh_2)$ (Figure 6.10). This particular porphyrin has at least four definitive bands (possibly six) in its 77 K emission spectrum. This is probably due to the fact that as the samples are frozen, rotation and tumbling will effectively stop, leading to sharper lines.

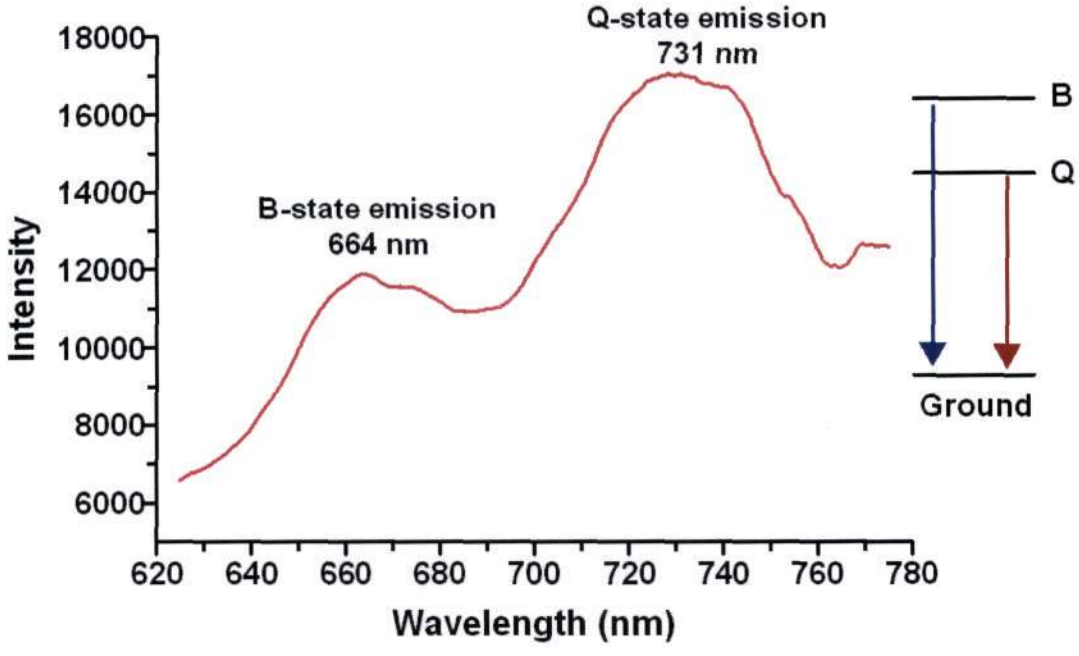

Figure 6.9: B and Q state emission bands for $H_2T(CHPh_2)P$ at room temperature, with a diagram showing the origin of the bands.

Therefore these multiple bands seen in the 77 K spectrum are due to the system being trapped in a frozen glass at low temperatures where rotational levels cannot blur the vibrational levels of the ground state. Only vibrations will occur and therefore transitions to vibrational levels are resolved. The occurrence of more definite bands can be seen for each of the 77 K spectra for each of the six *meso*-tetraalkylporphyrins in the series (Figures 6.3 to 6.8). However, the division of the B band is generally less prominent than the separation of the Q bands.

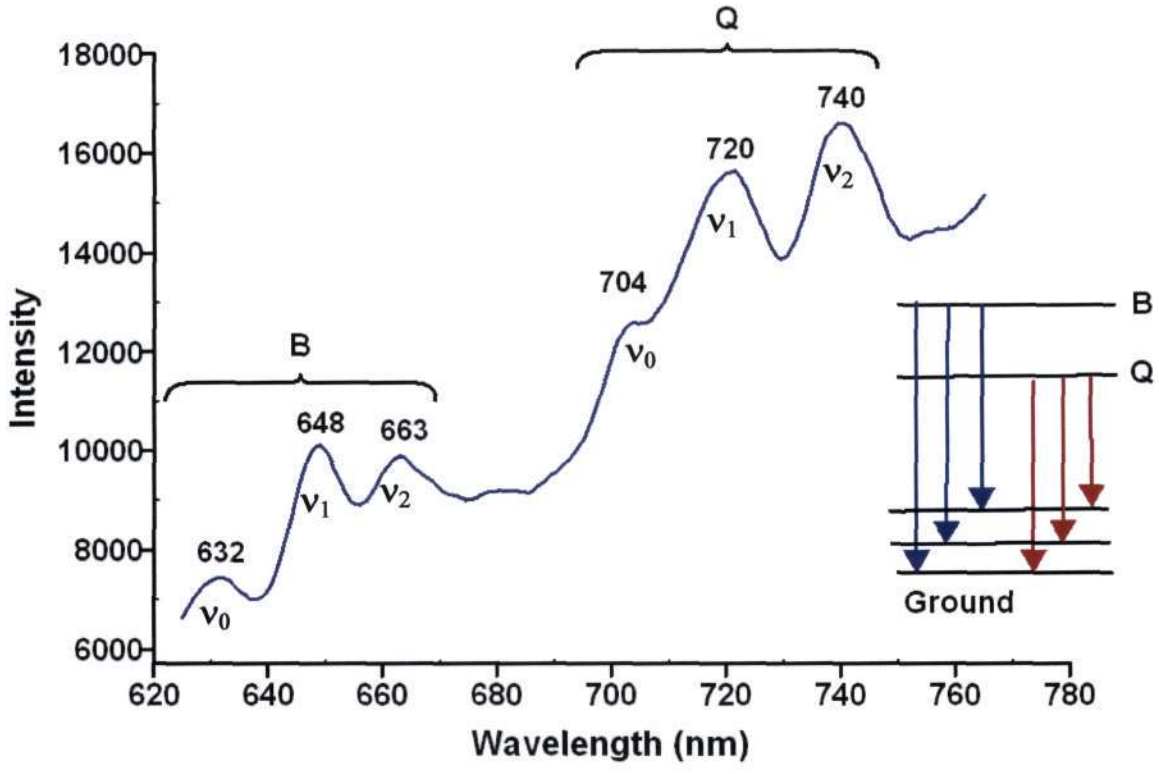

Figure 6.10: The multiple bands present for the B and Q state emission when $H_2T(CHPh_2)P$ is cooled to 77 K, with a diagram showing the origin of the bands.

For $H_2T(CH_2Ph)P$ and $H_2T(iPent)P$ in particular, only the B(0,0) band is clearly visible. For $H_2T(iBu)P$, $H_2T(iPr)P$ and $H_2T(cyHx)P$, emission from the B state is better resolved as there is a slight shoulder of the B(0,1) band present next to the more dominant B(0,0) band. In the case of $H_2T(CHPh_2)P$, however, division between the bands is the most pronounced, showing two definitive peaks for B(0,0) and B(0,1) (as seen in Figure 6.10). For B(1,0), the 0 denotes the zeroth level of the excited state and the 1 denotes the first excited vibrational level of the ground state. Evidently this porphyrin has widely spaced vibrational levels, more so than the other less severely crowded porphyrins in this series. The experimental evidence suggests that vibrational excitation of the porphyrin in its ground state is more difficult (larger energy quanta required), possibly due to limited flexibility engendered by the bulky *meso*-alkyl groups.

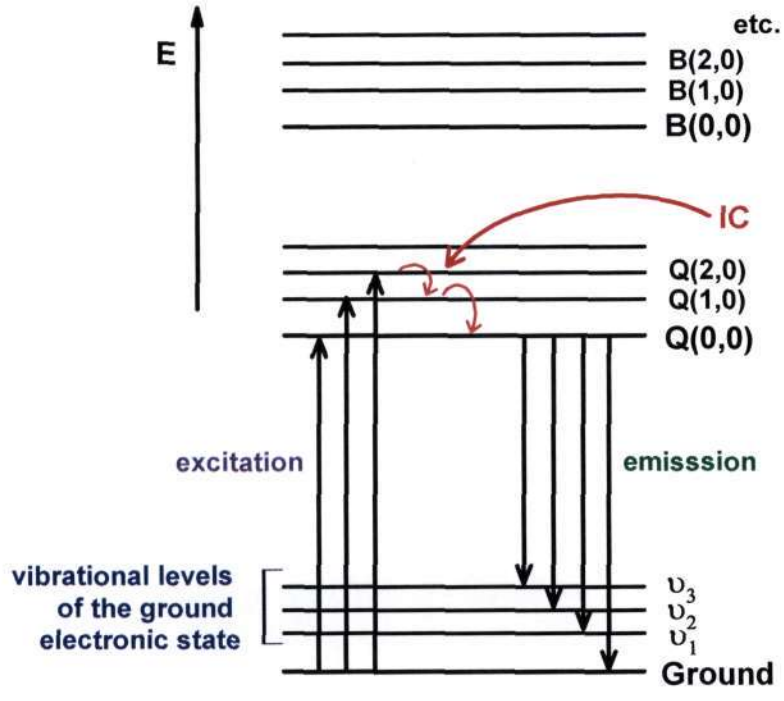

Figure 6.11: Excitation and fluorescent emission of the Q bands. IC ≡ internal conversion.

The emission from the Q bands (diagrammatically shown in Figure 6.11) at 77 K gives up to four definite bands in the spectra. All four, although not always clearly defined, are present in all the spectra. The best representation of all four Q bands is for $H_2T(CHPh_2)P$ (as seen in the enlarged spectrum, Figure 6.10). For $H_2T(iBu)P$, $H_2T(CH_2Ph)P$ and $H_2T(iPent)P$ (Figures 6.3, 6.4 and 6.5, respectively), the four bands can also be easily deciphered, whereas for $H_2T(iPr)P$ and $H_2T(cyHx)P$ (Figures 6.7 and 6.8, respectively), the exact position of two may be easily defined with the other two being slightly obscured. A calculation to determine the energy quantum of the $\nu_0 \rightarrow \nu_1$ vibrational transition to the ground electronic state may be done here for the Q bands. Such a calculation may also be done for the B bands. This is shown in Figure 6.12 for the emission spectrum of $H_2T(CHPh_2)P$ and will be done quantitatively in future work as part of our on-going research efforts with this series of porphyrins.

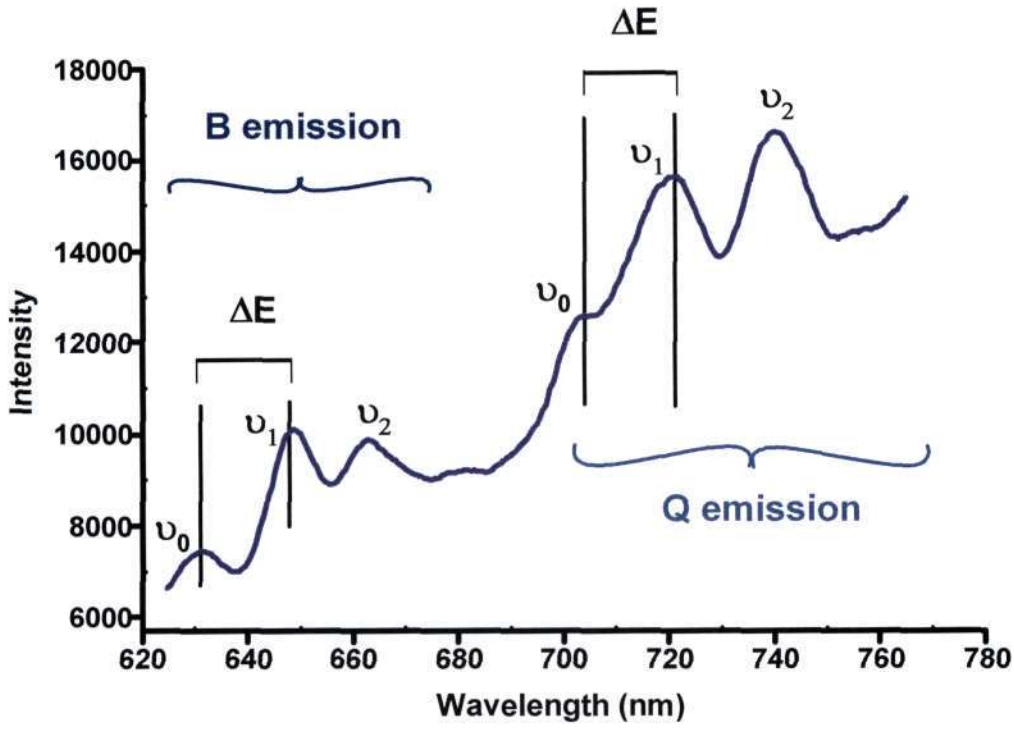

Figure 6.12: The 77 K emission spectrum for $H_2T(CHPh_2)P$ showing the energy quantum of the ground state: $\Delta E = \nu_1 - \nu_0$.

Clearly the emission spectra allow us to probe the vibrational levels of the ground state in these *meso*-tetraalkylporphyrins. Due to the multiple emission bands in the frozen glass, emission to several vibrational levels of the ground state is apparent. For $H_2T(CHPh_2)P$ the porphyrin core conformation is more rigid due to the bulky *meso*-alkyl groups, and the vibrational levels are well separated in energy. This is not true for the other *meso*-tetraalkylporphyrins and so the vibrational fine structure on the emission band is less well resolved for the less hindered porphyrins. The peaks seen in the emission spectra for each of the porphyrins at room temperature and at 77 K are given in Table 6.9.

Table 6.9: Wavelengths of the emission band maxima for each porphyrin at room temperature and at 77 K in CH_2Cl_2.

	Wavelength of emission at room temperature (nm)		Wavelength of emission at 77 K (nm)			
$H_2T(iBu)P$	665	736	654		727	
$H_2T(CH_2Ph)P$	665	737	658		738	
$H_2T(iPent)P$	664	733	652		725	
$H_2T(CHPh_2)P$	664	731	648	663	720	740
$H_2T(iPr)P$	667	741	657		743	
$H_2T(cyHx)P$	668	738	659		732	

For porphyrins the lowest energy excited states can be described in terms of 'normal' $\pi \rightarrow \pi^*$ character.[357] The absorption spectra of porphyrins show intense $\pi \rightarrow \pi^*$ transitions in the visible region. In the region 400 to 470 nm is the most intense, highest energy band (the B(0,0) band), and between 500 and 650 nm the Q(0,0) band, which is the lowest energy excited singlet state.[356,357,358] Consistent with the four-orbital model developed by Gouterman,[214] the B band can be assigned to the origin of the second singlet $\pi \rightarrow \pi^*$ excited state and the four Q bands are associated with the first singlet $\pi \rightarrow \pi^*$ excited state.[359] Therefore it is expected that the emission observed for this range of *meso*-tetraalkylporphyrins will be from the Q and B states and that it is singlet state emission (fluorescence) and therefore not phosphorescence (triplet state emission).

Most literature refers to metalloporphyrins; however, this work deals with free base *meso*-tetraalkylporphyrins. Thus the best comparison that can be made is with a free base *meso*-tetraarylporphyrin, H_2TPP. This porphyrin has two main emission bands at around 650 and 725 nm (excitation at a wavelength of 514 nm).[370] The emission spectra for the six porphyrins presented in this work also showed these two bands at similar wavelengths. We conclude that the *meso*-tetraalkylporphyrins behave similarly to the *meso*-tetraarylporphyrins with Q and B band emission.

There is a difference in the lifetimes of the two excited states, B and Q. Furthermore, radiative relaxation to the ν_0 and ν_1 vibrational levels from the Q and B states proceeds at different rates. Clearly, radiative relaxation to the first vibrationally excited state of the ground electronic state is always faster, irrespective of the emitting state (Q or B). The geometry of the ν_1 state probably better matches that of the zeroth vibrational levels of the Q and B excited states, thus facilitating fast e^- transfer back to the ground state.

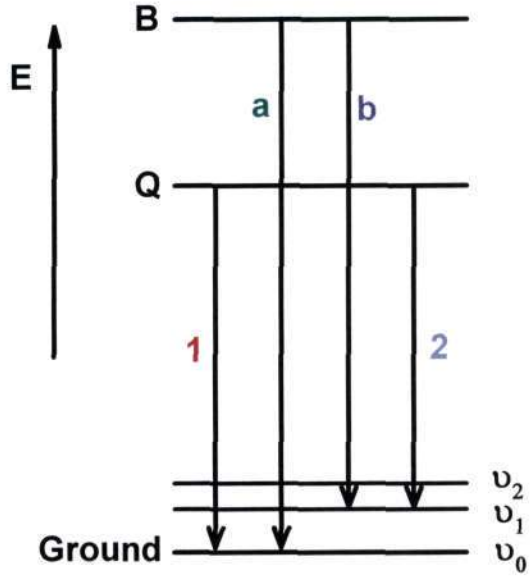

Figure 6.14: The origin and lifetimes for the B and Q states of *meso*-tetraalkylporphyrins. Lifetime data are for $H_2T(CHPh_2)P$ at 77 K.

An important property of this photoluminescence (phosphorescence and fluorescence) is the lifetime; the time period which it takes for the excited molecules to relax back to their ground state. These lifetimes were measured for the fluorescence of each of the porphyrins at each wavelength given in Table 6.9, at room temperature and at 77 K. The results are presented in Tables 6.10 and 6.11. The best and most direct way to measure a lifetime of an excited state is to actually create it; this can be done using short pulse or flash irradiation, which has a duration much shorter than the particular lifetime. The consequent disappearance of the excited species can then be observed and recorded. Absorption or emission of the radiation can be used to monitor the concentration of the excited species.

Table 6.10: Lifetimes for the *meso*-tetraalkylporphyrins in CH_2Cl_2 at each emission maximum at room temperature.

	Wavelength (nm)	Lifetime (μs)	Chi^{2*}	Wavelength (nm)	Lifetime (μs)	Chi^{2*}
$H_2T(iBu)P$	665	0.497(13)	4.232	736	0.721(9)	8.165
$H_2T(CH_2Ph)P$	665	0.382(14)	2.206	737	0.119(17)	1.801
$H_2T(iPent)P$	664	0.907(10)	12.08	733	0.411(14)	2.025
$H_2T(CHPh_2)P$	664	1.045(9)	16.01	731	0.435(13)	1.995
$H_2T(iPr)P$	667	0.631(16)	2.828	741	0.470(13)	2.325
$H_2T(cyHx)P$	668	0.454(14)	3.314	738	0.348(19)	3.679

*The chi-square distribution (also chi^2 or χ^2 distribution) is one of the most widely used theoretical probability distributions in probability theory and statistical significance tests.

Table 6.11: Lifetimes for the *meso*-tetraalkylporphyrins in CH_2Cl_2 at each emission maximum at 77K.

	Wavelength (nm)	Lifetime (μs)	Chi^{2*}	Wavelength (nm)	Lifetime (μs)	Chi^{2*}
$H_2T(iBu)P$	654	0.391(14)	6.992	727	0.885(12)	9.548
$H_2T(CH_2Ph)P$	658	0.334(12)	2.801	738	0.290(19)	1.924
$H_2T(iPent)P$	652	0.740(13)	5.601	725	0.580(14)	3.633
$H_2T(CHPh_2)P$	648	1.046(17)	8.882	720	0.650(15)	3.491
	663	0.581(12)	3.930	740	0.467(16)	1.818
$H_2T(iPr)P$	657	0.511(15)	2.101	743	0.560(12)	3.349
$H_2T(cyHx)P$	659	0.614(16)	2.613	732	0.562(15)	2.389

*The chi-square distribution (also chi^2 or χ^2 distribution) is one of the most widely used theoretical probability distributions in probability theory and statistical significance tests.

Lifetimes of around 1–100 μs are normally seen for triplet states in solution; they are often destroyed by external quenching as opposed to phosphorescence emission. Lifetimes of around 1–100 ns are common for upper singlet states, but these short times introduce instrumentation problems. Fluorescence intensity is used to monitor de-excitation to the ground state; the nanosecond pulses are low in energy which results in the detected signals being weak and having a large bandwidth; therefore high noise levels result. This can be improved with the use of repetition and signal-averaging techniques, which result in a comparatively low-noise plot of the intensity of the fluorescence as a function of time following each flash.[333]

The plots used in the determination of the lifetimes for this series of free base *meso*-tetraalkylporphyrins involved the use of an instrument response function (IRF). In this case LUDOX (colloidal silica, SiO_2) was used. By subtraction of the IRF from the intensity data, the decay of the analyte excited state(s) could be measured and quantified. The type of decay is found to be first order. An example of the curve used to determine the lifetimes is shown in Figure 6.15. Here the decay curve for $H_2T(CH_2Ph)P$ at 665 nm can be seen with the IRF, as well as the fit used to determine the lifetime.

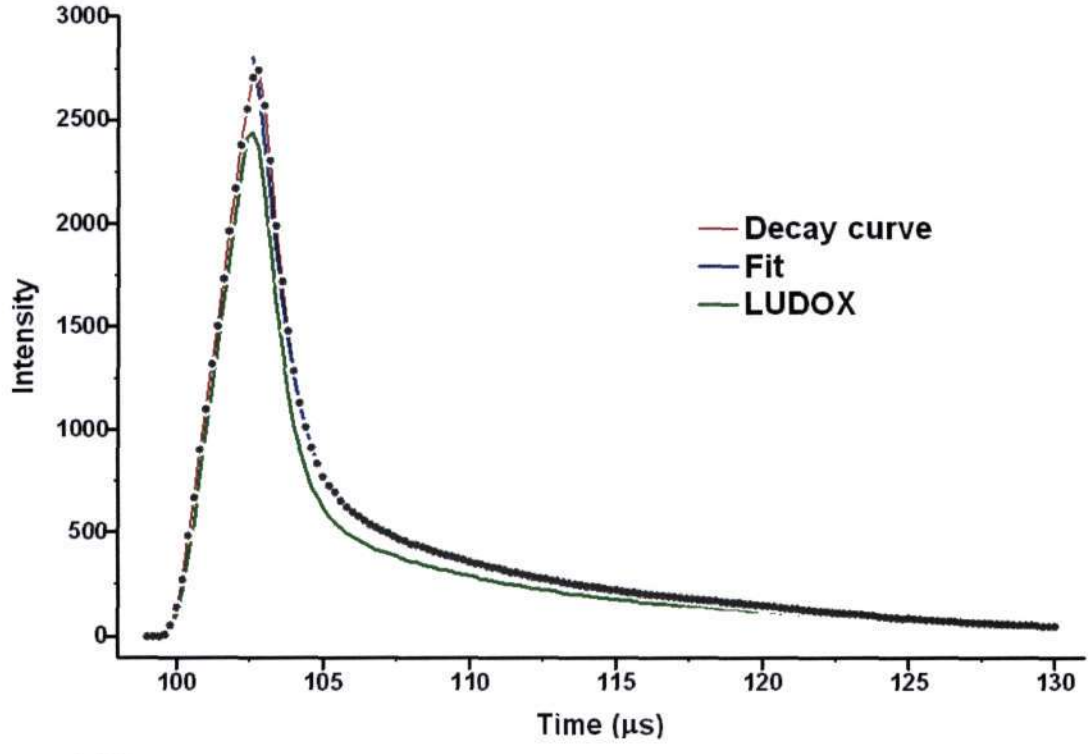

Figure 6.15: An example of the decay process for $H_2T(CH_2Ph)P$ at 665 nm. The excited state decays in a simple first-order process.

The lifetimes determined for this series of free base *meso*-tetraalkylporphyrins are rather long compared to the lifetimes seen for other porphyrins in the literature. The most common range seen for porphyrin fluorescence is from 10^{-12} to 10^{-9} s (singlet state emission). Phosphorescence (triplet state emission) has longer lifetimes and the literature values recorded for porphyrin phosphorescence are in the range of around 10^{-6} to 10^{-3} s. Phosphorescence has been seen for H_2TPP at 865 nm;[356] however, in this work, emission spectra for the range beyond 800 nm were not collected and therefore no phosphorescence has been observed for these *meso*-tetraalkylporphyrins. However, this will form part of the future experimental work. Previous work has shown that the fluorescence lifetimes for certain metallated porphyrins (e.g. Cu^{II} metalloporphyrins) can be less than 10 ps which can make the excited state decay difficult to observe.[357]

The lifetime determined for H_2TPP was shown to be 15 ns.[359] This is far shorter than the lifetimes observed for the *meso*-tetraalkylporphyrins of this work, which fall in the range of 100 ns to 1 μs. The lifetimes for the range of substituted tetraphenylporphyrins studied by Harriman and Hosie were all less than the lifetime for H_2TPP. Their range extended as low as about 16% of the lifetime for the unsubstituted tetraphenylporphyrin, i.e. 2.5 ns.[359] Looking at the results[356] for free base H_2TPP there is only one wavelength lifetime given; however, there are two clear peaks in the emission spectrum. The metallated tetraphenylporphyrins studied by Harriman[356,357,358] were either in the nanosecond range or even into the microsecond range (Tables 6.4 to 6.7). In the case of phosphorescence the longer lifetimes for these metalloporphyrins extended into the millisecond range.

When comparing the lifetimes measured at room temperature (Table 6.10) and at 77 K (Table 6.11) for both wavelengths, the discrepancy between corresponding pairs of values is generally small. Although none of the lifetimes are identical, they are all mostly within 0.1 to 0.2 μs of each other. At room temperature it was found that the lifetimes at the longer wavelength are generally shorter than those at the lower wavelength, except for $H_2T(iBu)P$. The errors for each lifetime are generally similar and the chi^2 values for the fitted experimental data are all as close to 1 as possible, with the highest being 16 for $H_2T(CHPh_2)P$.

The lifetimes determined for the porphyrins at 77 K are very similar with the highest chi^2 value just below 10; this is for $H_2T(iBu)P$. The lifetimes at the higher wavelength are also generally shorter than those at the shorter wavelength. This is true for all the porphyrins except $H_2T(iBu)P$ and now $H_2T(iPr)P$, which differs by only about 0.05 μs. The errors for each lifetime are all similar to each other, with no particular outliers.

6.5 Future work

Presented in this work are preliminary studies on the emission spectra and lifetimes of *meso*-tetraalkylporphyrins. Fluorescence, in particular, has been observed and discussed for these porphyrins. The emission spectra compare well with those of other studied metallated and free base porphyrins; however, the lifetimes differ by an order of magnitude.

This is novel work and therefore our future experimental and theoretical work will be to:

(1) obtain quantum yields for the fluorescence of each sample;
(2) calibrate our spectrofluorimeter (specifically all lifetimes measured using the Xeon pulse lamp) using pyrene which is expected to have a lifetime in the same range as was determined for this series of porphyrins (~ 100 ns);
(3) obtain emission spectra (with wavelength maxima) and lifetimes for the gold(III) metalloporphyrins (if quenching is absent);
(4) use peak-fitting methods to fully deconvolute and thus quantify the vibrational level spacings for the porphyrin ground states;
(5) correlate the lifetimes with any structural features of the compounds; and
(6) attempt to measure triplet state emission (phosphorescence) from this series of *meso*-tetraalkylporphyrins.

7. DFT Simulations

7.1 Introduction

Computational chemistry uses the fundamental laws of physics (either wholly or only partially) as its basis to predict chemical structures and reactions numerically. This then allows the study of chemical phenomena of these compounds and reactions by performing calculations instead of merely using experimental examinations. Thus computational chemistry can be used, not only as an independent study method, but also in conjunction with experimental investigations to further broaden experimental knowledge.[224] Molecular simulations are also useful because they do not merely help calculate the properties of synthesized compounds, but they can also predict the structures, energies and other features of unknown molecules.[371] These chemical calculation techniques are therefore significant applications that have often been used in chemical research.

There is an elementary distinction between experimental techniques and the calculations performed (quantum-mechanical or force field), because calculations can also be carried out on molecules that have no real existence; molecules that can either not exist under normal conditions or compounds that have yet to be synthesized.[371] Quantum chemical techniques are therefore especially useful when studying unstable species as these are not easily examined by conventional structure determination procedures; examples include reactive intermediates, excited states, transition states, etc.[272]

These types of calculations can provide extraordinary amounts of information compared with what chemists obtain from experimental techniques. For example, modern DFT calculations can give the molecular structure, heat of formation, dipole moment, ionization potentials, charge densities, bond orders and spin densities in one experiment. There is still, unfortunately, the possibility that these results obtained from calculations may be unreliable. However, for the most common methods, the

advantages and disadvantages have already been established and thus the probable accuracies can be sensibly predicted.[371]

There are two broad methodologies within computational chemistry; *molecular mechanics* and *electronic structure theory*, and both are primarily dedicated to the structure and reactivity of compounds. They both perform the same basic types of calculations: geometry optimizations, and computing the energy and vibrational frequencies. Molecular mechanics uses the laws of classical physics, while electronic structure methods use the laws of quantum mechanics. There are two major classes of electronic structure methods:[224]

Semi-empirical methods: e.g. AM1, PM3, used in programs like HyperChem and Gaussian, which use parameters already obtained from experimental data in order to simplify the calculation. They solve an approximate form of the Schrödinger equation according to their possession of suitable parameters for that specific system. They are largely characterized by their differing parameter sets.[224]

Ab initio methods: these use no experimental parameters in computations; rather, computations are founded exclusively on the laws of quantum mechanics—the name *ab initio* means "first principles"—and on a few physical constants (Planck's constant, speed of light, masses and charges of electrons and nuclei).[224] There are a few simplifying assumptions involved in *ab initio* theory, but the calculations are more comprehensive (and therefore more expensive) than those of semi-empirical methods.[371]

The *ab initio* procedure generally searches for exact solutions; all quantities in the calculation are computed as precisely as is numerically possible. The semi-empirical procedure seeks, from the beginning, only approximate solutions. Often the simplifications used may be quite radical, but they are nonetheless required to always be physically justified.[372] The basic steps for the execution of a typical *ab initio* or semi-empirical calculation are very similar.[371] Lately, a third class of electronic structure methods has been used in computations: Density Functional Theory (DFT). Density Functional Theory is not much different from the *ab initio* methods and the calculations need about the same total of computation resources as the Hartree-Fock

theory (the least expensive *ab initio* method).[224] DFT methods are more appealing due to their inclusion of the effects of electron correlation, whereas Hartree-Fock calculations regard this effect only in an average sense, which causes less accuracy for some system sorts. Therefore using DFT has the advantage and benefits of more expensive methods, but at the fee of Hartree-Fock theory.[224]

DFT based techniques draw from the quantum mechanics research of the 1920s (especially the Thomas-Fermi-Dirac model), and also from fundamental work in quantum chemistry done by Slater in the 1950s.[373] The approach of these DFT methods is founded on a strategy of modelling electron correlation using functionals of the density of these electrons.[224] In the last decade, methods based on DFT have gained steadily in popularity. In recent years, DFThas proved to be extremely useful and has been applied to a variety of problems that occur in porphyrin chemistry, often involving ground states. DFT can take electron correlation into account in a computationally efficient manner and hence provides practical results.[272] The best DFT methods achieve considerably better accuracy than Hartree-Fock methods with only a small increase in cost. DFT methods aim at providing, in one batch of self-consistent field (SCF) iterations, the real density distribution of correlated electrons in the ground state and the associated energy.[374]

Another role played by these theoretical studies is their usefulness in helping to understand structural details. This can be particularly applied to protein-active sites because this information is often not obtained at a high enough resolution from protein crystallography.[272] 'In this connection, the crucial role that quantum chemistry has played in elucidating the deformability of haem-bound carbon monoxide in carbonmonoxymyoglobin may be cited as an instructive example.'[272] There is also an interest in whether the observed structural packing is indeed a fundamental property of the molecule or merely a result of crystal packing forces. This is important particularly in the case of nonplanarity in porphyrins. It is possible for quantum chemistry to readily distinguish between such intramolecular and intermolecular effects. As a final point, quantum chemical computations supply us with the information to be able to understand molecular energetics or thermochemistry in terms of structural properties and molecular structure in terms of electronic structure.[272]

The foundation for DFT (as it is known today) was created in 1964 when a landmark paper appeared in the journal *Physical Review*.[375] All modern day density functional theories are based on the main theoretical support of the theorems that Hohenberg and Kohn proved in this publication.[373] This publication demonstrated the existence of a unique functional which can determine the ground state energy and density exactly.[224,376] It also showed that the ground state electronic energy is determined by the electron density, ρ,[376] implying then that there exists a one-to-one correspondence between the electron density of a system and any property of the system in its ground state, including energy.[374] This is different to using the wave function approach, where the number of coordinates is 3N in an N-electron system (3 for each electron and 4 including spin).[376] Squaring the wave function and integrating over the N–1 electron coordinates gives the electron density; it depends on three coordinates and is independent of the number of electrons.[376] Thus, while the complexity of a wave function increases according to the number of electrons, the electron density, independent of the system size, has the same number of variables.[376] There is, however, a problem. Although each different density produces a different ground state energy, which has been proven, the connecting functional of these two is not known.[376] The objective of DFT methods is to devise functionals connecting the electron density with the energy.[377]

There is a difference between a function and a functional; a function is a prescription for generating a number from a set of variables (coordinates) and a functional produces a number from a function (which in turn depends on variables).[376] In mathematics, functionals are defined as a function of a function. An energy that depends on an electron density or a wave function is a functional; and the electron density or wave function is a function.[376] DFT methods use general functionals of the electron density to compute electron correlation.[224]

In DFT, functionals are functions of the electron density which is itself a function of coordinates in real space. These functionals divide the electronic energy into several components which are each computed separately. In comparison with the wave mechanics method, it is evident that the energy functional may be divided into three parts. These three parts are kinetic energy, $T[\rho]$; attraction between the nuclei and electrons, $E_{ne}[\rho]$; repulsion between electrons, $E_{ee}[\rho]$ (in the Born-Oppenheimer

approximation the nuclear-nuclear repulsion is a constant);[376] and then there is also an exchange-correlation term to account for the remainder electron-electron interactions, $E_{xc}[\rho]$, (in most actual DFT formulations it is divided into separate exchange and correlation components).[224] A general equation for the energy functional is shown below:

$$E_{DFT} = T[\rho] + E_{ne}[\rho] + E_{ee}[\rho] + E_{xc}[\rho] \quad (1)$$

The second major paper of modern DFT, written by Kohn and Sham,[378] appeared about a year after that of Hohenberg and Kohn. This report proposed how the, up till then unheard of, universal functional could easily be handled. Their basic idea was to split the kinetic energy functional into two parts. One would be calculated exactly, while the other would be a small correction term. Their proposal was based on the acknowledgement of a common problem with direct density functionals (e.g. the Thomas-Fermi method) being associated with the way the kinetic energy is established.[373] Kohn and Sham therefore launched the idea of a non-interacting reference system made from a collection of orbitals; one electron functions. It had also been noted that orbital-based approaches such as the Hartree-Fock method performed a lot better in this respect. It permits the exact treatment of the majority of the contributions to the electronic energy of an atomic or molecular system, thus allowing the major part of the kinetic energy to be computed more accurately.[373]

In reality, however, the electrons are interacting and therefore the total kinetic energy is not provided, but the difference between the exact kinetic energy and that which is calculated, assuming non-interacting orbitals, is small.[376] The remainder is absorbed into an exchange-correlation term; it is merged with the non-classical contributions to the electron-electron repulsion. These are typically also small and include the non-classical fraction of the electron-electron interaction accompanied by the correction for the self-interaction and the component of the kinetic energy that is not included in the non-interacting reference system.[373] This method allows the maximum amount of information to be computed exactly so that only a small part need be calculated from an approximate functional.[373]

A few procedures have been promoted to deal with the Kohn-Sham equations: (1) the "scattered wave" (SW) or "multiple scattering" (MS) technique (founded on the so-called "muffin-tin" approximate potential); (2) the discrete variational method (DVM) (relying on the numerical sampling of Slater orbitals; and (3) as standard molecular orbitals, the expansion as linear combinations of Gaussian atomic functions.[374]

After the work done by Kohn and Sham, the approximate functionals used by present DFT methods divide the electronic energy into several terms, shown in the general expression:[224,376]

$$E_{DFT} = T_s[\rho] + E_{ne}[\rho] + J[\rho] + E_{xc}[\rho] \quad (2)$$

where $T_s[\rho]$ is the term for kinetic energy (from the motions of the electrons), $E_{ne}[\rho]$ includes terms for the repulsion between pairs of nuclei and the potential energy for the nuclear-electron attraction, $J[\rho]$ represents the electron-electron repulsion (also known as the Coulomb electron density self-interaction). The term $E_{xc}[\rho]$ represents exchange-correlation and also comprises the left over components of the electron-electron interactions. These include exchange energy evolving from the anti-symmetry of the quantum mechanical wavefunction, and dynamic correlation in the movement of individual electrons.[224,376]

If E_{DFT} is equated to the exact energy then it may be seen as the definition of E_{xc}; the portion which is left over after taking away the non-interacting kinetic energy, and the E_{ne} and J potential energy terms:[376]

$$E_{xc}[\rho] = (T[\rho] - T_s[\rho]) + (E_{ee}[\rho] - J[\rho]) \quad (3)$$

The kinetic correlation energy is shown in the first parenthesis and the second contains both the exchange and potential correlation energy.[376] This equation may be rewritten as:[224]

$$E_{xc}[\rho] = E^X[\rho] + E^C[\rho] \quad (4)$$

E_{xc} is determined entirely by the electron density and is usually divided into two parts. These are the exchange and correlation parts, which actually respectively correspond to the same-spin and mixed-spin interactions.[224] All three of the equation components are functionals of the electron density; the two terms on the right hand side are the exchange and correlation functionals, respectively. Both of these can be of two distinct types (1) local functionals (which depend only on ρ); and (2) gradient-corrected functionals which depend on ρ as well as its gradient.[224]

The advantage of DFT is that only the total density needs to be taken into account. However, to accurately calculate the kinetic energy, it is necessary that orbitals be reintroduced. Nonetheless, as previously mentioned, DFT has a computational cost which is similar to that of the least expensive *ab initio* method, Hartree-Fock theory, but it also has the advantage of possibly yielding more accurate results.[224,376] Despite the similarities, there is one important difference between *ab initio* methods, wave mechanics Hartree-Fock theory and DFT. DFT methods could give the exact total energy (including electron correlation) if the exact $E_{xc}[\rho]$ was known.[224,376] DFT methods are popular due to their inclusion of the effects of electron correlation in their model. These effects refer to the reality that electrons in a molecular system react to each other's motion and will try to stay out of the other's way. Therefore DFT methods have the ability to offer the benefits usually associated with more expensive *ab initio* methods at a Hartree-Fock cost.[224] Hartree-Fock theory considers this method only as an average (causing less accurate results for some types of systems) while methods that include electron correlation account for the instantaneous interactions of electron pairs with opposite spin.[224]

The reliable prediction and simulation of molecular structures is one of the most important applications of computational chemistry. A great deal of experience and knowledge has been gathered regarding the functioning and performance of each of the methods that have been employed. Therefore, as opposed to the early days of computational chemistry, it is now rather simple and easy to perform geometry optimizations on systems of more than 50 atoms. Most of these techniques generally have an accuracy performance of about 0.02 Å; this often improves for bond lengths where molecules that contain main group elements are involved.[224] It is now acknowledged (and has been for a long time) that bond lengths are predicted shorter

than they actually are by Hartree-Fock theory. Owing to the neglect of electron correlation, simulating multiple bonds is inclined to be complicated.[224] The precision of the bond energies acquired from the use of DFT calculations has been significantly enhanced by taking into account the nonuniformity of the electron density in the exchange and correlation functionals.[374] DFT methods differ according to the choice of the functional form of the exchange-correlation energy. Theory gives rather little guidance about how such functionals should be chosen and therefore many different potentials have been put forward. A variety of functionals have been defined in computational chemistry history and they are characterized by the means by which they deal with the exchange and correlation components.[224]

7.2 Functionals

7.2.1 Local Density Methods

Local exchange and correlation functionals engage only the values of the electron spin densities.[224] The Local Density Approximation (LDA) assumes the electron density is a slowly varying function, i.e. that the electron density locally can be treated as a hypothetical uniform electron gas.[373,376] The number of electrons and the gas volume are thought to move toward infinity, at the same time as the electron density remains finite and reaches a stable value.[373] LDA has been extended to the *Local Spin Density Approximation* (LSDA),[373] which is the unrestricted case where the spin densities, α and β, are not equal. It is also possible to write LSDA in terms of the total density and spin polarization. This LSDA will be equal to LDA for closed shell systems.[376]

For a number of different densities, by using Monte Carlo methods, the correlation energy of a uniform electron gas has been established.[373,376] It is necessary to have an appropriate analytic interpolation formula to use these results in DFT computations; similarly to that constructed by Vosko, Wilk and Nusair in 1980 (VWN),[379] which is a widely-used functional.[376] Often, instead of LDA defining the model of local density approximation, the acronym SVWN is used. The LSDA method does, unfortunately, have limitations. Although its results are mostly superior to that of the Hartree-Fock method, it has a tendency to overestimate outcomes.[373] This LSDA approximation,

unfortunately, has a tendency to underestimate the exchange energy by about 10%, which in turn causes errors larger than the whole correlation energy, which is itself overestimated (regularly by a factor close to 2). Consequently, the bond strengths will also be overestimated.[376] LSDA techniques may offer outcomes with comparable accuracy to those acquired from Hartree-Fock methods in spite of the simplicity of their fundamental assumptions.[224,376]

7.2.2 Gradient Methods

In the early eighties, the first successful expansions to the purely local approximations were developed.[373] To improve on the LSDA approach, a non-uniform electron gas needs to be considered. One way to do this is to make the correlation and exchange energies dependent on electron density *and* derivatives of the density; thus gradient-corrected functionals will entail electron spin densities as well as their gradients.[224,376] The name given to these processes is *Gradient Corrected or Generalized Gradient Approximation* (GGA) methods (also sometimes called *non-local* functionals in the literature which is somewhat misleading).[376]

In 1986, Perdew and Wang (PW86)[380] suggested altering the existing LSDA exchange expression. And in 1988 Becke[381] proposed a gradient-corrected correlation functional (B or B88) which became rather popular, followed by another widely-used functional (not a correction) by Lee, Yang and Parr (LYP) in the same year.[382] (These two forms were also combined to make the B-LYP method.) There is one empirical parameter in the LYP functional and it differs from other GGA functionals because it includes a few local components.[373] Another functional, with a correction to the LSDA energy, was proposed by Perdew and Wang in 1991,[224,376] PW91.[383] It should, however, be noted that quite a few of these propositioned functionals defied fundamental restrictions. P86 and PW91, for example, predict correlation energies for one-electron systems and for others, the exchange energy may be unsuccessful in cancelling the Coulomb self-repulsion.[376]

7.2.3 Hybrid Functionals

Generally, the exchange contributions are considerably larger in absolute numbers than the analogous correlation effects. Therefore, a prerequisite for acquiring useful outcomes from DFT is a precise expression for the exchange functional specifically.[373] A precise link can be made between the exchange-correlation energy and the corresponding potential connecting the non-interacting reference and actual system using the Hamiltonian and the definition of the exchange-correlation energy.[376] The resulting equation involves integration over a parameter that allows for the electron-electron interaction. This equation is known as the Adiabatic Connection Formula (ACF).[376]

The Half-and-Half method may be described by writing the exchange energy as a blend of LSDA, a gradient correction term and exact exchange. *Hybrid* methods frequently refers to models that include exact exchange. The *Adiabatic Connection Model* (ACM) and *Becke 3 parameter functional* (B3)[384] are therefore examples of hybrid models. These functionals operate well and thus the Half-and Half model is hardly ever used.[376] Several hybrid functionals define the exchange functionals as a linear combination of Hartree-Fock, local, and gradient-corrected exchange terms. This exchange functional is then joined with a local and/or gradient-corrected correlation functional.[224] Becke's three-parameter formulation, B3 (B3LYP),[384] is the best known of these hybrid functionals and these Becke style hybrid functionals have been found to be superior to the conventional functionals defined thus far.[224]

From the time of their manifestation in the early nineties these hybrid functionals have experienced unparalleled success.[373] One in particular, the B3LYP functional, has become a well known and extremely useful functional due to its surprisingly good performance in many chemical applications.[373] It was suggested by Stevens *et al.* in 1994[385] and has an unsigned error of only slightly above 2 kcal/mol (with respect to the G2 data base). It is related to that originally suggested by Becke (using B88 and PW91); however, the PW91 correlation functional has been exchanged for the LYP functional.[373]

In 1996 Becke made further progress by dropping the number of parameters to one where the amount of exact exchange was empirically ascertained. This resulted in the B1B95 functional.[386] Becke presented a new type of exchange-correlation functional founded on an intricate fitting procedure in the closing stages of his string of papers on density functional thermochemistry. It was aptly labelled B97.[387] Together, Schmider and Becke, then reparameterized this functional (with respect to the extended G2 set)[388] and the ensuing B98 functional preserves the good absolute average and low maximum errors (11.9 kcal/mol and 9.1 kcal/mol, respectively). Additional development was also carried out in the same year on the original B97 functional by Hamprecht *et al.*, they called their result B97-1.[373] The year 1998 also saw van Voorhis and Scuseria[389] offer a new exchange-correlation functional known as VSXC; it was dependent on the non-interacting kinetic energy density, as well as on ρ and its gradient, $\Delta\rho$.[373]

Development and research into the discovery of new and improved functionals continues. Some of the current functionals do have the ability to yield energy related results approaching alleged "chemical accuracy". This means that the results are within less than 2 kcal/mol, which is very high accuracy even for experimental results. There are many literature records showing high accuracy obtained by means of modern functionals and more are being published each year.[373]

Conversely, the regularly cited main shortfall of DFT is the official incapability to methodically progress the accuracy of quantitative predictions. There are a few key difficulties with DFT, which are clearly documented (weak interactions, excited states and highly degenerate systems). However, to forecast any other possible errors in DFT *a priori* is not possible without a thorough understanding of the fundamental aspects of the theory. Additionally, it has repeatedly been stated that when density functional methods do not succeed in a particular situation, then there is no exact course of action that may be followed to correct the imperfections in view of the fact that the underlying reasons for the limitations in the theory are a long way from being understood. This is true when the reason for failure is not the selection of the functional, integration grid, or basis set.[373]

7.3 Performing a calculation

The important requirement of a DFT method is the selection of an appropriate structure for the exchange and correlation energies.[376] It is possible to use a combination for the exchange and correlation energies; a LSDA form for one and a gradient form for the other. However, this is not actually uniform. The Dirac-Slater expression gives the exchange within the LSDA approximation, thus the only distinction is the interpolation function which is used in the reproduction of (very good) Monte Carlo results for the correlation.[376] The term LSDA is generally connected to the acronym SVWN, because the VWN formula is considered to be such a good interpolation function. Gradient corrected methods will typically use the B88 exchange functional or the B3/ACM hybrid, and this will be coupled with the LYP, P86 or PW91 correlation functional. Other related acronyms are BLYP, BP86, BPW91, **B3LYP**, B3P86, and B3PW91.[376]

LSDA methods do not usually perform as well as gradient corrected methods. There is a notable improvement attained by the addition of gradient terms and hybrid methods operate almost as well as the complex G2 model for some test situations.[376] Using the GGA methods for stable molecules usually presents geometries and vibrational frequencies of better or similar quality to those from perturbation methods like MP2 and the computational cost is analogous to that of Hartree-Fock.[376] Results of DFT procedures have been shown to produce outcomes that are as good as those of coupled cluster methods in multi-reference character systems, where MP2 generally does not succeed. DFT methods founded on unrestricted determinants for open shell systems have another advantage in that they are not as sensitive to "spin contamination".[376]

Current functionals inadequately describe weak interactions due to dispersion (van der Waals type interactions).[390] LDA predicts for example (though not very precisely) an attraction between rare gas atoms, whereas all gradient methods foretell a purely repulsive interaction (at least for the case of correction for basis set superposition error).[376] DFT methods account reasonably well for hydrogen bonding, which is mainly electrostatic. There are, however, indications that DFT methods less accurately predict relative energies and inadequately portray transition structures. Nevertheless,

it must be remembered that for DFT methods the number of systems for which it has been calibrated is still somewhat undersized.[376]

DFT computations (B3LYP/6-31G(d) level of theory) were, however, performed in 2003 by Oakes and Bell on the ground and excited triplet states of free base *meso*-tetraphenylporphyrin (H_2TPP), and some of its isotopomers. The calculated results for band positions (scaled accordingly) gave similar values to those determined experimentally; where errors could be avoided in the calculations, then even very small isotope shifts could be computed accurately. The success seen for these calculations, as compared to the experimental data for the extensive series of isotopomers, shows the usefulness of this approach. Thus DFT computations were shown to be of practical use and can therefore be applied to many other porphyrin systems, including β-substituted porphyrins and metalloporphyrins.[391]

And lastly, DFT methods at the moment are poorly matched for excited states that possess the same symmetry as the ground state. It is not easy to guarantee orthogonality between excited and ground states due to the deficiency of a wave function.[376] Theory does not provide much assistance in choosing functionals, thus numerous different potentials have been suggested. To determine the best performing functional involves a comparison with experiments of high-level wave mechanics calculations or with functionals known to have been successful for similar compounds in the past.

7.4 DFT and Porphyrins

High-quality geometry optimizations of large polycyclic molecules, such as porphyrins, are a somewhat more recent advance in computational chemistry.[392] These calculations were originally thought to be a technical feat,[392] however, in this day and age, they are routinely possible with the use of DFT methods.[393] There are methods, especially nonlocal DFT (NLDFT) methods, that yield structural information that is of such high quality that it is able to rival experimental data, like that acquired from high-quality crystallographic measurements.

In the last century, researchers used the energy levels of an electron in a circular ring, in a circular box, or a cyclic polyene to acquire qualitative comprehension of porphyrin electronic spectra.[272] Work on these highly simplified representations of the porphyrin macrocycle were performed from around 1949 to 1960.[272] In 1950 Longuet-Higgins and co-workers were the first to report data that accounted for the comprehensive shape of the porphyrin molecule in the form of Hückel calculations.[394] Gouterman expanded on the "four-orbital model" of porphyrin electronic spectra in the early 1960s. He did this by adding the main effects of configuration interaction into standard Hückel calculations.[211,214] According to this model, the two lowest unoccupied and two highest occupied molecular orbitals of a typical porphyrin are near-degenerate. These four orbitals are also all well separated from the other molecular orbitals. Porphyrin electronic structure has been based on the four-orbital model and the basic spectroscopic features can be explained in terms of transitions involving them, to a first approximation. Regular Hückel calculations eventually started to surrender after the 1960s to extended Hückel, Pariser-Parr-Pople, and semi-empirical treatments.[272]

The electronic structure of transition metal porphyrins was initially delineated by these extended Hückel calculations. They created the basis of an "electronic taxonomy" of the varied electronic spectra of transition metal porphyrins.[272] Semi-empirical calculations have made a chief contribution to the understanding of porphyrin electronic structure from the early 1970s, particularly for transition metal complexes and excited states.[272] These semi-empirical methods were and continue to be important in the theoretical work carried out on porphyrins and thus it is imperative to give emphasis to the way in which they compliment the ever more significant *ab initio* calculations.[272]

In the 1970s, the first *ab initio* calculations that were performed on porphyrins were recorded[395] and Gouterman forecast that this was just the beginning of many more to come that would eventually replace the extended Hückel calculations. During the later 1970s and early 1980s there were some *ab initio* calculations on other porphyrin-type molecules; however, by modern standards these were rather simple. They used small basis sets and electron correlation was not accounted for. There were further *ab initio* calculations that followed which used good basis sets and took electron correlation into account.[393] However, they were still impractical for numerous systems due to their

requirement of computational resources. They also continued to be unfeasible for complex porphyrin molecules and for studies that involve potential energy surfaces, including geometry optimizations and vibrational analyses. With the development of DFT (which takes electron correlation into account with a computationally efficient approach) a range of problems involving porphyrin-type molecules, primarily involving ground states, have been addressed.[393]

7.4.1 Nonplanar Porphyrins

The porphyrin macrocycle is flexible as far as out-of-plane distortions are concerned and can easily take on a broad range of nonplanar conformations according to its structure. The main conformations in which the porphyrin macrocycle will distort from the mean plane are known as ruffled, saddled, domed, and waved.[79] Due to the fact that several porphyrin and related tetrapyrrolemacrocycles have a tendency to distort their planarity in their protein environments, it is thought that nonplanarity may be a factor that fine-tunes the functional role of the cofactor.[71,72] This therefore makes the understanding of the actual cause of these distortions an essential objective in nonplanar studies. Some particular factors that may have an effect on planarity of the porphyrin macrocycle are the size of the central metal, steric hindrance between substituents and the type of metal-bonded axial ligands.[272] To determine the exact causes of the distortion is not easy and thus different methods need to be used to investigate the different possible factors; some investigations have already been done at the molecular mechanic level.[71]

It seems that DFT and molecular mechanics computations are very convenient and precise methods for the examination of porphyrin distortion from planarity. They can help to differentiate between solid state effects seen in the X-ray crystal data and effects that occur in the gas phase. The complex, $[Co(TPP)(BzNH_2)_2](SCN)$, has been studied by X-ray crystallography and DFT calculations (at the B3LYP/LACVP* level of theory) to show that it prefers a nonplanar conformation. Examining the crystal structure shows that the core conformation is a combination of ruffled and saddled distortions.[396]

Studies on a range of cobalt(III) metalloporphyrins, with various *meso*- and β-substituents,[397] showed that structures from ^{1}H NMR studies and molecular mechanics calculations agreed and that a single conformer is therefore preserved in solution. Complexes of this type showed axial ligands with hindered rotation and there were some unusual examples where the conformation influenced the orientations of axial ligands (these may find application as models when examining ligand orientation effects for biological systems).[397] A range of free base dodecasubstituted porphyrins were also shown to generally have analogous distorted macrocycles in both solution and crystal states; the structure of the substituents was also alike. This was determined from molecular mechanics calculations and ^{1}H NMR spectroscopy.[398] To date, no DFT simulations have been used to gauge the accuracy of the molecular mechanics simulations reported in these studies.

DFT studies were performed on four metalloporphyrins, the zinc and nickel derivatives of *meso*-tetra(trifluoromethyl)porphyrin and *meso*-tetra(pentafluoro-ethyl)porphyrin, to analyze the existence of multiple nonplanar conformations. Although the ruffled and saddled geometries are essentially equal in energy for the zinc complexes, the ruffled conformation is dominant for the nickel complexes; this is consistent with experimental data. However, for the nickel complexes of dodecaphenylporphyrins (mostly saddled conformations) both geometries are competitive. Thus, for particular metals, it seems that complexes display comparable nonplanar distortions.[399]

Studies on 5,10,15,20-tetraarylporphyrins have shown that the barrier for rotation of the *meso*-aryl rings varies according to the central core. Large metal ions, e.g. Zn(II), have a higher barrier than smaller metal ions, e.g. Ni(II), as do free bases compared to dication porphyrins.[400] The cause has been assigned to the extent to which the core substituents deform the macrocycle and variation of the porphyrin ring nonplanar distortions.[401] Computational studies performed by Haddad *et al.* convincingly show that, concerning very nonplanar *meso*-tetra(tert-butyl)porphyrin compared to *meso*-tetramethylporphyrin, the origin of large Soret band red shifts (40 nm) are mainly caused by nonplanar deformations and not by in-plane nuclear reorganization (IPNR).[402]

The original belief about the affect of distortions from planarity on electronic spectra was that red shifts would result. This was then challenged by DiMagno and co-workers[403] with semi-empirical AM1 studies of *meso*-tetra (perfluoroalkyl)porphyrins, but Parusel *et al.* presented density functional theory based configuration interaction singles calculations that agreed with the initial idea. It seems that these red shifts may be brought about by the nonplanarity-induced destabilization of the porphyrin HOMOs.[404] Shelnutt *et al.* also examined red shifts for a series of ruffled tetraalkylporphyrins with nickel and zinc. For the energy-optimized structures, the calculated transitions and experimental data were similar; however, for the structures that were ruffled by artificial constraints, only a fraction of the red shift is seen, consistent with DFT studies. The large red shifts were shown to result from the ruffled nonplanar deformations which are absent in the artificially constrained structures.[405]

The protonation behaviour of porphyrins has been studied with respect to the importance of nonplanar deformations.[406] Medforth *et al.* found a relationship between the amount of saddle deformation (tilting of the pyrrole rings) in the dication and the activation energy for intramolecular proton exchange. An increase in pH has also shown to increase nonplanarity of the porphyrin of nickel(II) microperoxidase-11 (NiMP-11).[407] Nonplanar cobalt(II) porphyrins that possess distinct cavities within their structures in a crystal may also retain these cavities when in solution. The cavities may modulate a range of porphyrin-substrate interactions. This gives them possible application in the synthesis of products with distinct ligand orientations and as regio- and stereoselective oxidation catalysts.[398]

7.4.2 Choosing the Functionals and Basis Sets

There is a founded fascination with porphyrins and their derivatives; they are remarkable compounds that have provoked all kinds of research concerning their properties and nature. Theoretical research in particular is motivated by the great biological importance of these molecules, their extensive coordination chemistry, and many other increasing practical applications.[272] Due to correlated *ab initio* calculations of sufficient quality being rather demanding with respect to computational resources, they therefore continue to be impractical for use with complex substituted porphyrins.

DFT, on the other hand, has shown itself to be very valuable and thus has been used in a variety of problems concerning porphyrin chemistry.[272]

The two variable parameters in DFT methods are the basis set and the variety of exchange-correlation potentials.[376] There are no set rules regarding which methods gives the best results for which systems. The best starting place is to ascertain whether any successful (or unsuccessful, in the case of elimination) calculations have been performed previously on similar systems. In the case of DFT calculations, there is evidence of its success for many different relevant metal porphyrins such as: CO, NO, HIm and O_2 adducts of haem proteins and models;[408] five coordinate deoxy haem derivatives;[409] model prototypes of haem for instance protoporphyrin-IX [Fe(PPIX)] and picket fence [Fe(TPivPP)(2-MeIm)];[410] cobalt(III) porphyrins;[411] iron(III) and manganese(III) porphyrins;[412] iron(II) porphyrins;[413] $[Fe(Por)(Im)O]^+$ and [Fe(Por)(Im)O];[414] models for the active centre of myoglobin;[410] [Fe(Por)O];[415] as well as a range including cytochrome P450: model ferryl species of cytochrome P450 and horseradish peroxidase (HRP);[416] the bonding of NO to Fe cytochrome P450;[417] and methylmercapate porphine model of cytochrome P450;[418] However, relatively fewer DFT studies have been reported for free base porphyrins.

In a recent study (2006), Hui and Yixin[419] reported some DFT (B3LYP and B3PW91 methods) and *ab initio* Hartree-Fock method optimizations on "Free-Base Porphyrin (H_2P)", with a range of basis sets. They showed that results from Hartree-Fock theory do not correlate well with experimental data for the porphyrin conformation and NMR shielding tensors. The DFT computations, however (where electron correlation is included), gave better results.[419] And in 2005 a range of free base *meso*-phenylporphyrins (5-monophenylporphine (H_2MPP), 5,15-diphenyporphine (H_2DOPP), 5,10-diphenyl porphine (H_2DAPP), 5,10,15-triphenylporphine (H_2TrPP), and 5,10,15,20-tetraphenylporphine (H_2TPP)) were studied with DFT computations (B3LYP/6-31G(d) level of theory) in order to test the affects caused by *meso*-phenyl substitution on the free base porphyrin. This included the electronic and vibrational spectra, as well as the conformations of the porphyrin macrocycles. These studies showed significant in-plane distortion and minor out-of-plane distortion of the porphyrin

ring. The predicted frequencies and electronic absorption peaks were similar to those from experimental data.[420]

In 1997 computations (local density functional and *ab initio* Hartree-Fock) for free base porphyrin, chlorin, bacteriochlorin, and isobacteriochlorin were reported by Ghosh. When looking at the optimized geometry of the low-symmetry trans-isobacteriochlorin by delocalized local density functional the advantage over Hartree-Fock theory is obvious. The DFT-calculated results concur with those of X-ray photoelectron spectroscopic (XPS) data. Although for a few molecules Hartree-Fock theory has produced comparable results to XPS, it gives poor results for molecular charge distributions for hydroporphyrins. Overall, for structural and electronic properties of hydroporphyrins, DFT theory is rather superior.[421]

The DFT-calculated absorption spectrum obtained by Sundholm agreed with recent *ab initio* calculations and experimental data for free base porphine.[422] In the same year (2000), structures, energetics, and triplet-triplet (T-T) spectra were calculated using DFT for the low-lying triplet states of free base porphine (H_2P) and some of its β-octahalogenated products: β-H_2X_8P; where X = F, Cl, Br. The gap for the singlet to triplet (S_0-T_1) obtained for H_2P by phosphorescence conformed well with that computed by DFT with the B3LYP functional.[423] A year later geometry optimization of octaethylporphyrin (OEP) was performed using DFT and produced a centrosymmetric molecule with local D_{2h} symmetry; this compared well with the X-ray structure obtained for H_2OEP.[424] Corresponding vibrational spectroscopic information was also obtained.

DFT computations (B3LYP/6-31G* level of theory) were run on free base porphyrin (H_2P) and free base tetraphenylporphyrin (H_2TPP) to determine the geometrical structures of their lowest triplet states. The same functional, but with the extended EPR-II basis set, was used for the calculation of hyperfine couplings. The results compared well with experimental data and it was noted that the presence of the phenyl groups did not overly effect the unpaired electron spin-density distribution.[425]

Porphyrins have found uses ranging from photovoltaic devices to multi-electron transfer catalysts; for these functions it is important to be able to modulate electron

transfer parameters. Sun and co-workers[426] have showed that controlling ion-pairing, axial ligation and electronic effects can help in selection of the electron transfer numbers using β-fluorinated porphyrin free bases. DFT calculations have been used, in conjunction with digital simulation and quantum electrochemical studies to show that these effects may cause inversion in porphyrins, which is a means to controlling multi-electron transfer reactions.[426]

Once it has been established that there have been successful DFT methods on related systems then the pros and cons of the different accessible basis sets have to be inspected. Therefore it is easy to use experimental data to guide the choices of the computational type. Most of the above work discussed on porphyrins used the B3LYP/6-31G(d) level of theory in the computations performed. The difference between the basis set, 6-31G(d), in this method and the basis set, 6-31G(d,p), is that former adds polarization functions to heavy atoms and the latter to hydrogen atoms as well. Both basis sets have 15 basis functions for first row atoms, but 6-31G(d,p) has 5 for hydrogen atoms whereas 6-31G(d) only has 2.[224] Thus for this work on free base porphyrins 6-31G(d,p) is the better and more useful choice.

Throughout the years, many basis sets have been generated in the context of wave function based approaches to quantum chemistry.[373] A basis set is defined as the mathematical description of the orbitals in a molecule (which in turn combine to approximate the total electronic wavefunction) used to carry out the theoretical calculation. The basis set thus restricts each electron to an exacting area of space; therefore the more accurate approximations are made by larger basis sets because they impose fewer restrictions on the locations in space.[224,376] The larger the basis set, however, the more computational resources required.[224] Therefore it is necessary to find the largest basis set possible, that will accomplishes the job with the best results, without calling for unmanageably large computational resources.

7.4.3 Computational Methods

DFT calculations (B3LYP functional,[384] 6-31G**[224] basis set, coarse/medium grid) were performed with Gaussian 03W[427] V 6.1, Rev. C.02 running on a dual core and

Athlon 64-bit machine under Windows XP-64. The 6-31G** basis set is a split valence basis set; it has two (or more) sizes of basis function for each valence orbital. It also adds polarization functions to the hydrogen atoms as well as all non-H atoms.[224]

The input files for porphyrin 2 ($H_2T(CH_2Ph)P$) contained coordinates from the X-ray structures of the synthesized compound, using the cif file created from the X-ray crystallography data. The input files for porphyrins 1, 3 and 5 ($H_2T(iBu)P$, $H_2T(iPent)P$ and $H_2T(iPr)P$, respectively) were altered forms of the not quite ideal crystal structures that were obtained. And the remaining porphyrins, 4 and 6 ($H_2T(CHPh_2)P$ and $H_2T(cyHx)P$), used input files that were generated in Arguslab,[428] both were PM3 optimized structures.

All input files contained the full structure of each porphyrin including all *meso*-substituents so that any effect that these substituents may have on the core of the macrocycle was factored into all the computations performed. In the case of porphyrin 4 ($H_2T(CHPh_2)P$), it was necessary to perform an ONIOM computation in order to save time and memory. This is a method used in order to overcome the limitations associated with large molecules. This method was first a part of Gaussian 98 and has subsequently been improved so that it may be used for even larger molecules. In this procedure two or three layers are defined within the actual structure and each layer is then dealt with at different levels of theory. Investigations have shown that the results computed using this method are comparable to those produced by the high accuracy method.[429] Unfortunately this was not an acceptable method for obtaining vibrational data and therefore only the optimized geometry of $H_2T(CHPh_2)P$ was obtained.

Each of the structures was symmetrized in order to make use of molecular point group symmetry and to reduce the number of basis functions in the calculation. Once the geometries had been optimized, frequency jobs were run on each structure to obtain the theoretical IR frequencies for each type of vibrational stretch or bend in the porphyrin molecule. An NMR job (GIAO method) was then used to determine the shielding tensors for each atom for ^1H and ^{13}C NMR spectra.

7.5 Objectives

The main goals of this chapter were to:

(1) optimize the geometries of the six synthesized *meso*-tetraalkylporphyrins and to compare them with those observed in the solid state;

(2) characterize the molecular orbitals of this series of porphyrins;

(3) compute the frequencies for each porphyrin to enable comparison of the theoretical and experimental IR spectra;

(4) calculate the NMR shielding tensors for each porphyrin to be compared to the experimentally obtained data; and

(5) determine the relative energies of all possible atropisomers of *meso*-tetraalkylporphyrins with sterically bulky substituent groups.

7.6 Results and Discussion

7.6.1 Introductory remarks

1970 saw the introduction of the first program in the GAUSSIAN series; and in 1971 it was made available via QCPE.[430] It was called GAUSSIAN70 and was capable of performing single-point calculations or optimizations (using Gaussian basis sets containing *s*- and *p*-orbitals) by cyclic variation of all parameters. This was the first *ab initio* program that found extensive approval. The basis sets, STO-3G and 4-31G, were the two most well-known to be built into the program. This program was subsequently used expansively externally to the laboratory in which it was produced due to the simplicity of the input structure and GAUSSIAN70's swiftness.[371]

The most current version of Gaussian was used for this work, Gaussian 03.[427] This is a very user-friendly version compared to earlier versions, all of the standard input is free-format and mnemonic with reasonable default settings. The output files are simply laid out and are self-explanatory. This version of Gaussian (and others) have found application by chemists, chemical engineers, biochemists, physicists and others where research is being carried out in other chemical interest areas.[429]

Gaussian 03W[427] is capable of predicting the energies, molecular structures, and vibrational frequencies of molecular systems. It is then also viable for numerous molecular properties to be derived from these basic computation types. These computations provide a wide range of spectra predictions including: IR, Pre-resonance Raman, NMR and harmonic and anharmonic vibration-rotation coupling. These computations can help in the analysis of compounds that may be difficult or impractical to examine experimentally and it is possible for the conditions of the studies to be altered, e.g. properties can be computed in the presence of particular solvents.[429]

In this work, DFT calculations that were performed with Gaussian 03W[427] were executed in order to acquire a correlation between the theory and the practically collected data. This included IR bands, NMR shielding tensors and possible X-ray structures for each of our synthesized porphyrins. Not only do such simulations help in the understanding of the specific data of the particular compound for which the calculations were carried out, but simulations at this level of theory facilitate the discovery of trends that may well occur in similar compounds.

All the values ascertained from these computations can be compared to experimental values; any possible discrepancies can then be investigated and their causes investigated. These calculations can help in the understanding of many different concepts related to the properties observed for the porphyrin in question due to the vast quantity of information that is obtainable from these types of computations.

Using these calculations it is possible for the conformers of the porphyrin macrocycles to be examined. The DFT-optimized coordination geometries and those obtained from X-ray crystallography in the solid state may be compared. There may be some notable differences between the final structures determined by these two techniques; which may often be attributed to the packing in the solid states. The structures determined by X-ray diffraction will take these packing effects into account; however, the computations are for the free structure in the gas phase (possible packing effects are ignored). This packing can result in either the flattening of the structure (planarity) or a distortion that pushes the structure out of its planar position (nonplanarity). Thus the observed difference will be a level of the distortion of planarity.

7.6.2 Geometry Optimizations

The results for the lowest energy conformations from the two techniques are given in Table 7.1 below and they are also displayed pictorially on the following pages. In these six figures the results for the DFT simulations are on the left and their relevant counterparts determined (or partially determined) from the crystal structures obtained from X-ray diffraction are on the right of the figures. Some literature structures have also been included.

Table 7.1: Summary of the lowest energy conformations from DFT computations and from crystal structures obtained from X-ray diffraction.

	DFT-calculated conformation	X-ray conformation
$H_2T(iBu)P$	Ruffled distortion	Planar with slight wave distortion component
$H_2T(CH_2Ph)P$	Planar with slight wave distortion component	Planar with slight wave distortion component
$H_2T(iPent)P$	Ruffled distortion	Planar with slight wave distortion component
$H_2T(CHPh_2)P$	Saddled distortion	–
$H_2T(iPr)P$	Ruffled distortion	Planar with slight ruffling
$H_2T(cyHx)P$	Ruffled distortion	Ruffled distortion

Figure 7.1: The structure of $H_2T(iBu)P$ from DFT (left) and X-ray diffraction (right), along the N-H axis of the molecule. (iBu groups have been omitted from the X-ray structure for clarity.)

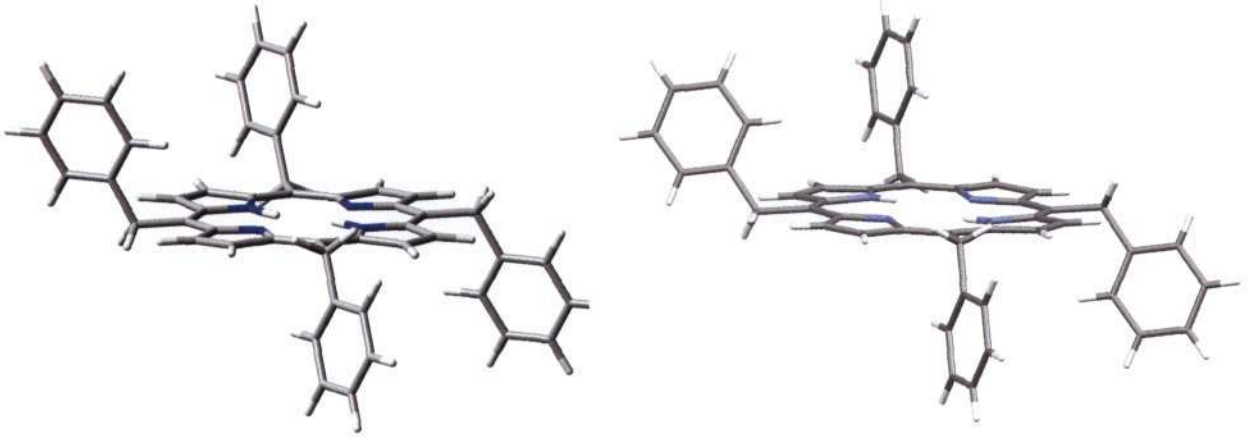

Figure 7.2: The structure of $H_2T(CH_2Ph)P$ from DFT (left) and X-ray diffraction (right).

Figure 7.3: The structure of $H_2T(iPent)P$ from DFT (left) and X-ray diffraction (right), along the N-H axis of the molecule.

Figure 7.4: Side-on and top-down views of the structure of $H_2T(CHPh_2)P$ from DFT simulations (no crystal structure was obtained).

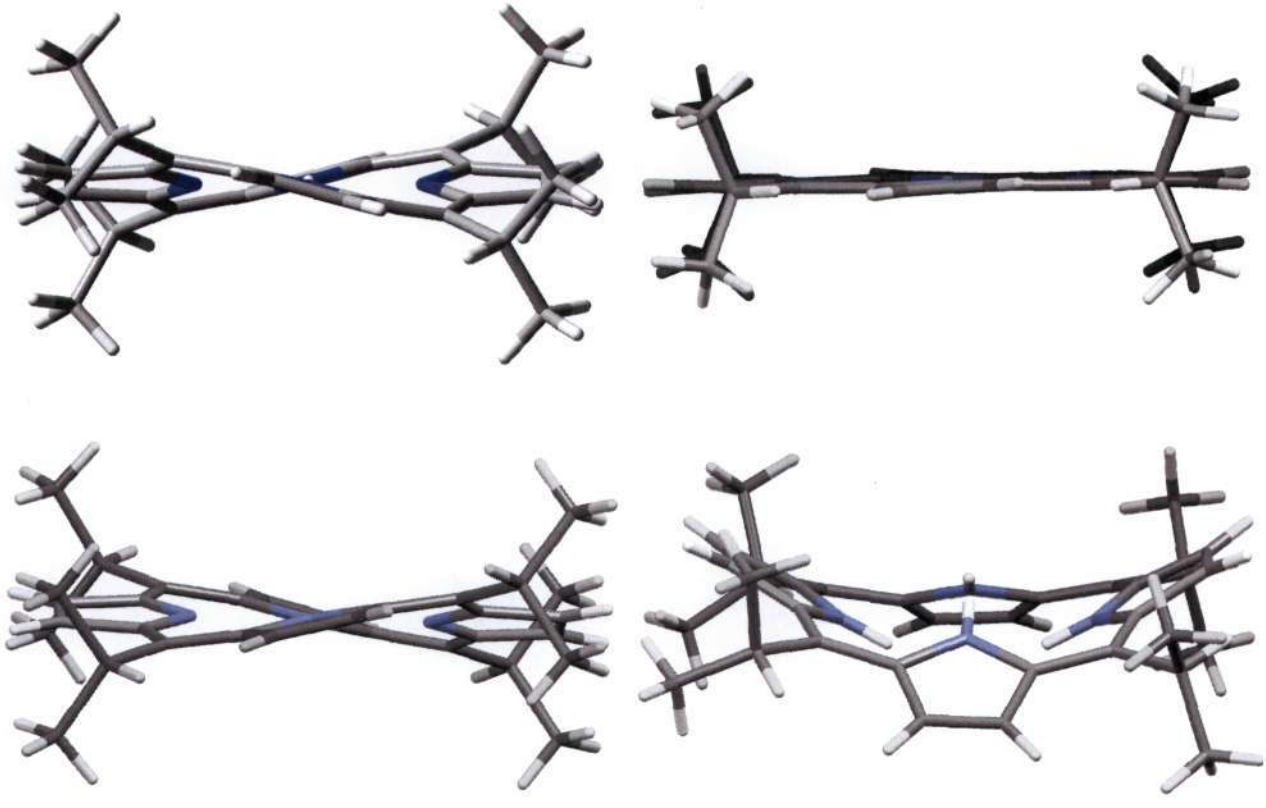

Figure 7.5: The structure of $H_2T(iPr)P$ from DFT (top left) and X-ray diffraction (top right), viewed along the N-H axis of the molecule. The two literature structures for the free base (bottom left; ruffled) and diacid (bottom right; saddled) analogues of this porphyrin.

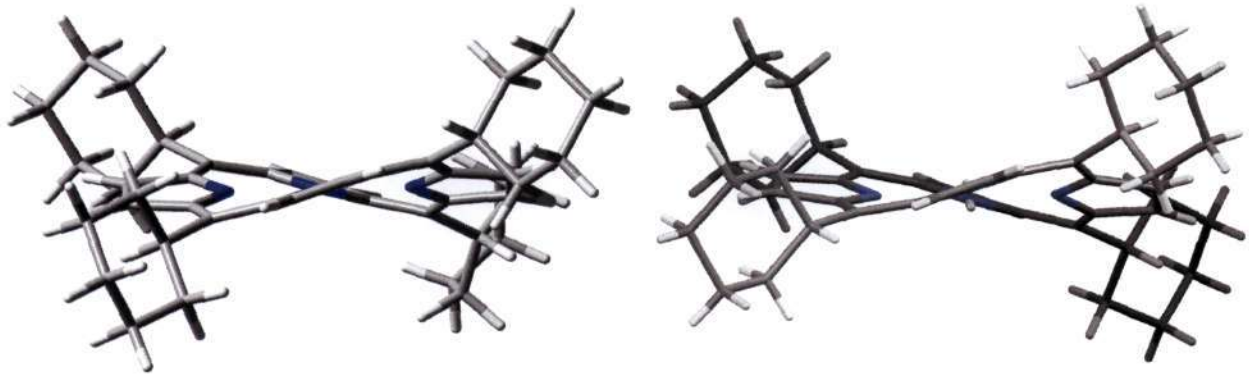

Figure 7.6: The structure of $H_2T(cyHx)P$ from DFT (left) and X-ray diffraction (right), along the N-H axis of the molecule.

The most noticeable differences (if any) between the X-ray structures and the DFT-calculated structures are the conformations of the porphyrin cores. From the final computed structures it was observed that for all six porphyrins, except for P2 ($H_2T(CH_2Ph)P$) and P4 ($H_2T(CHPh_2)P$), a core with a ruffled distortion was calculated. This was anticipated due to the type of aldehydes that had been purposefully used in the syntheses. However, there is also the possibility that the core distortion is under- or overestimated by the DFT calculations.

The crystal structure for P1 ($H_2T(iBu)P$) could not be fully resolved for the substituents and therefore only the core of the macrocycle for the X-ray crystal structure is represented in Figure 7.1. There is a rather obvious difference between these two structures of the macrocycles. The DFT calculations predict a ruffled geometry whereas the X-ray structure only shows a slight wave component. This may be due to the fact that there may be either an R- or S- enantiomer present at each of the *meso*-substituents due to the racemic mixture of the starting aldehyde that was used in the synthesis. This therefore means that the crystal structure may be an average of the different possible conformers formed by the different enantiomers at different positions. This might explain the flattening of the porphyrin core seen in the crystal structure and account for the ruffled conformation from the DFT simulation, which is predicted for the gas phase.

The theoretically determined and the experimentally determined conformations for P2 ($H_2T(CH_2Ph)P$) are almost identical. The structures can be superimposed using Hyperchem;[431] this has been done and the result is shown in Figure 7.7. The

porphyrin macrocycles of the two structures fit almost perfectly onto each other; however, there is a larger discrepancy between the phenyl ring substituents. This can be attributed to crystal packing interactions for the X-ray structure which are absent in the DFT simulation. The RMSD for the least squares fit of the two structures is 7.33 x 10^{-2} Å (24 non-H atoms of the porphyrin macrocycle).

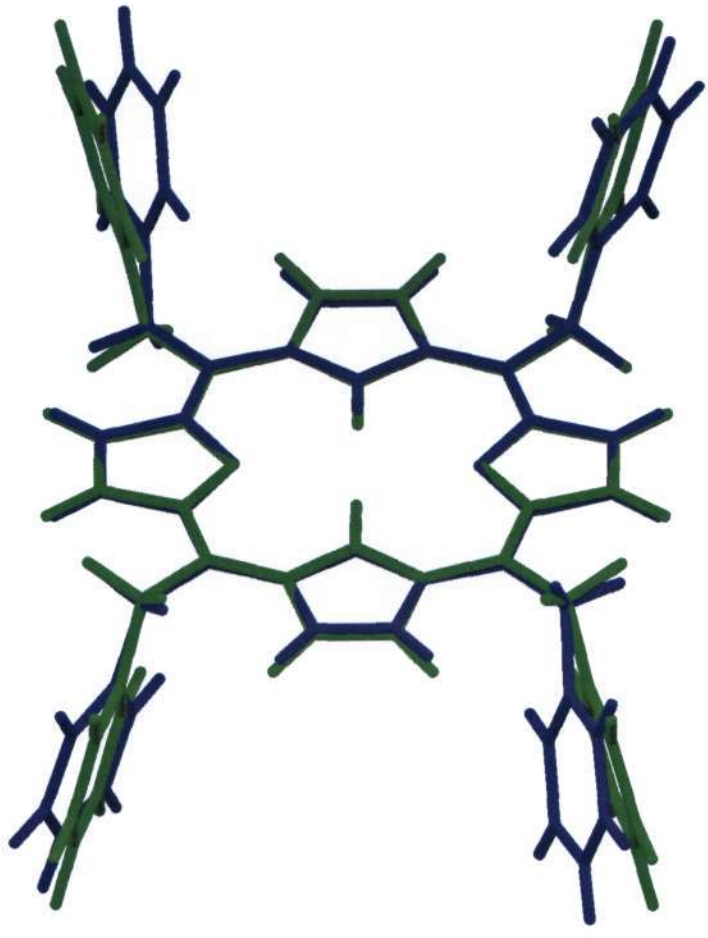

Figure 7.7: Least squares fit of the X-ray (blue) and DFT-calculated (green) structures of $H_2T(CH_2Ph)P$.

In the case of H_2T(iPent)P there is again a difference between the expected and obtained conformations; this is the same as what was seen for H_2T(iBu)P. This discrepancy may be due to the packing effects which may have a flattening effect on the ruffled structure which would be seen in the gas phase according to DFT. Alas, no X-ray quality crystal could be obtained for P4 ($H_2T(CHPh_2)P$) and therefore there are only DFT simulated structures in Figure 7.4. In this case where an appropriate crystal structure could not be obtained it is not possible to make a direct comparison of the

final geometries and thus only the results from the DFT calculation can be examined and compared to the other porphyrins. It will, however, be possible to compare their NMR and IR data with experimentally obtained results. The DFT computation does foresee a saddled conformation, which does not particularly agree with the predictions for most of the other *meso*-tetraalkylporphyrins. However, a saddle conformer is the favoured stereo-chemistry for sterically crowded systems. DFT simulations are currently in progress to calculate atropisomers for this system (and will be reported on at a later date).

The crystal structure for $H_2T(iPr)P$ shows a perfectly planar structure with substituents in the same conformation with the hydrogen atom lying in the mean plane of the macrocycle with one methyl group on either side of it. This structure could not be fully resolved due to the disorder which stems from the variety of different conformations that may be formed. The resulting structure is therefore an average of all these possible conformations (each conformation has an equal and opposite conformation thus the final structure is a perfect average). The DFT computes the structure expected in the gas phase for the conformation with the lowest energy and therefore a ruffled core with tilted substituents is predicted. The crystal structure reported in the literature for this free base porphyrin has a ruffled conformation (consistent with the DFT-calculated structure) and the diacid has a saddled conformation. See Chapter 5 (X-ray Crystallography).

The two structures for $H_2T(cyHx)P$ look very similar to each other; they are both ruffled and the cyclohexyl substituents all have the chair conformation. There is, however, a small difference in the degree of ruffling of the porphyrin macrocycle. Looking down the N-H bonds of the structure computed by DFT shows a perfect axis through the molecule; however, when doing the same for the crystal structure the N-H bonds do not line up with each other. Due to this slight discrepancy between the macrocycle distortions there is also a slight difference in the orientations of the cyclohexyl groups; however, the basic distortion is still the same.

The discrepancies between the experimental values obtained for each of the porphyrins and those calculated by DFT can mostly be explained by the effect that crystal packing has on the orientations of the *meso*-alkyl groups relative to the

porphyrin core. In cases where the calculated and observed core conformations differ markedly, disorder in the X-ray structure accounts for the difference in conformation. As expected, these effects are absent in the gas phase structures.

Although the substituents differ for each of the six *meso*-tetraalkylporphyrins the porphyrin core is the same in each case and therefore some similarities between the bond lengths and bond angles of each structure are expected. Structural parameters have already been compared for the X-ray structures (Chapter 5); but the values calculated by DFT for these variables are given in Tables 7.2 and 7.3.

Table 7.2: Average bond lengths (Å) calculated by the DFT simulations for each of the six *meso*-tetraalkylporphyrins.

	N-H	N-C_α	C_α-C_β	C_β-C_β	C_α-C_{meso}
H_2T(iBu)P	1.014(0)	1.373(5)	1.447(13)	1.360(9)	1.413(4)
H_2T(CH_2Ph)P	1.014(0)	1.372(5)	1.447(14)	1.360(9)	1.408(4)
H_2T(iPent)P	1.014(0)	1.374(4)	1.446(12)	1.361(9)	1.414(3)
H_2T($CHPh_2$)P	1.014(0)	1.374(6)	1.448(14)	1.360(8)	1.411(6)
H_2T(iPr)P	1.014(0)	1.373(4)	1.447(13)	1.360(9)	1.412(3)
H_2T(cyHx)P	1.014(0)	1.373(5)	1.447(14)	1.361(9)	1.414(4)

Table 7.3: Average bond angles (°) calculated by the DFT simulations for each of the six *meso*-tetraalkylporphyrins.

	C_α-N-H	C_α-N-C_α	C_α-C_β- C_β	N-C_α-C_β	C_α-C_{meso}- C_α	N-C_α-C_{meso}
H_2T(iBu)P	124.2(0)	109(3)	107.6(9)	108(2)	123.1(1)	126.4(3)
H_2T(CH_2Ph)P	124.6(0)	108(3)	107.4(9)	108(2)	124.9(0)	126.7(5)
H_2T(iPent)P	124.2(7)	109(3)	107.6(9)	108(2)	122.7(9)	126.5(5)
H_2T($CHPh_2$)P	124.5(2)	108(3)	108(1)	108(2)	124.3(0)	126.7(1)
H_2T(iPr)P	124.2(0)	109(3)	107.6(9)	108(2)	123.3(0)	126.5(4)
H_2T(cyHx)P	124.2(1)	109(3)	108(1)	108(2)	122.7(5)	126.3(5)

Chemically equivalent bond lengths are, as expected, very similar to one another; there are no significant outliers and most differ only in the third decimal place. However, $H_2T(CHPh_2)P$ does show slightly longer bond distances than the sample mean, except for C_β-C_β and C_α-C_{meso} (shorter than the sample mean). The bond angles are also all rather similar with the largest differences occurring for the N-C_α-C_β and C_α-C_{meso}- C_α angles; the rest differ on average by less than half a degree.

7.6.3 Molecular Orbitals

Also determined from the computations were the four frontier molecular orbitals (MOs) for each compound. Here, we are mainly interested in determining to what degree the *meso*-alkyl groups may perturb the frontier MOs of the porphyrin. Once the PM3 geometry optimization had converged, GaussView 3.09[225] was used to compute the surfaces for the four frontier molecular orbitals of each of the six synthesized *meso*-tetraalkylporphyrins. Although orbitals may be useful in the qualitative understanding of some molecules, they are merely mathematical functions that represent solutions to the Hartree-Fock equations for that molecule. It is possible for other orbitals to exist, which look quite different, yet produce the same energy and properties. There is no physical reality that can be connected with these images; individual orbitals are mathematical not physical constructs.[224]

These four frontier molecular orbitals include the highest and second-highest occupied molecular orbitals and the lowest and second-lowest unoccupied molecular orbitals. These are denoted HOMO, HOMO-1, LUMO, LUMO+1, respectively. For each porphyrin, these four orbitals are shown pictorially in Figures 7.8 to 7.13. Given that the frontier molecular orbitals for this series of *meso*-tetraalkylporphyrins are all rather similar, for brevity we shall present the discussion for $H_2T(iBu)P$ (P1):

The HOMO-1 is localized on the central porphyrin macrocycle with no contribution from the *meso*-substituents. Nodal planes run perpendicular to the viewing plane every 45° with one that is the molecular plane. The HOMO is more delocalized with some contributions from the substituents. The nitrogen *p* orbitals figure mainly at the centre of this orbital. They are all in phase due to the arrangement (aligning) of the

positive lobes. The LUMO and LUMO+1 are more similar to the HOMO than they are to the HOMO-1, but have more nodal planes due to their antibonding character. The LUMO and LUMO+1 orbitals have the same symmetry, differing only by a rotation of 90°.

In the standard D_{4h} symmetry labelling system for the frontier molecular orbitals of porphyrins,[432] the symmetry species of the HOMO (a_{2u}), HOMO-1 (a_{1u}), and LUMOs (e_g^*) of the present *meso*-tetraalkylporphyrin derivatives match those of most standard *meso*-tetraarylporphyrins such as H_2TPP and its metal analogues.

LUMO+1

LUMO

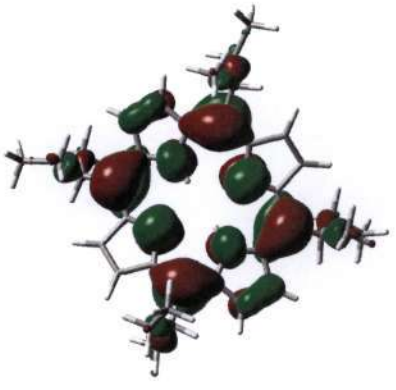

HOMO

HOMO–1

Figure 7.8: LUMOs (top) and HOMOs (bottom) calculated for $H_2T(iBu)P$ with GaussView 3.09.[225]

LUMO+1

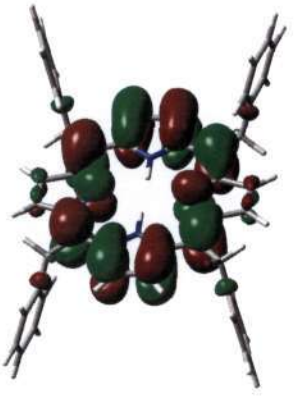

LUMO

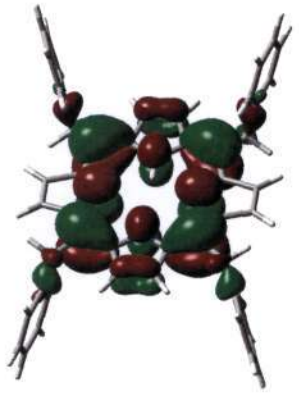

HOMO

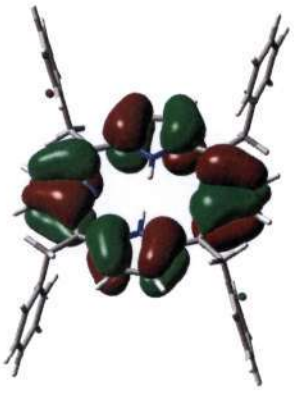

HOMO–1

Figure 7.9: LUMOs (top) and HOMOs (bottom) calculated for $H_2T(CH_2Ph)P$ with GaussView 3.09.[225]

LUMO+1

LUMO

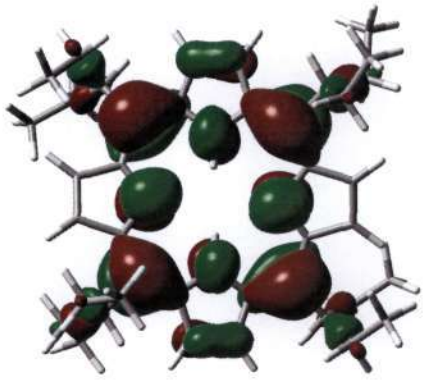

HOMO

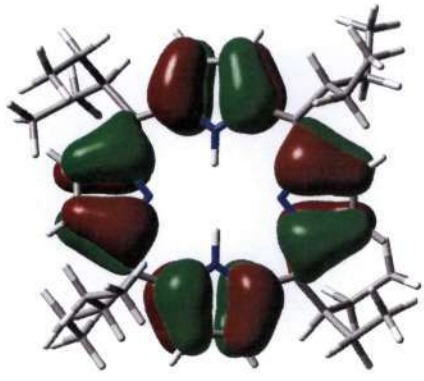

HOMO–1

Figure 7.10: LUMOs (top) and HOMOs (bottom calculated for $H_2T(iPent)P$ with GaussView 3.09.[225]

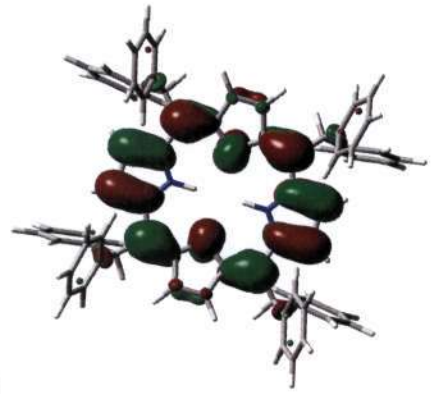

LUMO+1

LUMO

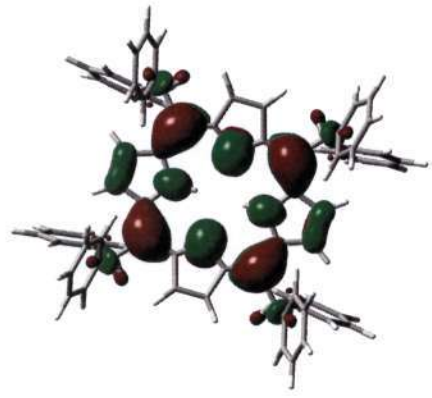

HOMO

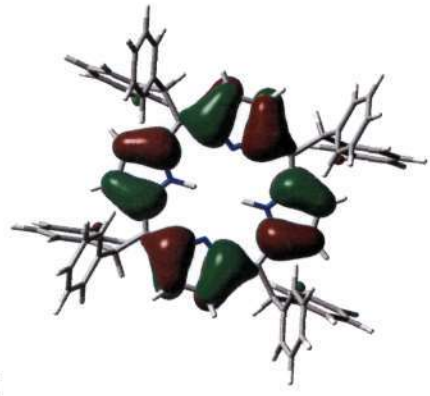

HOMO–1

Figure 7.11: LUMOs (top) and HOMOs (bottom) calculated for $H_2T(CHPh_2)P$ with GaussView 3.09.[225]

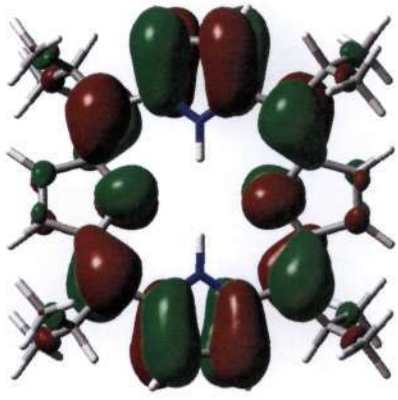

LUMO+1

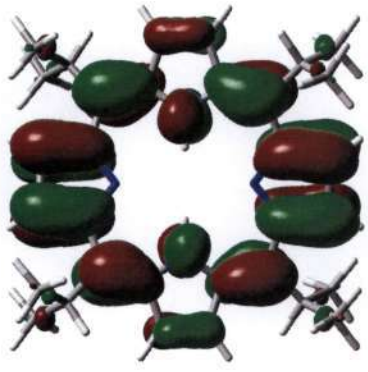

LUMO

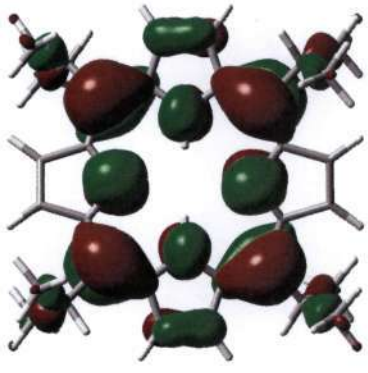

HOMO

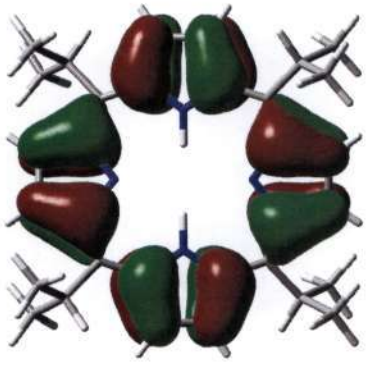

HOMO–1

Figure 7.12: LUMOs (top) and HOMOs (bottom) calculated for $H_2T(iPr)P$ with GaussView 3.09.[225]

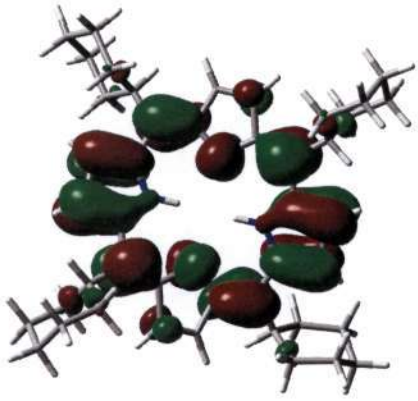

LUMO+1

LUMO

HOMO

HOMO–1

Figure 7.13: LUMOs (top) and HOMOs (bottom) calculated for $H_2T(cyHx)P$ with GaussView 3.09.[225]

As shown in Figures 7.8 to 7.13, the HOMO-1, HOMO, LUMO and LUMO+1 are similar for each porphyrin. They are localized mainly on the central ring of the macrocycle with little or no contribution from the alkyl-substituents, depending on the particular porphyrin and orbital. An orbital energy level diagram comparing the six porphyrins is depicted in Figure 7.14

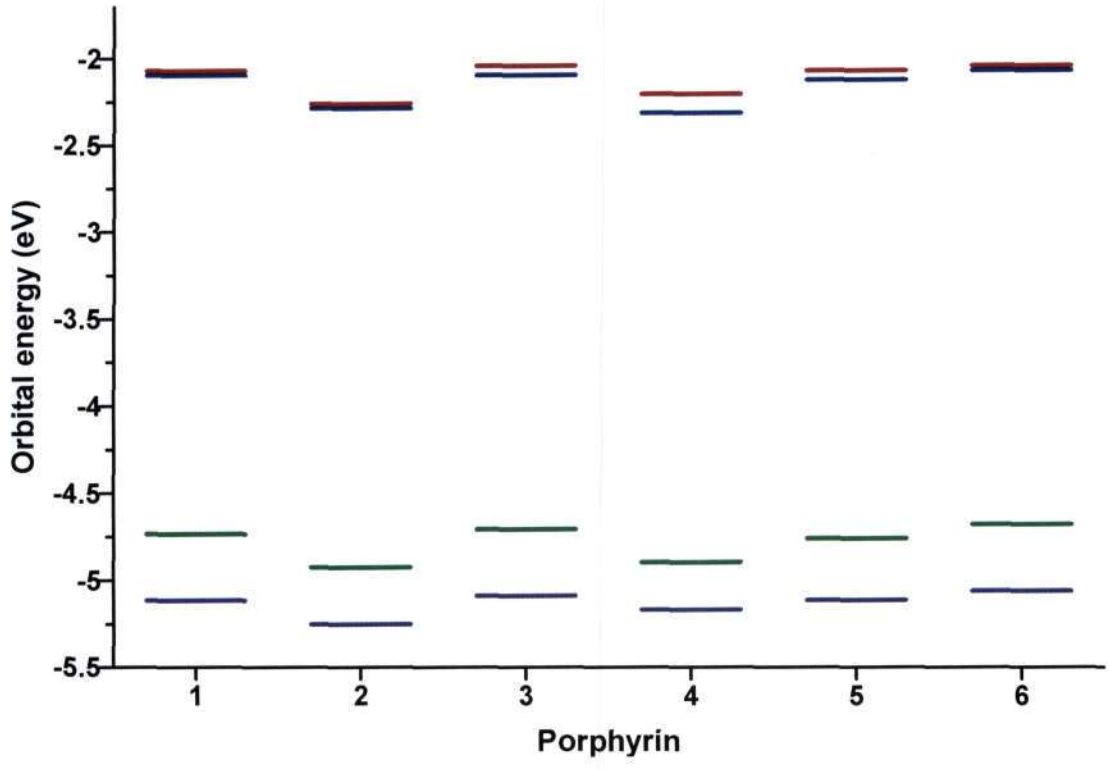

Figure 7.14: An orbital energy diagram for the series of six *meso*-tetraalkylporphyrins; where 1 = $H_2T(iBu)P$; 2 = $H_2T(CH_2Ph)P$; 3 = $H_2T(iPent)P$; 4 = $H_2T(CHPh_2)P$; 5 = $H_2T(iPr)P$; and 6 = $H_2T(cyHx)P$.

The bonding and antibonding MOs for the *meso*-tetraalkylporphyrins are partitioned into groups with marginal variations in absolute orbital energies. Two of the porphyrins, $H_2T(CH_2Ph)P$ and $H_2T(CHPh_2)P$, display MO energies that are somewhat lower than those of the congeners. These have planar and saddled conformations, respectively. Shown in Table 7.4 are the energy differences between the occupied and unoccupied orbitals for each porphyrin. Here the trend is rather different to that seen in the diagram. The energy difference is lowest for $H_2T(CHPh_2)P$; slightly higher for $H_2T(iPent)P$ and $H_2T(cyHx)P$; and the largest for $H_2T(iBu)P$, $H_2T(CH_2Ph)P$ and $H_2T(iPr)P$.

Table 7.4: The energy difference between the HOMO and the LUMO orbitals for each porphyrin.

Porphyrin	Energy gap / eV
$H_2T(iBu)P$	2.639
$H_2T(CH_2Ph)P$	2.639
$H_2T(iPent)P$	2.612
$H_2T(CHPh_2)P$	2.585
$H_2T(iPr)P$	2.639
$H_2T(cyHx)P$	2.612

7.6.4 IR

Geometry optimizations and energy calculations ignore vibrations in the molecular system, thus using an idealized view of nuclear position. In reality the nuclei in molecules are constantly in motion, these vibrations are regular and predictable in equilibrium states and thus can be used to identify molecules from their characteristic spectra. Gaussian 03 computes vibrational spectra for both the excited and ground states, besides predicting the frequency and intensity of spectral lines the program can also depict the displacements undergone by a system in its normal modes. This means it can predict the direction and magnitude of the nuclear displacements that occur when a system absorbs a quantum of energy.[224]

A significant application for modern quantum chemical methods is the computational forecast of vibrational spectra since it permits the elucidation and understanding of experimental spectra. This may then be used to assist with identification of unknown compounds or help to clarify the structures of already known compounds. There are two characteristics of vibrational spectra that need to be considered; the frequency of the absorbed incident light and how much is absorbed. To determine the frequency and intensity the harmonic vibrational frequencies of the particular molecule are calculated and accurate intensities must be supplied. For IR spectra, "the intensity is related to the square of the infinitesimal change of the electric dipole moment μ with respect to the normal coordinates".[224]

The crude frequency values calculated using the Hartree-Fock level have systematic errors because electron correlation is ignored, this results in overestimates of around 10-20%. Therefore it is normal for values that have been computed at the Hartree-Fock level to be scaled by an empirical factor of 0.8929. It has been found that the use of this factor results in good agreement with experimental values for a broad series of systems. For the particular level of theory used in this work, B3LYP/6-31G(d), the scale factor to be used is 0.9613.[224] This gave relatively good results that compared well to the experimental spectra in all six cases.

The spectra are all very similar, particularly in the fingerprint region, with only a few obvious differences. This therefore confirms a series of similar structures all based on the same macrocycle. There is better correlation in the fingerprint region than at the higher frequencies, which helps in assignment. The difference between the two methods (RMSD) for the values at lower frequencies is more than six times less than that at higher frequencies, although at higher frequencies there is still comparatively good correlation between the two methods. It was possible to use the DFT computations to make assignments for vibrations of the porphyrins in the IR region and to elucidate those obtained experimentally. The computed vibrations could be assigned exactly even if there was no marked evidence of these peaks in the experimental spectrum. A full comparison of the results obtained experimentally and those computed using DFT can be found in Chapter 3.2 (IR Spectroscopy).

7.6.5 NMR

Another property that can be computed in the context of a single point energy calculation using DFT is NMR shielding tensors. This refers to the result of a molecule being under the influence of an externally applied magnetic field. These important effects include how the local electronic currents induced by the externally applied magnetic field interact with a nuclear or electron spin. This interaction results in a *chemical shift*; which is the main component of nuclear magnetic resonance (NMR) experiments. However, the interaction of the spin of one nucleus with the electronic currents caused by another, known as coupling, is also an important source of information.[224]

Reliable chemical shifts will only be predicted if the geometries on which they are based are suitable and accurate. These chemical shifts have a clear response to structural variance and thus if the geometries are not close to perfect then determined values may be untrue. This sensitivity to geometry has already found application when identifying geometrical parameters of a target molecule.[224] A comparison of the experimental and theoretical spectra can help to make correct assignments and understand the basic chemical shift-molecular structure relationship. Density functional techniques are at the moment the only way, other than experimental procedures, in which realistically accurate results for NMR and electron spin resonance (ESR) properties can be acquired. This is particularly true regarding large molecules with transition-metal centres and/or complex electronic structure.[224]

The resulting output file gives the expected value of the chemical shift for each of the atoms in the molecule in turn. The shielding constants reported in literature are usually relevant to the standard compound tetramethylsilane (TMS), thus in order to compare our predicted computational results with those obtained experimentally the absolute shielding value for TMS must be determined using exactly the same model chemistry. Thereafter the corrected predicted shift is obtained by subtracting its absolute value from that which was calculated for the reference molecule. If the resulting shift is negative then there is more shielding in that particular atom of the molecule than in the reference molecule (TMS), and a positive number indicates less shielding than in the reference molecule.[224]

The computed NMR data were obtained for each of the porphyrins in the gas phase (with no solvent), but for a few, namely $H_2T(iBu)P$, $H_2T(iPr)P$ and $H_2T(cyHx)P$, NMR data were obtained using a solvent continuum model with chloroform. Mostly there was little difference between calculations with or without solvent. The isotropic shielding constants were converted to chemical shifts, tabulated, grouped according to the type of signal and finally averaged. These final values were then compared to the experimental values obtained for each porphyrin. These calculations of magnetic properties carry a common complexity in that the usual wave functions do not guarantee gauge invariance, thus in the simplest case it is possible for the results to depend on the position of the molecule in the Cartesian frame.[300]

For all the porphyrins the worst correlation for the proton NMR signals between the calculated value and the experimentally obtained value was for the pyrrole N-H, which exhibited a difference of more than 2 ppm. The rest of the calculated data for the ^{1}H and ^{13}C NMR shifts compare well to our experimental data, with small discrepancies of only about 0.5 ppm and 6 ppm or less, respectively. Thus for the majority of the signals, the agreement between theory and experiment is good at the chosen level of theory (B3LYP/6-31G**). A higher level of theory is therefore unwarranted for these large molecules; the NMR spectra have been successfully predicted. A complete discussion of the data can be found in Chapter 4 (NMR Spectroscopy).

7.7 Summary

In this work, DFT methods were used to compute the structures and electronic properties of the six *meso*-tetraalkylporphyrins. The data generally compared well with experimental variables (e.g., geometries, chemical shifts, and vibrational frequencies) measured in this work. More specifically, the simulations (a) facilitated assignment of the IR and NMR spectra, (b) delineated key differences between solution and solid state (X-ray structures), and (c) offered insights as to the preferred conformational isomers as well as their electronic structures (including FMO symmetries).

7.8 Future Work

Our on-going and future DFT simulations will be used to:

(1) obtain optimized structures, IR frequency data and NMR shielding tensors for the gold(III) metalloporphyrins of each porphyrin in the series; and

(2) calculate the most stable atropisomers and possibly the rotational barriers linking the minima on the potential energy surface for free base and gold(III) *meso*-tetraalkylporphyrins.

8. Metallation with gold(III)

8.1 Metallation of porphyrins

The two pyrrole N-H groups at the centre of free base porphyrins are readily ionized to form a dianion. Porphyrin dianions are capable of complexing a range of metal ions with the porphyrin mostly acting as a tetradentate ligand; thus the minimum coordination number of most metalloporphyrins will be four. The coordination number can be increased to five, six, seven or even eight with the uptake of either anionic or neutral ligands. In cases where there are only two axial ligands, there will usually be one on either side of the porphyrin plane (top *and* bottom). However, when more ligands are present it is common for them to all be on one side of the porphyrin (top *or* bottom).[310]

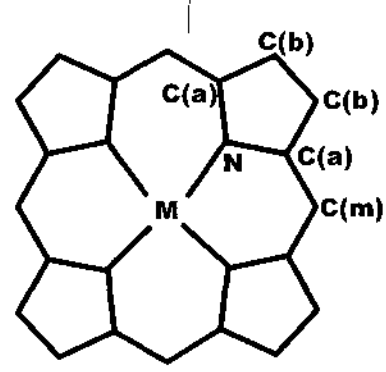

Figure 8.1: A skeleton of the macrocyclic centre showing the notation used for the chemically unique atoms in metallated porphyrin structures.

For the porphyrin structures discussed, the following general notation—as shown in Figure 8.1—will be used with regards to the labelling of the atoms of the central macrocycle skeleton in the structure. The α- and β-carbon atoms of the pyrrole rings are labelled C(a) and C(b), respectively, with C(m) being used for the *meso*-carbon atom. The central metal will be denoted as M and any bonds between these atoms will be referred to by the same notation. The hydrogen atoms in the structures will be named according to the atom to which they are bonded.

An interesting structural variable in metallated porphyrins is the length of the metal-nitrogen (M-N) bond. The size and complexing power of the metal, as well as the size of the porphyrin cavity, play a role in determining these bond lengths. Some metal ions will sit in the mean plane of the macrocycle, whereas others will be forced out.[310] With an increase in the metal ion size, the probability that it will be displaced out of the porphyrin plane, particularly if there is a single axial ligand, increases as it is less likely to be able to fit properly into the cavity formed by the four nitrogen atoms at the porphyrin core. This observed out-of-plane displacement can not, however, provide direct information about the detailed energy balance in the system, or about the 'strain' energy of the different deformations.[8]

Although porphyrin structures will usually oppose unwarranted radial expansion or contraction of the porphyrin core, they will more readily permit buckling of the porphyrin macrocycle, which may cause displacement of the metal ion from the porphyrin plane. For porphyrin ligands that do not have sterically demanding substituents, a nonplanar conformation will ease the strain for metals that have need of unusual M-N bond distances. For delocalized π-bonding in the core, such deformations are somewhat unfavourable, but are quite common in crystalline metalloporphyrins.[310] A pictorial view of the possible distortions of the porphyrin macrocycle can be found in Chapter 5 (X-ray Crystallography).

The size of the metal ion and—for transition metal complexes—the spin state of the ion will affect the stereochemistry of a metalloporphyrin. The effects of the electronic configuration on the geometry have been summarized by Scheidt.[36] Metalloporphyrins can generally be divided into separate groups of main group derivatives: transition metal derivatives and the lanthanide and actinide species.[36]

Certain factors have been found to have an affect on the metal ion's equilibrium position with respect to the plane of the macrocycle. These include the oxidation state, coordination number and the spin state of the specific metal used. These properties are crucial when determining the chemical, functional, and mechanistic properties of haem proteins, and newly synthesized metalloporphyrins. In the mid 1970's it was shown that resonance Raman (rR) frequencies were sensitive to the relative location of the metal ion in these metalloporphyrins complexes. For the metalloporphyrins that

were nonplanar with ruffled or domed configurations, the predicted frequencies were noticeably higher than those observed.[433]

8.2 Gold in medicinal history

Gold compounds have been used clinically in the alleviation of various symptoms and particularly those normally associated with rheumatoid arthritis. The use of gold for medicinal purposes has been documented throughout our history.[434] Treatment with gold based drugs is now accepted in modern medicine and is known as Chrysotherapy, derived from *chrysos*, which is the Greek word for gold. The earliest use of gold medicinally is believed to be by the Chinese in 2500 BC.[434] However, both Arabic and Chinese physicians documented the use of gold when treating an assortment of disorders. Alchemists in medieval Europe also used it in a variety of medicinal recipes.[435] The 17th century new pharmacopoeias showed a gold cordial which Nicholas Culpepper promoted for the treatment of ailments caused by a decrease in the 'vital spirits' (this included melancholy, fainting, fevers, and falling sickness). The late 19th century produced a treatment for syphilis with gold, this was a mixture (muriate) of gold chloride and sodium chloride, $Na[AuCl_4]$.[434]

The medicinal use of gold in the twentieth century started when gold cyanide $K[Au(CN)_2]$ was shown to be bacteriostatic towards *mycobacterium tuberculosis*.[434] This was discovered by the German bacteriologist Robert Koch in 1890 and illustrated the scientific basis for the pharmacological activity of gold compounds.[435] Then, in the 1920s, gold therapy for tuberculosis was established on the grounds that *mycobacterium tuberculosis* was a causative agent for rheumatoid arthritis. However, it soon proved to be unsuccessful. Further studies sponsored by the Empire Rheumatism Council nevertheless confirmed that gold compounds were effective in treating rheumatoid arthritis.[434]

Gold complexes were used for treating rheumatoid arthritis in the twentieth century, which, in 1985, resulted in the introduction of the oral drug Auranofin (Figure 8.3). Gold drugs also found use in the treatment of psoriatic arthritis (a form of arthritis associated with psoriasis), juvenile arthritis, palindromic rheumatism and discoid lupus

erythematosus.[436] Various inflammatory skin disorders (such as pemphigus, urticaria and psoriasis[437]) have also been treated using gold therapy.[434]

In spite of the fact that gold compounds have been useful in the treatment of rheumatoid arthritis, as well as having been used so much in both ancient and modern medicine, there is not much crystallographic evidence of their structures. This is due to the difficulty of obtaining X-ray quality crystals.[435] Interest in gold(III) complexes has now further developed due to the prospect of inorganic drug design and their use in studying biochemical reaction mechanisms.[438]

8.3 Gold as an Anti Cancer Drug

Platinum has long been the metal at the forefront of anticancer drug research, the anti-tumour activity of cisplatin, cis-$[PtCl_2(NH_3)_2]$ (Figure 8.2), was discovered in 1969.[439] Due to the success of cisplatin against a diversity of cancers (in cancer chemotherapy), investigations began for other alternative metal-containing anti-tumour drugs.[434,435] Gold compounds were considered a good choice for further investigation for anti-tumour activity/cytotoxicity as they were expected to produce favourable results due to their already founded anti-arthritic activity. However, this was not the only reason that interest was shown in gold compounds.[435]

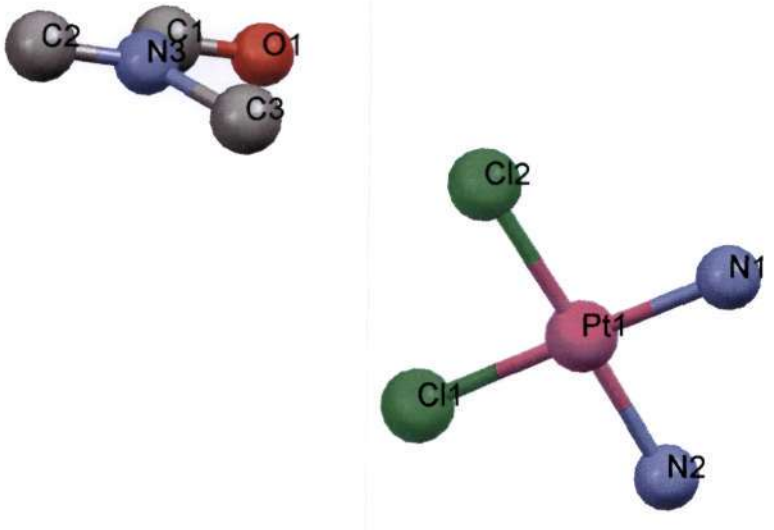

Figure 8.2: The planar structure of the anti-cancer drug: cisplatin, cis-$[PtCl_2(NH_3)_2]$; CSD reference code CUKRAB.

Gold(III) complexes are especially likely candidates for possible development and testing as anticancer drugs since they are isoelectronic with platinum(II) compounds.[440] Interest has therefore been focused on gold(III) complexes, particularly those that are isostructural to the platinum(II) compounds already studied.[441] The four-coordinate gold(III) complexes also bear a resemblance to that of the square planar form of cisplatin.[434,435,440,441,442] Due to the close structural and chemical correlations between these two types of compounds, it was thought that similar biological properties and favourable cytotoxic and anti-tumour properties might result.[443] The distinction, however, might be slight differences in the actual mechanism of action that could then possibly overcome platinum resistance and/or extend the range of anti-tumour activity.[441] The key difference between the mode of action of Au(III) and Pt(II) is the rate of ligand substitution reactions, with the gold(III) compounds generally being much faster.[440]

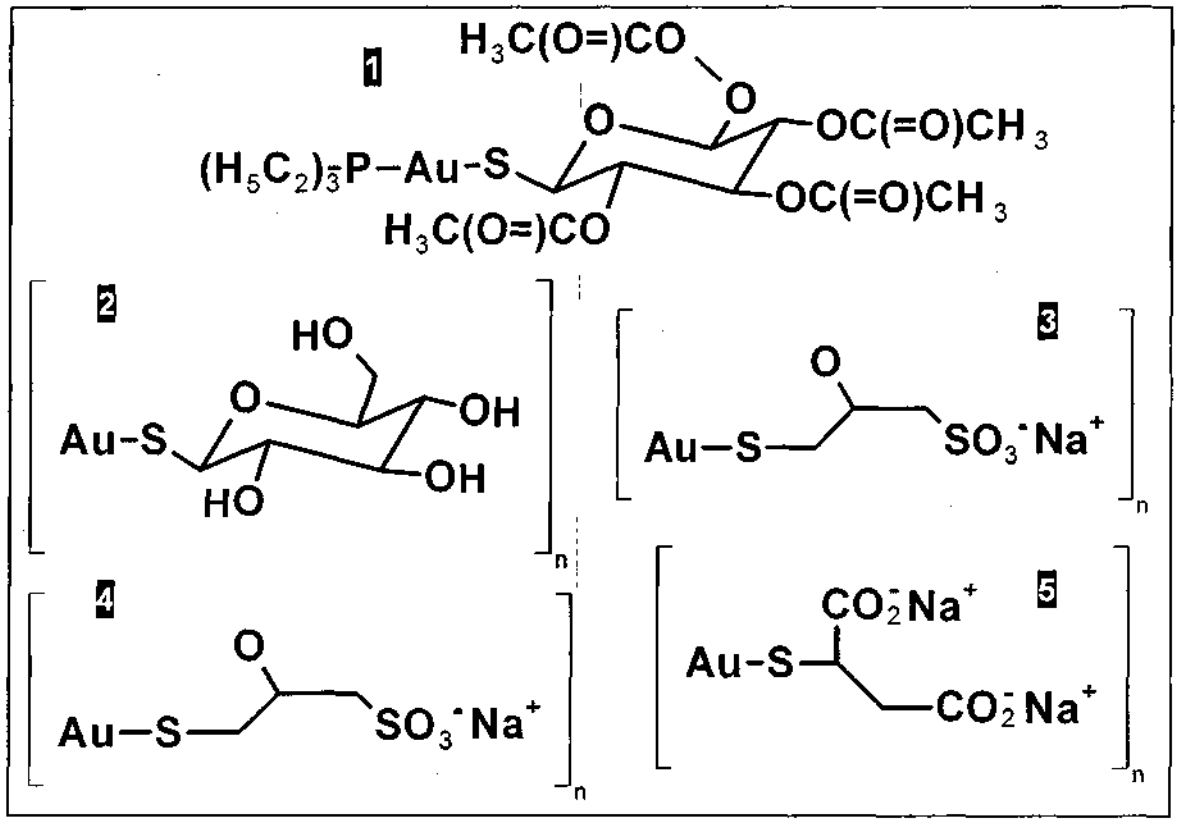

Figure 8.3: Chemical structures of examples of gold(I) thiolates that have been used in the treatment of rheumatoid arthritis: 1 = triethylphosphinegold(I) tetraacetatothioglucose (auranofin); 2 = aurothioglucose (solganol); 3 = aurothiosulphate (sanocrysin); 4 = aurothimpropanol sulphonate (allocrysin); and 5 = aurothiomalate (myocrisin).[435]

Gold(I) thiolates that were originally used in the treatment of rheumatoid arthritis were shown to have some activity against various tumours; however, their analogues appear to be more promising. This class of gold compounds, used in the treatment of rheumatoid arthritis, was the first to be screened for cytotoxicity. Most gold(I) compounds feature gold in a coordination geometry defined by 'soft' (easily polarisable) atoms, e.g. sulphur and/or phosphorus; some examples of these used in the treatment of rheumatoid arthritis are represented in Figure 8.3. Usually gold(III) compounds include 'hard' atom donors, e.g. nitrogen, oxygen and carbon, some examples of which are represented in Figure 8.4.[435]

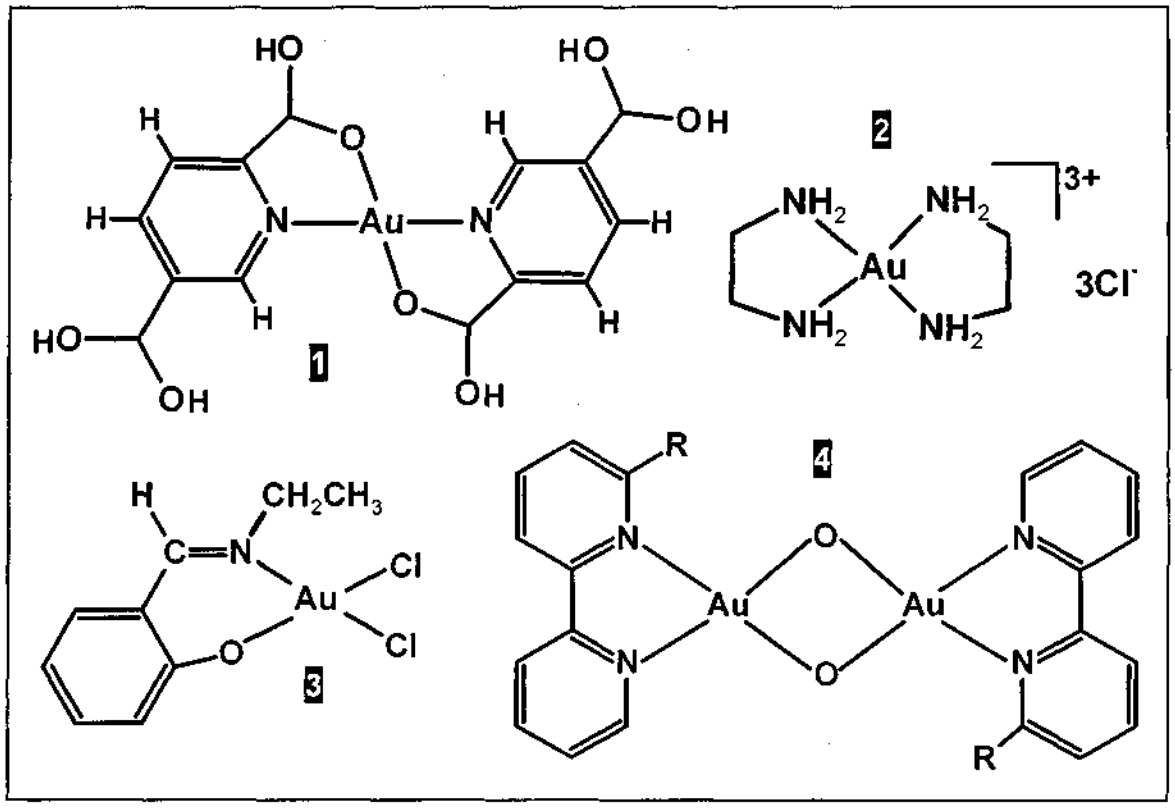

Figure 8.4: Chemical structures of some examples of gold(III) complexes: 1 = $[Au(2,5\text{-}pydca)_2]^+$;[444] 2 = $[Au(en)_2]Cl_3$;[440] 3 = $[AuCl_2(esal)]$;[441] and 4 = *trans*-$[Au_2(HL)_2(\mu\text{-}O)_2]^{2+}$.[445]

Only a few gold compounds exhibit good stability under physiological conditions due to the Au(III) to Au(I) reduction.[446] The mammalian environment is generally reducing and thus it is likely that gold(III) may be reduced *in vivo* to gold(I) and metallic gold, but with a suitable choice of ligand donors, gold(III) can be stabilized. Therefore there has been great interest in the anti-tumour/cytotoxicity activity of gold(III) compounds.

The screening for cytotoxicity/anti-tumour activity of these gold(III) compounds started in the mid-1970s.[435] However, studies have been somewhat mired, owing to relatively high kinetic lability and typically high redox potentials.[440]

The general belief is that the biological activity of anticancer metal complexes is firmly connected to their capability to bind DNA, thereby causing structural damage and thus harming its function.[447] This impairment of DNA functionality causes inhibition of replication and transcription processes. If the DNA lesions are not suitably and hastily repaired, then this will ultimately result in cell death. It is probable that platinum compounds operate via such a mechanism and therefore likely that gold(III) complexes closely related to these platinum(II) complexes will also do so.[440]

Further research has established that gold(III) compounds with square-planar geometries (as for cisplatin) may target DNA and provide new anti-tumour agents. More recently, some gold compounds have even been investigated for possible anti-HIV activity.[435] A number of synthesized gold(III) complexes have been evaluated against an in vitro panel of human tumour cell lines encompassing cells with different responses to cisplatin and of different tissue types.[448] Differential toxicity across the cell line panel is used as an indicator of potential anti-tumour activity, rather than non-selective toxicity. Biochemical studies indicate that there is a different mechanism of action between that of cisplatin and the gold complexes, which suggests that these are part of a potentially important novel group of metal-containing anti-tumour agents.[434]

Tiekink showed that although the gold(III) compound containing the ligand derived from glycylhistidine, HNR, was not as active as cisplatin, it was considerably more active than the cobalt(II), zinc(II), palladium(II) and platinum(II) derivatives.[435] A zinc porphyrin [Zn^{II}(TPP)] was found to be at least 100-fold less potent in killing cancer cells than several gold(III) porphyrins and the porphyrin ligand was also found to be essential for the anticancer activities. Che *et al.* reasoned that the porphyrin ligand should stabilize the Au(III) centre and carry the metal to its cellular target.[198]

One finding that significantly supports the prospect of gold(III) porphyrins as a promising lead for anticancer drug development was in 2003, when Che *et al.* synthesized a series of gold(III) tetraarylporphyrins, which were found to be stable in the presence of glutathione.[198] These workers showed that this group of para-substituted gold(III) *meso*-tetraarylporphyrins, stable against demetallation under physiological conditions, display 100-fold more powerful cytotoxicity against a panel of human cancer cell lines than the better known cisplatin. This includes the drug-resistant variants; multidrug- (KB-V1) and cisplatin-resistant cancer cells (CNE-1).[198] Many gold(III) complexes show significant cytotoxicities (determined by means of the MTT assay) against some recognized human cancer cell lines (including some drug resistant variants). Some lack of cross resistance was observed which suggested that the gold(III) porphyrins and cisplatin induce cytotoxicity *via* different mechanisms.[198]

One paper tried to define structure-function relationships for gold(III) compounds. In this context, it reported on the chemistry, the cytotoxicity and the DNA binding properties of three representative square planar gold(III) complexes with polyamine ligands.[448] This investigation of the cytotoxic properties of polyamine-gold(III) complexes demonstrated a different degree of biological activity for the various studied complexes, firmly dependent on their chemical structure. Two in particular, $[Au(en)_2]Cl_3$ and $[AuCl(dien)]Cl_2$, exhibit rather encouraging cytotoxic properties, because they are capable of overcoming resistance to cisplatin, to a certain degree. Comparison with previous studies of gold(III) complexes, indicated that both complexes were reasonably stable within a physiological environment, thus making them good candidates for further biological evaluation. The similar activity profiles of the other compounds suggest that the presence of a labile gold-chloride bond is not an essential feature for cytotoxicity. Rather excessive stabilization of the gold(III) centre by a polydentate ligand results in reduction (or possibly loss) of the biological activity.[440]

Gold compounds have also been of interest due to their general applicability for metal-based compounds. It is possible that when bioactive molecules coordinate metal centres, the resulting compound may have greater activity/therapeutic effects than the

original. This could be due to protection from the normal metabolic pathways and slow release mechanisms.[435] There are no particular or central uses for gold compounds to date and no special advances have been made since about 1985 (auranofin, Figure 8.3). The most interesting findings have been those from studies on their mechanism of action and their relationship to the biological chemistry of the gold drugs. There have also been discoveries regarding the effect of gold drugs on gene expression. The future of gold in medicinal chemistry will, hopefully, be more in the therapeutic areas—other than rheumatoid arthritis—with new research into the anticancer and antimicrobial activity of gold compounds.[434]

8.4 Objectives

Since Au(III) complexes of *meso*-tetraalkylporphyrins are very active against key cancer cell lines, our long-term objective is to evaluate the relative efficacy of Au(III) *meso*-tetraalkylporphyrins as anticancer drug candidates. We are also interested in synthesizing novel *meso*-tetraarylporphyrins with appended cell-targeting groups for chelation of Au(III) and evaluation as novel Au(III) anticancer compounds.

The present chapter describes our preliminary work on the synthesis and characterization of *meso*-tetraalkylporphyrin derivatives of Au(III). Experimental details have been given in Chapter 2.6 (Synthesis of Gold(III) Porphyrin Complexes).

The proposed research in this section therefore has the following aims:

(1) to synthesize and characterize novel gold(III) coordination compounds with planar aromatic ligands based on porphyrin derivatives,
(2) to characterize these new compounds using UV-vis, IR and NMR spectroscopy,
(3) to obtain X-ray quality crystals in order to determine the crystal structures of the new complexes.

8.5 Results and Discussion

8.5.1 General

The synthetic procedures that are required to metallate porphyrins with $K[AuCl_4]$, $NaAuCl_4.xH_2O$ or other Au(III) salts are already established in the literature. The Cambridge Structural Database (CSD) has three structurally characterized Au(III) porphyrins. These porphyrins, with their CSD reference codes, are: [Au(TPP)][$AuCl_4$] (FUJFEV),[449] [Au(TPP)](ClO_4) (ILIWIJ),[198] and [Au(TPP)][$Pt(S_2C_4N_2)_2$] (GAFTAI).[450] This indicates that other workers have already obtained X-ray quality crystals and hence that these Au(III) porphyrins are stable crystalline compounds that may be characterized by using X-ray diffraction.

The structure of [Au(TPP)](ClO_4) (ILIWIJ)[198] is shown in Figure 8.5. The Au(III) ion is clearly square planar in geometry and the porphyrin conformation is saddled due to crystal packing effects on the four aryl substituents. Each of the structures found in the Cambridge Structural Database is with the *meso*-tetraarylporphyrin, H_2TPP. Metallation of *meso*-tetraalkylporphyrins with Au(III) affords a novel series of derivatives, and this is a key goal of our work.

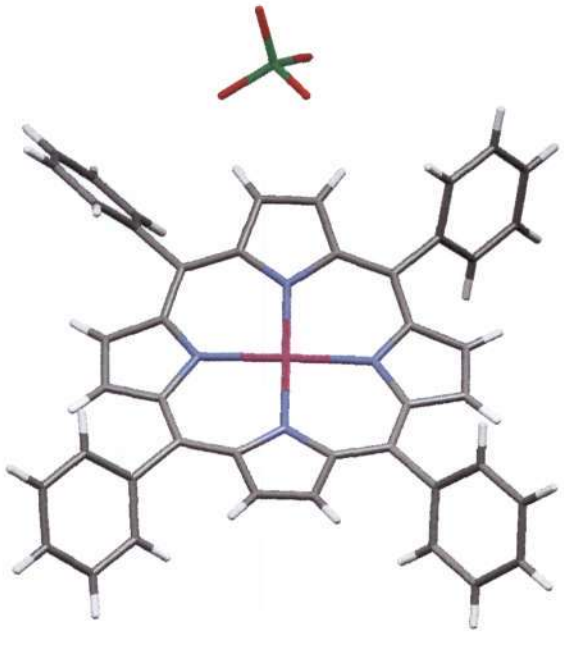

Figure 8.5: The saddled conformation of the X-ray structure of [Au(TPP)](ClO_4); CSD reference code ILIWIJ.

We expect most, if not all, of the Au(III) porphyrins to be cytotoxic in light of the fact that at least two worldwide patents exist for the use of some Au(III) porphyrins in cancer and HIV therapy,[451] and due to work done by Che *et al.*[198] These workers showed that the porphyrin ligand was necessary for this high cytotoxicity to be achieved and that the mode of action is likely to be DNA intercalation since [Au(TPP)]Cl had a high binding constant with calf thymus DNA. There have also been other reports that DNA intercalation occurs for water-soluble Au(III) porphyrins.[452] Therefore, we want to establish whether gold(III) tetraalkylporphyrins are more, or less active than the present benchmark systems ([Au(TPP)]Cl and cisplatin) and what particular alkyl groups favour enhanced cytotoxicity in vitro. Any metallated porphyrin found to have an activity higher than that of cisplatin would be studied further to establish its potential as a lead compound.

The original methods found for the metallation of gold(III) with various porphyrins[196,198] had numerous steps and were rather prolonged. They were both used in an attempt to metallate H_2T(iPent)P (P3); however, neither was successful. Therefore a simple one-step procedure involving the reflux of a gold(III) salt and the free base *meso*-tetraalkylporphyrin in DMF (monitored by TLC) was chosen. This method was successful, and therefore suitable for further use in our laboratory.

8.5.2 Metallation of *meso*-Tetraalkylporphyrins

The results for the attempted and successful metallations of the *meso*-tetraalkylporphyrin, H_2T(iPent)P, with gold(III) are presented below, as well as characterizations of [Au(T{iPent}P)]Cl:

Metallation of H_2T(iPent)P with Au(III)

The metallation of this porphyrin was performed in refluxing DMF for 2 hours, as shown in Scheme 8.1. The result was, after a silica gel column (dichloromethane containing 10% hexane as the elutant), a purple microcrystalline powder, which gave a predominant spot on TLC. The TLC also showed no sign of any unreacted free base porphyrin still present in the solution and therefore complete metallation was

assumed. If metallation is incomplete and ligand-induced reduction from Au^{III} to Au^{I} competed with metallation, then the product could be: $[Au^{III}(T\{iPent\}P)][Au^{I}Cl_2]$. This means that the chloride ion has instead been replaced by $[Cl–Au^{I}–Cl]^-$.[453]

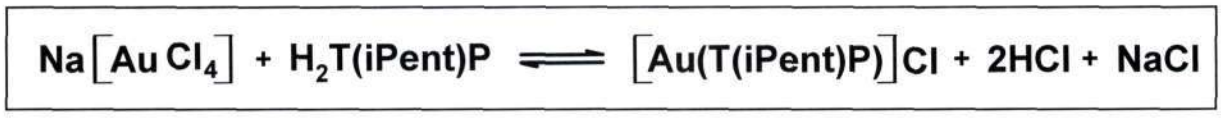

Scheme 8.1: The salt formed in the reaction of the free base $H_2T(iPent)P$ with gold(III).

The ^1H NMR spectrum of $H_2T(iPent)P$ suggests that there is not identical symmetry for each of the four *meso*-substituents. However, metallation is expected to raise the symmetry in the porphyrin due to the central metal giving four identical quarters of the molecule with no more division of the porphyrin according to the nitrogen atoms; with two bonded to a hydrogen atom and the other two not. Therefore with the metal at the centre, one expects four-fold symmetry and thus a simplified ^1H NMR spectrum. This is, however, not the case for [Au(T{iPent}P)]Cl. In fact the ^1H NMR spectrum is more complicated than that for the free base porphyrin.

The ^1H NMR spectrum obtained for the [Au(T{iPent}P)]Cl sample had numerous small peaks throughout the spectrum. Figure 8.6 shows a comparison between the ^1H NMR spectrum for the free base *meso*-tetraalkylporphyrin (—) and for the gold(III) metallated porphyrin (—). An explanation for the multiple peaks in the metallated spectrum is that due to possible dimerization favoured by $Au^{III}\cdots Au^{III}$ interactions and $\pi\cdots\pi$ interactions, there are dimers and possibly higher oligomers in solution. These interactions are schematically represented in Scheme 8.2. It is expected that the ^1H NMR spectrum of the metallated porphyrin would be simpler than that of the free base porphyrin due to the increased symmetry, which should exist in the metallated form. Due to the fact that the sample has been purified and therefore does not contain impurities, it is assumed that either more than one species must exist in this particular sample, or that these types of interactions are present.

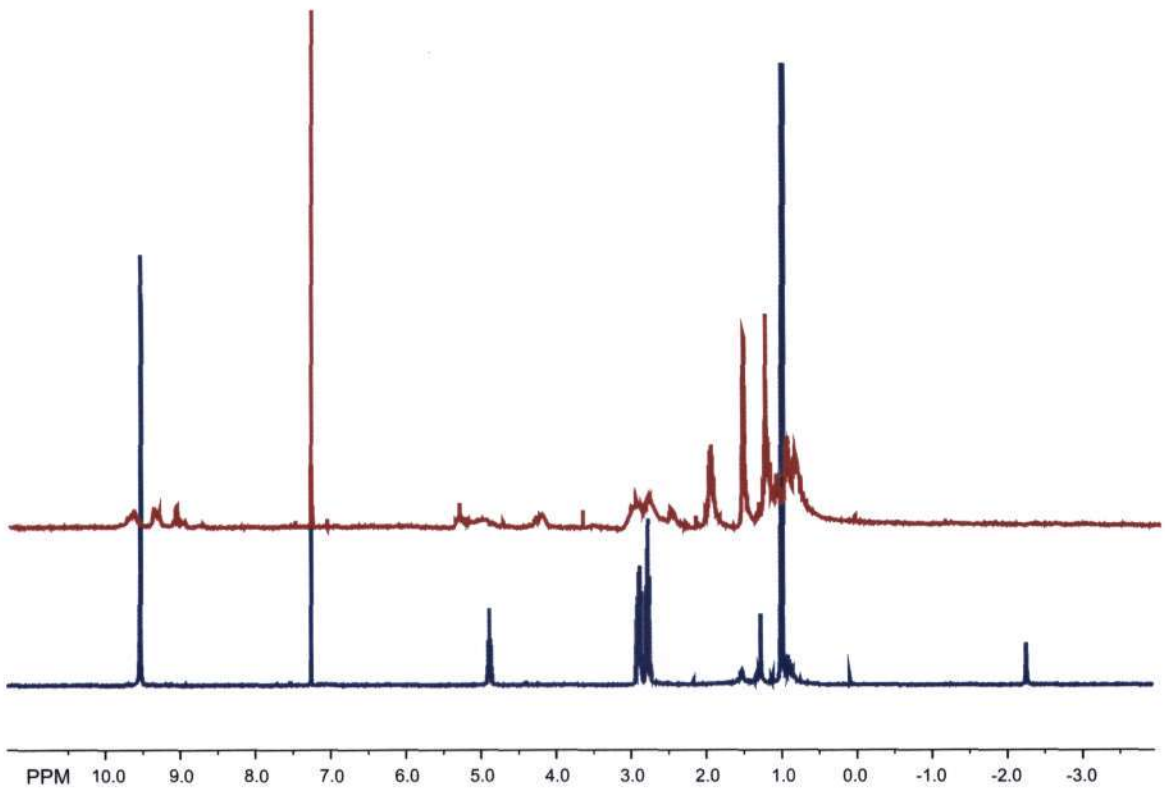

Figure 8.6: ^{1}H NMR spectra for the free base porphyrin, $H_2T(iPent)P$ (below —), and the metallated porphyrin [Au(T{iPent}P)]Cl (above —).

The two spectra in Figure 8.6 are aligned according to the prominent solvent peak of $CDCl_3$ and the small peak around 0 ppm (which has previously been attributed to a hydrocarbon contaminant, Chapter 4 (NMR spectroscopy)). Clearly there are differences between the two spectra. The most prominent of these differences is the absence of any definitive N-H proton resonances in the region around –2 ppm for the metallated porphyrin, as opposed to the clearly visible peak seen at –2.247 ppm for the free base. This suggests that the free base porphyrin ($H_2T(iPent)P$) was successfully metallated with the gold(III).

Similar impurities are evident in the 1 to 2 ppm region in both spectra (this has also been previously discussed, Chapter 4 (NMR spectroscopy)). However, as opposed to the spectrum for the free base, where an obvious signal for the CH_3 group of the *meso*-substituents was present in this region, none exists for the metallated porphyrin. The same is true for the CH group and CH_2 groups (of the *meso*-substituents) in their respective regions. There is also no definitive singlet peak for the pyrrole C-H protons in the region of ~ 9 ppm (as would have been expected), but rather three multiplets.

The integration across these three multiplets seems to correlate to the eight pyrrole protons; however, with three signals present, it can only be assumed that the pyrrole protons exist in different chemical environments.

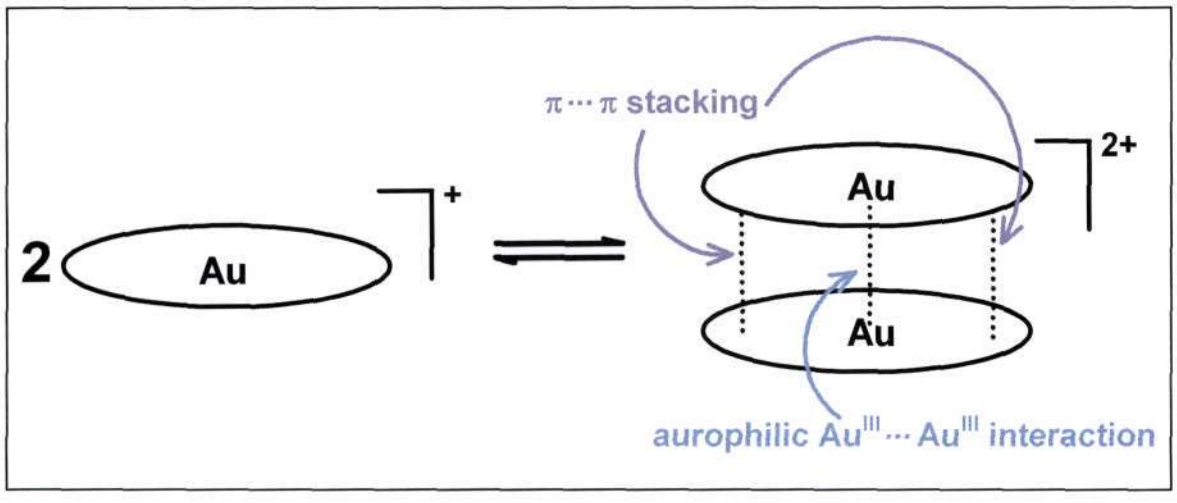

Scheme 8.2: The formation of gold(III) dimers.

In an attempt to determine if dimerization or some type of aurophilic interaction exists, the ^{1}H NMR spectrum was obtained for the sample with the solvent DMSO-d6. This was done since this particular solvent often disrupts oligermization whereas $CDCl_3$ tends to promote it. A simpler, cleaner spectrum in DMSO-d6 would confirm that aggregation in $CDCl_3$ leads to multiple signals in the NMR spectrum. However, it is obvious that there are similarities between the two spectra and that there has been no distinct decrease in the number of peaks present (Figure 8.7). The concentration used for the sample in DMSO-d6 was very dilute, and hence the solvent peaks (DMSO-d6: ~ 2.49 ppm and water: ~ 3.4 ppm) are of very high intensity. Clearly, since DMSO-d6 cannot coordinate to Au^{III} in this system, it is incapable of disrupting dimers or oligomers that are stabilized by aurophilic interactions. In a future experiment, we plan to use benzene-d6 (which will compete with porphyrin···porphyrin π-stacking) in an effort to monomerize the porphyrin for NMR characterization.

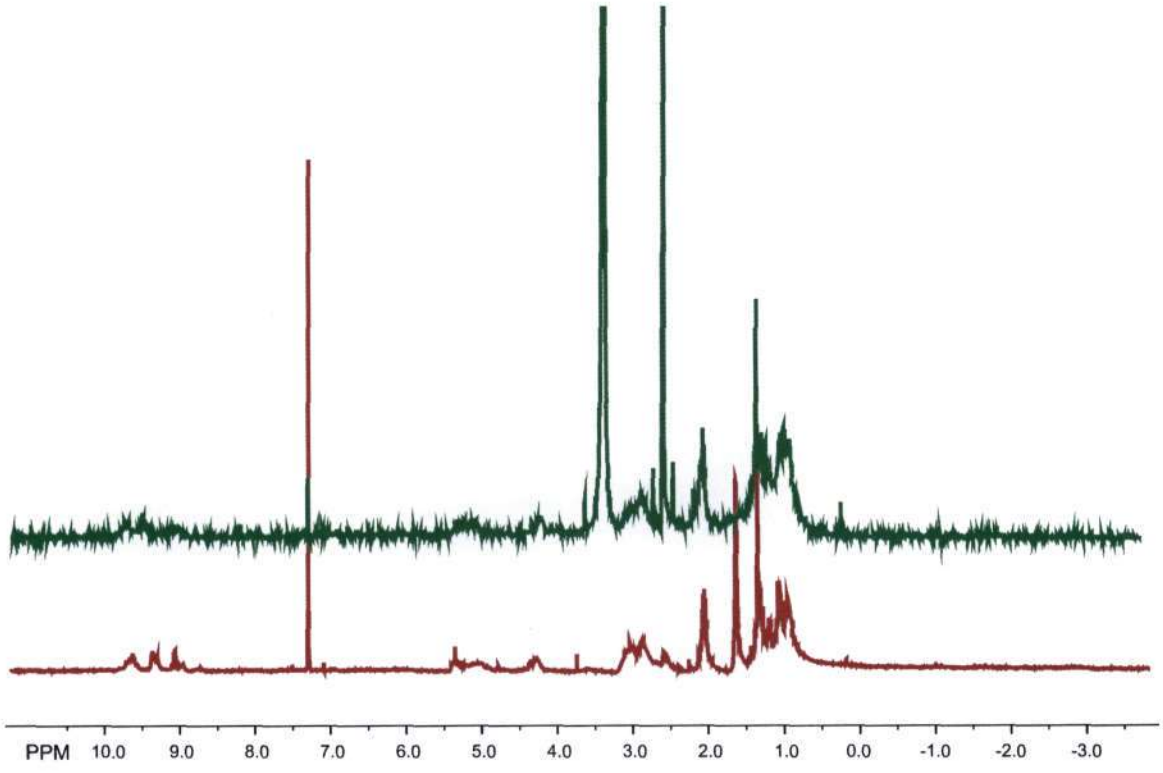

Figure 8.7: ^{1}H NMR spectra for the metallated porphyrin, [Au(T{iPent}P)]Cl, in dueterated chloroform (below —) and in DMSO-d6 (above —).

The ^{1}H NMR data given for [Au(TPP)](ClO_4) by Che *et al.* gave only the expected peaks for the pyrrole and aryl group protons.[198] There was no particular mention of any aurophilic interaction; however, several types of porphyrin aggregation are common. Different oligomers may easily form, particularly in concentrated solutions with non-coordinating solvents. Some of the most common examples are represented in Figure 8.8. The tendency of porphyrins and chlorins to aggregate is not a new concept and has previously been of considerable research interest. Porphyrins and metalloporphyrins often show dimerization and aggregation through attracting interactions between their highly polarizable π-clouds. Solution studies have shown the dependence of the aggregate structures on the nature of the metal ion, substituents and axial ligands.[454] Broad, multiple peaks have been seen for ^{1}H NMR spectra of aggregating porphyrins as are presented in this work.[455]

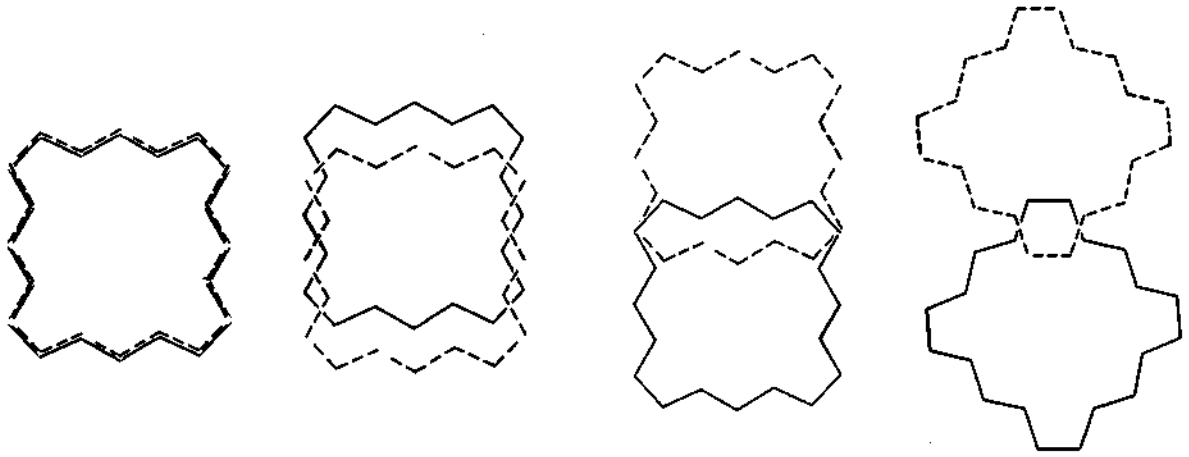

Figure 8.8: The assorted types of π overlap found in porphyrin aggregates (from left to right): four-on-four; slightly "slipped" four-on-four; two-on-two and one-on-one pyrrole overlap.[455]

In the present spectra for [Au(T{iPent}p)]Cl, numerous, broad peaks strongly suggest aggregation. This will be confirmed using a Beers Law experiment in future work to test for aggregation of the metalloporphyrin. A deviation from the straight line plot would be expected to prove aggregation of the system. If there is simple dimer formation then one can measure the dimerization constant from this data. A further test would be to induce aggregation in a UV-vis cell using $[NBu_4][ClO_4]$; increasing the ionic strength of the medium is known to promote $\pi-\pi$ dimer formation in ferric porphyrins and leads to marked changes in the electronic spectrum of the system.[456]

The UV-vis and IR spectra (Figures 8.9 and 8.10, respectively) were both obtained for the gold(III) complex. Interestingly, the UV-vis spectrum for [Au(T{iPent}P)]Cl (Figure 8.9) still shows four Q bands when essentially there should only be two present due to nominal four-fold symmetry. However, due to the outcome of the ^{1}H NMR spectrum showing the possibility of more than one species being present and the possibility that there might still be some difference in the conformations of the *meso*-substituents, it is possible that multiple bands in the visible region would result.

In the Q band region (450–700 nm) for the metallated porphyrin (Figure 8.9), and for the free base porphyrin (Figure 8.10), there are distinct differences between the spectra. The free base porphyrin has one Q band (527.5 nm) at a greater intensity than the rest, which are all at a similar, lower intensity. The metallated porphyrin, on

the other hand, seems to have the opposite, with three bands at a similar, greater intensity than one band (640 nm), which has a lower intensity. This obvious difference between the Q bands provides more evidence that metallation of $H_2T(iPent)P$ occurred. The wavelengths of these Q bands also all show shifts of about 10 nm to almost 30 nm between the free base and metallated derivatives of the porphyrin.

The UV-vis spectrum obtained for $[Au^{III}(TPP)]ClO_4$ by Che *et al.*[198] showed two bands, namely at 409 and 521 nm. The broad Soret band which has been blue-shifted by 8 nm from the free base H_2TPP corresponds well with that seen in our UV-vis spectrum for [Au(T{iPent}P)]Cl. The Soret band for [Au(T{iPent}P)]Cl in this work at 412.5 nm has been blue-shifted by 11 nm relative to the free base porphyrin. Both the broadness and the blue-shifting of the Soret band illustrate successful metallation of the porphyrin. The poor definition of the highest wavelength Q(0,0) band may possibly be due to some unreacted free base porphyrin or, more likely, aggregation. Aggregation often leads to band broadening, consistent with the changes in the UV-vis spectrum for the metallated porphyrin (compared with the free base porphyrin). One other possibility is population of multiple nonplanar conformers in solution.

As noted in Chapter 3.2, IR spectra for metallated porphyrins are expected to have fewer and relatively sharper bands than their corresponding free base porphyrins; this is generally true for the spectra presented here. The IR spectrum for the metallated porphyrin, (Figure 8.11), proved to be very similar to the free base, particularly in the fingerprint region (Figure 8.12). This was expected; however, the region 3000 to 3500 cm^{-1} region differed. The N-H stretch which occurs around 3300 cm^{-1} is clearly absent. In the IR spectrum for $H_2T(iPent)P$ there is a prominent peak at 3327 cm^{-1}; in the IR spectrum for [Au(T{iPent}P)]Cl there are two weak peaks at 3447 and 3255 cm^{-1}. The N-H stretch peak for the free base porphyrin is in the region 3300 cm^{-1}; however, neither this peak—nor any that is within 70 cm^{-1} of it—is present in the metallated porphyrin. It is therefore acceptable to assume that this N-H stretch is absent due to deprotonation of the porphyrin upon metallation. This is clear evidence that metallation of the free base porphyrin with gold(III) was successful.

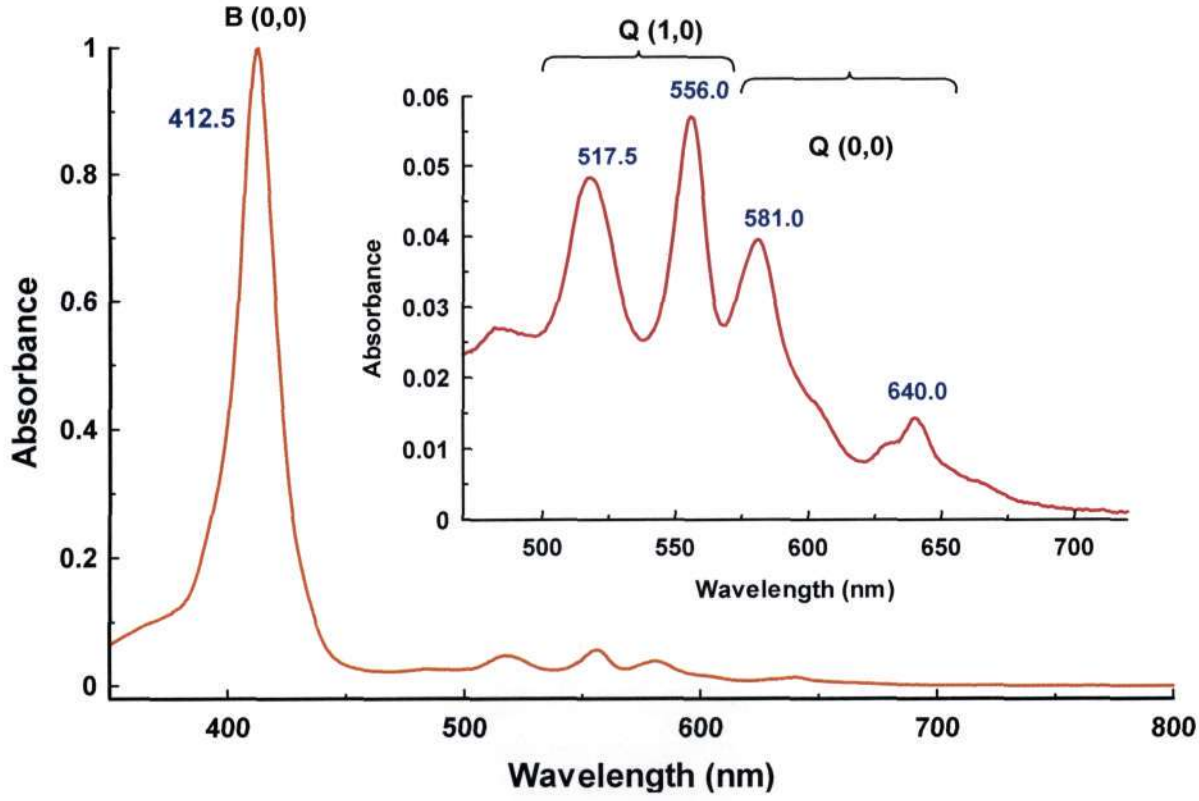

Figure 8.9: The UV-vis spectrum for [Au(T{iPent}P)]Cl in CH_2Cl_2 at 25 °C.

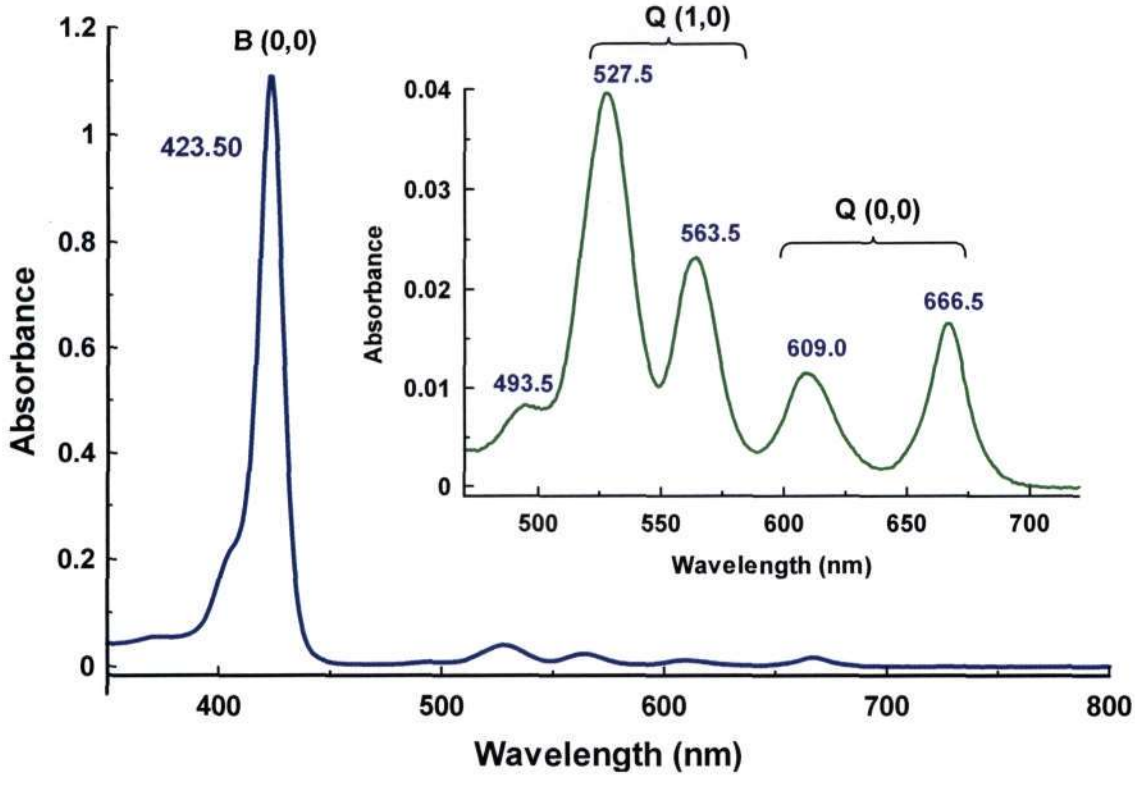

Figure 8.10: The UV-vis spectrum for $H_2T(iPent)P$ in CH_2Cl_2 at 25 °C.

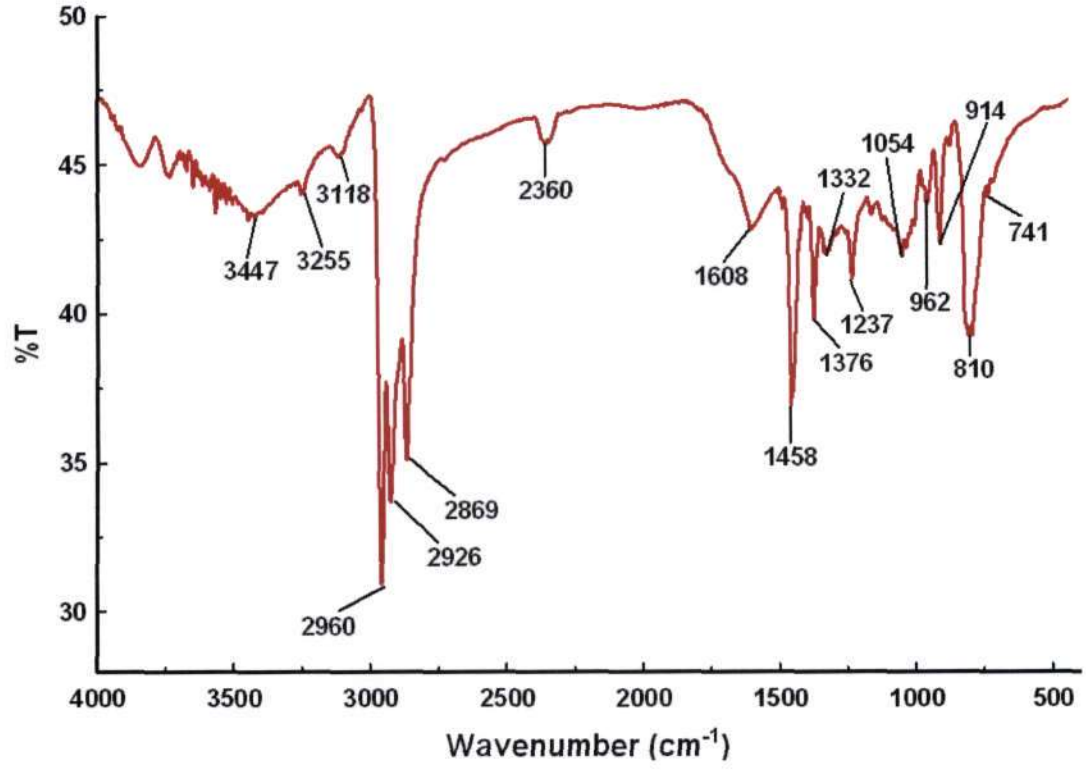

Figure 8.11: The IR spectrum for [Au(T{iPent}P)]Cl, showing the absence of the N-H stretch in the region 3300 cm^{-1}.

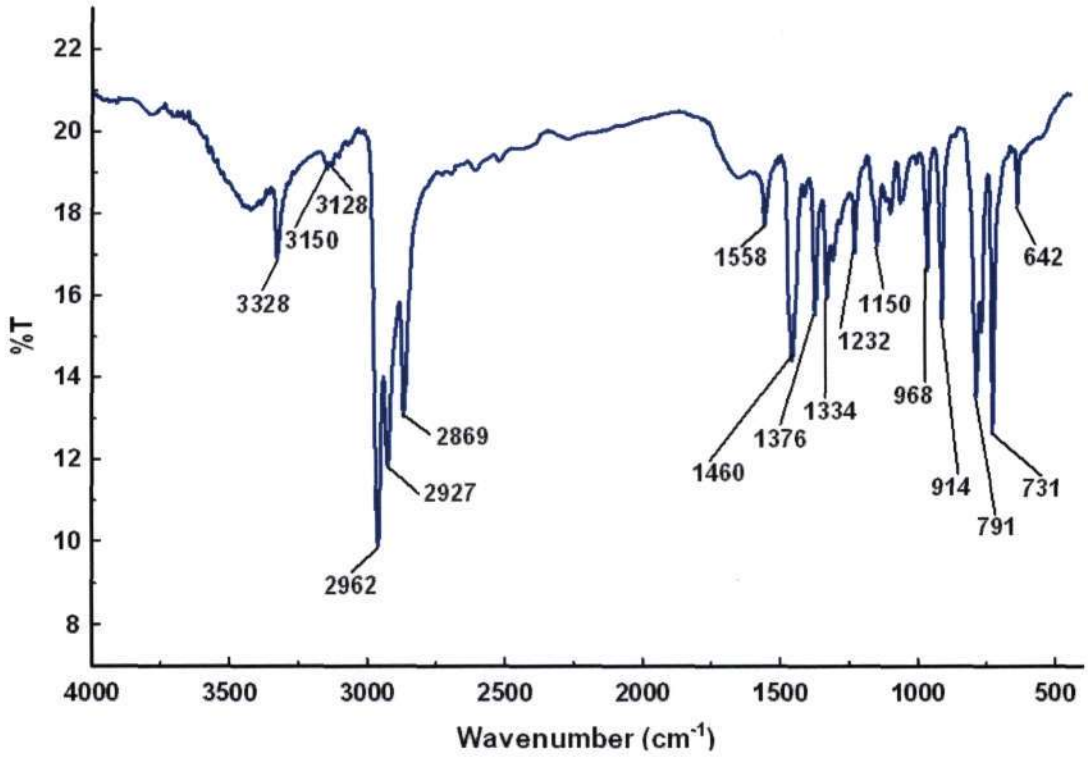

Figure 8.12: The IR spectrum for $H_2T(iPent)P$, showing the N-H stretch at 3328 cm^{-1}.

The purple powder of [Au(T{iPent}P)]Cl obtained from the metallation procedure did not give X-ray quality crystals when the solvent was allowed to slowly evaporate from the solution in a beaker or when test tubes were set up using a solution in dichloromethane with an inwardly diffusing layer of hexane. From other work with gold(III) metallations of porphyrins[453] it was noted that the crystals of a Schiff base with gold(III) needed a large counter ion in order to relieve stress caused in the structure. Since the chloride salt of $[Au(T\{iPent\}P)]^+$ failed to afford X-ray quality crystals, a plan to switch to a larger counter-anion (SbF_6^-, PF_6^- or BPh_4^-, etc.) in an effort to obtain a crystalline salt for X-ray diffraction studies will be explored.

A metathesis reaction was subsequently performed to replace the chloride ion with SbF_6^- (shown in Scheme 8.3). According to the suspected formation of silver chloride the method was successful. However, all attempts to obtain crystals (both by diffusion and slow evaporation) failed. Different solvents and concentrations were used, but still no crystals were formed. It seems that even the larger counter ion could not cause the sample to crystallize (although many attempts were made). Therefore we are in the process of ordering tetrabutylammonium tetraphenylborate (an extremely large counter ion) which will, hopefully, overcome aggregation and allow crystals of this novel gold(III) to be formed!

$$[Au(T\{iPent\}P)]Cl + AgSbF_6 \rightarrow [Au(T\{iPent\}P)]SbF_6 + AgCl(s)$$

Scheme 8.3: The metathesis reaction the chloride counter ion.

8.6 Future Work

The principal objective of this work is to metallate several *meso*-tetraalkylporphyrins with Au(III) to produce novel complexes. Therefore it will be necessary to employ a dependable method for the preparation of gold(III) metallated *meso*-tetraalkylporphyrins. The method used for [Au(T{iPent}P)]Cl is promising and may need relatively small optimizations before it is uniformly applicable to this class of porphyrins.

meso-Tetraalkylporphyrins other than those presented in this work will also be synthesized in order to extend the series of *meso*-tetraalkylporphyrins that has already been prepared. The derivatives with the four *meso*-substituents shown in Figure 8.13 will be the new target compounds for our future work. Thus, ten in total, new Au(III) porphyrins will be available for cytotoxicity testing. These new porphyrins include systems with biologically useful side-chains such as alcohols, ethers, and more exotic groups (e.g., uracil analogues).

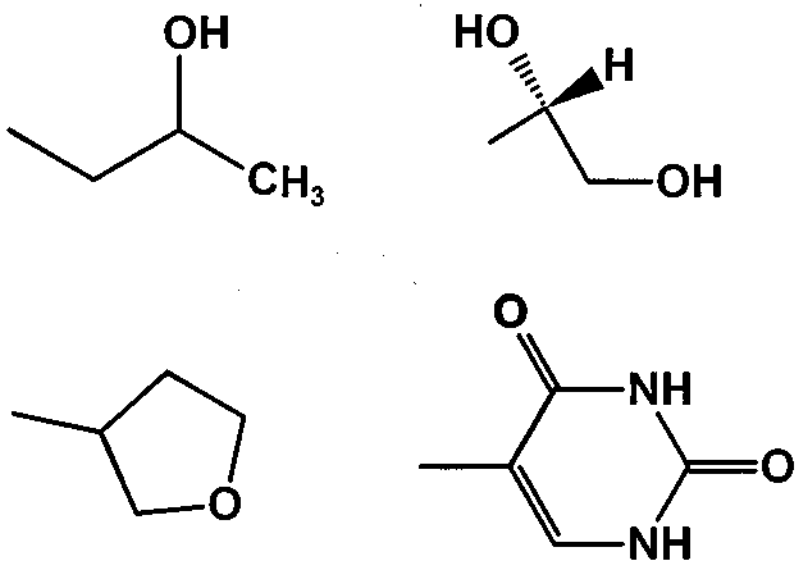

Figure 8.13: The derivatives with the above four *meso*-substituents will be the four new target compounds for future synthesis.

After characterization of the novel free base porphyrins that will be made from these synthons, metallation will be performed using the best yielding method in order to produce the target square planar Au(III) drug candidates. The final metallated structures will be fully characterized using UV-vis and IR spectra, as well as ^{1}H and ^{13}C NMR. Attempts will be made to obtain X-ray crystal structures of each of the synthesized porphyrins. DFT computational studies will be performed for each of these porphyrins and any ruffling that occurs will be observed and investigated using these DFT calculations and X-ray structures.

8.7 Long term Objectives

The proposed research in this section and the future work has the following aims:

(1) to synthesize and characterize a range of novel gold(III) coordination compounds with planar aromatic ligands based on porphyrin derivatives;

(2) to use DFT methods to compute the structures and electronic properties of all gold(III) porphyrins synthesized in this work;

(3) to run an NMR sample of [Au(T{iPent}P)]Cl in benzene-d6 in order to try prevent any aurophilic aggregation from occurring;

(4) to perform Beers Law experiments for the metalloporphyrins in order to check for aggregation in each system;

(5) to study $\pi \cdots \pi$ dimers formed at high ionic strength;

(6) to use larger counter ions in an attempt to allow X-ray quality crystals to form;

(7) to evaluate the compounds for cytotoxicity against a range of cancer cell lines; and

(8) to develop hit compounds into lead compounds through appropriate chemical modifications.

The overarching goal is therefore to use existing and new ligand systems in our laboratory for the coordination of Au(III) in an effort to find new drugs primarily for the treatment of cancer and possibly HIV.

9. Summary and Conclusions

The main aim of this work was to synthesize and fully characterize (structurally and spectroscopically) a range of *meso*-tetraalkylporphyrins (some novel and some known). A great deal of literature is available for *meso*-tetraarylporphyrins, which have many applications and uses. Therefore our long term proposition is to determine whether *meso*-tetraalkylporphyrins may be as practical, or possibly even better, for medicinal and other applications.

In this project, six *meso*-tetraalkylporphyrins were synthesized from a range of aldehydes using a locally improved literature method. UV-vis spectra, including the band maxima and extinction coefficients, were obtained for the resulting porphyrins. This data compared favourably with relevant literature and provided the experimental excitation wavelengths for subsequent photoluminescence work. The IR spectra obtained showed that the ground state conformations (ruffled or planar) of the porphyrin macrocycle had a measurable effect on the energy of the low-frequency modes in the IR spectra. The steric bulk of the alkyl-substituents also tended to modulate some of the vibrational modes. The most prominent bands, common to each porphyrin spectrum, were assigned by means of DFT computations (B3LYP functional, 6-31G** basis set). The agreement between the experimental and theoretical vibrational frequencies was generally between 0.5–5%.

These DFT simulations were utilized to determine the structural conformation of each porphyrin. They were also used to predict NMR shielding tensors for the ^{1}H and ^{13}C spectra. A favourable comparison was observed between the experimental and theoretical data. For all the ^{1}H NMR shifts, except for the N-H resonance (for which there was a larger, but consistent, difference for each porphyrin), there were small discrepancies of 0.5 ppm or less. Although larger than the ^{1}H NMR shift difference, the ^{13}C chemical shifts had acceptable differences (less than 6 ppm) between experimentally obtained and calculated values. Clearly, shielding tensors are more accurately calculated for the lighter nuclei in these compounds. This observation is consistent with similar data in the literature for the GIAO (Gauge-Independent Atomic

Orbital) method. The difference between the observed and calculated chemical shifts at the B3LYP/6-31G** level of theory is therefore small and of a consistent magnitude.

X-ray quality crystals could not be obtained for $H_2T(CHPh_2)P$; however, an X-ray structure with an *R*-factor of 6.98% was obtained for $H_2T(CH_2Ph)P$. The X-ray structures for the other porphyrins had *R*-factors above the publishable limit, often due to substantial disorder; these structures in general could not be fully refined. However, it was possible to determine key conformational data which could then be compared to the DFT simulated geometries. The porphyrin structures obtained using X-ray diffraction were generally planar, except for $H_2T(cyHx)P$, which exhibited a strongly ruffled conformation with significant atomic displacements from the plane of the macrocycle. However, the DFT-computed structures mostly exhibited ruffled conformations, with only one predominantly planar structure ($H_2T(CH_2Ph)P$) and one saddled conformation ($H_2T(CHPh_2)P$). The DFT simulations determine the conformation for the gas phase and therefore it can be assumed that packing interactions and inversion symmetry preclude ruffling of the porphyrin macrocycle in the solid state.

Preliminary studies on the emission spectra and lifetimes of *meso*-tetraalkylporphyrins at room temperature and at 77 K are reported in this work. The emission spectra at room temperature show two definite, smooth emission bands (B and Q bands) at ~ 665 nm and ~ 735 nm, respectively. At 77 K, multiple bands are seen due to the system being trapped in a frozen glass where rotational levels cannot blur the vibrational levels of the ground state. The division of the B band is generally less prominent than the separation of the Q bands. The origin of the B band can be assigned to the second singlet $\pi \rightarrow \pi^*$ excited state and the four Q bands are associated with the first singlet $\pi \rightarrow \pi^*$ excited state, consistent with the four-orbital model developed by Gouterman. The emission spectra generally compare favourably with data for *meso*-tetraarylporphyrins the literature; however, the lifetimes obtained for this series of porphyrins differ considerably from those found for H_2TPP. There is also a difference in the lifetimes between the two excited states, B and Q; however, both occur within the range of 0.1 to 1 μs. When comparing the lifetimes measured at room temperature and at 77 K for both wavelengths, the discrepancy between

corresponding pairs of values is generally small. Generally, the B state lifetimes are longer (sometimes up to more than 50% longer) than those of the Q state.

This work has therefore succeeded in producing a series of spectroscopically and structurally elucidated *meso*-tetraalkylporphyrins. It has also included novel DFT simulations and photoluminescence work on this class of porphyrins. The similarities and differences in this series of porphyrins have been noted, discussed and, where possible, explained. Some of the results have been unusual and remarkable. The promise of potential photophysical and medicinal applications therefore provides good basis for further investigation.

10. Future Work

As stated in relevant chapters, future work will involve: NMR, X-ray, fluorescence and DFT studies. The main goal of this work will, however, be the study of the gold(III) derivatives of the *meso*-tetraalkylporphyrins described in this thesis.

The NMR work will include variable temperature studies as well as DFT simulations for the elucidation (and theoretical study) of the porphyrin structures. The fluorescence work presented here for *meso*-tetraalkylporphyrins will continue including the determination of quantum yields as well as attempting to measure phosphorescence for this series of porphyrins. The spectrofluorimeter will be calibrated in order to confirm the results obtained and we will then try to correlate these results with possible structural features of the *meso*-tetraalkylporphyrins. Peak-fitting methods will be used to quantify the vibrational level spacings for the porphyrin ground states.

Attempts to obtain X-ray quality crystals will also continue for the porphyrins in order to obtain X-ray structures for the remaining five porphyrins for which this has not yet been possible.

Furthermore, future work will involve the metallation and characterization of these *meso*-tetraalkylporphyrins and others (from the extended series). Emission spectra and lifetime data will also be collected for the Au(III) metalled porphyrins (if their excited states are emissive) and DFT simulations will be used to predict their final geometries, vibrational data and chemical shifts. Finally, the resulting metalloporphyrins will be evaluated for their cytotoxicity against a range of cancer cell lines and hit compounds will be developed into lead compounds through appropriate chemical modifications.

References

[1] Milgrom, L. R. In *The Colours of life: An Introduction to the Chemistry of Porphyrins and related Compounds*; Oxford Uni. Press: Oxford, **1997;** pp 13–19.

[2] *Reader's Digest Universal Dictionary*, The Reader's Digest Association Limited: London, **1988;** pp 1202.

[3] Clayden, J.; Greeves, N.; Warren, S.; Wothers, P. *Organic Chemistry*; Oxford Uni. Press: Oxford, **2001;** pp. 1148–9, 1157, 1164.

[4] Smith, K. M. In *Porphyrins and Metalloporphyrins*; Smith K. M., Ed.; Elsevier: Amsterdam, **1975;** Chapter 1.

[5] Küster, W. *Physiol. Chem.* **1912**, *82*, 463.

[6] Fisher, H.; Zeile, K. *Ann. Chem.* **1929**, *98*, 468.

[7] Kuster, W.; Koppenhofer, G. *Berichte der Deutschen Chemischen Gesellschaft B* **1927**, *60B*, 1778–1781.

[8] Warshel, A. *Proc. Natl. Acad. Sci. U.S.A.* **1977**, *74*, 1789–1793.

[9] Olafson, B. D.; Goddard III, W. A. *Proc. Natl. Acad. Sci. U.S.A.* **1977**, *74*, 1315–1319.

[10] Song, Y.; Haddad, R. E.; Jia, S.; Hok, S.; Olmstead, M. M.; Nurco, D. J.; Schore, N. E.; Zhang, J.; Ma, J.; Smith, K. M.; Gazeau, S.; Pécaut, J.; Marchon, J.; Medforth, C. J.; Shelnutt, J. A. *J. Am. Chem. Soc.* **2005**, *127*, 1179–1192.

[11] Moustakali, I.; Tulinsky, A. *J. Am. Chem. Soc.* **1973**, *95*, 20, 6811–6815.

[12] Senge, M. O.; Renner, M. W.; Kalisch, W. W.; Fajer, J. *J. Chem. Soc. Dalton Trans.* **2000**, 381–385.

[13] Senge, M. O.; Ema, T.; Smith, K. M. *J. Chem. Soc. Chem. Commun.* **1995**, 733–734.

[14] Jentzen, W.; Simpson, M. C.; Hobbs, J. D.; Song, X.; Ema, T.; Nelson, N. Y.; Medforth, C. J.; Smith, K. M.; Veyrat, M.; Mazzanti, M.; Ramasseul, R.; Marchon, J.-C.; Takeuchi, T.; Goddard, III, W. A.; Schelnutt, J. A. *J. Am. Chem. Soc.* **1995**, *117*, 11085–11097.

[15] Song, X.-Z.; Jaquinod, L.; Jentzen, W.; Nurco, D. J.; Jia, S.-L.; Khoury, R. G.; Ma, J.-G.; Medforth, C. J.; Smith, K. M.; Schelnutt, J. A. *Inorg. Chem.* **1998**, *37*, 2009–2019.

[16] Richardson, T. H.; Dooling C. M.; Worsfold O.;Jones L. T.; Kato K.; Shinbo K.; Kaneko F.; Treggoning R.; Vysotsky M. O.; Hunter C. A. *Thin Solid Films* **2001**, *393*, 259–266.

[17] Bussetti, G.; Corradini, C.; Goletti, C.; Chiaradia, P.; Russo, M.; Paolesse, R.; Di Natale, C.; D'Amico, A.; Valli, L. *Physica Status Solidi B: Basic Solid State Physics* **2005**, *242*, 13, 2714–2719.

[18] Purrello, R.; Gurrieri, S.; Lauceri, R.; *Coordination Chem. Rev.* **1999**, *190-192*, 683–706.

[19] Bhyrappa, P.; Young, J. K.; Moore, J. S.; Suslick, K. S. *J. Am. Chem. Soc.* **1996**, *118*, 5708–5711.

[20] Elemans, J. A. A. W.; Claase, M. B.; Aarts, P. P. M.; Rowan, A. E.; Schenning, A. P. H. J.; Nolte, R. J. M. *J. Org. Chem.* **1999**, *64*, 7009–7016.

[21] Kaim, W.; Schwederski, B. In *Bioinorganic Chemistry: Inorganic Elements in the Chemistry of Life*; John Wiley & Sons: Chichester, **1994;** pp 39–43, 56–69, 88–99.

[22] Perutz, M. F.; Fermi, G.; Luisi, B.; Shaanan, B.; Liddington, R. C. *Cold Spring Harbor Symposia on Quantitative Biology* **1987**, *52*, 555–655.

[23] Article within a web site: Goldoni, A. "Elettra Highlights." AREA Science Park, 34012 Basovizza, Trieste, Italy. 2000–2001. <http://www.elettra.trieste.it/science/highlights/2001-2002/elettra_highlights_2001-2002-pg064.pdf>

[24] Scheidt, W. R.; Gouterman, M. In *Iron Porphyrins, Part 1;* Lever, A. B.; Gray, H. B., Eds.; Addison-Wesley Publishing: London, **1983;** pp 89–139.

[25] Hubbard, C. D.; Jones, J. G.; McKnight, J. *J. Chem. Soc. Dalton Trans.* **2000**, *18*, 3143–3148.

[26] Hill, C. L.; Williamson, M. M. *Inorg. Chem.* **1985**, *24*, 3024–3030.

[27] Lindsey, J. S.; Schreiman, I. C.; Hsu, H. C.; Kearney, P. C.; Marguerettaz, A. M. *J. Org. Chem.* **1987**, *52*, 827–836.

[28] Kwok, K. S. *Nanotoday.* **2003**, *Dec*, 20–27.

[29] Moresco, F.; Meyer, G.; Rieder, K.-H.; Tang, H.; Gourdon, A.; Joachim, C. *Phys. Rev. Lett.* **2001**, *86*, 672–675.

[30] Loppacher, C.; Guggisberg, M.; Pfeiffer, O.; Meyer, E.; Bammerlin, M.; Lüthi, R.; Schlitter, R.; Gimzewski, J. K.; Tang, H.; Joachim, C. *Phys. Rev. Lett.* **2003**, *90*, 1–4.

[31] Liang, X. L.; Flores, S.; Ellis, D. E.; Hoffman, B. M.; Musselman, R. L. *J. Chem. Phys.* **1991**, *95*, 403–417.

[32] Dougherty T. J. *J. Clin. Laser Med. Surg.* **1996**, *14*, 219–221.

[33] FDA Approval for Photofrin for Early NSCLC, *Oncology Times*. **1998**.

[34] Smith, K. M. In *Porphyrins and Metalloporphyrins*; Smith K. M., Ed.; Elsevier: Amsterdam, **1975;** Chapter 2.

[35] Arsenault, G. P.; Bullock, E.; MacDonald, S. F. *J. Am. Chem. Soc.* **1960**, *82*, 4384.

[36] Scheidt, W. R. In *The Porphyrin Handbook*; Kadish, K. M.; Smith, K. M.; Guilard, R., Eds.; Academic: New York, **2000;** Vol 3, Chapter 16.

[37] Web site (Professional): Washburn University, 1700 SW College Ave, Topeka, Kansas 66621. 16 April, 1996. Porphyrin Page. 11 Nov. 2002 <http://www.washburn.edu/cas/chemistry/sleung/porphyrin/porphyrin_page.html>

[38] Article within a web site: Vicente, M. G. H. "Porphyrin Functionalization." 31 Aug. 1997. KMS Group Website. <http://chemgroups.ucdavis.edu/~smith/research/porph_funct/WebPF1.html>

[39] Runge, S.; Senge, M. O. *Tetrahedron* **1999**, *55*, 10375–10390.

[40] Lindsey, J. S. In *The Porphyrin Handbook*; Kadish, K. M.; Smith, K. M.; Guilard, R., Eds.; Academic: New York, **2000;** Vol 1, Chapter 2.

[41] Geier, III, G. R.; Lindsey, J. S. *J. Chem. Soc. Perkin Trans. 2* **2001**, 677.

[42] Walker, D.; Hiebert, J. D. *Chem. Rev.* **1967**, *67*, 153.

[43] Fu, P. P.; Harvey, R. G. *Chem. Rev.* **1978**, *78*, 317.

[44] Peover, M. E. *J. Chem. Soc.* **1962**, 4540–7549.

[45] Thiele, J.; Günther, F. *Ann.* **1906**, *349*, 45.

[46] Braude, E. A.; Brook, A. G.; Linstead, R. P. *J. Chem. Soc.* **1954**, 3569.

[47] Cavaleiro, J. A. S.; Rocha Gonsalves, A. M. *J. Chem. Soc. Perkin Trans. 1* **1974**, 1771.

[48] Cavaleiro, J. A. S.; Kenner, G. W.; Smith, K. M. *J. Chem. Soc. Perkin Trans. 1* **1973**, 2478.

[49] Eisner, U.; Lichtarowicz, A.; Linstead, R. P. *J. Chem. Soc.* **1957**, 733.

[50] Bruckner, C.; Karunaratne, V.; Rettig, S. J.; Dolphin, D. *Can. J. Chem.* **1996**, *74*, 2182.

[51] McDonagh, A. F.; Palma, L. A. *Biochem. J.* **1980**, *189*, 193.

[52] Jackman, L. M. *Advan. Org. Chem.* **1960**, *2*, 329.

[53] Buckley, D.; Dunstan, S.; Henbest, H. B. *J. Chem. Soc.* **1957**, 4880.

[54] Oikawa, Y.; Yoshioka, T.; Yonemitsu, O. *Tetrahedron Lett.* **1982**, *23*, 889.

[55] Oikawa, Y.; Tanaka, T.; Horita, K.; Yoshioka, T.; Yonemitsu, O. *Tetrahedron Lett.* **1984**, *25*, 5393.

[56] Lindsey, J. S.; MacCrum, K. A.; Tyhonas, J. S.; Chuang, Y.-Y. *J. Org. Chem.* **1994**, *59*, 579.

[57] Ghosh, A. In *The Porphyrin Handbook*; Kadish, K. M.; Smith, K. M.; Guilard, R., Eds.; Academic: New York, **2000**; Vol 7, Chapter 47.

[58] Senge, M. O.; Bischoff, I.; Nelson, N. Y.; Smith, K. M. *J. Porphyrins Pthalocyanines.* **1999**, *3*, 99–116.

[59] Rothemund, P. *J. Am. Chem. Soc.* **1936**, *58*, 625.

[60] Rothemund, P. *J. Am. Chem. Soc.* **1939**, *61*, 2912–2915.

[61] Rothemund, P. *J. Am. Chem. Soc.* **1935**, *57*, 2010–2011.

[62] Fajer, J. *Chem. Ind. (Lond.)* **1991**, 869.

[63] Ravikanth, M.; Chandrashekar, T. K. *Struct. Bonding (Berlin)* **1995**, *82*, 105.

[64] Senge, M. O. *J. Photochem. Photobiol. B: Biol.* **1992**, *16*, 3.

[65] Barkigia, K. M.; Chantranupong, L.; Smith, K. M.; Fajer, J. *J. Am. Chem. Soc.* **1988**, *110*, 7566.

[66] Kratky, C., Waditschatka, R.; Angst, C.; Johansen, J.; Plaquevent, J. C.; Schreiber, J.; Eschenmoser, A. *Helv. Chim. Acta.* **1984**, *68*, 1312–1337.

[67] Waditschatka, R.;Kratky, C.; Jaun, B.; Heinzer, J.; Eschenmoser, A. *J. Chem. Soc. Chem. Commun.* **1985**, 1604–1607.

[68] Geno, M. K.; Halpern, J. *J. Am. Chem. Soc.* **1987**, *109*, 1238–1240.

[69] Furenlid, L. R.; Renner, M. W.; Smith, K. M.; Fajer, J. *J. Am. Chem. Soc.* **1990**, *112*, 1634–1635.

[70] Anderson, K. K.; Hobbs, J. D.; Luo, L.; Stanley, K. D.; Quirke, J. M. E.; Shelnutt, J. A. *J. Am. Chem. Soc.* **1993**, *115*, 12346–12352.

[71] Shelnutt, J. A.; Song, X.-Z.; Ma, J.-G.; Jia, S.-L.; Jentzen, W.; Medforth, C. *J. Chem. Soc. Rev.* **1998**, *27*, 31.

[72] Jentzen, W.; Ma, J.-G.; Shelnutt, J. A. *Biophysical Journal* **1998**, *74*, 753–763.

[73] Barkigia, K. M.; Berber, M. D.; Fajer, J.; Medforth, C. J.; Renner, M. W.; Smith, K. M. *J. Am. Chem. Soc.* **1990**, *112*, 8851.

[74] Sparks, L. D.; Medforth, C. J.; Park, M. –S.; Chamberlain, J. R.; Ondrias, M. R.; Senge, M. O.; Smith, K. M.; Shelnutt, J. A. *J. Am. Chem. Soc.* **1993**, *115*, 581.

[75] Evans, B.; Smith, K. M.; Fuhrhop, J.-H. *Tetrahedron Lett.* **1977**, *5*, 443.

[76] Barkigia, K. M.; Renner, M. W.; Furenlid, L. R.; Medforth, C. J.; Smith, K. M. Fajer, J.; *J. Am. Chem. Soc.* **1993**, *115*, 3627.

[77] Medforth, C. J.; Senge, M. O.; Smith, K. M.; Sparks, L. D.; Shelnutt, J. A. *J. Am. Chem. Soc.* **1992**, *114*, 9859.

[78] Ema, T.; Senge, M. O.; Nelson, N. Y.; Ogoshi, H.; Smith, K. M. *Angew. Chem. Int. Ed. Engl.* **1994**, *33*, 18, 1879–1881.

[79] Scheidt, W. R.; Lee, Y. J. *Struct. Bonding (Berlin)* **1987**, *64*, 1.

[80] Gentemann, S.; Medforth, C. J.; Ema, T.; Nelson, N. Y.; Smith, K. M.; Fajer, J.; Holten, D. *Chem. Phys. Lett.* **1995**, *245*, 441.

[81] Gentemann, S.; Nelson, N. Y.; Jaquinod, L.; Nurco, D. J.; Medforth, C. J.; Smith, K. M.; Fajer, J.; Holten, D. *J. Phys. Chem.* **1996**, *101*, 1247.

[82] Senge, M. O. *Z. Naturforsch.* **2000**, *55b*, 336–344.

[83] Rothemund, P.; Menotti, A, R. *J. Am. Chem. Soc.* **1941**, *63*, 267.

[84] Aronoff, S.; Calvin, M. *J. Org. Chem.* **1943**, *8*, 205.

[85] Calvin, M.; Ball, R. H.; Aronoff, S. *J. Am. Chem. Soc.* **1943**, *65*, 2259.

[86] Ball, R. H.; Dorough, G. D.; Calvin, M. *J. Am. Chem. Soc.* **1946**, *68*, 2278.

[87] Barnett, G. H.; Hudson, M. F.; Smith, K. M. *Tetrahedron Lett.* **1973**, 2887.

[88] Rousseau, K.; Dolphin, D. *Tetrahedron Lett.* **1974**, 4251.

[89] Barnett, G. H.; Hudson, M. F.; Smith, K. M. *J. Chem. Soc. Perkin Trans. 1* **1975**, 1401.

[90] Thomas, D. W.; Martell, A. E. *J. Am. Chem. Soc.* **1956**, *78*, 13335.

[91] Fukada, N. *Bull. Chem. Soc. Japan* **1961**, *34*, 884.

[92] Sharp, D. B. *U. S. Patent* 3,076,813 (**1963**).

[93] Johnson, A. W.; Kay, I. T. *J. Chem. Soc.* **1961**, 2418.

[94] Krol, S. *J. Org. Chem.* **1959**, *24*, 2065.

[95] Petit, A.; Loupy, A.; Mailard, Ph.; Momenteau, M. *Syn. Commun.* **1992**, *22*, 1137.

[96] Drain, C. M.; Gong, X. *Chem. Commun.* **1997**, 2117.

[97] Groves, J. T.; Nemo, T. E. *J. Am. Chem. Soc.* **1983**, *105*, 6243.

[98] Traylor, P. S.; Dolphin, D.; Traylor, T. G. *J. Chem. Soc. Chem Commun.* **1984**, 279.

[99] Adler, A. D.; Longo, F. R.; Shergalis, W. *J. Am. Chem. Soc.* **1964**, *86*, 3145–3149.

[100] Adler, A. D.; Longo, F. R.; Finarelli, J. D.; Goldmacher, J.; Assour, J.; Korsakoff, L. *J. Org. Chem.* **1967**, *32*, 476.

[101] Adler, A.-D.; Sklar, L.; Longo, F. R.; Finarelli, J. D.; Finarelli, M. G. *J. Heterocyclic Chem.* **1968**, *5*, 669.

[102] Kim, J. B.; Leonard, J. J.; Longo, F. R. *J. Am. Chem. Soc.* **1972**, *94*, 3986.

[103] Torrens, M. A.; Straub, D. K.; Epstein, L. M. *J. Am. Chem. Soc.* **1972**, *94*, 4160.

[104] Cavaleiro, J. A. S.; Condesso, M. F. P. N. ; Olmstead, M. M.; Oram, D. E.; Snow, K. M.; Smith, K. M. *J. Org. Chem.* **1988**, *53*, 5847.

[105] Young Jin Cho, Y. J.; Lee, S. H.; Bae, J. W.; Pyun, H.-J.; Yoon, C. M. *Tetrahedron Lett.* **2000**, *41*, 3915–3917.

[106] Herz, W.; Dittmer, K.; Cristol, S. J. *J. Am. Chem. Soc.* **1947**, *69*, 1698.

[107] Tabushi, I.; Yamamura, K. *Tetrahedron Lett.* **1978**, 1821.

[108] Kagan, N. E.; Mauzerall, D.; Merrifield, R. B. *J. Am. Chem. Soc.* **1977**, *99*, 5484.

[109] Guo, C.-C.; He, X.-T.; Zhou, G.-Y. *Org. Chem. Res. Bull.* (Youji Huaxue) **1991**, *11*, 416.

[110] Treibs, A.; Haberle, N. *Liebigs Ann. Chem.* **1968**, *718*, 183.

[111] Little, R. G. *J. Heterocyclic Chem.* **1981**, *18*, 833.

[112] Volz, H.; Herb, G. *Z. Naturforsch.* **1984**, *39b*, 1393.

[113] Volz, H.; Hassler, M. *Z. Naturforsch.* **1988**, *43b*, 1043.

[114] Kuroda, Y.; Murase, H.; Suzuki, Y.; Ogoshi, H. *Tetrahedron Lett.* **1989**, *30*, 2411.

[115] Lindsey, J. S.; Wagner, R. W. *J. Org. Chem.* **1989**, *54*, 828–836.

[116] Lindsey, J. S.; Hsu, H. C.; Schreiman, I. C. *Tetrahedron Lett.* **1986**, *27*, 41, 4969–4970.

[117] Li, F.; Yang, K.; Tyhonas, J. S.; MacCrum, K. A.; Lindsey, J. S. *Tetrahedron*, **1997**, *53*, 37, 12339–12360.

[118] Badger, G. M.; Jones, R. A.; Laslett, R. L. *Aust. J. Chem.* **1964**, *17*, 1028.

[119] Marchon, J.-C. Ramasseul, R.; Ulrich, J. *J. Heterocyclic Chem.* **1987**, *24*, 1037.

[120] Williamson, M. M.; Prosser-McCartha, C. M.; Mukundan Jr., S.; Hill, C. L. *Inorg. Chem.* **1988**, *27*, 1061.

[121] Littler, B. J.; Miller, M. A.; Hung, C.-H.; Wagner, R. W.; O'Shea, D. F.; Boyle, P. D.; Lindsey, J. S. *J. Org. Chem.* **1999**, *64*, 1319.

[122] Sobral, A. J. F. N.; Rebanda, N. G. C. L.; da Silva, M.; Lampreia, S. H.; Silva, M. R.; Beja, A. M.; Paixao, J. A.; Rocha Gonsalves, A. M. d'A. *Tetrahedron Lett.* **2003**, *44*, 3971.

[123] Porra, R. J. *Photochem. Photobiol.* **1997**, *65*, 492.

[124] Dolphin, D. *J. Heterocyclic Chem.* **1970**, *7*, 275.

[125] Evans, B.; Smith, K. M.; Fuhrhop, J.-H. *Tetrahedron Lett.* **1977**, *5*, 443.

[126] Nevé, R. A.; Labbe, R. F.; Aldrich, R. A. *J. Am. Chem. Soc.* **1956**, *78*, 691.

[127] Mauzerall, D. *J. Am. Chem. Soc.* **1960**, *82*, 2601–2605.

[128] Mauzerall, D. *J. Am. Chem. Soc.* **1960**, *82*, 2605–2609.

[129] Evans, B.; Smith, K. M. *Tetrahedron Lett.* **1977**, *5*, 443–446.

[130] Tabushi, I.; Sakai, K.-I.; Yamamura, K. *Tetrahedron Lett.* **1978**, *21*, 1821–1824.

[131] Lindsey, J. S. In *Metalloporphyrins Catalyzed Oxidations*; Montanari, F.; Casella, L., Eds., Kluwer Academic Publishers: The Netherlands, **1994;** pp 49–79.

[132] Wagner, R. W.; Lawrence, D. S.; Lindsey, J. S. *Tetrahedron Lett.* **1987**, *28*, 27, 3067–3070.

[133] Wagner, R. W.; Li, F.; Du, H.; Lindsey, J. S. *Org. Proc. Res. Dev.* **1999**, *3*, 28.

[134] Rabonovitz, M.; Grinvald, A. *Tetrahedron Lett.* **1971**, *7*, 641–644.

[135] Yates, K.; Stewart, R. *Can. J. Chem.* **1959**, *37*, 664–71.

[136] Chiang, Y.; Whipple, E. B. *J. Am. Chem. Soc.* **1963**, *85*, 2763.

[137] Chiang, Y.; Hinman, R. L.; Theodoropulos, S.; Whipple, E. B. *Tetrahedron* **1967**, *23*, 745.

[138] Wamser, C. A. *J. Am. Chem. Soc.* **1951**, *73*, 409.

[139] Reetz, M. T.; Hüllmann, M.; Massa, W.; Berger, S.; Rademacher, P.; Heymanns, P. *J. Am. Chem. Soc.* **1986**, *108*, 2405–2408.

[140] Gross, Z.; Kaustov, L. *Tetrahedron Letters*, **1995**, *36*, 21, 3735–3736.

[141] Pedersen, C. J. *J. Am. Chem. Soc.* **1967**, *89*, 7017–7036.

[142] Geier, III, G. R.; Lindsey, J. S. *J. Chem. Soc. Perkin Trans. 2* **2001**, 687.

[143] Geier, III, G. R.; Littler, B. J.; Lindsey, J. S. *J. Chem. Soc. Perkin Trans. 2* **2001**, 701.

[144] Geier, III, G. R.; Littler, B. J.; Lindsey, J. S. *J. Chem. Soc. Perkin Trans. 2* **2001**, 712.

[145] Geier, G. R.; Riggs, J. A.; Lindsey, J. S. *J. Porphyrins Pthalocyanines.* **2001**, *5*, 681–690.

[146] Farthing, A. C.; Reynolds, R. J. W. *J. Polymer Sci.* **1954**, *12*, 503–507.

[147] Rose, J. B. *J. Chem. Soc.* **1956**, 546–555.

[148] Miki, T.; Higashimura, T.; Okamura, S. *Bull. Chem. Soc. Jpn.* **1966**, *39*, 2480–2485.

[149] Collins, G. L.; Greene, R. K.; Berardinelli, F. M.; Ray, W. H. *J. Polymer Sci.: Polymer Chem. Ed.* **1981**, *19*, 1597–1607.

[150] Kihn-Botulinski, M.; Meunier, B. *Inorg. Chem.* **1988**, *27*, 209.

[151] Eastham, A. M. *J. Am. Chem. Soc.* **1956**, *78*, 6040–6042.

[152] Collman, J. P.; Gagne, R. R.; Reed, C. A.; Halbert, T. R.; Lang, G.; Robinson, W. T. *J. Am. Chem. Soc.* **1975**, *97*, 1427.

[153] Diekmann, H.; Chang, C. K.; Traylor, T. G. *J. Am. Chem. Soc.* **1971**, *93*, 4069.

[154] Collman, J. P. *Inorg. Chem.* **1997**, *36*, 5145.

[155] Rose, E.; Kossanyi, A.; Quelquejeu, M.; Soleilhavoup, M.; Duwavran, F.; bernard, N.; Lecas, A. *J. Am. Chem. Soc.* **1996**, *118*, 1567.

[156] Almog, J.; Baldwin, J. E.; Dyer, R. L.; Peters, M. *J. Am. Chem. Soc.* **1975**, *97*, 226.

[157] Little, R. G. *J. Heterocyclic Chem.* **1981**, *18*, 129.

[158] Rempel, U.; von Maltzan, B.; von Borczyskowski, C. *Chem. Phys. Lett.* **1995**, *245*, 253.

[159] Leznoff, C. C.; Svirskaya, P. I. *Angew. Ann. Chem. Int. Ed. Engl.* **1978**, *12*, 947.

[160] Kus, P.; Knerr, G.; Czuchajowski, L. *J. Heterocyclic Chem.* **1990**, *27*, 1161.

[161] Gross, Z.; Toledano, I. *J. Org. Chem.* **1994**, *59*, 8312.

[162] Werner, A.; Sanchez-Migallon, A.; Fruchier, A.; Elguero, J.; Fernandez-Castano, C.; Foces-Foces, C. *Tetrahedron* **1995**, *51*, 4779.

[163] Milgrom, L. R.; Dempsey, P. J. F.; Yahioglu, G. *Tetrahedron* **1996**, *52*, 9877.

[164] Zhilina, Z. I.; Vodzinskii, S. V.; Andronati, S. A. *Ukr. Khim. Zhur.* **1990**, *56*, 1084.

[165] Driaf, K.; Granet, R.; Krausz, p.; Kaouadji, M.; Thomasson, F.; Chulia, A. J.; Verneuil, B.; Spiro, M.; Blais, J.-C.; Bolbach, G. *Can. J. Chem.* **1996**, *74*, 1550.

[166] Pozzi, G.; Montanari, F.; Quici, S. *Chem. Commun.* **1997**, 69.

[167] Rocha Gonsalves, A. M. d'A.; Pereira, M. M. *J. Heterocyclic Chem.* **1985**, *22*, 931.

[168] Onaka, M.; Shinoda, T.; Izumi, Y.; Nolen, E. *Chem. Lett.* **1993**, 117.

[169] DiMagno, S. G.; Willliams, R. A.; Therien, M. J. *J. Org. Chem.* **1994**, *59*, 6943.

[170] Shinoda, T.; Onaka, M.; Izumi, Y. *Chem. Lett.* **1995**, 493.

[171] Johnstone, R. A. W. Nunes, M. L. P. G.; Pereira, M. M.; Rocha Gonsalves, A. M. d'A.; Serra, A. C. *Heterocycles* **1996**, *43*, 1423.

[172] Yalman, R. G. *U. S. Patent* 3, 579,533 (**1971**).

[173] Von Maltzan, B. *Ger. Offen.* 2,413,414 (See *Chem. Abstr. 84:* 17450d).

[174] Ulman, A.; Gallucci, J.; Fischer, D.; Ibers, J. A. *J. Am. Chem. Soc.* **1980**, *102*, 6852.

[175] Suh, M. P.; Swepston, P. N.; Ibers, J. A. *J. Am. Chem. Soc.* **1984**, *106*, 5164.

[176] Li, G. Q.; Govind, R. *Inorg. Chim. Acta* **1994**, *217*, 135.

[177] Neya, S.; Funasaki, N. *J. Heterocyclic Chem.* **1997**, *34*, 689.

[178] Frydman, L.; Olivieri, A. C.; Diaz, L. E.; Valasinas, A.; Frydman, B. *J. Am. Chem. Soc.* **1988**, *110*, 5651.

[179] Anderson, H. L. *Tetrahedron Lett.***1992**, *33*, 1101.

[180] Milogrom, L. R.; Rees, R. D.; Yahioglu, G. *Tetrahedron Lett.* **1997**, *38*, 4905.

[181] Edwards, L.; Gouterman, M.; Rose, C. B. *J. Am. Chem. Soc.* **1976**, *98*, 7638.

[182] Linstead, R. P.; Noble, E. G. *J. Chem. Soc.* **1937**, 933.

[183] Linstead, R. P. *J. Chem. Soc.* **1934**, 1016.

[184] Byrne, G. T.; Linstead, R. P. *J. Chem. Soc.* **1934**, 1017.

[185] Cook, A. H.; Linstead, R. P. *J. Chem. Soc.* **1937**, 929.

[186] Ficken, G. E.; Linstead, R. P. *J. Chem. Soc.* **1952**, 4846.

[187] Linstead, R. P.; Whalley, M. *J. Chem. Soc.* **1952**, 4839.

[188] Baguley, M. E.; France, H.; Linstead, R. P.; Whalley, M. *J. Chem. Soc.* **1955**, 3521.

[189] Marat, K. *SpinWorks*, Version 2.5.5, Copyright **1999-2006** and Version 2.4 PL2, Copyright **1999-2004**.

[190] *CrysAlis CCD* and *CrysAlis RED*, Version 170, Oxford Diffraction Ltd., Abingdon, UK, **2002**.

[191] Sheldrick, G. M. *SHELXS-97, Program for solution of crystal structures*, University of Göttingen, Germany, **1997**.

[192] Farrugia, L. J. *J. Appl. Crystallogr.* **1999**, *32*, 837–838.

[193] Sheldrick, G. M. *SHELXL-97, Program for refinement of crystal structures*, University of Göttingen, Germany, **1997**.

[194] *FeliX32 Analysis*, Version 1.1 (Build 51 BETA 8), **2003**.

[195] Veyrat, M.; Ramasseul, R.; Turowska-Tyrk, I.; Sheidt, W .R.; Autret, M.; Kadish, K. M.; Marchon, J. *Inorg. Chem.* **1999**, *38*, 1772–1779.

[196] Tyulyaeva, E. Yu.; Lomova, T. N. *Russian Journal of Coordination Chemistry*, **2001**, *27*, 6, 433–438. (Translated from Koordinatsionnaya Khimiya, 2001, *27*, 6, 465–470.)

[197] Rothemund, P. and Menotti, A.K., *J. Am. Chem. Soc.*, **1948**, *70*, 5, 1808.

[198] Che, C.-M.; Sun, R. W.-Y.; Yu, W.-Y.; Ko, C.-B.; Zhu, N.; Sun, H. *Chem. Commun.* **2003**, 1718–1719.

[199] MacCragh, A.; Koski, W. S. *J. Am. Chem. Soc.* **1965**, *87*, 2496.

[200] Fleischer, E. B.; Laszlo, A. *Inorg. Nucl. Chem. Lett.* **1969**, *5*, 373–376.

[201] Howarth, O. In *Theory of Spectroscopy*; Thomas Nelson and Sons Ltd.: London, **1973;** pp 1, 64–67.

[202] Friedel, R. A.; Orchin, M. In *Ultraviolet Spectra of Aromatic Compounds*; John Wiley & Sons: New York, **1951;** pp 1, 13, 14.

[203] Rao, C. N. R. In *Ultra-Violet and visible Spectroscopy 2nd ed.*; Butterworth & Co.: London, **1967;** pp 1, 13–16, 58, 76, 88, 97, 131–46, 175.

[204] Lewis, G. N.; Calvin, M. *Chem. Rev.* **1939**, *25*, 273.

[205] Soret, J. L. *Compt. Rend.* **1883**, *97*, 1267.

[206] Gamgee, A. *Zeitschrift fuer Biologie* (Munich) **1897**, *34*, 505–528.

[207] Stern, A.; Wenderlein, H. *Z. Physik. Chem.* **1936**, *A176*, 81.

[208] Jacobs, E. E.; Holt, A. S.; Rabinowitch, E. *J. Chem. Phys.* **1954**, *22*, 142.

[209] Ohno, K. *Theoretica Chimica Acta*. **1964**, *2*, 3, 219–227.

[210] Weiss, C.; Kobayashi, H.; Gouterman, M. *J. Molec. Spec.* **1965**, *16*, 2, 415–450.

[211] Gouterman, M.; Wagniere, G.; Snyder, L. *J. Molec. Spec.* **1963**, *11*, 2, 108–127.

[212] Gouterman, M. *J. Chem. Phys.* **1959**, *30*, 1139–1161.

[213] Gouterman, M. *J. Chem. Phys.* **1960**, *33*, 1523–1529.

[214] Gouterman, M. *J. Molec. Spec.* **1961**, *6*, 138–163.

[215] Veyrat, M.; Ramesseul, R.; Marchon, J. *New J. Chem.* **1995**, *19*, 1199–1202.

[216] Herschel, W. *Phil Transact. Roy. Soc.* **1800**, *90*, 284.

[217] Günzler, H.; Gremlich, H.-U. In *IR Spectroscopy*; Wiley VCH: Weinheim, **2002;** pp 1–3, 24, 95–99, 171, 176, 193, 225, 347.

[218] Lehrer, E. Z. *Techn. Phys.* **1942**, *23*, 169.

[219] Nakamoto, K. In *Infrared and Raman Spectra of Inorganic and Coordination Compounds. 5th ed. Part A*; John Wiley & Sons: New York, **1997;** pp 1–5.

[220] Nakamoto, K. In *Infrared and Raman Spectra of Inorganic and Coordination Compounds. 4th ed.*; John Wiley & Sons: New York, **1986;** pp 3–5, 213–221.

[221] Silverstein, R. M.; Webster, F. X. In *Spectometric Identification of Organic Compouns, 6th ed.*; John Wiley & Sons: New York, **1998;** pp 71–109, 144–246.

[222] Ogoshi, H.; Saito, Y.; Nakamoto, K. *J. Chem. Phys.* **1972**, *57*, 4194.

[223] Bürger, H. In *Porphyrins and Metalloporphyrins*; Smith K. M., Ed.; Elsevier: Amsterdam, **1975;** Chapter 11.

[224] Foresman, J. B.; Frisch, Æ. In *Exploring Chemistry with Electronic Structure Methods, 2nd ed.*; Gaussian Inc.: Pittsburgh, **1993;** pp 6, 9, 21, 61–63, 97, 100–103, 112, 118, 154–160, 272.

[225] *GaussView 3.09*, Gaussian Inc. Carnegie Office Park-Building 6, Pittsburgh, PA 15106, USA. Copyright **2000–2003**.

[226] Friebolin, H. In *Basic One- and Two-Dimensional NMR Spectroscopy*; VCH Verlagsgesellschaft: Weinheim, **1991**; pp 19, 37, 43, 61, 64, 83, 203.

[227] Pauling, L. *J. Chem. Phys.* **1936**, *4*, 673.

[228] Medforth, C. J. In *The Porphyrin Handbook*; Kadish, K. M.; Smith, K. M.; Guilard, R., Eds.; Academic: New York, **2000;** Vol 5, Chapter 35.

[229] Pople, J. A. *J. Chem. Phys.* **1956**, *24*, 1111.

[230] Becker, E. D.; Bradley, R. B. *J. Chem. Phys.* **1959**, *31*, 1413.

[231] *Porphyrins and Metalloporphyrins*; Smith K. M., Ed.; Elsevier: Amsterdam, **1975.**

[232] Ellis, J.; Jackson, A. H.; Kenner, G. W.; Lee, J. *Tetrahedron Lett.* **1960**, 23.

[233] Caughey, W. S.; Koski, W. S. *Biochemistry* **1962**, *1*, 923.

[234] Scheer, H.; Katz, J. J. In *Porphyrins and Metalloporphyrins*; Smith K. M., Ed.; Elsevier: Amsterdam, **1975;** Chapter 10.

[235] Abraham, R. J. *Mol. Phys.* **1961**, *4*, 145.

[236] Abraham, R. J.; Rowan, A. E.; Mansfield, K. E.; Smith, K. M. *J. Chem. Soc. Perkin trans. 2* **1991**, 515.

[237] Naksnishi, K. In *One-dimensional and Two-dimensional NMR Spectra*; Kodansha: Tokyo, **1990;** pp 2.

[238] Denniss, I. S.; Sanders, J. K. M.; Waterton, J. C. *J. Chem. Soc. Chem. Commun.* **1976**, 1049.

[239] Sanders, J. K. M.; Waterton, J. C.; Denniss, I. S. *J. Chem. Soc. Perkin Trans. 1* **1978**, 1150.

[240] Abraham, R. J.; Jackson, A. H.; Kenner, G. W.; Warburton, D. *J. Chem. Soc.* **1963**, 856.

[241] Smith, K. M.; Abraham, R. J.; Pearson, H. *Tetrahedron* **1982**, *38*, 2441.

[242] Abraham, R. J.; Smith, K. M.; Goff, D. A.; Lai, J.-J. *J. Am. Chem. Soc.* **1982**, *104*, 4332.

[243] Smith, K. M.; Bobe, F. W.; Minnetian, O. M.; Abraham, R. J. *Tetrahedron* **1984**, *40*, 3263.

[244] Hombrecher, H. K.; Horter, G.; Arp, C. *Tetrahedron* **1992**, *48*, 9451.

[245] Takeda, J.; Sato, M. *Tetrahedron Lett.* **1994**, *35*, 3565.

[246] Miura, M.; Majumder, S. A.; Hobbs, J. D.; Renner, M. W.; Furenlid, L. R.; Shelnutt, J. A. *Inorg. Chem.* **1994**, *33*, 6078.

[247] Somma, M. S.; Medforth, C.J.; Nelson, N. Y.; Olmstead, M. M.; Khoury, R. G.; Smith, K. M. *Chem. Commun.* **1999**, 1221–1222.

[248] Medforth, C. J.; Muzzi, C. M.; Shea, K. M.; Smith, K. M.; Abraham, R. J.; Jia, S.; Shelnutt, J. A. *J. Chem. Soc. Perkin Trans. 2* **1997**, 839–844.

[249] Takeda, J.; Sato, M. *Chem. Lett.* **1995**, 971.

[250] Smedarchina, Z.; Zgierski, M. Z.; Siebrand, W.; Kozlowski, P.W. *J. Chem. Phys.* **1988**, *109*, 1014.

[251] Vogel, E.; Köcher, M.; Schmickler, H.; Lex, J. *Angew. Chem. Int. Ed. Engl.* **1986**, *25*, 3, 257–259.

[252] Storm, C. B.; Teklu, Y.; Sokolski, E. A. *Ann. N. Y. Acad Sci.* **1973**, *206*, 631.

[253] Nurco, D. J.; Medforth, C. J.; Forsyth, T. P.; Olmstead, M. M.; Smith, K. M. *J. Am. Chem. Soc.* **1996**, *118*, 10918–10919.

[254] Takeda, J.; Sato, M. *Chem. Lett.* **1995**, 971.

[255] du Vernet, R.; Boekelheide, V. *Proc. Nat. Acad. Sci. U.S.A.* **1974**, *71*, 2961.

[256] Battersby, A. R.; Moron, J.; Mcdonald, E.; Feeney, J. *J. Chem. Soc. Chem. Commum.* **1972**, 920.

[257] Abraham, R. J.; Hawkes, G. E.; Smith, K. M. *J. Chem. Soc. Chem. Commum.* **1973**, 401.

[258] Abraham, R. J.; Hawkes, G. E.; Smith, K. M. *J. Chem. Soc. Perkin Trans. 2* **1974**, 627.

[259] Lincoln, D. N.; Wray, V.; Brockmann, H. Jr.; Trowitzsch, W. *J. Chem. Soc. Perkin Trans. 2* **1974**, *15*, 1920–1925.

[260] Strouse, C. E.; Kollman, V. H.; Matwiyoff, N. A. *Biochem. Biophys. Res. Commun.* **1972**, *46*, 328.

[261] Boxer, S. G.; Closs, G. L.; Katz, J. J. *J. Am. Chem. Soc.* **1974**, *96*, 7058.

[262] Battersby, A. R.; Hodgson, G. L.; Ihara, M.; Mcdonald, E.; Saunders, J. *J. Chem. Soc. Perkin Trans. 1* **1973**, 2923.

[263] Asakawa, M.; Toi, H.; Aoyama, Y.; Ogoshi, H. *J. Org. Chem.* **1992**, *57*, 5796–5798.

[264] Storm, C. B.; Teklu, Y. *J. Am. Chem. Soc.* **1972**, *94*, 5, 1745–1747.

[265] Eaton, S. S.; Eaton, G. R. *J. Am. Chem. Soc.* **1977**, *99*, 5, 1601–1604.

[266] Hennig, J.; Limbach, H.-H. *J. Am. Chem. Soc.* **1984**, *106*, 2, 292–298.

[267] Wehrle, B.; Limbach, H.-H.; Köcher, M.; Ermer, O.; Vogel, E. *Angew. Chem. Int. Ed. Engl.* **1987**, *26*, 9, 934–936.

[268] Becker, E. D.; Bradley, R. B.; Watson, C. J. *J. Am. Chem. Soc.* **1961**, *83*, 3743.

[269] Abraham, R. J.; Burbidge, P. A.; Jackson, A. H.; Mcdonald, D. B. *J. Chem. Soc.* **1966**, 620.

[270] Braun, J.; Schlabach, M.; Wehrle, B.; Kocher, M.; Vogel, E.; Limbach, H.-H. *J. Am. Chem. Soc.* **1994**, 6593.

[271] Braun, J.; Limbach, H.-H.; Williams, P. G.; Morimoto, H.; Wemmer, D. E. *J. Am. Chem. Soc.* **1996**, *118*, 7231.

[272] Ghosh, A. In *The Porphyrin Handbook*; Kadish, K. M.; Smith, K. M.; Guilard, R., Eds.; Academic: New York, **2000;** Vol 1, Chapter 2.

[273] Furuta, H.; Ishizuka, T.; Osuka, A.; Dejima, Nakagawa, H.; Ishikawa, Y. *J. Am. Chem. Soc.* **2001**, *123*, 6207–6208.

[274] Robertson, J. *J. Chem. Soc.* **1936**, 1195.

[275] Corwin, A.; Quattlebaum, M. *J. Am. Chem. Soc.* **1936**, *58*, 1081.

[276] Erdman, J.; Corwin, A. *J. Am. Chem. Soc.* **1946**, *68*, 1885.

[277] Ghosh, A. *Acc. Chem. Res.* **1998**, *31*, 189.

[278] Falk, J. E.; Willis, J. B. *Aust. J. Sci. Res., Ser.* **1951**, *A*, 4, 579.

[279] Badger, G. M.; Harris, R. L. N.; Jones, R. A.; Sasse, J. M. *J. Chem. Soc.* **1962**, 4329.

[280] Abraham, R. J.; Hawkes, G. E.; Smith, K. M. *Tetrahedron Lett.* **1974**, 1483.

[281] Sarai, A. *J. Chem. Phys.* **1982**, *76*, 5554.

[282] Butenhoff, T.; Moore, C. B. *J. Am. Chem. Soc.* **1988**, *110*, 8336.

[283] Butenhoff, T.; Chuck, R.; Limbach, H.-H.; Moore, C. B. *J. Phys. Chem.* **1990**, *94*, 7847.

[284] Braun, J.; Hasenfratz, C.; Schwesinger, R.; Limbach, H.-H. *Angew. Chem. Int. Ed. Engl.* **1994**, *33*, 2215.

[285] Irving, C. S.; Lapidot, A. *J. Chem. Soc. Chem. Commun.* **1977**, 184.

[286] Gust, D.; Roberts, J. D. *J. Am. Chem. Soc.* **1977**, *99*, 3637.

[287] Hennig, J.; Limbach, H.-H. *J. Am. Chem. Soc. Faraday Trans. 2* **1979**, *75*, 752.

[288] Vangberg, T.; Ghosh, A. *J. Phys. Chem.* **1997**, *101*, 1496.

[289] Ghosh, A.; Almlöf, J. *J. Phys. Chem.* **1995**, *99*, 1037.

[290] Kasha, M. *J. Chem. Soc. Faraday Trans. 2* **1986**, *82*, 2379–2392.

[291] Völker, S.; Macfarlane, R. M. *J. Chem. Phys.* **1980**, *73*, 4476.

[292] Braun, J.; Schwesinger, R.; Williams, P. G.; Morimoto, H.; Wemmer, D. E.; Limbach, H.-H. *J. Am. Chem. Soc.* **1996**, *118*, 11101.

[293] Harris, R. K.; Kennedy, J. D.; McFarlane, W. In *NMR and the periodic table*; Harris, R. K.; Mann, B. E., Eds.; Academic Press: London, **1978**; pp 342–377 and references therein.

[294] Jameson, C. J.; Gutowsky, H. S. *J. Chem. Phys.* **1964**, *40*, 1714.

[295] Liu, I.-C.; Chen, J.-H.; Wang, S.-S.; Wang, J.-C. *Polyhedron* **1996**, *15*, 22, 3947–57.

[296] Abraham, R. J.; Barnett, G. H.; Hawkes, G. E.; Smith, K. M. *Tetrahedron* **1976**, *32*, 2949.

[297] Columbus, I.; Biali, S. E. *J. Org. Chem.* **1993**, *58*, 7029.

[298] Hugo E. Gottlieb, H. E.; Kotlyar, V.; Nudelman, A. *J. Org. Chem.* **1997,** *62*, 7512–7515.

[299] Ditchfield, R. *Mol. Phys.* **1974**, *27*, 789.

[300] Wolinski, K.; Hilton, J. F.; Pulay, P. *J. Am. Chem. Soc.* **1990**, *112*, 8251.

[301] Pople, J. A., *Discuss. Faraday Soc.* **1962**, *34*, 7.

[302] London, F. *J. Phys. Radium, Paris* **1937**, *8*, 397.

[303] Columbus, I.; Cohen, S.; Biali, S. E. *J. Am. Chem. Soc.* **1994**, *116*, 22, 10306–10307.

[304] Columbus, I.; Biali, S. E. *J. Org. Chem.* **1994**, *59*, 8132–8138.

[305] Crute, M. B. Acta. Crystallogr. **1959**,*12*, 24.

[306] Robertson, J. M. *J. Chem. Soc.* **1936**, 1195.

[307] Robertson, J. M.; Woodward, I. *J. Chem. Soc.* **1937**, 219.

[308] Robertson, J. M.; Woodward, I. *J. Chem. Soc.* **1940**, 36.

[309] Hoard, J. L. In *Porphyrins and Metalloporphyrins*; Smith K. M., Ed.; Elsevier: Amsterdam, **1975;** Chapter 8.

[310] Handbook Sheidt, W. R. In *The Porphyrin Handbook*; Kadish, K. M.; Smith, K. M.; Guilard, R., Eds.; Academic: New York, **2000;** Vol 1, Chapter 2.

[311] Cambridge Crystallographic Data Centre, CSDS **2006** release. 12 Union Rd, Cambridge CB21EZ, UK.

[312] Collman, J. P. *Acc. Chem. Res.* **1977**, *10*, 265–272.

[313] Fleischer, E.; Miller, C.; Webb, L. *J. Am. Chem. Soc.* **1964**, *86*, 2342.

[314] Hamor, T. A.; Caughey, W. S.; Hoard, J. L. *J. Am. Chem. Soc.* **1965**, *87*, 2305.

[315] Stone, A.; Fleischer, E. B. *J. Am. Chem. Soc.* **1968**, *90*, 2735–2748.

[316] Scheidt, W. R.; Lee, Y. J. *Struct. Bonding (Berlin),* **1987**, *64*, 1–70.

[317] Jentzen, W.; Song, X.-Z.; Shelnutt, J. A. *J. Phys. Chem.* **1997**, *101*, 1684–1699.

[318] Barkigia, K. M. Fajer, J.; Adler, A. D.; Williamsic, G. J. B. *Inorg. Chem.* **1980**, *19*, 2057–2061.

[319] Codding, P. W.; Tulinsky, A. *J. Am. Chem. Soc.* **1972**, *94*, 12, 4151–4157.

[320] Kano, K.; Fukuda, K.; Wakami, H.; Nishiyabu, R.; Pasternack, R. F. *J. Am. Chem. Soc.* **2000**, *122*, 31, 7494–7502.

[321] *Mercury*, version 1.4, Cambridge Crystallographic Data Centre, Cambridge, UK, **2005**.

[322] Yoshids, Y.; Matsui, S.; Takagi, Y.; Mitani, M.; Nakano, T.; Tanaka, H.; Kashiwa, N.; Fujita, T. *Oranometallics* **2001**, *20*, 4793–4799.

[323] Wołowiec, S.; Latos-Grazynski, L.; Toronto, D.; Marchon, J.-C. *Inorg. Chem.* **1998**, *37*, 724–732.

[324] Rao, C. N. R. In *Ultra-Violet and visible Spectroscopy 3rd ed.*; Butterworth & Co.: London, **1975;** pp 143.

[325] Jaffé, H. H.; Miller, A. L. *J. Chem. Educ.* **1966**, *43*, 469.

[326] Article within a web site (Anonymous): "Fluorescence." Answers.com. 2007 <http://www.answers.com/topic/fluorescence-in-various-sized-cdse-quantum-dots-png>

[327] Chamberlin, G. J.; Chamberlin, D. G. In *Colour;* Heyden: London, **1980;** pp 2.

[328] Schenk, G. H. In *Absorption of light and ultraviolet radiation: Fluorescence and Phosphorescence emission*; Allyn and Bacon: Boston, **1973;** pp 97–100, 149.

[329] Hirschlaff, E. In *Fluorescence and Phosphorescence*; Methuen & Co.: London, **1938;** pp 1, 2, 18, 39.

[330] Article within a web site (Anonymous): "Fluorescence." BERTHOLD TECHNOLOGIES GmbH & Co. 2006. <http://www.bertholdtech.com/ww/en/pub/bioanalytik/biomethods/fluor.cfm>

[331] Article within a web site (Anonymous): "Fluorescence spectroscopy." 21 May 2007. Wikipedia. 2007. <http://en.wikipedia.org/wiki/Fluorescence_spectroscopy>

[332] Lever, A. B. P. In *Inorganic Electronic Spectroscopy 2nd ed.*; Elsevier: Amsterdam, **1984;** pp 194–196.

[333] Crooks, J. E. *The spectrum in chemistry;* Academic Press: London, **1978**; pp 124–138.

[334] Phillips, D.; Salisbury, K. In *Spectroscopy*; Straughan, B. P.; Walker, S., Eds., John Wiley & Sons: New York, **1976;** pp 161–198.

[335] Khalil, G. E.; Thompson, E. K.; Gouterman, M.; Callis, J. B.; Dalton, L. R.; Turro, N. J.; Jockusch, S. *Chem. Phys. Lett.* **2007**,*435*, 45–49.

[336] Qi, M.-H.; Liu, G.-F, *J. Porphyrins Phthalocyanines*, **2004**, *8*, 10, 1187–1195.

[337] Qi, M.-H.; Liu, G.-F, *Solid State Sciences* **2004**, *6*, 3, 287–294.

[338] Rusakova, N. V.; Korovin, V. Yu.; Zhilina, Z. I.; Vodzinskii, S. V.; Ishkov, Yu. V. Bogatskii, A. V. *J. Appl. Spec.* **2004**, *71*, 4, 506–511.

[339] Korovin, Yu. V.; Rusakova, N. V.; Zhilina, Z. I.; Vodzinskii, S. V.; Ishkov, Yu. V. *Ukrainskii Khimicheskii Zhurnal (Russian Edition)* **2002**, *68*, 75–78.

[340] He, H.-S.; Zhao, Z.-X.; Wong, W.-K.; Li, K.-F.; Meng, J.-X.; Cheah, K.-W. *J. Chem. Soc. Dalton Trans.* **2003**, *5*, 980–986.

[341] Gouterman, M.; Hanson, L. K.; Khalil, G. E.; Buchler, J. W.; Rohbock, K.; Dolphin, D. *J. Am. Chem. Soc.* **1975**, *97*, 11, 3142–3149.

[342] Eastwood, D.; Gouterman, M *J. Molec. Spec.* **1970**, *35*, 3, 359–375.

[343] Gouterman, M; Mathies, R. A.; Smith, B. E.; Caughey, W. S. *J. Chem. Phys.* **1970**, *52*, 7, 3795–3802.

[344] Pan, S.; Rothberg, L. J. *J. Am. Chem. Soc.* **2005**, *127*, 16, 6087–6094.

[345] Li, G.; Jin, W.. *Fenxi Huaxue* **2002**, *30*, 12, 1515–2150.

[346] Zhang, X.; Wasinger, E. C.; Muresan, A. Z.; Attenkofer, K.; Jennings, G.; Lindsey, J. S.; Chen, L. X. *Abstracts of Papers, 233rd ACS National Meeting*, United States, March 25–29, **2007**, PHYS-512.

[347] Burgner, R. P.; Ponte Goncalves, A. M. Eds: Longo, F. R. *Porphyrin Chem. Adv.* **1979**, 29–42.

[348] von Borcyskowski, C.; Rempel, U.; Zenkevich, E.; Shul'ga, A.; Chernook, A. *Ultrafast Processes in Spectroscopy*, **1996**, 71–74.

[349] Song, H.-E.; Cissell, J. A.; Vaid, T. P.; Holten, D. *J. Phys. Chem. B* **2007**, *111*, 9, 2138–2142.

[350] Hoshino, M.; Seki, H. *Chem. Phys. Lett.* **1984**, *110*, 4, 413–416.

[351] Cunningham, K. L.; McNett, K. M.; Pierce, R. A.; Davis, K. A.; Harris, H. H.; Falck, D. M.; McMillin, D. R. *Inorg. Chem.* **1997**, *36*, 4, 608–613.

[352] Allison, J. B.; Becker, R. S. *J. Chem. Phys.* **1960**, *32*, 1410–1417.

[353] Khairutdinov, R. F.; Serpone, N. *J. Phys. Chem. B* **1999**, *103*, 5, 761–769.

[354] Tsvirko, M. P.; Solov'ev, K. N.; Gradyushko, A. T.; Dvornikov, S. S. *USSR. Zhurnal Prikladnoi Spektroskopii* **1974**, *20*, 3, 528–530.

[355] Flamigni, L.; Ventura, B.; Tasior, M.; Gryko, D. T. *Inorg. Chim. Acta.* **2007**, *360*, 3, 803–813.

[356] Harriman, A. *J. Chem. Soc. Faraday Trans. 1* **1980**, *76*, 1978–1985.

[357] Harriman, A. *J. Chem. Soc. Faraday Trans. 1* **1981,** *77*, 369–377.

[358] Harriman, A. *J. Chem. Soc. Faraday Trans. 2* **1981,** *77*, 1281–1291.

[359] Harriman, A. *J. Chem. Soc. Faraday Trans. 1* **1981**, *77*, 1695–1702.

[360] Gouterman, M.; Khalil, G. E. *J. Mol. Spec.* **1974**, *53*, 88.

[361] Quimby, D. J.; Longo, F. R. *J. Am. Chem. Soc.* **1975**, *97*, 5111.

[362] Gouterman, M.; Schwarz, F. P.; Smith, P. D. *J. Chem. Phys.* **1974**, *61*, 3491.

[363] Stickler, S. J.; Berg, D. J. *J. Chem. Phys.* **1962**, *37*, 814.

[364] Harriman, A.; Porter, G.; Richoux, M.-C. *J. Chem. Soc. Faraday Trans. 2* **1981**, *77*, 1175.

[365] Gouterman, M.; Schwarz, F. P.; Smith, P. D.; Dolphin, D. *J. Chem. Phys.* **1973**,*59*, 676.

[366] Harriman, A.; Porter, G.; Richoux, M.-C. *J. Chem. Soc. Faraday Trans. 2* **1981**,*77*, 833.

[367] Pekkarinen, L.; Linshitz, H. *J. Am. Chem. Soc.* **1960**, *82*, 2407. Madge, D.; Windsor, M. W.; Holten, D.; Gouterman, M. *Chem. Phys. Letters* **1974**, *29*, 183.

[368] Platt, J. R.; *J. Opt. Soc. Am.* **1953**, *43*, 252.

[369] César. F.; Polo, A. L.; Frisardl, E. R.; Resnlk, A.; Schoua, E. M.; Alcira M. del C. B. *Clin. Chem.* **1988**, *34*, 4, 757–760.

[370] Du, H.; Fuh, R. A.; Li, J.; Corkan, A.; Lindsey, J. S. *A. Soc. Photobio. J.* **1998**, *68*, 141–142.

[371] Clark, T. In *A Handbook of Computational Chemitry–A Practical guide to Chemical Structure and Energy Calculations;* John Wiley & Sons: USA, **1949;** pp 1, 99, 233, 242.

[372] Wagnière, G. H. In *Introduction to Elementary Molecular Orbital Theory*; Springer-Verlag: Berlin, **1976;** pp 3.

[373] Koch, W.; Holthausen, M. C. In *A Chemist's Guide to Density Functional Theory*; Wiley-VCH: Weinheim, **2000;** pp 30, 41, 70–85, 117–119, 191, 195, 199, 212.

[374] Handbook Lecomte, C.; Rohmer, M.-M.; Bénard, M. In *The Porphyrin Handbook*; Kadish, K. M.; Smith, K. M.; Guilard, R., Eds.; Academic: New York, **2000;** Vol 7, Chapter 48.

[375] Hohenberg, P.; Kohn, W. *Phys. Rev. B.* **1994**, *136*, 846–871.

[376] Jensen, F. In *Introduction to Computational Chemistry*; John Wiley & Sons: Chichester, **1999;** pp 177.

[377] Ziegler, T. *Chem. Rev.* **1991**, *91*, 651–667.

[378] Kohn, W.; Sham, L. J. *Phys. Rev. A.* **1965**, *140*, 1133–1138.

[379] Vosko, S. J.; Wilk, L.; Nusair, M. *Can. J. Phys.* **1980**, *58*, 1200.

[380] Perdew, J. D.; Wang, Y. *Phys. Rev. B.* **1986**, *33*, 8800–8802.

[381] Becke, A. D. *Phys. Rev. B.* **1988**, *38*, 3098–3100.

[382] Lee, C.; Yang, W.; Parr, R. G. *Phys. Rev. B.* **1988**, *37*, 785–789.

[383] Perdew, J. P.; Chevary, J. A.; Vosko, S. H. ; Jackson, K. A. ; Pederson, M. R.; Singh, D. J.; Fiolhias, C. *Phys. Rev. B-Cond. Matter.* **1992**, *46*, 6671–6687.

[384] Becke, A. D. *J. Chem. Phys.* **1993**, *98*, 5648–5652.

[385] Stevens, P. J.; Devlin, J. F.; Chabalowski, C. F.; Frisch, M. J. *J. Phys. Chem.* **1994**, *98*, 11623.

[386] Becke, A. D. *J. Chem. Phys.* **1996**, *104*, 1040.

[387] Becke, A. D. *J. Chem. Phys.* **1997**, *107*, 8554.

[388] Schmider, H. L.; Becke, A. D. *J. Chem. Phys.* **1998**, *108*, 9624.

[389] van Voorhis, T.; Scuseria, G. E. *J. Chem. Phys.* **1998**, *109*, 400.

[390] Meijer, E. J.; Sprik, M. *J. Chem. Phys.* **1996**, *105*, 8684.

[391] Oakes, R. E.; Bell, S. E. J. *J. Phys. Chem.* A **2003**, *107*, 10953–10959.

[392] Almlöf, J.; Fischer, T. H.; Gassman, P. G.; Ghosh, A.; Häser, M. *J. Phys. Chem.* **1993**, *97*, 10964.

[393] Ghosh, A. *Acc. Chem. Res.* **1998**, *31*, 189.

[394] Longuet-Higgins, H. C.; Rector, C. W.; Platt, J. R. *J. Chem. Phys.* **1950**, *18*, 1174.

[395] Dedieu, A.; Rohmer, M.-M.; Veillard, A. *Adv. Quantum Chem.* **1982**, *16*, 43.

[396] Munro, O. Q.; Pearson, N. *J. Porphyrins Phthalocyanines* **2004**, *8*, 8, 1067–1079.

[397] Medforth, C. J.; Muzzi, C. M.; Shea, K. M.; Smityh, K. M.; Abraham, R. J.; Jia, S.; Shelnutt, J. A. *J. Chem. Soc. Perkin Trans 2* **1997**, *4*, 833–837.

[398] Medforth, C. J.; Hobbs, J. D.; Rodriguez, M. R.; Abraham, R. J.; Smith, K. M.; Shelnutt, J. A. *Inorg. Chem.* **1995**, *34*, 6, 1333–1341.

[399] Wondimagegn, T.; Ghosh, A. *J. Phys. Chem. A* **2000**, *104*, 19, 4606–4608.

[400] Eaton, S. S.; Eaton, G. R. *J. Am. Chem. Soc.* **1977**, *99*, 6594. Dirks, J. W.; Underwood, G.; Matheson, J. C.; Gust, D. *J. Org. Chem.* **1979**, *44*, 2551. Freitag, R. A.; Whitten, D. G. *J. Phys. Chem.* **1983**, *87*, 3918.

[401] Medforth, C. J.; Haddad, R. E.; Muzzi, C. M.; Dooley, N. R.; Jaquinod, L.; Shyr, David C.; Nurco, D. J.; Olmstead, M. M.; Smith, K. M.; Ma, J.-G.; Shelnutt, J. A. *Inorg. Chem.* **2003**, *42*, 7, 2227–2241.

[402] Haddad, R. E.; Gazeau, S.; Pecaut, J.; Marchon, J.-C.; Medforth, C. J.; Shelnutt, J. A. *J. Am. Chem. Soc.* **2003**, *125*, 5, 1253–1268.

[403] DiMagno, S. G.; Wertsching, A. K.; Ross, II, C. R., *J. Am. Chem. Soc.* **1995**, *117*, 8279.

[404] Parusel, A. B. J.; Wondimagegn, T.; Ghosh, A. *J. Am. Chem. Soc.* **2000**, *122*, 27, 6371–6374.

[405] Shelnutt, J. A.; Haddad, R.; Medforth, C. J. *Abstracts of Papers, 225th ACS National Meeting*, New Orleans, LA, United States, March 23–27, **2003**, GEOC-065.

[406] Medforth, C. J.; Somma, M. S.; Shyr, D. C.; Smith, K. M.; Goodrow, M. H.; Haddad, R.; Qiu, Y.; Shelnutt, J. A. *224th ACS National Meeting*, Boston, MA, United States, August 18–22, **2002**, INOR-113.

[407] Zhang, J.; Ma, J.-G.; Jia, S.-L.; Lu, Y.; Shelnutt, J. A.; Vanderkooi, J. M. *Book of Abstracts, 217th ACS National Meeting*, Anaheim, Calif., March 21–25 **1999**, INOR-126.

[408] Patchkovskii, S.; Ziegler, T. *Inorg. Chem.* **2000**, *39*, 5354–5364.

[409] Kozlowski, P. M.; Spiro, T. G.; Zgierski, M. Z. *J. Phys. Chem. B* **2000**, *104*, 10659–10666.

[410] Rovira, C.; Parrinello, M. *Int. J. Quantum Chem.* **2000**, *80*, 1172–1180.

[411] Munro, O. Q.; Shabalala, S. C.; Brown, N. J. *Inorg. Chem.* **2001**, *40*, 3303–3317.

[412] Ghosh, A.; Vangberg, T.; Gonzalez, E.; Taylor, P. *J. Porphyrins Pthalocyannnes* **2001**, *5*, 345–356.

[413] Lui, Y. P. *J. Chem. Info. Computer Sciences* **2001**, *41*, 22–29.

[414] Kuramochi, H.; Noodleman, L.; Cae, D. A. *J. Am. Chem. Soc.* **1997**, *119*, 11442–11451.

[415] Ohta, T.; Matsuura, K.; Yoshizawa, K.; Morishima, I. *J. Inorg. Biochem.* **2000**, *82*, 141–152.

[416] Filatov, M.; Harris, N.; Shaik, S. *J. Chem. Soc. Perkin Trans. 2* **1999**, *3*, 399–410.

[417] Scherlis, D. A.; Cymeryng, C. B.; Estrin, D. A. *Inorg. Chem.* **2000**, *39*, 2352–2359.

[418] Harris, D.; Loew, G.; Waskell, L. *J. Am. Chem. Soc.* **1998**, *120*, 4308–4318.

[419] Hui, R.; Yixin, Q. *Jisuanji Yu Yingyong Huaxue* **2006**, *23*, 5, 431–435.

[420] Zhang, Y.-H.; Ruan, W.-J.; Li, Z.-Y.; Wu, Y.; Zheng, J.-Y. *Chem. Phys.* **2005**, *315*, 1-2, 201–213.

[421] Ghosh, A. *J. Phys. Chem. B* **1997**, *101*, 16, 3290–3297.

[422] Sundholm, D. *Phys. Chem. Chem. Phys.* **2000**, *2*, 10, 2275–2281.

[423] Nguyen, K. A.; Day, P. N.; Pachter, R. *J. Phys. Chem. A* **2000**, *104*, 20, 4748–4754.

[424] Schluecker, S.; Koster, J.; Nissum, M.; Popp, J.; Kiefer, W. *J. Phys. Chem. A* **2001**, *105*, 41, 9482–9488.

[425] Kay, C. W. M. *J. Am. Chem. Soc.* **2003**, *125*, 45, 13861–13867.

[426] Sun, H.; Smirnov, V. V.; Nelson, A. P.; Biffinger, J. C.; DiMagno, S. G. *Abstracts of Papers, 229th ACS National Meeting*, San Diego, CA, United States, March 13–17, **2005**, ORGN-290.

[427] *Gaussian 03W*, version 6.1. Gaussian Inc. Carnegie Office Park-Building 6, Pittsburgh, PA 15106, USA. Copyright **1995–2004**.

[428] *Arguslab 4.0.1*, version 1.2. Thompson M. and Planaria Software LLC. Copyright **1997–2004**.

[429] Web site (Professional): gaussian.com. 31 July 2007. Gaussian 03. 15 March 2005.
<http://www.gaussian.com>

[430] Hehre, W. J.; Lathan, W. A.; Ditchfield, R.; Newton, M. D.; Pople, J. A. QCPE Program No. 236.

[431] *HyperChem*, Release 6.03 for Windows. Hypercube Inc. Copyright **2000**.

[432] Walker, F. A. In *The Porphyrin Handbook*; Kadish, K. M.; Smith, K. M.; Guilard, R., Eds.; Academic: New York, **2000;** Vol 5, Chapter 36.

[433] Mylrajan, M.; Andersson, L. A.; Sun, J.; Loehr, T. M.; Thomas, C. S.; Sullivan, E.P.; Thomson, M. A.; Long, K. M.; Anderson, O. P.; Strauss, S. H. *Inorg. Chem.* **1995**, *34*, 3953–3963.

[434] Fricker, S. P. *Gold Bulletin* **1996**, *29*, 2, 53–59.

[435] Tiekink, E. R. T. *Crit. Rev. Oncology/Hematology* **2002**, *42*, 225–248.

[436] Champion, G.D.; Graham, G.G.; Ziegler, J.B. *Ballieres Clin. Rheumatol* **1990**, *4*, 491.

[437] Thomas, R. E.; Papandrea, R. A. *Med. J Aust.* **1993**, *158*, 720.

[438] Liu, H.-Q.; Cheung, T.-C.; Peng, S.-M.; Che, C.-M. *J. Chem. Soc. Chem. Commun.* **1995**, 1787–1788.

[439] Shaw, III, C. P. In *Metal Compounds in Cancer Therapy;* Pricker, S. P. Ed.; Chapman and Hall: London, **1994;** pp 46.

[440] Carotti, S.; Guerri, A.; Mazzei, T.; Messori, L.; Mini, E.; Orioli, P. *Inorg. Chim. Acta* **1998**, *128*, 90–94.

[441] Calamai P.; Guerri, A.; Messori, L.; Orioli, P.; Speroni, G. P. *Inorg. Chim. Acta* **1999**, *285*, 309–312.

[442] Rossignoli, M.; Bernhardt, P. V.; Lawrance, G. A.; Maeder, M. *J. Chem. Soc. Dalton Trans.* **1997**, 323–327.

[443] Sadler, P. J.; Sue, R. E. *Metal-based Drugs 1* **1994**, 107.

[444] Dar, A.; Moss, K.; Cottrill, S. M.; Parish, R. V.; McAuliffe, C. A.; Pritchard, R. G.; Beagley, B.; Sandbank, J. *J. Chem. Soc. Dalton Trans.* **1992**, 1907–1913.

[445] Cinellu, M. A.; Minghetti, G.; Pinna, M. V.; Stoccoro, S.; Zucca, A.; Manassero, M. *J. Chem. Soc. Dalton Trans.* **2002**, 1261–1265.

[446] Guo, Z.; Sadler, P. J. *Angew. Chem., Int. Ed.* **1999**, *38*, 1512.

[447] Keppler, B.K. In *Metal Complexes in Cancer Chemotherapy* Holler, B.K. Ed.; VCH: Weinheim, **1993**; pp 37.

[448] Parish, R. V.; Howe, B.P.; Wright, J .P.; Mack, J.; Pritchard, R.G.; Buckley, R.G.; Elsome , A. M.; Pricker, S. P. *Inorg. Chem.* **1996**, *35*, 1659.

[449] Schacter, A. M.; Fleischer, E. B.; Haltiwanger, R. C. *Acta Crystallogr., Sect.C: Cryst. Struct. Commun.* **1987**, *C43*, 1876.

[450] Zhong, Z. J.; Nishida, Y.; Okawa, H.; Kida, S. *Mem. Fac. Sci. Kyushu U., Ser. C* **1987**, *16*, 19.

[451] Che, C. Patent No. WO 2004024146, Kind A1, **2004**. Laster, B. H.; Shani, G.; Faraggi, M.; Golan, Y. Patent No. WO 2003063757, Kind A2, **2003**.

[452] Gibbs, E. J. ; Maurer, M. C.; Zhang, J. H.; Reiff, W. M.; Hill, D. T.; Malicka-Blaszkiewicz, M.; McKinnie, R. E.; Liu, H. Q.; Pasternack, R. F. *J. Inorg. Biochem.* **1988**, *32*, 39.

[453] Barnholtz, S. L.; Lydon, J. D.; Huang, G.; Venkatesh, M.; Barnes, C. L.; Ketring, A. R.; Jurisson, S. S. *Inorg. Chem.* **2001**, *40,* 972–976.

[454] Migita, K.; La Mar, G. N. *J. Phys. Chem.* **1980**, *84*, 2953–2957.

[455] Abraham, R. J.; Rowan, A. E.; Smith, N. W.; Smith, K. M. *J. Chem. Soc. Perkin Trans.* 2 **1993**, 1047–1059.

[456] Munro, O. Q.; Marques, H. M. *Inorg. Chem.* **1996**, *35*, 3768–3779.

APPENDIX A

A1 – Conversions

Energy conversions:

All DFT-calculated energies are given in Hartrees in the computational output data files. They are then converted to electron volts (eV) by convention.

1 Hartree = 27.211 eV

APPENDIX B

Appendix B1

Figure B1-1: UV-vis spectrum of $H_2T(iBu)P$.

Figure B1-2: UV-vis spectrum of $H_2T(CH_2Ph)P$.

Figure B1-3: UV-vis spectrum of $H_2T(iPent)P$.

Figure B1-4: UV-vis spectrum of $H_2T(CHPh_2)P$.

Figure B1-5: UV-vis spectrum of $H_2T(iPr)P$.

Figure B1-6: UV-vis spectrum of $H_2T(cyHx)P$.

Appendix B2

Figure B2-1: IR spectrum of $H_2T(iBu)P$.

Figure B2-2: IR spectrum of $H_2T(CH_2Ph)P$.

Figure B2-3: IR spectrum of $H_2T(iPent)P$.

Figure B2-4: IR spectrum of $H_2T(CHPh_2)P$.

Figure B2-5: IR spectrum of $H_2T(iPr)P$.

Figure B2-6: IR spectrum of $H_2T(cyHx)P$.

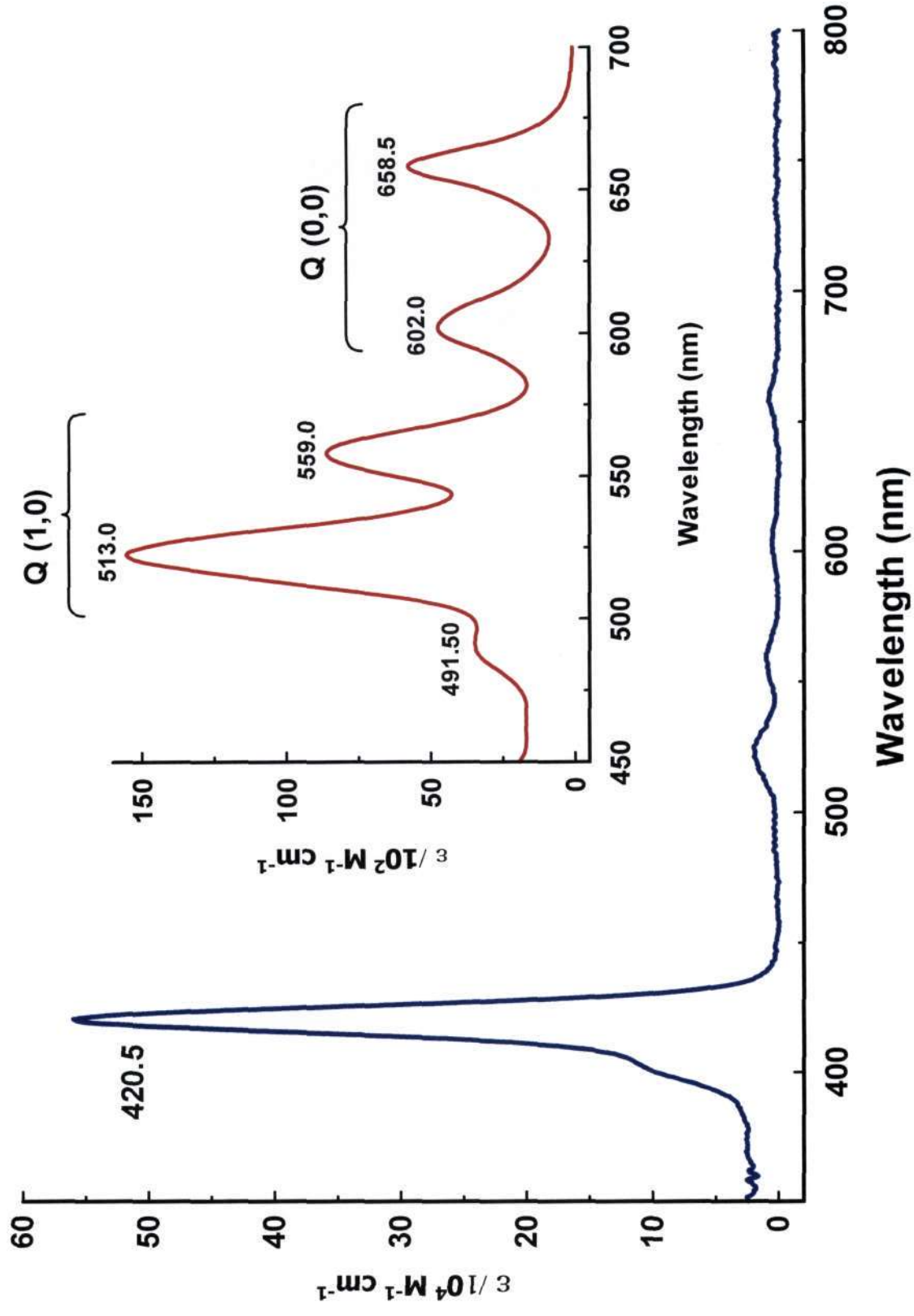

Figure B1-1: UV-vis spectrum of $H_2T(iBu)P$.

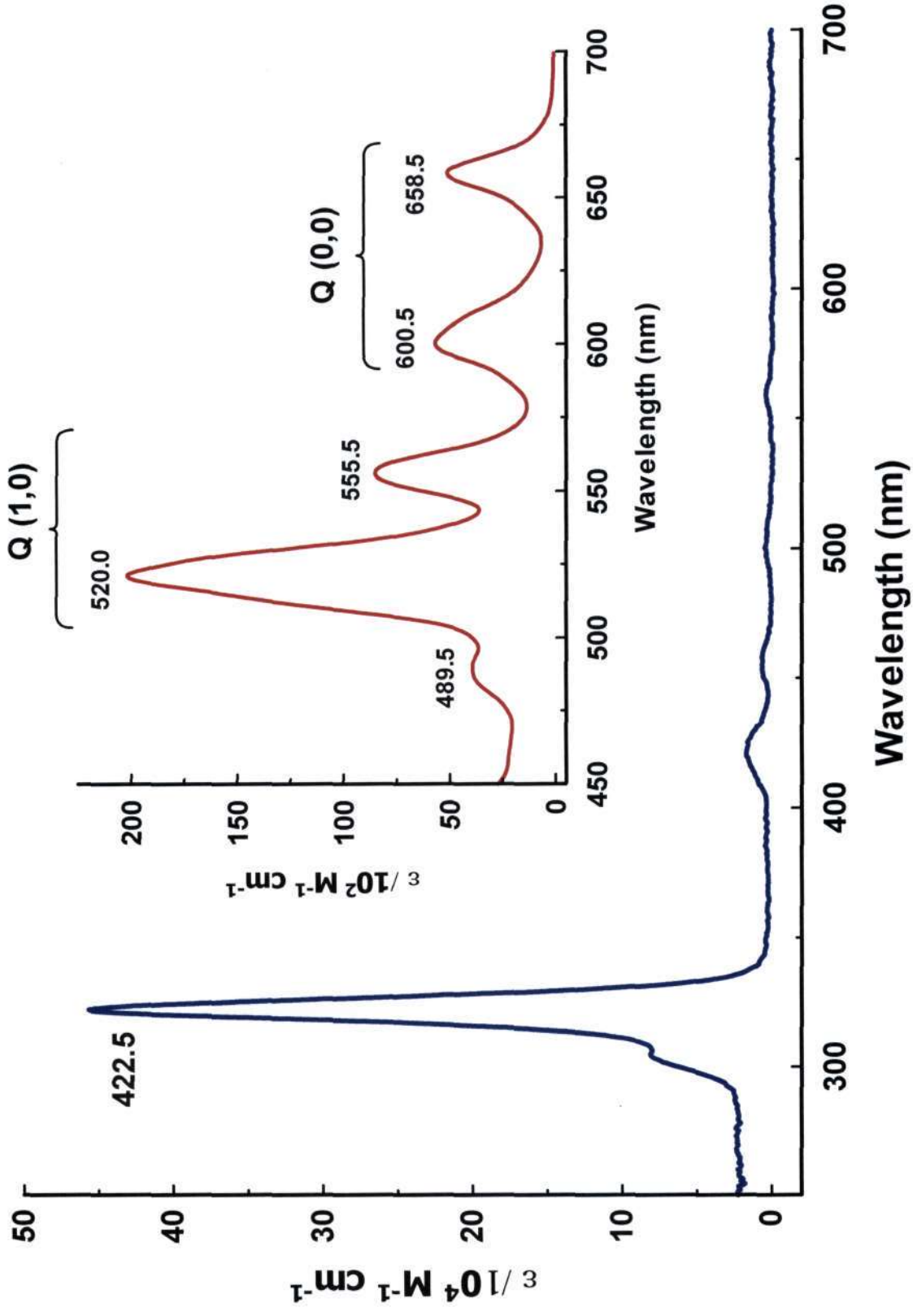

Figure B1-2: UV-vis spectrum of $H_2T(CH_2Ph)P$.

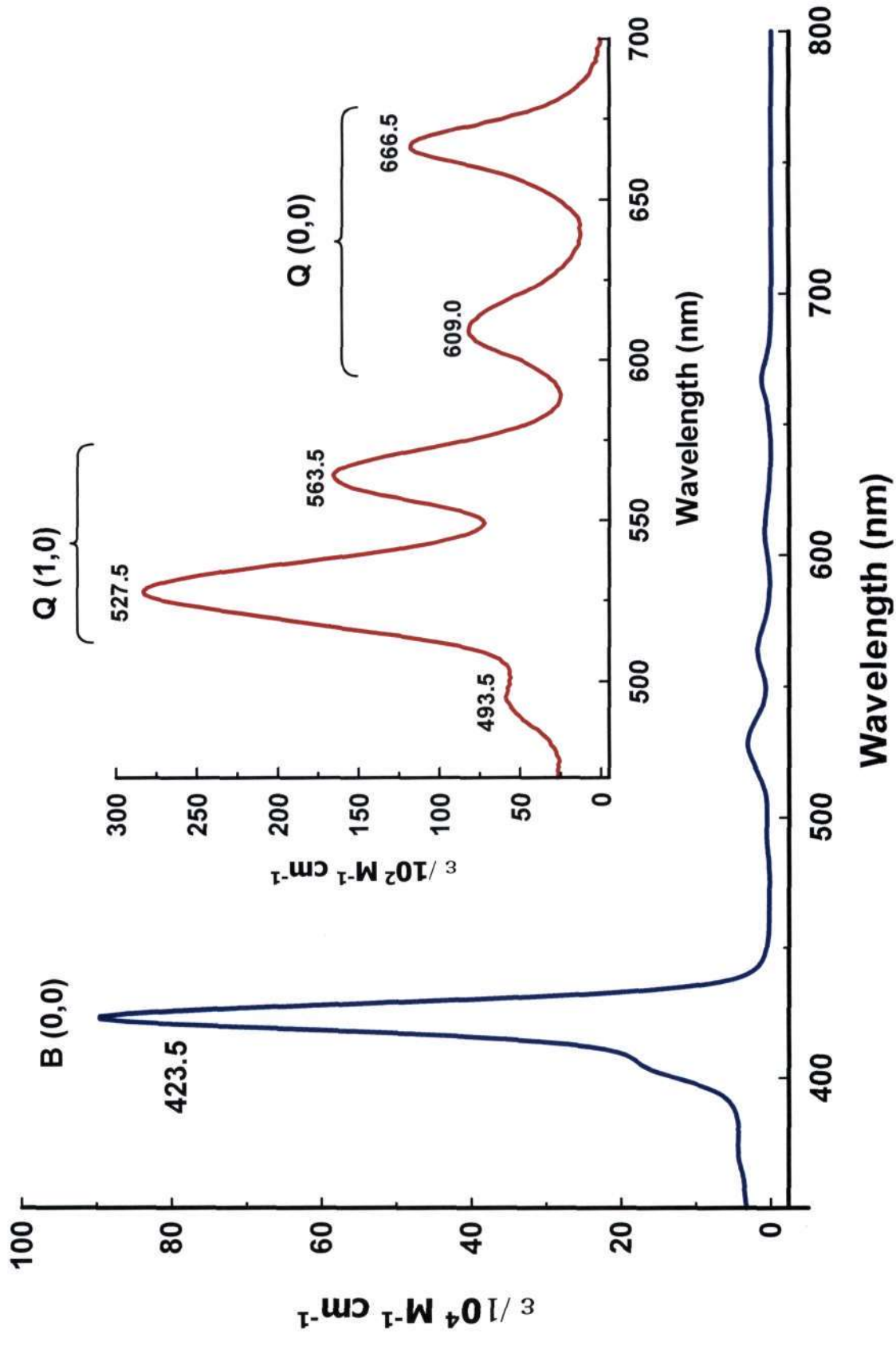

Figure B1-3: UV-vis spectrum of $H_2T(iPent)P$.

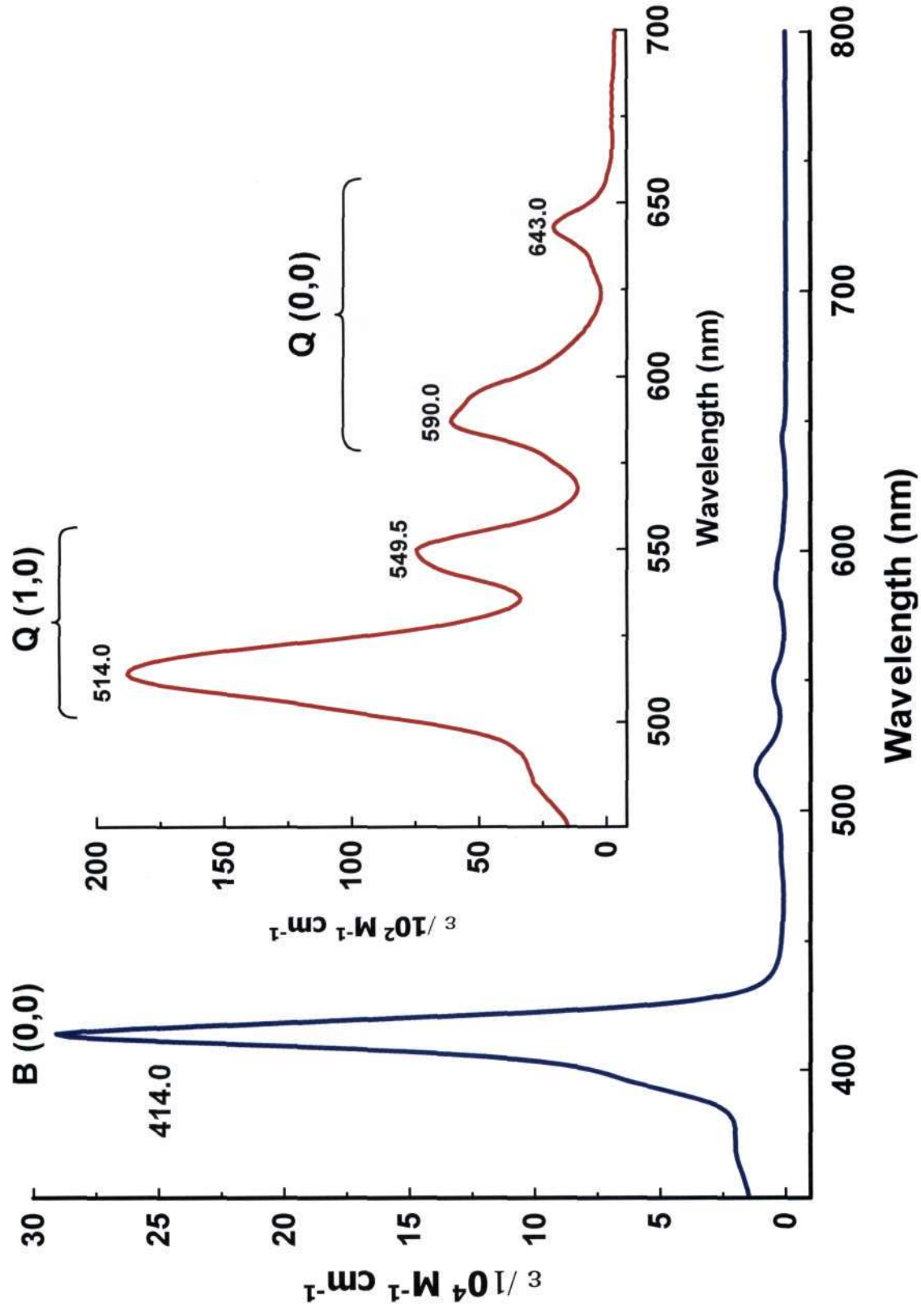

Figure B1-4: UV-vis spectrum of $H_2T(CHPh_2)P$.

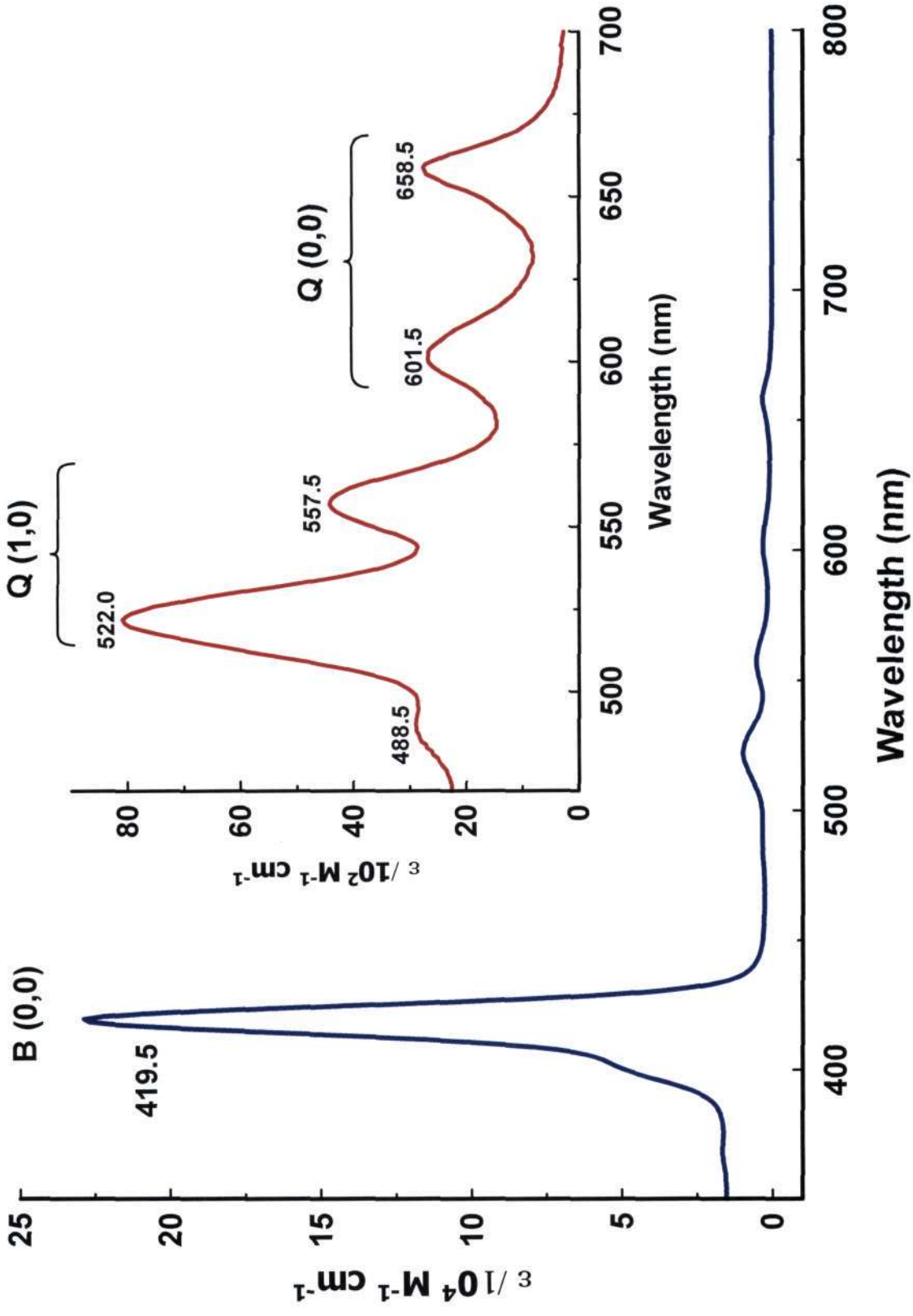

Figure B1-5: UV-vis spectrum of $H_2T(iPr)P$.

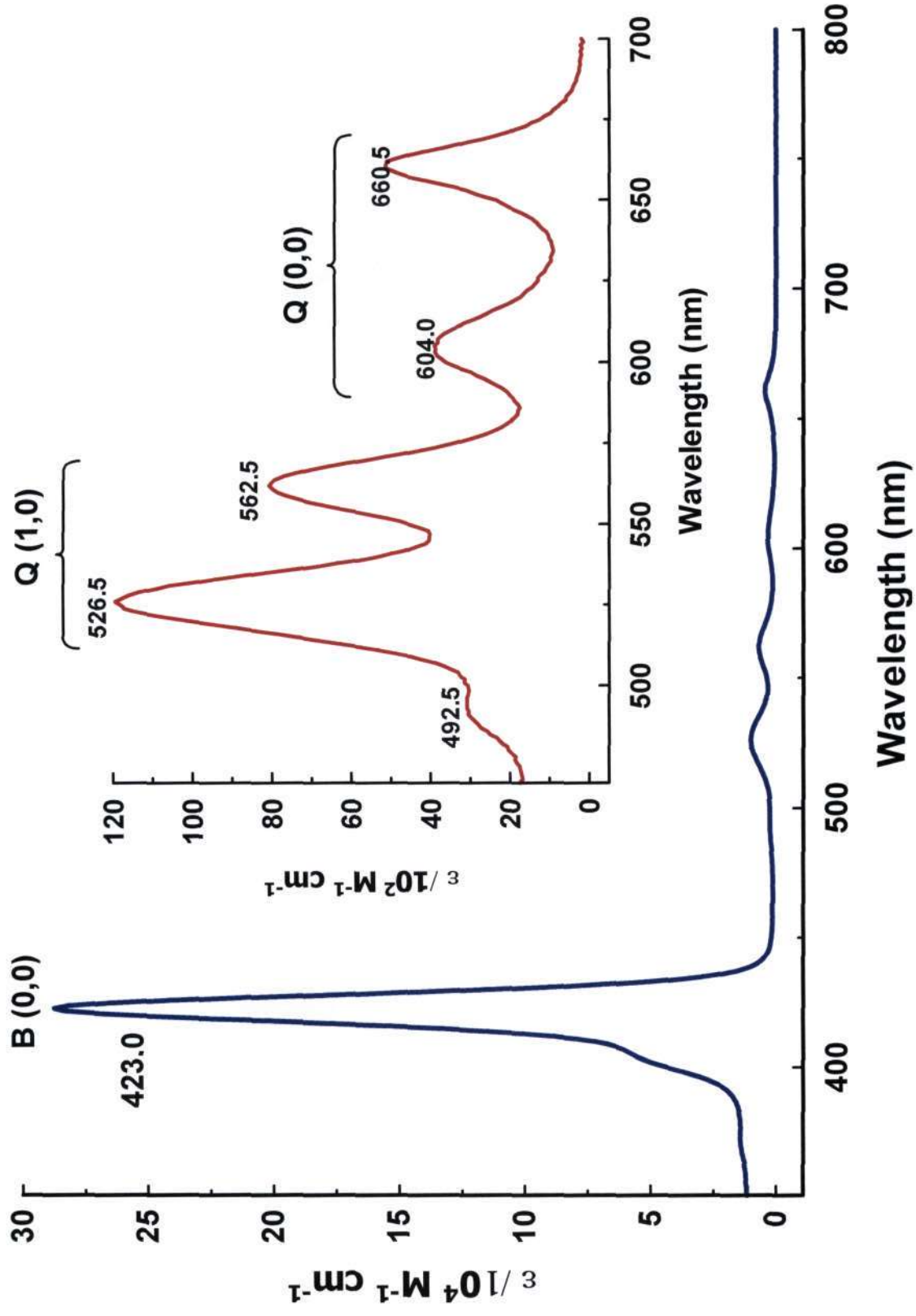

Figure B1-6: UV-vis spectrum of $H_2T(cyHx)P$.

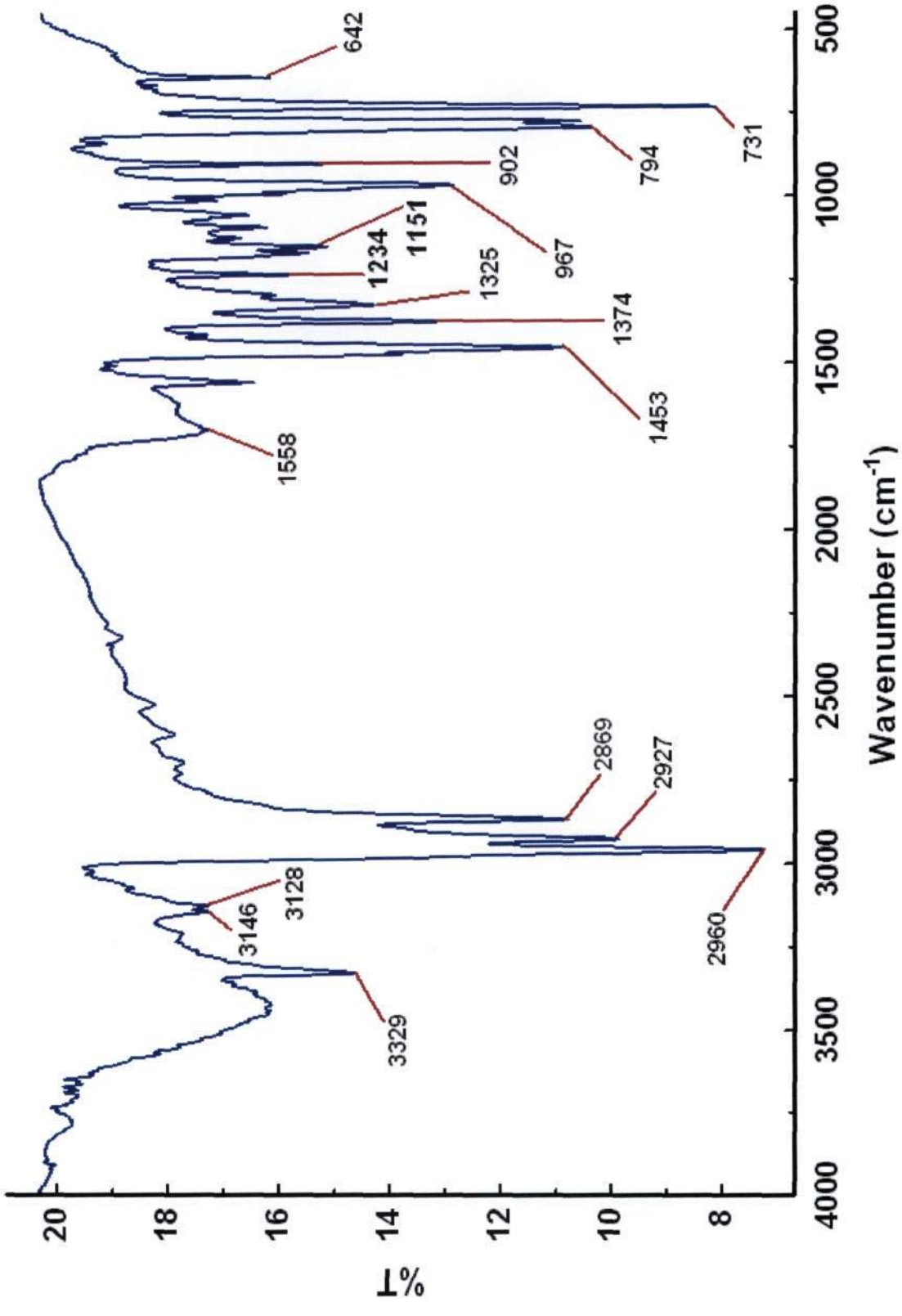

Figure B2-1: IR spectrum of $H_2T(iBu)P$.

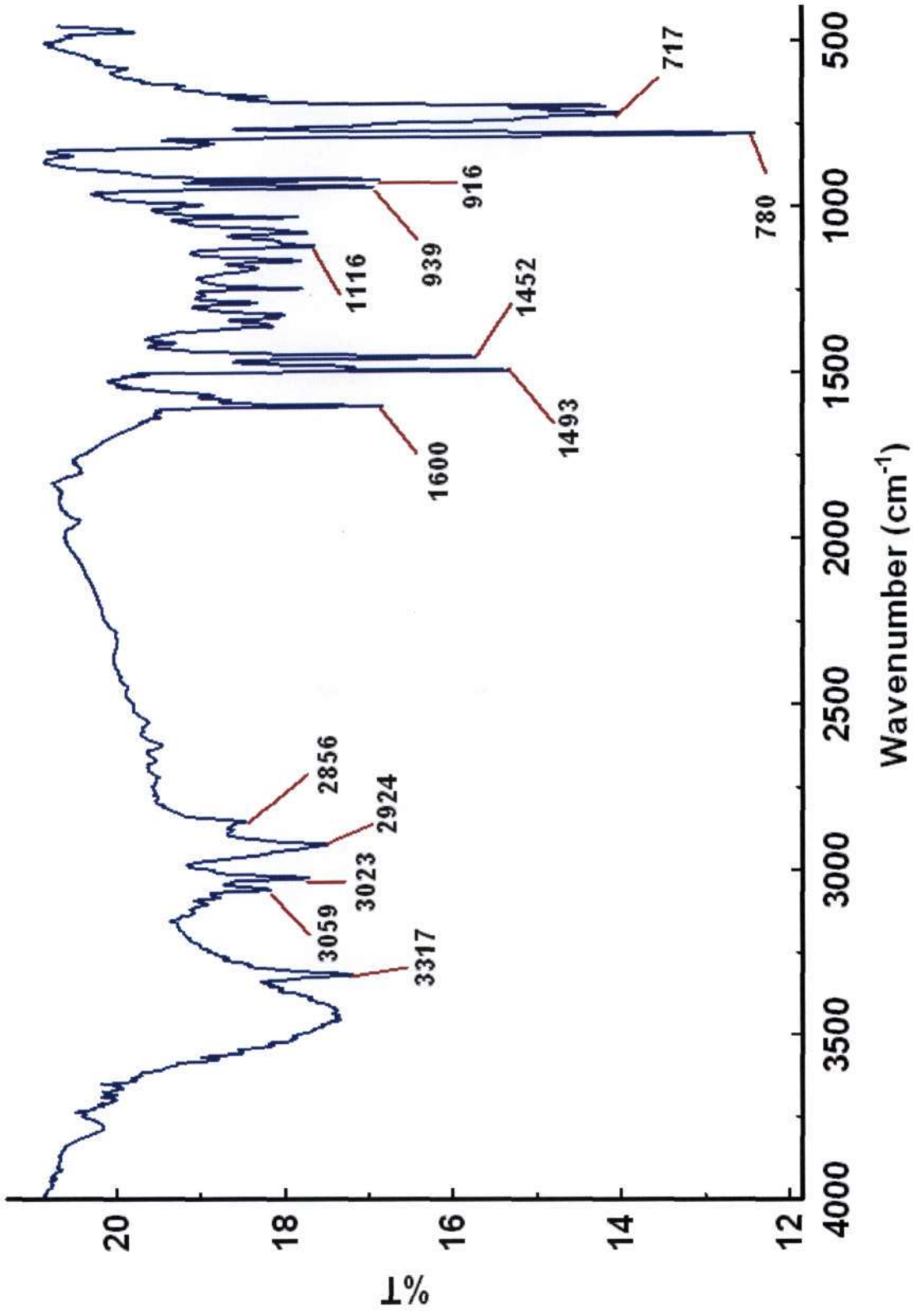

Figure B2-2: IR spectrum of $H_2T(CH_2Ph)P$.

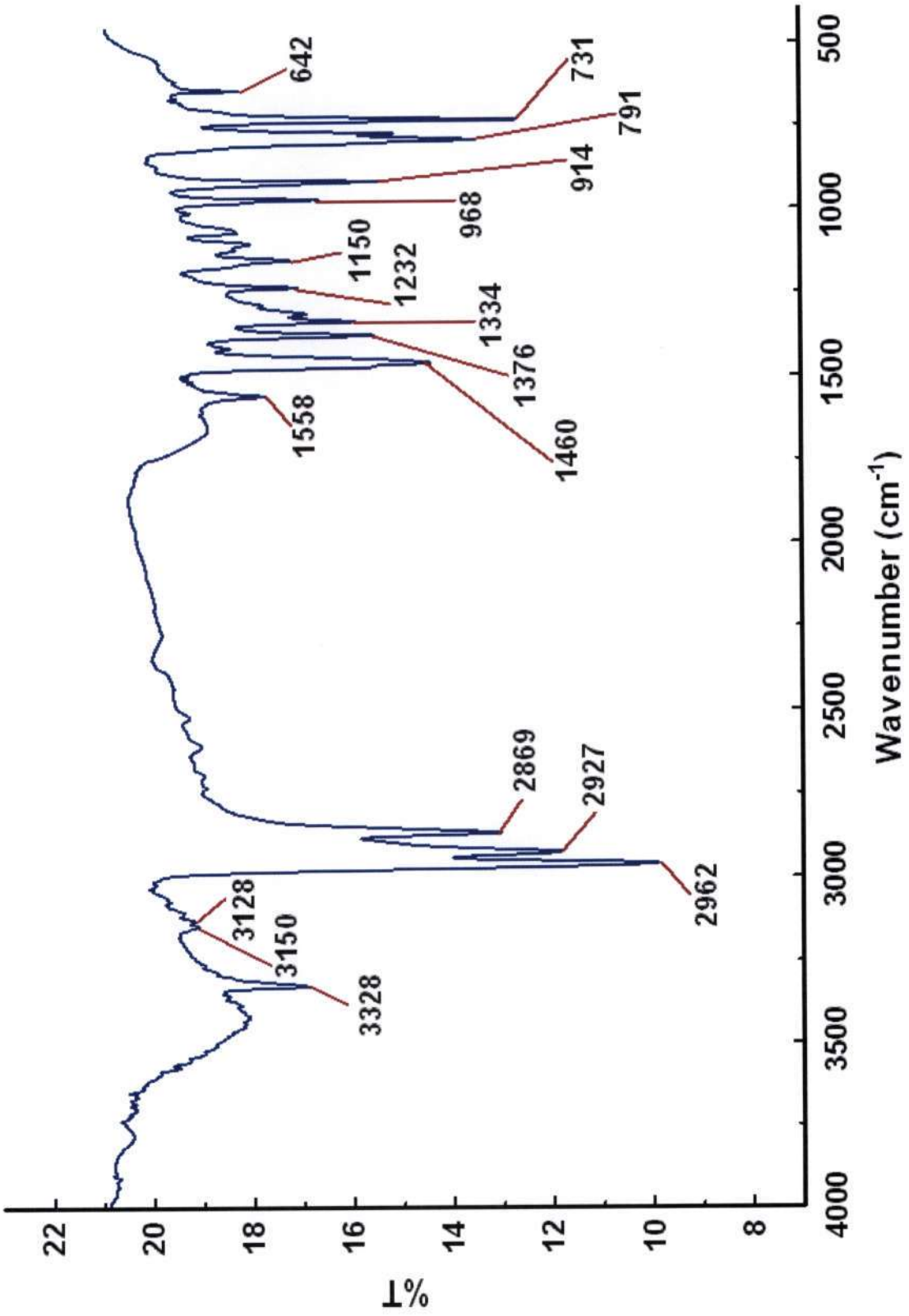

Figure B2-3: IR spectrum of $H_2T(iPent)P$.

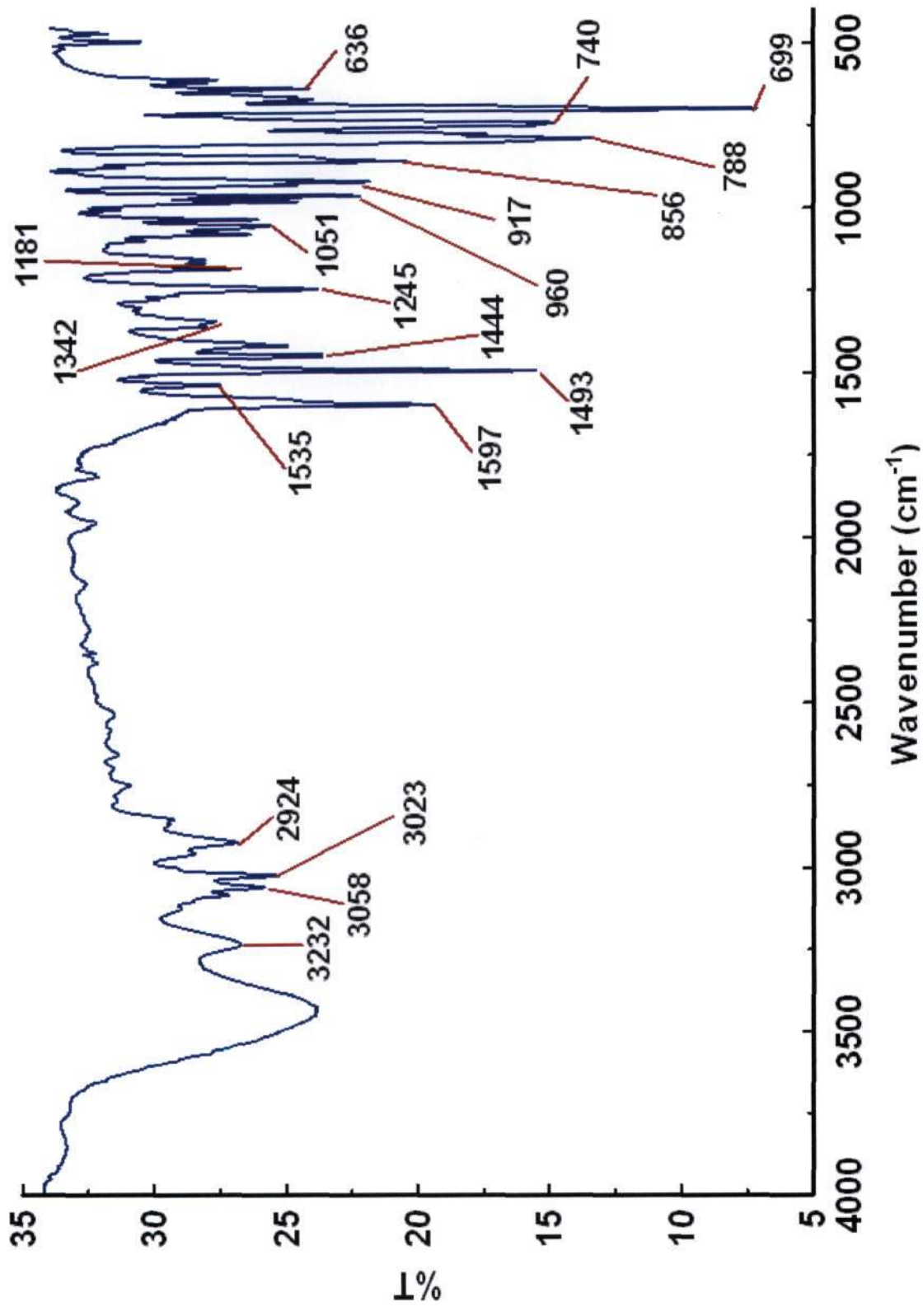

Figure B2-4: IR spectrum of $H_2T(CHPh_2)P$.

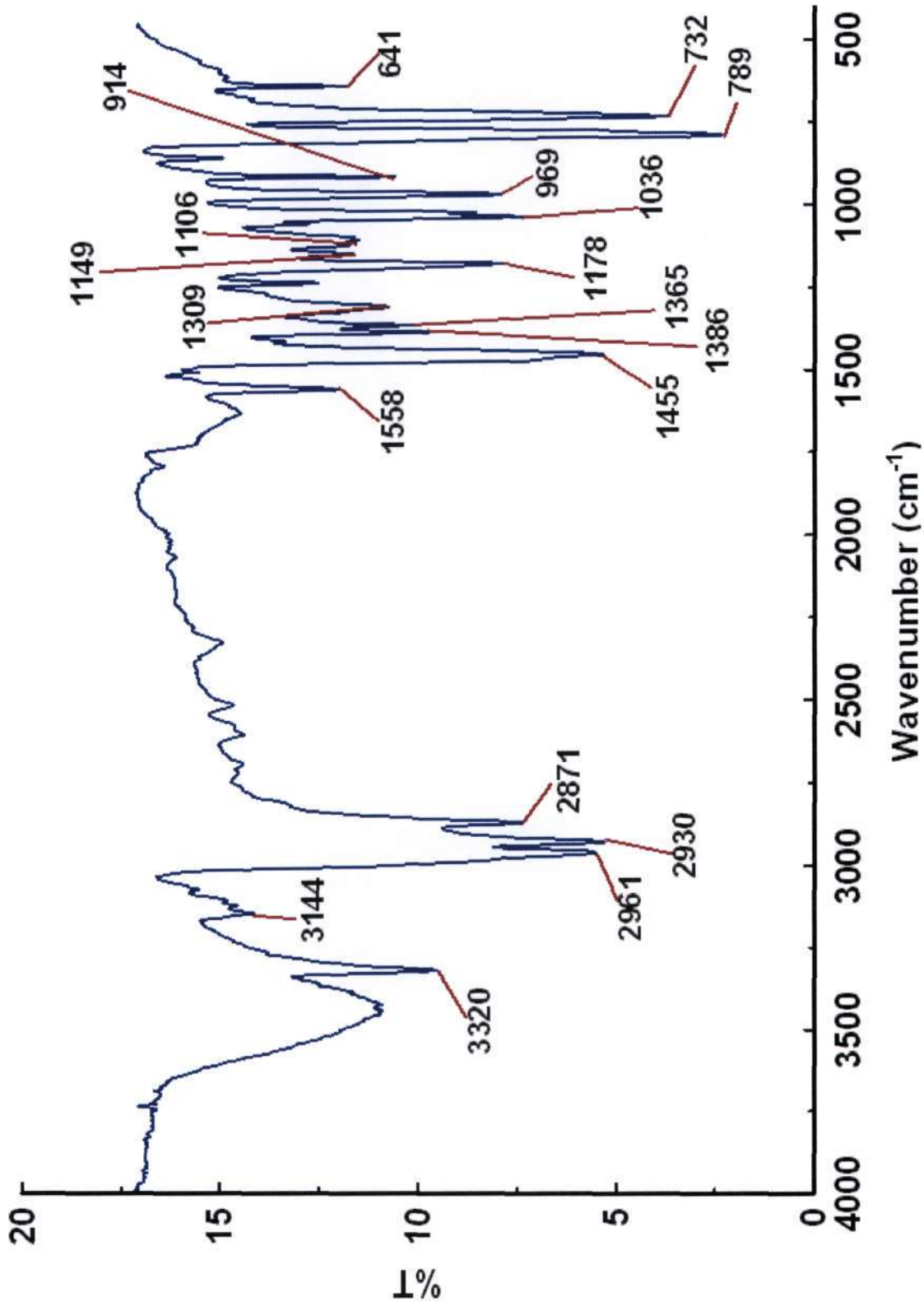

Figure B2-5: IR spectrum of $H_2T(iPr)P$.

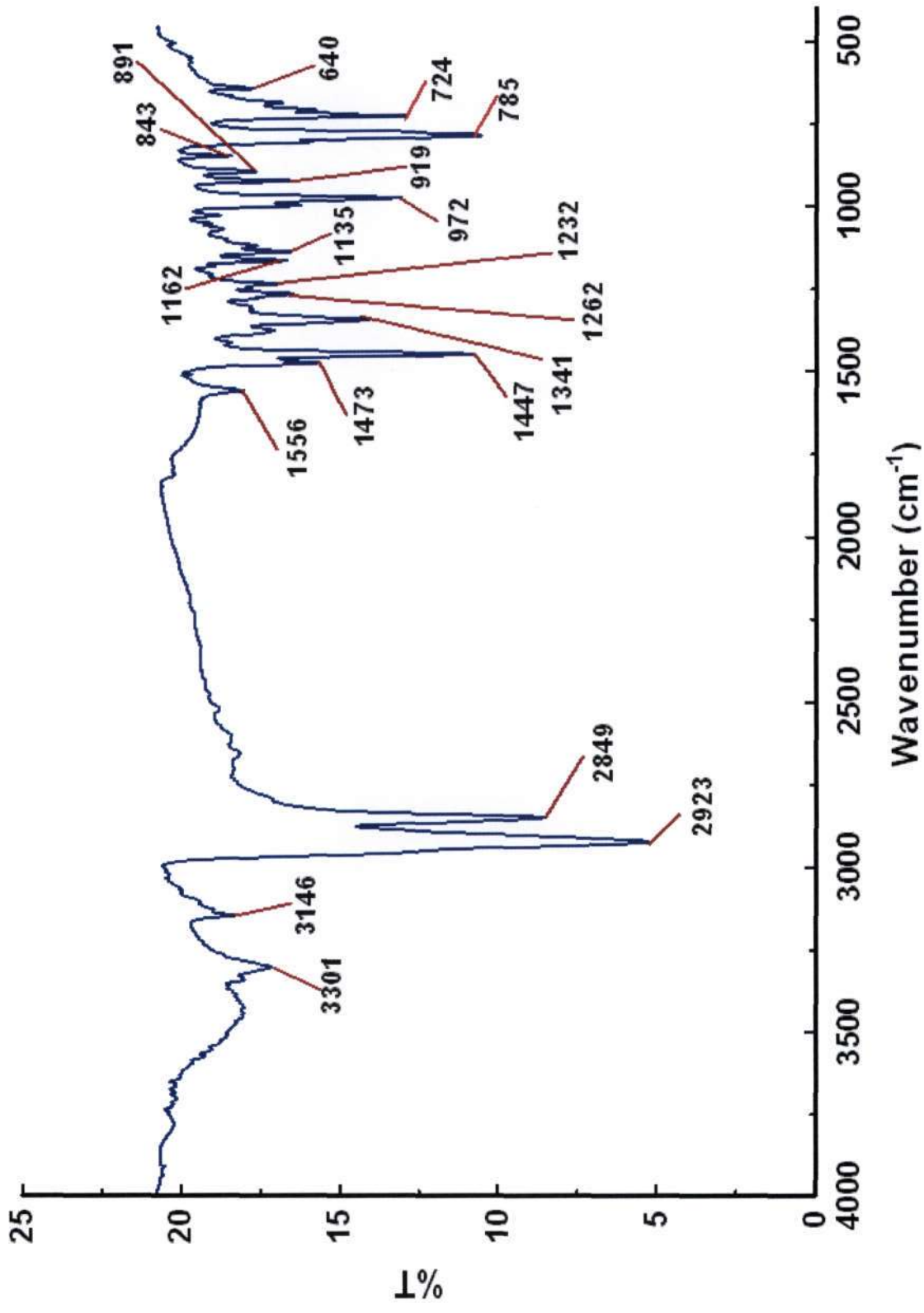

Figure B2-6: IR spectrum of $H_2T(cyHx)P$.

APPENDIX C

Appendix C1

Figure C1-1: COSY spectrum for $H_2T(iBu)P$.

Figure C1-2: HSQC spectrum for $H_2T(iBu)P$.

Figure C1-3: DEPT spectrum for $H_2T(iBu)P$.

Appendix C2

Figure C2-1: COSY spectrum for $H_2T(CH_2Ph)P$.

Figure C2-2: HSQC spectrum for $H_2T(CH_2Ph)P$.

Appendix C3

Figure C3-1: COSY spectrum for $H_2T(iPent)P$.

Figure C3-2: HSQC spectrum for $H_2T(iPent)P$.

Figure C3-3: DEPT spectrum for $H_2T(iPent)P$.

Appendix C4

Figure C4-1: COSY spectrum for $H_2T(CHPh_2)P$.

Figure C4-2: HSQC spectrum for $H_2T(CHPh_2)P$.

Appendix C5

Figure C5-1: COSY spectrum for $H_2T(iPr)P$.

Figure C5-2: HSQC spectrum for $H_2T(iPr)P$.

Appendix C6

Figure C6-1: COSY spectrum for $H_2T(cyHx)P$.

Figure C6-2: HSQC spectrum for $H_2T(cyHx)P$.

Figure C6-3: DEPT spectrum for $H_2T(cyHx)P$.

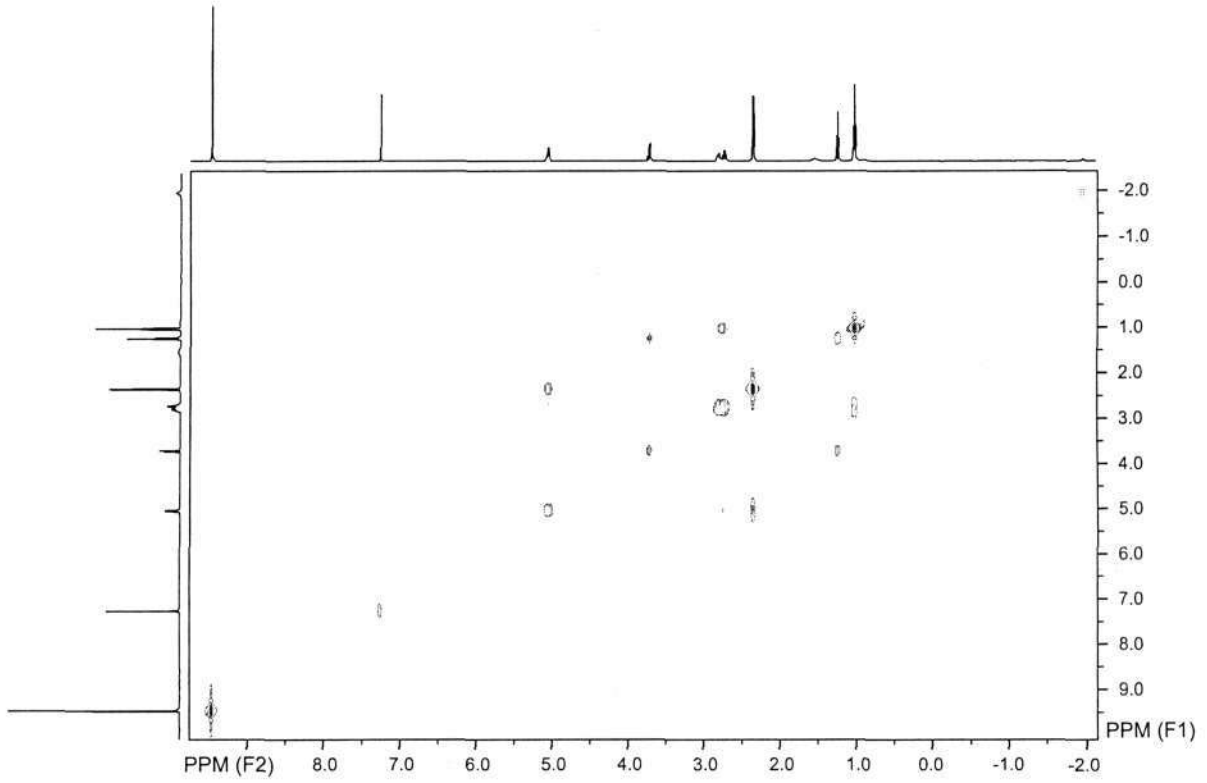

Figure C1-1: COSY spectrum for $H_2T(iBu)P$.

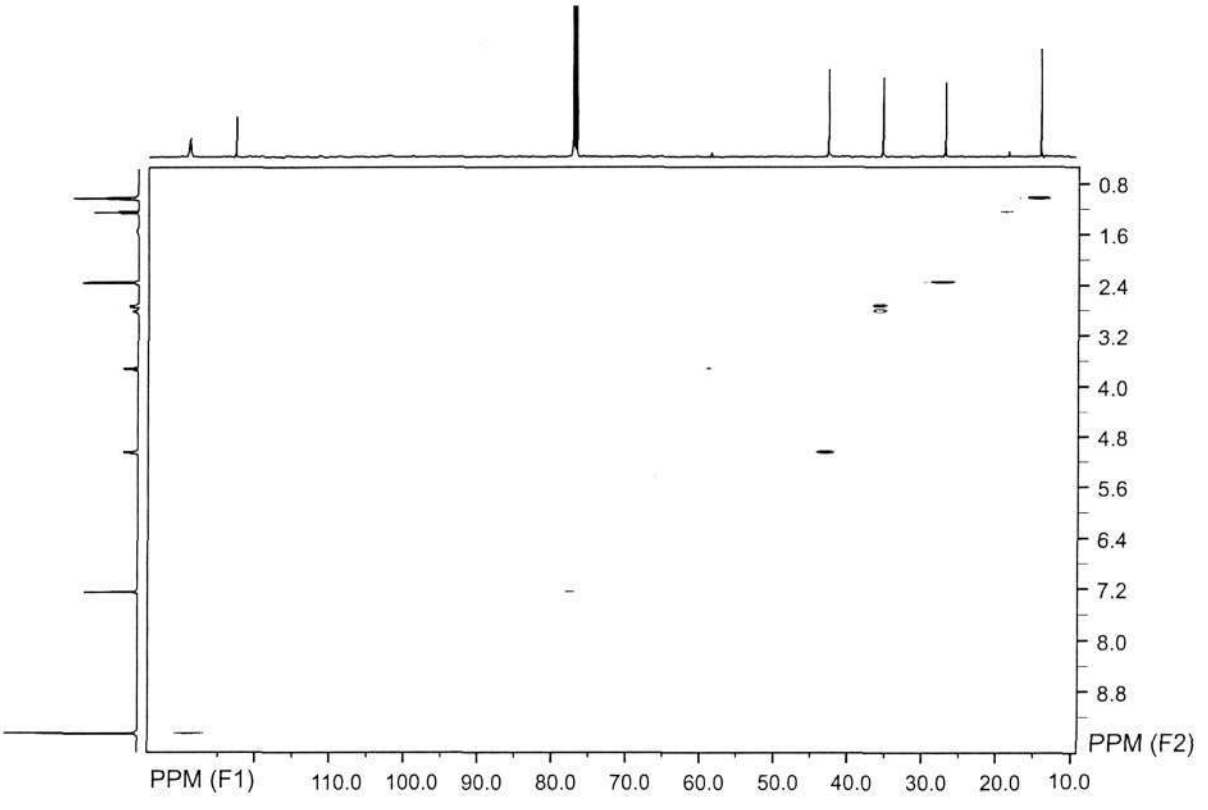

Figure C1-2: HSQC spectrum for $H_2T(iBu)P$.

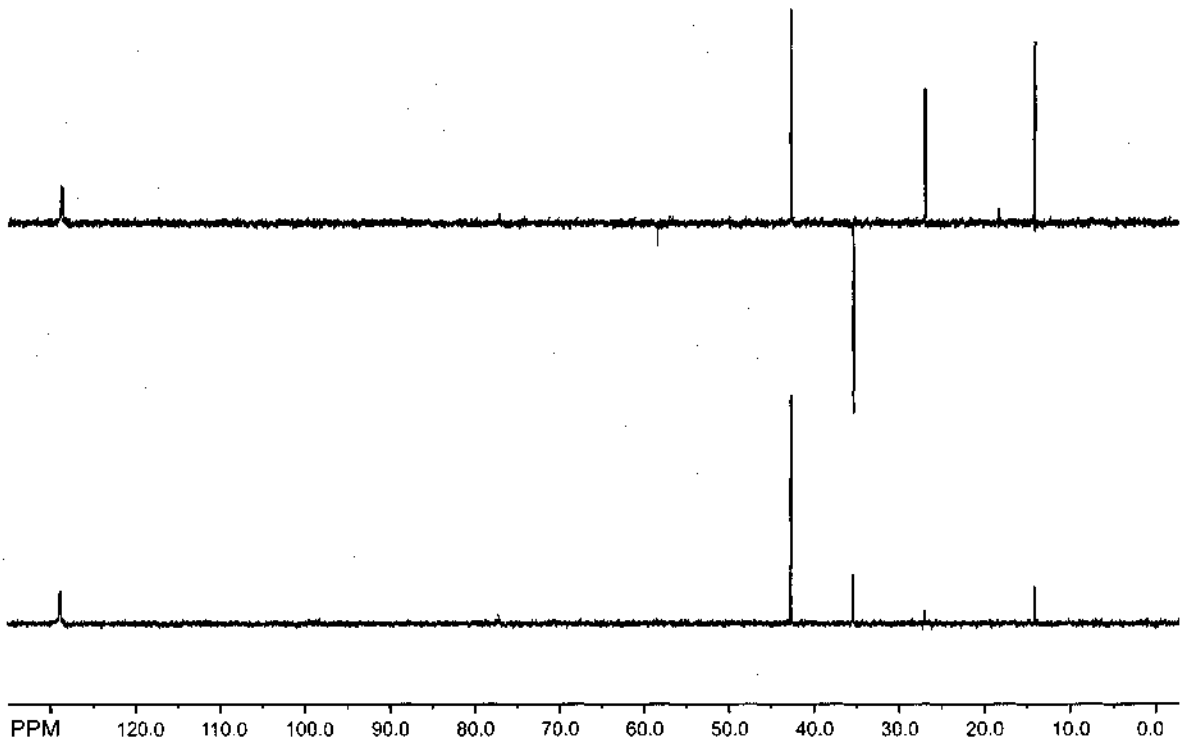

Figure C1-3: DEPT spectrum for $H_2T(iBu)P$.

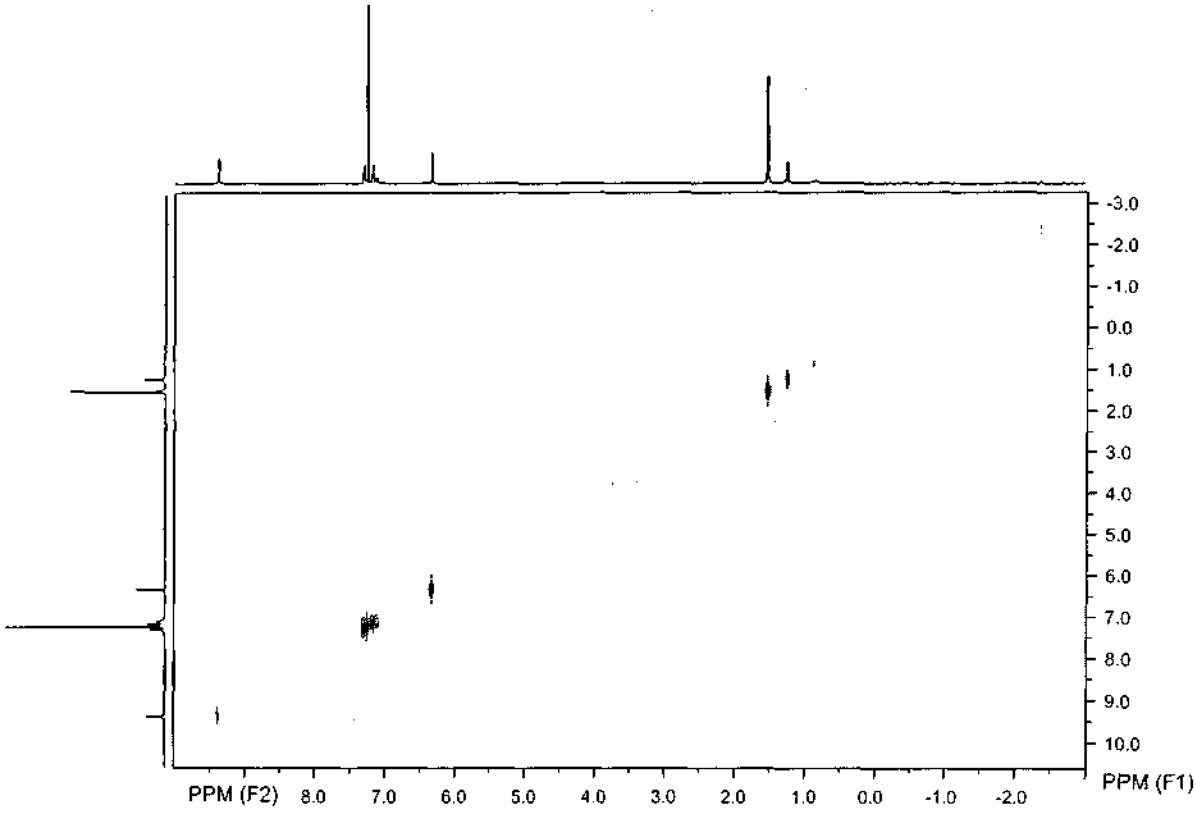

Figure C2-1: COSY spectrum for $H_2T(CH_2Ph)P$.

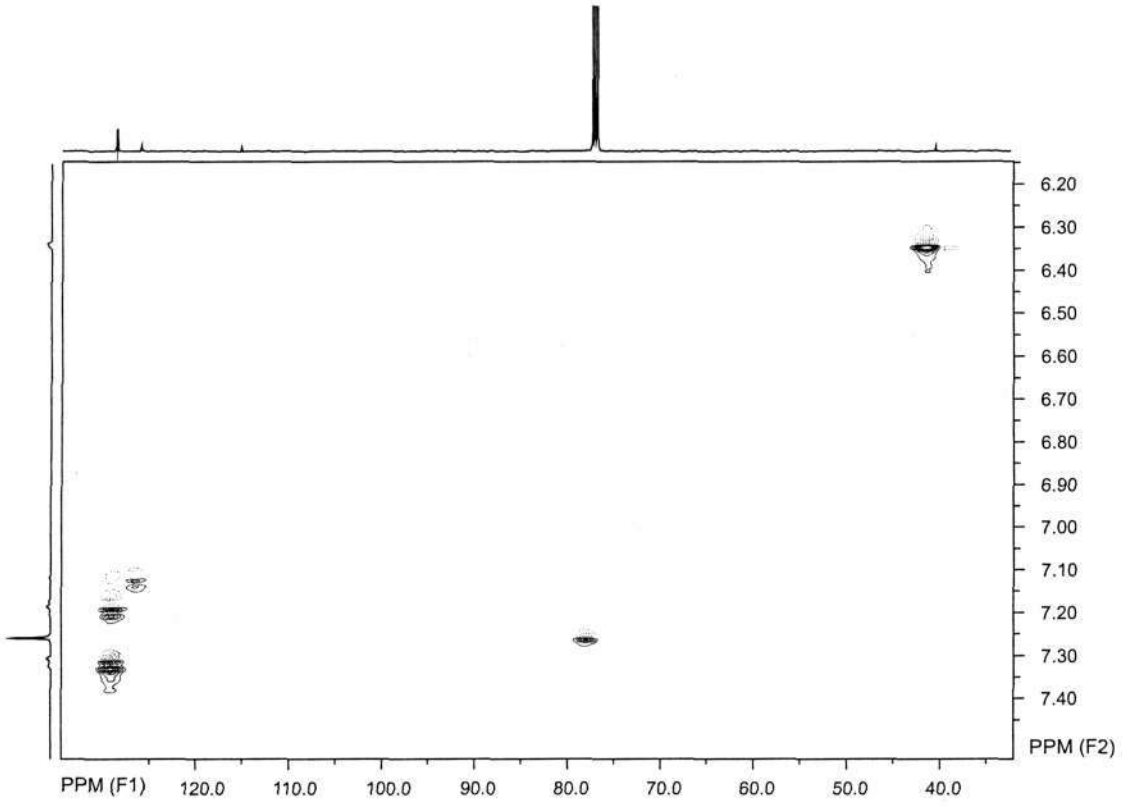

Figure C2-2: HSQC spectrum for $H_2T(CH_2Ph)P$.

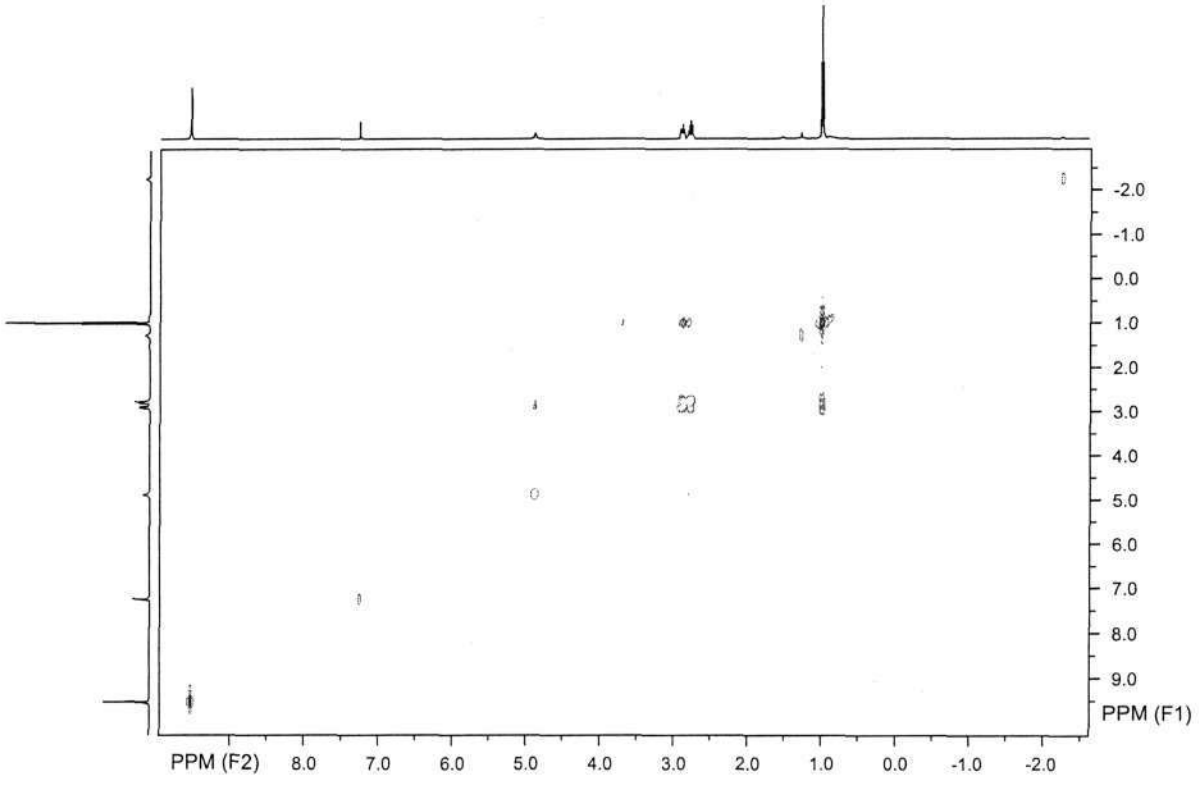

Figure C3-1: COSY spectrum for $H_2T(iPent)P$.

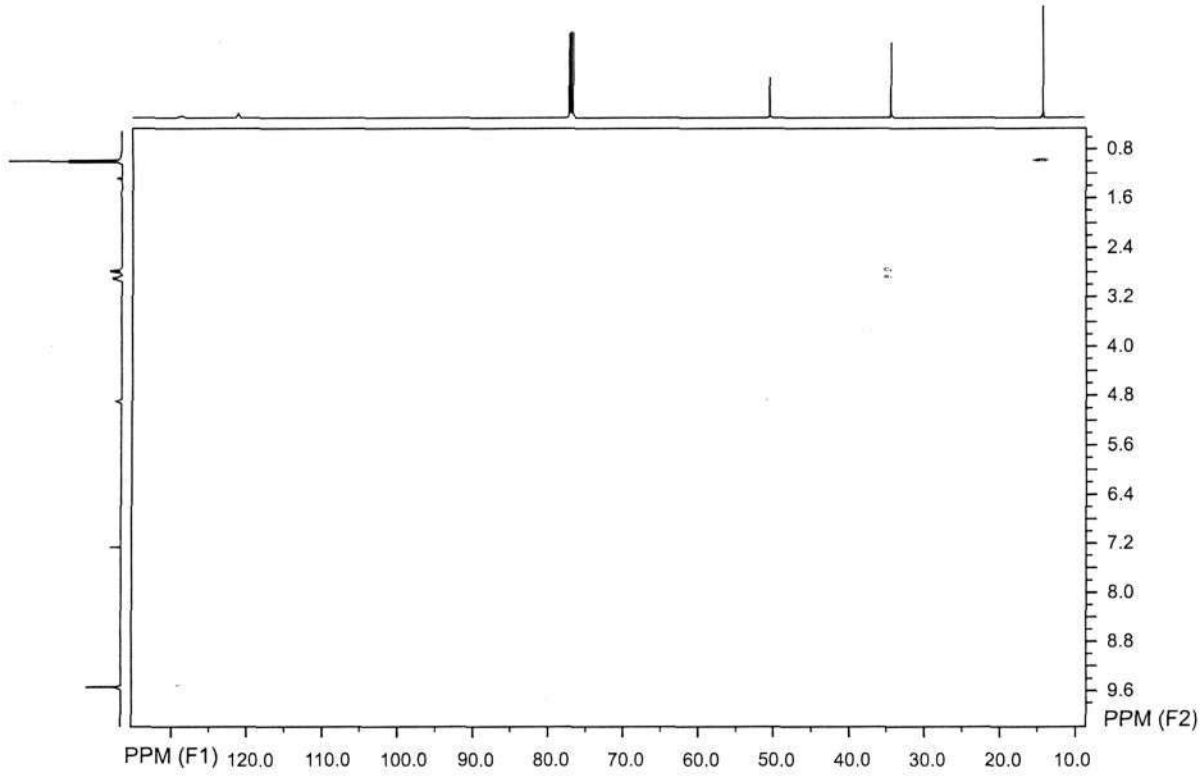

Figure C3-2: HSQC spectrum for H_2T(iPent)P.

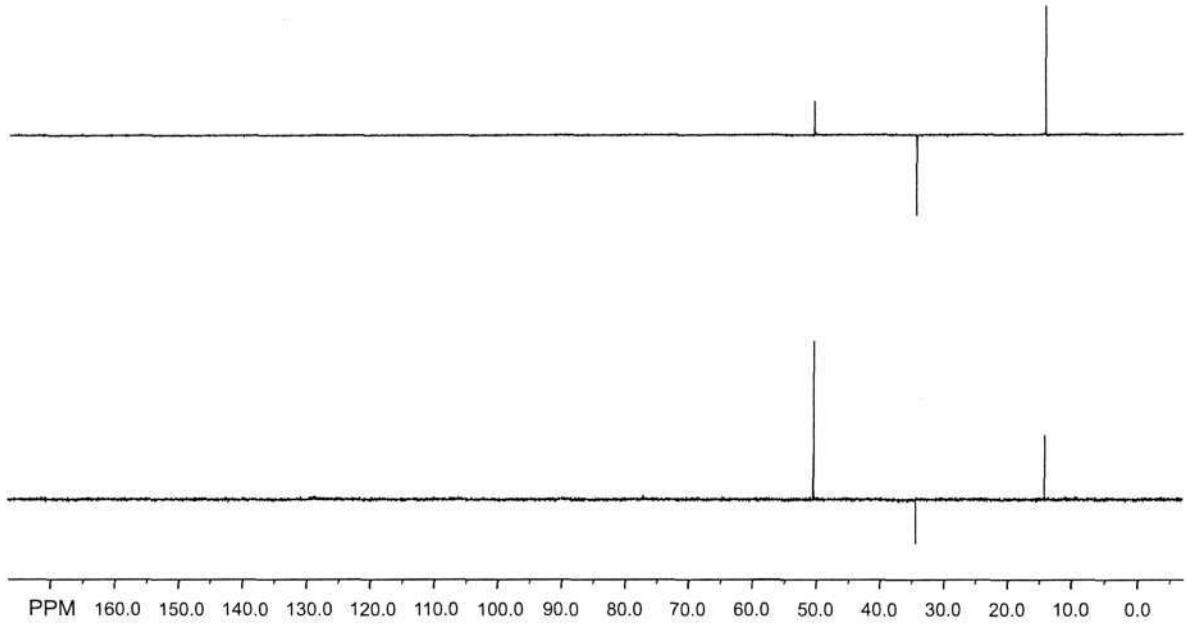

Figure C3-3: DEPT spectrum for H_2T(iPent)P.

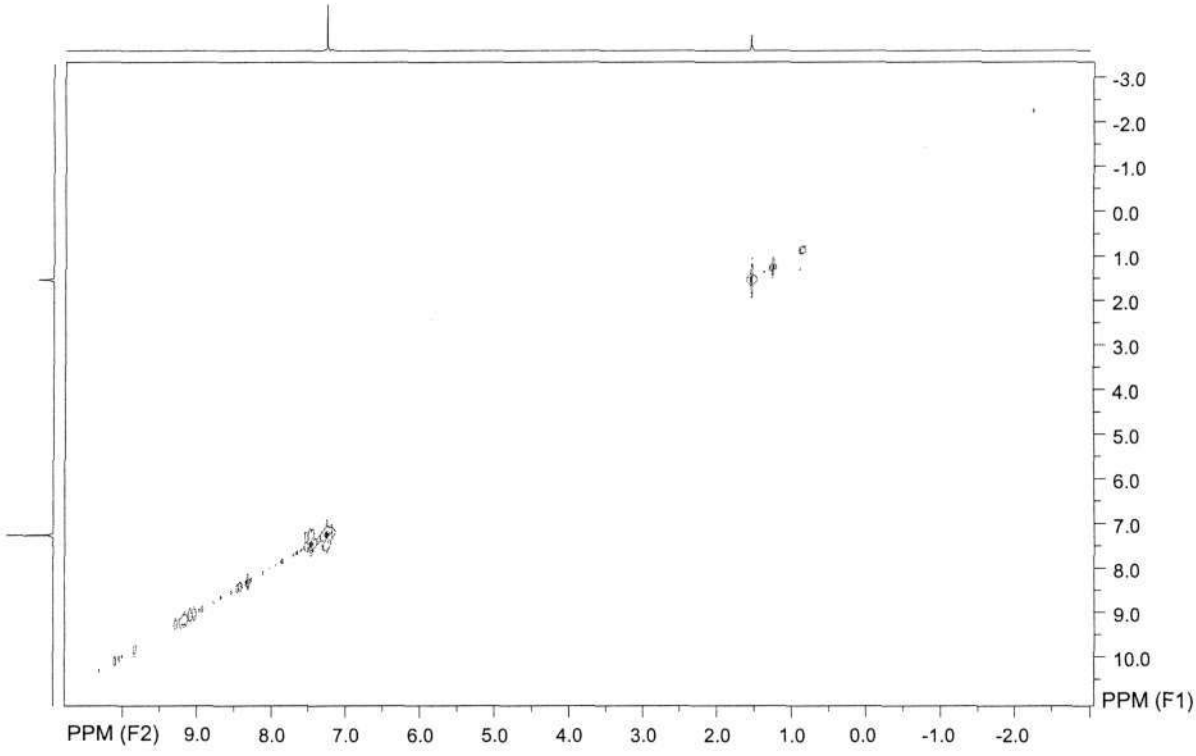

Figure C4-1: COSY spectrum for $H_2T(CHPh_2)P$.

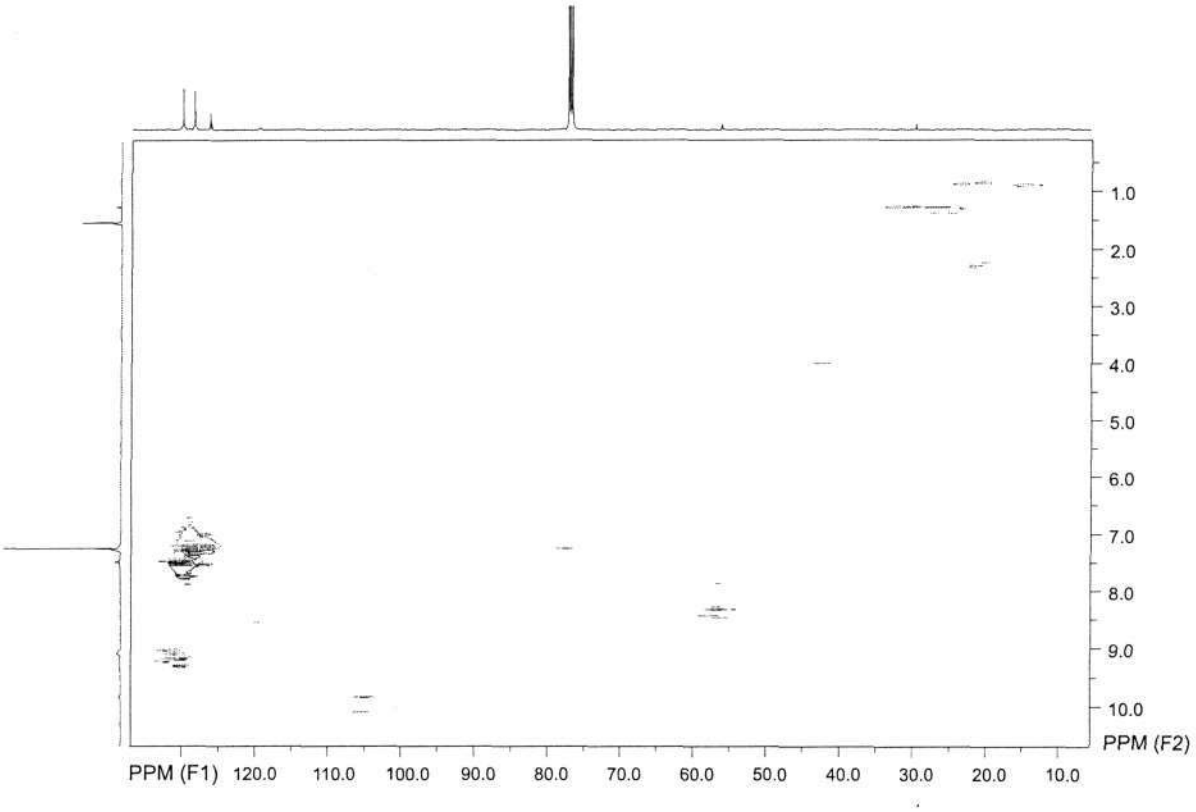

Figure C4-2: HSQC spectrum for $H_2T(CHPh_2)P$.

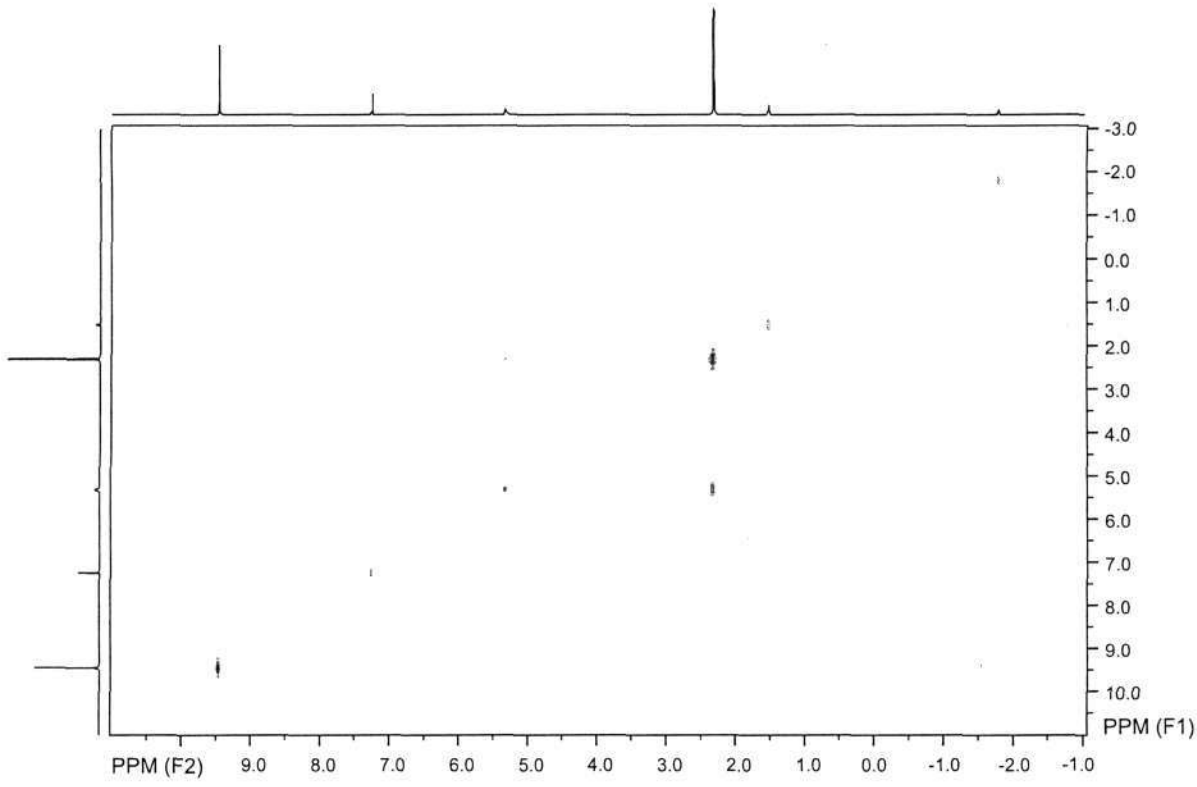

Figure C5-1: COSY spectrum for $H_2T(iPr)P$.

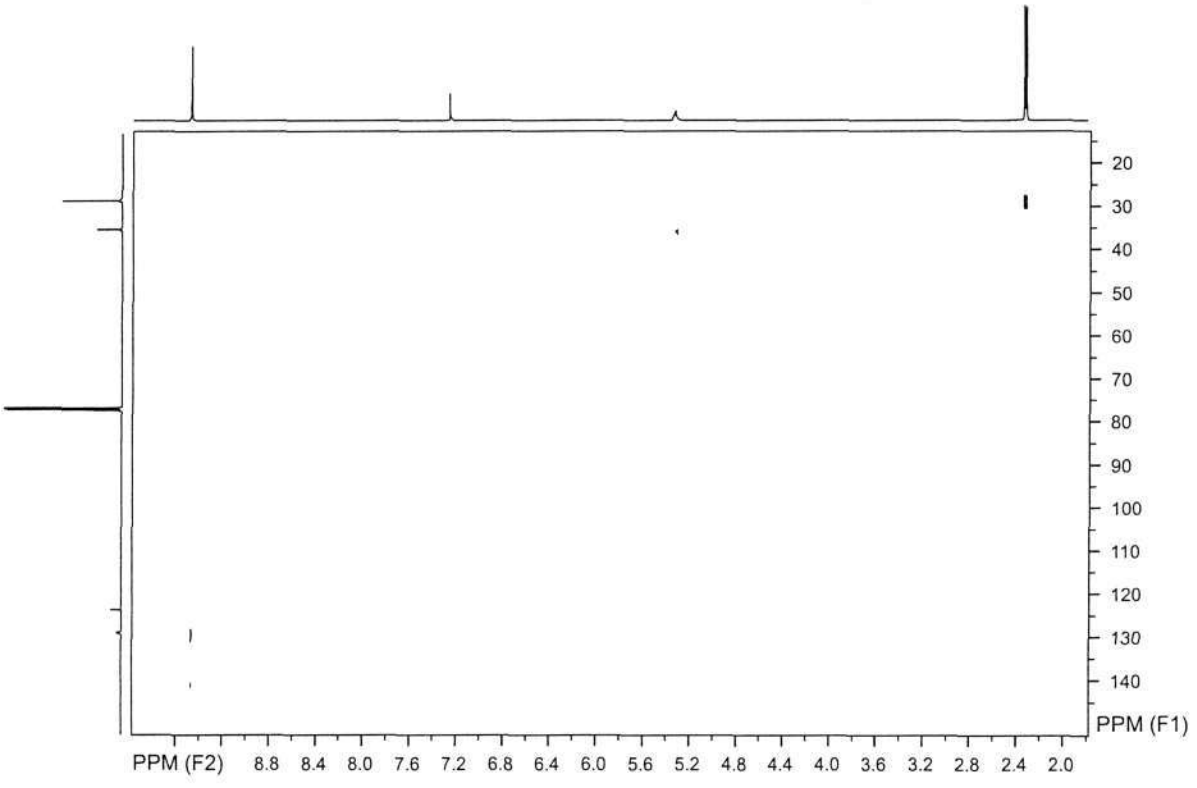

Figure C5-2: HSQC spectrum for $H_2T(iPr)P$.

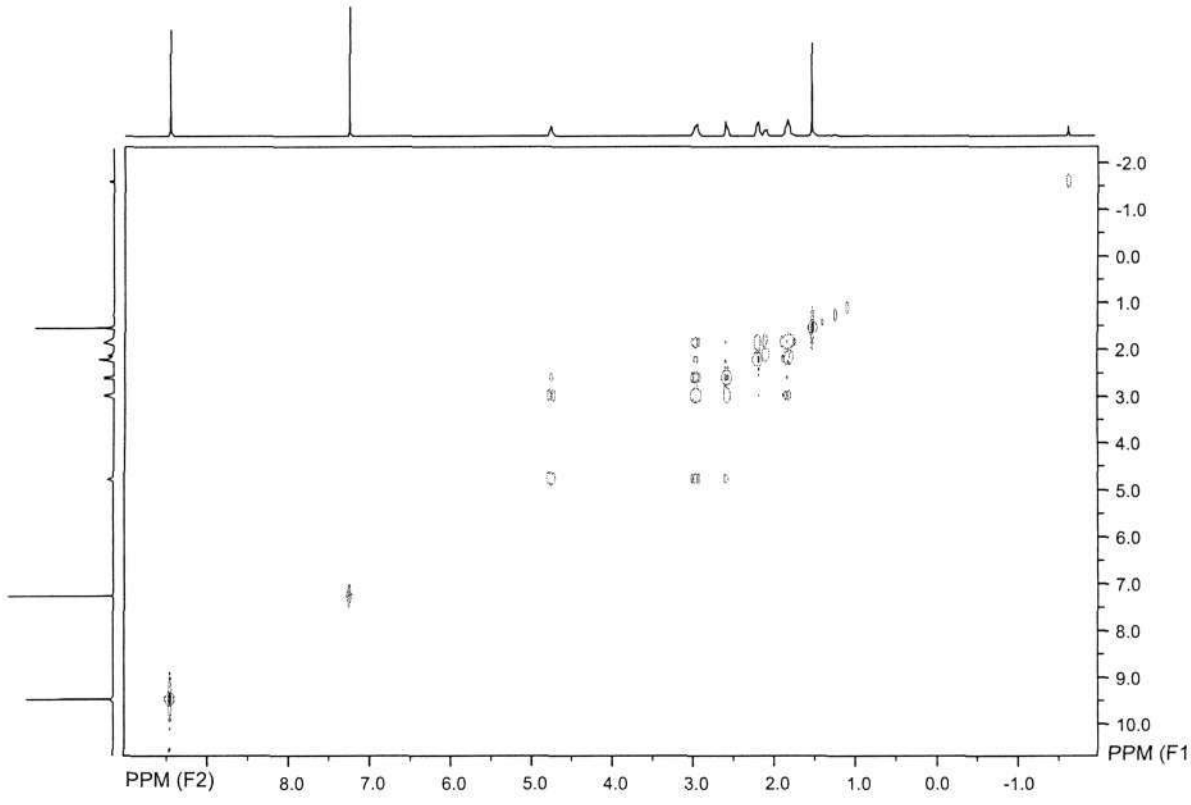

Figure C6-1: COSY spectrum for $H_2T(cyHx)P$.

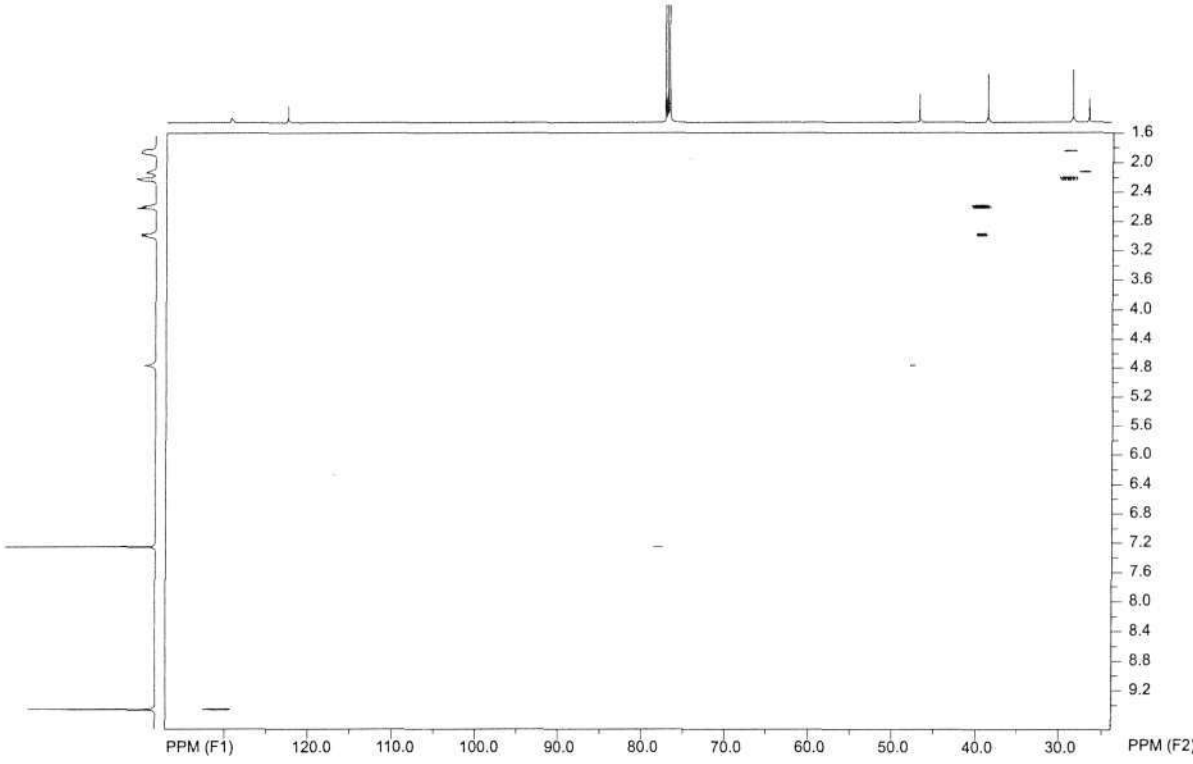

Figure C6-2: HSQC spectrum for $H_2T(cyHx)P$.

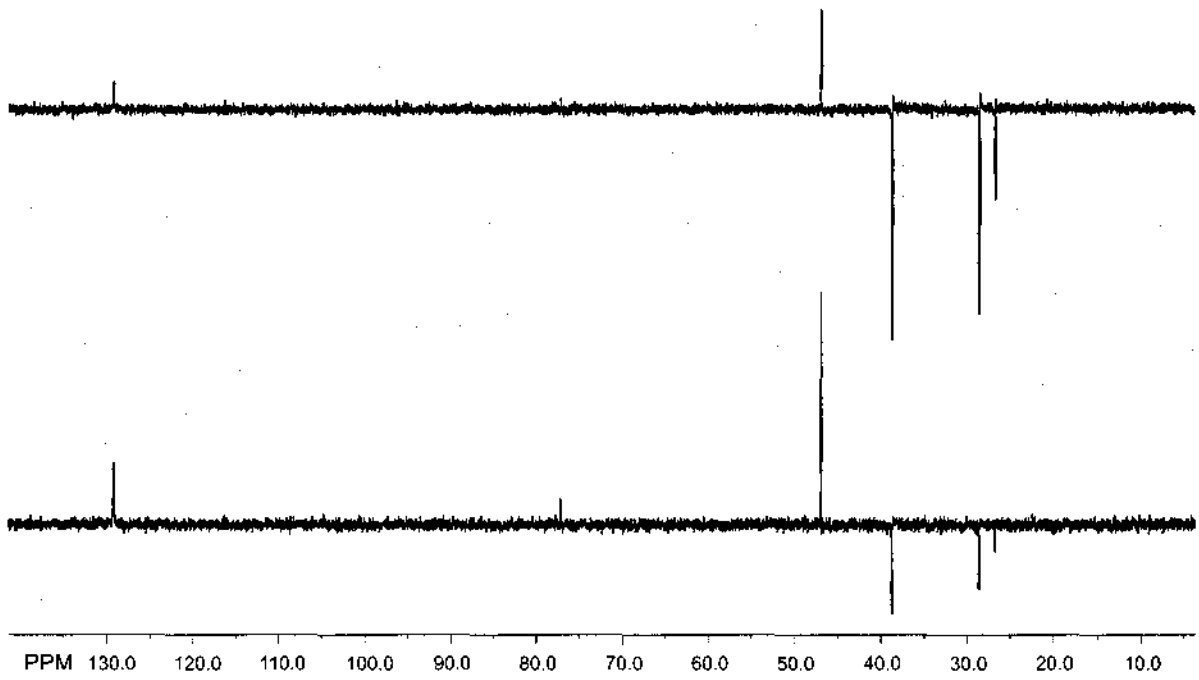

Figure C6-3: DEPT spectrum for $H_2T(cyHx)P$.

APPENDIX D

D1 – Crystallographic data tables for $H_2T(CH_2Ph)P$

Table D1-1: Crystal data and structure refinement for $H_2T(CH_2Ph)P$.

Table D1-2: Atomic coordinates (x 10^4) and equivalent isotropic displacement parameters ($Å^2$ x 10^3) for benzyl. U(eq) is defined as one third of the trace of the orthogonalized U^{ij} tensor.

Table D1-3: IUCR CIF check report.

D2 – Crystallographic data tables for $H_2T(iPent)P$

Table D2-1: Crystal data and structure refinement for $H_2T(iPent)P$.

Table D2-2: Atomic coordinates (x 10^4) and equivalent isotropic displacement parameters ($Å^2$ x 10^3) for ipent1. U(eq) is defined as one third of the trace of the orthogonalized U^{ij} tensor.

D3 – Crystallographic data tables for $H_2T(cyHx)P$

Table D3-1: Crystal data and structure refinement for $H_2T(cyHx)P$.

Table D3-2: Atomic coordinates (x 10^4) and equivalent isotropic displacement parameters ($Å^2$x 10^3) for p6_new2_red1b. U(eq) is defined as one third of the trace of the orthogonalized U^{ij} tensor.

Table D1-1: Crystal data and structure refinement for $H_2T(CH_2Ph)P$.

Identification code	benzyl	
Empirical formula	$C_{48}H_{38}N_4$	
Formula weight	670.82 amu	
Temperature	100(2) K	
Wavelength	0.71073 Å	
Crystal system	Triclinic	
Space group	$P\bar{1}$	
Unit cell dimensions	a = 5.952(2) Å	α = 91.76(3)°
	b = 12.076(4) Å	β = 100.16(3)°
	c = 12.188(5) Å	γ = 97.75(3)°
Volume	853.0(5) $Å^3$	
Z	1	
Density (calculated)	1.306 Mg/m^3	
Absorption coefficient	0.077 mm^{-1}	
F(000)	354	
Crystal size	0.20 x 0.15 x 0.02 mm^3	
Theta range for data collection	4.12 to 25.05°	
Index ranges	$-6 \le h \le 7$	
	$-14 \le k \le 14$	
	$-14 \le l \le 11$	
Reflections collected	5627	
Independent reflections	2991 [R_{int} = 0.1051]	
Completeness to theta = 25.00°	99.3 %	
Absorption correction	None	
Max. and min. transmission	0.9985 and 0.9848	
Refinement method	Full-matrix least-squares on F^2	
Data / restraints / parameters	2991 / 0 / 236	
Goodness-of-fit on F^2	0.886	
Final R indices [$I > 2\sigma(I)$]	R_1 = 0.0698, wR_2 = 0.1491	
R indices (all data)	R_1 = 0.1383, wR_2 = 0.1724	
Largest diff. peak and hole	0.268 and -0.271 e $Å^{-3}$	

Table D1-2: Atomic coordinates (x 10^4) and equivalent isotropic displacement parameters ($Å^2$ x 10^3) for benzyl. U(eq) is defined as one third of the trace of the orthogonalized U^{ij} tensor.

	x	y	z	U(eq)
C(11)	9313(7)	7086(3)	7390(3)	26(1)
C(12)	8230(7)	6942(3)	6153(3)	26(1)
C(13)	9645(8)	7271(3)	5384(3)	36(1)
C(14)	8718(8)	7169(4)	4240(3)	39(1)
C(15)	6440(8)	6744(4)	3870(3)	35(1)
C(16)	5037(8)	6422(4)	4620(3)	48(1)
C(17)	5959(7)	6536(4)	5768(3)	39(1)
C(21)	9065(7)	1709(3)	9472(3)	27(1)
C(22)	8761(7)	1147(3)	8310(3)	22(1)
C(23)	10564(6)	629(3)	8042(3)	22(1)
C(24)	10329(7)	68(3)	7002(3)	26(1)
C(25)	8320(7)	26(3)	6225(3)	30(1)
C(26)	6533(7)	556(3)	6482(3)	29(1)
C(27)	6763(7)	1100(3)	7528(3)	24(1)
C(101)	3917(6)	7414(3)	9678(3)	20(1)
C(102)	6377(6)	6996(3)	8639(3)	22(1)
C(103)	8397(6)	5362(3)	8365(3)	22(1)
C(104)	8311(6)	3626(3)	9047(3)	23(1)
C(201)	4469(6)	8388(3)	9063(3)	23(1)
C(202)	5989(7)	8131(3)	8431(3)	24(1)
C(203)	10081(7)	4787(3)	7953(3)	27(1)
C(204)	10051(7)	3768(3)	8364(3)	28(1)
C(301)	7961(6)	6444(3)	8171(3)	21(1)
C(302)	7723(7)	2673(3)	9610(3)	23(1)
N(1)	5078(5)	6567(2)	9405(2)	22(1)
N(2)	7392(6)	4618(2)	9026(2)	23(1)

Table D1-3: IUCR CIF check report.

IUCR CheckCIF/PLATON report (full structural check)

No syntax errors found.

Datablock: benzyl

Bond precision: C-C = 0.0054 A Wavelength=0.71073

Cell: a=5.952(2) b=12.076(4) c=12.188(5)
alpha=91.76(3) beta=100.16(3) gamma=97.75(3)

	Calculated	Reported
Volume	853.1(5)	853.0(5)
Space group	P -1	P -1
Hall group	-P 1	-P 1
Moiety formula	C48 H38 N4	C48 H38 N4
Sum formula	C48 H38 N4	C48 H38 N4
Mr	670.82	670.82
Dx,g cm-3	1.306	1.306
Z	1	1
Mu (mm-1)	0.077	0.077
F000	354.0	354.0
F000'	354.12	
h,k,lmax	7,14,14	7,14,14
Nref	3012	2991
Tmin,Tmax	0.986,0.998	0.985,0.998
Tmin'	0.985	

Correction method= 'NONE'

Data completeness= Ratio = 0.99 Theta(max)= 25.05

R(reflections)= 0.0698(1441) wR2(reflections)= 0.1724(2991)

S = 0.886 Npar= 236

The following ALERTS were generated. Each ALERT has the format
test-name_ALERT_alert-type_alert-level.

Alert level C

RINTA01_ALERT_3_C The value of Rint is greater than 0.10 Rint given 0.105
PLAT020_ALERT_3_C The value of Rint is greater than 0.10 ..... 0.10
PLAT026_ALERT_3_C Ratio Observed / Unique Reflections too Low .... 48 Perc.
PLAT066_ALERT_1_C Predicted and Reported Transmissions Identical . ?
PLAT166_ALERT_4_C S.U's Given on Coordinates for calc-flagged H2
PLAT340_ALERT_3_C Low Bond Precision on C-C bonds (x 1000) Ang ... 5

---

0 **ALERT level A** = In general: serious problem
0 **ALERT level B** = Potentially serious problem
6 **ALERT level C** = Check and explain
0 **ALERT level G** = General alerts; check

1 ALERT type 1 CIF construction/syntax error, inconsistent or missing data
0 ALERT type 2 Indicator that the structure model may be wrong or deficient
4 ALERT type 3 Indicator that the structure quality may be low
1 ALERT type 4 Improvement, methodology, query or suggestion

Publication of your CIF

A full structural check has been run on your CIF. This includes checks on:

- CIF syntax and construction
- Cell and geometry details
- Space-group symmetry
- Anisotropic displacement parameters

These full checks give an indication of potential problems with your CIF. Please note that if you intend to submit your CIF for publication in Acta Crystallographica Section C or E, you must make sure that full publication checks are run on the final version of the CIF prior to submission.

If you intend to submit to another section of Acta Crystallographica, Journal of Applied Crystallography or Journal of Synchrotron Radiation, you should make sure that at least basic structural checks are run on the final version of your CIF prior to submission.

To submit your CIF for publication in an IUCr journal click here.

PLATON version of 12/04/2005; check.def file version of 22/03/2005
Datablock benzyl - ellipsoid plot

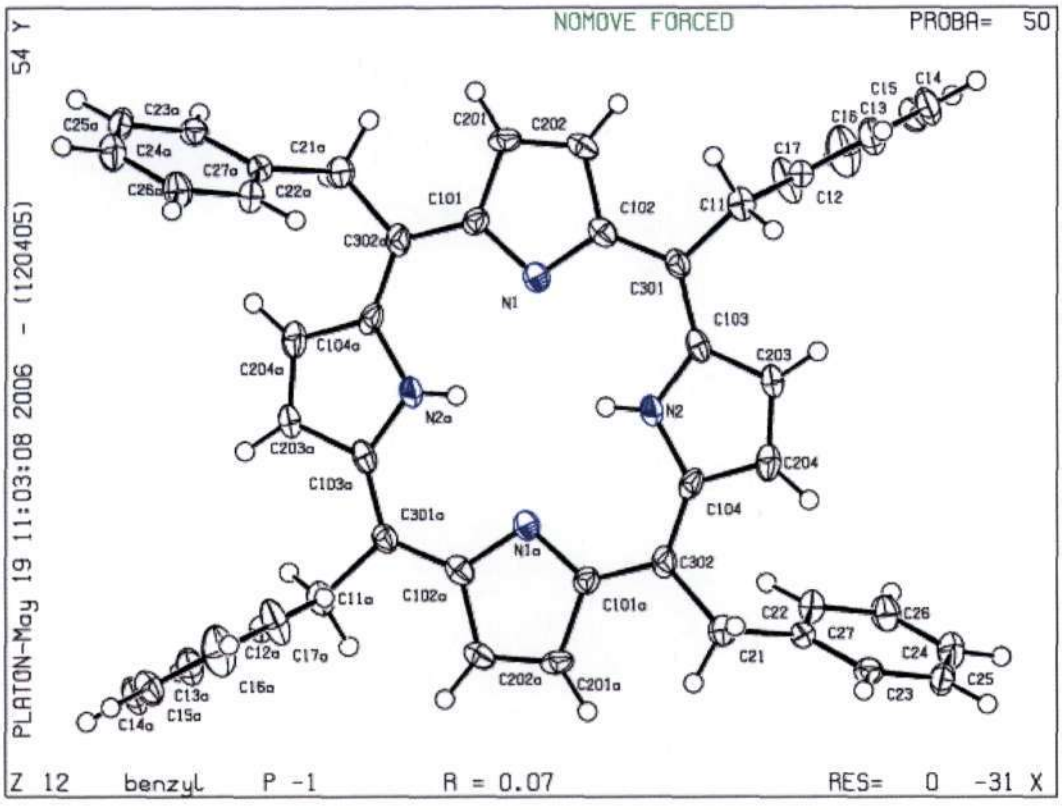
NOMOVE FORCED
PROBA= 50
54 Y
PLATON-May 19 11:03:08 2006 - (120405)
Z 12 benzyl P -1 R = 0.07
RES= 0 -31 X
C14
C15
C13
C16
C17
C12
C11
C201
C202
C101
C102
C301
C103
C203
N1
N2
C104
C204
C21a
C22a
C23a
C24a
C25a
C26a
C27a
C302a
C104a
C204a
N2a
C203a
C103a
C301a
N1a
C11a
C102a
C101a
C12a
C17a
C16a
C13a
C14a
C15a
C202a
C201a
C21
C22
C27
C26
C24
C25
C23

D2 – Crystallographic data tables for $H_2T(iPent)P$

Table D2-1: Crystal data and structure refinement for $H_2T(iPent)P$.

Identification code	ibup1	
Empirical formula	$C_{40}H_{54}N_4$	
Formula weight	590.87 amu	
Temperature	100(2) K	
Wavelength	0.71073 Å	
Crystal system	Monoclinic	
Space group	$P2_1/c$	
Unit cell dimensions	a = 11.328(11) Å	α = 90°
	b = 10.448(10) Å	β = 98.02(8)°
	c = 14.179(12) Å	γ = 90°
Volume	1662(3) $Å^3$	
Z	2	
Density (calculated)	1.181 Mg/m^3	
Absorption coefficient	0.069 mm^{-1}	
F(000)	644	
Crystal size	0.40 x 0.30 x 0.02 mm^3	
Theta range for data collection	4.30 to 25.15°	
Index ranges	-12 ≤ h ≤ 13	
	-12 ≤ k ≤ 11	
	-16 ≤ l ≤ 14	
Reflections collected	9412	
Independent reflections	2944 [R_{int} = 0.1837]	
Completeness to theta = 25.00°	99.3 %	
Max. and min. transmission	0.9986 and 0.9730	
Refinement method	Full-matrix least-squares on F^2	
Data / restraints / parameters	2944 / 6 / 199	
Goodness-of-fit on F^2	0.971	
Final R indices [$I > 2\sigma(I)$]	R_1 = 0.1340, wR_2 = 0.3256	
R indices (all data)	R_1 = 0.2601, wR_2 = 0.3855	
Largest diff. peak and hole	1.077 and -0.364 $e.Å^{-3}$	

Table D2-2: Atomic coordinates (x 10^4) and equivalent isotropic displacement parameters ($Å^2$ x 10^3) for ipent1. U(eq) is defined as one third of the trace of the orthogonalized U^{ij} tensor.

	x	y	z	U(eq)
C(11)	4027(11)	2173(10)	5301(5)	89(4)
C(12)	4736(9)	1794(10)	4443(7)	77(3)
C(13)	5998(11)	2066(14)	4678(8)	113(4)
C(14)	3993(11)	3476(16)	5505(7)	120(5)
C(15)	3723(10)	3777(13)	6454(6)	102(4)
C(21)	-1179(6)	1940(7)	1743(4)	36(2)
C(22)	-307(7)	1516(8)	1061(4)	55(2)
C(23)	-934(8)	1401(8)	37(4)	54(2)
C(24)	-1432(8)	3386(7)	1691(5)	53(2)
C(25)	-2371(9)	3853(9)	2225(5)	72(3)
C(101)	1681(6)	-607(6)	6873(4)	33(2)
C(102)	2504(7)	735(7)	5976(4)	40(2)
C(103)	1886(6)	1839(7)	4419(4)	33(2)
C(104)	277(6)	1747(6)	3270(4)	32(2)
C(201)	2866(7)	-345(7)	7348(5)	41(2)
C(202)	3400(7)	477(8)	6807(5)	47(2)
C(203)	2070(7)	2707(6)	3658(4)	39(2)
C(204)	1093(7)	2635(7)	2973(5)	40(2)
C(301)	2705(7)	1588(7)	5234(5)	45(2)
C(302)	-864(6)	1434(6)	2777(4)	33(2)
N(1)	1492(5)	74(5)	6030(3)	35(2)
N(2)	780(5)	1325(5)	4167(3)	33(2)

D3 – Crystallographic data tables for $H_2T(cyHx)P$

Table D3-1: Crystal data and structure refinement for $H_2T(cyHx)P$.

Identification code	p6_new2_red1b	
Empirical formula	$C_{44}H_{54}N_4$	
Formula weight	638.91 amu	
Temperature	293(2) K	
Wavelength	0.71073 Å	
Crystal system	Orthorhombic	
Space group	*P* bca	
Unit cell dimensions	*a* = 10.5218(12) Å	α = 90°
	b = 12.7805(14) Å	β = 90°
	c = 53.917(6) Å	γ = 90°
Volume	7250.4(14) $Å^3$	
Z	**8**	
Density (calculated)	1.171 Mg/m^3	
Absorption coefficient	0.068 mm^{-1}	
F(000)	2768	
Crystal size	0.05 × 0.3 × 0.5 mm^3	
Theta range for data collection	3.71 to 25.07°	
Index ranges	-12 ≤ h ≤ 12	
	-15 ≤ k ≤ 15	
	-63 ≤ l ≤ 64	
Reflections collected	65864	
Independent reflections	6407 [R_{int} = 0.1528]	
Completeness to theta = 25.00°	99.7 %	
Refinement method	Full-matrix least-squares on F^2	
Data / restraints / parameters	6407 / 0 / 441	
Goodness-of-fit on F^2	1.176	
Final R indices [$I > 2\sigma(I)$]	R_1 = 0.2285, wR_2 = 0.4640	
R indices (all data)	R_1 = 0.2769, wR_2 = 0.4785	
Largest diff. peak and hole	0.553 and -0.650 $e.Å^{-3}$	

Table D3-2: Atomic coordinates (x 10^4) and equivalent isotropic displacement parameters ($Å^2$x 10^3) for p6_new2_red1b. U(eq) is defined as one third of the trace of the orthogonalized U^{ij} tensor.

	x	y	z	U(eq)
C(301)	10932(12)	1929(9)	1855(2)	20(3)
C(11)	11216(13)	1537(11)	2118(2)	30(3)
C(12)	12563(13)	1773(10)	2204(2)	26(3)
C(13)	12732(15)	1420(13)	2472(3)	45(4)
C(14)	12381(16)	307(12)	2521(3)	46(5)
C(15)	11013(15)	104(15)	2437(3)	52(5)
C(16)	10794(14)	383(12)	2155(3)	36(4)
C(21)	12402(14)	151(11)	854(2)	32(3)
C(22)	13253(13)	702(10)	667(3)	30(3)
C(23)	14225(13)	-10(10)	553(2)	26(3)
C(24)	13617(16)	-984(11)	437(3)	43(4)
C(25)	12803(14)	-1533(12)	625(3)	45(4)
C(26)	11842(13)	-860(9)	750(3)	29(3)
C(31)	7022(12)	3362(10)	569(2)	24(3)
C(32)	7630(13)	3909(10)	343(2)	24(3)
C(33)	6661(15)	4140(12)	138(2)	37(4)
C(34)	6005(17)	3137(13)	61(3)	52(5)
C(35)	5308(14)	2628(11)	285(2)	33(3)
C(36)	6249(14)	2388(12)	490(2)	37(4)
C(41)	9250(11)	6325(9)	1603(2)	20(3)
C(42)	8032(12)	6734(10)	1723(2)	26(3)
C(43)	8249(14)	7826(11)	1843(3)	32(3)
C(44)	8763(15)	8579(13)	1655(3)	47(4)
C(45)	9962(15)	8218(11)	1533(3)	40(4)
C(46)	9758(13)	7118(10)	1414(2)	28(3)
C(102)	10388(11)	2908(9)	1830(2)	16(3)
C(01)	9719(11)	4437(9)	1673(2)	15(3)
C(104)	11632(11)	892(9)	1244(2)	16(3)
C(103)	11341(11)	1338(9)	1652(2)	16(3)
C(106)	8875(11)	2407(9)	766(2)	14(3)
C(105)	10497(11)	1368(8)	855(2)	15(3)
C(108)	8655(12)	4959(9)	1291(2)	18(3)

Table D3-2: Continued.

	x	y	z	U(eq)
C(107)	7976(11)	3962(9)	963(2)	15(3)
C(202)	10277(13)	3679(11)	2036(2)	30(3)
C(201)	9922(13)	4576(12)	1936(2)	31(3)
C(204)	12410(12)	245(9)	1397(2)	17(3)
C(203)	12193(10)	475(10)	1641(2)	19(3)
C(206)	9180(12)	1795(10)	547(2)	21(3)
C(205)	10197(13)	1207(9)	594(2)	22(3)
C(208)	7747(12)	5545(12)	1150(2)	30(3)
C(207)	7301(12)	4959(9)	961(2)	19(3)
C(302)	11461(12)	824(10)	990(2)	24(3)
C(303)	7972(11)	3202(10)	777(2)	19(3)
C(304)	9214(12)	5201(9)	1513(2)	20(3)
N(1)	10003(9)	3424(7)	1610(2)	15(2)
N(2)	10993(10)	1542(9)	1405(2)	21(2)
N(3)	9685(9)	2112(7)	956(2)	16(2)
N(4)	8747(10)	3997(7)	1170(2)	16(2)

APPENDIX E

Table E-1: Final coordinates for the DFT optimization of $H_2T(iBu)P$.

Table E-2: Final coordinates for the DFT optimization of $H_2T(CH_2Ph)P$.

Table E-3: Final coordinates for the DFT optimization of $H_2T(iPent)P$.

Table E-4: Final coordinates for the DFT optimization of $H_2T(CHPh_2)P$.

Table E-5: Final coordinates for the DFT optimization of $H_2T(iPr)P$.

Table E-6: Final coordinates for the DFT optimization of $H_2T(cyHx)P$.

Table E-1: Final coordinates for the DFT optimization of $H_2T(iBu)P$.

Stoichiometry C36H46N4
Framework group C1[X(C36H46N4)]
Deg. of freedom 252
Full point group C1 NOp 1
Largest Abelian subgroup C1 NOp 1
Largest concise Abelian subgroup C1 NOp 1

Standard orientation:

Center Number	Atomic Number	Atomic Type	Coordinates (Angstroms) X	Y	Z
1	6	0	-2.264297	1.822438	-0.420059
2	6	0	-0.381902	2.851965	0.343967
3	6	0	1.977669	2.086984	0.492249
4	6	0	3.038213	0.251591	-0.063021
5	6	0	-2.529943	3.226826	-0.301535
6	6	0	-1.410092	3.839860	0.189898
7	6	0	3.403066	2.403939	0.513053
8	6	0	4.054057	1.280881	0.132512
9	6	0	-3.170914	0.798392	-0.758425
10	6	0	0.966856	3.058104	0.695653
11	7	0	-0.954056	1.655620	-0.028750
12	7	0	1.790879	0.775998	0.148057
13	6	0	2.385831	-2.140927	-0.200411
14	6	0	0.416377	-3.209840	0.200381
15	6	0	-1.945805	-2.458805	0.041913
16	6	0	-2.907525	-0.575686	-0.535986
17	6	0	2.642061	-3.551363	-0.123444
18	6	0	1.464154	-4.190245	0.152211
19	6	0	-3.361322	-2.752940	-0.154853
20	6	0	-3.948370	-1.599517	-0.548618
21	6	0	3.335863	-1.107010	-0.325662
22	6	0	-0.968343	-3.444752	0.320661
23	7	0	1.030241	-1.995290	-0.008977
24	7	0	-1.706834	-1.128684	-0.181849
25	6	0	-2.297366	-4.970570	1.945934
26	6	0	-1.690492	-4.348335	3.207186
27	6	0	-1.378654	-4.877053	0.701078
28	6	0	-1.906247	-5.705907	-0.489807
29	1	0	-3.465556	3.709336	-0.527261
30	1	0	-1.304082	4.892537	0.389804
31	1	0	3.858368	3.356906	0.737450
32	1	0	5.120675	1.167201	0.029740
33	1	0	-0.472152	0.763652	-0.014666
34	1	0	3.606652	-4.024510	-0.219980
35	1	0	1.339373	-5.255151	0.269606
36	1	0	-3.847351	-3.708331	-0.046085
37	1	0	-4.995064	-1.466710	-0.777593
38	1	0	0.544397	-1.105739	-0.021854

Table E-1: Continued.

39	1	0	-3.273226	-4.516311	1.754064
40	1	0	-2.488733	-6.036999	2.125499
41	1	0	-2.350480	-4.490797	4.068921
42	1	0	-0.723577	-4.804047	3.450006
43	1	0	-1.528335	-3.273418	3.083768
44	1	0	-0.461794	-5.377593	1.021058
45	1	0	-1.187204	-5.693139	-1.314879
46	1	0	-2.054917	-6.748537	-0.186904
47	1	0	-2.855962	-5.334052	-0.880290
48	6	0	1.392763	4.423651	1.259558
49	6	0	1.510621	5.521795	0.170985
50	6	0	2.182858	6.811755	0.654828
51	6	0	0.576100	4.852425	2.498669
52	6	0	4.760790	-1.545384	-0.699713
53	6	0	5.307565	-0.820971	-1.958913
54	6	0	6.525076	-1.514931	-2.580471
55	6	0	5.735768	-1.551443	0.497764
56	6	0	-4.546806	1.177577	-1.330233
57	6	0	-5.528387	1.713680	-0.255808
58	6	0	-6.978569	1.831195	-0.738892
59	6	0	-4.456703	2.059644	-2.595471
60	1	0	2.404273	4.281430	1.644970
61	1	0	0.524593	5.759424	-0.242705
62	1	0	2.090483	5.105248	-0.661426
63	1	0	1.589842	7.324108	1.418848
64	1	0	2.321181	7.511441	-0.175716
65	1	0	3.171569	6.609257	1.083605
66	1	0	0.506914	4.025285	3.211375
67	1	0	-0.442201	5.168264	2.262601
68	1	0	1.070809	5.685575	3.006918
69	1	0	4.678781	-2.587486	-1.017833
70	1	0	4.501261	-0.781685	-2.700989
71	1	0	5.560819	0.219683	-1.737728
72	1	0	7.389897	-1.510216	-1.909404
73	1	0	6.826758	-1.011176	-3.504403
74	1	0	6.304393	-2.559256	-2.830874
75	1	0	5.315951	-2.133314	1.324213
76	1	0	5.944245	-0.549064	0.878707
77	1	0	6.690196	-2.009981	0.220229
78	1	0	-4.985831	0.244726	-1.688706
79	1	0	-5.490441	1.030962	0.601636
80	1	0	-5.192071	2.685072	0.122227
81	1	0	-7.638344	2.124582	0.084002
82	1	0	-7.346073	0.875702	-1.131675
83	1	0	-7.090532	2.578994	-1.530173
84	1	0	-4.149993	3.087322	-2.390204
85	1	0	-5.427265	2.098506	-3.099114
86	1	0	-3.735583	1.636663	-3.301240

Table E-2: Final coordinates for the DFT optimization of $H_2T(CH_2Ph)P$.

Stoichiometry $C_{48}H_{38}N_4$
Framework group C2H[C2(N.N),SGH(H2N2),X(C48H36)]
Deg. of freedom 67
Full point group C2H NOp 4
Largest Abelian subgroup C2H NOp 4
Largest concise Abelian subgroup C2H NOp 4
Standard orientation:

Center Number	Atomic Number	Atomic Type	Coordinates (Angstroms) X	Y	Z
1	6	0	1.368500	3.260053	3.529581
2	6	0	0.369218	4.353112	3.896696
3	6	0	0.839002	5.613893	4.289312
4	6	0	-0.044810	6.622539	4.673672
5	6	0	-1.420036	6.386103	4.668654
6	6	0	-1.899393	5.135463	4.276913
7	6	0	-1.012978	4.127923	3.893965
8	6	0	1.368500	3.260053	-3.529581
9	6	0	0.369218	4.353112	-3.896696
10	6	0	0.839002	5.613893	-4.289312
11	6	0	-0.044810	6.622539	-4.673672
12	6	0	-1.420036	6.386103	-4.668654
13	6	0	-1.899393	5.135463	-4.276913
14	6	0	-1.012978	4.127923	-3.893965
15	6	0	-0.418313	-1.008452	2.873639
16	6	0	0.418313	1.008452	2.873639
17	6	0	1.040718	2.687228	1.133227
18	6	0	1.040718	2.687228	-1.133227
19	6	0	-0.262130	-0.623546	4.273931
20	6	0	0.262130	0.623546	4.273931
21	6	0	1.484974	3.974697	0.684080
22	6	0	1.484974	3.974697	-0.684080
23	6	0	0.919233	2.263819	2.466758
24	6	0	0.919233	2.263819	-2.466758
25	7	0	0.000000	0.000000	2.049726
26	7	0	0.770220	1.954184	0.000000
27	6	0	-1.368500	-3.260053	-3.529581
28	6	0	-0.369218	-4.353112	-3.896696
29	6	0	-0.839002	-5.613893	-4.289312
30	6	0	0.044810	-6.622539	-4.673672
31	6	0	1.420036	-6.386103	-4.668654
32	6	0	1.899393	-5.135463	-4.276913
33	6	0	1.012978	-4.127923	-3.893965
34	6	0	-1.368500	-3.260053	3.529581
35	6	0	-0.369218	-4.353112	3.896696
36	6	0	-0.839002	-5.613893	4.289312
37	6	0	0.044810	-6.622539	4.673672
38	6	0	1.420036	-6.386103	4.668654

Table E-2: Continued.

39	6	0	1.899393	-5.135463	4.276913
40	6	0	1.012978	-4.127923	3.893965
41	6	0	0.418313	1.008452	-2.873639
42	6	0	-0.418313	-1.008452	-2.873639
43	6	0	-1.040718	-2.687228	-1.133227
44	6	0	-1.040718	-2.687228	1.133227
45	6	0	0.262130	0.623546	-4.273931
46	6	0	-0.262130	-0.623546	-4.273931
47	6	0	-1.484974	-3.974697	-0.684080
48	6	0	-1.484974	-3.974697	0.684080
49	6	0	-0.919233	-2.263819	-2.466758
50	6	0	-0.919233	-2.263819	2.466758
51	7	0	0.000000	0.000000	-2.049726
52	7	0	-0.770220	-1.954184	0.000000
53	1	0	0.450576	0.992296	0.000000
54	1	0	2.297831	3.736228	3.203278
55	1	0	1.643542	2.715540	4.436449
56	1	0	1.909705	5.806566	4.295543
57	1	0	0.341251	7.593236	4.972060
58	1	0	-2.111425	7.170193	4.963113
59	1	0	-2.968341	4.941992	4.265174
60	1	0	-1.397888	3.161545	3.583638
61	1	0	1.643542	2.715540	-4.436449
62	1	0	2.297831	3.736228	-3.203278
63	1	0	1.909705	5.806566	-4.295543
64	1	0	0.341251	7.593236	-4.972060
65	1	0	-2.111425	7.170193	-4.963113
66	1	0	-2.968341	4.941992	-4.265174
67	1	0	-1.397888	3.161545	-3.583638
68	1	0	-0.497169	-1.221581	5.141956
69	1	0	0.497169	1.221581	5.141956
70	1	0	1.737196	4.802873	1.328132
71	1	0	1.737196	4.802873	-1.328132
72	1	0	-0.450576	-0.992296	0.000000
73	1	0	-2.297831	-3.736228	-3.203278
74	1	0	-1.643542	-2.715540	-4.436449
75	1	0	-1.909705	-5.806566	-4.295543
76	1	0	-0.341251	-7.593236	-4.972060
77	1	0	2.111425	-7.170193	-4.963113
78	1	0	2.968341	-4.941992	-4.265174
79	1	0	1.397888	-3.161545	-3.583638
80	1	0	-1.643542	-2.715540	4.436449
81	1	0	-2.297831	-3.736228	3.203278
82	1	0	-1.909705	-5.806566	4.295543
83	1	0	-0.341251	-7.593236	4.972060
84	1	0	2.111425	-7.170193	4.963113
85	1	0	2.968341	-4.941992	4.265174
86	1	0	1.397888	-3.161545	3.583638
87	1	0	0.497169	1.221581	-5.141956

Table E-2: Continued.

88	1	0	-0.497169	-1.221581	-5.141956
89	1	0	-1.737196	-4.802873	-1.328132
90	1	0	-1.737196	-4.802873	1.328132

Table E-3: Final coordinates for the DFT optimization of $H_2T(iPent)P$.

Stoichiometry C40H54N4
Framework group C1[X(C40H54N4)]
Deg. of freedom 288
Full point group C1 NOp 1
Largest Abelian subgroup C1 NOp 1
Largest concise Abelian subgroup C1 NOp 1
Standard orientation:

Center Number	Atomic Number	Atomic Type	Coordinates (Angstroms) X	Y	Z
1	7	0	-2.068775	-0.002542	-0.033951
2	7	0	-0.098580	-2.127283	-0.036961
3	6	0	-1.217087	-2.867191	0.279639
4	6	0	-2.888820	-1.024076	0.374215
5	6	0	-2.507304	-2.373310	0.572726
6	6	0	-4.265221	-0.549836	0.464842
7	6	0	-4.672660	-3.762724	0.116933
8	6	0	-0.816334	-4.240888	0.167412
9	6	0	-4.054512	-3.073629	2.517603
10	6	0	-3.523871	-3.403220	1.096796
11	7	0	-0.041427	2.005887	-0.125972
12	6	0	-1.114951	2.796844	-0.468645
13	6	0	-2.880802	1.077716	-0.256482
14	6	0	-2.455864	2.379802	-0.620168
15	6	0	-4.263746	0.733605	0.037221
16	6	0	-4.126396	4.366652	-0.126246
17	6	0	-0.616112	4.143224	-0.486723
18	6	0	-4.251954	3.081721	-2.434563
19	6	0	-3.406147	3.462474	-1.174627
20	7	0	1.931964	-0.126080	-0.096053
21	6	0	0.971659	-2.934739	-0.352719
22	6	0	2.742863	-1.206568	-0.324811
23	6	0	2.305339	-2.527250	-0.588379
24	6	0	4.139792	-0.827699	-0.159352
25	6	0	4.046165	-4.443316	-0.049093
26	6	0	0.485981	-4.281102	-0.248843
27	6	0	3.963573	-3.369853	-2.469153
28	6	0	3.232373	-3.644189	-1.113918

Table E-3: Continued.

29	6	0	1.089285	2.757971	0.100082
30	6	0	2.762908	0.920112	0.203426
31	6	0	2.384383	2.272731	0.370792
32	6	0	4.151589	0.475708	0.203773
33	6	0	4.576983	3.570669	-0.193479
34	6	0	0.697952	4.123046	-0.105847
35	6	0	3.921078	2.999253	2.266634
36	6	0	3.422724	3.306659	0.828130
37	6	0	-5.616679	2.385876	-2.355215
38	6	0	-5.036781	3.770503	0.952648
39	6	0	-4.203718	-4.273074	-1.248805
40	6	0	-2.953499	-2.944593	3.574665
41	6	0	5.248504	-2.541964	-2.590032
42	6	0	5.079639	-3.765007	0.856261
43	6	0	4.679580	5.037964	-0.626695
44	6	0	4.708622	4.149306	2.902839
45	1	0	-5.126183	-1.106599	0.794213
46	1	0	-5.280740	-4.537806	0.602118
47	1	0	-5.338481	-2.908650	-0.034227
48	1	0	-1.442651	-5.100271	0.343069
49	1	0	-4.653407	-2.158438	2.510270
50	1	0	-4.738219	-3.883254	2.805330
51	1	0	-2.971047	-4.335003	1.236100
52	1	0	-0.061243	-1.114622	-0.051304
53	1	0	-5.110389	1.392630	-0.014441
54	1	0	-4.695221	5.114341	-0.696242
55	1	0	-3.339272	4.926406	0.394434
56	1	0	-1.188799	5.027858	-0.717318
57	1	0	-3.599413	2.501042	-3.097981
58	1	0	-4.418805	4.037160	-2.950274
59	1	0	-2.713204	4.167503	-1.637789
60	1	0	-0.087858	0.995574	-0.059989
61	1	0	4.993245	-1.472085	-0.259427
62	1	0	4.539742	-5.262601	-0.590174
63	1	0	3.308709	-4.922684	0.607258
64	1	0	1.061138	-5.177729	-0.418505
65	1	0	3.215557	-2.946633	-3.151155
66	1	0	4.189759	-4.369119	-2.865910
67	1	0	2.523788	-4.400008	-1.456555
68	1	0	5.022881	1.074540	0.414953
69	1	0	4.431846	2.949407	-1.081919
70	1	0	5.536766	3.260596	0.239337
71	1	0	1.341527	4.984222	-0.020532
72	1	0	4.530491	2.089869	2.271111
73	1	0	3.045630	2.777350	2.888787
74	1	0	2.888040	4.252936	0.932515
75	1	0	-6.090851	2.424950	-3.342275
76	1	0	-6.295834	2.883626	-1.655494
77	1	0	-5.543344	1.334109	-2.075525

Table E-3: Continued.

78	1	0	-5.931448	3.293999	0.541657
79	1	0	-5.377996	4.570508	1.618869
80	1	0	-4.511164	3.033821	1.565776
81	1	0	-3.615900	-3.517207	-1.778022
82	1	0	-5.059758	-4.534548	-1.879293
83	1	0	-3.579863	-5.168723	-1.151864
84	1	0	-3.383906	-2.768778	4.565819
85	1	0	-2.279723	-2.112701	3.349504
86	1	0	-2.346958	-3.855841	3.631931
87	1	0	5.082242	-1.476928	-2.422467
88	1	0	5.644587	-2.652655	-3.605779
89	1	0	6.031038	-2.881422	-1.903930
90	1	0	4.636784	-2.964109	1.453463
91	1	0	5.923796	-3.348510	0.299100
92	1	0	5.489889	-4.505638	1.551696
93	1	0	3.758602	5.367050	-1.121269
94	1	0	5.502798	5.185672	-1.333775
95	1	0	4.852474	5.700427	0.228292
96	1	0	4.107170	5.064426	2.953768
97	1	0	5.620742	4.382441	2.343162
98	1	0	5.008952	3.894585	3.924409

Table E-4: Final coordinates for the DFT optimization of $H_2T(CHPh_2)P$.

```
Stoichiometry    C72H54N4
 Framework group  C2[X(C72H54N4)]
 Deg. of freedom   193
 Full point group                              C2      NOp   2
 Largest Abelian subgroup                C2      NOp   2
 Largest concise Abelian subgroup   C2      NOp   2
                        Standard orientation:
```

Center Number	Atomic Number	Atomic Type	Coordinates (Angstroms) X	Y	Z
1	6	0	4.555175	2.114386	-0.150608
2	6	0	3.178723	1.414615	-0.107874
3	6	0	3.117121	0.012300	-0.177254
4	6	0	4.220417	-0.904844	-0.212764
5	1	0	5.259558	-0.623974	-0.232346
6	6	0	3.724586	-2.176551	-0.218469
7	1	0	4.300053	-3.086105	-0.241853
8	6	0	2.291387	-2.105877	-0.185097
9	7	0	1.975790	-0.763128	-0.163607
10	1	0	1.032184	-0.391548	-0.145693

Table E-4: Continued.

11	6	0	1.390796	-3.182927	-0.122239
12	6	0	2.048923	2.257247	0.027543
13	6	0	2.154331	3.687897	0.304378
14	6	0	0.894550	4.175384	0.299277
15	6	0	0.011175	3.045445	0.020099
16	1	0	0.601027	5.189259	0.526422
17	1	0	3.052361	4.240933	0.535358
18	7	0	0.736001	1.890336	-0.098315
19	6	0	-0.011175	-3.045445	0.020099
20	6	0	-0.894550	-4.175384	0.299277
21	1	0	-0.601027	-5.189259	0.526422
22	6	0	-2.154331	-3.687897	0.304378
23	1	0	-3.052361	-4.240933	0.535358
24	6	0	-2.048923	-2.257247	0.027543
25	7	0	-0.736001	-1.890336	-0.098315
26	6	0	-3.178723	-1.414615	-0.107874
27	6	0	-3.117121	-0.012300	-0.177254
28	6	0	-4.220417	0.904844	-0.212764
29	1	0	-5.259558	0.623974	-0.232346
30	6	0	-3.724586	2.176551	-0.218469
31	1	0	-4.300053	3.086105	-0.241853
32	6	0	-2.291387	2.105877	-0.185097
33	7	0	-1.975790	0.763128	-0.163607
34	6	0	-1.390796	3.182927	-0.122239
35	1	0	-1.032184	0.391548	-0.145693
36	1	0	4.336096	3.133287	-0.475184
37	6	0	5.499744	1.618631	-1.262984
38	6	0	7.184642	0.859209	-3.391579
39	6	0	5.010838	1.537943	-2.576232
40	6	0	6.848975	1.323601	-1.037931
41	6	0	7.683097	0.942599	-2.093307
42	6	0	5.841411	1.161654	-3.628860
43	1	0	3.966453	1.766391	-2.770407
44	1	0	7.254092	1.389262	-0.033888
45	1	0	8.726089	0.712871	-1.893854
46	1	0	5.439441	1.104234	-4.636487
47	1	0	7.833161	0.563848	-4.211116
48	6	0	5.221488	2.276565	1.220200
49	6	0	6.497999	2.695350	3.700789
50	6	0	5.995739	3.424727	1.452707
51	6	0	5.093319	1.346578	2.259035
52	6	0	5.727066	1.553494	3.486363
53	6	0	6.630090	3.634175	2.676154
54	1	0	6.105742	4.160463	0.659209
55	1	0	4.486919	0.459368	2.117568
56	1	0	5.609990	0.819502	4.278613
57	1	0	7.221740	4.532108	2.830293
58	1	0	6.986059	2.856126	4.657576
59	6	0	-1.935368	4.627182	-0.184150

Table E-4: Continued.

60	**1**	**0**	-1.082170	5.228435	-0.503408
61	**6**	**0**	-2.335996	5.210436	1.175474
62	**6**	**0**	-3.025176	6.408023	3.635042
63	**6**	**0**	-2.170753	6.589690	1.382240
64	**6**	**0**	-2.844754	4.442422	2.229646
65	**6**	**0**	-3.187544	5.036206	3.446663
66	**6**	**0**	-2.512771	7.185616	2.594892
67	**1**	**0**	-1.773880	7.203332	0.576690
68	**1**	**0**	-2.965765	3.372066	2.108587
69	**1**	**0**	-3.577162	4.418883	4.251160
70	**1**	**0**	-2.373487	8.254614	2.728867
71	**1**	**0**	-3.288420	6.866559	4.583688
72	**6**	**0**	-2.951579	4.886412	-1.314003
73	**6**	**0**	-4.678779	5.436922	-3.473434
74	**6**	**0**	-2.624845	4.486536	-2.619071
75	**6**	**0**	-4.152609	5.575846	-1.112956
76	**6**	**0**	-5.010838	5.844883	-2.183393
77	**6**	**0**	-3.477422	4.756419	-3.686745
78	**1**	**0**	-1.695401	3.952039	-2.795445
79	**1**	**0**	-4.424064	5.905721	-0.115961
80	**1**	**0**	-5.940448	6.377124	-2.001905
81	**1**	**0**	-3.203372	4.434538	-4.687505
82	**1**	**0**	-5.345287	5.646533	-4.304851
83	**6**	**0**	-4.555175	-2.114386	-0.150608
84	**1**	**0**	-4.336096	-3.133287	-0.475184
85	**6**	**0**	-5.499744	-1.618631	-1.262984
86	**6**	**0**	-7.184642	-0.859209	-3.391579
87	**6**	**0**	-5.010838	-1.537943	-2.576232
88	**6**	**0**	-6.848975	-1.323601	-1.037931
89	**6**	**0**	-7.683097	-0.942599	-2.093307
90	**6**	**0**	-5.841411	-1.161654	-3.628860
91	**1**	**0**	-3.966453	-1.766391	-2.770407
92	**1**	**0**	-7.254092	-1.389262	-0.033888
93	**1**	**0**	-8.726089	-0.712871	-1.893854
94	**1**	**0**	-5.439441	-1.104234	-4.636487
95	**1**	**0**	-7.833161	-0.563848	-4.211116
96	**6**	**0**	-5.221488	-2.276565	1.220200
97	**6**	**0**	-6.497999	-2.695350	3.700789
98	**6**	**0**	-5.093319	-1.346578	2.259035
99	**6**	**0**	-5.995739	-3.424727	1.452707
100	6	0	-6.630090	-3.634175	2.676154
101	6	0	-5.727066	-1.553494	3.486363
102	1	0	-4.486919	-0.459368	2.117568
103	1	0	-6.105742	-4.160463	0.659209
104	1	0	-7.221740	-4.532108	2.830293
105	1	0	-5.609990	-0.819502	4.278613
106	1	0	-6.986059	-2.856126	4.657576
107	6	0	1.935368	-4.627182	-0.184150
108	1	0	1.082170	-5.228435	-0.503408

Table E-4: Continued.

109	**6**	**0**	2.951579	-4.886412	-1.314003
110	**6**	**0**	4.678779	-5.436922	-3.473434
111	**6**	**0**	4.152609	-5.575846	-1.112956
112	**6**	**0**	2.624845	-4.486536	-2.619071
113	**6**	**0**	3.477422	-4.756419	-3.686745
114	**6**	**0**	5.010838	-5.844883	-2.183393
115	**1**	**0**	4.424064	-5.905721	-0.115961
116	**1**	**0**	1.695401	-3.952039	-2.795445
117	**1**	**0**	3.203372	-4.434538	-4.687505
118	**1**	**0**	5.940448	-6.377124	-2.001905
119	**1**	**0**	5.345287	-5.646533	-4.304851
120	**6**	**0**	2.335996	-5.210436	1.175474
121	**6**	**0**	3.025176	-6.408023	3.635042
122	**6**	**0**	2.844754	-4.442422	2.229646
123	**6**	**0**	2.170753	-6.589690	1.382240
124	**6**	**0**	2.512771	-7.185616	2.594892
125	**6**	**0**	3.187544	-5.036206	3.446663
126	**1**	**0**	2.965765	-3.372066	2.108587
127	**1**	**0**	1.773880	-7.203332	0.576690
128	**1**	**0**	2.373487	-8.254614	2.728867
129	**1**	**0**	3.577162	-4.418883	4.251160
130	**1**	**0**	3.288420	-6.866559	4.583688

Table E-5: Final coordinates for the DFT optimization of $H_2T(iPr)P$.

```
Stoichiometry    C32H38N4
 Framework group  D2[C2(NH.HN),C2"(N.N),X(C32H36)]
 Deg. of freedom    54
 Full point group                                 D2      NOp   4
 Largest Abelian subgroup                 D2      NOp   4
 Largest concise Abelian subgroup      D2      NOp   4
                        Standard orientation:
```

Center Number	Atomic Number	Atomic Type	Coordinates (Angstroms) X	Y	Z
1	**7**	**0**	2.011227	0.000000	0.000000
2	**7**	**0**	0.000000	0.000000	-2.076223
3	**6**	**0**	1.104857	0.274108	-2.851416
4	**6**	**0**	2.832226	0.263746	-1.063849
5	**6**	**0**	2.422118	0.491343	-2.398786
6	**6**	**0**	4.229502	0.179786	-0.651695
7	**1**	**0**	5.098637	0.336779	-1.268810
8	**6**	**0**	4.379982	-0.192855	-3.939654
9	**1**	**0**	4.995637	0.157232	-4.775968

Table E-5: Continued.

10	1	0	3.804840	-1.058641	-4.282675
11	1	0	5.052850	-0.539734	-3.152528
12	6	0	0.659674	0.180720	-4.212631
13	1	0	1.270272	0.327485	-5.089575
14	6	0	4.185085	2.234343	-3.109093
15	1	0	4.880477	2.121102	-2.275861
16	1	0	3.476030	3.023275	-2.840104
17	1	0	4.758270	2.578844	-3.977074
18	6	0	3.435440	0.933236	-3.468161
19	1	0	2.845530	1.205621	-4.344994
20	1	0	0.000000	0.000000	-1.062729
21	7	0	0.000000	0.000000	2.076223
22	6	0	1.104857	-0.274108	2.851416
23	6	0	2.832226	-0.263746	1.063849
24	6	0	2.422118	-0.491343	2.398786
25	6	0	4.229502	-0.179786	0.651695
26	1	0	5.098637	-0.336779	1.268810
27	6	0	4.379982	0.192855	3.939654
28	1	0	4.995637	-0.157232	4.775968
29	1	0	3.804840	1.058641	4.282675
30	1	0	5.052850	0.539734	3.152528
31	6	0	0.659674	-0.180720	4.212631
32	1	0	1.270272	-0.327485	5.089575
33	6	0	4.185085	-2.234343	3.109093
34	1	0	4.880477	-2.121102	2.275861
35	1	0	3.476030	-3.023275	2.840104
36	1	0	4.758270	-2.578844	3.977074
37	6	0	3.435440	-0.933236	3.468161
38	1	0	2.845530	-1.205621	4.344994
39	1	0	0.000000	0.000000	1.062729
40	7	0	-2.011227	0.000000	0.000000
41	6	0	-1.104857	-0.274108	-2.851416
42	6	0	-2.832226	-0.263746	-1.063849
43	6	0	-2.422118	-0.491343	-2.398786
44	6	0	-4.229502	-0.179786	-0.651695
45	1	0	-5.098637	-0.336779	-1.268810
46	6	0	-4.379982	0.192855	-3.939654
47	1	0	-4.995637	-0.157232	-4.775968
48	1	0	-3.804840	1.058641	-4.282675
49	1	0	-5.052850	0.539734	-3.152528
50	6	0	-0.659674	-0.180720	-4.212631
51	1	0	-1.270272	-0.327485	-5.089575
52	6	0	-4.185085	-2.234343	-3.109093
53	1	0	-4.880477	-2.121102	-2.275861
54	1	0	-3.476030	-3.023275	-2.840104
55	1	0	-4.758270	-2.578844	-3.977074
56	6	0	-3.435440	-0.933236	-3.468161
57	1	0	-2.845530	-1.205621	-4.344994
58	6	0	-1.104857	0.274108	2.851416

Table E-5: Continued.

59	6	0	-2.832226	0.263746	1.063849
60	6	0	-2.422118	0.491343	2.398786
61	6	0	-4.229502	0.179786	0.651695
62	1	0	-5.098637	0.336779	1.268810
63	6	0	-4.379982	-0.192855	3.939654
64	1	0	-4.995637	0.157232	4.775968
65	1	0	-3.804840	-1.058641	4.282675
66	1	0	-5.052850	-0.539734	3.152528
67	6	0	-0.659674	0.180720	4.212631
68	1	0	-1.270272	0.327485	5.089575
69	6	0	-4.185085	2.234343	3.109093
70	1	0	-4.880477	2.121102	2.275861
71	1	0	-3.476030	3.023275	2.840104
72	1	0	-4.758270	2.578844	3.977074
73	6	0	-3.435440	0.933236	3.468161
74	1	0	-2.845530	1.205621	4.344994

Table E-6: Final coordinates for the DFT optimization of $H_2T(cyHx)P$.

Stoichiometry C44H54N4
Framework group C1[X(C44H54N4)]
Deg. of freedom 300
Full point group C1 NOp 1
Largest Abelian subgroup C1 NOp 1
Largest concise Abelian subgroup C1 NOp 1
Standard orientation:

Center Number	Atomic Number	Atomic Type	Coordinates (Angstroms) X	Y	Z
1	6	0	4.100315	2.374455	1.081261
2	6	0	6.195748	3.744977	0.609537
3	6	0	5.209853	3.702052	2.945571
4	6	0	5.963728	4.540197	1.902523
5	6	0	3.878393	3.170546	2.392131
6	6	0	4.879540	3.203808	0.029410
7	1	0	6.870832	2.903366	0.822916
8	1	0	5.841848	2.856160	3.252628
9	1	0	5.378968	5.442582	1.672290
10	1	0	3.195930	4.010830	2.234266
11	1	0	4.269906	4.039461	-0.330862
12	1	0	4.784397	1.574399	1.379424
13	1	0	6.704570	4.367354	-0.136352
14	1	0	5.026226	4.294178	3.850111
15	1	0	6.920314	4.886496	2.311831

Table E-6: Continued.

16	1	0	3.393836	2.518557	3.128215
17	1	0	5.080064	2.574612	-0.845894
18	6	0	2.841777	1.678427	0.548759
19	6	0	2.968149	0.300138	0.277433
20	6	0	4.182661	-0.459849	0.197958
21	6	0	3.877098	-1.713109	-0.258879
22	6	0	2.458555	-1.806429	-0.423519
23	7	0	1.962128	-0.563821	-0.091594
24	6	0	1.691783	-2.945166	-0.735841
25	6	0	1.656578	2.409217	0.290489
26	6	0	1.598440	3.865179	0.213117
27	6	0	0.347092	4.185023	-0.190567
28	6	0	-0.389725	2.929268	-0.298547
29	1	0	-0.034117	5.182968	-0.347513
30	7	0	0.434725	1.873857	-0.016706
31	6	0	0.299739	-3.014967	-0.458367
32	6	0	-0.432025	-4.277706	-0.393336
33	6	0	-1.671466	-3.983435	0.063056
34	6	0	-1.732556	-2.533222	0.208538
35	7	0	-0.517586	-1.979250	-0.099100
36	6	0	-2.919080	-1.821235	0.506296
37	6	0	-3.054789	-0.432526	0.296512
38	6	0	-4.275068	0.319545	0.231037
39	6	0	-2.550318	1.708854	-0.288145
40	7	0	-2.050742	0.454856	-0.014443
41	6	0	-1.785346	2.867161	-0.534629
42	6	0	-4.173415	-2.545533	1.010557
43	6	0	-6.261752	-3.907789	0.486554
44	6	0	-5.274165	-3.949987	2.822146
45	6	0	-6.025037	-4.750880	1.748053
46	6	0	-3.945545	-3.391624	2.288738
47	6	0	-4.948578	-3.337733	-0.072510
48	1	0	-6.941439	-3.078762	0.732157
49	1	0	-5.909539	-3.118998	3.161244
50	1	0	-5.436469	-5.641342	1.483515
51	1	0	-3.259826	-4.222252	2.096559
52	1	0	-4.334745	-4.155903	-0.463972
53	1	0	-4.861804	-1.761907	1.340872
54	1	0	-6.767352	-4.503910	-0.282600
55	1	0	-5.087554	-4.575325	3.703403
56	1	0	-6.979785	-5.116784	2.144400
57	1	0	-3.462650	-2.767098	3.049294
58	1	0	-5.152506	-2.676910	-0.923378
59	6	0	-2.487193	4.147036	-1.002023
60	6	0	-3.878260	5.329420	-2.772107
61	6	0	-3.823370	6.233525	-0.403460
62	6	0	-4.668604	6.054524	-1.672958
63	6	0	-3.270103	4.893684	0.107018
64	6	0	-3.339994	3.975035	-2.284375

Table E-6: Continued.

65	1	0	-3.037513	5.963120	-3.089126
66	1	0	-2.984980	6.910180	-0.623745
67	1	0	-5.568493	5.470979	-1.429703
68	1	0	-4.096956	4.275490	0.474932
69	1	0	-4.183184	3.298751	-2.112805
70	1	0	-1.691560	4.830639	-1.309278
71	1	0	-4.505836	5.182408	-3.659262
72	1	0	-4.413100	6.718623	0.383630
73	1	0	-5.019399	7.028060	-2.035752
74	1	0	-2.607836	5.058066	0.965058
75	1	0	-2.726412	3.506713	-3.062718
76	6	0	2.870200	-5.263073	-0.331548
77	6	0	3.254471	-4.019885	-2.591335
78	6	0	5.117107	-5.391007	-1.486721
79	6	0	4.773208	-4.207656	-2.401727
80	6	0	4.392159	-5.283197	-0.138658
81	6	0	2.315567	-4.215637	-1.351326
82	1	0	2.938891	-4.769184	-3.328607
83	1	0	4.820189	-6.330814	-1.974570
84	1	0	5.236904	-3.297909	-2.008091
85	1	0	4.727891	-4.389301	0.400885
86	1	0	2.581968	-6.257823	-0.700184
87	1	0	3.052948	-3.046975	-3.051218
88	1	0	6.201958	-5.447861	-1.337956
89	1	0	5.224764	-4.356628	-3.390212
90	1	0	4.656122	-6.134604	0.500485
91	1	0	1.447203	-4.699883	-1.793910
92	1	0	2.362547	-5.135586	0.629796
93	1	0	2.402858	4.557130	0.401641
94	1	0	-5.266054	-0.067850	0.408520
95	1	0	-2.466993	-4.687628	0.243490
96	1	0	-0.052725	-5.265731	-0.608052
97	1	0	4.573032	-2.515043	-0.415885
98	1	0	5.173309	-0.095475	0.420019
99	1	0	0.978625	-0.319188	-0.110554
100	1	0	-1.064089	0.221857	-0.026948
101	6	0	-3.974156	1.597647	-0.155974
102	1	0	-4.682558	2.395762	-0.300375